

**PETROLOGY OF THE PLUTONIC ROCKS OF THE
MACQUARIE ISLAND COMPLEX**



C. CHRISTODOULOU

**Thesis submitted to the University of Adelaide in
fulfilment of the requirements for the degree of
Doctor of Philosophy**

**University of Adelaide
Department of Geology and Geophysics**

1990

This thesis contains no material which has been accepted for the award of any other degree or diploma in any other University, nor to the best of my knowledge and belief, contains material published or written by any other person, except where due reference is made in the text.

C. Christodoulou

CONTENTS

	<u>Page</u>
Abstract	i
List of Figures	ii
List of Tables	iii
List of Plates	iv

CHAPTER ONE : INTRODUCTION

1.1 Previous work	1.1
1.2 Scope of the present study	1.2
1.3 Acknowledgements	1.3

CHAPTER TWO : GEOLOGY OF MACQUARIE ISLAND

2.1 Regional Setting and Tectonics	2.1
2.2 Geology of Macquarie Island	2.5
2.2.1 Previous Work	2.5
2.2.2 Layered Sequence	2.6
2.2.3 Peridotites	2.7
2.2.4 Upper Level Gabbro	2.8
2.2.5 Volcanic Rocks	2.9
2.2.6 Dyke Swarms	2.9
2.2.7 Minor Rock Units	2.10
2.3 Structural Geology	2.11
2.3.1 Layered Rocks	2.12
2.3.2 Lavas and Dyke Swarms	2.12
2.3.3 Shear Zones	2.13
2.3.4 Synthesis	2.14

CHAPTER THREE : PRIMARY PETROGRAPHY

3.1 Harzburgite	3.1
3.2 Layered Troctolites and Gabbros	3.2
3.3 Massive Gabbros	3.4

CHAPTER FOUR : IGNEOUS MINERALOGY

4.1	Olivine	
4.1.1	Harzburgite	4.1
4.1.2	Layered Rocks	4.2
4.1.3	Massive Gabbros	4.3
4.1.4	North Mountain Wehrlite	4.3
4.1.5	Lavas	4.3
4.2	Chrome-spinel	
4.2.1	Introduction	4.4
4.2.2	Harzburgite	4.5
4.2.3	Layered Troctolites	4.5
4.2.4	North Mountain Wehrlite	4.7
4.2.5	Lavas	4.7
4.2.6	Discussion	4.9
4.3	Pyroxenes	
4.3.1	Harzburgite	4.10
4.3.2	Cumulate Rocks and Massive Gabbros	4.11
4.3.3	Lavas	4.12
4.4	Plagioclase	
4.4.1	Layered Rocks	4.12
4.4.2	Upper Level Gabbro	4.13
4.4.3	Iron and magnesium substitution	4.13
4.4.4	Lavas and Dykes	4.14
4.5	Discussion	4.15

CHAPTER FIVE : METAMORPHIC MINERALOGY

5.1	Introduction	5.1
5.2	Layered Rocks and Massive Gabbros	5.1
5.3	Serpentinized Harzburgite	5.4
5.4	Chemical Effects of Alteration	5.6

CHAPTER SIX : GEOCHEMISTRY OF PLUTONIC ROCKS

6.1	Introduction	6.1
6.2	Peridotites	6.2
6.3	Layered Rocks	6.4
6.4	North Mountain Wehrlite	6.7

6.5	Massive Gabbros	6.7
6.6	Discussion	6.11

CHAPTER SEVEN : BASALTS AND DOLERITE DYKES

7.1	Mineralogy	7.1
7.2	Metamorphism	7.2
7.3	Geochemistry	7.4
	Geochemical Characteristics	7.8

CHAPTER EIGHT : CRYSTALLISATION MODELLING

8.1	Introduction	8.1
8.2	Geothermometry and subsolidus equilibria	8.1
	8.2.1 The olivine - spinel geothermometer	8.2
	8.2.2 Olivine - spinel geospeedometry	8.7
	8.2.3 Pyroxene thermometry	8.9
8.3	Mineral - Melt Equilibria	8.14
	8.3.1 Olivine-melt equilibrium	8.15
	Petrologic Applications	8.19
	8.3.2 Spinel-melt equilibrium	8.23
	Spinel synthesis	8.24
	Petrologic Applications	8.25
8.4	Crystallisation Models	8.30
	Olivine crystallisation	8.31
	Equilibrium crystallisation	8.31
	Fractional crystallisation	8.33
8.5	Conclusions	8.36

CHAPTER NINE : PETROGENESIS

9.1	Introduction	9.1
9.2	Phase diagram considerations	9.6
	9.2.1 The CaO-MgO-Al ₂ O ₃ -SiO ₂ (CMAS) system	9.7
	9.2.2 The pseudoliquidus OL-PLAG-DI-SI system	9.15
9.3	Partial melting modelling	9.23
	9.3.1 FeO - MgO modelling	9.23
	9.3.2 Transition metals	9.25
	9.3.3 Source composition	9.29
9.4	Trace element petrogenesis	9.32
	9.4.1 Fractional crystallisation	9.33
	9.4.2 Partial melting	9.35

9.5	Assessment of the processes controlling the compositions of Macquarie Island basalts	9.37	
9.5.1	Partial melting and mantle source	9.38	
9.5.2	Fractional crystallisation at low pressures		9.42
9.5.3	Magma mixing	9.45	
9.5.4	High pressure clinopyroxene fractionation	9.50	
9.6	Dynamics of melt segregation in the upper mantle	9.51	

CHAPTER TEN : MACQUARIE ISLAND AND OPHIOLITES

10.1	Mineralogic variability amongst ophiolite and abyssal peridotites. Comparisons with the Macquarie Island peridotites		10.1
10.2	Geologic and Mineralogic characteristics of ophiolitic cumulates - Oceanic gabbroic suites - Macquarie Island layered rocks.		10.7
10.3	Geochemistry of ophiolitic and abyssal peridotite-gabbro suites. Relationships to the Macquarie Island plutonic suite		10.10
10.4	Mid-ocean Ridge basalts, Ophiolitic lavas and the Macquarie volcanic suite. Petrologic characteristics and petrotectonic implications	Island	10.13
10.5	The concept of crustal magma chambers.		
10.5.1	Introduction		10.17
10.5.2	Geophysical considerations		10.18
10.5.3	Thermal models		10.18
10.5.4	Magma chamber models		10.19
10.5.5	Dynamics of magma chambers		10.20
10.6	Conclusions		10.23
	REFERENCES		1-25
	FIGURES		F2.1-F10.6
	TABLES		T5.1-T9.9d
	PLATES		P1-P11

APPENDICES

	<u>Page</u>
APPENDIX 1 : Sample descriptions	A.1
(A). Layered Sequence	A.2
(B). Upper Level Gabbro	A.6
(C). Peridotites and Gabbroic Mylonite	A.8
(D). Island Lake Gabbro	A.12
(E). Sandy Bay Gabbroic Unit	A.13
(F). North Mountain to Mount Blair: Gabbros and Werhlite	A.14
(G). East Coast: Nuggets Point to Sandy Bay	A.16
(H). Lavas and Dykes	A.16a
APPENDIX 2 : X-Ray Fluorescence and Atomic Absorption Analysis. Techniques and Results.	
(A). Preparation of samples	A.17
(B). Analytical techniques for major elements analysis	A.17
(C). Analytical techniques for trace elements	A.18
(D). FeO determination	A.18
(E). Results and CIPW normative mineralogy	A.19
(A). Layered Sequence	A.21-a.1
(B). Upper Level Gabbro	A.21-a.8
(C). Harzburgite	A.21-a.7
(D). Island Lake Gabbro	A.21-a.11
(E). Sandy Gabbro Unit	A.21-a.13
(F). Massive Gabbros and Werhlite	A.21-a.14
(G). East Coast	A.21-a.15
(H). Dolerite Dyke Swarm	A.21-a.17
(I). Dolerite Dykes in Layered Sequence and Upper Level Gabbro	A.21-a.18
(J). Dolerite and Gabbroic Dykes in Harzburgite	A.21-a.19
(K). Basalts	microfiche
APPENDIX 3 : Electron Microprobe Analysis and Results.	
(A). Instrumentation and precision levels of wavelength (WDS) and energy (EDS) dispersive systems.	A.22
(B). Olivine	microfiche
(C). Spinel	*
(D). Feldspars	*
(E). Pyroxenes	*
(F). Amphiboles	*

ABSTRACT

Macquarie Island is the only exposed part of the Macquarie Ridge Complex, which extends from the south of New Zealand to the Indian-Pacific-Antarctic triple junction. The island lies in the central sector of the Ridge Complex. Identification of the magnetic Anomaly 7 along the island suggests that the island formed at the Australian-Antarctic spreading ridge 27 Ma (Williamson et al., 1981). Radiometric dating of lavas and dykes gave ages of 9.7 ± 0.3 – 11.5 ± 0.3 Ma (Duncan and Varne, 1988).

The dominant structural feature on the island is faulting at every scale. Lavas and dykes make up two thirds of the island. In the northern third of the island, a sequence of plutonic rocks is exposed next to the lavas and dykes. It is this plutonic complex which represents the main theme of this thesis.

An idealised cross section (across the northern third) reveals the following lithological associations; at the base, peridotites which are overlain by a sequence of layered rocks. The layered rocks comprise a series of troctolites, olivine-gabbros and laminated olivine-free gabbros. The thickness of the cumulate pile is estimated to about 1.5km. The layered rocks are followed by a zone of massive gabbros and then a complex of sheeted dykes (dyke swarms) which are finally topped by volcanics. The volcanic section consists mainly of pillow lavas and massive lava flows.

Well developed macroscopic layering is the dominant feature of the outcropping layered rocks. A characteristic feature of the layering is the intrusive character of the layers themselves. The layers are isomodal and discontinuous and of limited lateral extent. Alternations of olivine-rich and plagioclase-rich layers typify the troctolite layering. The olivine-free gabbros at the top of the sequence show prominent igneous lamination. The transition between layered and massive gabbros is abrupt. On one side of the contact, the gabbro shows good planar lamination and on the other, the gabbro has a massive structure. The unit of massive gabbro is overlain by sheeted dykes. The contact between these two units is mutually intrusive. Dykes and lavas are normally porphyritic with large plagioclase phenocrysts and minor amounts of smaller olivine and occasionally clinopyroxene phenocrysts.

The petrography of the layered rocks reveals the following crystallisation sequence; chromite, olivine, plagioclase, clinopyroxene. The compositions of these minerals exhibit limited variations. Olivine is Fo_{90-81} and plagioclase An_{91-75} . Clinopyroxene has $Mg/(Mg+Fe)$ ratios of 0.92-0.83. Chromite is only an accessory phase and has 38.5-41%wt Cr_2O_3 ; its $Mg/(Mg+Fe^{2+})$ ratio ranges from 0.6 to 0.4. The composition of plagioclase from the massive gabbros varies from An_{86} to An_{56} , and the clinopyroxene displays similar $Mg/(Mg+Fe)$ ratios to the cumulus clinopyroxene. The peridotites are serpentized harzburgites and show metamorphic textures microscopically. Their mineralogy is very refractory; olivine is Fo_{92} , enstatite has $Mg/(Mg+Fe)$ ratios of 0.91 and the high-Ca pyroxene is even more magnesian, maintaining $Mg/(Mg+Fe)$ ratios of 0.92-0.93. Accessory spinel is aluminous with $Cr/(Cr+Al)$ ratios of 0.4-0.5.

The whole rock chemistry of the layered rocks is a reflection of their modal mineralogy. TiO_2 is always exceptionally low. The ferromagnesian trace elements show high contents, but the incompatible element concentrations are at extremely low levels. The mineralogy and geochemistry of these rocks support an accumulative origin. The massive gabbros show tholeiitic differentiation trends and some of them important Fe, Ti and incompatible element enrichments. The chemistry of these gabbros may thus represent primary melt compositions. The harzburgites are high in MgO, Cr and Ni and depleted in alkalis, Ti and incompatible elements. Both, mineralogy and bulk rock chemistry argue for a residual origin. The lavas and dykes can be divided in two groups according to their mineralogy and geochemistry, a tholeiitic and alkaline group. The tholeiitic rocks have moderate $Mg/(Mg+Fe)$ ratios and lower Ni and incompatible element concentrations than the alkaline rocks. On the basis of phase diagram relations and trace element abundances, it is suggested that the two groups are not related genetically.

Various geothermometers used to establish the crystallisation temperatures of the plutonic rocks. Magmatic temperatures range from 1165° to 1287°C. The layered troctolites and olivine-gabbros and the residual harzburgites have however re-equilibrated to subsolidus temperatures. Estimated blocking temperatures are less than 800°C and as low as 650°C. Therefore, these rocks cooled slowly over a long period of time; estimated cooling rates are less than 0.01°C per year. Mineral-melt equilibria indicate that liquids parental to the layered rocks must have had $Mg/(Mg+Fe)$ ratios of 0.72, high CaO/Na_2O ratios, $\geq 16\%$ wt Al_2O_3 , low TiO_2 ,

>300ppm Ni and >500-700ppm Cr. The effect of olivine crystallisation on the Mg/(Mg+Fe) ratios and Ni-contents of basalts and dolerite dykes has been determined. 2-5% olivine fractional crystallisation can account for the Mg/(Mg+Fe) ratios and Ni-contents of the most magnesian basalts and dykes; 5-10% fractionation accounts for basalts with moderate to low Mg/(Mg+Fe) ratios, from 0.56 to 0.66. Least squares calculations indicate that low pressure olivine+ plagioclase+ clinopyroxene fractionation controls the compositions of both basalts and dolerite dykes; the respective proportions of the fractionating minerals are 10-20%, 55-65% and 15-30%. These percentages are in very good agreement with their observed proportions in the layered rocks. Consequently, troctolites are complementary plutonics of basalts and dolerites.

Phase relations in synthetic and natural systems indicate that the tholeiitic and alkalic basalts are not related by any low-pressure and/or high-pressure fractionation process. Combined data from basalts, troctolites and harzburgites favor moderate to low degrees of partial melting (from 20% to less than 15%) under low fO_2 conditions (possibly less than the FMQ buffer). It is also inferred from the mineralogy of harzburgites that partial melting took place in the Ol-En-Di-Sp-Liq phase volume. The source peridotite composition was estimated from different fractions of basalt and harzburgite; calculations indicate that the source is similar to a spinel-lherzolite with $\approx 39\%wt$ MgO, $\approx 3.5\%wt$ Al_2O_3 , $<2\%wt$ CaO and $<0.2\%wt$ TiO_2 . Partial melting of such a source lherzolite at 10-15kbar produces melts similar to the most primitive glasses/basalts/dolerites, and MORBs as well, with $\approx 10\%wt$ MgO. These magnesian melts show a wide range of silica saturation. Low-pressure olivine and/or ol+plag+cpx fractionation produces residual liquids which are compositionally identical to the evolved basalts and dolerites. The two groups of basalts, tholeiitic and alkalic, have been produced by different degrees of partial melting. Although the alkalic basalts resemble P-type MORBs, there is no evidence for source region heterogeneity. The incompatible element characteristics of the alkalic basalts have been produced by small degrees of partial melting at considerable depths, possibly more than 50-60km. The tholeiitic basalts represent liquids derived from shallow depth melting, $<30-40km$, where decompression melting results in a significant increase of the melt fractions. The trends shown by the most primitive basalts/dolerites on phase diagrams are due to variable degrees of partial melting and

subsequent mixing over a wide range of depths, and not polybaric olivine fractionation from parental picritic melts.

The presence of a thick succession of cumulate rocks indicates the existence and operation of a magma chamber. The various layering features of these cumulate rocks suggest in-situ crystallisation in a small sized magma reservoir. This is also supported by the lithostratigraphy and the geochemical trends of the layered rocks. The thickness of this zone is less than 1.5 km. Finally, it must be emphasized that the exposed oceanic crust on Macquarie Island shows several and notable differences (such as crystallisation sequence of cumulus minerals, petrographic and geochemical characteristics of basalts) to ophiolites. This makes Macquarie Island distinct from other ophiolite complexes, and also a reference point for oceanic crust generated in a major oceanic basin.

LIST OF FIGURES

<u>Figure</u>	<u>Page</u>
2A Geological map of Macquarie Island	pocket
2B Geological map of the northern part of the island	pocket
2.1 Regional setting of Macquarie Island	F 2.1
2.2 Sketch of layering styles	F 2.2
2.3 Projections of structural measurements	F 2.3
2.4 Orientation of harzburgite faulting	F 2.4
2.5 Structural data of:	
(A) dolerite dykes cutting harzburgite,	F 2.5
(B) gabbroic dykes cutting harzburgite and	F 2.5
(C) gabbroic foliation	F 2.5
2.6 Correlation of orientation maxima	F 2.6
2.7 Synthesis of structural data	F 2.7
2.8 Relative plate motions in the South Pacific	F 2.8
4.1 Histograms of olivine compositions	F 4.1
4.2 NiO - Fo-content plots for olivine	F 4.2
4.3 (A). Small scale compositional variation in olivine	F 4.3
(B). Olivine composition variation in troctolites	F 4.3a
4.4 Cr-spinel composition plots:	
(A) $100\text{Mg}/(\text{Mg}+\text{Fe}^{2+}) - 100\text{Cr}/(\text{Cr}+\text{Al})$,	F 4.4
(B) $100\text{Mg}/(\text{Mg}+\text{Fe}^{2+}) - 100\text{Fe}^{3+}/(\text{Cr}+\text{Al}+\text{Fe}^{3+})$ and	F 4.4a
(C) Trivalent cation Cr, Al, Fe^{3+} projection	F 4.4b
4.5 $\text{TiO}_2 - 100\text{Cr}/(\text{Cr}+\text{Al})$ plot for Cr-spinels	F 4.5
4.6 $\text{TiO}_2 - 100\text{Mg}/(\text{Mg}+\text{Fe}^{2+})$ plot for Cr-spinels	F 4.6
4.7 Compositional variation of Cr-spinels according to the grain size (mm) and their $100\text{Mg}/(\text{Mg}+\text{Fe}^{2+})$ ratios	F 4.7
4.8 (A). Crystallisation paths of Cr-spinels according to grain size	F 4.8
(B). Core-rim variation in spinel phenocrysts	F 4.8a
4.9 (A). Pyroxene quadrilateral plot,	F 4.9
(B). $\text{Cr}_2\text{O}_3 - 100\text{Mg}/(\text{Mg}+\text{Fe}^{2+})$ plot in the layered rocks	F 4.9a
(C). $\text{Al}_2\text{O}_3 - 100\text{Mg}/(\text{Mg}+\text{Fe}^{2+})$ plot	F 4.9a
(D). $\text{TiO}_2 - 100\text{Mg}/(\text{Mg}+\text{Fe}^{2+})$ plot	F 4.9a
(E). $\text{Cr}_2\text{O}_3 - 100\text{Mg}/(\text{Mg}+\text{Fe}^{2+})$ and $\text{Al}_2\text{O}_3 - 100\text{Mg}/(\text{Mg}+\text{Fe}^{2+})$ plots in pyroxenes from harzburgites	F4.9a

(F). Si versus Al ^{IV} cation plot for magmatic clinopyroxenes	F 4.9b
(G). Coexisting clinopyroxenes and exsolved orthopyroxenes projected in the pyroxene quadrilateral	F 4.9c
4.10 Plagioclase composition histograms	F 4.10
4.11 (A). Compositional range for cumulus plagioclase	F 4.11
(B). Plagioclase composition in Upper level gabbro	F 4.11a
4.12 An FeO versus An-content plot for plutonic plagioclases	F 4.12
4.13 (A). Cation Ca-Al plot for plutonic plagioclase,	F 4.13
(B). Cation Ca - (Al+Fe)+2Mg plot,	F 4.13a
(C). Cation Ca-Si plot and	F 4.13b
(D). Cation Ca - (Si-Mg-Fe) plot	F 4.13c
4.14 Cryptic variation of principal mineral phases	F 4.14
5.1 A Mg/(Mg+Fe ²⁺) versus Si plot of amphiboles	F 5.1
5.2 A (Na+K) _A versus Si plot of amphiboles	F 5.2
6.1 Major oxide variation in respect to the MgO content of Macquarie Island harzburgites	F 6.1
6.2 AFM diagram for all plutonic rocks	F 6.2
6.3 MgO variation diagrams for the layered rocks	F 6.3
6.4 MgO - TiO ₂ diagram for the layered rocks	F 6.4
6.5 MgO content versus Cr and Ni concentrations (layered rocks)	F 6.5
6.6 Variation of Sc and Y concentrations with Ti-content according to lithology (layered rocks)	F 6.6
6.7 Plot of Sc against Y contents for the layered rocks	F 6.7
6.8 Variation of Zr and Y concentrations with Ti according to lithology (layered rocks)	F 6.8
6.9 Plot of Zr and Y concentrations for the layered rocks	F 6.9
6.10 MgO variation diagrams for the massive gabbros	F 6.10
6.11 Fe ₂ O ₃ +FeO - Mg/(Mg+Fe ²⁺) and TiO ₂ - Mg/(Mg+Fe ²⁺) plots for the massive gabbros	F 6.11
6.12 Diagrams of Cr and Ni contents versus Mg/(Mg+Fe ²⁺) ratios for the massive gabbros	F 6.12
6.13 (A). TiO ₂ -Sc, TiO ₂ -Y and Sc-Y plots for the Upper Level Gabbros	
(B). TiO ₂ -Zr, TiO ₂ -Y and Zr-Y plots * *	F 6.13
6.14 A plot of Sc versus Y plot for all massive gabbros	F 6.14
6.15 A plot of Zr versus Y plot for all massive gabbros	F 6.15
6.16 (A). An Al ₂ O ₃ -MgO diagram for Macquarie Island plutonics and extrusives	F 6.16
(B). A CaO-MgO diagram	F 6.16
(C). A TiO ₂ -MgO diagram	F 6.16
6.17 Stratigraphic variation of Ni, Ti and Zr contents	F 6.17

6.18	A $(C_1/C_0)_{Ti}$ versus percent of crystallisation diagram	F 6.18
7.1	Covariance of Sc and V concentrations in dolerite dykes	F 7.1
7.2	Plots of $Mg/(Mg+Fe^{2+})$ ratios versus FeO^t and TiO_2 contents of dolerite dykes	F 7.2
7.3	Cr-Ni and Cr-Zr plots for dolerite dykes	F 7.3
7.4	Zr-Y and Zr-Nb correlations in dolerite dykes	F 7.4
7.5	A plot of Sc and V contents in basalts	F 7.5
7.6A	Major (TiO_2 and MnO) and transition metal concentrations in basalts and dolerite dykes	F 7.6a
7.6B	Minor and Trace element concentrations in basalts	F 7.6b
7.7	A TiO_2 -MnO- P_2O_5 plot for basalts and dolerites	F 7.7
7.8	A Y versus $Ti/1000$ plot of Macquarie Island basalts	F 7.8
7.9	(A). A Ti-Y plot for plutonic and extrusive rocks	F 7.9
	(B). A $\log Ti$ - $\log Y$ plot for plutonic and extrusive rocks	F 7.9
8.1	An $\ln K_D$ versus $Cr/(Cr+Al+Fe^{3+})$ plot of plutonic spinels	F 8.1
8.2	Profiles of coexisting olivines and spinels in troctolites	F 8.2
8.3	A plot of spinel grain size versus the calculated temperature for troctolites (A) and harzburgites (B), wehrlite (C) and lavas (C)	F 8.3 F 8.3a
8.4	Plutonic pyroxenes projected on the pyroxene quadrilateral according to the method of Lindsley and Anderson (1983)	F 8.4
8.5	A plot of $Cr/(Cr+Al+Fe^{3+})$ versus $Mg/(Mg+Fe^{2+})$ ratios for selected spinels from troctolites and basalts	F 8.5
8.6	A NiO versus $Mg/(Mg+Fe^{2+})$ plot for Macquarie Island lavas and calculated liquid lines of descent during olivine equilibrium crystallisation from MgO-rich parental melts	F 8.6
8.7a-b	Liquid lines of descent (Mg^* -Ni plot) during olivine fractional crystallisation assuming parental liquid basalt 236	F 8.7a
8.7c-d	Liquid lines of descent (Mg^* -Ni plot) during olivine fractional crystallisation assuming parental liquid basalt 38188	F 8.7b
8.8	Mg^* -Ni liquid path during olivine fractional crystallisation with changing distribution coefficients with dropping temperature	F 8.8
8.9	A Fo-NiO plot for calculated and natural olivines	F 8.9

9.1 (a). The basalt tetrahedron of Yoder and Tilley	F 9.1
(b). The Fo-Di-An-SiO ₂ tetrahedron	F 9.1
(c). Joins An-Di-Fo and An-Fo-SiO ₂	F 9.1
9.2 Projection of the Macquarie Island data on the Di-An-Fo join	F 9.2
9.3 * * * * * Fo-An-Q join	F 9.3
9.4 Phase relations in the Di-An-Fo-Q tetrahedron	F 9.4
9.5 Projections in the PL-CPX-OL ternary	F 9.5
9.5 Phase relations in the olivine-diopside-silica projection of the Ol-Di-Plag-Si tetrahedron of Walker et al.	F 9.6
9.6 Phase relations in the olivine-plagioclase-silica projection of the Ol-Di-Plag-Si tetrahedron of Walker et al.	F 9.7
9.8 Ol-Di-Si projection of Macquarie Island data	F 9.8
9.9 FeO-MgO plot for basalts and harzburgites	F 9.9
9.10 Transition metal abundances in basalts and harzburgites	F 9.10
9.11 Calculated Nb and Zr abundances in residual liquid during batch partial melting	F 9.11
9.12 Observed Nb and Zr contents of tholeiitic basalts and calculated Nb and Zr contents in residual liquids	F 9.12
9.13 Observed Nb and Zr contents of alkalic basalts and calculated Nb and Zr contents in residual liquids	F 9.13
9.14 Zr/Nb-Y/Nb and Zr/Nb-Zr/Y plots for basalts	F 9.14
9.15 Major element variation diagrams for Macquarie Island glasses	F 9.15
9.16 Calculated geotherms of McKenzie & Bickle, temperature distribution beneath a ridge axis, degrees of partial melting (Ahern & Turcotte), and Di-Ol-Q projections of Walker et al.	F 9.16
10.1 Stratigraphy of Macquarie Island and other ophiolites	F 10.1
10.2 Spinel composition in ophiolites and Macquarie Island	F 10.2
10.3 (a). A plot of the Al ₂ O ₃ content in spinel versus the Al ₂ O ₃ content in enstatite for the Macquarie Island harzburgites	F 10.3
(b). Correlation of the Mg/(Mg+Fe ²⁺) and Al ₂ O ₃ of enstatites	F 10.3
10.4 AFM diagram for Macquarie Island massive gabbros, abyssal gabbros and Skaergaard rocks	F 10.4
10.5 A discriminating FeO/(FeO+MgO) - TiO ₂ plot for massive gabbros according to Serri (1980)	F 10.5
10.6 A Cr/(Cr+Al) versus Mg/(Mg+Fe ²⁺) plot for spinels from the Macquarie Island lavas and ophiolitic lavas	F 10.6

LIST OF TABLES

<u>Table</u>	<u>Page</u>
5.1 Olivine and serpentine compositions	T 5.1
5.2 Analyses of zeolite from veins	T 5.1
5.3 Epidote and zoisite analyses	T 5.1
5.4 Lizardite composition	T 5.2
5.5 Bastite analyses after orthopyroxene	T 5.2
7.1 Elemental ratios for selected basalts	T 7.1
Elemental ratios for selected dolerites	T 7.1a
7.2 Summary of the Ti/Zr, Zr/Nb, Zr/Y and Y/Nb ratios of Macquarie Island basalts and dolerites, and oceanic basalts from the Mid-Atlantic Ridge, the Indian Ocean and Oceanic Islands	T 7.2
7.3 Least squares mixing calculations	T 7.3
8.1a Calculated equilibration temperatures from the olivine-spinel geothermometer for troctolites	T 8.1
8.1b Calculated equilibration temperatures from the olivine-spinel geothermometer for harzburgites	T 8.1
8.2 Geothermometric Equations	T 8.2
8.3 Mg [#] ratios and Ni- & Cr- contents of primitive basalts, dolerites and glasses from Macquarie Island	T 8.3
9.1 Harzburgite and basalt addition - mixing calculations	T 9.1
Recalculated basalt composition after olivine addition	T 9.1a
Calculated source composition	T 9.1b
9.2 Selected peridotite compositions (worldwide)	T 9.2
9.3 Compositions of experimental basaltic melts	T 9.3
9.4a Observed and estimated Macquarie Island harzburgite compositions	T 9.4a
9.4b Calculated source compositions	T 9.4b
9.5 Rayleigh fractionation modelling for Zr & Nb	T 9.5
9.6 Geochemical characteristics of basalts and dolerites	T 9.6
9.7 Primitive Macquarie Island basalts and the 10 kb melts of Fujii & Scarfe (1985)	T 9.7
9.8 Observed natural peridotite compositions	T 9.7
9.9 Least squares mixing calculations	T 9.9a-d

LIST OF PLATES

<u>Plate</u>	<u>Page</u>
2.1 Layering characteristics of troctolites, Eagle Bay - Half Moon Bay	P.1
2.2 * * * *	P.2
2.3 * * * *	P.3
2.4 * * * *	P.4
2.5 Layering in olivine gabbros at Half Moon Bay	P.5
2.6 Layering features in olivine gabbros at Handspike Pt.	P.6
2.7 Layering features in olivine-gabbros at Handspike Pt.	P.7
2.8 Peridotite outcrop at Eagle Pt.	P.8
2.9 Contact relationships between dolerite dykes from the dyke swarm and the Upper Level Gabbro, south of Nuggets Pt.	P.9
2.10 Pillow lavas and sheeted dykes	P.10
2.11 Mylonites and sheared gabbros from Langdon Bay	P.11

CHAPTER ONE: INTRODUCTION



1.1 PREVIOUS WORK

Macquarie Island is located in the central part of the Macquarie Ridge Complex which extends from the south of New Zealand to the Indian-Pacific-Antarctic triple junction. The island is made up of rock types typical of oceanic crust and residual upper mantle; basalts, dolerites, gabbros, troctolites and peridotites. Similar rock associations are recognised among ophiolite complexes. The oceanic setting of Macquarie Island presents the challenge of studying a piece of oceanic lithosphere in an oceanic environment.

Previous studies on the geology of the island were presented by Mawson (1943), Varne et al. (1969) and Varne and Rubenach (1972). A study on the igneous petrology of basalts and dolerite dykes appeared by Griffin and Varne (1980). A detailed investigation of the metamorphism of lavas and dykes was presented by Griffin (1982). The magnetic properties of the extrusives have been investigated by Butler et al. (1976) and Levi et al. (1978). Geophysical studies were carried out by several people (Williamson, 1974, 1978; Williamson and Rubenach, 1972; Williamson et al., 1981). Ages have been obtained from fossils in calcareous oozes which are intercalated with lavas (Quilty et al., 1973). More recently, K-Ar and $^{40}\text{Ar}/^{39}\text{Ar}$ ages from lavas and dolerite dykes have been reported by Duncan and Varne (1988).

1.2 SCOPE OF THE PRESENT STUDY

This thesis presents a detailed study on the petrology and petrogenesis of the plutonic rocks of Macquarie Island. The relationship between plutonics and basalts is examined. New models on basalt genesis are also considered and applied. The geology of the island, the field relations and the regional tectonics in the region are outlined and discussed in chapter two; the nature of the layering of the cumulate rocks is presented in detail for first time, also in the second chapter. Chapter three describes the primary mineralogy and chapter four the mineral chemistry of the plutonic rocks. The metamorphism of the Macquarie Island plutonic rocks is examined in chapter five. Chapter six is a very detailed account of the geochemistry of these rocks. An overview, a review accompanied by presentation of new data, of the igneous and metamorphic petrology of the lavas and dolerite dykes is presented in chapter seven. Mineral-melt equilibria and crystallisation models are examined and discussed in chapter eight. Chapter nine is devoted to petrogenesis; various experimental studies are analysed and different petrogenetic scenarios are assessed on the basis of phase equilibria, phase chemistry and dynamic models. Chapter ten presents a comprehensive review of ophiolite lithologies, and compares the mineralogy and geochemistry of the Macquarie Island plutonic rocks and lavas to those of the ophiolite complexes and oceanic plutonics and extrusives.

Access to the island was provided by the Antarctic Division, Tasmania. Fieldwork was carried out during the 1983 and 1984 summer seasons. Permission to collect material from the island was granted by the National Parks and Wildlife Service of Tasmania.

1.3 ACKNOWLEDGEMENTS

I wish to thank my supervisor Dr. J. Foden, for suggesting and supporting this project. His encouragement and support have contributed the most to the completion of this thesis. I also wish to thank the Head of the Department of Geology and Geophysics for providing the departmental facilities.

I extend my thanks to the Antarctic Division of the Department of Science and Technology for providing transport to Macquarie Island and logistic support in the field during the summer visits of 1982-83 and 1983-84.

I would like to thank many persons in the Department of Geology and Geophysics of The Adelaide University for their significant contribution during this study. In particular, the assistance of P. McDuire and Dr. K. Turnbull in analytical chemistry techniques. The assistance of Mr. J. Stanley in X-Ray fluorescence analysis is highly acknowledged. My special thanks go to Mr. G. Trevelyan and W. Mussared for preparing a considerable amount of thin and polished-thin sections. I am indebted to Dr. B. Griffin for instruction and assistance in the electron microprobe, as well as many useful discussions on the mineralogy and geochemistry of the Macquarie Island lavas and dykes.

Dr. R. Varne of the University of Tasmania is thanked for providing unpublished data on Macquarie Island geology in the early stages of this project.

This project was sponsored by a research grant from the University of Adelaide.

Finally, I wish to express my thanks to the members of the technical staff of the Department of Geology and Geophysics for the preparation of this thesis; Mr. R. Barrett and Mrs. S. Proferes. The assistance of my colleague B. Morrison in computer programs is greatly acknowledged.

CHAPTER TWO : GEOLOGY OF MACQUARIE ISLAND

2.1 Regional Setting and Tectonics

Macquarie Island lies approximately 1100 km south-southwest of New Zealand and is the only exposed part of the Macquarie Ridge Complex, an arcuate system of ridges and trenches approximately 1800 km long (figure 2.1). The Macquarie Ridge Complex (MRC) formed by the movement of the Indian and Pacific plates relative to each other, and at present times represents the boundary between the Indian-Australian and the Pacific plates. The MRC extends from the Alpine Fault of the South Island of New Zealand to the triple junction of the Indian-Pacific-Antarctic plates near 62°S - 162°E (Sykes, 1970). The MRC has a complicated morphology. It consists of three principal segments. In the central segment between 47°S and 57°S, the ridge (Macquarie Ridge) is normally 2000 m below sea level, but in one case (Macquarie Island, together with the Bishop Islands to the south and the Judge and Clerk Islands to the north), it rises above sea level (Summerhayes, 1967; Hayes and Talwani, 1972). Macquarie Island trends almost parallel to the ridge. To the east of the Macquarie Ridge extends the Macquarie Trench, a 550 km long trough. In the northern segment of the MRC, a trough (Puysegur Trench) lies to the west of the ridge; in the southern segment, from 57°S to 62°S, a deep trench (Hjort Trench) lies to the west of the ridge. The bathymetry around Macquarie Island shows very steep gradients to the east towards the Macquarie Trench, but smooth gradients to the west (Summerhayes, 1967). It is inferred that there is no sediment cover on the Macquarie Ridge and that the Macquarie Trench contains undisturbed sediments of variable thickness (Hayes and Talwani, 1972; Houtz et al. 1972). Basalt, peridotite and gabbro have been dredged from the Macquarie Ridge to the south of Macquarie Island; these rocks are similar to those exposed

on Macquarie Island (Summerhayes, 1969; Watkins and Gunn, 1970). It is therefore very likely that the ridge consists of such rock types.

The Macquarie Ridge Complex is associated with relatively high seismic activity. Analysis of focal earthquake solutions have been carried out by Sykes (1967, 1970), Banghar and Sykes (1969), Johnson and Molnar (1972), and Jones and McCue (1988). These studies indicate that the earthquakes occur at shallow depths, and in the northern and central parts of the MRC most of the earthquakes were located along the ridge. In the northern segment, north of 51°S, the fault motion indicates the underthrusting of the Tasman sea floor (Johnson and Molnar, 1972); Jones and McCue (1988) inferred fault motion along reverse dip-slip faults and incipient subduction beneath the northern part of the ridge. In the central segment and the Macquarie Island area, the interpretation of the fault plane solutions indicates right-lateral strike-slip motion (Johnson and Molnar, 1972; Jones and McCue, 1988). In the southern segment of the MRC, right-lateral strike-slip motion predominates. The previous studies on earthquake fault plane solutions are all consistent with the rotation of the Pacific plate relative to the Indian-Australian plate in an anticlockwise manner and around a pole of rotation located to the east of the central segment of the ridge at 57°S (Johnson and Molnar, 1972) or 60.5°S (Minster and Jordan, 1978).

Williamson and Johnson (1974) reported marine gravity data from the Macquarie Ridge Complex, and Williamson and Rubenach (1972) from Macquarie Island. Inversion of the gravity data revealed thickening of the Indian plate oceanic crustal layer from west to east and towards the Macquarie Ridge, and asymmetry in the gravity profile of the central MRC. Williamson (1988) compared the asymmetry of the gravity profiles from Macquarie Ridge and specific regions around the world known to be related to different stages of subduction, and concluded that the structure of the central segment of the MRC is suggestive of incipient subduction. This is consistent with the shallow depth of earthquakes, and also indicates a compressional regime at the central part of

the ridge. It is inferred that the Indian - Pacific plate boundary lies at the Macquarie Trench. The uplift of Macquarie Island (primarily the formation of Macquarie Ridge) is a result of the transpressive regime in the central MRC between the Indian and Pacific plates.

Recent data on SEASAT geoid anomalies over the MRC suggest incipient subduction (although the definition of the geoid anomalies is poor) in the central ridge segment, and a well developed oblique subduction zone at the Hjort Trench (Ruff and Cazenave, 1985).

The compressional regime at the central segment of the MRC indicated by the crustal thickening at this part of the ridge, resulted in the uplift of rocks from the ocean floor by 5-10 km. Tilting of these rocks took place during the uplift of Macquarie Island. Paleomagnetic data indicate that the southern block of the island was rotated 55° clockwise about a vertical axis relative to the central block (Williamson, 1978). Paleomagnetic pole positioning inferred from the Macquarie Island data suggests that the island is part of the Indian plate (Williamson, 1978), but no unique solution can be obtained (Williamson, 1988).

The magnetic properties of the Macquarie Island basalts are comparable to the magnetic properties of basalts dredged from present day spreading ridges (Butler et al., 1976; Levi et al., 1978). The magnetisation of the lavas provides the major contribution to the sea-floor spreading anomalies (Williamson, 1978).

Sea-floor spreading magnetic anomalies in the Southern Indian Ocean, the Southwest Pacific Ocean and the Macquarie Ridge Complex have been investigated by Weissel and Hayes (1971), and Weissel et al. (1977). To the west of the Macquarie Ridge Complex and south of 48°S, the magnetic anomaly lineations have been traced from the Indian- Antarctic Ridge to Anomaly 21 (according to the magnetic reversal time-scale of Heirtzler et al., 1968). Magnetic anomaly patterns for the Macquarie Island region and the island itself

have been reported by Williamson et al. (1981). The magnetic anomaly profile along Macquarie Island correlates with the marine magnetic profiles to the west of the island. The identification of Anomaly 7 in the marine magnetic profiles and the similar magnetic anomaly data on the island, indicate that the anomaly profile on Macquarie Island is part of Anomaly 7, and the remanent sea-floor spreading anomalies are preserved in the rocks of the island. The remanent magnetisation of volcanics is similar to the sequence of reversals about Anomaly 7; it was interpreted as suggestive of the formation of the Macquarie Island rocks at the Indian - Antarctic spreading ridge at about Anomaly 7 time (Williamson et al., 1981).

The age of Macquarie Island inferred from the identification of magnetic Anomaly 7 is approximately 27 Ma B.P. (Williamson et al., 1981; Heirtzler et al., 1968). Williamson (1988) believes that this age is correct within ± 3 Ma (revision is made to account for probable misinterpretation of Anomaly 7 as being either Anomaly 6 or 8). Cocoliths from calcareous oozes found as thin intercalations to the pillow lavas of North Head, indicate an Early-Middle Miocene age (Quilty et al., 1973). Recently, Duncan and Varne (1988) obtained K-Ar and $^{40}\text{Ar}/^{39}\text{Ar}$ ages from the lavas and dykes. Fresh lavas which have suffered only low grade alteration (ocean floor weathering) from North Head and Mawson Pt., gave $^{40}\text{Ar}/^{39}\text{Ar}$ "plateau" ages of 9.7 ± 0.3 Ma B.P. and 11.5 ± 0.3 Ma B.P. respectively. These ages were interpreted by Duncan and Varne (loc. cit.) as original magmatic. A K-Ar age for a hornblende separate from a dyke (Pyramid Peak) gave an age of 11.5 ± 0.3 Ma B.P. Lavas and dykes from stratigraphically deeper parts of the section, have suffered greenschist facies metamorphism, and their ages, less than 7.2 Ma, simply reflect the end of metamorphism. The radiometric ages indicate that the oldest volcanic activity dates to 11.5 ± 0.3 Ma (Pyramid Peak lavas). The fresh lavas at North Head suggest younger volcanic activity possibly off-axis broadly correlatable with their alkalic character (Duncan and Varne, 1988). The radiometric ages,

approximately Middle Miocene, are compatible with the Early-Middle Miocene age inferred from the fossils. There is however a discrepancy with the Upper Oligocene age (27 Ma) inferred from the sea floor spreading Anomaly 7 from geophysical studies. The reasons for such a discrepancy could be related to sampling problems, diachronous igneous activity at the spreading-ridge, and the complex tectonic history of the Macquarie Ridge. Additional work is required to resolve the contradicting ages.

2.2 Geology of Macquarie Island

2.2.1 Previous Work

The first geological study on Macquarie Island appeared in 1943 by Douglas Mawson. Almost all rock types have been described in some detail, and a distinction was made between the "older" and the "younger" basic groups. A more recent and comprehensive geological study of the island was presented by Varne and Rubenach (1972). They recognised sections of dyke swarms and volcanic rocks, and reported on the metamorphism of lavas and dolerite dykes. The dyke swarms correspond to Mawson's "older" basic group and the volcanics to his "younger" group of Mawson. A more detailed account on the metamorphism of the volcanics and dolerite dykes from the dyke swarms can be found in Griffin (1982).

Two thirds of the island are made up of volcanics (figure 2A). The dolerite dykes, either in swarms or crosscutting other units, comprise the second most abundant rock type. Layered and massive gabbroic lithotypes, together with minor peridotite outcrops, constitute a considerable part of the outcrop in the northern third of the island.

2.2.2 Layered Sequence

The layered rocks are exposed along Eagle Bay, Half Moon Bay and at Handspike Point. (figure 2A). The layered rocks comprise a sequence of melatroctolites, troctolites and some minor occurrences of anorthosite. Layering in igneous rocks has been considered to indicate origin by cumulus processes (Wager et al., 1960). The classical concept maintains that the crystals are separated from the melt and are precipitated due to their greater density. The introduced rock classification by Wager and others was mainly genetic. Later, crystal settling has been questioned and alternative mechanisms have been proposed (Campbell, 1978; McBirney and Noyes, 1979). The terminology adopted here is only descriptive, has no genetic implications and follows Irvine (1982).

The layers are isomodal, consisting essentially of olivine and plagioclase. Clinopyroxene is only a minor constituent phase. A typical feature is the common alternations of olivine+plagioclase isomodal layers (plates 2.1A, B and C). The forms of layers are planar and discontinuous. Drag faulting is common and suggests ductile behaviour of layers adjacent to faults (plates 2.1B, C). The angles between the fault planes and the layering range from 24° to 60° . Mineral and size graded layers are normally absent. Layer contacts are modal (plates 2.2A, B, C). In places, some layers show well developed igneous lamination (plate 2.2C). The irregularity of layer repetition is demonstrated by the modal changes of olivine and plagioclase and is better illustrated in plates 2.3A, B, C and D. Sections normal to the plane of layering reveal flattening of olivine and plagioclase on this plane. Rhythmic layering, a typical feature of the large continental intrusions, is absent. The general style of layering shows that the modal character dominates the outcrop (plates 2.4A, B and C). The lateral extent of the layers themselves is limited to a few meters. The unique style of layering however is the intruding character of individual layers (plates 2.5A, B). A layer is normally injected to a set of parallel layers at an angle without showing any contact thermal effects.

The layered rocks around Handspike Point comprise olivine-gabbros, gabbros and laminated olivine-free gabbros. Minor anorthosite is also present. The layers are again isomodal and discontinuous. They taper out over a short distance. Layer contacts are either modal or phase. No grain sized layers occur, although some grain size variation is locally observable (plate 2.6A). The intrusive nature of the layering is present here as well (plates 2.6). It is best demonstrated by mafic layers intruding and intersecting other generation layers (plates 2.7A, B, C). Two sketches are redrawn after photographs in figure 2.2, and demonstrate sufficiently well this complexity. In the olivine-free gabbros, planar lamination is well developed by the alignment of tabular plagioclase and pyroxene. Lineate lamination is present in several places as well.

2.2.3 Peridotites

The peridotite outcrops are exposed along Langdon Bay, and Unity and Eagle peninsulas. Smaller occurrences of peridotite are encountered in several other localities in the northern third part of the island (figure 2B). In outcrop, the rocks develop black weathering surfaces. In handspecimen, pale green enstatites are set in a black cementing material, serpentized olivine. Long fibres of iridescent blue-green asbestos are formed next to fault surfaces. A typical feature of the outcrop is the close spaced faulting (plate 2.8A). Compositional layering is observed at Eagle Point. It is defined by sharp changes in the amounts of olivine and enstatite between adjacent layers. These layers are usually a few centimeters thick (plate 2.8B). The overall range is from around 50cm to less than 1cm. The very thin layers are almost monomineralic. The lateral extent of individual layers can be traced for approximately 2m.

2.2.4 Upper Level Gabbro

This unit of massive gabbro (ULG) is sandwiched between the dyke swarm complex and the sequence of the layered rocks. The main outcrop extends from Hasselborough Bay to Scoble lake (figure 2B). In outcrop, it is a massive and coarse-grained rock type; it consists mainly of plagioclase and clinopyroxene. Hydrothermal alteration results in the replacement of pyroxene by secondary pale green amphibole (uralite) which produces greenish colourations.

Dolerite dykes of variable sizes, from a few centimeters to about 1m in width, are very frequent throughout the entire outcrop. The dolerite dykes increase in frequency towards the top of the outcrop. The contact between the massive ULG and the dolerite dykes of the dyke swarm is best exposed along Hasselborough Bay and to the south of Nuggets Point. The actual contact is a broad zone of changing amounts of gabbro and dyke. Gabbroic screens occur throughout the lower horizons of dolerite dykes, becoming more frequent towards the contact zone (to the ULG). The percentage of gabbro increases downsection, till gabbro and dolerite occur in approximately equivalent amounts. The dolerite dykes further diminish in abundance and become the minor lithology of the outcrop. An intrusive relation between the two rock types is observed throughout this zone. Not only the dolerite dykes crosscut the massive gabbro, but the dolerite dykes themselves are penetrated by gabbroic material in a similar manner (plates 2.9A and B). This mutually intrusive character suggests a plastic environment of formation. Segregations of plagioclase in the form ^{of} lenses are also encountered across this transitional zone (plate 2.9C). Contact relations indicate that the ULG postdates the dolerite dykes.

There is a sharp contact between the ULG and the uppermost laminated gabbros of the layered series. Massive gabbro sits on a poorly layered (very weak planar lamination) gabbroic type. Only a few meters away, tabular plagioclase and pyroxene display strong planar lamination.

2.2.5 Volcanic Rocks

The dominant volcanic rock types are pillow lavas, volcanic breccias and massive lava flows. The pillow lavas are preserved in excellent exposures around North Head, Eagle Point, Caroline Cove and Green Gorge (figure 2A). The size of the pillows varies considerably among different outcrops, but is almost uniform within the same outcrop (plate 2.10A). The pillows are either closely packed or loosely packed. The interstitial material of the loosely packed pillows is reddish mudstone, calcareous ooze and hyaloclastite. Glassy rims are well preserved, together with ropy and contraction cracks.

Massive lava flows are well exposed at Mawson Point. A notable feature of the outcrop is the total lack of feeder dykes. Lenses of volcanoclastic sediments are included in these flows and are of variable size. The lenses are normally small but occasionally extend to several meters (laterally), and range from siltstone to volcanic conglomerate. Fine-grained sediments show well developed bedding and are truncated and convoluted. The more coarse-grained sediments resemble rubble deposits. The volcanic breccias consist of broken pillows. They resemble talus breccias accumulated at the base of fault scarps.

2.2.6 Dyke Swarms

The best exposures of the dyke swarms, or according to several authors sheeted dykes, are encountered at Hasselborough Bay, at Gadgets Gully, around Lusitania Bay and along the east coast, from the Nuggets Point to Sandy Bay (figure 2A). The unit underlies the extrusive sequence without a clearly defined contact. Nevertheless, Varne and Rubenach (1972) pointed out that the dolerite dykes crosscut interbedded lava flows and sediments at acute angles to the bedding planes. The lower contact of the unit is transitional to the massive gabbros.

The internal structure of the dyke swarm complex has been described by Varne and Rubenach (1972) and Griffin (1982). The main characteristic of the complex is the parallel intrusion of dykes amongst other dykes. The dykes show chilled margins facing the same direction. The width of individual dykes is not constant (plate 2.10B). Commonly, the dykes have porphyritic central zones passing to aphyric ones, and then to chilled margins. The most frequent phenocryst phase is plagioclase. Its size decreases from the centre to the margin of the dyke.

2.2.7 Minor Rock Units

Several outcrops of gabbroic bodies are exposed on the plateau of the island and along the east coast of the northern part of the island. The largest is the unit around Island lake. A unit to the northwest of Sandy Bay, extending to the south of Mount Power and around trigonometric 318, is also of considerable size; this unit will be referred to as the *318-gabbro* hereafter. Smaller gabbroic bodies are exposed between Sandy Bay and Nuggets Point, and also between North Mountain and Mount Blair (figure 2B).

The exposure of the massive gabbro unit around Island Lake is poor and the rocks are highly altered. The lithologies are medium-grained to coarse-grained gabbros. Screens of finer grained gabbro alternate with coarser rock types. In handspecimen, pyroxenes show the effects of alteration. They become grey-green to pale-green as they are being replaced by amphiboles. Plagioclase alters to epidote and prehnite. Dolerite dykes are frequent, but their width never exceeds 30cm.

Along the west slopes of Island Lake, the gabbro develops good foliation. Plagioclase and pyroxene are replaced by prehnite and biotite respectively. The foliated gabbro extends from Langdon Bay to Eagle Bay, where it is interbanded with harzburgite. The style of the exposed mylonitic structures is depicted in plates 2.11B and 2.11C. A zone of cataclasite is

= mylonite

exposed to the east of Langdon Bay. The cataclasite is a recrystallised and fine-grained rock, and shows prominent slickensided surfaces (plate 2.11A). The harzburgite interleaves with the mylonitic gabbros in a complex manner. Recrystallised gabbroic veins in harzburgite and detached harzburgitic blocks of variable sizes in the mylonitic gabbros are very frequent (plates 2.11C and 2.11D).

There are several small gabbro exposures in the northern third of the island. The gabbroic body *J18-gabbro*, to the northwest of Sandy Bay, another smaller body to the south of North Mountain and a few more gabbroic outcrops scattered along the east coast. These gabbros are massive, medium-grained to coarse-grained and in most cases very altered. About 1km to the north of Sandy Bay, there is a narrow zone of gabbro which shows typical doleritic textures.

2.3 Structural Geology

It is shown in figure 2A that more than two thirds of the island is made up of volcanics. Their stratigraphy and structure was studied by Varne and Rubenach (1972). The predominant strike directions in the central island are westerly - northwesterly, and southwesterly. The dips range from near horizontal to steep (nearly vertical) and change over a short distance. The steepest dips however measured in interbedded lava flows and sediments, therefore most reliable values, and are not more than 45° . The lavas therefore were tilted. Dolerite dykes cutting pillow lavas and lava flows interbedded with sediments show near parallel strikes. The angles between the planes of the dykes and the bedding planes of the lavas, irrespective of the high inclination of the latter, are always large. Consequently, the axes about which tilting occurred must have been parallel to the dyke - lava plane intersections, and assuming an original near horizontal deposition of the lavas, the axes of rotation must have

been horizontal (Varne and Rubenach, 1972). Later tectonic movements associated with the uplift of the island resulted in rotations around vertical axes which caused the strike variations.

The thickness of the volcanic section was estimated to about 1.6km by Griffin and Varne (1980). It was pointed out however by Griffin and Varne that the reconstruction of the volcanic section, based on two incomplete sections and the distribution of metamorphic mineral assemblages, must be treated sceptically.

2.3.1 Layered Rocks

The layering orientation of the troctolite exposure at Eagle Bay – Half Moon Bay is consistent over the entire outcrop. The dip angles however, are variable. The layered–laminated gabbros at Handspike Point have different layering orientation. Structural measurements are plotted on a lower hemisphere equal area projection (figure 2.3A). The compositional banding of the harzburgite from the Eagle Point outcrop, best correlates to the layering orientation of the troctolites from the nearby Eagle Bay exposure (figure 2.3A).

2.3.2 Lavas and Dyke Swarms

Structural measurements on the pillow lavas and the dyke swarms are taken from the data set of Varne and Rubenach (1972) and are plotted in equal area projections (figures 2.3C and 2.3B respectively). The bedding and dip measurements of the lavas from the southern part of the island are not consistent with those from the central island (Green Gorge area). Over the same outcrop, bedding and dips correlate well with those of the associated sediments. However, the dips are variable and range from shallow to steep even for the same area.

The attitudes of the dyke swarms from different parts on the island are usually consistent. The main dyke swarm complex consisting of the large

exposures at Hasselborough Bay and Gadgets Gully, strikes SE – NW. At Lucitania Bay, the sheeted dykes strike and dip in a similar way (figure 2.3B). The other dyke swarm exposure however, at Mount Martin, shows characteristically different dip directions (caused by tilting?).

2.3.3 Shear Zones

It has been before that a characteristic feature of the harzburgite outcrop is the frequent all-scale faulting. The orientations of the fault planes are plotted in figure 2.4. Although they show a wide scatter, two groups are distinguished.

At Unity and Eagle peninsulas, the harzburgite is interleaved with gabbro. The gabbroic foliation develops well to the south of Eagle Bay. The orientation of the gabbroic foliation is shown in figure 2.5C. Along a major fault zone, the rocks are crushed and recrystallised. The resulting *mylonite* zone has an orientation conformable with that of the gabbroic foliation (figure 2.5C). The mylonitization of the gabbro was probably synchronous to the development of the cataclasites. Away from the fault zone, the gabbros are strongly sheared. Moving further away the rocks still show the effects of dynamic metamorphism, but progressively decreasing with distance.

The dolerite and gabbroic dykes crosscutting harzburgite do not show consistent attitudes (figure 2.5A, B). Some of the gabbroic dykes show an overall conformity with the gabbroic foliation and could be related to each other by a common episode. In Langdon Bay, the gabbroic and dolerite dykes show similar orientations.

2.3.4 Synthesis

It is generally believed today that at any given spreading ridge environment the lavas are extruded on the ocean floor nearly horizontal, the dolerite dykes form steeply inclined intrusions and the plutonic rocks accumulate in a magma chamber.

The strikes of the dykes SE (ESE) are broadly consistent with the strike – around 170° – of the lavas from the south part of the island (south of Double Pt.), but inconsistent with the westerly strikes of lavas from central island (Mawson Pt. – Green Gorge). The SE (ESE) striking direction of the dykes corresponds to the orientation of the marine magnetic lineations around Macquarie Island (mainly to the west) and furthermore to the axis of the spreading ridge at anomaly 7 time (Williamson, 1974).

The density maxima of the various lithological units are combined in figure 2.6. A possible solution in agreement with the generally accepted stratigraphy, is inferred in figure 2.6. The troctolite exposure at Eagle Bay – Half Moon Bay, the dyke swarm unit at Gadgets Gully and the lava section of the south block of the island are consistent with the assumed stratigraphy. It is also inferred from figure 2.6 that the angle between the plane of the troctolite layering and the attitude of the dyke swarm is about 66° . The bedding planes of the lavas are comparable to the layering of the troctolites. The angle between the bedding density maximum of the lava section and the attitude of the dyke swarm unit is about 70° . This is in good agreement with the angles of more than 60° (mean 72°) measured in the field (Griffin, 1982).

The bedding of the lavas from the central part of the island neither correlates to the troctolite layering nor to the attitude of the main dyke swarm (Gadgets Gully). Assuming that the different dips caused by rotations around near-horizontal axes, then the strikes of the central island lavas must be rotated about a vertical axis at an angle of 60° clockwise, in order to coincide with the strike of the lavas from the southern island. This is in agreement with

the paleomagnetic reconstruction of Williamson (1978), who showed that the south part of the island has been rotated around a vertical axis about 55° in a clockwise sense relative to the central island.

It is generally accepted today that the present day relative motion of the Pacific and Indian plates along the Macquarie Ridge is right-lateral strike slip, and the motion of the Antarctic plate relative to the Pacific plate along the Antarctic - Pacific fracture zone is left-lateral strike slip. The magnetic lineations of the Antarctic plate extend from 1 to 18. The along strike lengths of the lineations record the total extent of the Southeast Indian Ridge during the last 45 million years (Weissel et al., 1977). The anomaly 5, 6 and 8 lineations on the Indian plate are shorter than their Antarctic counterparts. This means that the portion of the Indian plate which is younger than the lithosphere corresponding to anomaly 9, is missing. The missing Indian lithosphere is either subducted beneath or incorporated into the Pacific plate.

The configuration of the triple junction and the sea floor magnetic anomaly patterns can be used to determine the finite rotations and the Euler poles between plate pairs. Since anomaly 5 time, the finite rotation between the Pacific-Antarctic plates and the Indian-Antarctic plates has been 9.5° and 6.7° around Euler poles at $68.7^\circ\text{S}-100.3^\circ\text{E}$ and $9.7^\circ\text{N}-36.3^\circ\text{E}$ respectively. These finite rotations can be used to determine the the relative motion between the Pacific plate and the Indian-Antarctic spreading ridge system. The rotation since anomaly 5 time has been approximately 5° around a Euler pole at $70^\circ\text{S}-160^\circ\text{E}$. This pole is close but to the south of the triple junction. It is therefore concluded that since anomaly 5 time, the Pacific plate must have been overriding the site of mantle upwelling once occupied by the Indian-Antarctic spreading ridge. Because of the proximity of the Euler pole to the region, the overridden ridge system rotates clockwise with respect to the Pacific plate.

In order to test the credibility and accuracy of these deductions, the structural elements at the present day ridge are rotated about a Euler pole

70°S-160°E. Rotation of the lava bedding and the troctolite layering around this axis at an angle of 10° (which is the rotation of the ridge since anomaly 5 time) clockwise, brings point L to point L₁ (figure 2.7). The angle between point L₁ and the lava maximum is about 52°. The tilting between the central island block and that from the southern island is corrected by a simple rotation about a vertical axis by 50°. This magnitude is very close to that inferred by Williamson (1978), who concluded that the south island block was rotated 55° around a vertical axis relative to the central island block in an anticlockwise sense.

In summary, structural measurements on lavas, dykes and layered rocks indicate that the different rock units are tilted in their present day position, in agreement with Varne and Rubenach (1972); the island consists of three blocks in agreement with palaeomagnetic data (Williamson, 1978), and the southern block has been rotated relative to the central block around a vertical axis. The northern block is thrown on the central block along major fault zones. The different radiometric ages obtained from the central island volcanics (Pyramid Peak, Mawson Pt.) and those of the northern part of the island (north Head) suggest that these two blocks represent two non-synchronous pieces of oceanic crust which are found today in fault contact possibly as a result of transform faulting. A tentative explanation may be the following; the oldest central island block formed and started moving away from the ridge about 11.5 Ma. A younger piece of oceanic lithosphere (the northern block), formed later possibly at the proximity of a transform, is thrown onto the moving older lithosphere along a fault zone when the older lithospheric crust crosses the transform. The regional configuration of the plates and their respective motions from Anomaly 5 time to present day are shown in figure 2.8. There are numerous transform faults transecting the Australian-Pacific spreading ridge. The two blocks could represent oceanic crust forming in this spreading ridge but at different times, and being displaced along these transcurrent faults. These two diachronous blocks are then subjected to interactions with the Pacific plate

and are eventually uplifted together. Marginal interactions during their ascent could be responsible for the major fault zones observed on the west coast. Hence, although they are in actual fault contact, they represent non-synchronous lithosphere.

CHAPTER THREE : PRIMARY PETROGRAPHY

3.1 Harzburgite

The harzburgite mineralogy is fairly uniform. Olivine makes up 70% or more of the rock by volume and orthopyroxene accounts for 25-30%. Clinopyroxene is a minor constituent (<5%) and spinel is always less than 1%. The optical properties of the orthopyroxene make it of an enstatite composition. Pervasive serpentinization results in bastite pseudomorphs after orthopyroxene and mesh-textured lizardite after olivine.

The rocks are coarse grained. Individual enstatites are as long as 10mm. Porphyroclastic or mylonitic textures common in peridotites from ophiolites, are not present here. Instead, olivine forms large domains of strained crystals and enstatite is rounded with lobate grain boundaries, poikiloblastically enclosing smaller olivines. Exsolution lamellae of a Ca-poor phase parallel to (100) are usually fine, less than 10 μm , but in a few samples (eg. 161) they form blebs up to 0.05 mm wide. Olivine exhibits strain effects such as deformation lamellae and kink bands. In a second group of samples, small polygonal olivine crystals form trails along enstatite grain boundaries.

Reddish-brown spinel is closely associated with enstatite. It is always anhedral, interstitial and intergranular, and shows worm like shapes. Its irregular - interstitial character as well as its association with enstatite argue for a residual origin (Dick, 1977). Subhedral spinel crystals occur however as inclusions in larger enstatite crystals (eg. sample 179). Clinopyroxene forms cusped grains, always interstitial to enstatite and olivine.

3.2 Layered Troctolites and Gabbros

Both troctolites and olivine gabbros exhibit cumulus textures as well as planar lamination in thin section. The troctolites are olivine-plagioclase adcumulates, while the olivine gabbros range from adcumulates to mesocumulates. Adcumulate olivine-free gabbros from the top section of the layered sequence show prominent igneous lamination. The four primary minerals -olivine, chromite, plagioclase, pyroxene- show considerable modal variations from the lower to the upper parts of the sequence.

Troctolites range from melatroctolites (olivine \geq 70-75%) to felsic troctolites (plagioclase $>$ 65%). In general, the rocks are coarse grained. Cumulus olivine and plagioclase are subhedral with grain sizes ranging from 1 mm to 5 mm and 2 mm to 20 mm respectively. The olivine is either partly or wholly serpentinized. Plagioclase displays typical multiple albite twinning and is not optically zoned. Chromite is always an accessory phase (\leq 1%). It is commonly euhedral to subhedral, opaque, and is either included in olivine or plagioclase. Sometimes, it occurs at the boundaries of the much larger olivine and plagioclase crystals. It is the first phase to crystallize (possibly co-crystallised with olivine) in accord with observations in ocean floor tholeiites (Sigurdsson and Schilling, 1976), ophiolites (Pallister and Hopson, 1981) and experimental studies on melting of primitive basaltic glasses (Bender et al., 1978; Fujii and Bougault, 1983). The grain size varies from 0.1 mm to 0.3 mm. When chromite is enclosed in plagioclase however, its grain size reaches 0.9mm. The clinopyroxene is diopside. It forms highly interstitial grains, more than 3 mm across, although irregular blebs with a width of less than 0.02mm are also present. Assuming that clinopyroxene represents the crystallisation product of trapped liquid, the layered rocks can be classified on the basis of their

clinopyroxene content (Irvine, 1982). Modal diopside is less than 7% and therefore the troctolites are adcumulates.

In the olivine gabbros from the Handspike Pt. outcrop, olivine decreases in amount (5-15% of the mode) and chromite is not present. Clinopyroxene accounts for 30% of the volume and poikilitically encloses small euhedral plagioclases, less than 0.5 mm long. Exsolution lamellae of a Ca-poor phase are observed parallel to (100). The width of the lamellae is less than 5 μm , but occasionally they coalesce to larger blebs, 0.02mm wide. In very high resolution (SEM observation), two sets of lamellae are distinguished. The first is typically parallel to (100). The other is observed at an angle to the first and is very fine, less than 5 μm in width. Tabular plagioclase and clinopyroxene crystals are aligned with their long axes on the plane of layering. The planar lamination is best displayed in the olivine-free gabbros. Anorthositic layers, alternating with the olivine gabbros, display also strong igneous lamination. These layers consist entirely of plagioclase without any interstitial phase, and hence are extreme plagioclase adcumulates.

Intrusive mafic layers are emplaced at an angle to the layering of the olivine gabbros. They are made up of plagioclase, olivine, clinopyroxene and tiny chromite euhedra. Plagioclase accounts for 60-65% of the mode. Olivine is a cumulus phase and always less than 25%. Clinopyroxene is coarse-grained, poikilitic and accounts for up to 30% of the mode.

The observed crystallisation order is chromite + olivine \rightarrow plagioclase \rightarrow clinopyroxene. This is similar to the crystallisation sequence of the MgO-rich MORBs at pressures of less than 5 kbar (Bender et al., 1978).

The North Mountain wehrlite is medium grained. Cumulus olivine is subhedral to euhedral. It is either enclosed in large intercumulus clinopyroxene crystals or forms discrete domains. Interstitial plagioclase and accessory amounts of reddish-brown Cr-spinel make up the rest of the

mode. The texture resembles that of an orthocumulate (Wager and Brown, 1967).

3.3 Massive Gabbros

The Upper level gabbro is coarse-grained and consists of plagioclase (60-70%) and augitic clinopyroxene (30-40%). Rare olivine is present in accessory amounts. The Island Lake and Sandy Bay gabbros are medium to coarse grained and have similar modal mineralogies. A few samples however, contain minor olivine (up to 5%) and opaques. Typical hypidiomorphic textures characterize these rocks. Clinopyroxene, normally poikilitic, is partially or wholly replaced by uralitic amphibole. Very fine exsolution of an orthorhombic phase is present in most crystals. Plagioclase forms tabular crystals of varying sizes (0.2 mm - 3 mm long) and shows strong optical zoning. It alters to massive brownish aggregates. Sample 221A displays a subophitic texture. The medium grain size and the doleritic texture suggest that this gabbro is transitional to dolerite. A small gabbro outcrop occurs to the north of Sandy Bay. The rock is medium grained with doleritic texture. It contains primary kaersutite, green hornblende, strongly zoned plagioclase, minor amounts of sphene and apatite, and lesser amounts of skeletal ilmenite.

Most of the samples show the effects of the superimposed low grade metamorphism, and some the effects of deformation and shearing. Sample 209A has a typical mortar texture, where large granular grains are surrounded by finer grained plagioclase and augite. Increasing shearing results in the texture of sample 218, where plagioclase and augite augen are set in a fine-grained recrystallised matrix.

CHAPTER FOUR : IGNEOUS MINERALOGY

This chapter presents new mineral data on harzburgites, layered troctolites, layered olivine-gabbros, wehrlite Upper Level gabbro and other massive gabbros, and finally basalts. Mineral analyses obtained by microprobe analysis using a JEOL 733 electron microanalyser at the University of Adelaide. Details on the technique and the precision limits of the wavelength (WDS) and the energy dispersive (EDS) systems together with complete tables of mineral analyses are given in appendix 3. Analytical data on phenocryst phases from basalts and dolerites were presented by Cameron et al. (1980), Griffin and Varne (1980), and Griffin (1982). New mineral data on phenocryst phases from the lavas have been obtained and are presented in this chapter. One lava (sample M14) shows significant olivine and spinel accumulation. The spinel phenocrysts occur as isolated phenocrysts and glomerocrysts; the term xenocrysts (or megacrysts) is however more appropriate, because these olivines and spinels are not in equilibrium with the host lava.

4.1 Olivine

4.1.1 Harzburgite

Olivines in the harzburgite are chemically homogeneous. The compositions presented here are core crystal analyses. The range of major and minor oxide variations is relatively limited. No compositional variation was detected between alternating orthopyroxene-rich and olivine-rich layers. Fo-content [the atomic ratio $100 \cdot \text{Mg}/(\text{Mg} + \text{Mn} + \text{Fe}^{2+})$] ranges from 90.5 to 92 (figure 4.1). NiO increases with increasing $\text{Mg}/(\text{Mg} + \text{Fe}^{2+})$, and varies from 0.39% to 0.45%wt (figure 4.2). MnO shows a typical anticorrelation to Fo-content, and varies from 0.10% to 0.15%wt. The concentrations of CaO, Al_2O_3 and Cr_2O_3 are at extremely low levels.

4.1.2 Layered Rocks

The olivine composition in troctolites spans a limited range, $Fo_{87.5} - Fo_{89.7}$ (figure 4.1). NiO varies sympathetically with the Fo-content, ranging from 0.20% to 0.30%wt (figure 4.2). MnO content is between 0.15% and 0.20%wt, while Cr_2O_3 is always less than 0.01%wt. CaO and Al_2O_3 contents are very low, 0.007%-0.04%wt and 0.004%- 0.01%wt respectively (refer to appendix 3). The variation of olivine Fo-contents within a thin section is of the order of 1 mole%. Such a variation is very close to the analytical error. Core to rim variation in large olivines is minor. In one case however, when chrome-spinel is enclosed in or is adjacent to olivine, the $Mg/(Mg+Fe^{2+})$ ratio of olivine increases towards the chrome-spinel boundary. Olivine inclusions in chrome-spinel are more magnesian (Fo_{90-91}) suggesting subsolidus re-equilibration with the host mineral.

Small scale stratigraphic compositional variation of Fo-content is limited (figure 4.3A). The overall variation in sample 324 is 1.2% and in sample 393 merely 0.6%. In the well exposed troctolite outcrop at Eagle Bay, the thickness of the exposed section of the layered rocks is approximately 100 meters. Cryptic variation from the base to the top of this section is shown in figure 4.3B. At the base of this section, in the interval from sample 312 to sample 315, there appears to be progressive increase in the olivine Fo-content (pattern I). A minor decrease in the Fo-content follows, from sample 315 to sample 316 (pattern II). A reset of the olivine composition towards more MgO-rich compositions follows (samples 316 to 323). At the top of the section, patterns I and II are not clear because of the consistency in olivine composition (marked by ? in figure 4.3B). Although these variations are very limited, it appears that after an interval of olivine fractionation, the liquid becomes depleted in MgO and thus the olivine crystallising from this MgO-poorer liquid has a less forsteritic composition (pattern II). Pattern I (from sample 316 to

323) results from the resetting of the liquid $Mg/(Mg+Fe^{2+})$ ratio to higher values possibly by mixing with slightly more primitive melts.

In the olivine-gabbros from Handspike Pt., olivine displays lower $Mg/(Mg+Fe^{2+})$ ratios. Its composition lies between $Fo_{81.3}$ and $Fo_{85.3}$. NiO content ranges from 0.11% to 0.18%wt, and MnO from 0.20% to 0.26%wt.

4.1.3 Massive Gabbros

Three samples from the Upper Level Gabbro unit contain olivine. Fresh olivine has been analysed from two of these samples. It is $Fo_{72.9}$ to Fo_{81} in composition (figure 4.1). NiO and MnO range from 0.09% to 0.13%wt and from 0.27% to 0.38%wt respectively (figure 4.2). CaO, Al_2O_3 and Cr_2O_3 concentrations are very low. Olivine from the NW of Sandy Bay massive gabbro body (318-gabbro unit) maintains a uniform composition, Fo_{75} .

4.1.4 North Mountain Wehrlite

Cumulus olivine from the North Mountain wehrlite exposure has a composition of Fo_{83-87} . Its NiO content is high, 0.20%-0.26%wt. MnO is variable, showing a minimum value of 0.15% and a maximum of 0.25%wt.

4.1.5 Lavas

Olivine occurs as phenocrysts in both lavas and dolerite dykes. Fresh olivine has a composition of $Fo_{85.1}$ - $Fo_{89.5}$ (Griffin and Varne, 1980; Cameron et al., 1980). Both, forsterite content and NiO content are well within the observed range in the troctolites and the olivine-gabbros. One lava (sample M14) carries an unusually high proportion of olivine xenocrysts (megacrysts). These olivines are fresh, usually rounded, reaching up to 5mm in size. They contain a variety of chrome-spinel and glass inclusions. Compositionally, they are MgO-rich (Fo_{90}) with high NiO contents, 0.30- 0.34%wt. Their MnO contents span a limited range from 0.13% to 0.16%wt, whereas their Cr_2O_3 contents are

low, 0.05-0.06%wt, but higher than those in the troctolite olivines. These olivine "megacrysts" are only slightly more magnesian, but richer in NiO than their associates in troctolites.

4.2 Chrome-spinel

4.2.1 Introduction

Perfect spinel stoichiometry is assumed for the recalculation of the ferric and ferrous iron from the total iron of the microprobe analyses. The general formula of spinels is $(R^{2+})_8(R^{3+})_{16}O_{32}$ and deviations from it are considered to be minor (Irvine, 1965). The normal cation distribution, eight R^{2+} cations in the tetrahedral sites and sixteen R^{3+} cations in the octahedral sites, is also assumed. Therefore, the cation sum $R^{2+}+R^{3+}+R^{4+}$ equals 24, where R^{4+} represents the quadrivalent cations titanium and vanadium. $R^{2+}=8+R^{4+}$ and $R^{3+}=16-2R^{4+}$. Divalent cations of interest are the Mg, Fe^{2+} and Mn, and trivalent cations are Al, Cr and Fe^{3+} . Mossbauer spectra results justify such assumptions (Osborne et al., 1981).

Spinel analysed using the energy-dispersive system (EDS) of the electron microprobe. To ensure however the analytical precision and consistency of the results, half of the samples analysed using the wavelength procedure (WDS) as well. For analysis of minor oxides, the WDS method is more accurate with lower detection limits than the EDS. The only significant difference between the two methods was the higher V_2O_5 content indicated by the EDS method.

Cr-spinels lack higher reflectivity rims and 'ferritechromite' is generally absent. The development of 'ferritechromite' is a very common feature of the high Cr-spinels in serpentinized peridotites from ophiolites (Engin and Aucott, 1971; Onyeagocha, 1974) as well as stratiform complexes

(Beeson and Jackson, 1969). The most altered Cr-spinels in troctolites show the development of a very thin rim of higher reflectivity. This rim is patchy, and consists of a silicate- ferritechromite- magnetite mix. Euhedral spinel xenocrysts in basalts have black rims, suggesting disequilibrium with the surrounding basalt.

Cr-spinel analyses are projected in the compositional prism of Stevens (1944). The three projections used in this study are, the trivalent cation Cr-Al-Fe³⁺ triangle, the Cr/(Cr+Al) - Mg/(Mg+Fe²⁺) and the Mg/(Mg+Fe²⁺) - Fe³⁺/(Al+Cr+Fe³⁺) plots. Microprobe data are listed in appendix 3.

4.2.2 Harzburgite

Cr-spinels from harzburgites are Al-rich and plot in the chromian spinel field (figure 4.4C). Their 100-Cr/(Cr+Al) [abbreviated as cr*] ratios range from a minimum of 37 to a maximum of 53, but most of the analysed crystals have cr* ratios between 42 and 48. The ratio 100-Mg/(Mg+Fe²⁺) [abbreviated as mg*] varies from 55 to 71 (figure 4.4A). In general, there is an Al-Cr reciprocity at constant mg*, a feature very common among ophiolitic harzburgite - lherzolite and alpine-type peridotite Cr-spinels. The oxidation ratio 100-Fe³⁺/(Al+Cr+Fe³⁺) [abbreviated here as fe*] is always less than 10 (figure 4.4B). TiO₂ is consistently less than 0.05%wt. NiO content is also low and mostly less than 0.16%wt. The overall chemistry compares well with that of the abyssal and ophiolite peridotite Cr-spinels (Dick and Bullen, 1984).

4.2.3 Layered Troctolites

The spinel crystals in troctolites are always euhedral to subhedral, and occur as inclusions in either olivine or plagioclase; sometimes however, they are sandwiched at the boundaries of larger olivine and plagioclase crystals. Their chemistry was studied in detail according to their textural

habit. Individual crystals are internally homogeneous. Chemical zoning, from core to rim, was detected for grains enclosed in olivines.

Compositional data are plotted in figures 4.4A, 4.4B and 4.4C. The $mg^{\#}$ ratio increases with increasing $cr^{\#}$, and decreases with increasing $fe^{\#}$; $mg^{\#}$ ranges from 37 to 66 and $cr^{\#}$ from 42 to 58. The oxidation ratio $fe^{\#}$ is always below 15. The Cr_2O_3 content of all analysed Cr-spinels varies from 36.2% to 41.5%wt. TiO_2 contents are low, but significantly variable from 0.62% to 2.5%wt. MnO averages 0.35%wt. Cr-spinels from the intrusive melanocratic layers at Handspike Pt. contain less Cr_2O_3 (34.8-37.25%wt) and more TiO_2 (1.98-3.32%wt) and MnO (0.40%wt). In the trivalent cation diagram, there is a general trend away from the Al apex and towards compositions richer in Cr and Fe^{3+} (figure 4.4C). The variation of TiO_2 contents relative to the $cr^{\#}$ (figure 4.5) is similar to that observed in Cr-spinels from abyssal peridotites (Dick and Bullen, 1984). In addition, TiO_2 shows a good negative correlation with the $mg^{\#}$ ratio (figure 4.6). NiO is always low, 0.07-0.15%wt, and correlates positively with MgO.

The composition of Cr-spinels depends on their textural habit and their size as well. The size of those crystals which are enclosed in plagioclase is significantly smaller than the size of spinels (at similar $mg^{\#}$) enclosed in olivine. Assuming that the smaller the crystal size the later the generation of the crystal, then this relationship suggests that Cr-spinels included in olivine are higher temperature crystallisation phases (or cocrystallised with olivine), than those included in plagioclase. In addition, Cr-spinels included in plagioclase have higher $mg^{\#}$ (at equal grain size) than those included in olivine. This relationship between crystal size and $mg^{\#}$ ratio is well displayed in figure 4.7. Grain size and $mg^{\#}$ show a positive correlation. Specifically, the smaller the grain size the lower the $mg^{\#}$. This trend is better displayed by Cr-spinels included in plagioclases.

Compositional changes during the course of crystallisation are presented in figure 4.8A. Crystallisation paths of Cr-spinels are inferred from their sizes. Late crystallised Cr-spinels are less magnesian (lower $mg^{\#}$) and more Cr-rich (higher $cr^{\#}$) than the larger early crystals. The variation of $cr^{\#}$ and $mg^{\#}$ from core to rim is also shown for some of the larger grains. Rims usually have higher $cr^{\#}$ and lower $mg^{\#}$ ratios. This trend is similar to the "reverse zoning" observed in spinel phenocrysts from the Mid-Atlantic Ridge basalts (Sigurdsson, 1977).

4.2.4 North Mountain Wehrlite

Minor amounts of cumulus reddish-brown chrome-spinel occur in the North Mt. wehrlite as well. The crystal size ranges from 20 μ m to 0.2mm and is considerably smaller than the spinel size in troctolites. Core analyses show that these spinels have higher $mg^{\#}$ and lower $cr^{\#}$ compared to spinels from troctolites. The larger grains, more than 60 μ m, have high $mg^{\#}$ ratios (70-72) and low $cr^{\#}$ ratios (24-26) (figures 4.4A and 4.4B). The $cr^{\#}$ increases with decreasing grain size, while at the same time $mg^{\#}$ decreases. The smaller the grain size, the higher the $fe^{\#}$ ratio. TiO_2 variation is always inconsistent, 0.10-0.27%wt, whereas NiO averages 0.20%wt. MnO increases with decreasing $mg^{\#}$, and is always limited between 0.15 and 0.25%wt.

4.2.5 Lavas

Subhedral Cr-spinel crystals occur as small discrete phenocrysts and as rounded to euhedral inclusions in either olivine or plagioclase or both. Their compositional variation in terms of their $cr^{\#}$, $mg^{\#}$ and $fe^{\#}$ ratios is presented in figure 4.4. These spinels have higher $mg^{\#}$ ratios and lower $cr^{\#}$ and $fe^{\#}$ ratios than those from the troctolites. They also have lower TiO_2 contents (figure 4.5). Their lower $fe^{\#}$ ratios indicate less oxidising conditions during their formation than those in troctolites.

The lava M14 contains numerous Cr-spinel xenocrysts (megacrysts). Two types of xenocrysts are distinguished. Resorbed crystals (200 μm in diameter or less) with Al_2O_3 contents of 38%wt, and euhedral crystals or glomerocrysts with black rims (silicate - oxide intergrowth) and Al_2O_3 contents of 36-38%wt. Both types are not in equilibrium with their host basalt. Red-brown spinel xenocrysts having 27%wt Al_2O_3 have variable sizes. The cores of the high-alumina xenocrysts show the highest $\text{mg}^\#$ ratios (≈ 80) and the lowest $\text{cr}^\#$ ratios (≈ 30) (figure 4.4A). The low- Al_2O_3 spinels have $\text{mg}^\#$ ratios about 75 and $\text{cr}^\#$ between 40 and 50.

TiO_2 contents (core analyses only) are lower in the high-Al spinels, 0.12-0.14%wt, and higher in the Al-poor spinels, up to 0.20%wt (figure 4.5). The overall NiO-content range is from 0.20% to 0.26%wt, and hence is relatively higher than that of troctolite Cr-spinels. MnO contents are normally between 0.14% and 0.18%wt, though the more Al-rich spinels have MnO content as low as 0.11%wt. Rims have strikingly higher MnO, more than 0.30%wt, and lower NiO contents, less than 0.09%wt. Core-rim variation is shown in figure 4.8B for some of the xenocrysts. There is a dramatic decrease in $\text{mg}^\#$ ratios from cores to rims with a lesser increase in the $\text{cr}^\#$ ratio. $\text{Mg}/(\text{Mg}+\text{Fe}^{2+})$ drops from 0.8 in the core to less than 0.6 in the rim and is accompanied by a $\text{cr}^\#$ increase from 32-38 to 45. Similarly, TiO_2 shows a considerable increase from the cores (<0.2%wt) to the rims (up to 0.7%wt).

Equilibrium spinel phenocrysts in a basaltic glass from North Head (sample NH2) have $\text{Al}_2\text{O}_3 \approx 27\%$ wt, $\text{Cr}_2\text{O}_3 \approx 34\%$ wt, and 14.5%wt MgO. Their TiO_2 content is always more than 1%wt. In comparison to the spinel xenocrysts in the lavas (eg. sample M14), they have lower $\text{mg}^\#$ ratios, higher $\text{fe}^\#$ ratios, lower Al_2O_3 and higher TiO_2 contents. They are compositionally similar to the magnesiocromites of Sigurdsson and Schilling (1976). These phenocrysts are in equilibrium with glass having an $\text{Mg}/(\text{Mg}+\text{Fe})$ ratio of 0.64 and a TiO_2 content

of about 1.6%wt. They therefore represent lower temperature - higher fO_2 crystals in comparison to the high- Al_2O_3 spinel xenocrysts of the lavas.

4.2.6 Discussion

Spinel phenocrysts in basalts exhibit considerable textural and chemical variability. Abyssal basalts contain accessory spinel as inclusions in either olivine or plagioclase, and as individual euhedral crystals in variolitic groundmass (Sigurdsson, 1977; Dick and Bryan, 1978; Furuta and Tokuyama, 1983). Sigurdsson and Schilling (1976) described three types of spinel phenocrysts in MAR basalts. Chromian spinels with $cr^{\#}$ ratios of 22-26, magnesiochromites with $cr^{\#}$ ratios of 45-55 and titaniferous magnesiochromite with intermediate $cr^{\#}$ ratios. "Normal" zoning (decreasing $cr^{\#}$ from core to rim) and "reverse" zoning (increasing $cr^{\#}$ and decreasing $mg^{\#}$ from core to rim) were detected.

The spinel xenocrysts/megacrysts of the Macquarie Island lavas are chromian spinels and have a zoning pattern (figure 4.8B) similar to the "reverse" type of Sigurdsson and Schilling (1976).

The crystallisation of Cr-spinels from basaltic melts is a function of temperature, melt composition and oxygen content of the system. Experimental studies on the crystallisation of Cr-spinels from such melts were performed by Hill and Roeder (1974) and Fisk and Bence (1980). The results of Hill and Roeder (1974) suggest that with increasing fO_2 at constant temperature, the $cr^{\#}$ ratio and the MgO content of spinel decrease and the ferric iron increases. At constant fO_2 , decreasing temperature results in Cr_2O_3 , Al_2O_3 and MgO decreases and total iron and TiO_2 increases. Fisk and Bence (1980) synthesized high-Cr spinels, with $cr^{\#}$ ratios of 42-47, from a FAMOUS olivine-tholeiite having $Mg/(Mg+Fe^{2+})$ of 0.68. They established the following composition trend with decreasing temperature: decrease in $mg^{\#}$ and $cr^{\#}$ ratios and increase in $fe^{\#}$ ratios.

The spinel megacrysts of the Macquarie Island lavas are chromian spinels and have a zoning pattern (figure 4.8B) similar to the "reverse" type of Sigurdsson and Schilling (1976). According to the results of Hill and Roeder (1974) and Fisk and Bence (1980), during low pressure fractional crystallisation the $cr^{\#}$ and $mg^{\#}$ ratios of spinel decrease and the TiO_2 content and total iron increase. Ferric iron and TiO_2 content do indeed increase and the $mg^{\#}$ ratio decreases from core to rim in the Macquarie Island spinel phenocrysts, but the $cr^{\#}$ ratio increases as well. The $cr^{\#}$ pattern is not a temperature trend, but possibly relates to the crystallisation of plagioclase which results in an Al_2O_3 decrease in the melt and consequently in a reciprocal $cr^{\#}$ increase in the spinel (Fisk and Bence, loc.cit.). The observed zoning patterns of spinels from the lavas and the troctolites, considering only the (large) megacrysts and not those crystals included in olivines, are essentially identical. Because of this similarity, it is inferred that the zoning patterns shown by the plutonic spinels are of primary magmatic origin and not a subsolidus feature.

4.3 Pyroxenes

4.3.1 Harzburgite

The large enstatites have 100-Mg/(Mg+ Σ Fe) ratios from 90.5 to 91.5. Their CaO contents are between 1% and 3%wt. In the pyroxene quadrilateral diagram, they plot in the enstatite field (figure 4.9A). Cr_2O_3 content is less than 1%wt, while Al_2O_3 spans from 1.5% to 3.2%wt (figure 4.9E). TiO_2 is negligible and NiO never exceeds 0.1%wt.

Interstitial clinopyroxene has slightly higher 100-Mg/(Mg+ Σ Fe) from 92 to 94 and plots in the diopside field (figure 4.9A). Its Cr_2O_3 and Al_2O_3 contents vary from 2% to 4%wt and 0.5% and 1.5%wt respectively (figure 4.9E).

There are no chemical differences between the interstitial diopsides and the exsolved Ca-rich lamellae in large enstatites.

4.3.2 Cumulate Rocks and Massive Gabbros

Clinopyroxene from the layered rocks is in composition a diopsidic augite. The most magnesian types come from the melatroctolites where it is a minor and interstitial phase. Its $100\text{-Mg}/(\text{Mg}+\Sigma\text{Fe})$ ratio lies between 89.5 and 92. The composition range in terms of Ca, Mg, and Fe is from $\text{Ca}_{49.2}\text{Mg}_{45.9}\text{Fe}_{4.9}$ to $\text{Ca}_{46.5}\text{Mg}_{48.3}\text{Fe}_{5.2}$ (figure 4.9A). Cr_2O_3 and Al_2O_3 contents range from 0.5% to 1.5%wt and 2.5% to 4%wt respectively (figures 4.9B and 4.9C). Exsolved Ca-poor pyroxene is bronzite in composition, with $100\text{-Mg}/(\text{Mg}+\Sigma\text{Fe})$ of 89-90 and CaO contents of less than 0.9%wt (figure 4.10A). It has typically lower Al_2O_3 (1.2%-2%wt) and Cr_2O_3 (always less than 0.5%wt) than its host diopside.

The clinopyroxene from the olivine-gabbros and the laminated olivine-free gabbros, is less magnesian. The entire range of the $100\text{-Mg}/(\text{Mg}+\Sigma\text{Fe})$ ratios is from 89.3 to 83.3. The determined compositional range is depicted in the pyroxene quadrilateral (figure 4.9A). Cr_2O_3 content is usually less than 1%wt (figure 4.9B). The Al_2O_3 and TiO_2 contents are lower than those in the troctolite diopsides (figures 4.9C and 4.9D). The exsolved Ca-poor phase has Mg-values of 82-84. The Macquarie Island clinopyroxenes show distinctly higher TiO_2 contents than their counterparts from ophiolite complexes and ocean-floor gabbroic rocks (Coleman, 1977; Hodges and Papike, 1976; Hebert et al., 1983).

Figure 4.9F is a plot of substitutions of Al and Si in the tetrahedral sites for clinopyroxenes from troctolites (Kushiro, 1960; Malpas, 1978). The tetrahedral Al is low and consequently all the analysed diopsides-augites plot in the tholeiitic field. Coexisting pairs of Ca-rich (host) and Ca-poor (exsolved phase) are plotted in the pyroxene quadrilateral (figure 4.9G). The Ca-rich pyroxenes are displaced to the Ca-rich side of the solidus trend shown by the

pyroxenes of the Skaergaard intrusion (Wager and Brown, 1967; Atkins, 1969). The exsolved Ca-poor pyroxenes are also displaced towards less calcic compositions than the primary Ca-poor pyroxenes from the same intrusion. The broader miscibility gap defined by the Macquarie pyroxenes suggests significant subsolidus re-equilibration. The Ca-rich pyroxenes define a trend approximating the 800°C solvus of Ross and Huebner (1975).

Clinopyroxene from the massive gabbros has comparable major and minor element contents to that of the olivine-gabbros and the laminated gabbros from the layered series.

4.3.3 Lavas

The rare clinopyroxene phenocrysts in lavas are augites. Core analyses show limited variation. They usually have 100-Mg/(Mg+ΣFe) ratios of 86.6-89 (Griffin and Varne, 1980). In terms of quadrilateral components and minor oxide concentrations, the phenocrysts resemble the clinopyroxenes from the layered rocks (figures 4.9B, C and D). Reversed distribution of Cr₂O₃ between cores and rims was also observed (Griffin, 1982).

4.4 Plagioclase

4.4.1 Layered Rocks

In the layered troctolites, plagioclase is bytownite to anorthite in composition, An_{82-90.5}, (figure 4.10). In the olivine-gabbros, its composition ranges from An₇₄ to An₈₉ (figure 4.10), reaching a composition of An_{91.2} in an olivine gabbro from Handspike Pt. (figure 4.11A). The overall compositional range within individual sections is shown in figure 4.11A, a ternary diagram of the system CaAl₂Si₂O₈-NaAlSi₃O₈-KAlSi₃O₈. Iron and magnesium are detectable. The distribution of Mg is erratic. On the contrary, FeO shows a good positive

correlation with decreasing An-content (figure 4.12). Similar relationships were reported for plagioclase phenocrysts in abyssal basalts (Kuo and Kirkpatrick, 1982) and gabbros (Hodges and Papike, 1976) from the mid-Atlantic. Many traverses across plagioclase crystals of different orientations reveal complex zonation. The distribution of Ca and Na is highly irregular from core to rim. Even within the same section, a unique pattern is not defined. Although the cores are usually more calcic, in several cases the rims appear more calcic. Representative microprobe analyses are listed in appendix 3.

4.4.2 Upper Level Gabbro

The plagioclase composition from this gabbroic unit varies from An₆₆ and An₉₆. The end member component is illustrated in the An-Ab-Or ternary plot, figure 4.11B, for eleven selected samples. Core to rim variation in terms of An-content is even more irregular than in the plagioclase from the troctolites. FeO content is higher than that from the troctolites, and reaches a maximum value of 0.60%wt (figure 4.12). Plagioclase from a gabbroic screen in the dolerite dykes (sample 202) is significantly more Na-rich, reaching An₅₆. The entire range in this sample is from An₈₄ to An₅₆. In the other massive gabbro units, plagioclase spans the range observed in the layered rocks and the Upper Level Gabbro.

4.4.3 Iron and magnesium substitution

The substitutions in the two plagioclase end members, anorthite and albite, are of the type $R^{2+}(R^{3+})_2Si_3O_8$ and $R^+R^{3+}Si_3O_8$ respectively. R^{2+} cations are Ca, Mg and Fe^{2+} , and R^{3+} cations are represented by Al, Fe^{3+} . The only R^+ cation present is Na. Because microprobe analyses do not distinguish between Fe^{2+} and Fe^{3+} , stoichiometric considerations are employed to infer the type of substitution. In figure 4.13A, Ca cations are plotted against Al cations (analyses recalculated on the basis of 32 oxygens). Substitution of the

anorthite type is assumed. The Ca excess over Al, especially in the more Na-rich compositions, suggests that not all iron substitutes for Ca in the octahedral sites as Fe^{2+} . The agreement between predicted and calculated Fe distribution is better in the calcic plagioclases from the troctolites and the olivine-gabbros than that in the ULG plagioclase, suggesting that the amount of ferric iron, at least in the An-rich plagioclases, is very low.

Figure 4.13B is a plot of the Ca cations against the cation sum $\text{Al} + \text{Fe} + 2\text{Mg}$. If all iron was to substitute for Al in the tetrahedral sites as Fe^{3+} , then the relation $\text{Ca} = \text{Al} + \text{Fe} + 2\text{Mg} - 4$ would be true. It is clear that there is a shift of the data points to the right of the predicted distribution line, and a poorer correlation than that of figure 4.13A. The next two figures (4.13B and 4.13D) illustrate the correlation of Ca with Si, and Ca with $\text{Si} - \text{Mg} - \text{Fe}^{\text{tot}}$. All four diagrams show that iron is not exclusively in either Fe^{2+} or Fe^{3+} state. If only a small amount of iron is considered as Fe^{3+} , then the required rotation of the data points in figure 4.13A could be achieved. The amount of Fe^{3+} in the Upper Level gabbro plagioclase is higher than that in the troctolite plagioclase; therefore, the conditions were more oxidising during the formation of the Upper Level Gabbros than those prevailing during the accumulation of the layered rocks.

Based on similar arguments, Bryan (1974) concluded that most of the iron in plagioclase microphenocrysts from oceanic basalts is in the ferrous state, and also that both Fe and Mg substitute in the tetrahedral sites. On the hand, Hodges and Papike (1976) inferred that the iron of plagioclases from the abyssal gabbros at DSDP site 334 is mainly present in the ferric state.

4.4.4 Lavas and Dykes

Plagioclase is the most abundant phenocryst in both lavas and dolerite dykes. It is more frequent however in the tholeiitic basalts. The phenocrysts are usually tabular, zoned and corroded in their centres. Their size

is highly variable (2-6mm), reaching 30mm in the alkalic lavas. Core compositions are in the range An_{87-72} (Griffin, 1982). Cameron et al. (1980) reported more calcic compositions, An_{92-70} . Groundmass plagioclase reaches a compositions of An_{43} . Phenocryst rims and microphenocrysts span the entire compositional range.

4.5 Discussion

The composition range of olivine and enstatite from harzburgites is very restricted. Both phases are very magnesian and minor diopside is even more magnesian. The only phase showing composition variation is Cr-spinel, which shows a wide range in Cr/Al ratios. Cr-spinel is an accessory phase and consequently any compositional changes would not influence the bulk rock composition, with the exception of the rock chromium. For this reason, Cr-spinel composition, specifically its Cr/Al, Mg/Fe and Ti-content, will be more affected than the composition of any other phase during partial melting or fractional crystallisation. The geochemical behaviour of Ni and Cr is different from that of Ti. Ni and Cr partition to the solid relative to the liquid during partial melting or fractional crystallisation, because of their high crystal field stabilization energies and resulting strong octahedral site preference; Ni is enriched in olivine and Cr in spinel (Burns, 1973). Ti is enriched in the liquid, increasing with differentiation. The Ni content of harzburgite olivines is significantly higher than that of troctolite olivines. The Ti content of the Cr-spinel in harzburgites is extremely low and uniform, in contrast to the much higher (and variable) TiO_2 content of Cr-spinels in the overlying cumulates. Partial melting and fractional crystallisation produce lithologies with restricted phase compositions. During fractional crystallisation however, the precipitated phases show successive composition changes towards more

differentiated compositions. During partial melting the changes in phase compositions involve Mg, Ni and Cr increases (incorporated in the residual phases) and Al, Ti, Na, K, Fe decreases (enter preferentially in the melt); that is, phase compositions become more refractory. The differences in mineral chemistry (and textures as well) between harzburgites and troctolites indicate that harzburgites are residues of partial melting after the separation of basaltic melts.

Experimental studies on the crystallisation of olivine from primitive basaltic glasses confirm that at low pressures, from 1atm to 10 kbars, olivine is always the liquidus phase (Bender et al., 1978; Green et al., 1979). Bender et al. (loc. cit.) studied the phase boundaries and liquidus phase compositions of a primitive tholeiitic glass, with $Mg/(Mg+Fe) = 0.68$, from the FAMOUS area of MAR in the pressure range 1atm - 15 kbars. Olivine $Fo_{89.1}$ appears on the liquidus at 1265°C and 1atm. With decreasing temperature, olivine becomes less forsteritic; for instance, at 1205°C its composition is $Fo_{84.1}$. Green et al. (1979) also determined the liquidus phases of another primitive glass, with $Mg/(Mg+Fe) = 0.695$, from the South Atlantic. Again, olivine Fo_{88} is the liquidus phase at 1230°C and 1atm. At 1210°C, olivine becomes less Mg-rich, $Fo_{86.5}$. Plagioclase is the second phase to appear in the crystallisation order of these two tholeiitic glasses at 1atm. Bender et al. (loc. cit.) reported a liquidus plagioclase composition of An_{89} at 1235°C, An_{81} at 1218°C and An_{79} at 1208°C. Green et al. (loc. cit.) reported that the first plagioclase appears at 1210°C and has a composition of An_{79} . There is thus good agreement in the determined plagioclase composition at the respective temperature between the two studies, considering the slightly differing initial glass compositions. The only discrepancy is the reported plagioclase An_{89} by Bender et al. (loc.cit.), for which Langmuir and Hanson (1981) argued that it was not stoichiometric.

The composition of olivine in the Macquarie Island troctolites and gabbros as well as basalts is identical to that crystallising from primitive basaltic liquids, such as the two tholeiitic glasses, at 1 atm, whose phase relations discussed before. The plagioclase composition in troctolites is considerably more calcic than that observed by Bender et al. (loc. cit.) and Green et al. (loc. cit.). Similar calcic plagioclase is present in the plutonic suites of many ophiolites. Second stage *Q*-normative and *O1*-normative basaltic liquids have sufficiently high $Mg/(Mg+Fe)$ and CaO/Na_2O ratios to produce the magnesian olivines and the very calcic plagioclases observed in Macquarie Island and other ophiolites. Such "second stage" melts can be produced by melting a depleted mantle peridotite at shallow depths, less than 15 km (Duncan and Green, 1980).

The mineral cryptic variation throughout the sequence of the layered rocks and the overlying massive gabbros (Upper Level Gabbro unit) is shown in figure 4.14. The stratigraphic section was reconstructed on the basis of several traverses in the northern third of the island, from Langdon Bay to Hasselborough Bay. The variation in olivine composition (Fo-contents) is limited throughout the cumulates; nevertheless, the olivine Fo-content decreases progressively from the base to the top of the layered sequence. A similar pattern is shown by the $Ca/(Ca+Na)$ ratio of plagioclases; there is a progressive decrease in the An-content from the cumulates to the massive gabbros, although the within-sample observed compositional variation of plagioclases is much greater than that of olivines. The restricted decrease in olivine Fo-contents up-section and the overlap of the plagioclase compositions suggest that the $Mg/(Mg+Fe)$ and CaO/Na_2O ratios of the fractionating magma in the crustal magma chamber maintained relatively uniform composition, possibly because of mixing with primitive magmas (with high $Mg/(Mg+Fe)$ and CaO/Na_2O ratios) constantly feeding the magma chamber.

The textures of Upper Level Gabbros, the strongly zoned plagioclase, the variable amounts of Fe-Ti oxides and the presence of primary amphiboles indicate that these rocks are not cumulates, but crystallised directly from basaltic melts at higher fO_2 than the cumulates and possibly higher fH_2O . These rocks could possibly represent melts.

CHAPTER FIVE: METAMORPHIC MINERALOGY

5.1 Introduction

This thesis is focused on the primary mineralogy and igneous geochemistry of the plutonic rock types. In order to validate the arguments regarding the igneous processes, it is necessary to assess the hydrothermal effects on mineralogy and especially on the concentrations of the major and trace elements. The following discussion is aimed towards this direction, and by no means is a detailed study of the oceanic metamorphism beneath a mid-oceanic ridge. The hydrothermal alteration of troctolites, gabbros and harzburgites is examined in this section. Secondary minerals have been analysed and the mineralogic changes are discussed. The hydrothermal effects on the rock chemistry, major oxide concentrations and trace element abundances, are evaluated. The serpentinization of the harzburgites is also addressed.

5.2 Layered Rocks and Massive Gabbros

The troctolites and gabbros are altered to variable degrees. The extent of alteration depends on the stratigraphic position within the sequence and the proximity to fault zones. Cumulus olivine is variably fractured and altered. Alteration commences from the cracks and proceeds inwards producing a net of serpentine and magnetite dust. Four minerals are produced during the hydration process, lizardite, chlorite, talc and iddingsite. Iddingsite has a distinct brown colour in thin section and is usually superimposed to serpentine. Table 5.1 gives microprobe analyses of unaltered olivine and the surrounding lizardite, iddingsite and talc from samples 331A and 349.

Plagioclase alters to a fine grained cloudy brownish mixture. In the anorthositic layers, the original plagioclase is totally replaced by brown

patches and minor prehnite. In sample 319, thomsonite veins (table 5.2) crosscut plagioclase, now a mixture of clay minerals and clinozoisite. Similar replacement products have been described from the Equatorial Mid-Atlantic gabbros (Honnorez and Kirst, 1975). Clinopyroxene is either rimmed or replaced by colourless amphibole along its cleavage traces and around its periphery. The secondary amphibole always mimics the clinopyroxene precursor. Extreme lower temperature hydration of augites next to fracture zones results in dark brown aggregates.

Three types of amphiboles are present in the plutonic rocks. A colourless variety replacing augites, a green hornblende forming veins and a primary brown amphibole. The uralitic amphibole is commonly pale green to colourless with low Al_2O_3 (<4%wt) in the troctolites. In the massive gabbros, it is an actinolite with pale brown to pale green colours (figure 5.1). Veins of green hornblende are common in the Upper Level Gabbro and absent in the troctolites. Colourless actinolite-tremolite occurs in cracks and amygdaloid fillings. It shows euhedral shapes and is high in Al_2O_3 , more than 10%wt. Needle like fibers of tremolitic actinolite form patches in altered plagioclases. The observed compositional field is shown in figures 5.1 and 5.2, according to the classification of Leake (1978). The recalculation of the ferric iron, Al^{IV} and Al^{VI} were carried by the fortran program of Spear and Kimball (1984). In sample 726, the primary brown amphibole is kaersutite. It has more than 4%wt TiO_2 and 2%wt Na_2O .

In the massive gabbros, chlorite is a common secondary mineral. It occurs in patches and complex (multiple layer) veins. Compositionally, it is a clinochlore type with $\frac{\text{Fe}_{(\text{tot})}}{\text{Fe}_{(\text{tot})}+\text{Mg}}$ ratios from 0.10 to 0.22. Other frequently occurring metamorphic phases include epidote, clinozoisite (table 5.3) and recrystallised plagioclase of andesine (An_{50}) composition in sheared samples.

Minor sulphides are represented by chalcopyrite, pyrite and galena, and occur in the most altered samples.

Metamorphic conditions.

In troctolites, the secondary hornblende has high Al_2O_3 contents (>10%wt), while the actinolite from the massive gabbros has always less than 4%wt Al_2O_3 . This is in agreement with experimental studies in basaltic systems, which showed that the Al-content of the amphibole increases with increasing grade of metamorphism (Liou et al., 1974; Moody et al., 1983). In troctolites, the hornblende probably formed above 550°C (Liou et al., loc.cit.). This is the upper temperature stability limit of chlorite and represents the transition from greenschist to amphibolite assemblages (Moody et al., loc.cit.). The disequilibrium textures and the coexistence of hornblende, actinolite and chlorite indicate retrogression.

The greenschist facies assemblage actinolite+chlorite+ epidote+ albite has an upper temperature boundary of 475°C (Liou et al., loc.cit.). This assemblage characterises the massive gabbros, although albite is not present. The metamorphic assemblage of troctolites is therefore suggestive of metamorphism at the onset of amphibolite facies. The metamorphic assemblage of the gabbros indicates greenschist facies, or upper actinolite facies according to Stern and Elthon (1979). The presence however of chlorite and zeolite veins in the troctolites, suggest a later retrograde event. This is attributed to the successive changes in temperature, which were possibly governed by readjustment to different depths. This is also the case for the massive gabbros, where chlorite coexists with actinolite+sulphide.

5.3 Serpentinized Harzburgite

The style of serpentinization in harzburgites is similar to that described from oceanic ultramafics (Aumento and Loubat, 1971). Olivines are cut by a multiple network of cracks and fractures along which alteration proceeds inwards. Pervasive alteration results in mesh and hour-glass textures of serpentine after olivine, and bastite pseudomorphs after enstatite. The serpentine shows typical undulatory extinction and fibrous development. It is a length fast type. With increasing deformation mesh textures change to ribbon. The bastites show inward zoning (ie. sample 107). The development of sequential zones from the rims to the centres, and the relict enstatite cores suggest progressive replacement of the original crystals. Compositions of lizardite are listed in tables 5.4 and 5.5. Bastites have higher Al_2O_3 and Cr_2O_3 contents than lizardite replacing primary olivine. Fresh chromite is usually reddish brown. Alteration produces very dark brown to opaque crystals.

An important aspect of serpentinization is whether it is a constant volume or isochemical process (Thayer, 1966). Moody (1976) inferred that serpentinization takes place under constant volume and chemical composition at the same time. A second important aspect is the introduction of the fluid phase. In oceanic environments, seawater penetrates the crust to considerable depths through the extensive fracture system. The depth of fluid penetration varies between fast and slow spreading ridges because of the different fracture patterns. Alteration is more advanced in fast spreading ridges (Moody, 1979). The pervasive serpentinization of Macquarie Island harzburgites indicates sufficient supply of a fluid phase through an extensive and well developed fracture system. The relatively fresh nature of the olivine-gabbros is in contrast to the altered character of harzburgites. This difference is a reflection of the situation at the ridge. The deepest seated harzburgites are intensely faulted at a first stage. This stage is followed by the uplift of the

harzburgite blocks to such crustal levels where serpentinization commences. The next stage is the squashing of these blocks to the overlying crustal sequences. The final episode was accompanied by the development of numerous faulting at every scale, well preserved in the exposure along Langdon Bay.

The hydration reactions taking place during serpentinization are summarized by Coleman (1977). Hydration of olivine and orthopyroxene results in lizardite (\pm chrysotile) and brucite. Brucite is important because it defines the lower limit of serpentinization. It is however absent in these Macquarie Island rock samples which have been studied. Iron is partially oxidised and released during olivine alteration, resulting so in secondary magnetite. Moody (1976) has shown that the presence of magnetite is related to high temperature and low oxygen fugacity. Otherwise, iron substitution takes place into brucite. Coleman and Keith (1971) examined the effects of serpentinization in dunites and harzburgites in terms of modal mineralogy, MgO/SiO₂ ratios and major oxide concentrations. They concluded that SiO₂, MgO, FeO* (total iron), Al₂O₃, Cr₂O₃ and NiO have not changed during serpentinization, although calcium loss has been observed. The Macquarie Island harzburgites have similar MgO/SiO₂ ratios to those reported by Coleman and Keith (1971). Also, the bastites have similar Cr₂O₃ and Al₂O₃ contents to the unaltered enstatites (table 5.5).

The typical metamorphic assemblage of the Macquarie harzburgites is lizardite+chrysotile+ magnetite. Experimental evidence suggests that this paragenesis formed at temperatures less than 350°C (Evans, 1977). It is also similar to the type-3 assemblage of Wicks and Whittaker (1977), although brucite is not present. Antigorite forms above 500°C during prograde metamorphism. It is not observed in Macquarie serpentinites.

An experimental study on the direct interaction of seawater with fresh harzburgite (80% olivine and 15% enstatite) at 300°C and 500 bars was carried by Seyfried and Dibble (1980). The results are consistent with the predicted phase changes in the MgO-SiO₂-H₂O system for pressures lower than

1kbar (Johannes, 1968). The characteristic assemblage is lizardite+ magnetite+ minor anhydrite. This paragenesis strikingly resembles that of the Macquarie harzburgites, apart from the apparent incoming of minor anhydrite.

Most of the oceanic serpentinites are enriched in chlorine and boron, thus suggesting interaction with sea water (Sanford, 1981). Some chlorine was detected in the microprobe analyses of bastites (table 5.5).

In summary, the magnesium, total iron, aluminium and chromium contents of the Macquarie Island harzburgites were probably unaffected (or only slightly modified) by the serpentinization processes. The temperature and total pressure conditions of retrogression were 300°-350°C and less than 1kbar respectively. There are no indications of shearing during the hydration of harzburgites.

5.4 Chemical Effects of Alteration

Low temperature alteration of basalts is a complex process. It usually involves increases in Fe_2O_3 and H_2O , removal or addition of alkalis, leaching of potassium and rubidium, and decreases in SiO_2 , Al_2O_3 and CaO (Hart et al., 1974; Saunders et al., 1980). Griffin (1982) concluded that during the metamorphism of Macquarie Island lavas and dykes water was gained and the $\text{Fe}^{2+}/\text{Fe}^{3+}$ ratios changed. The elements Ti, Zr, Y, Nb and REE are known to be immobile during low temperature metamorphism (Pearce and Cann, 1973; Pearce and Norry, 1979). Griffin (1982) found very good correlations between the immobile Zr, P, Ti and the alkali elements. Zr, Y and Ti also correlate well amongst themselves and with the major oxides as well. This suggests that the original abundances of these elements in the lavas and dykes have not been destroyed by hydrothermal processes.

In gabbroic rocks, metamorphosed from greenschist to amphibolite facies, certain chemical changes took place. Introduction of Na, K, H_2O and

removal of Ca has been demonstrated for hydrothermally altered gabbros from the mid-Cayman Rise (Ito and Anderson, 1983). Leaching of several elements may occur according to Stern and Elthon (1979). The alteration of the Macquarie Island troctolites and gabbros is not pervasive. Olivine and augite are more susceptible to alteration than plagioclase. The replacement of olivine involves the addition of at least Al, Ca and H₂O and the removal of Mg and iron. Similarly, the alteration of pyroxene by amphibole requires H₂O and Al addition, and a sink for Si. If element losses and gains are accounted for, then it appears that they balance each other. The only exception is the necessary introduction of H₂O, and minor Na and Cl. Percolating sea water is the only source of supply for OH⁻, Na, and K and Cl. Sea water is also capable of transporting Ca, Mg and Fe (Ito and Anderson, 1983).

Examination of the bulk compositions of fresh and altered rocks shows no differences in both major and minor oxide concentrations. Certain immobile elements such as Zr, Y, P and Ti show good positive correlations amongst themselves under a wide range of metamorphic conditions. Similar good correlations are displayed by the Macquarie Island plutonic rocks (chapter 6). Other elements occurring in trace concentrations such as Cr, Ni and Sc, V show covariances which are anticipated from the modal mineralogy. It is concluded that the penetration of sea water into the oceanic crust and its interaction with the layer of the gabbroic rocks, is the cause for the development of the observed metamorphic assemblages. Secondly, the bulk rock compositions have not been modified during the alteration process. The removal of certain elements from specific primary minerals is limited to the scale of a few centimeters.

CHAPTER SIX : GEOCHEMISTRY OF PLUTONIC ROCKS

6.1 Introduction

This chapter examines the bulk rock chemistry of cumulate rocks, massive gabbros and harzburgites. A set of 60 samples from the layered rocks (Half Moon Bay and Handspike Pt. area), 78 samples from the various massive gabbro units (Upper Level Gabbro, Island Lake unit, North Mountain outcrop, Mount Blair outcrop, *318-gabbro* unit to the northwest of Sandy Bay, Rookery Creek outcrop), two samples from the North Mt. wehrlite and ten harzburgite samples (Langdon Bay, Eagle peninsula) were analysed by XRF techniques (see appendix 2 for details on sample preparation and analytical technique). In addition, fifteen dolerite dykes intruding harzburgite, layered rocks and massive gabbros were also analysed; major and trace element data of dolerite dykes were presented in chapter seven. Complete tables with the analytical data and CIPW normative mineralogies are included in appendix 2.

The chemical changes taking place during hydrothermal alteration were assessed in the previous chapter. Serpentinization of harzburgites is mainly responsible for H₂O increases and oxidation of ferrous iron to ferric iron. Altered samples as well as samples containing veins of metamorphic minerals and sulphides were excluded. The effects of alteration and metamorphism on the bulk rock composition of troctolites and olivine-gabbros as well as massive gabbros were discussed in chapter five. It was inferred that major element concentrations have remained nearly constant during submarine hydrothermal alteration. When the modal mineralogy and mineral chemistry are combined, then the estimated concentrations of major elements compare well with the measured major oxide contents in most rock samples. The loss on ignition (LOI) varies from 0.8% to 3%wt. Melatroctolites however, show higher LOI contents, up to 12%wt because of the advanced stage of olivine

serpentinization. Samples from the vicinity of fault zones and shear zones have been excluded.

The elements Ti, Zr, Nb are known to be immobile during metamorphism. The elements K, Rb, Cs, Ba, light rare earths (LREE) and Th were named large ion lithophile (LIL) by Schilling (1973). Wood et al. (1979) preferred the term "hygromagmatophile", and distinguished two groups; the "more hygromagmatophile" elements comprising the group of Rb, K, Th, Ta, Nb, LREE and the "less hygromagmatophile" group including Zr, Y, Ti, Sr and HREE. Their classification is based on the bulk distribution coefficients which are less than 0.01 for the first group and about 0.1 for the second group of elements. Saunders et al. (1980) argued that the previous scheme did not consider the atomic structure of the elements. They proposed the following grouping of elements according to the radius/charge ratio; elements with radius/charge ratio of less than 0.2 are named "high field strength" (HFS) and those having radius/charge ratio of more than 0.2 "low field strength" (LFS). HFS elements include the Zr, Hf, Ti, P, Nb, Ta and LFS the Rb, Cs, Ba, Sr, REE.

6.2 Peridotites

The Macquarie Island "tectonite" peridotites, mostly harzburgites, have been affected by hydrothermal alteration. The rocks are serpentinized and have average LOI (loss on ignition) values of 12%. The alteration effects on their bulk chemistry have been discussed in chapter five. It has been inferred that the principal process during serpentinization is the hydration of primary mineral phases, resulting in increases in the H₂O content and the Fe₂O₃/FeO ratios, and possibly the introduction of CO₂ and chlorine. For this reason the bulk analyses were adjusted to water free basis. The amounts of SiO₂, MgO, FeO^t (total iron), Al₂O₃, Ni and Cr remained relatively constant, in agreement with deductions for serpentinized peridotites from ophiolites (Coleman and

Keith, 1971). It is however possible that some Al_2O_3 and TiO_2 have been lost (Miyashiro et al., 1969b).

The $\text{MgO}/(\text{MgO}+\text{FeO}^{\dagger})$ ratios range from 0.84 to 0.81, and the $\text{Mg}/(\text{Mg}+\Sigma\text{Fe})$ ratios from 0.89 to 0.91. The Al_2O_3 (1% - 1.3%wt) and CaO (0.06% - 0.6%wt) content is a function of the modal amount of spinel and pyroxenes. Ti is always very low, less than 150 ppm. In order to evaluate the chemical characteristics of the harzburgites, major oxides are plotted in figure 6.1. The major oxide variations in respect to MgO content are shown together with compositional data from ocean floor peridotites. It is apparent that the Macquarie Island rocks form a group towards the more refractory compositions of the ocean floor peridotites (higher MgO and lower Al_2O_3 , CaO and alkali contents). In an AFM diagram (figure 6.2) the harzburgites plot on the MgO-FeO sideline and towards the MgO corner.

The concentrations of the compatible elements Ni and Cr average 2100ppm and 2550ppm respectively. The abundances of the transition metals Sc and V range from 9ppm to 14ppm and from 33ppm to 58ppm respectively. Concentrations of the incompatible elements Zr, Y, Nb, and Rb are extremely low and usually below the detection limit of the analytical technique (less than 1ppm).

In terms of major and trace element contents, the Macquarie Island harzburgites are very similar to the tectonised peridotites from ophiolite complexes and also to peridotites recovered from the ocean floor. It is generally accepted that the whole rock chemistry of these peridotites indicates that such rocks are refractory residues left behind after the removal of basaltic liquids from an initially undepleted upper mantle peridotite source (Dick, 1977; Hamlyn and Bonatti, 1980).

6.3 Layered Rocks

The concentrations of both major and trace elements from a representative set of samples including layered melatroctolites- troctolites, plagioclase-rich troctolites, olivine-gabbros, minor anorthosites and laminated olivine-free gabbros are presented here. Major oxide variation reflects the variation in the modal amounts of olivine, plagioclase and clinopyroxene. The correlation between the major oxide concentrations and the MgO content is shown in figure 6.3. The olivine-rich rocks show typically high MgO contents and low to very low CaO, alumina and alkalis. The plagioclase-rich and clinopyroxene-rich gabbros have lower MgO contents and higher CaO, Al₂O₃ and alkali contents.

In an AFM diagram (figure 6.2) the layered rocks define a rock trend away from the MgO-FeO sideline and towards more iron-rich compositions. The melatroctolites plot on the MgO-FeO sideline, the troctolites and olivine-gabbros towards more iron and alkali rich compositions, and the uppermost layered gabbros partly overlap the compositions of the least differentiated massive gabbros. Melatroctolites have high MgO contents (38-40.2%wt) and low to very low alumina, alkalis and CaO (figure 6.3). Troctolites have lower MgO contents (9-30%wt), and higher CaO (9-15%wt) and alumina (11.5-27%wt) contents. The alkali content is always very low. These variations reflect the changes in the modal amounts of olivine and plagioclase. The MgO content of olivine-gabbros ranges from 7% to 15%wt. The layered rocks define a general trend of decreasing MgO with increasing CaO, Al₂O₃, SiO₂ and Na₂O. The best correlation is shown by MgO and CaO contents. K₂O is less than 0.01%wt in the melatroctolites and between 0.1% and 0.5%wt in the troctolites; its concentration however could reflect secondary alteration effects. In fresh olivine-gabbros which show the minimum alteration effects under the microscope and the lowest loss on ignition values of all analysed samples from

the layered sequence, K_2O ranges from 0.03% to 0.04%wt. The MnO content of troctolites varies from 0.05% to 0.10%wt. It increases progressively in the olivine-gabbros, and it reaches a maximum value of 0.19%wt in the uppermost laminated olivine-free gabbros.

The TiO_2 content of melatroctolites is very low, always less than 0.05%wt (240-440ppm Ti); in troctolites, TiO_2 ranges from 0.06% to 0.1%wt (220-850ppm Ti), increasing progressively in the olivine-gabbros and gabbros, where it varies from 0.11% to 0.2%wt. TiO_2 content increases steadily with decreasing MgO content (figure 6.4). P_2O_5 is very low in all analysed cumulate rocks (0.00-0.02%wt). The extremely low P_2O_5 contents of the cumulates in comparison with those of basalts (0.15-0.65%wt) suggest that P_2O_5 was efficiently transferred to the intercumulus liquid. Similarly, TiO_2 must have been concentrated in the intercumulus liquid and hence it should be depleted in the cumulates. The very low TiO_2 content of the cumulates is in accord with such an interpretation. In addition, the intercumulus liquid in troctolites is very low. These rocks are thus adcumulates (Wager and Brown, 1967), formed by a process whereby selective diffusion of appropriate components from the magma to the crystallising olivine and plagioclase operates simultaneously with the removal of the interstitial liquid. The $Mg/(Mg+Fe^{2+})$ ratios of the troctolites will therefore be similar to those of the cumulus olivine. The $Mg/(Mg+Fe^{2+})$ ratios of troctolites are from 0.90 to 0.95, slightly higher than those of the constituent olivines (0.88-0.9) because serpentinization of olivine results in the formation of secondary magnetite and hence increases in the ferric iron content of the rock.

Two anorthosites from Handspike Point show the lowest MgO contents (0.1%wt) and the highest Al_2O_3 (32%wt) and Na_2O (2%wt) contents. These rocks have the lowest TiO_2 and total iron contents.

The concentrations of chromium and nickel show considerable variation from the base to the top of the layered sequence. The Ni content of

cumulates is high, reaching a maximum of 1645ppm in melatroctolites (figure 6.5). It decreases to 122ppm in the olivine-free gabbros. Cr shows a general increase with increasing MgO (figure 6.5). The dispersion of the data reflects variations in the amount of Cr-spinel and clinopyroxene, the two major phases accommodating Cr, in troctolites, and modal clinopyroxene in the olivine-gabbros. Anorthosites have the lowest Cr and Ni contents (figure 6.5).

The transition metals scandium and vanadium increase from the base to the top of the cumulate pile. Sc varies from 7ppm to 15ppm in troctolites and V from 15ppm to 42ppm. In the olivine-gabbros, Sc and V concentrations reach a maximum of 46ppm and 140ppm respectively. The concentrations of Sc and V show a positive correlation with Ti (figure 6.6). Sc and V concentrations increase steadily from troctolites to olivine-gabbros; the highest concentrations are observed in the clinopyroxene-rich laminated gabbros. Intrusive melanocratic layers in the olivine-gabbros (at Handspike Point) have similar contents to the olivine-gabbros. The chemical affinity of both elements and their intercorrelation (figure 6.7) suggest that Sc and V are mainly concentrated in clinopyroxene. Cu and Zn abundances are in the range of 30-88ppm and 13-46ppm respectively in troctolites. Olivine-gabbros have higher Cu (53-150ppm), but similar Zn (15-47ppm) concentrations.

The hygromagmatophile elements Rb, Nb, Zr, and Y are in extremely low concentration levels. Zr and Y correlate in a positive manner with Ti (figure 6.8); they increase from troctolites to laminated gabbros. Melatroctolites and troctolites have the lowest Zr and Y contents (<2ppm), olivine-gabbros have slightly but clearly higher contents, and the mafic intrusive layers from Handspike Point intermediate contents. Although the detected concentrations are very low and subject to analytical uncertainties, Zr and Y show an overall good positive correlation (figure 6.9), suggesting increases for both elements with increasing modal plagioclase and clinopyroxene. The abundances of Nb and Rb are below 1ppm. The observed

concentrations in trace elements are thus consistent with previous inferences that these rocks are adcumulates containing extremely low to negligible amount of intercumulus liquid.

The Sr content of troctolites is very low, a minimum of 1ppm was detected in melatroctolites. It increases with increasing modal plagioclase and reaches a maximum value of 200ppm in the anorthosites from Handspike Point. Ba shows a minimum of 1ppm in melatroctolites and a wide range in troctolites, from 10ppm to 90ppm, always increasing with increasing modal plagioclase. In the olivine-gabbros, it varies from 15ppm to 55ppm, and shows no definitive correlation with the amount of plagioclase; an anorthosite interlayered with the olivine-gabbros at Handspike Point, has only 5ppm Ba.

6.4 North Mountain Wehrlite

Two wehrlite samples from the North Mountain outcrop are also plotted in figure 6.3. They have high MgO content (33.8-34.7%wt), low CaO (3.6-4%wt) and low alumina (6.8-7%wt Al_2O_3) contents (figure 6.3). Their TiO_2 content is in the range of 0.29%-0.21%wt. Average Ni and Cr contents are 1300ppm and 2380ppm respectively. Sc and V concentrations are low, less than 15ppm and 70ppm respectively. Hygromagmatophile element abundances are very low; on average, Zr is about 11ppm, Y is less than 5ppm and Nb less than 2ppm. Such low concentrations compare with those of the cumulate rocks.

6.5 Massive Gabbros

Representative samples of massive gabbros from the Upper Level Gabbro unit, the Island Lake Gabbro exposure, the gabbroic unit to the northwest of Sandy Bay (*318-gabbro*), the small gabbro outcrop at North

Mountain, and the smaller exposures of doleritic gabbros along the east coast were selected for whole rock element analysis. The stratigraphic position of the Upper Level Gabbro unit, overlying the layered rocks and underplating the dyke swarms, is important because the stratigraphic position of the other gabbroic units is not known. For this reason, the compositional characteristics of all other units are related to those of the Upper Level Gabbro.

Major oxide variation diagrams are shown in figure 6.10; they illustrate the compositional trends of the different gabbroic units. Overall, there is a poor negative correlation between MgO and SiO₂, Na₂O and K₂O. In the Al₂O₃-MgO and CaO-MgO plots, there are no clearcut correlations; a poor positive correlation is shown by the Island Lake gabbros in both diagrams. The Upper Level Gabbros span the entire compositional range. Their MgO, CaO, Al₂O₃ and Na₂O contents range from 5.3% to 12.5%wt, 10% to 17%wt, 16.5% to 25.2%wt and 0.15% to 3%wt respectively; their TiO₂ content shows a considerable range (0.12-1.42%wt) and their P₂O₅ content is uniformly low (0.01-0.05%wt). Sample 221A shows enrichment in both TiO₂ (1.42%wt) and P₂O₅ (0.39%wt).

Two felsic samples (711 and 727) form leucocratic segregations in the Upper Level Gabbro unit at Nuggets Point; they have less than 3%wt MgO, have 2.6% to 6.2%wt Na₂O and K₂O 0.37% to 1.1%wt. A doleritic gabbro (sample 726) from a minor outcrop on the east coast (north of Sandy Bay) is significantly enriched in K₂O (0.36%wt), Na₂O (3.9%wt), TiO₂ (1.94%wt) and P₂O₅ (0.4%wt).

The Mg/(Mg+Fe²⁺) ratio of the gabbros is plotted against their total iron and TiO₂ content in figure 6.11. There is a progressive increase of Ti with decreasing Mg/(Mg+Fe²⁺) in all rock samples. This trend resembles a typical tholeiitic (liquid) trend during fractionation. Advanced differentiation of tholeiitic magmas produces rocks with abundant Fe-Ti oxides, such as ferro-gabbros and ilmenite-gabbros. Such gabbros have been recovered from the ocean

floor along the Mid-Atlantic Ridge (Prinz et al., 1976; Miyashiro et al., 1970). The Fe and Ti enrichment trends in the Macquarie Island massive gabbros are less pronounced; the two samples from the North Mountain exposure show the highest total iron ($12 \pm 0.5\%$ wt). In the AFM diagram of figure 6.2, the massive gabbros define a trend from MgO-rich compositions towards Fe-rich compositions with rising alkalies.

Minor and trace element concentrations vary greatly amongst samples from different localities. The Cr and Ni contents of the Upper Level Gabbros range from 257ppm to 1600ppm and from 80ppm to 290ppm respectively. The Cr and Ni concentrations from all analysed massive gabbros show a positive correlation to the $Mg/(Mg+Fe^{2+})$ ratios (figure 6.12). The lowest Cr and Ni contents are observed in a doleritic gabbro (sample 726); Cr is less than 5ppm and Ni is 37ppm. Sc and V range from 29ppm to 61ppm and from 77ppm to 227ppm respectively in the Upper Level Gabbros. The concentrations of Sc and V increase with increasing Ti-content, and show a good positive correlation among themselves (figure 6.13A). The two alkali-rich and Ti-rich samples (221A and 236) have comparable Sc contents with the other gabbros. Figure 6.14 is a Sc-V plot for all massive gabbros. The data points show a poor positive correlation. The lowest V concentrations are observed in the leucocratic samples 711 and 727.

The abundances of hygromagmatophile elements Zr, Y, Nb and Rb are lower than those in basalts, and higher than those in the cumulate rocks. In most gabbros, the Zr-content is usually between 4ppm and 15ppm, but it reaches higher concentrations in the Upper Level Gabbros, up to 74ppm (figure 6.13B). The Zr content of sample 221A is 127ppm. The doleritic gabbro (sample 726) has 139ppm Zr. Both Zr and Y increase with increasing TiO_2 content (figure 6.13B). Y ranges from 2ppm to 17ppm in most gabbros (figure 6.15). Samples 221A and 726 have 23ppm and 30ppm Y respectively. The gabbros from the North Mountain unit have average Zr and Y concentrations of 56ppm and 26ppm

respectively (figure 6.15). The abundances of Nb and Rb are usually very low in all massive gabbros. The Nb contents of the Upper Level Gabbros are less than 2ppm. Similarly, Rb is always limited to less than 3ppm, although a few altered samples show much higher contents. Two exceptions are notable; samples 221A and 726 contain 42ppm and 45ppm Nb respectively. These rocks contain minor sphene, where Nb proxies for Ti.

The concentration of Ba in the Upper Level Gabbros varies from 20ppm to 60ppm; sample 221A shows a maximum of 73ppm. The Ba content of all other gabbros is well within the range of Upper Level gabbros; the Ba content of sample 726 is 121ppm. Because of its large ionic radius cannot replace Ca, but can be captured in K-bearing phases. Ba shows higher concentrations in the alkali rich samples. The two felsic segregations from the higher parts of Upper Level Gabbro have 100–170ppm Ba; the sample with the highest Ba content (170ppm) has also the highest K₂O (1.1%wt) and Sr (365ppm) contents.

The Sr content of Upper Level Gabbros ranges from 112ppm to 299ppm. The overall range in massive gabbros is from 91ppm to 316ppm. Samples 711 and 727 have 365ppm and 394ppm respectively. Sr is mostly concentrated in plagioclase in the early stages of differentiation, but in the later stages is captured in K-bearing phases, mainly potash feldspar. In most analysed gabbros, Sr increases with increasing CaO and reaches highest values in the plagioclase-rich rocks which have the higher K₂O contents as well.

The normative mineralogy of the Upper Level Gabbros consists of 4–13% olivine, 28–57% anorthite, 12–40% diopside, 1–8% hypersthene, and minor amounts of magnetite (<2.5%) and ilmenite (<2.7%). Those rocks that are not *Hy*-normative, are nepheline normative (≤2% Ne). The Island Lake and *318-gabbro* (NW of Sandy Bay) are *Hy*-normative, whereas the North Mountain gabbros are *Ne*-normative (2–4% Ne). The alkali-rich doleritic gabbro (sample 726) has hypersthene (7%) and olivine (8%) in its norm.

6.6 Discussion

Major oxide variation diagrams in volcanic rocks can be used qualitatively to predict the fractionating minerals and the liquid paths. The major oxides CaO, Al₂O₃ and TiO₂ of the layered rocks, the massive gabbros, the lavas and the dolerite dykes from the dyke swarms are plotted against their MgO contents in figure 6.16. The trends defined by the massive gabbros, the dolerite dykes and the lavas suggest that their compositions are mainly controlled by olivine fractionation, although fractionation of plagioclase can not be ruled out. It is also shown in figure 6.16 that the liquids which produced the layered olivine-gabbros (lying on the MgO-poor side of the layered sequence array) are controlled almost exclusively by olivine fractionation of MgO-rich melts. Such a graphical method however is only qualitative; even so, it illustrates that the dominant phase controlling the compositions of lavas and massive gabbros (at least in terms of the oxides concerned) is olivine. It also precludes the possibility of a crystal extract consisting of either clinopyroxene or clinopyroxene+olivine.

Fractionation in a closed system magma chamber such as the Skaergaard intrusion, would result in simple relations between major and minor element concentrations (trace element concentrations as well). If magma mixing is an important process as the mineralogic data suggest (chapter four), then the differentiation paths of the erupted liquids would be better ascribed to an open system magma chamber model, such as the Rhum intrusion (Wager and Brown, 1967). The concentrations of the major elements as well as those of the minor elements Ni, Cr and Sr correlate with the proportions of the constituent minerals, whereas the concentrations of the incompatible elements Ti and Zr are very low in all cumulates. Figure 6.17 shows the stratigraphic variation of Ni, Ti and Zr in the plutonic rocks. Ni always correlates with the amount of modal olivine. Ti and Zr show no enrichment up-section and are

maintained at extremely low contents throughout the layered sequence. The abundances of Ti and Zr increase in the Upper Level Gabbros, but only in the uppermost stratigraphic horizons there are significant enrichments for both elements. Fractionation of a single batch of magma in a closed system would result in steady Ti increases upwards. The up-section Ti variation within the layered sequence is not comparable to the trend expected during closed system fractionation (figure 6.18). The fractionating assemblage in the model calculations was 20% olivine, 45% plagioclase, and 35% clinopyroxene, and the Ti content of the liquid was calculated from the TiO_2 content of the clinopyroxene assuming a $K^{T(cpx-llq)}$ of 0.3 (Pearce and Norry, 1979). Fractionation of olivine alone cannot reproduce the observed trend either. The observed Ti trend of the layered rocks suggests that crystal fractionation and magma mixing are the predominant processes; crystal fractionation of a single batch of magma in a closed system is ruled out. Repeated replenishment and magma mixing with liquids already undergoing crystal fractionation in an open system magma reservoir is more consistent with the present data than crystal fractionation processes of a single batch of magma in a closed (in both time and space) system.

CHAPTER SEVEN : BASALTS AND DOLERITE DYKES

This chapter reviews the previous works of Mawson (1943), Varne and Rubenach (1972), Griffin and Varne (1980), Cameron et al. (1980), and Griffin (1982) on the mineralogy, metamorphism and geochemistry of basalts and dolerite dykes. Additional data have been collected during the course of this study in order to complement the existing data set. Selected samples from the dolerite dykes have been analysed for major and trace elements. They were chosen on the basis of their position in the crustal section. Thirty basalt samples from the collection of the Geology Department, University of Tasmania, were run on the Siemens™ SRS-1 spectrometer of the Geology Department at Adelaide University. The analytical results showed good consistency between the two laboratories. The trace element concentrations given in Griffin (1982) are used in the following discussion; the reason for such a preference was to utilize all the trace element data on lavas and dykes obtained from one laboratory only. The abundances of scandium, vanadium and titanium (on pressed pellets) in basalts have also been determined at Adelaide University using the techniques described in appendix 2.

7.1 Mineralogy

The petrography of the lavas and dolerite dykes has been described by Mawson (1943), Varne and Rubenach (1972), and Cameron et al. (1980). Both basalts and dolerite dykes show a continuous gradation from porphyritic to aphyric types. The basalts also show a range from crystalline to glassy. The dolerite dykes are coarser than the basalts and have ophitic textures. The textures of the basalts range from ophitic and subvariolithic. Griffin (1982) distinguished two groups of basalts on the basis of their

petrography; one showing tholeiitic variants and a second with alkalic variants. The first group is characterised by subhedral plagioclase laths, augite displaying purplish rims, some skeletal titanomagnetite and interstitial glass ponds. The second group is distinguished by the occurrence of purplish titanaugites, phenocrystal and groundmass olivine and skeletal ilmenite- titanomagnetite. Basalts showing alkalic variants dominate the central part of the island. In the southern part of the island, the basalts are mainly tholeiitic (Griffin, loc.cit.).

The most common phenocryst phase is plagioclase ranging in composition from An_{87} to An_{70} (Griffin and Varne, 1980). Cameron et al. (1980) reported plagioclase phenocryst compositions of An_{90-70} . Phenocryst rims and groundmass crystals are always more sodic (An_{70-43}) than the phenocryst cores. Olivine (Fo_{85-89}) and clinopyroxene ($En_{55}Wo_{45}Fs_5 - En_{50}Wo_{38}Fs_{12}$) also appear as phenocryst phases, but in lesser amounts (Griffin and Varne, 1980). Occasionally, tiny spherical glass inclusions are present in the olivine phenocrysts. Reddish-brown Cr-spinel, $Cr/(Cr+Al) < 50$, is occasionally present as phenocryst as well. It is more frequent in the alkalic basalts and occurs as inclusions in either plagioclase or olivine phenocrysts.

The Macquarie Island basalts and dolerite dykes show similar textures and have comparable mineral chemistry to ocean floor basalts from the Mid-Atlantic Ridge system (Miyashiro et al., 1969a and 1970; Bryan et al., 1976; Rhodes et al., 1979; Bryan et al., 1979a and 1979b; Shibata et al., 1979a).

7.2 Metamorphism

The metamorphism of basalts and dolerites was described by Varne and Rubenach (1972) and Griffin and Varne (1980). The first study on

this subject was presented by Varne and Rubenach (loc.cit.). They distinguished two major groups. One showing development of greenschist and lower amphibolite facies assemblages and a second group showing only limited alteration, smectite weathering. Lower greenschist facies assemblages dominate in the southern block of the island and along the west coast from Langdon Pt. to Sandell Bay area. The observed lower greenschist facies paragenesis is, chlorite + albite + sphene + epidote + K-feldspar + sericite. The chlorite FeO/MgO ratio increases with increasing depth and reaches the highest values in those samples containing epidote and actinolite. Zeolite facies assemblages are common in the central part of the island and the east coast. The lavas around Pyramid Peak and Green Gorge show typical zeolite facies alteration. The metamorphic assemblage consists of Na,Ca,K zeolites + smectites + carbonate + sericite + chlorite. The highest grades occur around Caroline Cove (Griffin, 1982).

Upper greenschist to amphibolite facies assemblages are found in dolerites from the dyke swarm complex exposed at Gadgets Gully (Varne and Rubenach, 1972). Pyroxene is replaced by actinolite. Plagioclase is relatively unaltered, although development of chlorite in cracks took place. Sphene rims titanomagnetite. An Fe-rich amphibole, ferroactinolite-hornblende, appears in higher grades. In the dyke swarm to the southeast of Mt. Blair, the metamorphic assemblage is hornblende + chlorite + plagioclase + opaques (Varne and Rubenach, loc.cit.).

Pillow basalts from the North Head exposure are affected by ocean floor weathering (or low grade sub-zeolite facies alteration) according to Griffin (1982). Olivine alteration is pervasive. In holocrystalline rocks, olivine is replaced by yellow - orange smectites and calcite whereas plagioclase remains unaltered. Interstitial glass alters to smectite and carbonate. In hyaloclastites, the glassy rims around pillows are replaced by palagonite.

The uppermost boundary of zeolite development occurred at a depth of 300 m to 500 m and temperatures of more than 40°C. The lowermost boundary is placed at about 230°C. The greenschist facies assemblages indicate a minimum temperature of 230°C and a maximum of 300°C. A preliminary metamorphic map of Macquarie Island can be found in Varne and Rubenach (*loc.cit.*), and a more recent in Griffin (*loc.cit.*). The least altered lavas from North Head represent the uppermost part of the volcanic sequence. The increasing metamorphic grade from zeolite to lower greenschist facies in the rest of the island indicates deeper positions in the volcanic pile. Lavas from the west coast and southern block of the island represent the stratigraphically deepest lavas in the volcanic sequence.

7.3 Geochemistry

The whole rock chemistry of basalts and dolerite dykes was presented in detail elsewhere (Varne and Rubenach, 1972; Griffin and Varne, 1980). New data on the scandium and vanadium concentrations of both basalts and dolerites are presented here. In addition, fifteen samples of selected dolerite dykes have been analysed for major and trace elements. These samples were chosen on the basis of their host lithology; they include dykes crosscutting harzburgite, layered troctolites and gabbros, and massive gabbros from the Upper Level Gabbro unit.

Both basalts and dolerites grade from *O1*- and *Hy*-normative to *Ne*-normative; *Q*-normative rocks are rare. Griffin and Varne (1980) pointed out that "the normative transition from *O1*- and *Hy*-bearing to *Ne*-bearing rocks corresponds with the appearance of groundmass olivine and titanite". Their Mg/(Mg+Fe) ratios range from 0.51 to 0.72. Varne and Rubenach (*loc.cit.*) and Griffin and Varne (*loc.cit.*) have employed

discriminant plots to elaborate their chemical characteristics. Based on the concentrations of the incompatible elements (Ti, Zr, Y and Nb) they inferred that most of the basalts and dolerites are geochemically similar to ocean-floor basalts. Those basalts that plot outside the ocean-floor basalt field are *Ne*-normative, and have high Nb contents, low Zr/Nb and Y/Nb ratios, and relatively low Ti/Zr ratios.

The Sc and V abundances of dolerites range from 25 ppm to 44 ppm and from 148 ppm to 395 ppm respectively. When the two elements are plotted against each other, they show a good positive correlation (figure 7.1). Figure 7.2 is a plot of the $Mg/(Mg+Fe^{2+})$ ratio against the FeO^t (total iron) content of dolerite dykes. The five groups shown in figure 7.2 represent dolerite dykes crosscutting harzburgite, layered rocks, massive gabbros, pillow lavas and also dolerites from the dyke swarm complex. Total iron increases with decreasing $Mg/(Mg+Fe^{2+})$. In the $Mg/(Mg+Fe^{2+})$ against TiO_2 diagram (also shown in figure 7.2), the Ti-content increases with decreasing $Mg/(Mg+Fe^{2+})$. In both plots, there is no grouping of the samples according to their host lithology. The compatible elements Cr and Ni correlate in a positive manner (figure 7.3). The abundances of the incompatible trace elements Zr, Y, and Nb are plotted in figure 7.4; Zr and Nb show a positive correlation in samples with Nb contents of less than 30 ppm, whereas the not so well constrained positive correlation in the Zr-Y plot is continuous. All these diagrams demonstrate that dolerite dykes from distinctly different stratigraphic units do not define separate clusters. It is inferred that dolerite dykes from the dyke swarms and those crosscutting pillow lavas are neither more nor less differentiated than those crosscutting harzburgites and cumulate rocks. Furthermore, the differentiated or not character of each dolerite dyke is independent of its stratigraphic position in the crustal sequence.

The abundances of vanadium and scandium in basalts are in the range of 141-327 ppm and 24-40 ppm respectively. Figure 7.5 is a Sc-V plot and shows a general positive correlation between the abundances of these two elements. The abundances of the other transition metals Ni, Cr, Co show typical MORB ranges, from 52 ppm to 302 ppm, from 103 ppm to 663 ppm, and from 30 ppm to 49 ppm respectively. The incompatible elements Zr, Y, Nb are immobile during low temperature sub-sea floor hydrothermal alteration (Pearce and Cann, 1973). The ranges of the Zr, Y and Nb concentrations are 32-163 ppm, 11-45 ppm and 1-73 ppm respectively (after Griffin 1982). A summary of selected major oxide and trace element variations is presented graphically in figures 7.6A and 7.6B. The lavas are divided into two groups. The first group comprises the central island volcanics (Green Gorge, Aurora Pt., North Head) which are mainly alkalic, and the second the southern island volcanics (Mawson Pt., Hurd Pt., Caroline Cove) which are mainly tholeiitic in character. The variations of TiO_2 with P_2O_5 , Zr with TiO_2 and Y, and Nb with Ti and Zr show the consistently enriched character of the alkalic basalts relative to the tholeiitic basalts. The elemental ratios of the determined incompatible elements from representative basalts and dolerites are given in table 7.1.

Varne and Rubenach (1972) first noted on the spatial distribution of the tholeiitic lavas (their "typical ocean-floor basalt") and alkalic lavas (their "unlike typical ocean-floor basalt"). The first group represents the volcanics of the central island mainly around Green Gorge and to the south of Brothers Pt.; alkalic basalts also occur at North Head. The second group consists of the lavas exposed at the southern part of the island, from Lucitania Bay to Hurd Pt. and around Caroline Cove.

The discriminant diagrams employed by Griffin and Varne (1980) utilized the concentrations of the trace elements Ti, Zr, Y, Nb and Sr (following Pearce and Cann, 1973). Major elements have also been used to

distinguish the petrotectonic environment of basaltic volcanics (Pearce et al., 1975; Pearce et al., 1977; Mullen, 1983). The TiO_2 - MnO - P_2O_5 ternary diagram developed by Mullen (1983) is the most useful, because it discriminates successfully among three tectonic settings, oceanic islands, mid-ocean ridges and island arcs, and does not suffer the drawbacks of the other major element discriminating plots. Ti is immobile during alteration processes. MnO and P_2O_5 contents are found to change insignificantly during low temperature alteration; even in spilitized basaltic rocks, the MnO and P_2O_5 contents are not largely changed. The TiO_2 , MnO and P_2O_5 compositions of Macquarie Island basalts and dolerites are plotted in the TiO_2 - MnO - P_2O_5 ternary (figure 7.7). The fields of MORB, ocean island tholeiites (OIT), ocean island alkalic basalts (OIA), island arc tholeiites (IAT) and calc-alkaline basalts (CAB) are also shown. The Macquarie Island rocks form a cluster in the centre of the diagram plotting in the MORB, IAT and OIT-OIA fields. This cluster shows a general trend from the MORB field to the ocean island field.

Early olivine fractionation in MORBs removes MnO, and subsequent olivine+plagioclase+clinopyroxene fractionation removes MnO and TiO_2 from the initial melt. The fractionated melts will therefore show depletion in MnO and TiO_2 , and a relative enrichment of TiO_2 with respect to MnO, while P_2O_5 remains unchanged; P_2O_5 will change much later due to fractionation of P-bearing phases. Titanomagnetite fractionation occurs at high $f\text{O}_2$ and removes more TiO_2 than MnO. The resulting trend with fractionation in island arc magmas will be relative enrichment of MnO with respect to TiO_2 . Oceanic island basalts, in particular the subalkaline, follow the MORB trend during fractionation, but their higher P_2O_5 contents can only be related to small degrees of partial melting and source composition characteristics. The trend of the Macquarie Island data from the MORB field to the OIA field cannot be accommodated by models invoking crystal fractionation of the

constituent phases of cumulates. The high $Mg/(Mg+Fe)$ ratios and the high TiO_2 and P_2O_5 contents of the alkalic basalts must therefore reflect varying degrees of partial melting, preferably small.

Geochemical Characteristics

The Macquarie Island tholeiitic basalts form a group with typical "depleted" characteristics like the N-type MORB from normal segments (Sun et al., 1979), with normative *OI+Hy*, low Ti-contents and low concentrations of incompatible elements (in particular Zr and Nb). The Macquarie Island alkalic basalts are *Ne*-normative with incompatible element enrichments, low Zr/Nb ratios ≈ 3.5 , and compare with the "enriched" (P-type) or "transitional" (T-type) MORBs (table 7.2).

The range of incompatible element abundances and the range of Ti/Zr, Zr/Nb and Y/Nb ratios are the result of partial melting and fractional crystallisation processes. Incompatible element ratios are known to be insensitive to fractional crystallisation. The layered troctolites consist mainly of olivine and plagioclase and their Zr, Y and Nb contents are extremely low (chapter 6). Even though major element concentrations can be accounted for by olivine \pm plagioclase \pm clinopyroxene fractionation as suggested by least squares mixing calculations employing the compositions of the minerals in the cumulates (table 7.3), incompatible element concentrations tell a different story. Extensive olivine (\pm plagioclase) fractionation from the most primitive basalts would not change the incompatible element concentrations significantly (see also chapter 9, section 9.4); moreover, the observed variation of the incompatible element ratios of basalts cannot be accounted for by olivine (\pm plagioclase \pm clinopyroxene) fractionation. Some of the basalts listed in table 7.1 are the least differentiated, having the highest $Mg/(Mg+Fe)$ ratios, and therefore

they must have experienced the minimum amount of olivine fractionation. Basalts with such high $Mg/(Mg+Fe)$ ratios could represent near primary or relatively undifferentiated melts; for example basalt 38288 with $Mg/(Mg+Fe)$ of 0.72 has Zr/Nb and Y/Nb ratios of 2.6 and 0.78 respectively, and basalt 38188 with $Mg/(Mg+Fe)$ ratio of 0.74 has Zr/Nb and Y/Nb ratios of 2.8 and 0.9 respectively. The Zr/Nb, Y/Nb and Ti/Zr ratios of some basalts are even lower than chondritic (table 7.2). Such low Zr/Nb and Y/Nb ratios are unlike those of typical depleted MORBs from normal segments, which are characterised by significantly higher Zr/Nb ratios; N-type MORBs from the American- Antarctic Ridge have Zr/Nb ratios in the range of 17-78 and from the Southwest Indian Ridge 17-64 (table 7.2). The Macquarie Island basalts and dolerites are more likely the enriched MORBs from transitional segments, and some of them even compare with MORBs from plume-type segments such as Bouvet and Azores. It is therefore clear that the considerable variations in the elemental ratios of the incompatibles have not been caused by olivine and plagioclase fractionation. They could reflect source region heterogeneities. Alternatively, low to very low degrees of partial melting can be invoked to explain the incompatible element concentrations of the alkalic basalts.

Low degrees of partial melting (small to very small) can cause systematic variations in the incompatible element contents and ratios if garnet or clinopyroxene are residual phases (Pearce and Norry, 1979; Shibata et al., 1979b). Complex melting episodes such as "dynamic melting" can also modify significantly the elemental ratios of incompatible elements (Langmuir et al., 1977). LeRoex et al. (1981) found that the degree of partial melting can account for some of the observed variation within a particular group of basalts. The wide variation in Ti/Zr (52-119) and Y/Nb (0.35-15) ratios, and the continuous compositional range of the Macquarie Island basalts, as well as their much lower than Bulk Earth Ti/Zr and Zr/Nb ratios

suggest that moderate to large degrees of partial melting of a depleted source commonly favoured for MORBs (eg. Malpas, 1978; Green et al., 1979) is not a viable mechanism for generating the observed compositional characteristics of the Macquarie Island basalts (in particular those of the alkalic basalts); these features can be assigned to one of the following processes, complex partial melting processes, very small to moderate increments of melts of a homogeneous source but with varying residual mineralogy and varying percentages of retained melt in the residue, and finally to melting of a heterogeneous source. The ratios of radiogenic isotopes however will not change during these processes and will reflect these ratios in the source (Hofmann and Hart, 1978). The concept of mantle heterogeneity has gained considerable attention and support lately; it is however mainly supported by isotopic data (eg. Sun et al., 1979; Wood, 1979; leRoex et al., 1985). This source heterogeneity is normally accounted for by a "depleted" and an "enriched" component. Griffin (1982) arrived at a broadly similar conclusion for the tholeiitic and alkalic basalts of Macquarie Island based on their Zr/Nb and La/Sm ratios. Isotopic data are required to evaluate the different sources of basalts.

The effects of metamorphism on the abundances of the incompatible elements (Ti, Zr, Y, Nb and LREE) are known to be very limited (Pearce and Norry, 1979). A few REE data have been obtained by Griffin (1982) for a group of selected basalts and dolerites, whose Zr/Nb ratios span the entire composition range, and have been metamorphosed from greenschist facies to sub-zeolite facies. Samples metamorphosed to greenschist facies conditions have lower La/Sm and La/Yb ratios than those suffered zeolite facies alteration. The highest La/Sm ratios are observed in the least altered samples, affected by ocean floor alteration only. LREE show good positive correlations with Zr and Nb suggesting that the REE concentrations are a primary characteristic rather than an alteration effect.

The $(La/Sm)_{CF}$ ratios of the Macquarie Island basalts which have been affected by lower greenschist facies alteration range from 0.86 to 1.56; dolerites metamorphosed to lower upper greenschist facies have similar ratios. The least altered samples, affected by ocean floor alteration, show $(La/Sm)_{CF}$ ratios in the range of 2.56-4.82.

Schilling et al. (1983) presented a comprehensive review on the geochemistry of Mid-Atlantic Ridge (MAR) basalts. They noted the systematic variation in both major and trace elements of MAR basalts with latitude; the enrichments in incompatible elements and radiogenic isotopes in basalts from the Azores and Jan Mayen regions. N-type basalts from MAR have $(La/Sm)_{CF}$ ratios of less than 0.7, T-type basalts from 0.7 to 1.8 and enriched P-type basalts (Azores plateau, Jan Mayen fracture zone, Oceanographer fracture zone) more than 1.8. The high $(La/Sm)_{CF}$ ratios of the Macquarie Island alkalic lavas compare only with the hot spot influenced volcanics of MAR.

The abundances of the transition metals Ni, Cr, Sc, Ti, V have also been determined with sufficient accuracy by XRF methods. Because these cations are usually immobile during alteration (Shervais, 1982 and references therein), their abundances are indicative of the extent of partial melting and crystal fractionation processes. Titanium (Ti^{4+}) is a HFS cation with small radius/charge ratio and very small crystal/liquid partition coefficients for most ferromagnesian minerals and feldspars (Saunders et al., 1980). The other transition metals have similar geochemistry (similar ionic radii and similar charges) and occur in octahedrally coordinated sites, thus behaving as compatible elements. Vanadium occurs in three valence states V^{3+} , V^{4+} and V^{5+} . V^{3+} has similar ionic radius and radius/charge ratio with Cr^{3+} and Fe^{3+} , thus substituting for these trivalent cations in clinopyroxene and spinel. The oxidised cations V^{4+} and V^{5+} behave similarly to Ti^{4+} . At low fO_2 , Fe-WO buffer, vanadium occurs mainly as V^{3+} , while at

higher fO_2 ($\geq 10^{-5}$ atm) the predominant cation is either V^{4+} or V^{5+} . Because of the different geochemistry of the titanium and vanadium, the incompatible character of Ti^{4+} and the dependence of the vanadium cation valence on the oxidation state (fO_2) of the system, Ti-V diagrams can be used to distinguish among volcanic suites from different tectonic settings, mid-oceanic ridges, island arcs, back arc basins, etc. (Shervais, 1982), and also to test the crystal fractionation effects in the concentrations of Ti and V under low fO_2 conditions. Figure 7.8 shows the variation of Ti contents with those of V for the Macquarie Island basalts. Constant Ti/V ratio trends are also shown. The Macquarie Island basalts have Ti/V ratios between 25 and 55. MORBs have Ti/V ratios of 20-50, irrespective of being N-type, T-type or P-type. Arc-tholeiites from mature island arcs have Ti/V ratios of less than 20.

The concentrations of V and Ti in the Macquarie Island cumulates, massive gabbros, basalts and dolerites are plotted in figure 7.9. The trend defined in the logarithmic plot (figure 7.9B) between cumulates and dolerites -tholeiitic basalts suggests a genetic relationship (Montigny et al., 1973). Fractionation of olivine plus plagioclase (troctolite accumulation) would result in the trend (a) of figure 7.9A. This trend has been calculated from the Rayleigh fractionation equation, $C_{liq} = C_o * f^{(D-1)}$ where C_{liq} is the concentration of an element in the liquid, C_o is the original concentration of the element in the melt, D is the bulk distribution coefficient for this element and f is the fraction of liquid remaining after crystallisation (Shaw, 1970), adopting the mineral/melt distribution coefficients of Shervais (1982). The fractionation trend (a) almost parallels a constant Ti/V ratio (≈ 29), line (c) in figure 7.9A. Basalts and dolerites with intermediate V and Ti contents (155-230 ppm V and 5000-7000 ppm Ti) can be derived from an initial melt having 140 ppm V and 4000ppm Ti by 10-40% olivine plus plagioclase segregation. Higher V and Ti concentrations

can be produced by gabbroic fractionation, trend (b) in figure 7.9A. Trend (b) has also been calculated from the Rayleigh fractionation equation for a gabbroic extract consisting of 15% olivine + 25% clinopyroxene + 70% plagioclase, very similar to the average mineral mode of the layered rocks. Trend (b) has been calculated for initial V and Ti concentrations of 200 ppm and 6000 ppm respectively. Both trends, (a) and (b), can account for the Ti and V contents of the tholeiitic basalts and dolerite dykes by either olivine + plagioclase or olivine + plagioclase + clinopyroxene fractionation. The alkalic basalts define a different trend, trend (d) of figure 7.9A. Such a trend is not consistent with olivine ± plagioclase ± clinopyroxene fractionation models, which dictate constantly increasing Ti and V contents from the initial (primary) melt values. Trend (d) can be only accounted for by (i) variable degrees of partial melting of a relatively homogeneous source (uniform Ti/V ratios), (ii) a source with different initial Ti/V ratios and (iii) a combination of (i) and (ii).

In summary, the dolerite dykes are more differentiated than the basalts, and the chemical character of each dolerite (primitive/evolved) does not correlate with its stratigraphic position. Major element concentrations of both basalts and dolerites show ol ± plag ± cpx control. In particular, the major element and compatible trace element contents of the tholeiitic basalts are controlled by ol ± plag ± cpx fractionation; the proportions of the fractionating minerals are identical to the modal amount of these minerals in the cumulates. The geochemistry of the tholeiitic basalts, mainly their trace element concentrations, compares with that of the "normal" MORBs, whereas the geochemical features of the alkalic basalts are only comparable with those of the "enriched" MORBs from transitional or plume type segments. Isotopic data are needed to verify the sources and partial melting processes of the tholeiitic and alkalic basalts.

CHAPTER EIGHT : CRYSTALLISATION MODELS

8.1 Introduction

This chapter discusses the conditions of crystallisation of the Macquarie Island plutonic rocks. The first part is an outline of subsolidus equilibria with particular emphasis on the Fe-Mg partitioning between spinel and olivine. Applications of the methods for estimating equilibration temperatures are discussed and tested. In the second part, a detailed assessment of mineral-melt equilibria is presented. Crystallisation models are examined in the third part. Finally, parental liquid compositions are assessed and liquid lines of descent for possible parental liquids are calculated.

8.2 Geothermometry and subsolidus equilibria

The exchange of cations among coexisting minerals has been a popular method in calibrating crystallisation temperatures for the minerals concerned. Two of the best studied geothermometric methods are the olivine - spinel geothermometer and the pyroxene solid solutions. These two methods showed the most consistent results on application to Macquarie Island data, and are described in detail in this section. The plagioclase-liquid thermometer on the other hand showed considerable deviations from the results obtained by the previous two methods. For this reason, there is no discussion on the plagioclase-liquid thermometry methods.

8.2.1 The olivine-spinel geothermometer

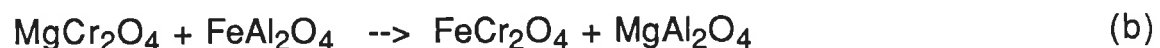
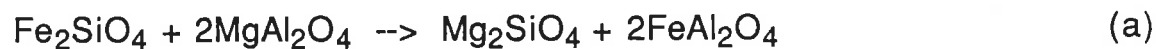
The exchange of Mg and Fe²⁺ between coexisting (Mg,Fe²⁺)₂SiO₄ olivine and (Mg,Fe²⁺)(Al,Cr,Fe³⁺)₂O₄ spinel is expressed by the distribution coefficient $K_D(\text{ol-sp})$ where $K_D(\text{ol-sp}) = \frac{(X_{\text{Mg}}^{\text{ol}} \cdot (X_{\text{Fe}^{2+}}^{\text{sp}})^2)}{(X_{\text{Fe}^{2+}}^{\text{ol}} \cdot (X_{\text{Mg}}^{\text{sp}})^2)}$ (8.1), where X_i^k is the mole fraction of component i in phase k. Irvine (1965)

pointed out that the Fe²⁺ - Mg partitioning between olivine and spinel is also a function of the trivalent cation content of spinel. He considered the effect of the trivalent cations on the distribution coefficient K_D , assuming ideal solid solution of Fe²⁺ and Mg in both olivine and spinel, and derived the following expression,

$$\ln K_D = \ln K_a + Y_{\text{Cr}}^{\text{sp}} \cdot \ln K_b + Y_{\text{Fe}^{3+}}^{\text{sp}} \cdot \ln K_c \quad (8.2),$$

where Y^{sp} is the mole fractions of trivalent cations in spinel.

Equation (8.2) shows the dependence of K_D on the equilibrium constants K_a , K_b , and K_c of the following reactions,



Jackson (1969) utilised the equations produced by Irvine (1965) and the then available thermochemical data to calibrate the thermometric expression 8.3 (table 8.2). Although equation 8.3 produced geologically acceptable temperatures for the Stillwater complex, in the case of the Kilauea volcanics the calculated temperatures were in excess of 2000°C (Evans and Wright, 1972).

Medaris (1975) and Evans and Frost (1975) studied the applicability of the Irvine-Jackson modelling in metamorphosed ultramafic rocks and found a linear relation between $\ln K_D$ and Y_{Cr}^{sp} . Evans and Frost (1975) assigned a value of 0.05 in the Y_{Cr}^{sp} ratio and then normalised the K_D to a ferric free basis according to the relationship:

$$\ln K_D^* = \ln K_D - 4 \cdot Y_{Cr}^{sp} \quad (8.4),$$

where the coefficient 4 is the value of $\ln K_C$ (Irvine, 1965). The end-member chromite $\{FeCr_2O_4\}$ is a very important component of natural spinels, but determinations of its free energy values show considerable variation (Roeder et al., 1979). Roeder et al. (1979) suggested that the value of the $\ln K_C$ is closer to 2 at 1200°C. In the following calculations the latter value is preferred, because it is constrained by a better set of free energy of formation values for spinel end-members and especially for chromite. Therefore, the normalised $\ln K_D^*$ is given by the equation,

$$\ln K_D^* = \ln K_D - 2 \cdot Y_{Cr}^{sp} \quad (8.4a).$$

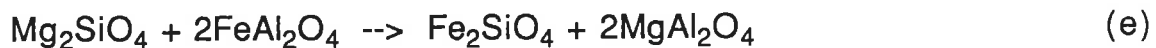
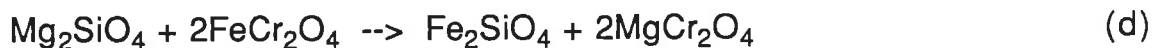
Fujii (1978) produced experimental data for olivine-spinel pairs for temperatures in the range of 1200°C - 1350°C and pressures of 1 atm-15 kbars. He derived the thermometric relation 8.5 (table 8.2). His thermometer appears to fit best peridotites.

Fabries (1979) attempted an empirical calibration of the olivine - spinel thermometer for peridotitic rocks. He derived expression 8.6 (table 8.2).

Roeder et al. (1979, 1980) re-evaluated the geothermometer on the basis of new experimental and thermodynamic data. They

emphasized the inconsistencies of the thermodynamic data, particularly the different free energy (ΔG) values of the spinel group end-members. Their experimental results suggest that olivine and spinel continue to re-equilibrate to temperatures as low as 500°C. The revised geothermometer is expressed by equation 8.7 (table 8.2).

Lehmann (1983) criticized the weaknesses of the previous geothermometers, in particular the assumptions on the ideality of solid solutions for both olivine and spinel. He considered the deviations from ideality by using the olivine solid solution model of Nafziger and Muan (1967), and the spinel solid solution model of Vannier (1977). He utilized the following reactions for expressing the Fe²⁺-Mg partitioning between olivine and spinel,



and the following two spinel solid solutions,



and produced two thermometric relations, (8.8) and (8.9), where R is the gas constant (1.987 cal · K · mol⁻¹), ΔG_1 and ΔG_2 refer to reactions (f) and (g) respectively, $\Delta G_3 = -(\Delta G_1 + \Delta G_2)$, [Mg] is the mole fraction of Mg in the phase concerned, and p is the pressure in kbar.

Figure 8.1 is a plot of normalized $\ln K_D^*$ (calculated from equation 8.4a) against the Cr/(Cr+Al+Fe³⁺) ratios of spinels from troctolite mineral pairs. The 700°C and 1200°C isotherms of Evans and Frost (loc. cit.) and Roeder et al. (1979) are also plotted. Two groups are distinguished, one showing high normalized distribution coefficients and another with lower normalized K_D^* s. The first group defines a low temperature trend which approximates the 700°C

isotherm of Roeder et al. (loc. cit.), while the latter defines a higher temperature trend. Both olivine and spinel compositions represent core analyses. The high normalized distribution coefficient group represents spinels included in olivine; the olivine composition was obtained at least 200 microns away from the spinel crystal boundary. The low $\ln K_D^*$ group represents spinels included in plagioclase; the olivine composition, which was employed in the calculations, was measured at a distance of not less than 300 μm from the spinel crystals. The much higher normalized distribution coefficients of the first group at similar Y_{Cr}^{Sp} indicate that spinels included in olivines have re-equilibrated at significantly lower temperatures than the spinels occurring as inclusions in large plagioclases. A third group is also shown. It represents "isolated" spinels lying at the crystal boundaries of much larger olivines and plagioclases. The data from the third group are transitional to the previous groups, and span almost the entire range from the high to the low $\ln K_D^*$ groups.

Temperature estimates from representative olivine-spinel pairs in troctolites are presented in table 8.1a. Core spinel compositions were used in the following calculations. The olivine composition was the average of several analyses obtained at a distance of more than 200 μm from the spinel crystals. The calculated temperatures from the most magnesian spinels ($\text{Mg}/(\text{Mg}+\text{Fe}^{2+}) > 0.60$) are in the range 1010°-1251°C according to equation 8.7 (Roeder et al., 1979). The calculated temperatures for similar olivine composition and less magnesian spinels ($\text{spinel } 100 \cdot \text{Mg}/(\text{Mg}+\text{Fe}^{2+}) = 43.5-44.5$) range from 626°C to 722°C. Temperatures estimated from the expression of Jackson (loc. cit.) are too high (1400°-1669°C) to be considered realistic. The geothermometers of Fujii (loc. cit.) and Fabries (loc. cit.)

give temperatures which differ $\pm 100^\circ\text{C}$ from those estimated from equation 8.7. Equation (8.8) gives temperatures between 1165° and 1259°C for the magnesian spinels ($\text{Mg}/(\text{Mg}+\text{Fe}^{2+}) > 0.60$), whereas equation 8.9 gives considerably lower temperatures, 700° - 740°C , for similar spinel compositions. The temperature range estimated from equation (8.9) for the majority of spinel compositions is 640° - 725°C . Coexisting olivine-spinel pairs in the intrusive layers at Handspike Point, indicate temperatures of 730° - 766°C according to equation 8.7.

Calculated equilibration temperatures for harzburgites are listed in table 8.1b. Temperatures range from 669°C to 914°C (using equation 8.7). Lehmann's equations 8.8 and 8.9 (table 8.2) give temperatures in the range of 962°C - 1121°C and 597°C - 630°C respectively. Estimated temperatures from the expressions of Fujii (loc. cit.) and Fabries (loc. cit.) are also subsolidus (table 8.1b). Olivine - spinel pairs from the North Mountain wehrlite indicate much higher equilibration temperatures, 1129° - 1355°C (estimated from equation 8.7). When the composition of the larger spinel crystals is employed in the calculations, the temperature range is between 1210° and 1287°C . Coexisting olivine (Fo_{87-88}) and spinel ($\text{mg}\# \geq 64$) phenocrysts from the glasses indicate temperatures of 1225° - 1235°C , very similar to those obtained from olivine-spinel pairs from the troctolites.

These results indicate that spinel included in olivine exchanged Fe^{2+} and Mg with the host mineral down to very low temperatures. Spinels included in plagioclase are more magnesian than those included in olivine, because the diffusion of both Fe^{2+} and Mg to plagioclase is very limited. These included spinels are thought to be of magmatic origin and hence the calculated temperatures from such spinels and the average olivine composition are high. It is argued that such temperatures could reflect original crystallisation temperatures,

possibly in the range of 1165°-1259°C. It is therefore clear that the use of the olivine-spinel geothermometer is only suitable for calibrating initial crystallisation temperatures when subsolidus diffusional Fe-Mg exchange between spinel and olivine is prevented. When this is not the case, such Fe-Mg exchange can provide information on the cooling history of the rocks.

8.2.2 Olivine - Spinel Geospeedometry

Recent studies on tectonite peridotites (Ozawa, 1983), spinel-lherzolite xenoliths (Takahashi, 1980; Smith and Roden, 1981) and ultramafic cumulates (Wilson, 1982) have emphasized the chemical heterogeneity of constituent minerals and the discrepancies in the estimated temperatures from different geothermometers. The development of zoning patterns between ferromagnesian silicate phases and included chromite was also emphasized.

The Macquarie Island cumulate troctolites represent rocks which underwent slow cooling over a period of time. The intercrystalline cationic exchange between olivine and spinel during such continuous cooling is a function of the diffusion rates of Fe²⁺ and Mg. Diffusion is expressed by Fick's law, $(s^i)_x = -D^i \cdot \frac{\partial c^i}{\partial x}$, which states that the rate of flow per unit time in a direction x, $(s^i)_x$, is proportional to the concentration gradient per unit surface in that direction $(\partial c^i / \partial x)$ (Carmichael et al., 1974). D^i is the diffusion coefficient of component i in the concerned phase. The diffusion coefficient is strongly dependent on temperature; its variation with temperature is represented by an Arrhenius type equation,

$D^i = D_0 \cdot \exp \frac{-Q}{kT}$ ($\text{cm}^2 \cdot \text{sec}^{-1}$), where D_0 is a frequency constant, Q is the activation energy (eV) and k is Boltzmann's constant. The Fe^{2+} -Mg diffusion between olivine and spinel depends on the values of the diffusion coefficients for Fe^{2+} and Mg and the equilibrium boundary compositions; according to the conservation of matter, elemental fluxes between olivine and spinel at the crystal boundaries must be equal,

$$(D^i)_{\text{ol}} \cdot \frac{\partial(c^i)_{\text{ol}}}{\partial x} = (D^i)_{\text{sp}} \cdot \frac{\partial(c^i)_{\text{sp}}}{\partial x}$$

where $(D^i)_{\text{ol}}$ and $(D^i)_{\text{sp}}$ are the diffusion coefficients of element i in olivine and spinel respectively. Ozawa (1984) assumed a spherical spinel core and a semi-infinite shell of olivine surrounding this spinel core. He formulated a kinetic model for the diffusion controlled Fe^{2+} -Mg exchange between olivine and spinel based on the previous differential equations.

Compositional zoning profiles in olivine and spinel across their mutual grain boundaries from the Macquarie Island troctolites are shown in figure 8.2. The $\text{Mg}/(\text{Mg}+\text{Fe}^{2+})$ in olivine increases towards the boundary, while the spinel $\text{Mg}/(\text{Mg}+\text{Fe}^{2+})$ decreases. Calculated compositional profiles in olivine and spinel (Ozawa, 1984) match the measured profiles from troctolites and harzburgites. It was pointed out by Ozawa (1984) and Wilson (1982) that Fe^{2+} -Mg zoning starts to develop at less than 850°C and the blocking temperatures range from 600° to 800°C . The shape of the $\text{Mg}/(\text{Mg}+\text{Fe}^{2+})$ profile depends on the cooling rate and the spinel composition (Ozawa, 1983). The spinel grain size is an important parameter which relates the compositional zoning to the cooling rates, because the $\text{Mg}/(\text{Mg}+\text{Fe}^{2+})$ ratio of spinel is more sensitive to smaller cooling rates than that of olivine, and the changes in $\text{Mg}/(\text{Mg}+\text{Fe}^{2+})$ ratios are simply a function of time during which

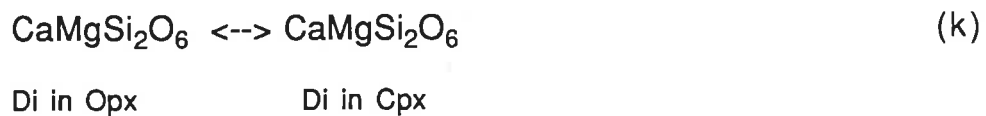
continuous cooling took place. In figure 8.3, computed cooling rates are correlated with the calculated temperatures (using the equation of Roeder et al., 1979) and the spinel grain size. The initial Y_{Cr} of the spinels was assumed to be equal to 0.5 (almost identical to that of most analysed spinels), and the olivine $Mg/(Mg+Fe^{2+})$ ratio was taken equal to 0.9, a value similar to that of the olivine from the harzburgites and the basal troctolites.

The data from the troctolites indicate that the rate of cooling was on average $0.001^{\circ}C$ per year ($\pm 10^{-1}^{\circ}C/year$). The data from harzburgites show cooling rates of the same order of magnitude. The North Mountain wehrlite on the other hand cooled rapidly, at about $10^3(^{\circ}C)$ per year. It therefore represents the fastest cooled plutonic rock, suggesting that it is a high level intrusion, also corroborated by field evidence. Data for a basalt carrying olivine and spinel xenocrysts are also shown in figure 8.3. Olivine and spinel do not show zoning. The cooling rate for this basalt is high, more than $10^4 (^{\circ}C)$ per year at temperatures of $1200^{\circ}C$ ($\pm 60^{\circ}$). The very slow cooling rates of troctolites and harzburgites suggest continuous cooling for long periods. If the initial magmatic temperatures were about $1200^{\circ}C$, then these rocks attained their present equilibrium state after 100,000 years. Assuming a half spreading rate of 1cm/yr, then these rocks must have been re-equilibrating for at least 1km away from the ridge.

8.2.3 Pyroxene thermometry

Temperatures of equilibration have been determined for a wide range of igneous and metamorphic rocks using the clinopyroxene (Cpx) and orthopyroxene (Opx) compositions in these rocks. Various methods have been employed but the more frequently applied one is

based on the diopside-enstatite solvus (Davis and Boyd, 1966). The join diopside (Di) -enstatite (En) is Fe-free and therefore provides a satisfactory fit to Mg-rich pyroxene pairs. The phase relations in the Di-En system have been determined by numerous researchers over a wide pressure-temperature range (Lindsley and Dixon, 1976; Mori and Green, 1975; Huebner, 1980; Lindsley, 1980; Lindsley et al., 1981; Jenner and Green, 1983, and many others). Temperature estimations are accomplished by employing the phase diagram of this system or a solution model. The two reactions governing the phase equilibria in this system are the following:



A solution model based on equation (l) was developed by Wood and Banno (1973), who assumed ideal mixing in clinopyroxene. Wells (1977) revised the formulation of Wood and Banno (1973) on the basis of newer experimental data. Some of the assumptions of the previous authors however, notably the large enthalpy for the reaction orthoenstatite = clinoenstatite, were in error (Holland et al., 1979; Davidson et al., 1982). Kretz (1982) presented an improved thermometer (in the Di-En join) which uses igneous pyroxene compositions (Skaergaard intrusion) together with experimental data (Lindsley and Dixon, 1976). He produced the following two thermometric equations for a portion of the Ca-rich side of the solvus,

$$T = \frac{1000}{0.468 + 0.246[X]_{\text{Cpx}} - 0.123 \ln(1-2[\text{Ca}]_{\text{Cpx}})} \quad \text{(8.10a)}$$

$$T = \frac{1000}{0.054 + 0.608[X]^{Cpx} - 0.304 \ln(1-2[Ca]^{Cpx})} \quad (8.10b)$$

where $[X]^i$ is the atomic fraction of $Fe^{2+}/(Fe^{2+}+Mg)$ in phase i , and $[Ca]^{Cpx}$ is the cation ratio $Ca/(Ca+Mg+Fe^{2+})$ in Cpx. Equation 8.10a represents to the high temperature part of the solvus, more than $1080^\circ C$, and equation 8.10b to the lower part, for temperatures less than $1080^\circ C$.

An improved solution model in the Di-En system was published by Lindsley et al., (1981). It incorporates revised values for the various thermodynamic parameters and an asymmetric Margules formulation for the clinopyroxene solid solution. They give the following thermometric equation (based on reaction I) for coexisting Ca-poor and Ca-rich pyroxene pairs,

$$T = -273.15 + \left\{ (3.561 + 0.0355p + 2W_{G1}[X_{En}]^{Cpx} \cdot ([X_{Di}]^{Cpx})^2 + W_{G2}([X_{Di}]^{Cpx})^2 \cdot (1 - 2[X_{En}]^{Cpx}) - W_G([X_{Di}]^{Opx})^2) / \{ 0.0091 - R \cdot \ln([X_{En}]^{Cpx}/[X_{En}]^{Opx}) \} \right\} \quad (8.11)$$

where p is the total pressure in kbars, $W_{G1} = 25.484 + 0.0812 \cdot p$, $W_{G2} = 31.216 - 0.0061 \cdot p$ and $W_G = 25$ kJ.

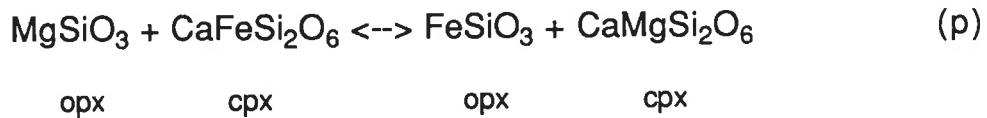
Nominal temperatures for the troctolites, olivine-gabbros and harzburgites estimated using the equations of Lindsley et al. (loc. cit.) and Kretz (loc. cit.). The most magnesian augites [$100 \cdot Mg/(Mg+Fe) = 90-92$] in the troctolites deliver temperatures of $750^\circ-820^\circ C$ using equations 8.10. Employing these equations for the less magnesian augites [$100 \cdot Mg/(Mg+Fe) = 85-88$] of the olivine-gabbros, the calculated temperatures are in the range $830^\circ-910^\circ C$. Bulk pyroxene compositions from the olivine-gabbros give temperatures between 1090° and $1130^\circ C$.

Application of equation 8.11 results in considerably lower subsolidus temperatures for both troctolites (630°-670°C) and olivine-gabbros (600°-660°C). The apparently higher temperatures obtained from the olivine-gabbros could be accounted for a shorter period of subsolidus equilibration.

Lindsley and Andersen (1983) devised a graphical thermometer and a projection method which incorporates all other components of natural pyroxenes. Pyroxene analyses from Macquarie Island have been recalculated according to the method of Lindsley and Andersen (1983), and projected on the pyroxene quadrilateral (figure 8.4). The augites from troctolites plot between the 880°C and 1040°C isotherms, whereas those from the olivine-gabbros between the 960°C and 1045°C isotherms. Bulk pyroxene compositions obtained with a defocused electron beam. Such compositions approximate the original magmatic subcalcic pyroxene compositions. These indicate temperatures of 1060°C-1125°C and 1120°C-1165°C for troctolites and olivine-gabbros respectively. The exsolved Ca-poor phase in the augites from troctolites approximates the 900°C isotherm. The estimated temperature range in troctolites is 840°-920°C and in gabbros 870°-900°C.

The pyroxene assemblage of harzburgites permits estimation of the exsolution temperature. The calculated temperatures from the solvus method of Kretz (1982) range from 620°-795°C. The expression of Lindsley et al. (1981) delivers similar subsolidus temperatures (620°-705°C). In the graphical thermometer of Lindsley and Andersen (1983), the enstatites project between the 800° and 1100°C isotherms. The exsolved Ca-rich phase plots about the 1000°C isotherm (range 1000±60°C).

A different method for temperature estimations is based on the Fe²⁺-Mg and associated Ca exchange between coexisting low-Ca and high-Ca pyroxenes, and is expressed by the reaction,



The temperature dependence of the distribution coefficient has been determined by Kretz (1982) and is expressed as follows,

$$K_D = \frac{X^{\text{Opx}}}{1-X^{\text{Opx}}} \cdot \frac{1-X^{\text{Cpx}}}{X^{\text{Cpx}}}, \quad \text{where } X \text{ is the atomic ratio } \text{Fe}^{2+}/(\text{Fe}^{2+}+\text{Mg}).$$

He gives the following relation between K_D and temperature,

$$T = \frac{1130}{\ln K_D \cdot [X]^{\text{Opx}} + 0.505} \quad (8.12)$$

Application of this equation to augites and exsolved Ca-poor pyroxene pairs from the olivine-gabbros produces temperatures in the range of 1035°-1155°C. Pyroxene pairs from an intrusive melanocratic layer in these olivine-gabbros give the highest recorded temperature, 1170°C. The troctolite pyroxenes deliver an average temperature of 1125°C.

The olivine-spinel and pyroxene Fe-Mg and unmixing relationships suggest that harzburgite, troctolites and olivine-gabbros underwent slow cooling to "blocking temperatures" of the order of 650°-800°C. Both methods yield magmatic temperatures in the range of 1100°-1200°C. Evidence presented suggests that initiation of pyroxene exsolution occurred at temperatures less than 1170°C. This is in agreement with experimental studies; crystallisation of a subcalcic clinopyroxene from primitive FAMOUS basalts occurs at 1193°-1170°C at low pressures (Grove and Bryan, 1983). The harzburgites continuously re-equilibrated down to low temperatures. The estimated minimum exsolution temperature is around 700°C. Comparable

subsolidus temperatures were inferred from other ophiolitic peridotites (Sinton, 1977; Dick, 1977; Quick, 1981).

8.3 Mineral - Melt Equilibria

Crystal-liquid equilibria provide invaluable information on the chemical composition of the liquids from which the various phases crystallised. The dominant phases in both volcanic and plutonic rocks from Macquarie Island are olivine, plagioclase and clinopyroxene. Experimental studies on olivine-liquid equilibria have produced very consistent results. Thus, the composition of olivine crystallising from different melts can be accurately estimated. Spinel is only a minor phase in the Macquarie Island rocks, but its composition is very important in constraining the Cr-content, the $\text{Fe}^{3+}/\text{Fe}^{2+}$ ratio and possibly the Al_2O_3 content of the liquid from which it crystallised. In the light of recent detailed studies on spinel synthesis from MORB liquids, assessment of these parameters is possible. The plagioclase-liquid and clinopyroxene-liquid equilibria on the other hand are not so well constrained. The following discussion is consequently concentrated in the olivine-liquid and spinel-liquid equilibria.

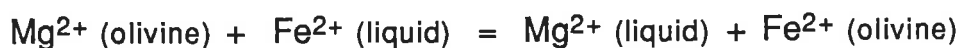
The harzburgites had a more complex history than the cumulates since they were affected by solid state ductile deformation possibly at higher temperatures (and higher pressures?) prior to their final subsolidus re-equilibration. Liquids in equilibrium with residual mantle peridotites, such as the Macquarie Island harzburgites, can be identified if the $\text{K}^{\text{Fe-Mg}}$ and the Ni partition coefficient are well known.

8.3.1 Olivine-melt equilibrium

The Mg/(Mg+Fe) ratios and nickel content of silicate melts are important petrogenetic parameters. They have been used to identify the compositions of primitive basaltic melts separated from mantle peridotites, and to constrain models involving olivine fractionation at low and elevated pressures. Ni²⁺ is strongly fractionated to olivine relative to the liquid during crystallisation of basaltic magmas, because of its large crystal field stabilization energy and consequent strong octahedral site preference energy (Burns, 1970).

Fe²⁺-Mg²⁺ distribution between olivine and melt.

The partitioning of Fe²⁺ and Mg²⁺ between olivine and melt is expressed as the concentration ratio $K_{MO} = \frac{(MO)^{ol}}{(MO)^{liq}}$, where M=Fe²⁺ and Mg²⁺ and parentheses denote cation mole fractions. The partitioning of Fe²⁺ and Mg²⁺ can also be treated as an ion exchange reaction of the form,



The distribution coefficient of Fe²⁺ and Mg²⁺ between olivine and melt is expressed as:

$$K_{D(FeO-MgO)}^{ol-liq} = \frac{(X^{FeO}/X^{MgO})^{ol}}{(X^{FeO}/X^{MgO})^{liq}},$$

where $(X^{MO})^i$ is the mole fraction of MO in phase i, or as

$$K_{D(Fe^{2+}-Mg)}^{ol-liq} = \frac{(Fe^{2+}/Mg^{2+})^{ol}}{(Fe^{2+}/Mg^{2+})^{liq}}. \text{ Experimental studies on natural basaltic systems indicate that } K_{D(Fe^{2+}-Mg)}^{ol-liq} \text{ is a function of temperature,}$$

pressure and melt composition (Roeder and Emslie, 1970; Roeder, 1975; Mysen, 1975; Longhi et al., 1975; Bickle et al., 1977; Bender et al., 1978). The experiments of Roeder and Emslie (loc. cit.) indicate that for a wide range of temperatures (1150°-1300°C), oxygen fugacities ($10^{-0.6}$ - 10^{-12} atm) and basaltic compositions, the $K_{D(\text{Fe}^{2+}\text{-Mg})}^{\text{ol-liq}}$ is 0.3.

Bender et al. (1978) determined the variation of $K_{D(\text{Fe}^{2+}\text{-Mg})}^{\text{ol-liq}}$ during low pressure olivine crystallisation from a primitive basaltic glass; $K_{D(\text{Fe}^{2+}\text{-Mg})}^{\text{ol-liq}}$ ranges from 0.266 at 1268°C to 0.299 at 1205°C and 1 atm.

They also commented on the $K_{D(\text{Fe}^{2+}\text{-Mg})}^{\text{ol-liq}}$ increase with pressure, from 0.27 at 1 atm to 0.31 at 10 kbar and 1290°C. At constant temperature, the distribution coefficient varies with the silica and alkali content of the liquid, and at constant liquid composition, the $\ln K_{D(\text{Fe}^{2+}\text{-Mg})}^{\text{ol-liq}}$ is a function of the inverse temperature (Roeder, 1975; Leeman, 1978; Takahashi, 1978). Bender et al. (1978) derived the following expression which relates temperature and $K_{D(\text{Fe}^{2+}\text{-Mg})}^{\text{ol-liq}}$,

$$\log K_{D(\text{Fe}^{2+}\text{-Mg})}^{\text{ol-liq}} = \frac{1671}{T^{\circ}\text{K}} - 1.679 \quad (8.13)$$

Because of the importance of the Fe^{2+} - Mg distribution coefficient in modelling crystallisation and partial melting processes, the selection of the appropriate $K_{D(\text{Fe}^{2+}\text{-Mg})}^{\text{ol-liq}}$ values must be made carefully. For basaltic systems at low oxygen fugacities ($f\text{O}_2$), pressures from 1atm to 10 kbar and over a considerable range of magmatic temperatures (1200°-1290°C), $K_{D(\text{Fe}^{2+}\text{-Mg})}^{\text{ol-liq}}$ varies from 0.27 to 0.30. At higher pressures, 10-20 kbar, $K_{D(\text{Fe}^{2+}\text{-Mg})}^{\text{ol-liq}}$ increases to

0.29-0.34. The average value of 0.33 is generally accepted at such high pressures (Irvine, 1977).

Ni²⁺ Partitioning between olivine and melt.

The partitioning of nickel between olivine and silicate melt can be expressed by the concentration ratio, $\frac{(\text{NiO})^{\text{ol}}}{(\text{NiO})^{\text{liq}}}$. Hart and Davis (1978) examined the partitioning of Ni between olivine and silicate melt in the system Forsterite-Anorthite-Albite for temperatures ranging from 1250°C to 1450°C and pressure of 1atm. They found that the Ni partition coefficient $D^{\text{Ni}} = \frac{(\text{Ni})^{\text{ol}}}{(\text{Ni})^{\text{liq}}}$ is strongly dependent on the melt composition, but not on the Ni concentration. The variation of D^{Ni} with the liquid MgO content at constant temperature is expressed by the relation,

$$D^{\text{Ni}} = \frac{124}{\text{MgO}} - 0.9 \quad (8.14).$$

The temperature dependence of D^{Ni} was found to be significant in coexisting olivines and quenched liquids from basalts of the Makaopuhi lava lake in Hawaii (Hakli and Wright, 1967). Leeman and Lindstrom (1978) presented experimental data for natural basaltic compositions and the systems Forsterite-Anorthite-Silica and Diopside-Albite-Anorthite. They concluded that the Ni partition coefficient is strongly dependent on temperature, and at constant temperature it depends on the liquid composition, increasing with the alkali content of the liquid. Hart and Davis (1978) found the following relationship for the temperature dependence of D^{Ni} ,

$$\ln D^{\text{Ni}} = \frac{12345}{T} - 5.593 \quad (8.15a)$$

where the temperature T is given in degrees Kelvin. Leeman and Lindstrom (1978) give a similar (in terms of regression parameters) relation for natural basaltic compositions,

$$\ln D^{\text{Ni}} = \frac{12242}{T} - 5.55 \quad (8.15b).$$

The variation of the estimated D^{Ni} between expressions 8.15a and 8.15b, is less than ± 0.3 . Therefore, results obtained by using anyone of these relations would not show considerable deviations. The expression 8.15b is preferred here however, because it is based on a larger data set than the other.

The previous studies confirmed that the Ni partitioning follows Henry's law over a large concentration range. Mysen (1979) reported that Henry's law is followed in the range of 10 ppm to 1000 ppm in olivine, and changes dramatically for concentrations of more than 100 ppm in the liquid. Nevertheless, subsequent studies on natural basaltic compositions (primitive glasses from the mid-Atlantic) by Nabelek (1980) and Drake and Holloway (1981) confirmed the Henry's law behaviour of Ni for both olivine and liquid over a considerable concentration range, from 10 ppm to 60,000 ppm in olivine.

The pressure dependence of D^{Ni} was investigated by Mysen and Kushiro (1979). They found that the D^{Ni} decreases with increasing pressure. They reported on an abrupt decrease in D^{Ni} above 15kbar. Any melt generated at such high pressures will have much higher Ni contents than those estimated from the 1atm experiments and derived relations.

In order to minimize the dependence of the Ni partition coefficient on the composition of the coexisting liquid, D^{Ni} can be normalized to Mg (Sato, 1977). The normalized Ni partition coefficient is expressed by the following relation: $k_{D(\text{Ni-Mg})}^{\text{ol-liq}} = \frac{(\text{Ni/Mg})^{\text{ol}}}{(\text{Ni/Mg})^{\text{liq}}}$, for

which there is less temperature dependence (Sato, loc. cit.). Irvine and Kushiro (1976) however, examined the Ni-Mg partitioning in the join $\text{Mg}_2\text{SiO}_4\text{-K}_2\text{O}\cdot 6\text{SiO}_2$ of the $\text{Mg}_2\text{SiO}_4\text{-K}_2\text{O}\text{-SiO}_2$ system and showed that even the $K_{\text{D}(\text{Ni-Mg})}^{\text{ol-liq}}$ depends on the liquid composition. They inferred that the $K_{\text{D}(\text{Ni-Mg})}^{\text{ol-liq}}$ increases as the liquid becomes richer in SiO_2 and alkalis. Takahashi (1978) confirmed the compositional dependence of $K_{\text{D}(\text{Ni-Mg})}^{\text{ol-liq}}$ in the join $(\text{Mg}_{0.5}\text{Fe}_{0.5})_2\text{SiO}_4\text{-K}_2\text{O}\cdot 4\text{SiO}_2$ and for seven basaltic compositions and argued for a small temperature dependence; the $K_{\text{D}(\text{Ni-Mg})}^{\text{ol-liq}}$ for an Hawaiian tholeiite and an abyssal tholeiite is 2.7. The temperature dependence of the exchange partition coefficient was emphasized by Leeman and Lindstrom (1978), who gave the following inverse relationship between $K_{\text{D}(\text{Ni-Mg})}^{\text{ol-liq}}$ and temperature for natural basaltic compositions,

$$\ln K_{\text{D}(\text{Ni-Mg})}^{\text{ol-liq}} = \frac{4396}{T} - 1.94 \quad (8.16).$$

In the temperature range $1300^\circ\text{C}\text{--}1200^\circ\text{C}$, $K_{\text{D}(\text{Ni-Mg})}^{\text{ol-liq}}$ varies from 2.4 to 2.8.

Petrologic Applications

The olivine composition in basalts (phenocrysts/xenocrysts) and troctolites (cumulus phase) can be employed to estimate the $\text{Mg}/(\text{Mg}+\text{Fe})$ ratio and the Ni-content of the melt from which these olivines crystallised. It was concluded in the previous section (8.2) that the troctolites and harzburgites re-equilibrated at subsolidus temperatures. The subsolidus equilibration of these rocks was inferred from the compositional characteristics of spinel included in olivine, as

well as the exsolution features of clinopyroxenes. Olivine is a major constituent phase in troctolites. It is very unlikely that the olivine composition changed during subsolidus equilibration because of the limited Fe-Mg exchange between olivine and plagioclase; the olivine composition did however change at a narrow boundary zone around the spinel grains. In the latter case, Fe-Mg exchange produced the observed compositional profiles. The average olivine composition however remained unchanged, as is evidenced by the consistency of the forsterite and Ni contents within single layers and across successive layers. The incoming of clinopyroxene in the olivine-gabbros could have influenced the olivine composition. The uniform Mg/(Mg+Fe) ratios of olivine and clinopyroxene, and the very similar olivine and high-Ca pyroxene compositions crystallising from primitive basaltic melts at low pressures as documented by melting studies, suggest that the Fe-Mg exchange between these two minerals was negligible. Additionally, olivine from adjacent olivine-rich and plagioclase-rich layers in troctolites, and layers with variable modal clinopyroxene in the olivine-gabbros, has consistent Fo-content and Ni content.

The harzburgites had a more complex history than the cumulate rocks since they were affected by solid state ductile deformation possibly at higher temperatures and pressures prior to their final subsolidus re-equilibration. Liquids in equilibrium with residual mantle peridotites, such as the Macquarie Island peridotites, can be identified when the $K_{D(\text{Fe}^{2+}\text{-Mg})}^{\text{ol-liq}}$ (abbreviated as $K^{\text{Fe-Mg}}$) and D^{Ni} are well constrained. Because of the $K^{\text{Fe-Mg}}$ and D^{Ni} dependence on temperature, pressure and $f\text{O}_2$, the appropriate values at any given P-T conditions are not adequately constrained. Values of 0.3-0.33 for the $K^{\text{Fe-Mg}}$ and 9-10

for the D^{Ni} seem reasonably appropriate for low fO_2 , high temperatures ($>1200^\circ C$) and pressures up to 20kbar.

The average composition of the most magnesian cumulus olivine in troctolites is $Fo_{89.6}$, the composition range being from $Fo_{89.9}$ to $Fo_{88.6}$. Melts in equilibrium with these olivines would have had $Mg/(Mg+Fe^{2+})$ ratios of 0.7-0.68 assuming a K^{Fe-Mg} of 0.27. For a K^{Fe-Mg} of 0.3, the $Mg/(Mg+Fe^{2+})$ ratio would have been 0.70-0.72. Similarly, the olivines (Fo_{84-82}) from the olivine-gabbros at Handspike Pt., precipitated from melts having $Mg/(Mg+Fe^{2+})$ ratios of 0.59-0.55 (assuming $K^{Fe-Mg}=0.27$). The more FeO-rich olivines (Fo_{77-73}) from the Upper Level gabbros crystallised from melts with 0.48-0.42 $Mg/(Mg+Fe^{2+})$ ratios (at $K^{Fe-Mg} = 0.27$) or 0.50-0.46 (at $K^{Fe-Mg} = 0.3$). The MgO-rich olivine xenocrysts in basalt M14 must have crystallised from melts with $Mg/(Mg+Fe^{2+})$ ratios of 0.73-0.74 assuming $K^{Fe-Mg} = 0.3$. Melts expelled from residual harzburgite, containing olivine $Fo_{90.8-91.6}$, must have had $Mg/(Mg+Fe^{2+})$ ratios of 0.77-0.75 assuming the low pressure K^{Fe-Mg} of 0.3.

The Ni-content of basaltic melts is an important parameter in the identification of primary melts segregated from upper mantle peridotites and has also been used to assess fractional crystallisation processes (Sato, 1977). The olivine from the Macquarie Island harzburgites has 0.40-0.45%wt NiO (3140-3536 ppm Ni), on average 0.42%wt (3300 ppm Ni). The liquid Ni-content in equilibrium with these olivines is estimated from expression 8.15b. At a temperature of $1280^\circ C$ which is only slightly higher than that determined for liquidus olivine precipitating from primitive basaltic glasses (Bender et al., 1978; Green et al., 1979), melts in equilibrium with harzburgite olivine would have had at least 300 ppm Ni and as much as 345 ppm Ni; on average, 320 ppm Ni. The most magnesian olivines in troctolites have

on average, 0.22%wt NiO (1730 ppm Ni). Assuming crystallisation at about the same temperature (1280°C), these olivines must have crystallised from melts having ≈ 170 -180ppm Ni. If olivine crystallisation had occurred at the temperature range 1270° -1235°C, then the estimated Ni-content of the melt would have been 160-133 ppm Ni. The less magnesian olivines in the olivine-gabbros have NiO contents of 0.12-0.14%wt (943-1100 ppm Ni); they could crystallise from melts having as much as 107 ppm Ni and as little as 73 ppm Ni in the temperature range 1270° -1210°C. The olivine megacrysts in basalt M14 have 2357-2670 ppm Ni. Assuming crystallisation at the temperature range 1280°C - 1220°C, the estimated melt Ni-content would be 240 ± 20 ppm to 200 ± 10 ppm respectively. They therefore crystallised from melts which segregated from relatively "fertile" mantle peridotite, and not the refractory Macquarie Island harzburgites.

Some of the Macquarie Island basalts and dolerite dykes have sufficiently high Mg/(Mg+Fe) ratios and Ni and Cr contents to qualify as parental melts to the cumulate troctolites and olivine-gabbros. Their Mg/(Mg+Fe²⁺) ratios and Ni and Cr contents are listed in table 8.3. The basalts 38188, 38291, 236 and 38284, the glasses 47979 and 155, and the dolerite 220 can be identified as possible parental magmas of the layered rocks. However, even the most primitive basalts and dolerites could not be in equilibrium with the mineralogy of the residual harzburgites. The Ni-contents of both basalts and dolerites are considerably lower than those expected for liquids in equilibrium with residual harzburgite. In addition, no basalt or dolerite could crystallise the MgO-rich and NiO-rich olivine xenocrysts of basalt M14. The most magnesian basalts/dolerites (>9%wt) are therefore capable of generating the sequence of layered troctolites- olivine-gabbros, but

even the most primitive were not the last melts to equilibrate and been extracted from the residual harzburgites.

8.3.2 Spinel-melt equilibrium

The partitioning of Cr, Al, Mg and iron between basaltic liquid and spinel at various temperatures and oxygen fugacities is discussed in this section. Experimental studies by Hill and Roeder (1974), Fisk and Bence (1980) and Maurel and Maurel (1982-84) suggest that at constant temperature the Cr/(Cr+Al) ratio and the MgO content of spinel decrease with increasing fO_2 ; at constant fO_2 , spinel Cr_2O_3 and Al_2O_3 contents decrease with decreasing temperature. The spinel ferric iron content increases with increasing fO_2 and decreasing temperature.

The chromium content of basaltic liquids is a function of temperature and fO_2 . At 1200°C and 10^{-8} atm, 200-300ppm Cr can be dissolved in a basaltic liquid (Hill and Roeder, 1974). The partition coefficient $D^{Cr} = \frac{(Cr_2O_3)^{sp}}{(Cr_2O_3)^{liq}}$ increases with increasing temperature at constant fO_2 and decreases with decreasing fO_2 at constant temperature (Maurel and Maurel, 1982b). At an fO_2 of less than $10^{-9.5}$ atm, spinel does not crystallise (Fisk and Bence, 1980).

The aluminium partition coefficient $D^{Al} = \frac{(Al_2O_3)^{sp}}{(Al_2O_3)^{liq}}$ increases with decreasing fO_2 (Fisk and Bence, 1980). Maurel and Maurel (1982a) have found that the relation:

$$(Al_2O_3)^{sp} = 0.035 \cdot ((Al_2O_3)^{liq})^{2.42} \quad (8.17)$$

expresses with sufficient accuracy the exchange of Al_2O_3 between spinel and basaltic liquid.

The distribution of ferrous iron between spinel and magma depends on the temperature, fO_2 , the total iron content, MgO content and

the ratio $\text{Fe}^{3+}/\text{Fe}^{2+}$ of the magma. Maurel and Maurel (1984b) showed that the partition coefficient

$D^{\text{Fe}^{2+}} = \frac{(\text{FeO})^{\text{sp}}}{(\text{FeO})^{\text{liq}}}$ correlates with the MgO and FeO contents of the melt

according to the following expression:

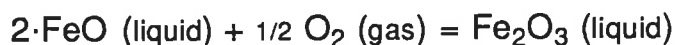
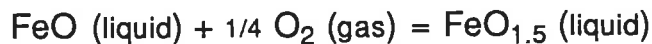
$$\ln D^{\text{Fe}^{2+}} = 5.83 - 1.93 \cdot \ln(\text{MgO})_{\text{liq}} + \left(0.059 \cdot ((\text{MgO})_{\text{liq}} - 1) \right) \cdot \ln(\text{FeO})_{\text{liq}} \quad (8.18).$$

The Fe_2O_3 content of spinel is also a function of the total iron content and the $\text{Fe}^{3+}/\text{Fe}^{2+}$ ratio of the melt, and the temperature and $f\text{O}_2$. The temperature dependence of $D^{\text{Fe}^{3+}} = \frac{(\text{Fe}_2\text{O}_3)^{\text{sp}}}{(\text{Fe}_2\text{O}_3)^{\text{liq}}}$ is given by the

following expression according to Maurel and Maurel (1984a),

$$D^{\text{Fe}^{3+}} = \frac{4813}{T} - 2.39 \quad (8.19).$$

The ferric to ferrous iron ratio ($\text{Fe}^{3+}/\text{Fe}^{2+}$) of the silicate melt is an important parameter which monitors the composition of the spinel. The $\text{Fe}^{3+}/\text{Fe}^{2+}$ ratio is sensitive to temperature, pressure, $f\text{O}_2$ and liquid composition. The following two reactions give two different approaches in expressing the ferric to ferrous oxide equilibrium,



The first reaction was adopted by Fudali (1965). Sack et al. (1980) considered the second reaction and formulated the following expression which relates the $\text{Fe}^{3+}/\text{Fe}^{2+}$ to temperature, $f\text{O}_2$ and liquid composition at 1atm pressure:

$$\ln \frac{\text{Fe}^{3+}}{\text{Fe}^{2+}} = a \cdot \ln(f\text{O}_2) + \frac{b}{T} + c + d_i X_i \quad (8.20)$$

where a, b, c and d are constants and X_i is the mole fraction of component i in the silicate melt.

Spinel synthesis

Hill and Roeder (1974) synthesized Cr-bearing spinel from the Hawaiian olivine-tholeiite 1921 (8.1%wt MgO, 13%wt Al₂O₃, 500 ppm Cr). They found that at 1200°C, increasing fO_2 results in increasing the Fe₂O₃ and decreasing the Cr₂O₃ content of spinel. Spinel is the liquidus phase at high temperatures (>1200°C) and 10^{-9} - 10^{-11} atm fO_2 . Spinel crystallised at 1200°C and fO_2 of $10^{-9.5}$ and 10^{-8} atm had 43% and 35-36% Cr₂O₃ respectively. Decreasing temperature at a constant fO_2 of 10^{-7} atm results in increases in FeO, Fe₂O₃ and TiO₂ and decreases in Cr₂O₃, Al₂O₃ and MgO.

Fisk and Bence (1980) synthesized Cr-spinel from the FAMOUS basalt 527-1-1 (MgO>9.5%wt, Mg/(Mg+Fe²⁺)=0.68, 510 ppm Cr). This basalt contains three types of spinel phenocrysts, an Al-rich variety having Cr/(Cr+Al) ratios of 0.22-0.32 (group I), a Cr-rich type with Cr/(Cr+Al) ratios of 0.42-0.47 (group II), and a third group (group III) with intermediate Cr/(Cr+Al) and Mg/(Mg+Fe²⁺) ratios. Fisk and Bence found that spinel is the liquidus phase at fO_2 $10^{-8.5}$ atm and higher, but did not crystallise at fO_2 of less than $10^{-9.5}$ atm. They duplicated experimentally the group II spinels at temperatures of 1230° -1250°C and fO_2 of 10^{-9} atm, but failed to synthesize the group I spinels. They concluded that the group I spinels must have crystallised at high temperatures (>1250°C), low fO_2 (\leq QFM) and possibly high pressures from MgO-rich melts (Mg/(Mg+Fe²⁺) \geq 0.74). Group III spinels are similar to those synthesised at 1200°C and $10^{-8.5}$ atm fO_2 .

PETROLOGIC APPLICATIONS

The composition of spinel phenocrysts in basalts represents liquidus composition, and as such can be employed to assess the liquid

Cr-content. Spinel is a minor phase (<1% by volume) in troctolites while olivine is a major constituent mineral. Spinel compositions are affected by subsolidus Fe-Mg exchange with olivine. Not all of them however can represent liquidus spinel compositions. Spinels wholly enclosed in plagioclases on the other hand, must have not exchanged Mg and Fe with the surrounding phase; hence, and their compositions were the least, if at all, changed during subsolidus equilibration. The composition of spinel megacrysts in the lavas, the phenocrysts in the glasses and the most magnesian spinels in troctolites are used to assess liquid Cr-contents and other parameters.

Comparison of Macquarie Island spinels with experimentally crystallised spinels.

The high-Al spinel xenocrysts of Macquarie Island lavas (eg. sample M14) with 32-36%wt Al_2O_3 and 28-30%wt Cr_2O_3 , and high $\text{Mg}/(\text{Mg}+\text{Fe}^{2+})$, 0.75-0.80, and low $\text{Cr}/(\text{Cr}+\text{Al})$, ≈ 0.3 , ratios compare with the group I spinel phenocrysts of Fisk and Bence (1980) from basalt 527-1-1. Representative spinel core compositions from the lavas are plotted in figure 8.5. Also shown in figure 8.5 are the fields of the experimental spinels from Fisk and Bence (loc.cit.). The similar compositions of Macquarie Island high-Al spinels and the group I spinels of 527-1-1 basalt suggest broadly similar genetic conditions; high temperatures, more than 1250°C , and low $f\text{O}_2$, approximately FMQ buffer. The composition of the melt from which such spinels crystallised is governed by high $\text{Mg}/(\text{Mg}+\text{Fe}^{2+})$ ratios (≥ 0.74), high Al_2O_3 (>16%wt), and Cr-contents of 500 ppm or higher.

The most magnesian spinels in troctolites occur in a thin chromite band (segregation) within plagioclase layers in sample 324. They are likely to represent liquidus spinels, although minor subsolidus

re-equilibration cannot be ruled out. These spinels have $Mg/(Mg+Fe^{2+})$ ratios of more than 0.65-0.66 and Cr_2O_3 and Al_2O_3 contents in the range of 34-38%wt and 27-31%wt respectively. Their TiO_2 content is limited between 0.7% and 0.8%wt. Compositionally, they grade towards the less magnesian spinel "megacrysts" from the lavas (figure 4.6). They are very similar to the group II spinel phenocrysts from basalt 527-1-1 (Fisk and Bence, 1980). Synthetic spinels similar to the Macquarie Island plutonic spinels and the group II spinels of Fisk and Bence (loc.cit.) crystallised from basalt 527-1-1 at temperatures of 1250°-1200°C and fO_2 of $10^{-8.5}$ - $10^{-9.5}$ atm; they had 35-38%wt Cr_2O_3 at $fO_2 \approx 10^{-9.5}$ atm and temperature 1230°-1250°C. Spinel crystallised from the olivine tholeiite 1921 at 1200°C and $fO_2 = 10^{-8}$ - $10^{-9.5}$ atm had 35-40%wt Cr_2O_3 , a maximum of 43%wt (Hill and Roeder, 1974).

A direct comparison of the Macquarie Island spinels with those synthesised experimentally from MgO-rich magmas indicates that the Al-rich, Mg-rich spinel "megacrysts" in the lavas crystallised at high temperatures, in excess of 1250°C, low $fO_2 \approx$ FMQ buffer from melts with high $Mg/(Mg+Fe^{2+})$ ratios, ≥ 0.74 , and around 500 ppm Cr. The most magnesian spinels in troctolites crystallised from melts with lower MgO contents at lower temperatures and possibly at 1 atm; provided that the most Cr-rich spinels crystallised from basalt 1921 had about 40%wt Cr_2O_3 , the Macquarie Island plutonic spinels must have crystallised from melts with around 500 ppm Cr. The less magnesian ($Mg/(Mg+Fe^{2+})=0.5-0.6$), lower-alumina ($Al_2O_3=20-22\%$ wt) and high-Cr ($Cr_2O_3=39-41\%$ wt) spinels in the chromite band from troctolite 324, are compositionally similar to the synthetic spinels at 1200°C and fO_2 of 10^{-8} - 10^{-9} atm from basalt 1921 (Hill and Roeder, 1974), and those crystallised at about 1200°C and $10^{-8.5}$ - $10^{-7.5}$ atm fO_2 from basalt 527-1-1. Assuming that their compositions have not been modified by

subsolidus Fe-Mg exchange with olivine, these spinels must have crystallised at temperatures of about or less than 1200°C and fO_2 of around 10^{-8} atm.

Inverse method

An inverse method approach has been undertaken in order to compare the compositions of spinels crystallising from tentative parental magmas with the Macquarie Island liquidus spinels.

The Fe^{3+}/Fe^{2+} ratio of the melt was computed from the total iron content using the formulation of Sack et al. (1980), equation 8.20; the values of the constants a, b, c and d, were taken from the better defined data set of Kilinc et al. (1983). The spinel FeO and Fe_2O_3 contents were estimated from equations 8.18 and 8.19 respectively. The ferric and ferrous iron content of the melt calculated for a range of temperatures and fO_2 , from 1180°-1300°C and $10^{-5.5}$ - 10^{-11} atm respectively. The estimated spinel FeO and Fe_2O_3 contents were calculated for each T- fO_2 step. The spinel Al_2O_3 content estimated from equation 8.17, and the Cr_2O_3 content was calculated for a range of melt Cr-contents, from 300 ppm to 1500 ppm Cr. Although a direct comparison of fictive and liquidus spinels is not a *a priori* guarantee for constraining precisely the liquid composition, it does however provide some information on the liquid composition.

Several tentative parental melt compositions were tested. The Macquarie Island glass NH2 contains in equilibrium spinel phenocrysts. Microprobe analyses of coexisting glass and spinel phenocrysts provide an excellent opportunity to estimate the Ds for Al_2O_3 , MgO and FeO. The equations of Maurel and Maurel (loc.cit.) have been applied to spinel-glass pairs from this sample. When basaltic glass 527-1-1 is tested as parental melt, and the calculated spinel composition compares with the

compositions of the synthesized spinels for different temperatures and fO_2 . In both cases, it is found that the calculated spinel Al_2O_3 content is overestimated by $\approx 0.5-1\%$ from equation 8.17; equation 8.17 predicts spinel Al_2O_3 content of $\approx 31.5\%wt$ from liquid 527-1-1; this value is in the middle of the observed range of group II spinels and group I spinel rims, inferred to be liquidus spinels at $10^{-8.5} - 10^{-9}$ atm fO_2 . The liquidus Macquarie Island lava spinels must have crystallised from melts with about $17\% Al_2O_3$ according to 8.17. The FeO content is reproducible within $\pm 0.6\%$ (equation 8.18), but the Fe_2O_3 content is underestimated (equation 8.19). The calculated spinel FeO content from liquid 527-1-1 for the temperature range $1220^\circ-1300^\circ C$ and $10^{-9} - 10^{-9.5}$ atm fO_2 is about $12-13\%wt$, and approximates the FeO content of group II spinels ($\approx 12\%wt$). The Macquarie Island spinels from the lavas have similar FeO contents ($12-13\%wt$), and hence could have been crystallised from melts with similar FeO contents to the basalt 527-1-1. The Fe^{3+}/Fe^{2+} ratio of the liquid is an important factor controlling the FeO content of the crystallising spinel. The lower this ratio the better the agreement of observed and calculated (from equation 8.18) spinel compositions. The Cr content of the liquid which crystallised the high-Al spinels from the lavas was estimated to be the range of $500-700$ ppm.

Oxidation States

The very low Fe_2O_3 contents of spinel "xenocrysts" in the Macquarie Island lavas and phenocrysts in glasses suggest very low fO_2 possibly $\leq FMQ$ at the source regions of the melts from which these spinels crystallised. Previous studies (including direct Fe^{3+}/Fe^{2+} measurements) on the oxidation states of mantle peridotites (Arculus and Delano, 1981) and basaltic glasses (Dmitriev et al., 1984; Christie

et al., 1986) showed that fO_2 is about and/or lower than the FMQ buffer. The Macquarie Island data show excellent agreement with these studies. The Al-rich, MgO-rich, Ti-poor character of these spinels necessitates parental liquids with high Mg/(Mg+Fe) ratios, also inferred from the composition of the olivine xenocrysts/megacrysts, high Al_2O_3 contents ($\geq 17\%$ wt) and generating at high temperatures, $\geq 1250^\circ C$, and low fO_2 , possibly around the FMQ buffer. The spinels in troctolites indicate crystallisation from melts at higher fO_2 and hence shallower depths.

8.4 Crystallisation Modelling

Low pressure fractional crystallisation of MgO-rich basaltic melts (MgO $\geq 9\%$ wt) is widely considered as the most effective process for generating the compositional diversity of MORBs (for a review see Wilkinson, 1982). The well defined basaltic glass trend of decreasing MgO with falling Al_2O_3 and CaO and increasing total iron and TiO_2 provides strong support to fractional crystallisation of olivine+plagioclase+clinopyroxene especially for less magnesian glass compositions (MgO $< 7\%$ wt). Least squares calculations corroborate the control of olivine+plagioclase+clinopyroxene fractionation in the compositions of the evolved basaltic glasses (Bence et al., 1979; Perfit and Fornari, 1983). Experimental confirmation of the crystallisation temperatures of these minerals comes from a number of studies (Bender et al., 1978; Green et al., 1979; Fujii and Bougault, 1983). Olivine is the liquidus phase at low pressures (≤ 5 kb) and is followed by plagioclase 20-30 $^\circ C$ below the liquidus, and clinopyroxene at about 50 $^\circ C$ below the liquidus. The phase relations of MgO-rich basalts (MgO $\geq 9\%$ wt) are suggestive of olivine and plagioclase removal from such melts; these two phases together with

clinopyroxene at lower temperatures must exert a major control on the composition of MORBs. In particular, the $Mg/(Mg+Fe)$ ratios of MORBs (mostly $Mg\# < 63$) must be controlled by olivine fractionation. The presence of olivine+plagioclase and olivine+plagioclase +clinopyroxene cumulates in Macquarie Island offers clear circumstantial evidence for such fractionation and an excellent opportunity to test whether the most MgO-rich basalts relate (and to what extent) to the more evolved via olivine and plagioclase fractionation.

Olivine Crystallisation

The crystallisation of olivine from MgO-rich melts parental to the olivines of the cumulate troctolites is tested. Two cases are considered in this section, equilibrium crystallisation and fractional crystallisation. Fractional crystallisation has long been considered as the dominant process generating the observed compositional diversity of MORBs. Removal of olivine, plagioclase and clinopyroxene at low pressures has been modelled by least squares approximations and found to be essential for producing the wide major element variations of MORBs. Most of the relevant studies employed phenocryst compositions in modelling the liquid changes during fractionation of these three phases. The cumulate rock sequence exposed on Macquarie Island provides a unique opportunity to test the effectiveness of the various crystallisation models.

Case for Equilibrium Crystallisation

The compositional changes of a liquid during equilibrium crystallisation of olivine from a primitive MgO-rich melt are modelled in terms of $Mg/(Mg+Fe)$ ratios and NiO contents. A melt in equilibrium with the average olivine ($Fo_{89.7}$, Ni=1730ppm) of the lowermost layered troctolites undergoes olivine crystallisation. The initial melt $Mg/(Mg+Fe)$

and Ni-content are estimated from the olivine composition. Partition coefficients for Mg, Fe and Ni are estimated from the regressions of Leeman and Lindstrom (1978), Leeman (1978) and Jones (1984) at two temperatures, 1220° and 1280°C.

Mass balance requirements necessitate that the concentration of an element i in the resulting melt after olivine crystallisation from an initial melt is expressed by the following relation,

$$C_{i.o} = C_{rliq}^i \cdot (1-x) + C_{oliv}^i \cdot x \quad (8.21)$$

where C_o^i is the concentration of element i in the initial melt, C_{rliq}^i is the concentration of element i in the residual melt, C_{oliv}^i is the concentration of element i in olivine, and x is the fraction of olivine crystallising.

The changes in the Mg/(Mg+Fe) ratio and Ni-content of the initial liquid during olivine equilibrium crystallisation are calculated from expression 8.21. The olivine composition is fixed at Fo_{89.7}. The liquid path is calculated for an increment of olivine crystallisation of 1%. Residual liquid compositions are plotted in figure 8.6. The liquid paths for 1% to 14% olivine crystallisation at the two different temperatures of interest (1220° and 1280°C) have different slope than that shown by the basalts. Separation of olivine from the residual liquid would contribute to a greater depletion in the liquid Ni-content thus resulting in the rotation of curves 1 and 2 towards curve SS. It is evident from figure 8.6 that equilibrium crystallisation of olivine cannot account for the observed compositional trend of basalts. Segregation of olivine from MgO-rich melts is suggested by field evidence, presence of cumulate melatroctolites - troctolites;

olivine segregation is also indicated by the trends of $Mg/(Mg+Fe)$ ratios and Ni contents of basalts. Geological observations and chemical inferences are thus in good agreement.

Case for Fractional Crystallisation

During fractional crystallisation of olivine, both liquid and olivine compositions change incrementally. Olivine precipitated from each residual liquid will be more Fe-rich than previous olivines. It was inferred in section 8.3 that liquids in equilibrium with the troctolite olivines would have had $Mg/(Mg+Fe^{2+})$ ratios of 0.7-0.72 and Ni-contents of more than 170 ppm. Some of the basalts have similar $Mg/(Mg+Fe^{2+})$ ratios and Ni-contents. They therefore can be parental liquids to the cumulate rocks. These basalts are the initial liquids. The olivine composition in equilibrium with these basalts is firstly estimated. The calculated olivine Fo-content is reduced by 0.5 Fo units to account for the $Mg/(Mg+Fe)$ ratio of the next residual liquid. A weight percentage (2% in the following calculations) of this olivine composition is then subtracted from the initial liquid composition to estimate the residual liquid composition, $Mg/(Mg+Fe)$ ratio and Ni-content. The resulting residual liquid will be in equilibrium with a less magnesian olivine; the composition of olivine is again calculated and then its composition (minus 0.5 Fo units) subtracted from the liquid composition, thus resulting in a new residual liquid and so on. Olivine compositions used in the following calculations are real compositions from the troctolite olivines.

Two cases of olivine fractionation are tested and the results are plotted in figures 8.7 and 8.8. In the first case, the K^{Fe-Mg} and D^{Ni} are assumed constant. The value of K^{Fe-Mg} is taken equal to 0.3, and D^{Ni} equal to

11. The value of D^{Ni} represents a temperature of $\approx 1270^\circ\text{C}$, estimated from expressions 8.15a and 8.15b. Figure 8.7 shows the successive liquid changes during fractional crystallisation of olivine from two magnesian basalts, samples 236 and 38188 (table 8.3). The liquid path is calculated by successively subtracting 2 wt% olivine composition. Figures 8.7a and 8.7b show fractionation paths of an initial liquid 236. After 5% fractionation, the liquid Ni-content is reduced to half. Only after 4% fractionation, the liquid becomes so depleted in Ni, that the crystallising olivine (Fo_{88}) has just 0.14% NiO. The liquid path interpolates the compositional trend defined by most basalts and dolerites. Figures 8.7c and 8.7d show the liquid paths during olivine fractionation from an initial liquid similar to 38188. Basalt 38188 has higher MgO (11.17%wt) and Ni (199 ppm) than basalt 236 (7.99%wt MgO, 164ppm Ni); basalt 38188 can be parental to basalt 236 via 2% olivine fractionation. It is shown in figure 8.7 that most basalts are derivatives of such initial liquids. The majority of basalts can be derived from basalt 38188 through 2-10% olivine fractionation, and the most evolved basalts ($\text{Mg}/(\text{Mg}+\text{Fe}^{2+}) \approx 0.60 \pm 0.02$) can be produced by $14 \pm 1\%$ fractionation. Similarly, most basalts can be derived from basalt 236 via 1-10% olivine fractionation. The same holds true for dolerites. Almost all but one dolerite are derived from initial liquids such as basalts 236 and 38188 by 2-12% fractionation. The most evolved dolerite, sample 391 ($\text{Mg}/(\text{Mg}+\text{Fe})=0.47$, $\text{Ni}=27\text{ppm}$), is derived by 16% olivine fractionation from basalt 38188.

In the second case, the $K^{\text{Fe-Mg}}$ and D^{Ni} are considered to change progressively as temperature falls. The calculated values for D^{Ni} (from expression 8.15b) change considerably as temperature drops, in contrast to the minor change of $K^{\text{Fe-Mg}}$ with decreasing temperature. $K^{\text{Fe-Mg}}$ is estimated from the relation of Bender et al. (1978), expression 8.13. Resulting liquid

paths during olivine fractionation from basalt 38188, are plotted in figure 8.8. Because of the increasingly higher D^{Ni} with decreasing temperature, calculations carried out using as initial temperature $1265^{\circ}C$; there is a marked depletion in the liquid Ni-content as temperature drops, and the resulting liquid path is significantly different than the liquid lines of descent shown in figure 8.7. The liquid path does not approximate the basalt trend, but instead lies in the $Mg/(Mg+Fe)$ -rich side of the basalt cluster. 12% olivine fractionation depletes the liquid in Ni too much; the estimated Ni values (<32 ppm) are even lower than those observed in the most differentiated basalts ($Mg/(Mg+Fe) \approx 0.60$).

The successive changes in the olivine composition during fractional crystallisation from a possible parental melt such as basalt 38188, are illustrated in figure 8.9. The first olivine to crystallise from basalt 38188 has the same composition as the in-equilibrium olivine, $Fo_{90.4}$. Fractional crystallisation of this olivine will result in a residual liquid which then crystallises a less magnesian olivine. The olivine composition estimated assuming a K^{Fe-Mg} value of 0.3. Two cases are shown in figure 8.9. In the first case, the olivine composition path is calculated using a D^{Ni} of 9; a D^{Ni} of 12 is used to calculate the olivine path in the second case. The calculated olivine composition is plotted for 2% fractionation intervals. Representative olivine compositions from the Macquarie Island layered troctolites, olivine-gabbros and harzburgites are also plotted. The calculated olivine trend and the cumulus olivine trend (real) have distinctly different slopes. The calculated trend shows that after 6% fractionation, the liquid is in equilibrium with olivine $Fo_{88.5}$. This olivine however has only 0.13-0.14%wt NiO. Cumulus olivine from the cumulate rocks has around 0.20%wt NiO for similar Fo contents. After 8% fractionation, the liquid can only crystallise olivine ($Fo_{87.6}$) with 0.11%wt NiO. Such Ni-

contents are the lowest detected in cumulus olivines, but correspond to Fo contents of 81-82.

The real olivine compositions lie on the concave side of the calculated olivine trend; they are always less forsteritic but with higher Ni-content than the calculated olivines. Also, these actual olivines maintain similar Ni-contents over a wide range of Fo-contents. These chemical characteristics are suggestive of continuous replenishment of the magma conduit/chamber with fresh batches of unfractionated melts, which mix with the existing (and fractionating) magma continuously. As a result the Fo- and the Ni- contents are reset towards higher values continuously during the course of magma differentiation. Such a conclusion is also in agreement with previous inferences (chapter 4, eg. figure 4.3B).

8.5 Conclusions

The Fe-Mg exchange between olivine and spinel continues for considerable time down-temperature (after the original crystallisation of these two minerals at some high temperature) when spinel is included in olivine. Olivine-spinel pairs from the Macquarie Island harzburgites give subsolidus temperatures of 670°-910°C. In troctolites, the most magnesian spinels ($\text{mg}\# > 60$) and the averaged olivine compositions, which are very similar to the spinel and olivine phenocryst compositions from the glasses, indicate temperatures of 1165°-1250°C. Coexisting spinel and olivine phenocrysts from the glasses give very similar temperatures, approximately 1230°C. Calculated temperatures from the averaged olivines and the less magnesian spinels ($\text{mg}\# < 50$) of troctolites are clearly subsolidus, on average 700°±50°C. The estimated temperatures from the olivine -spinel pairs in the North Mt. wehrlite are in the range of 1210°-

1287°C, and possibly represent original crystallisation temperatures. The pyroxene compositions from the Macquarie Island harzburgites, troctolites and olivine-gabbros have also been employed for calculating crystallisation temperatures. The different methods applied yield original magmatic temperatures of 1100°-1170°C and blocking temperatures of less than 800°C for troctolites and olivine-gabbros. Subsolidus temperatures (650°-800°C) are indicated by the pyroxene assemblage of harzburgites.

Examination of the compositional profiles in both spinel and olivine, and the Fe-Mg diffusion rates between these two phases suggest that the cooling rate of the Macquarie Island harzburgites and troctolites was $\leq 0.001^\circ\text{C}/\text{year}$. The North Mt. wehrlite cooled fast, estimations suggest around $1000^\circ\text{C}/\text{year}$; therefore, it is possibly a high level intrusion, in agreement with its observed stratigraphic position.

Consideration of the olivine-liquid equilibria indicates that liquids in equilibrium with the troctolite olivines would have had Mg/(Mg+Fe) ratios of 0.69-0.72 and Ni contents of around 180ppm. Similarly, liquids equilibrated with (or extracted from) the refractory harzburgites would have had Mg/(Mg+Fe) ratios of 0.75-0.76 and Ni contents of about 320ppm. Some of the basalts and dolerite dykes have sufficiently high Mg/(Mg+Fe) ratios and Ni contents to qualify as parental melts to the cumulate troctolites and olivine-gabbros (table 8.3). The basalts 38188, 38291, 236 and 38284, the glasses 47979 and 155, and the dolerite 220 can be parental magmas of the layered rocks. However, even the most primitive basalts and dolerites could not be in equilibrium with the mineralogy of the residual harzburgites. The Ni-contents of both basalts and dolerites are considerably lower than those expected for liquids in equilibrium with residual harzburgite. In addition, no basalt or dolerite could crystallise the MgO-rich and NiO-

rich olivine xenocrysts of basalt M14. The compositions of the liquidus spinels indicate that this mineral crystallised from liquids rich in MgO ($\geq 9\%$ wt), with high Al_2O_3 ($\approx 17\%$ wt) and Cr-content ($> 500\text{--}700\text{ppm Cr}$), and under very low $f\text{O}_2$ conditions ($\leq \text{FMQ}$).

Equilibrium and fractional crystallisation of olivine from MgO-rich melts, aphyric basalts and glasses, has been tested. It was inferred that fractional crystallisation of olivine can account for the $\text{Mg}/(\text{Mg}+\text{Fe})$ ratios and Ni-contents of the less magnesian basalts and dolerites. The amount of fractionating olivine depends on the $\text{Mg}/(\text{Mg}+\text{Fe})$ ratio and Ni-content of each basalt/dolerite. The moderately differentiated basalts/dolerites, with $\text{Mg}/(\text{Mg}+\text{Fe})=0.7\text{--}0.64$, can be derived from a primitive melt (such as basalts 38188 and 236) through 2-10% olivine fractionation. The low $\text{Mg}/(\text{Mg}+\text{Fe})$ (≈ 0.6) basalts/dolerites can be derived from such primitive melts after 12-14% olivine fractionation. The most differentiated sample (dolerite 391) can be derived from basalt 38188 via 16% olivine extraction. The $\text{Mg}/(\text{Mg}+\text{Fe})$ ratios and Ni-contents of basalts/dolerites can be accounted for by different proportions of olivine fractionation. The fractionating olivine has a composition similar to that of the cumulus olivine in troctolites. The accumulation of troctolites has thus controlled the $\text{Mg}/(\text{Mg}+\text{Fe})$ ratios and Ni-contents of basalts and dolerites, and these layered rocks can be considered as complementary to the volcanics.

CHAPTER NINE : PETROGENESIS

9.1 Introduction

The mineralogy, chemistry and genesis of mid-ocean ridge basalts (MORBs) have been the centerpoint of innumerable studies. Discussions on the genesis of these basalts, predominantly tholeiitic, concentrated in defining their phase relations at given P/T conditions and comparing their liquidus or near-liquidus phases with the mineral phases of mantle peridotites; attempting to identify the composition and mineralogy of the source upper mantle peridotites and the extent of partial melting; discussing their low pressure fractionation paths; and assessing the chemical effects of magma mixing in open-system magma chambers located at some shallow depth beneath the spreading ridge. The literature is enormous; for this reason, very few selected studies are considered in the following discussion. The most recent reviews on the genesis of MORBs are those of Wilkinson (1982), Thompson (1987) and the Basaltic Volcanism Study Project (1981).

Primary basaltic melts generated by partial melting of upper mantle peridotite must have high Mg# values ($Mg\# = 100 \cdot Mg / (Mg + Fe^{2+})$), high Ni and Cr contents, and to be in equilibrium with suitable upper mantle peridotite mineralogies. Primitive MORBs have Mg# ratios of 70-73, more than 200 ppm Ni and 500 ppm Cr. These characteristics interpreted by Kay et al. (1970) to indicate that these basalts are relatively undifferentiated liquids. The compositions of basaltic liquids with less than 7% MgO follow the 1 atm cotectics of olivine, plagioclase and clinopyroxene, and so are mainly controlled by low pressure fractionation of these phases (Walker et al., 1979). Basaltic liquids with more than 9.5% MgO are rare; they could be either primary

magmas directly derived by melting upper mantle peridotite or differentiated products (mainly through olivine fractionation) of even more magnesian melts (picrites). Most MORBs however have MgO contents between 7% and $\leq 9.5\%$; they are therefore fractionated liquids.

Residual peridotites produced by partial melting of "fertile" upper mantle peridotite are lherzolites and harzburgites as is evidenced by the tectonite peridotites from the base of ophiolite complexes and dredged ultramafics from the ocean floor. Tectonised harzburgite is the dominant lithology of ophiolite ultramafic rocks; these rocks have been subjected to asthenospheric flow. Lherzolite is the predominant ultramafic rock from the ocean floor. Harzburgite always contains up to 5% modal clinopyroxene. Basaltic melts extracted from such peridotites must have olivine and orthopyroxene, the two major constituent phases of lherzolite and harzburgite, as liquidus phases at the P/T conditions of interest.

Melting experiments of magnesian MORBs show that olivine is the liquidus phase from 1 atm to 10 kbar anhydrous; it is followed by plagioclase and clinopyroxene (Bender et al., 1978; Green et al., 1979; Fujii and Bougault, 1983). At about 10 kbar, olivine is replaced by clinopyroxene on the liquidus. Clinopyroxene persists as a liquidus phase up to 15 kbar. Bender et al. (1978) showed that the basaltic (tholeiitic) glass 527-1-1 (Mg#=68; Ni=232 ppm) from the FAMOUS area has clinopyroxene at its liquidus from 10.5 to 15 kbar. At 1310°C and 15 kbar, orthopyroxene crystallises after clinopyroxene. Fujii and Bougault (1983) determined the phase relations of the basaltic glass ARP 74-10-16 (an olivine-tholeiite) with mg#= 69 ($mg\# = 100 \cdot Mg / (Mg + \Sigma Fe)$) and 240 ppm Ni from Mount Venus in the FAMOUS area. They found that olivine, clinopyroxene, orthopyroxene and plagioclase

crystallise within 10°C from the liquidus. Orthopyroxene is not a liquidus phase at any pressure, from 1 atm to 15 kbar. Green et al. (1979) studied the phase relations of glass 3-18-7-1 from DSDP Site 18, South Atlantic. This basaltic glass (mg#=69.5) shows only clinopyroxene as a liquidus phase from 10 to 15 kbar; clinopyroxene is followed by plagioclase with decreasing temperature. Green and his colleagues added up to 9% orthopyroxene before orthopyroxene appeared on the liquidus. Orthopyroxene was found as a liquidus phase at 9 kbar from the olivine tholeiite II (Mg#=69.8) of Green and Ringwood (1967). Kushiro and Thompson (1972) also reported a Ca-poor pyroxene (mg#=84.4) to crystallise from the olivine-tholeiite T-87 (mg#=64.3) at 7.5 kbar. Fujii and Kushiro (1977a) also found orthopyroxene (mg#=86) to crystallise from a less magnesian olivine tholeiite (mg#=57.2) after olivine, plagioclase and clinopyroxene within 10°C from the liquidus.

Various models have been proposed for the genesis of MORBs based on their phase relations at low and high pressures. The predominant models fall in two categories, (1): All sampled MORBs, even and the most magnesian with 9.5-11%wt MgO, are derived from parental picritic melts via olivine fractionation polybarically. Picritic magmas generate in the mantle at pressures between 15 and 30 kbar (60-100 km). This model is supported by the studies of O'Hara (1968), Green et al. (1979), Stolper (1980), Elthon and Scarfe (1984), and others. (2): Some of the most magnesian MORBs (MgO >9.5%wt; Ni >200 ppm) are primary melts generated by partial melting of suboceanic mantle peridotite at pressures 9-11 kbar (25-35 km). This model is preferred by Presnall et al. (1979), Fujii and Bougault (1983) and Takahashi and Kushiro (1983).

Presnall et al. (1979) investigated the phase relations of magnesian tholeiites in the system CaO-MgO-Al₂O₃-SiO₂ (CMAS). At the intersection of spinel-lherzolite and plagioclase-lherzolite solidi (≈ 9 kbar), there is a cusp; Takahashi and Kushiro (1983) also found two cusps on the peridotite HK66 solidus, at the points where the subsolidus assemblages change. Presnall and his colleagues favoured the generation of magnesian MORBs at the ≈ 9 kbar cusp by merit of its invariancy, forsterite +diopside +enstatite +anorthite +spinel +liquid.

Green et al. (1979) carried orthopyroxene and olivine addition experiments in a magnesian basalt (3-18-7-1) to test at which temperature and pressure this basalt would be saturated with both olivine and orthopyroxene, and thus a primary magma. They concluded that basalt 3-18-7-1 was saturated with both olivine and orthopyroxene at 20 kbar and $\approx 1430^\circ\text{C}$. They proposed generation of tholeiitic picrites at 20 kbar ($\approx 70\text{km}$), and formation of all MORBs from parental picritic magmas through olivine fractionation.

Fujii and Bougault (1983) performed melting experiments on a magnesian olivine tholeiite (ARP 74-10-16) from the FAMOUS area. They found that this basalt has near liquidus olivine, orthopyroxene, clinopyroxene, spinel and plagioclase at 10 kbar; ARP 74-10-16 has also high Ni content (≥ 240 ppm). Fujii and Bougault suggested that such magnesian MORBs could be primary magmas generated at ≈ 10 kbar, at the P/T interval where the peridotite subsolidus assemblage changes from spinel lherzolite to plagioclase lherzolite.

Elthon and Scarfe (1984) arrived at different conclusions. They presented high pressure phase equilibria for a MgO-rich basalt (NT-23) with more than 16.5wt% MgO from the Tortuga ophiolite. They showed that at 25 kbar, olivine+orthopyroxene+clinopyroxene+garnet are the liquidus phases. They proposed that even the most primitive MORBs

with $\text{MgO} > 9.5\%$ are derivatives of primary high-MgO magmas generated by melting of mantle peridotite at 15-25 kbar.

Significant progress has been made in experimental techniques in the meantime. Subsequent melting experiments used a new experimental method; the peridotite-basalt sandwich technique. A thin basalt wafer is encapsulated in peridotite. In this way, there are less equilibration and incipient crystallisation problems than the previous techniques using Pt or graphite capsules (Thompson, 1984).

Stolper (1980) studied the phase equilibria of the primitive basaltic glass ALV-519-4-1 ($\text{MgO} = 9.6\%$ wt) from the FAMOUS area of MAR. The basalt was embedded in a matrix of olivine+orthopyroxene, similar to a residual harzburgite, and melted from 10 to 20 kbar. Liquids produced at different pressures were saturated with olivine and orthopyroxene. Stolper combined his high pressure data with those of Green et al. (1979) and established the olivine+orthopyroxene cotectic in the normative OL-CPX-OPX-PLAG tetrahedron. He superimposed the MORB compositions on the determined phase boundaries, and drew very specific conclusions. He argued that although the MORB cluster comes very close to the olivine+orthopyroxene+clinopyroxene cotectic at ≈ 10 kbar, even the most primitive MORB compositions do not lie on this cotectic and hence cannot be primary melts generated at the low pressure range, from 8 to 11 kbar.

Takahashi and Kushiro (1983) studied the melting behaviour of a Hawaiian spinel-lherzolite (HK66) at anhydrous conditions using the sandwich method. The melts produced at 8-10 kbar are olivine tholeiites very similar (almost indistinguishable) to MORBs. They supported generation of MORBs at pressures of 8-10 kbar. Melts produced at pressures between 15 and 20 kbar are alkali olivine basalts; at low pressures (≤ 5 kbar), the melts are quartz- tholeiites.

Fujii and Scarfe (1985) also used the sandwich method to test whether peridotite bulk composition (by varying the amount of constituent minerals) influences the melt composition. The experiments carried out at 10 kbar pressure. The peridotite was reconstructed from mineral separates of olivine, orthopyroxene, clinopyroxene and spinel. The olivine-tholeiite ARP-74-10-16 (Fujii and Bougault, 1983) was used as the sandwiched basalt. The equilibrated liquids (coexisting with olivine+orthopyroxene+ clinopyroxene+spinel) with different peridotite-basalt mixtures showed a range of compositions. This led Fujii and Scarfe (loc.cit.) to suggest that partial melting of mantle lherzolite is not isobarically invariant (or "pseudoinvariant"). Some of these 10 kbar liquids are compositionally similar (a few are identical) to magnesian MORBs.

9.2 Phase Diagram Considerations

The compositions of basaltic, peridotitic rocks and gabbroic rocks can be sufficiently well represented by phase diagrams which have the major constituent oxides as end member components. Crystalline and liquid paths during partial fusion and crystallisation processes have been studied for a number of simplified binary and ternary systems. Crystallisation under perfect equilibrium and perfect fractional conditions can be studied graphically on such ternary phase diagrams. There is a number of diagrams for projecting basaltic compositions for studying their phase relations and crystallisation paths. The iron -free system $\text{CaO-MgO-Al}_2\text{O}_3\text{-SiO}_2$ (CMAS) is a good basaltic analogue because the principal constituent minerals of basalts - peridotites - gabbros can be satisfactorily approximated. The system

Fo-An-Di-Q (Mg_2SiO_4 - $\text{CaAl}_2\text{Si}_2\text{O}_8$ - $\text{CaMgSi}_2\text{O}_6$ - SiO_2) shown in figure 9.1b, part of the larger CMAS system, is a simplified analogue for polycomponent basaltic - peridotitic compositions and is employed here for studying the crystallisation paths of Macquarie Island basalts and testing the various scenarios regarding their genesis.

Yoder and Tilley (1962) classified basalts by using this simplified system in an extended version (the five component system Na_2O - CaO - MgO - Al_2O_3 - SiO_2) and the CIPW normative basalt mineralogy (figure 9.1a). In this diagram, forsterite becomes olivine, anorthite becomes plagioclase and diopside becomes clinopyroxene. The normative basalt tetrahedron shows three volumes; the alkali-basalt volume (nepheline-bearing rocks), the olivine-tholeiite and tholeiite volumes for olivine-normative to quartz-normative basalts. In the following projections, the normative minerals are combined. The phase relations in the normative basalt tetrahedron are considered by analogy to the simplified synthetic CMAS system in section 9.2.1.

Walker et al. (1979) used the pseudoliquidus diagram OL-PLAG-DI-SI (olivine -plagioclase -diopside -silica) for studying the phase equilibria, the crystallisation paths and the genesis of basaltic magmas. They preferred a projection method which utilizes the combined molecular proportions of the major constituent oxides. Phase relations in this system and implications from the Macquarie Island data are discussed in section 9.2.2.

9.2.1. The CaO-MgO-Al₂O₃-SiO₂ (CMAS) System

The liquidus phase relations in the CaO-MgO-Al₂O₃-SiO₂ system (CMAS) are shown in figure 9.1b. The ternary Fo-An-Di (figure 9.1c)

contains the three principal phases (olivine-clinopyroxene-plagioclase) of basaltic and peridotitic rocks. This plane Fo-An-Di corresponds to the *OI-Di-Plag* plane of the normative basalt tetrahedron. The *OI-Di-Plag* plane is the plane of silica undersaturation and has been considered as a "thermal divide" (liquids on either side of this plane cannot fractionate on the other side) between tholeiitic and alkalic basalts at low pressures, for experiments carried at 1 atm. By analogy, the Fo-An-Di plane can be considered as a low pressure thermal divide between tholeiitic and alkalic basalts in the simplified CMAS system. The ternary Fo-An-SiO₂ is also very important in considering phase equilibria in basaltic melts because it contains as end member component SiO₂, hence the silica saturation of liquids can be modelled, and also because it illustrates the olivine reaction relation with the liquid. Liquidus phase boundaries in this ternary are shown in figure 9.1c. The low temperature point E is a ternary eutectic. The line An-En can be considered as the trace of the plane of silica saturation. The Fo-Ab-Q or its expanded version *OI-Plag-Q* plane of the basalt tetrahedron is equivalent to the simplified Fo-An-SiO₂ system.

Macquarie Island data from the layered rocks, the massive gabbros, the dolerite dykes, the basalts and the few analysed glasses are plotted in the Fo-An-Di ternary in figure 9.2 and the Fo-An-SiO₂ ternary in figure 9.3, by combining the end member components for each phase; hence, Fo represents olivine (*Fo+Fa*), An represents plagioclase (*An+Ab*) and Di is clinopyroxene (*Wo+En+Fs*).

The layered troctolites form an array almost paralleling the Fo-An sideline in the Fo-An-Di join (figure 9.2), and the olivine-gabbros show a broad cluster reflecting their modal olivine. The laminated gabbros from the uppermost parts of the layered sequence show an array towards piercing point E; their trend intersects the An-

Fo sideline to a point which has 0.85 parts of An. The massive gabbros plotted in figure 9.2G are mainly from the Upper Level Gabbro unit; selected samples from other exposures are also plotted. The alkali gabbro 726 is also shown on this projection. The trend defined by the massive gabbros is away from the An-Fo sideline and towards the piercing point E of this ternary. A troctolitic-gabbro intrusion (sample 380) into the layered olivine-gabbros at Handspike Pt., projects in the olivine liquidus volume (figure 9.2F).

The majority of dolerite dykes plot in the anorthite liquidus volume, An+L (figure 9.2B). Both, glasses and basalts project in the An+L volume. The glasses (figure 9.2A) show a trend towards the An-Di sideline. The tholeiitic basalts, mainly samples from the southern part of the island, cluster in the An+L volume and close to the spinel primary phase field and show a trend towards the An-Fo boundary (figure 9.2B). The alkalic basalts, mainly from the Green Gorge area and the central part of the island, cluster around the low pressure An-Sp univariant curve (figure 9.2D). The aphyric alkalic basalts define a cotectic parallel to the An-Sp cotectic. Examination of the liquid and solid paths during equilibrium and fractional crystallisation always provides invaluable information (assuming that the piercing point E as a true eutectic and ignoring the Sp+L field).

During equilibrium crystallisation of a liquid in the Fo+L volume, the liquid path is away from the Fo apex. The rock type formed is a dunite. With further decrease in temperature, the liquid arrives at the An-Fo cotectic boundary and anorthite starts crystallising. The solid/liquid proportion is given by the tangent to the An-Fo boundary. The rock now consists of forsterite and anorthite. As the liquid moves towards the isobarically invariant point of the system (Fo+An+Di+L), the rock composition becomes progressively more An-rich. When the

liquid reaches the system's eutectic, then diopside commences crystallising. Olivine-gabbro is thus produced. The rock path is continuous and the rock types produced become progressively richer in An.

The liquid path during fractional crystallisation is similar with that in the equilibrium crystallisation case. The rock paths are however different. When the liquid moves from its initial composition towards the An-Fo cotectic boundary, a dunite is formed. On reaching the An-Fo boundary, the liquid follows the down temperature path towards the invariant point. The solid extract now consists of anorthite and forsterite; the proportions of these phases are given by a point on the An-Fo sideline, a point which is the intersection of the tangent to the An-Fo boundary and the An-Fo sideline. The rock type is a plagioclase-rich allivalite. There is therefore a jump in the rock composition (or a "rock hop" following Morse, 1980). When the liquid arrives at the piercing point E, diopside starts crystallising and the rock that is now produced is an olivine-gabbro. When the liquid moves along the An-Fo boundary towards point E, the solid extract composition remains fixed at constant proportions of anorthite and forsterite. When diopside commences crystallising, there is another rock jump from an anorthite+forsterite solid extract to an anorthite+forsterite+ diopside solid extract, an olivine-gabbro. The rock path is thus discontinuous. The intermediate allivalite is very similar to the Macquarie Island layered troctolite, and unlike the intermediate solid extracts produced during equilibrium crystallisation. Although there are olivine-rich troctolites at the base of the layered sequence (five such samples are shown in figure 9.2E and 9.3) the overall troctolite section is high in modal plagioclase. Therefore, fractional

crystallisation of a basaltic melt better approximates the formation of the layered rocks compared to equilibrium crystallisation.

The layered troctolites and olivine-gabbros plot as an array from Fo-rich side to An-rich compositions in the Fo-An-SiO₂ ternary as well (figure 9.3). Sample 380 plots again in the olivine primary phase field. The massive Upper Level gabbros plot in the An phase volume. The dolerites and basalts plot mainly in the An+L volume, but also extending to the spinel field, Sp+L. The dolerites as a group are more silica saturated than the basalts. They come close to the plane of silica saturation, line An-En, but they do not cross it. Assuming that addition of other components to the system, such as Na₂O, would displace the equilibria towards more undersaturated compositions, some of the dolerites would lie on the right hand side of the An-En plane, achieving so silica saturation.

Because the natural olivine, plagioclase, and diopside are solid solutions and their compositions lie off the Fo-An-Di plane, the isobarically invariant point is not a true eutectic and the system Fo-An-Di is not a true ternary. Consequently, phase relations are better illustrated and understood by resorting to the quaternary Fo-An-Di-SiO₂ system. In the Fo-An-Di-SiO₂ quaternary, the temperature maximum (t) on the univariant cotectic a-p was determined to be located on the SiO₂-rich side of the An-Fo-Di plane at 1 atm pressure (Presnall et al., 1978), and the invariant point a lies on the SiO₂-poor side of this plane. Therefore, the thermal divide (located at the temperature maximum t when Fo, An and Di cocrystallise) is located slightly on the SiO₂-rich side of the An-Fo-Di plane and is graphically depicted as Di_{ss}-Fo-An in figure 9.4. Fractional crystallisation of a melt in the tholeiitic volume would produce a more silica rich residual liquid; alternatively, a melt in the silica poor side would fractionate to

a more silica undersaturated liquid. Therefore, the tholeiitic basalts and the majority of the dolerites (Hy-normative) cannot be related to the alkalic basalts (Ne-normative) by low pressure fractionation of the cumulus minerals. The dolerites are as a group more differentiated than the tholeiitic basalts; they could thus be derived by low pressure fractionation from the more magnesian tholeiitic basalts.

The phase relations in the Fo-An-Di-SiO₂ system change considerably with rising pressure. In the An-Fo-Di join, Presnall et al. (1978) showed that the primary phase fields of An and Fo contract and the Di primary volume (Di+L field) expands with increasing pressure, till the An+L field disappears between 15 and 20 kbar. In the An-Fo-SiO₂ join, a similar change in the primary phase fields of An and Fo has been observed with increasing pressure (Sen and Presnall, 1984). The enstatite (En+L) and SiO₂ primary volumes expand at the expense of the An and Fo fields, till the An+L field disappears at 10 kbar. Hence, melts formed at increasingly higher pressures become progressively poorer in SiO₂. Fractional crystallisation of such liquids at high pressures produce less silica saturated residual liquids.

In the Fo-An-Di-SiO₂ quaternary, increasing pressure causes the thermal maximum (t) to move towards the silica poor side of the An-Fo-Di plane and the invariant point a to move towards the SiO₂ rich side of this plane. Presnall et al. (1978) estimated that these points meet at around 4-5 kbar and hencefore the thermal divide disappears at this pressure interval. Fractional crystallisation at pressures between 4 and 12 kbar produces tholeiitic from alkalic basalts. The minimum pressure range for the generation of alkalic basalts was placed by Presnall et al. (1978) between 10 and 13.5 kbar, or approximately at 12 kbar. At this pressure range, the primary En field penetrates the An-Fo-Di plane or the field of alkalic basalts. Primary alkalic basalts can be

partial melts of a four phase (Ol+Opx+Cpx+Sp) peridotite at pressures of more than 12-13.5 kbar. The Macquarie Island alkalic basalts could be partial melts of such peridotites at this high pressure range.

Fractional crystallisation of such alkalic liquids at high pressures, less than 12-13.5 kbar, would produce tholeiitic basalts as residual liquids. The alkalic basalts are hence favoured of being primary at high pressures and could be parental to the tholeiitic basalts via high pressure fractionation.

The order of appearance of the cumulus minerals in troctolites, chromite+olivine-> plagioclase-> clinopyroxene, and the absence of a thick succession of dunite cumulates suggest that the parental magma composition was very close to the divariant surface *abcdp* in the Fo-An-Di-SiO₂ system (figure 9.4) and in the olivine primary phase volume. The presence of cumulus chromite in troctolites and also chromite phenocrysts and magnesian "xenocrysts" in lavas preceding or cocrystallising with olivine, does not imply that the parental melts had to lie in the spinel liquidus volume (Sp+L) or the Sp-Fo cotectic surface. The reason is that the Macquarie Island chromites are Cr₂O₃-rich solid solutions with significant FeO content and not the MgAl₂O₄ spinels of the simplified CMAS system. The succession of troctolites is followed by clinopyroxene-bearing troctolites. The appearance of clinopyroxene comes shortly after the crystallisation of plagioclase. The segregation of cpx-troctolites persists for a longer period of time than that of troctolites. Typical olivine-gabbros appear later in the cumulate succession. The crystallisation sequence of the minerals and the relative thickness of the various units indicate that parent melt remained on the divariant surface *abcdp* while segregating troctolites and shortly afterwards moved to the Fo-An-Di cotectic a-p where olivine, plagioclase and clinopyroxene co-crystallised.

Turning to natural basaltic compositions now, the position of the cotectic a-p will be a function of the Na_2O and FeO content of the melt. Addition of Na_2O to the system will move the equilibria to more silica undersaturated compositions (Hoover and Presnall, 1982). Because natural diopsides and augites are solid solutions, the Macquarie Island Ca-rich pyroxenes have high enough Al_2O_3 (>2%wt) and hypersthene component (figure 4.9), the coprecipitation of olivine + plagioclase + clinopyroxene (assuming that olivine is free of CaO and plagioclase is free of MgO which is the case for Macquarie Island cumulus olivines and plagioclases) will occur along the Ol-Plag-Cpx cotectic curve paralleling the a-p cotectic (Biggar, 1983), and the modal composition of the olivine-gabbros will be defined by the intersection of this cotectic with the Di_{SS} -Plag-Ol plane (figure 9.4). Olivine disappears in the laminated gabbros of the layered sequence, suggesting a reaction relation with the liquid. Low-Ca pyroxene is absent however, suggesting that the residual liquids did not arrive at the invariant point p of the system; the residual liquids were thus still silica undersaturated.

In figure 9.5, the fields of Macquarie Island basalts, dolerites and glasses are shown in the Plag-Ol-Cpx ternary. The inferred olivine-plagioclase cotectic of Shido et al. (1971) for abyssal tholeiites, and the cotectic defined by FAMOUS glasses (Bryan, 1979) are also shown in figure 9.5. The Macquarie Island glass field is on the plagioclase side of these two olivine-plagioclase cotectics. The trend of the aphyric alkalic basalts mimics the An-Sp cotectic in the simplified system Fo-An-Di; it is not analogous to the trend shown by the Macquarie Island glasses. The trend of the tholeiitic basalts is away from plagioclase - olivine and towards pyroxene, approaching the olivine-plagioclase cotectic of Shido et al. (1971). The field of dolerites overlaps that of

tholeiitic basalts. A few selected samples are also plotted in figure 9.5. The magnesian Hy-normative basalt 38284 (Mg#=70, Hy-normative ≈ 5 , Zr=121ppm) and the differentiated basalt 108C (Mg#=61, Hy-normative ≈ 5 , Zr=78ppm) plotted in figure 9.5 show a subparallel trend to the olivine-plagioclase cotectic of Shido et al. (1971), but on the plagioclase side. The primitive dolerite dyke 220 (mg#=71, Hy-normative ≈ 0.34 , Zr=46ppm) and the differentiated dyke 153 (mg#=60, Hy-normative ≈ 9 , Zr=135 ppm) also define a trend on the plagioclase side of the previous two ol-plag cotectics and the Macquarie glass field. The displacement of the fields of both dolerites and tholeiitic basalts to the plagioclase side of inferred glass cotectics suggests that their compositions must be controlled by plagioclase accumulation. This may be true for the plagioclase-phyric basalts and dolerites; both are largely plagioclase phyric. Aphyric basalts and dolerites (Hy-normative) however are also displaced on the plagioclase side of the glass field and there is no evidence for olivine control in the compositions of either primitive or evolved basalts, dolerites and glasses. The magnesian - evolved pairs shown in figure 9.5, suggest that other processes must have been operating together with low pressure fractionation. The trend shown by the aphyric alkalic basalts is almost at right angles to the Macquarie glass trend and also the inferred olivine-plagioclase cotectics from abyssal glasses from the Mid-Atlantic Ridge. Such a trend cannot represent a low temperature fractionation trend of olivine+ plagioclase+ Ca-rich pyroxene.

9.2.2. The pseudoliquidus OL-PLAG-DI-SI system

Walker et al. (1979) used the plagioclase - olivine - diopside - silica tetrahedron for plotting basalt compositions. Their projection technique does not utilise CIPW normative minerals. Instead, the percentages of the four end members are calculated by combining the molecular proportions of the major oxides.

Selected data from the Macquarie Island basalts and dolerites are plotted in the OL-DI-SI and OL-PL-SI projections in figures 9.6 and 9.7 respectively. The tholeiitic basalts and dolerites show a trend from tholeiitic to mildly silica undersaturated compositions. The alkalic basalts and the glasses extend from olivine-normative towards nepheline-normative compositions. The primitive basalts 38284 (mg#=70, ≈15% normative olivine) and 234 (mg#=72, ≈12% normative olivine) project on the 15Kbar *ol-di* cotectic. The primitive dolerite 38334 (mg#=69, ≈11% normative olivine) projects on the 15 kbar *opx-di* cotectic. Also plotted in figures 9.6 and 9.7 are the primitive abyssal glasses of Bender et al. (1978), Green et al. (1979) and Stolper (1980). They come close to the 10 kbar cotectic. The composition 3-18-7-1 + 17% olivine Fo₉₀ of Green et al. (1979) plots about the 16 kbar *ol-opx* cotectic (composition G in figure 9.6 and 9.7).

The *ol-opx* cotectic moves from Q-normative to olivine-tholeiitic compositions in the pressure range 1 atm - 10 kbar. Between 10 and 15 kbar, the *ol-opx* cotectic moves towards silica undersaturated compositions and between 15 and 20 kbar, towards alkalic (Ne-normative) compositions. In the pressure range 10-15 kbar, tholeiitic liquids will fractionate (eventually) to silica undersaturated liquids (towards the left hand side of the OL-DI-PL plane) along the *ol-cpx* cotectic (Stolper, 1980). At pressures of more than 15 kbar, liquids multiply saturated with *ol+opx+di* become progressively silica-undersaturated, and at 20 kbar the cotectic *ol+opx+di* crosses the

plane of silica saturation (OL-PL-DI); the petrogenetic implication is that olivine-tholeiites fractionate to alkali-basalts and liquids formed at around 20 kbar are Ne-normative.

The multiply saturated point $ol+opx+cpx+liq$ moves towards the OL-PL-DI plane with increasing pressure. At some pressure more than 15 kbar, this point crosses the OL-PL-DI plane; at this pressure range, liquids fractionate from olivine-tholeiitic to alkalic compositions. The exact location of the 10 kbar $ol+opx+cpx$ cotectic is crucial and hotly debated. If the most primitive MORBs ($MgO > 9.5\%wt$) lie on this cotectic, then can be primary melts generated at around 10 kbar pressure; such an interpretation is favoured by Fujii and Bougault (1983). If they do not approach this cotectic but only come close as suggested by Stolper (1980), then they are not primary melts generated at the low pressure range but derivative melts produced from primary picritic melts (formed at high pressures $\approx 20kbar$) by extensive olivine fractionation; this model is supported by Green and his colleagues.

An olivine-rich normative basalt such as composition G (27% normative olivine) can produce the dolerite 38334 by polybaric olivine fractionation; the liquid path will be away from the OL apex and will cross the $ol-opx$ cotectics at different pressures. It can also be produced by a more olivine-rich melt by greater amounts of olivine fractionation. Another way of deriving the dolerite 38334 is from a less magnesian liquid saturated with $ol+opx$ at pressures between 12 and 15 kbar and fractionating only a minimal amount of olivine. The most magnesian *Hy*-normative Macquarie Island basalts and dolerites plot close to the primitive abyssal glass compositions b, g and s. These samples can be produced by olivine-rich normative liquids saturated with $ol+opx$ at pressures of more than 10 kbar, such as composition G, by olivine fractionation. All these models or derivation scenarios

involve only olivine extraction from parental olivine-rich normative liquids, segregating from source peridotite at high pressures (15-20 kbar) and leaving behind a residue of ol+opx, a residual harzburgite; such a petrogenetic scenario is in agreement with the model of Green et al. (1979).

Other models can also be considered and are permissible by phase relations. Basalts plotting between the 10 and 15 kbar *ol-opx* cotectics could be derived from liquids saturated with ol+opx+di and segregating from their source at pressures of less than 15 kbar. Such liquids would fractionate opx+cpx, that is fractionate along the *opx-cpx* cotectic; in this case, they would produce liquid compositions similar to basalts 38284 and 234, and leave behind a lherzolite residue. Basalt 38284 could have been derived from a parent melt such as composition G, via ol+opx crystallisation at 15 kbar and then opx+cpx crystallisation at 15 kbar (liquid following the respective cotectics); in this case, the residue would be made of olivine+orthopyroxene. Such models however require high pressure clinopyroxene fractionation. The perils of high pressure cpx fractionation are discussed in a following section of this chapter.

Returning to the 10 kbar multiply saturated liquids, they plot as points, variably described as cotectics or "pseudoinvariant" points. It is apparent that the origin of the most primitive MORB compositions relate to the nature of these cotectic or "pseudoinvariant" points, and furthermore on the melting process. Presnall et al. (1979) considered that the partial melting of a simplified peridotite (Fo+En+Di+Sp±An) at the 9 kbar cusp is isobarically invariant. Fujii and Scarfe (1985) showed that this is certainly not the case during partial melting of natural peridotite compositions. Melts produced by direct melting of peridotite at 10 kbar

do not project as points in the OL-DI-SI and OL-PL-SI diagrams, but occupy areas. Presnall and Hoover (1984) on the other hand attributed the variations in the normative mineralogy and silica saturation of magnesian MORBs to analytical uncertainties and "real variations in the possible compositions of primary magmas produced from mantle peridotite at a given pressure". The Fe^{2+} and Fe^{3+} content of the Macquarie Island basalts and dolerites have been calculated from the total iron content assuming that $\text{Fe}_2\text{O}_3 = 15\%$ of total iron. If the $\text{Fe}^{2+}/\text{Fe}^{3+}$ ratios are even higher than the estimated ones as is suggested by the recent work of Christie et al. (1986), then most of the Macquarie Island *Hy*-normative basalts and dolerites would change to more olivine-rich normative compositions. For instance, basaltic glass 47979 has 7% *Hy* and 10% *OI* in its norm. Assuming all iron as Fe^{2+} , then the recalculated norm mineralogy would consist of 3% *Hy* and 17% *OI*. Similarly, basalt 38284 has 5.5% normative hypersthene and 15% normative olivine; assuming all iron in the ferrous state, normative olivine increases to 22% and normative hypersthene reduces to 1%. The normative mineralogy could thus be a source of error. An interesting discussion on this topic was presented by Thompson (1987).

In summary, following the findings of Fujii and Scarfe (1985) which indicate that the cotectics at any given pressure are not points but isobaric curves, it is possible that some of the most magnesian MORB compositions ($\text{MgO} \geq 9.5\%$ wt) could be direct partial melts from mantle peridotite at around 10 kbar. Some of the most magnesian basalts and dolerites from Macquarie Island such as 234, 47979, 38288, 38284, 38334 could have been derived from primary melts originating at around 10 kbar through small degrees of olivine fractionation. However, there is always the possibility of deriving these basalts by extensive olivine fractionation from primary picritic

melts. The basalts and dolerites that lie close to the 1 atm cotectic represent liquids that have been derived by low pressure fractionation of olivine + plagioclase + clinopyroxene.

The Macquarie Island harzburgites and the most magnesian glasses and (close to aphyric) basalts and dolerites are plotted in the OL-DI-SI projection together with data from primitive abyssal glasses and experimentally studied peridotite compositions in figure 9.8. The basalts show variable degrees of silica saturation for similar Mg# values. Examination of the following table shows that the most magnesian aphyric basalts-dolerites range from *Hy-* to *Ne-*normative,

<u>Sample</u>	<u>MgO</u>	<u>Hy</u>	<u>Ne</u>
38334	9.5%	11.7%	-
47979	9.3%	7%	-
234	9.45%	6%	-
38284	9.4%	5.5%	-
38306	9.5%	1.5%	-
38288	≈9%	-	0.3%
38188	11.2%	-	0.4%

It is also shown in figure 9.8 that most of the experimentally produced 10 kbar melts of Fijii and Scarfe (1985) form an array. The spinel-lherzolite HK66 and the 10.5 kbar melts produced by direct melting of HK66 (Takahashi and Kushiro, 1983) are also plotted in figure 9.8.

Phase relations in this ternary (OL-DI-SI) suggest that if pyrolite is the source and melting takes place at 20 kbar (and assuming a multiply saturated liquid lying at the 20 kbar *ol+opx+cpx* pseudoinvariant point), then the residual peridotites will be very similar to the Macquarie harzburgites. If melting of the same source occurs at 15 kbar, then the residue will be more olivine- rich. Finally,

if melting takes place at lower pressures and approximately at 10 kbar, the residue will be even more dunitic. Assuming now a source similar to the HK66 spinel-peridotite (Takahashi and Kushiro, 1983), the residues produced at 10, 15 and 20 kbar will be more silica rich than those produced from pyrolite at the respective pressure interval.

The model of Green et al. (1979) dictates generation of picritic melts at ≤ 20 kbar and subsequent fractionation of large amounts of olivine to arrive even in the most primitive MORB compositions. Following the phase relations in the OL-DI-SI projection (figure 9.8), melts formed at ≈ 20 kbar cannot produce the entire array of the most primitive Macquarie Island basalts via extensive olivine fractionation. They can however leave behind a residue similar to the Macquarie Island harzburgites. Melts produced at high pressures 15-20 kbar from small percentages of melting of a pyrolite source will be *Ne*-normative. In such a case however, the residues will be lherzolites and not harzburgites. Melts produced at less than 15 kbar will be *OI*-normative and will fractionate to more silica saturated liquids. The Macquarie basalts-dolerites show a continuous range from *Ne*- to *Hy*- normative compositions. At high pressures 15-20 kbar, isobaric ol+cpx fractionation is required to produce some of the most primitive undersaturated basalt compositions (figure 9.8). The complete lack of any evidence for ol+cpx high pressure fractionates in both Macquarie Island and oceanic samples are not in favour of such a high pressure fractionation scenario.

The 10.5 kbar melts produced from the HK66 sp-lherzolite (Takahashi and Kushiro, 1983) would produce more silica-rich compositions upon olivine fractionation. These liquids will be more silica-rich than the primitive *Hy*-normative Macquarie Island

compositions (trend d-e-f in figure 9.8). The residues so produced will also be more silica-rich than the Macquarie Island harzburgites.

Small amounts of melting of a pyrolite source at pressures between 15 and 20 kbar will produce liquids in equilibrium with cpx-poor lherzolite which will eventually become a harzburgite on further melting and will be like the Macquarie harzburgites. If melting was at low pressures, <12 kbar, and the source still a pyrolite then the residues would be more olivine-rich than any of the Macquarie harzburgites (figure 9.8). If however under these lower pressure conditions, the source were the spinel-lherzolite HK66 (Takahashi and Kushiro, 1983) then again the residues would be like the Macquarie harzburgites.

Based on these arguments, it is difficult to determine the precise pressure range within which the Macquarie Island harzburgites were formed. The trend of the Macquarie Island basalts and dolerites clearly does not reflect fractionation because the array does not represent any consistent trend of Mg# values. As a consequence the basalt trend is interpreted as the result of polybaric melt evolution.

Finally, certain differences in liquids and liquid paths between the CMAS and the OL-DI-PLAG-SI systems are worth noting. In the OL-DI-SI projection, inferences from natural basaltic compositions indicate that tholeiitic liquids fractionate to alkalic liquids via olivine+ clinopyroxene crystallisation at 10-15 kbar pressure (Stolper, 1980). In the CMAS system, alkalic liquids fractionate to tholeiitic in the same pressure range (Presnall et al., 1979). If such a discrepancy reflects on the higher Ol/Di ratios of the natural basaltic compositions relative to the simplified ones, or the spinel crystallisation (suggested by Presnall but not favoured by the Macquarie Island data presented

here) is still uncertain. Analytical uncertainties could also play an important role.

9.3 Partial melting modelling

Major elements constitute more than 99% of MORBs and their source composition. The behaviour of major elements during partial melting of oceanic upper mantle peridotite is therefore invaluable for constraining the chemistries of the source peridotite and the generated partial melts. Phase diagrams have been employed by Presnall (1969) to model the partial melting processes on simplified systems. Hanson and Langmuir (1978) used mineral-melt distribution coefficients, mass balance considerations and the olivine stoichiometry to constrain the FeO and MgO distribution during partial melting of a model upper mantle peridotite composition. This section examines the variation of FeO and MgO during partial melting of a source peridotite model composition and its bearing on the compositions of partial melts and residues. The distribution of transition metal abundances in basalts and harzburgites; model source calculations for producing these abundances. The source composition is then evaluated on the basis of the Macquarie Island residual harzburgite and most MgO-rich basalt compositions.

9.3.1 FeO-MgO modelling

The modelling of partial melting using the approach of Hanson and Langmuir (1978) permits the construction of fields for partial melts and residues from a model mantle peridotite composition. Figure

9.9 has been constructed after the method of Hanson and Langmuir (loc.cit.) for a source peridotite of model pyrolite composition. The FeO and MgO contents of model pyrolite are from Ringwood (1975). Partial melting curves have been constructed for batch melting and drawn for minimum (0% melting) and maximum (assuming that olivine is the only phase in the residue) melting percentage. Olivine fractionation curves are superimposed. The residue field is contoured for percent of melting and temperature.

The FeO and MgO contents of Macquarie Island aphyric lavas, glasses and harzburgites are plotted in figure 9.9. Most of the lavas and glasses plot below the 0% melting curve at temperatures of around 1200°C; they therefore cannot represent unfractionated melts formed by melting of a pyrolite source. Two samples plot on the 10% melting curve; these are basalt 38188 and glass 47979. Glass 47979 plots at a lower temperature than basalt 38188. These two samples can represent melts generated by partial fusion of pyrolite. The most MgO-rich basalts suggest that their parental melts fractionated around 10% olivine. The Macquarie Island harzburgites plot between the 10% and 20% melting curves and the 1000°-1200°C temperature curves. Most samples indicate that they are the residues of 15-20% melting at around 1200°C.

The melt field is fixed for a given parent composition and constant distribution coefficients at a particular pressure. The distribution coefficients however increase with increasing pressure. As a result, the melt field changes with increasing pressure. The value of the Fe-Mg exchange distribution coefficient applicable to the conditions of formation of Macquarie Island rocks should be in the range of 0.27-0.3. For this range, the change in the melt field is minor (Hanson and Langmuir, 1978). The liquidus and solidus temperatures of

the parent pyrolite increase with increasing pressure. Because the composition of pyrolite is fixed on the FeO-MgO diagram and the melt field upper bound isothermal line must pass through the pyrolite composition, increasing pressure will raise the isothermal lines within the melt field, but will not change the melt field (Langmuir and Hanson, 1980). The 1 atm melt field in figure 9.9 can thus be used for high pressures as well. The parent composition also influences the melt field; increasing MgO results in narrowing the melt field, and increasing FeO shifts the melt field towards higher FeO/MgO ratios (Langmuir and Hanson, 1980).

If the source was less fertile than the pyrolite, say a depleted spinel-lherzolite with higher MgO-content than pyrolite, then the two basalts plotting on the 10% melting curve in figure 9.9, would plot at a melting curve of less than 10% partial melting. Basalt 38188 could represent a higher pressure melt than glass 47979. The subparallel to the FeO axis trend of the less magnesian basalts could suggest derivation from a more FeO-rich source than the last two basalts. The harzburgites do not show any trend towards FeO rich compositions, thus denying this possibility. The more MgO-rich basalts would be derived by a parental melt similar to basalt 38188 through olivine fractionation.

9.3.2 Transition Metals

The transition metal (TM) Sc, V, Ti, Mn, Ni, Co and Cr abundances are high in both basalts and harzburgites, and accurately measurable by XRF techniques. The concentrations of TM in basalts and harzburgites can thus be employed for constraining the source

concentrations of these elements. The TM concentrations in basalts are not however process independent, that is differentiation processes - primarily crystal fractionation- do influence their abundances in the residual liquids. This problem is minimized if data on the most primitive (MgO-rich) basalts are utilised. It was inferred in a previous section that the most primitive Macquarie Island basalts have fractionated only olivine+spinel; therefore, their Ni and Cr contents might have been modified. Sc and V abundances are controlled by the amount of clinopyroxene in the residue and the percent of clinopyroxene crystallisation. The concentrations of Sc and V in the basal troctolites are very low, ≈ 10 ppm and < 40 ppm respectively (figure 6.6). Because the least fractionated basalts could only be controlled by the olivine-rich troctolite cumulates, it is inferred that Sc and V abundances in basalts are unlikely to have been modified by olivine (+minor spinel) and plagioclase accumulation. Ti behaves as an incompatible element, and the Mn content of basaltic melts is controlled by olivine fractionation.

The transition metal abundances of Macquarie Island harzburgites and most magnesian basalts are normalised to C1 carbonaceous chondrites (normalising values from Anderson, 1983) and plotted in figure 9.10A. The harzburgite pattern shows a marked Ti depletion; sample 163 shows only a minor Ti anomaly. The basalt pattern shows a positive Ti anomaly and a negative Cr anomaly; such a pattern is similar to that of the least fractionated basalts from the Mid-Atlantic Ridge (Langmuir et al., 1977). Sun et al. (1979) and Langmuir et al. (1977) commented on the uniform TM contents of the most primitive basalts from mid-oceanic ridges and ocean islands, and the relatively constant mantle abundances.

The transition metal abundances in liquid and residue during partial melting of a mantle peridotite were modelled using the batch melting equation (Shaw, 1970), $\frac{C^{liq}}{C_o} = \frac{1}{D_o + F * (1-P)}$, where C^{liq} is the concentration of an element in the liquid, C_o the concentration of this element in the initial solid, F is the fraction of the liquid produced, and D_o is the bulk distribution coefficient. $D_o = \sum x^a K^{a/liq}$, where $K^{a/liq}$ is the crystal-liquid distribution coefficient for the element of interest between mineral a and liquid, and x^a is the initial weight fraction of mineral a . $P = \sum p^a * K^{a/liq}$, where p^a is the fraction of liquid contributed by mineral a . The values for the distribution coefficients utilised in the modelling and the source TM abundances are from Sun et al. (1979). In addition, the mass balance equation $C_{res} = \frac{C_o - C^{liq} * F}{1 - F}$ where C_{res} , C_o and C^{liq} are the concentrations of a given element in residue, source and liquid respectively was also employed in the calculations assuming a residue consisting of 69% olivine, 25% opx, 5-2% cpx and 1% spinel, a mode similar to that of Macquarie Island harzburgites. The observed patterns (figure 9.10A) are reproduced by 20% melting of a lherzolite source consisting of 70% olivine, 12% opx, 16% cpx and 2% spinel; the calculated values in source, liquid and residue are normalised to C1 chondrites and plotted in figure 9.10B. The less refractory harzburgite 163 can be produced by 15% melting of a similar source lherzolite with 18% modal cpx. There is very good agreement between the calculated and observed patterns. Partial melting of a peridotite with transition metal abundances very similar to those of spinel-lherzolite xenoliths in basalts (Frey and Prinz, 1978; Maaloe and Aoki, 1977) can generate the observed basalt and harzburgite concentrations.

The negative Cr anomaly of basalts is either caused by the presence of residual spinel or by the early spinel separation from basaltic melts. Variations in the source mantle Cr-contents could also influence the Cr contents of basalts. The value of 2600 ppm in the source peridotite was selected, because it is intermediate to the values given by Jagoutz et al. (1979) and Anderson (1983), 3150 ppm and 1970 ppm respectively. By varying the source Cr content between these limiting values, the estimated liquid Cr-content shows only minor changes; its normalised value changes by a factor of two. It is therefore likely that the negative Cr anomaly of basalts is related to two superimposed effects, the amount of spinel in the residue and the early chromite crystallisation from a basaltic magma.

The negative Ti anomaly of harzburgites simply indicates that Ti was incorporated into the liquid. The Ti and V abundances of basalts are however more variable. The distribution coefficients for these elements in mantle minerals are not well constrained and are also dependent on fO_2 (Shervais, 1982). Langmuir et al. (1977) suggested that the observed Ti and V variation in basalts can be explained by melting of a mantle which is heterogeneous in Ti and V abundances. This is supported by the different Ti/V ratios of tholeiitic basalts, alkali basalts and spinifex textured peridotites (Nesbitt and Sun, 1980). Basaltic melts produced by melting of a homogeneous source and fractionating olivine under low fO_2 (QFM and lower) would be displaced along constant Ti/V trends. The trends shown by the Macquarie Island basalts in figures 7.8 and 7.9, suggest that the tholeiitic basalts, plotting along constant Ti/V trend lines, had a source with uniform Ti and V abundances. The alkalic basalts, crossing constant Ti/V lines, derived from sources with varying Ti/V ratios; their source regions were not homogeneous in respect to the Ti and V abundances.

Model calculations based on the concentrations of TM in basalts and harzburgites suggest an initial source peridotite containing about 70% olivine, 12% opx, 16-18% cpx and 1-2% spinel. Moderate degrees of partial melting (15-20%) of such a source peridotite are also inferred. This initial peridotite had relatively uniform concentrations of transition metals except for Ti and V. The source regions of tholeiitic and alkalic basalts had different abundances of Ti and V; tholeiitic basalts are derived from a homogeneous source, and alkalic basalts from a source with Ti and V heterogeneities.

9.3.3 Source composition

Experimental studies on basaltic systems show that an original "fertile" upper mantle lherzolite produces basaltic magma on partial fusion, and leaves behind a residue consisting mainly of olivine, orthopyroxene and clinopyroxene (\pm spinel or plagioclase). The Macquarie Island harzburgites consist of olivine and orthopyroxene (opx), with minor interstitial clinopyroxene (cpx) and spinel. Studies on the modal mineralogy and mineral chemistry of abyssal tectonised peridotites suggest that they are predominantly harzburgites and lherzolites, and that their opxs are saturated with a high-Ca cpx even in the most refractory rocks (Dick and Fisher, 1984; Michael and Bonatti, 1985). This observation led Dick and Fisher to conclude that melting in the oceanic upper mantle occurred in the four phase field olivine-opx-cpx-spinel. The mineralogy of Macquarie Island harzburgites suggests that the partial melting process ended before the entire amount of cpx was consumed. Assuming an initial cpx content of 20% in the original undepleted mantle lherzolite, then the degree of melting would be in

the range of around 15-20%. Similar percentages of melting have been inferred before from major and trace element modelling. A lherzolite with 20% modal cpx, would be compositionally very similar to the peridotites *PPM-1* and *PPM-2* (table 9.3) and peridotite-basalt mixtures SM2 and SM4 (table 9.2) of Fujii and Scarfe (1985); these reconstructed peridotites are however very "fertile", as is the spinel-lherzolite studied by Takahashi and Kushiro (1983).

By combining the compositions of the Macquarie Island basalts and harzburgites, the source composition can be evaluated. Four basalts were selected on the basis of their high mg# ratios and different degree of silica saturation. These are the MgO-rich basalts 38188, 38284 and 234 and the magnesian basaltic glass 47979. They range from mildly Ne-normative to Ol- Hy-normative (table 9.1). The composition of glass 47979 is from microprobe analysis (Griffin, 1982). Two representative harzburgites, samples 107 and 163, were also selected for the following calculations. Sample 107 has lower FeO* (total Fe), Al₂O₃, Ti and higher MgO than sample 163, and is probably more depleted. The basalts are not melts at equilibrium with the harzburgite olivines; also, they cannot crystallise the very magnesian olivine xenocrysts of basalt M14. Their MgO and Ni contents are thus modified by olivine fractionation. It was inferred in the previous chapter that all these basalts have fractionated small amounts (2-5%) of olivine. For this reason, 2-5% of olivine Fo₉₀ was added to their bulk composition. The recalculated basalt compositions (after olivine addition) are also listed in table 9.1. The resulting composition has higher MgO and Ni than the starting basalt composition; changes in Al₂O₃, CaO, Na₂O contents are too small (<0.3%) to exert any influence in the calculated source composition. The latter basalt composition is then combined with the harzburgite composition.

The source composition was calculated for different proportions of basalt-harzburgite, and results for combining 15 parts basalt and 85 parts harzburgite are listed in table 9.1.

Several peridotite compositions are listed in table 9.2. They range from very refractory (low CaO, Na₂O, Al₂O₃ and high MgO) to relatively "fertile" (low in MgO and NiO, and relatively high in CaO, Al₂O₃, Na₂O and FeO*). The estimated source composition from the combined Macquarie Island harzburgite-basalt data compares with the composition of pyrolite, although pyrolite has higher CaO and Na₂O and slightly lower MgO. The estimated source composition is less depleted than the average continental spinel-lherzolite of Maaloe and Aoki (1977) and Tinaquillo lherzolite (composition from Jaques and Green, 1980). The spinel+plagioclase lherzolite 77PAII-1 from Hawaii has higher MgO, lower FeO* and Na₂O than the estimated Macquarie Island mantle source, but comparable Al₂O₃ and CaO. Sen (1982) showed that this depleted lherzolite begins to melt at 1210°C (9 kbar pressure) and produces melts compositionally similar to primitive/primary MORBs (table 9.3). The spinel-lherzolite HK66 studied by Takahashi and Kushiro (1983) is more fertile than the 77PAII-1 lherzolite; melts produced above the solidus of HK66 kbar are olivine-tholeiites at 8-10 kbar and alkali-olivine basalts at 15-20 kbar. The 8-10 kbar melts are very similar to primitive MORBs (table 9.3). The starting compositions pyrolite minus 40% olivine and Tinaquillo lherzolite minus 40% olivine of Jaques and Green (1980) are considerably more fertile than the pyrolite, spinel-lherzolite 77PAII-1, garnet-lherzolite PHN 1611 and the source composition estimated from the Macquarie Island basalt-harzburgite data. The peridotite-basalt mixtures SM2 and SM4 of Fujii and Scarfe (1985) are made up of 15 parts of basalt and 85 parts of peridotite, and are equally fertile to those of Jaques and Green (1980).

Melts formed at 10 kbar and temperatures between 1250°-1300°C, display wide compositional variations particularly for Al_2O_3 and MgO ; these 10 kbar melts are identical to magnesian MORBs (table 9.3). It is evident from the melting experiments of Takahashi and Kushiro (loc.cit.) and Fujii and Scarfe (loc.cit.) that the different degree of mantle fertility exerts a major control on the melt composition, a point already raised by Thompson (1987).

Similar results are obtained for the source composition if the constituent mineral compositions of harzburgites (according to their respective modal proportions) are used instead of the whole rock chemistry. Representative mineral analyses (average of several microprobe analyses) of olivine, opx, cpx and spinel from the harzburgites are combined to give an average "estimated" harzburgite composition (table 9.4a). The source compositions estimated by this method are listed in table 9.4b. They have higher MgO and CaO , lower FeO , similar alumina content and comparable Na_2O , TiO_2 , MnO and NiO contents than the calculated compositions from the whole rock harzburgite concentrations. The minor differences can be justified by the very low contents of Na_2O , TiO_2 , MnO and NiO in the constituent minerals. The estimated compositions show higher MgO , and lower TiO_2 , Al_2O_3 , CaO and Na_2O than the peridotite- basalt mixtures of Fujii and Scarfe (1985), and the starting compositions pyrolite-40% olivine and Tinaquillo lherzolite-40% olivine of Jaques and Green (1980). They are more depleted than the pyrolite and spinel-lherzolite HK66. They are however comparable to lherzolite 77PAII-1 and Tinaquillo lherzolite with similar oxide contents except for Na_2O and TiO_2 .

9.4 Trace Element Petrogenesis

The abundance of trace elements in basaltic magmas is a function of (1) their abundance in the source upper mantle peridotite, (2) the extent of partial melting of this source, (3) the kind of partial melting (equilibrium or fractional) and (4) any subsequent magmatic processes such as fractional crystallisation and intermixing of magmas. Two extreme positions are currently held by petrologists. These are, (i) primitive basalts are direct mantle derived melts and (ii) all basalts, even the most primitive, are the result of fractionation and mixing at open system magma chambers located at high crustal levels. The trace element abundances of Macquarie Island basalts are examined in this section to assess possible crystal fractionation or partial melting controls.

9.4.1 Fractional Crystallisation

The effects of fractional crystallisation are tested by mineral-melt equilibria (chapter eight) and least squares mixing methods (chapter seven and section 9.5 of this chapter). It is documented that compositional differences amongst spatially associated basalts can be accounted for by olivine+plagioclase±clinopyroxene fractionation. The effect of fractional crystallisation of these phases on the concentrations of the incompatible trace elements in basalts is assessed in this section.

The immobile incompatible elements Zr and Nb have very low crystal/liquid distribution coefficients (for ferromagnesian minerals and plagioclase) and therefore their concentrations are the least affected by fractionation of such phases. Both elements show a wide

range in abundances in the Macquarie Island basalts. Some of the most magnesian basalts could relate to the evolved basalts by gabbroic fractionation (mixing calculations - tables 9.9). The bearing of gabbroic fractionation on the abundances of Zr and Nb in the residual liquids is tested for Rayleigh fractionation using the expression $C^{liq} = C^0 \cdot f^{(D-1)}$ (Shaw, 1970); C^{liq} concentration of an element in the resulting liquid, C^0 initial concentration of this element in the magma and f is the fraction of remaining melt. Selected results are listed in table 9.5. Basalt 38288 has 96ppm Zr and 37ppm Nb; a residual liquid produced from this MgO-rich basalt via $\approx 30\%$ gabbroic fractionation, gabbroic extract consisting of 64%plag + 22%ol + 14%cpx, will have similar Zr and Nb concentrations with the differentiated 38307 basalt; a similar percentage of gabbroic fractionation is indicated by major element least squares calculations. There is thus good agreement between major and incompatible element contents. Similar conclusions are drawn for basalts 38284 and 38434 from the same locality. Fractionation of gabbroic rocks from the primitive basalts 38188 and 234 results in residual liquids with Zr and Nb contents similar to some of the evolved basalts and dolerites such as basalts 108, 147, 119 and others. Thus, some of the observed incompatible element variations are attributed to closed system gabbroic fractionation.

Nevertheless, not all compositional variations can be accounted for by crystal fractionation. Some of the compositional features of the most magnesian basalts are listed in table 9.6. Basalts 234 and 38288 have similar mg# ratios, comparable Ni content, but very different Zr and Nb content; in addition, basalt 234 is *Hy*-normative and basalt 38288 is *Ne*-normative. It requires 58% gabbro fractionation to derive the high-Nb basalt 38288 from the low-Nb basalt 234. Such an amount of crystal fractionation is ruled out by the Ni content of these basalts.

Unrealistic percentages of crystal fractionation are required when attempting to relate the other basalts listed in table 9.6. The dolerite 38334 cannot be related by any crystal fractionation model to the most primitive basalts, at both high and low pressures. These differences can only be attributed to compositionally different parental magmas and therefore different source region geochemical characteristics. Two groups of basalts-dolerites can be distinguished on the basis of their Zr/Nb ratios, (i) a high Zr/Nb (3-15) group and (ii) a low Zr/Nb (2-3) group. In the low Zr/Nb group, the Zr and Nb contents of basalts are in the ranges of 50-70ppm and 1-20ppm respectively. It has also been inferred from several detailed studies of oceanic basalts that their Zr/Nb ratios, as well as other incompatible element and isotopic ratios, reflect those of the source peridotite (Erlank and Kable, 1976; Schilling et al., 1983).

9.4.2 Partial Melting

It was inferred in the previous section that not all incompatible element abundances of Macquarie Island basalts and dolerites can be attributed to low pressure crystal fractionation. The variation of Zr/Nb and other incompatible element ratios suggest that the range of the incompatible element ratios is a partial melting effect. Table 9.6 gives a summary of the range of Zr and Nb contents, and Zr/Nb and mg# ratios for some of the most magnesian Macquarie Island basalts and dolerites. The very different Zr/Nb ratios for similar mg# ratios provides strong evidence for the influence of partial melting processes.

The effects of the degree of partial melting on the concentrations of Zr and Nb have been examined for batch melting and Rayleigh melting. The batch melting equation $\frac{C_{liq}}{C_o} = \frac{1}{D_o + F*(1-D_o)}$ and the Rayleigh melting expression $\frac{C_{liq}}{C_o} = \frac{1}{D_o*(1-F)^{(1/D_o-1)}}$ (Shaw, 1970) were used in the calculations. The source region was modelled for a "depleted" composition similar to the less refractory Macquarie Island peridotite and a "less-depleted" composition similar to that inferred from the transition metal abundances, and for primordial mantle and upper mantle Zr and Nb concentrations. The degree of melting was estimated from 2% to 30%. Results for batch partial melting are plotted in figure 9.11. The batch melting results are combined with the Macquarie Island data from the volcanic rocks. Figure 9.12 shows the variation of Zr with Nb for the tholeiitic basalts; superimposed are the melting curves for the two different source mineralogies and source Zr and Nb abundances. The Macquarie Island data from the tholeiitic basalts suggest a "less depleted" mantle source with low Zr contents ≈ 11 ppm, intermediate Nb contents 0.6-2ppm, and moderate degrees of partial melting 10-30%. Data from the alkalic basalts are shown in figure 9.13. The calculated partial melting curves for a relatively "fertile" mantle source with a high Zr concentration (27ppm) are inconsistent with the trend shown by the alkalic basalts. The best approximation of the observed trend is obtained by a low Zr (11ppm) source and relatively fertile in Nb source, ≈ 2 ppm Nb (figure 9.13B). The alkalic basalts lie on the concave side of the curve suggesting that mixing of different melt fractions, from $>2\%$ to $<18\%$, could be an important process in the formation of some of the observed compositional variations.

Figure 9.14 is a plot of the Zr/Nb versus the Zr/Y ratios of the Macquarie Island basalts. The data points show a good correlation, defining a hyperbola. Such a trend suggests mixing between two end member components, a "depleted" and a relatively "enriched" component. Binary mixing was tested by the method of Langmuir et al. (1978) using as end member components the depleted basalt 210 and the less depleted basalt 38288. Basalt 38288 has a low Zr/Nb ratio, 2.6, and basalt 210 a high, 12.7 (see also table 7.1). It is shown that the calculated mixing curve is very similar to the best fit curve to the data. In the companion plot of Zr/Nb versus Y/Nb, also shown in figure 9.14, the Macquarie Island data show a good positive correlation. The calculated mixing line from the "depleted" basalt 210 and the "less depleted" basalt 38288 is identical to the best fit line. The excellent agreement between the observed data trends and the calculated binary mixing curves in both plots suggests that binary mixing between such two end member components, can account for the observed range of the Macquarie Island basalt Zr/Nb ratios. The petrogenetic implications dictate two possible processes; binary mixing between a "depleted" and an "enriched" component representing either melts derived from different source regions (a depleted and an enriched respectively), or magmas derived from the same mantle source but from different degrees of partial melting. In the latter case, the enriched component would represent small degrees of melting possibly at greater depths than those required for the generation of tholeiitic basalt magmas. Isotopic data are required to evaluate the most likely process.

9.5 Assessment of Processes Controlling the Compositions of Macquarie Island Basalts

The observed compositional spectrum of oceanic basalts can be assigned to two complementary processes: (1) partial melting of an upper mantle peridotite which yields primary basaltic magmas and (2) magmatic processes which modify the compositions of these primary magmas. The composition of a primary magma originated at the upper mantle will be a reflection of the given peridotite mineralogy and the degree of partial melting. The ratios of the incompatible elements would reflect the ratios of the mantle source. The dominant magmatic process is known to be fractional crystallisation at low pressures, ≤ 1 -2 kbar and possibly up to 5 kbar (Wilkinson, 1982). Another magmatic process recognised later, but recently attracting considerable attention, is the mixing of primitive with evolved magmas en route to the crust or at shallow located crustal magma reservoirs. These processes are discussed in some detail in this section and compared with inferences from phase equilibria.

9.5.1 Partial melting and mantle source

Experimental partial melting studies of natural peridotites provide a framework for assessing the compositional characteristics of partial melts forming at different P-T conditions. An overview of the studies of Stolper (1980) and Takahashi and Kushiro (1983) was presented in the introduction of this chapter (section 9.1). Jaques and Green (1980) showed that direct melting of a model pyrolite-40% olivine (Fo_{90}) and the Tinaquillo lherzolite-40% olivine (Fo_{90}) produces olivine-rich normative melts at moderate degrees of partial melting; olivine-tholeiites at 10-15 kbar pressure and silica saturated (tholeiites - Q-tholeiites) melts at pressures of 2-5 kbar. The

normative character of the partial melts is a function of the degree of melting and the fertility of the source. Olivine tholeiites are produced by 15-30% melting at pressures in the range from >8 kbar to 15 kbar, and alkali basalts by <15% melting at pressures in the range of >10 kbar to 15 kbar.

The FeO and MgO data of Macquarie Island basalts and harzburgites are suggestive of 15-20% melting of a peridotite source similar to model pyrolite. The concentrations of transition metals are also suggestive of 15-20% melting of a "fertile" peridotite, having $\approx 16\%$ modal diopside. The mineralogy of harzburgites, in particular the Al_2O_3 content of pyroxenes and the $\text{Cr}/(\text{Cr}+\text{Al})$ ratios of spinels, compares with the residual mineralogy produced at 5-10 kbar and temperatures of $1200^\circ\text{-}1300^\circ\text{C}$ from the starting peridotite compositions of Jaques and Green (loc. cit.). When the inferences from phase diagrams are combined with those from melting studies of primitive basalts, the results are consistent with the generation of the alkalic basalts at pressures of more than 12-13.5 kbar. All available data indicate that the Macquarie Island alkalic basalts formed at pressures of 12-15kbar and temperatures of $1250^\circ\text{-}1350^\circ\text{C}$, by small degrees of melting, $\leq 15\%$.

Turning now to tholeiitic basalt compositions, melting experiments of primitive MOR tholeiites and phase equilibria studies are not always consistent with a unique genetic model. Assuming isobarically invariant melting of a four phase (ol+opx+cpx+sp) mantle lherzolite in the simplified CMAS system, then magnesian tholeiites (mg#=70-72) are primary melts produced at low pressures, 9-10 kbar (Presnall et al., 1979). Melting of natural peridotites has also been assumed as approximately isobarically invariant or "*pseudoinvariant*" (Stolper, 1980). Recently, it is becoming increasingly acceptable that

a range of silica saturated melts is produced at any given pressure (Fujii and Scarfe, 1985; Thompson, 1987). Fujii and Scarfe (1985) have shown that the compositions of liquids change progressively with increasing temperature (degree of melting) at constant pressure, and therefore they are not invariant liquids. Consequently, partial melting of natural peridotites cannot be treated as isobarically "pseudoinvariant". Thus, the melt compositions depend on the source composition to a great extent. It must be pointed out that there appears to be serious inherent limitations in the models of Green and his colleagues; they developed their model by assuming that addition and/or subtraction of olivine does not affect the melt compositions. This is not however the case; it has been shown that addition of even small percentages of Na_2O shifts the phase equilibria towards more silica undersaturated compositions (Hoover and Presnall, 1982).

The most primitive Macquarie Island liquids (glasses and aphyric lavas) as well as MOR tholeiitic glasses show considerable variation in silica saturation. The different degrees of silica saturation reflect on the varying source composition (fertile to depleted) and the variable degrees of melting. Tholeiitic basalts can thus generate over the pressure range 8-12 kbar by variable degrees of melting, 15-30%. The picritic model of Green et al. (1979) on the other hand, suffers certain drawbacks. Green and his colleagues considered cpx-free harzburgite as the residual mantle peridotite lithology. The Macquarie Island harzburgites contain $\approx 2\%$ diopside and the enstatites are saturated in diopside molecule. Recent data from oceanic tectonised peridotites indicate that diopside (although in small percentages) is always present (Dick et al., 1984; Dick and Fisher, 1984; Michael and Bonatti, 1985). Thompson (1987) argued that tholeiitic picrites forming at high pressures 15-20 kbar, must fractionate significant

amounts of enstatite in addition to olivine if they were to produce the wide spectrum of silica saturation observed in primitive MOR tholeiites. The phase relations in the pseudoliquidus Ol-Di-Pl-Si system of Walker et al. (1979) discussed in section 9.2.2 corroborate Thompson's argument. Although such tholeiitic picrites could represent possible parental melts of MOR tholeiites, they are by no means the only available candidates as has been categorically stated by Green et al. (loc.cit.). They probably represent a small only percentage of parental magmas. This possibility is further explored in the discussion of section 9.5.6.

The extent of mantle peridotite fertility (or depletion) cannot be evaluated so easily. It was inferred that the Macquarie Island transition metal abundances in both basalts and harzburgites suggest a very fertile source peridotite with around 2% modal diopside. Estimations of the source composition by combining 85 parts of harzburgite and 15 parts of basalt (that is equivalent to the small to moderate degrees of of partial melting) suggest a source with low TiO_2 (<0.26%wt), low CaO (1.9%wt), low Na_2O (<0.45%wt), relatively high Al_2O_3 (\approx 3.5%wt), high MgO (\approx 38-40%wt) and FeO^* (\approx 9-10%wt) contents (see table 9.1). Such a composition is considerably more fertile than that of the Tinaquillo lherzolite and other natural lherzolites (table 9.2), but not as fertile as that of the reconstructed peridotites of Fujii and Scarfe (1985) and the basalt+HK66 peridotite mixture of Takahashi and Kushiro (1983). Both starting peridotite and reconstructed peridotite compositions of Fujii and Scarfe (loc. cit.) are considerably more fertile than the average source composition estimated from the Macquarie Island data. Partial melting of peridotites having compositions similar to those of SM2 and SM4 at pressures of around 10 kbar, produces basaltic melts which are very similar to the very

magnesian tholeiitic basalts from Macquarie Island (table 9.7). The Macquarie Island basalts have slightly higher FeO^* and TiO_2 content than those 10 kbar melts, possibly reflecting low depth oxidation of Fe^{2+} to Fe^{3+} and source region Ti-enrichments respectively. High magnesia ($\approx 10\%$ wt MgO) tholeiitic basalts showing different degrees of silica saturation are thus very likely to have been produced at around 10kbar pressure and temperatures of $1250^\circ\text{-}1350^\circ\text{C}$. Such tholeiitic liquids can be parental to the Macquarie Island basalts through low pressure fractionation.

When the Macquarie Island data are compared with the data of Fujii and Scarfe (loc.cit.), it seems that the Macquarie Island source composition must have been less depleted than that of the average composition of the less-depleted oceanic lherzolites of Maaloe and Aoki (1977) and Michael and Bonatti (1985) (table 9.8). In fact, the estimated peridotite composition is very similar to that of the average less-depleted Zabargad spinel-lherzolite (Bonatti et al., 1986). The estimated Macquarie Island source peridotite requires $\approx 20\%$ partial melting to produce the average less-depleted oceanic lherzolite, assuming a basalt composition similar to the most magnesian Macquarie Island glasses and aphyric basalts. Such a percent of partial melting is consistent with previous inferences. Additionally, the similarity of the Zabargad spinel-lherzolites with the estimated source composition from the Macquarie Island basalt-harzburgite mixes suggests that such an estimated composition is not too fertile to be considered unrealistic.

9.5.2 Fractional crystallisation at low pressures

Most of the oceanic basalts are olivine and plagioclase phenocrystal; minor amounts of clinopyroxene and spinel phenocrysts are also present. Melting studies of basaltic glasses reveal that the crystallisation sequence is olivine-> plagioclase-> clinopyroxene at 1atm pressure. Most of the abyssal tholeiites have compositions clustering along 1atm phase boundaries in various liquidus phase diagram projections, hence their compositions are largely controlled by fractional crystallisation of these three phases. Major oxide variation diagrams also provide strong support to low pressure crystal fractionation; the trends of most abyssal basalts and glasses show that with decreasing MgO (or Mg#), Ti and total iron increase and Al and Ca decrease. All these characteristics of oceanic basalts are consistent with crystal fractionation at low pressures. Earlier (Miyashiro et al., 1969a; Shido et al., 1971) and recent studies (Sigurdsson, 1981; Perfit and Fornari, 1983) attributed the compositional variation of spatially associated basalts in olivine + plagioclase and often clinopyroxene crystallisation. Common practice has been the testing of various fractionation models by least squares approximations; a primitive and a differentiated composition are normally employed in such calculations.

Griffin and Varne (1980) and Griffin (1982) have shown that the dominant phenocryst phase in both basalts and dolerites from Macquarie Island is plagioclase, followed by olivine and to a lesser extent by clinopyroxene; the general trends of basalts in major element variation diagrams show that with decreasing Mg#, Al, Ca, Ni decrease and Ti, Mn, P and total Fe increase; trends consistent with low pressure crystal fractionation of the phenocryst phases. The presence of the cumulate troctolites can be considered as a *prima facie* evidence for low pressure fractionation of olivine+plagioclase. Clinopyroxene is

interstitial in troctolites, but becomes a cumulus phase in the olivine-gabbros. Fractionation models have been tested by least squares calculations utilising a primitive lava composition (high in mg# and Ni) and an evolved lava composition (low in mg# and Ni) from the same locality but from different stratigraphic positions; compositions of cumulus minerals from the troctolites have been employed in the calculations. Aphyric and close to aphyric lavas were used only. Selected results are listed in tables 9.9.

A differentiated basalt such as 38307 (mg#=58.7) can be derived from a more primitive basalt such as 38288 (mg#=69) by 30-35% fractionation of olivine + plagioclase + clinopyroxene. These samples are from the volcanic section Mount Martin - Saddle Pt. The proportions of the minerals themselves vary as a function of their composition. When the fractionating minerals are olivine Fo_{88} , plagioclase An_{85} and clinopyroxene with $Mg/(Mg+\Sigma Fe)=88$, their respective proportions are 20.8%, 64.4% and 14.8%; if less MgO-rich olivine (Fo_{85}) and clinopyroxene ($Mg/(Mg+\Sigma Fe)=86$) fractionate, then the mineral proportions will be, olivine 21.4%, plagioclase 65.4% and clinopyroxene 13.2%. A MgO-rich basalt (mg#= 71) from Green Gorge (sample 38188) correlates with the spatially associated and evolved basalt 38303 (mg#= 61) through olivine + plagioclase + clinopyroxene subtraction. The crystal extract is about 20%; the proportions of the minerals in the crystal extract are olivine $\approx 55\%$, plagioclase $\approx 17\%$ and clinopyroxene $\approx 28\%$. Similarly, basalt 38284 (mg#= 67) from Davis Pt. can yield the more evolved basalt 147 (mg#= 56) after the removal of about 35% crystal extract; the proportions of fractionating minerals are 24.5% olivine, $\approx 63\%$ plagioclase and $\approx 12.5\%$ clinopyroxene. The crystal extracts required to yield the most evolved compositions (mg# 55-57) from the primitive basalts (mg# 69-71) are in the range of 30-

35%. The mode of these crystal extracts is very similar to the cumulate troctolites and olivine-gabbros. It is also evident that clinopyroxene is always a necessary fractionating phase. Similar conclusions are drawn from least squares calculations using glass compositions. The evolved glass 38390 (mg#= 57) requires removal of $\approx 31.5\%$ crystal extract from the primitive glass 47979 (mg#= 66.7); the crystal extract itself will be made of 18% olivine, 52% plagioclase and 30% clinopyroxene.

The crystal extracts required by the least squares approximations must contain $20\pm 5\%$ olivine, $60\pm 7\%$ plagioclase and 10-15% clinopyroxene. These mineral percentages are comparable with those of the combined cumulates, troctolites and olivine-gabbros. The results of such modelling are therefore in good agreement with the observed mineralogy of the cumulates.

9.5.3 Magma mixing

The original compositions of mantle derived magmas can be further complicated by mixing with magmas produced by source peridotites which are variably depleted or enriched (for instance the spreading ridge overrides a mantle region of an ascending plume); also, by magmas derived from the same source but at different pressures; and finally, by mixing with differentiated magmas which resulted through fractionation of olivine or olivine+plagioclase and olivine+plagioclase+clinopyroxene at moderate and low pressures. Mixing of magmas enroute to the surface in conduits located within the uppermost mantle or in crustal magma chambers is hence an important process in generating some of the observed compositional variations in

the chemistry of MORBs. The possibility of high pressure clinopyroxene fractionation is discussed in the following section. In this section, intermixing of magmas is examined in the low pressure end (2 kbar and less). Such a process is believed to take place in shallow level magma reservoirs.

The presence of olivine, plagioclase and clinopyroxene "xenocrysts" that are not in equilibrium with their host liquids, considering only glasses and aphyric basalts, the high residuals in least squares calculations when attempting to relate a primitive and an evolved basalt through olivine and plagioclase subtraction, and the consequently compulsory clinopyroxene fractionation to account for mathematically acceptable solutions, the lower $\text{CaO}/\text{Al}_2\text{O}_3$ ratios of the evolved glasses than these of the primitive ones, the significant enrichments in TiO_2 , K_2O and P_2O_5 in evolved glasses, the very high (almost anomalous) concentrations of Ti, Zr, Nb and REE in the evolved melts relative to those expected from crystal fractionation modelling of suitable minerals (usually compositions of phenocrysts) and suitable parental melts have all been used to argue that magma mixing in crustal magma reservoirs is an important process (Dungan and Rhodes, 1978; Rhodes et al., 1979; Rhodes and Dungan, 1979; Stakes et al., 1984; O'Hara, 1977).

Most of the relevant studies concentrated in relating the compositionally intermediate and evolved basalts and glasses to a common parent. This parental magma has been identified as a high MgO (>8.5%wt), low TiO_2 ($\approx 0.70\%$ wt), high CaO and Al_2O_3 (12-13%wt and 15-17%wt respectively), low Na_2O (<2%wt) melt; it will therefore have high $\text{CaO}/\text{Al}_2\text{O}_3$ (>0.7) and $\text{CaO}/\text{Na}_2\text{O}$ (>6) ratios. These studies also assumed consanguineous magmas. Stakes et al. (1984) suggested that mixing of a primitive glass with an evolved glass could account for the

intermediate glasses from the FAMOUS, AMAR and Narrowgate areas of the Mid-Atlantic Ridge.

Turning now to the Macquarie Island data, magma mixing hypotheses are evaluated on the basis of petrological evidence from basalts and glasses. The following factors are evaluated, the chemistry of phenocrysts in basalts and dolerites, the chemical characteristics of the layered troctolites and gabbros, and the major and trace element chemistry of basalts and glasses. The chemistry of the three types of phenocrysts in both basalts and dolerites was presented in chapter four. It was shown that the compositions of these phenocrysts overlap those of the cumulus minerals from troctolites and gabbros. The only exception is the rare spinel phenocrysts in some of the lavas. The composition of these spinels suggests that they formed at higher pressure (and temperature) than the cumulus spinels in troctolites.

The concentrations of certain elements (like Ti) in the cumulates suggest that close system fractionation cannot account for their observed distribution (figure 6.18).

The geochemistry of basalts and dolerites can be analysed by examining, (a) elements which preferentially enter the minerals and (b) elements which are constantly enriched in the liquid. It was inferred in chapter 8 that olivine fractionation and accumulation controls the Mg# ratios and Ni contents of basalts, glasses and dolerites. The TiO_2 contents and $\text{CaO}/\text{Al}_2\text{O}_3$ ratios of basalts are not influenced by olivine fractionation. Crystallisation of plagioclase or clinopyroxene has opposing effects on the $\text{CaO}/\text{Al}_2\text{O}_3$ ratio; plagioclase crystallisation increases this ratio whereas clinopyroxene crystallisation decreases it. Figure 9.12 shows that the $\text{CaO}/\text{Al}_2\text{O}_3$ ratios of glasses decrease with progressing differentiation (either decreasing Mg# or increasing TiO_2). Clinopyroxene is the only phase that can lower this ratio. This

cryptic crystallisation of clinopyroxene was considered as "paradox" because of its general absence as a phenocryst (Dungan and Rhodes, 1978). Furthermore, least squares modelling dictates that clinopyroxene is an important crystallising phase, even for spatially associated basalts which lack clinopyroxene phenocrysts. The trends shown in figure 9.15 suggest that primitive and evolved glasses relate to each other by olivine and plagioclase fractionation, respective decreases in mg# and CaO/Na₂O ratios. The apparent decrease of CaO/Al₂O₃ ratios with progressing fractionation suggests that clinopyroxene must have been crystallising and separating from the melt as well. This possibility is tested by least squares calculations (tables 9.9). The moderately evolved glass 38390 (mg#=61, CaO/Al₂O₃=0.66, TiO₂=1.71%) can be derived by the more magnesian glass 47979 (mg#=70, CaO/Al₂O₃=0.73, TiO₂=1.06%) by olivine Fo₈₈, plagioclase An₈₅ and clinopyroxene subtraction; the respective proportions of these minerals are ≈18%, ≈52% and ≈30%. Because the subtracted mineral compositions are the actual mineral compositions of the cumulus phases, it is clear that there is no such problem as the clinopyroxene "paradox". The compositions of the primitive and evolved Macquarie Island liquids can be related to each other by removal of a crystal extract consisting of various proportions of cumulus minerals. It seems appropriate to emphasize that the "phantom" clinopyroxene subtraction and by implication crystallisation inferred from numerous studies of mid-ocean ridge basalts is not phantom at all, but simply a reflection of the sampling problems associated with the drilling of the ocean floor.

Another complication arising when correlating primitive with moderately evolved and evolved basalts (always assuming consanguineous magmas) is the considerable enrichments of the

concentrations of the magmaphile elements in the evolved basalts, usually referred to as the "magmaphile element excess". The concentrations of trace elements in several Macquarie Island basalts have been tested for simple fractional crystallisation. It was inferred in the previous section that basalt 38307 can be derived from the primitive basalt 38288 through 21% olivine + 64% plagioclase + 15% clinopyroxene separation. The bulk distribution coefficients for Zr and Nb have been estimated using the same mineral percentages, and mineral-melt partition coefficients from Sun et al. (1979) and le Roex et al. (1981). The observed Zr and Nb abundances in basalt 38307 are 138ppm and 57ppm respectively. 30% simple fractional crystallisation of the crystal extract 21% olivine+ 64% plagioclase+ 15% clinopyroxene from basalt 38288 results in a residual liquid with 135ppm Zr and 53ppm Nb. The observed and calculated contents are almost identical. Least squares calculations (previous section) suggest that the evolved basalt 38434 can be derived from the primitive basalt 38284 via 20% fractionation of a crystal extract made up from 16% olivine, 61% plagioclase and 23% clinopyroxene. The bulk D^{Zr} and D^{Nb} have been estimated for such a crystal extract. 20% fractional crystallisation of will result in residual liquids with 149ppm Zr and 51ppm Nb; the observed Zr and Nb concentrations in basalt 38307 are 145ppm and 42ppm respectively. Although the observed and calculated value of the Zr content are almost identical (18.5% fractionation is required to match the observed value), the calculated Nb content is higher than the observed. The observed Nb value is reproduced by 2% fractionation only. Not all differentiated basalt Zr and Nb contents however can be derived from those of the spatially associated primitive basalts. Nevertheless, simple fractional crystallisation does account for the high Zr and Nb contents of some of the Macquarie Island basalts.

9.5.4 High pressure clinopyroxene fractionation

Typical MORB tholeiites are almost always free of high pressure "xenoliths". Occasionally however, resorbed and embayed phenocrysts of olivine, clinopyroxene and spinel occur and have been variably interpreted as high pressure "restites" or low pressure magmatic phases. Clinopyroxene occurs as anhedral "megacrysts" in MAR (Mid-Atlantic Ridge) basalts (Donaldson and Brown, 1977). These megacrysts are usually rounded and resorbed indicating that they are in a reaction relationship to the host basalt; compositionally, they are MgO-rich, high Al_2O_3 Cr-rich diopsides. They could represent either disaggregated upper mantle peridotite crystals incorporated in the liquid while it was ascending through the mantle peridotite, or low-pressure magmatic phases. Wilkinson (1982) reviewed this topic in detail and favoured a restite origin for such Mg-Cr-rich clinopyroxene megacrysts. Thompson (1987) argued for a magmatic origin.

The Macquarie Island basalts contain clinopyroxene phenocrysts (or megacrysts) which are too magnesian to be in equilibrium with their host liquids. They are normally rounded and embayed. Their chemistry was discussed in chapter four. It was shown that they have a similar composition with the cumulus clinopyroxenes from layered troctolites and olivine-gabbros. Therefore, it is inferred that they can only be low-pressure magmatic phases.

9.6 Dynamics of Melt Segregation in the Upper Mantle

The formation and segregation of magma in the upper mantle is by and large controlled by the fluid dynamics of the convecting mantle. It has long been known that adiabatic decompression melting begins at the low velocity zone (LVZ), at some depths of more than 60-70km. At shallower depths, the degree of melting increases significantly in the region of extensive melting. The physical processes governing partial fusion in the mantle were however unknown. The depth of formation, the extraction, and the percolation and migration of magma depend on both physical and chemical properties of the mantle-melt system. As a consequence, petrologic models dealing with basalt generation must take into account the fluid-dynamical constraints.

Melting by upwelling occurs in a continuously convecting mantle. Melts form at various depths and are then expelled from the gravitationally compacting matrix due to their differential buoyancy. A model on magma formation and migration beneath the ridge axis was presented by Ahern and Turcotte (1979). The model predicts initiation of melting at depths of more than 70km and small fractions of melts. Considerations of the mantle permeability also favour small melt fractions (Maaloe, 1981). Large amounts of partial melts cannot be retained in the matrix according to Ahern and Turcotte (1979). Their model dictates that small melt fractions segregate and migrate upwards faster than the matrix, and as a result mix during their ascent with partial melts forming at shallower depths. The distribution of partial melting gradients beneath a ridge axis is shown in figure 9.16D. The petrologic implications of such a model are significant. Models envisaging (or requiring) large degrees of melting are at odds with the fluid-dynamical conditions in the upper mantle. Small degrees of

melting in a convecting mantle can explain the disparities in the trace element abundances and ratios (in particular those of incompatible elements) of MORBs; large degrees of melting in the extensive melting region can account for the major element compositions of these liquids. The melts that reach the surface are thus a mixture of these two sequential melting processes, coupled with continuous mixing.

The compositional diversity of the Macquarie Island basalts-glasses-dolerites seems to favour such a multiple fusion - mixing model. The diverse ratios of incompatible elements, the concentrations of these elements, the MgO-rich Ne-normative basalts with high contents of incompatible elements, the uniformity in the major element compositions of the tholeiitic basalts which are relatively enriched in incompatibles and other geochemical features discussed before, suggest that the Macquarie liquids could well be the end product of different melting-degree partial melts which mixed during their ascent to the base of the crust, where either entered a crustal plumbing system or reached the surface.

Subsequent advances in the decompression melting theme beneath oceanic ridges progressed to very detailed treatments of the subject and reached comprehensive levels of understanding the processes involved. A detailed treatment of this topic is however beyond the scope of this thesis, but in the light of the importance of these studies and the significance of their petrologic implications, a brief reference seems inevitable. A short comprehensive review of the subject is given by Thompson (1987). Dan McKenzie in a series of contributions (1984, 1985a, 1985b) and McKenzie and Bickle (1988) analysed the physics of decompression melting beneath spreading ridges and reached some very important conclusions. McKenzie estimated the mean temperatures in the upper mantle, the porosity of

the matrix, the depths of formation of partial melts, the likely compositions of these melts, the lithospheric thickness that these melts can generate, and calculated geotherms for a convecting mantle. McKenzie and Bickle (1988) estimated a potential temperature of 1280°C beneath the ridge axis, a depth of melting of 40km, a degree of melting of less than 25% and also the major element composition of these partial melts. They argue that these magmas with about 10%wt MgO can produce a 7km thick oceanic crust, leaving as residual peridotite a harzburgite with small amounts of diopside; and also, that about half of the melt must be removed as gabbro to account for a 3-4km thick gabbroic layer. Figure 9.16E shows the calculated temperature distribution beneath a ridge axis; it is in good agreement with the temperature (and melt fraction distribution) profile of Ahern and Turcotte (1979).

The Macquarie Island data presented in the previous chapters and the theoretical modelling and calculations of McKenzie and McKenzie and Bickle are in a surprisingly excellent agreement. The small degree of melting inferred from the Macquarie data is very similar to that estimated by McKenzie. The mantle potential temperature of 1280°C and the mean major element composition of the melts of McKenzie and Bickle are identical to those inferred for Macquarie liquids. The observed (Macquarie basalts/glasses) and predicted (McKenzie and Bickle) melt compositions are plotted in the Di-Ol-Si diagram of Walker et al. (1979) and shown in figures 9.16B and C. The Ne-normative Macquarie liquids could result from small degrees of partial melting; with increasing fraction of melt, the melt becomes progressively less silica undersaturated and moves towards the cotectic composition. This is precisely what McKenzie and Bickle found. Their initial melts are Ne-normative; with increasing melt fraction,

the melt composition changes along a straight line, from the initial Ne-normative melt to the cotectic melt composition (shown in figure 9.16C), due to mixing with compositionally distinct melts (lower Na_2O and TiO_2). The Macquarie harzburgites are the residues of a previous partial melting episode (presumably more than one episodes), and contain a minor amount of diopside. It was inferred that harzburgites are the residues of small degrees of partial melting, about 20%, and that melting beneath the ridge did not progress to the stage of diopside elimination. Melting therefore was constrained in the Ol-En-Di-Sp (+Liq) phase volume. The calculations of McKenzie and Bickle show that melting is around 24% (and possibly less) and that the residual peridotite is a harzburgite with a small amount of diopside. The most MgO-rich Macquarie basalts-dolerites have >9%wt MgO. It was argued that these liquids have fractionated only small amounts of olivine, <2-5%. The agreement between the observed (from Macquarie Island) and calculated (from McKenzie and Bickle) liquid - residue compositions is more than satisfactory when the various uncertainties are taken into consideration. The data discussed so far permit the formulation of an intergrated spreading-ridge - magma-generation model for the Macquarie Island oceanic lithosphere.

The preferred model can be briefly described as follows. Upwelling mantle begins to melt in the LVZ. The melt fractions are extremely small, and are presumably retained in the matrix. With further upwelling, the adiabat intersects the solidus and extensive melting commences. The calculated convective geotherms of McKenzie and Bickle are shown in figure 9.16A. The crossing of the solidus occurs at a depth of around 40km, as can be inferred from figure 9.16A. From this point onwards, the degree of melting increases gradually and approaches a maximum of $\approx 25\%$ at a depth possibly corresponding to

the spinel-lherzolite - plagioclase-lherzolite transition. Partial melts formed earlier by small percentages of melting have alkalic compositions, and mix in this zone of extensive melting with large-melting-degree melts which have a tholeiitic composition. The aggregate liquid composition lies on a mixing line between a Ne-normative and a cotectic liquid. The Macquarie Island alkalic basalts represent such aggregate liquid compositions; the tholeiitic rocks are partial melts produced in the extensive melting region. The most magnesian liquids have 9.5-10%wt MgO. Low pressure fractional crystallisation of olivine, plagioclase and clinopyroxene disperses their compositions towards more silica-undersaturated and more silica-saturated compositions respectively. The crustal thickness produced is estimated to 5-6km from the Macquarie Island stratigraphy.



CHAPTER TEN : MACQUARIE ISLAND AND OPHIOLITES

This chapter compares Macquarie Island with the best known and studied ophiolite complexes. The lithologies present in ophiolites as well as their mineralogy and geochemistry are described in some detail and compared to those of Macquarie Island. In addition, abyssal plutonic and basaltic rocks recovered from the ocean floor are described and compared with those from Macquarie Island; their mineralogy and geochemistry is also discussed. Inferences are drawn from the similarities or differences between the ophiolite and abyssal rock associations and the Macquarie Island rock types. Finally, magma chamber models are discussed and their validity is evaluated on the basis of the available data from Macquarie Island.

10.1 Mineralogic variability amongst Ophiolitic and Abyssal Peridotites. Comparisons with the Macquarie Island Peridotites

The best known examples of ophiolites are encountered along the Tethyan ophiolite belt. This belt stretches from Spain to Iran and possibly to the Himalayas. Well preserved ophiolite complexes occur in the Appenines, Alps, Dinarides, Hellinides, Anatolides, Taurides, Oman Mountains and the Zagros Range. Some of the better studied and documented complexes of this belt are the Vourinos ophiolite in Greece, the Troodos complex in Cyprus and the Samail ophiolite in the Oman Mountains. Most of them show complete stratigraphy; a basal tectonite peridotite overlain by magmatic cumulates, massive gabbros, plagiogranites, sheeted dykes and capped by volcanics with intercalated sediments (figure 10.1).

The basal ophiolitic metamorphic peridotite is represented by harzburgite, spinel-lherzolite and dunite. All rocks display metamorphic fabrics.

Flow foliation is defined by the flattening of minerals and lineation by the direction of mineral elongation. Recrystallisation of olivine and orthopyroxene is common. Porphyroclastic, protoclastic and mylonitic textures have been reported from Vourinos (Ross et al., 1980), Newfoundland ophiolites (Girardeau and Nicolas, 1981) and Semail (Boudier and Coleman, 1981). Isoclinal folding is also present. These fabrics are indicative of a high-temperature low-stress environment, and have been attributed to plastic flow in the uppermost mantle immediately beneath the ridge (Nicolas and Le Pichon, 1980). These structures are observed in the main peridotite body and away from thrust zones. At the proximity of thrust zones, dynamothermal (low-temperature and high-stress) deformation features are superimposed on the high-temperature fabrics.

The mineral chemistry of the ophiolitic peridotites is uniform and highly refractory. Olivine is always the major constituent and has a composition Fo_{89-93} ; its NiO content is more than 0.30%wt. Orthopyroxene is enstatite in composition, and shows limited variation in $100\text{-Mg}/(\text{Mg}+\Sigma\text{Fe})$ ratios, from 90 to 93. Ca-rich pyroxene (usually diopside) occurs in interstitial grains and is a minor constituent (<5% of the mode). It is more magnesian than the enstatite, $100\text{-Mg}/(\text{Mg}+\Sigma\text{Fe}) = 89-95$. Accessory spinel is always present and shows a large compositional variation in terms of Cr_2O_3 and Al_2O_3 contents; its $\text{Cr}/(\text{Cr}+\text{Al})$ ratios range from 0.20 to 0.90 (figure 10.2a). The TiO_2 content is uniformly low, mostly less than 0.30%wt (England and Davies, 1973; Menzies and Allen, 1974; Menzies, 1975; Jackson et al., 1975; Dickey, 1975; Malpas and Strong, 1975; Boudier and Coleman, 1981; Dick, 1977; Quick, 1981; Jaques, 1981; and many others). Spinel is a key mineral in ophiolite-type peridotites because its composition critically depends on the bulk rock composition. Additionally, it consists of elements that are critical for the bulk rock composition and represents a minor phase. Because of its accessory character, its composition is very sensitive to partial melting processes. Thus, it can reflect compositional changes during partial melting episodes which would not affect (or would have

only a minor effect) the compositions of the other silicate phases. The textural character of spinel, interstitial to olivine and pyroxenes, suggests an origin after incongruent melting of clinopyroxene and enstatite (Dick, 1977). The large variation in the $Cr/(Cr+Al)$ and $Mg/(Mg+Fe^{2+})$ ratios of spinel, and the pattern of increasing $Cr/(Cr+Al)$ with decreasing $Mg/(Mg+Fe^{2+})$ in spinel always accompanied by increasing the $Mg/(Mg+Fe)$ of the coexisting olivine, indicate that equilibration of olivine and spinel took place during partial melting (Irvine, 1965, 1967; Dick, 1977).

The tectonite peridotites are therefore residual rocks after partial melting and extraction of basaltic melts, left behind as "fossil mantles". Gabbroic, websterite and feldspathic dykes and veins have been observed throughout this unit (Boudier and Coleman, 1981; Quick, 1981). They are considered as trapped melts produced by melting a more "fertile" upper-mantle peridotite, and sometimes they have produced metasomatic effects in the host depleted peridotite (Evans, 1985).

Alpine-type peridotites, the "root zone" peridotites of Den Tex (1969), differ from the ophiolite peridotites in that they are predominantly clinopyroxene rich lherzolites. They have higher alumina and alkali contents compared to ophiolite peridotites, and are overlain by granulites (Nicolas and Jackson, 1972). Typical examples of such peridotites are the Ronda intrusion in Spain, and the Lanzo, Balmuccia and Baldissero massifs in Northern Italy. The spinel in these lherzolites is Al_2O_3 rich (up to 66%wt), with $Cr/(Cr+Al)$ ratios of less than 0.6 (figure 10.2c). Both enstatite and clinopyroxene have higher Al_2O_3 and Na_2O contents than those in ophiolite peridotites (Boudier, 1978; Shervais, 1979). These compositional characteristics suggest that the "root zone" lherzolites are less depleted than the ophiolitic peridotites, and therefore the sub-continental upper mantle is more "fertile" than the oceanic upper mantle. The strikingly different mineral compositions between alpine-type peridotites

and Macquarie Island harzburgites suggest that the Macquarie Island harzburgites had a different genetic evolution from the sub-continental peridotites.

Peridotites have also been recovered from the world's oceanic ridge system and have been named "abyssal peridotites" (or oceanic). These peridotites are very similar to the ophiolitic peridotites. Abyssal peridotites have been dredged from the Equatorial Mid-Atlantic Ridge near 45°N and 43°N (Aumento and Loubat, 1971; Shibata and Thompson, 1986), the Vema and Romanche Fracture Zones (Prinz et al., 1976), the Northern Mid-Atlantic Ridge (Sinton, 1979; Michael and Bonatti, 1985), the Owen Fracture Zone (Hamlyn and Bonatti, 1980), the Indian Ocean Ridge system and the Carlsberg Ridge (Dick and Fisher, 1984), the Garret Transform Fault near the East Pacific Rise (Hebert et al., 1983), and elsewhere. They comprise a group of spinel-lherzolites, plagioclase-lherzolites, harzburgites and dunites. These rocks display similar structure, mineralogy and geochemistry to the ophiolite peridotites (Hamlyn and Bonatti, 1980). Their principal difference to the ophiolite tectonised peridotites is their higher modal clinopyroxene, usually more than 3%. Spinel shows considerable Al-Cr variation; its Cr/(Cr+Al) ratios are less than 0.6 and its Mg/(Mg+Fe²⁺) ratios very limited (figure 10.2b). TiO₂ contents are variable, from less than 0.1% to more than 1.5%wt (Dick and Bullen, 1984), a notable difference to the uniform and always low TiO₂ contents of spinel from ophiolitic peridotites. Olivine has a composition of Fo₈₉₋₉₂, with NiO contents from 0.2 to 0.4%wt. The orthopyroxene is enstatite, Mg/(Mg+ΣFe) ratios in the range 89-92, and the clinopyroxene is a diopside having Mg/(Mg+ΣFe) ratios of 89-93. Both pyroxenes show variable Al₂O₃ and CaO contents. Enstatites in peridotites dredged from the Carlsberg Ridge, have 3-6.5%wt Al₂O₃ and diopsides 4.4-7%wt Al₂O₃ (Hamlyn and Bonatti, 1980).

The Macquarie Island harzburgites display similar textural and compositional features to the ophiolitic and abyssal peridotites. Protogranular textures are characteristic, and spinel is always interstitial to olivine and enstatite. Olivine is MgO-rich, Fo₈₉₋₉₃, and characteristically shows high NiO

contents, 0.4-0.45%wt. Enstatite has high $100\text{-Mg}/(\text{Mg}+\Sigma\text{Fe})$ ratios, 89-92, and moderate Al_2O_3 contents. Interstitial diopside is always more magnesian than the coexisting enstatite; its $100\text{-Mg}/(\text{Mg}+\Sigma\text{Fe})$ ratios range from 92 to 94. Spinel has $\text{Cr}/(\text{Cr}+\text{Al})$ ratios of 37-53 (figure 10.2b), and very low TiO_2 contents (<0.05%wt). The composition of olivine and enstatite is thus comparable to that of both ophiolitic and abyssal peridotite olivine and enstatite. The Cr-spinel composition compares with that of abyssal peridotite spinel and to some extent to the ophiolitic spinel.

Evidence provided by the mineral chemistries of ophiolitic and abyssal peridotites suggest that the spinel and pyroxene compositions change progressively during partial melting. The spinel and pyroxene compositions reflect the degree of depletion of the peridotite. In spinel- and plagioclase-bearing lherzolites, enstatite has higher CaO and Al_2O_3 contents compared to enstatite from more refractory peridotites (harzburgites). The progressive decrease in Al_2O_3 and CaO contents is accompanied by an increase in the $\text{Mg}/(\text{Mg}+\Sigma\text{Fe})$ ratios. It has been observed that all silicate minerals become more MgO-rich, and the spinel $\text{Cr}/(\text{Cr}+\text{Al})$ ratio increases in the more refractory peridotites; also the spinel $\text{Cr}/(\text{Cr}+\text{Al})$ ratio shows a good negative correlation to the enstatite Al_2O_3 content (Michael and Bonatti, 1985). In addition, modal variations correlate well with mineral chemistry. Modal olivine increases with increasing spinel $\text{Cr}/(\text{Cr}+\text{Al})$ ratio, and modal clinopyroxene decreases with increasing spinel $\text{Cr}/(\text{Cr}+\text{Al})$ ratio (Dick et al., 1984; Michael and Bonatti, 1985). These trends are in agreement with anticipated variations and correlations in mineral chemistry during partial melting, and also trends documented from experiments on direct partial melting of Tinaquillo lherzolite and hypothetical pyrolite (Jaques and Green, 1980).

The variation of Al_2O_3 with the $\text{Mg}/(\text{Mg}+\text{Fe})$ ratio in enstatites from abyssal and ophiolitic peridotites is shown in figure 10.3a. Enstatites from ophiolitic peridotites extend to more refractory compositions than those in

abyssal peridotites. The Macquarie Island enstatites from the harzburgites span a limited range and plot in the middle of the observed fields, but towards the more depleted abyssal peridotite compositions. Figure 10.2b shows the correlation between the Al_2O_3 contents of spinel and enstatite. The abyssal peridotite field extends towards higher Al_2O_3 contents, while the ophiolite peridotite field towards more refractory compositions. Data from Macquarie Island harzburgites cluster in the middle of the ophiolitic field and towards the more depleted compositions of abyssal peridotites. The Macquarie Island data suggest that the harzburgites have intermediate refractory compositions and therefore must represent refractory residues of moderate degrees (10-20%) of partial melting. The Al_2O_3 contents of enstatite and spinel in ophiolitic peridotites are always lower than those in abyssal peridotites; a good linear correlation is displayed in the $(\text{Al}_2\text{O}_3)^{\text{spinel}} - (\text{Al}_2\text{O}_3)^{\text{enstatite}}$ plot; abyssal peridotites usually contain diopside, and when diopside is not present as a separate phase, then enstatite is saturated with diopside; these features together with phase diagram considerations led Dick and Fisher (1984) to conclude that abyssal peridotites are the residues of partial melting constrained by the $\text{Ol}+\text{En}+\text{Di}+\text{Sp}+\text{Liq}$ pseudoinvariant point; ophiolitic peridotites are residues of melting constrained by the $\text{Ol}+\text{En}+\text{Sp}+\text{Liq}$ point. Melting in the suboceanic mantle was therefore less advanced than the partial melting events which produced the ophiolitic peridotites. The characteristics of the Macquarie Island harzburgites indicate that they are the residues of partial melting of mantle lherzolite and that the partial melting event(s) occurred in the $\text{Ol}-\text{En}-\text{Di}-\text{Sp}-\text{Liq}$ phase volume; they are also less depleted than the residual ophiolitic peridotites, where partial melting progressed into the three phase volume $\text{Ol}-\text{En}-\text{Sp}-\text{Liq}$.

10.2 Geologic and Mineralogic characteristics of Ophiolitic

Cumulates - Oceanic Gabbroic Suites -

Macquarie Island Layered Rocks.

A zone of ultramafic cumulates overlies the tectonised peridotites. It is known as the "transition" or "critical" zone (Moore, 1969) and consists mainly of dunite with minor chromitite, wehrlite and pyroxenite. The lower level of cumulate dunite defines the petrological Moho. The thickness of this zone is highly variable among different ophiolite complexes; in the Smail ophiolite, it is limited to few meters (Boudier and Coleman, 1981), and in the Massif du Sud, New Caledonia, is about 600m (Prinzhofer et al., 1980). In the Bay of Islands ophiolite massif, the critical zone is 3000 meters thick (Girardeau and Nicolas, 1981). The base of the transition zone is a sudden change to peridotite tectonite. The upper boundary is a gradational zone of interfingered layers of dunite in clinopyroxenite and wehrlite, and massive dunites with websteritic and gabbroic lenses. Podiform chromite deposits of economic potential are located at the basal dunites, frequently extending downwards to harzburgites. The origin of podiform chromitites has been the subject of many studies (Dickey, 1975; Greenbaum, 1977; Neary and Brown, 1980; Cassard et al., 1981; Lago et al., 1982; Christodoulou and Hirst, 1985; Ceuleneer and Nicolas, 1985). The transition zone has been interpreted by many geologists as resulting from magmatic processes due to its cumulate textures (Coleman, 1977). This position has been challenged by Nicolas et al. (1980) and Nicolas and Prinzhofer (1983). They argued for a residual origin based on detailed structural studies in many ophiolite complexes. Recent detailed studies on the Zambales ophiolite critical zone suggest a magmatic origin of this zone (Abrajano et al., 1989). The absence of a transition zone in Macquarie Island is a notable feature. The lack of any chromite pods or segregations in Macquarie contrasts with the large podiform chromitite ore bodies encountered in most ophiolites. The chemistry of chromite in the

Macquarie Island troctolites also contrasts that of the chromite from the basal ophiolitic cumulates and chromitites. In the latter, chromite has typically high Cr_2O_3 content, more than 50%wt and usually up to 60%wt, and low TiO_2 , normally from 0.05%wt to 0.25%wt; the Macquarie chromites have lower Cr_2O_3 and distinctly higher TiO_2 contents suggesting a different physicochemical environment of formation. This is particularly important because chromite composition is sensitive to melt composition as well as $f\text{O}_2$ conditions.

The magmatic cumulates in ophiolites comprise sequences of layered pyroxenites, troctolites, olivine-gabbros, anorthosites, gabbros, gabbronorites and norites. The textures of the cumulates are usually adcumulus. The layered rocks are overlain by massive gabbros, hornblende-gabbros and feldspathic rock associations such as trondjemites, diorites and granophyres. The thickness of the magmatic sequence is variable; for instance, the cumulate section in Oman ranges from 1.5 km to 3.5 km (Pallister and Hopson, 1981). The cumulate pile in the Vourinos Ophiolite is 1500 m thick, and is arranged in 24 cyclic units (Jackson et al., 1975). A more detailed examination of the magmatic stratigraphy revealed that the cyclic units reported by Jackson and others are either incomplete or interrupted by non-cyclic lithologies (Rassios et al., 1983).

The four principal mineral phases are; olivine, plagioclase, clinopyroxene and orthopyroxene. Minor chromite is always present. The crystallisation order varies from one ophiolite complex to another. Olivine is followed by plagioclase and then clinopyroxene in some complexes; in other ophiolites, the order of crystallisation is olivine \rightarrow orthopyroxene \rightarrow clinopyroxene or olivine \rightarrow clinopyroxene \rightarrow plagioclase. Olivine is always forsteritic Fo_{80-90} . Clinopyroxene and orthopyroxene are always magnesian, $\text{Mg}/(\text{Mg}+\text{Fe}) > 0.90$ and 0.80 respectively. Plagioclase is characteristically very calcic; in the basal cumulates, it is normally more than An_{90} in composition. Plagioclase shows systematic Ab-enrichments up-section (Pallister and Hopson, 1981; Jaques, 1981; Beccaluva et al., 1984). In the Samail ophiolite, olivine shows a

composition range from Fo₉₁ to Fo₇₀ and plagioclase ranges from An₉₅ down to An₇₁; clinopyroxene has Mg/(Mg+Fe) ratios between 0.92 and 0.81 and orthopyroxene is in the range En₈₈₋₇₁ (Smewing, 1981). In the Antalya ophiolite, the olivine in the plutonic rocks is Fo₈₇₋₈₃ and the plagioclase An₉₄₋₈₄ (Juteau and Whitechurch, 1980). Intrusive relations between adjacent layers, very similar to those observed in Macquarie Island, have been reported from the Antalya ophiolite. Juteau and Whitechurch favoured multiple intrusions of fresh magma into the magma chamber. On the basis of the mineralogic features of the ophiolitic plutonic rocks, Duncan and Green (1980) proposed that such layered series can be accumulated by melts produced by "second stage" melting of an already depleted mantle source. They argued that OI- and Q-tholeiites are the most likely parental melts.

Plutonic rocks with relict cumulate textures have been recovered by deep sea drilling. Dominant rock types are dunites, troctolites, olivine-gabbros, noritic gabbros and hornblende-gabbros (Hodges and Papike, 1976; Miyashiro and Shido, 1980; Prichard and Cann, 1982; Ito and Anderson, 1983; Hebert et al., 1983). Olivine-gabbros from the Mid-Atlantic have olivine Fo₈₂₋₈₇, plagioclase An₇₁₋₉₂ and clinopyroxene with Mg/(Mg+Fe) ratios 74-89 (Hodges and Papike, 1976; Tiezzi and Scott, 1980).

There is an overall correspondence between the cumulate lithologies, adcumulate textures, mineral compositions and geochemistry of Macquarie Island plutonics (layered rocks) and the cumulate series of ophiolites. Some differences are however notable. The absence of pyroxene-rich cumulates and the absence of late stage differentiates such plagiogranites- trondjemites, from Macquarie contrast the common occurrence of such rock types in ophiolite complexes. The absence of chromite segregations in Macquarie is also of great importance. The Macquarie plagioclase is less sodic than that in ophiolites, and cumulus spinel is also significantly less Cr₂O₃-rich than that found in ophiolites, commonly in deposits of economic importance. These features indicate that crystallisation of

the cumulate rocks took place in a different physicochemical (and presumably geotectonic) environment than that of most ophiolites.

10.3 Geochemistry of Ophiolitic and Abyssal Peridotite-Gabbro Suites. Relationships to the Macquarie Island Plutonic Suite.

In ophiolite complexes, the tectonised peridotites underlying the cumulate sections are remarkably refractory. They have $MgO/(MgO+FeO^*)$ ratios of more than 0.8 ($Mg/(Mg+Fe) > 0.9$). Al_2O_3 and CaO contents are usually less than 2%wt, and Na_2O and K_2O are less than 0.01%wt. Cr_2O_3 and NiO contents range from 0.3% to 0.6%wt. The TiO_2 content is always extremely low. The incompatible trace element Zr, Rb, Nb concentrations are less than 1ppm. Oceanic (abyssal) peridotites are similarly depleted in alkalis and incompatible elements and high in MgO, Cr, Ni. They show variable degrees of depletion on a regional scale. Michael and Bonatti (1985) examined the modal variation and igneous mineralogy of abyssal peridotites from the North Atlantic between 0° and $79^\circ N$. They found evidence for regional variations of the peridotite chemistry. Peridotites dredged from $34^\circ-45^\circ N$ are more depleted than peridotites from other localities. The possible influence of the Azores region in the recorded pronounced depletions was suggested. Peridotites dredged from other localities close to hot spots are also more depleted than those recovered away from such regions (Dick et al., 1984). High degrees of melting have been favoured by Dick et al. to explain the pronounced depletions of these peridotites. Alternatively, melting of an already depleted source could cause such severe depletions.

Sequences of layered rocks reminiscent of the layered series of the continental stratiform complexes are well documented in many ophiolites such as the Vourinos complex (Jackson et al., 1975) and the Samail complex (Pallister

and Hopson, 1981). A typical sequence of lithologies comprises (from the base to the top of the sequence) dunites, wehrlites, olivine-pyroxenites, pyroxenites, troctolites, anorthosites, norites, olivine-gabbros, gabbros, hornblende-gabbros. A unit of massive (or isotropic) gabbros overlies the cumulate rocks. These rocks are typical granular cpx-plag gabbros; hornblende gabbros, microgabbros and doleritic gabbros are also present. Mafic rocks have been dredged from ocean floor at the proximity of fracture zones. Various lithotypes have been reported from the North Atlantic and the East Pacific. These include troctolites, olivine-gabbros, hypersthene-gabbros, norites and ilmenite-gabbros (Miyashiro et al., 1970; Hodges and Papike, 1976; Prinz et al., 1976; Vanko and Batiza, 1982; Hebert et al., 1983). A nepheline bearing gabbro has also been reported by Honnorez and Bonatti (1970). Hodges and Papike (1976) reported cumulate troctolites and olivine-gabbros from the Mid-Atlantic Ridge at 37°N. The rocks have high Mg/(Mg+Fe) ratios, 0.84-0.87, and are very depleted in TiO₂, K₂O, P₂O₅ and show typical tholeiitic enrichment trends. Gabbroic rocks from the Kane Fracture Zone have FeO*/MgO ratios from 0.32 to 2.8 and TiO₂ contents from 0.05% to 9.5%wt (Miyashiro and Shido, 1980).

Tiezzi and Scott (1980) examined the possible genetic relations of the gabbroic cumulates and basalts from DSDP Site 7 in the North Atlantic (26°N). They found that although the basalts continue the iron enrichment trend of the gabbros, hence possible by products of later stage gabbroic fractionation, clinopyroxene crystallisation is required to produce the observed chemical variations in the basalts; cpx however does not occur as a phenocryst phase. Based on this reasoning they concluded that the chemical variations in basalts cannot be reproduced by crystal fractionation at shallow magma chambers. On the other hand, data presented in chapters 6, 7 and 9 of this thesis strongly suggest that the Macquarie Island basalts-dolerites and cumulates are complementary. The absence of cpx as a phenocryst phase from MORBs is not

evidence for its crystallisation or not at low pressures, and possibly at crustal magma reservoirs.

Figure 6.1 shows that the Macquarie Island harzburgites represent some of the most refractory rock types; high in MgO and low in alkalis and Al_2O_3 . Their $\frac{\text{Mg}}{\text{Mg}+\text{Fe}^{2+}}$ ratios are between 0.90 and 0.92. Macquarie Island gabbros and Atlantic gabbros are compared in figure 10.4. The Macquarie Island gabbros show less Fe enrichment than the Atlantic Ridge gabbros. Both trends are almost parallel to the Skaergaard rock trend.

Serri (1981) plotted the FeO^*/MgO ratio versus the TiO_2 content of gabbros from ophiolites and the ocean floor. He suggested that this diagram can be used as a discriminant for the tectonic setting of ophiolite complexes. High-Ti ophiolites are formed at major oceanic spreading centres and low-Ti ophiolites are formed at marginal basins or back-arc spreading centers. Figure 10.5 is a $\frac{\text{FeO}}{\text{MgO}+\text{FeO}}$ versus TiO_2 plot for the Macquarie Island gabbros, and for gabbroic rocks from the Mid-Atlantic Ridge and the Indian ocean. The Macquarie rocks plot in the high-Ti field and show a similar trend to the Mid-Atlantic Ridge gabbros. The latter however, show much higher TiO_2 contents and $\frac{\text{FeO}}{\text{FeO}+\text{MgO}}$ ratios.

The crystallisation sequence in Macquarie Island is olivine (+chromite) \rightarrow plagioclase \rightarrow clinopyroxene. The crystallisation sequence of low-Ti ophiolites is olivine \rightarrow opx \rightarrow cpx \rightarrow plagioclase, and that of high-Ti ophiolites is olivine \rightarrow plagioclase \rightarrow cpx. The apparent resemblance of Macquarie Island with the high-Ti (or MORB-type) ophiolites is also confirmed by the order of appearance of mineral phases. In the majority of ophiolite complexes, pyroxenes precede plagioclase crystallisation; this contrasts the low-pressure crystallisation order of MORB liquids, and suggests an island-arc related setting (or supra-subduction) for the vast majority of these ophiolite complexes (Pearce et al., 1984).

In general, evidence presented so far from the Macquarie Island oceanic lithosphere is in agreement with the low-pressure crystallisation sequence of the MORB-like liquids, and support the presence of crustal magma chambers of relatively small size as well as the complementarity of tholeiitic lavas and cumulate gabbroic rocks.

In summary, Macquarie Island data on lithologies, mineral chemistry of cumulus phases, crystallisation order of these phases, geochemistry of plutonic rocks (cumulates and massive/isotropic gabbros) are in good agreement with lithologic and petrologic data obtained from abyssal plutonics. The plutonic ophiolite stratigraphy and the observed sequence of rock types (pyroxenites, websterites, gabbronorites, plagiogranites) are not comparable to those of Macquarie Island. The compositions of the cumulus minerals from Macquarie plutonics and ophiolitic plutonics differ substantially. A notable example is the high-Cr spinel (chromite) from the ophiolite ultrabasic cumulates (transition zone rocks). All this evidence suggests that the majority of ophiolite complexes formed at a different tectonic setting than that inferred for Macquarie Island. The similarities between the Macquarie Island plutonic rocks and abyssal plutonics from major oceanic spreading ridges, indicate the relationship of the lithosphere exposed on Macquarie Island to a major oceanic spreading ridge. On the other hand, the petrologic characteristics of ophiolite plutonics indicate an island-arc or subduction (marginal basin) related environment of formation.

10.4 Mid-ocean Ridge Basalts, Ophiolitic Lavas and the Macquarie Island Volcanic Suite. Petrologic Characteristics-Similarities and Petrotectonic Implications

Studies on ocean floor basalts have been intensified since the sixties. Systematic sampling of the Mid-Atlantic Ridge (MAR), east Pacific Rise (EPR),

Indian ocean and elsewhere has been undertaken to establish the petrography, mineralogy and geochemistry of basaltic lavas. Today there is a mountainous literature on the petrology of oceanic basalts. Inevitably, only some selected studies are referenced here. Early studies emphasized the predominance of tholeiitic (subalkaline) basalts with large ion lithophile element depletion, hence the name "abyssal tholeiites". The compositional uniformity of mid-ocean ridge basalts was challenged by Miyashiro et al. (1969a). Basalts with alkalic affinities were recognised later; Aumento (1968) described tholeiitic and alkalic basalts from the MAR at 45°N.

Bryan et al. (1976) summarized data from basalts drilled in the North and South Atlantic and the Indian Ocean. They recognised two groups; a group of typical abyssal tholeiites with LIL depletions (I), and a second group of basalts with LIL enrichments (II). Phenocrysts of plagioclase An_{90-90} , olivine Fo_{85-90} , diopsidic augite and Al and Mg-rich spinel are present in both groups. They noted the petrographic and mineralogic differences between the two groups, particularly the higher Ti-content of group (II) augites. In a survey study of basaltic glass compositions from the Atlantic, Pacific and Indian oceans, Melson et al. (1976) showed that the majority of the glasses have $\frac{100-Mg}{Mg+Fe^{2+}}$ ratios between 50 and 65. Tholeiitic basalts enriched in incompatible elements and alkali basalts (Ne-normative) strongly enriched in incompatible elements have been described from MAR at 43°N by Shibata et al. (1979b).

Sun et al. (1979) subdivided MORBs to three groups on the basis of their incompatible element ratios, REE abundances and isotopic ratios ($^{87}Sr/^{86}Sr$); "Normal" MORBs, incompatible element depleted tholeiites, "Plume" type MORBs, incompatible element enriched basalts, and "Transitional" type MORBs, a group of intermediate geochemical characteristics.

Subsequent studies emphasized the compositional diversity of the ocean floor basalts. The well studied FAMOUS area in the North Atlantic is an

appropriate example. LeRoex et al. (1981) recognised picritic, olivine-phyric, plagioclase-phyric and plagioclase-pyroxene basalts. Based on petrologic and geochemical evidence, they concluded that the parental magmas of these three groups were distinct. There is thus evidence for compositional variation even within a site.

Studies of basalts from fracture zones truncating ridges indicate a great compositional variability, from typical magnesian MORBs to ferrobasalts and FeTi basalts (Natland, 1980; Christie and Sinton, 1981; Bender et al., 1984).

Basalts erupted at the proximity of hotspot areas include enriched (P-type) and transitional (T-type). LeRoex et al. (1985), Humphris et al. (1985), and Thompson and Humphris (1984) examined the geochemistry of basalts from the America-Antarctic spreading ridge close to the Bouvet plume, and from the MAR at the vicinity of Tristan da Cunha plume respectively. They emphasized the incompatible element enrichments in these basalts and suggested that the observed compositional variation can be accounted for by mixing of enriched and depleted basalt components at regional scale. Schilling et al. (1983) summarized the available geochemical and isotopic data for the MAR from 29°N to 73°N. They concluded that the mantle at the proximity of hotspots is enriched in most incompatible elements and radiogenic isotopes of Sr and Pb relative to LIL element depleted mantle source of typical MORBs.

The petrology of the ophiolite extrusives is diverse and intriguing. The Troodos complex is one of the better exposed ophiolites. A sheeted dolerite complex is overlain by a thick volcanic succession which comprises two units, the Lower (LPL) and the Upper Pillow lavas (UPL) (Gass and Smewing, 1973). The UPL contain phenocrysts of olivine Fo_{86-89} , plagioclase An_{70-84} (An_{95} reported by Gass, 1958) and augite, and are more primitive than the LPL. Euhedral phenocrysts of forsteritic olivine Fo_{89-93} and pigeonite with $Mg/(Mg+Fe)$ ratios of 0.84-0.86 occur at the top of the sequence (Cameron et al. 1980; Cameron, 1985). Orthopyroxene phenocrysts En_{88-89} and pigeonite microphenocrysts

($Mg^{\#}=84-86$) are also encountered. Miyashiro (1973) proposed an island arc environment for the Troodos complex, based only on major element variations. Subsequent geochemical and isotopic studies indicated a subduction related tectonic setting (Robinson et al., 1983; McCulloch and Cameron, 1983; Thy et al., 1985; Rautenschlien et al., 1985). The Jurassic Vourinos complex in Greece has also been interpreted as an island-arc ophiolite (Noiret et al., 1981; Beccaluva et al., 1984).

Pearce et al. (1984) summarised the geochemical characteristics of ophiolite complexes studied up to date. They concluded that most ophiolites have geochemical characteristics of island arc tholeiites and formed in oceanic basins located in fore- arc, inter- arc and back- arc settings. They named these complexes "supra-subduction zone" ophiolites (SSZ-ophiolites).

The petrologic and geochemical features of the Macquarie Island basalts and dolerites have been briefly presented in chapter seven. The dolerites and the tholeiitic basalts resemble the group I of Bryan et al. (1976), but the alkalic basalts compare with the group II. The REE patterns of the alkalic basalts show significant LREE enrichments and the tholeiitic minor enrichments. The very interesting feature of some of these basalts is their very low Zr/Nb ratios (see chapter seven). Figure 10.6 is a plot of $Cr/(Cr+Al)$ versus $Mg/(Mg+Fe^{2+})$ ratios of spinel phenocrysts from Macquarie Island lavas, abyssal basalts and from Troodos lavas. The distinctly different composition of the Troodos spinel phenocrysts and the Macquarie Island spinel phenocrysts, as well as differences in phenocryst and groundmass phases strongly support previous inferences for the different tectonic setting of these two complexes. The compositional correspondence of the Macquarie Island and abyssal basalt spinels is apparent.

The petrography, mineral chemistry and geochemistry of ophiolitic lavas and Macquarie Island lavas show considerable differences. These differences reflect on the different character of their parental melts and by implication on the different geotectonic setting of formation.

Aumento (1968) suggested that tholeiitic lavas are the early extrusives along the rift valley, and the alkali lavas (high in normative nepheline) mark the end of the eruptive cycle always topping the tholeiitic cores. Stakes et al. (1984) presented a detailed study of the FAMOUS rift valley. They concluded that primitive melts are extruded at an early stage in the history of the spreading ridge when no magma chamber exists. When a magma chamber forms, the mantle derived primitive melts are buffered and so the extruded lavas become slightly evolved. As the magma chamber expands, the melts become moderately evolved due to crystal fractionation and magma mixing. When a steady state magma chamber develops, the expelled melts are fractionated, although primitive melts can still reach the surface carrying with them xenocrysts from the cumulus minerals. The model of Stakes et al. (loc.cit.) seems appropriate for Macquarie Island, because it can account for the stratigraphy and to some extent petrology of the extrusives; in addition, such a model invokes small and ephemeral magma chambers.

10.5 The Concept of Crustal Magma Chambers

10.5.1 Introduction

Evidence for the existence of magma reservoirs under the axial rift valleys is provided by the thick cumulate successions of many ophiolite complexes. The stratigraphy and structure of many well preserved ophiolites further constrain the size, shape and longevity of such magma chambers. A magma chamber is usually visualized as a variably thick zone where injection of mantle derived melts, fractionation, mixing and segregation of layered rocks take place (Greenbaum, 1972; Vine and Moores, 1972; Cann, 1974; Dewey and Kidd, 1977). Seismic studies along the East Pacific Rise (EPR) and the Mid-

Atlantic Ridge (MAR) reveal a different story. The presence of a thick succession of layered troctolites, olivine-gabbros, anorthosites and strongly laminated cpx-plag cumulates on Macquarie Island suggests cumulus crystallisation in a shallow level magma reservoir.

10.5.2 Geophysical Considerations

Geophysical studies on the MAR at 37°N and 45°N are summarised by Nisbet and Fowler (1978). They concluded that "large magma chambers cannot be present beneath the median valley of MAR, but smaller magma bodies having a combined diameter of less than 2 km cannot however be excluded". The combined geophysical and petrological data presented by Nisbet and Fowler (loc.cit.) suggest narrow and transient magma chambers. Their "infinite leak" model can be summarised as follows; melting commences at about 60 km depth beneath the ridge axial valley. The system mantle-melt starts moving towards higher levels. As the diapir ascends, the degree of melting increases. Magma segregates at 15 to 25 km depth (5-8 kb) and rises to a depth of 6-8 km where it ponds at the bottom of the crust.

Recent seismic studies along the EPR failed to detect any axial magma bodies (Bratt and Solomon, 1984; Buhl et al. 1986; Mutter et al. 1986). These studies indicate that any tentative magma reservoir beneath the ridge must be of small size, <3 km in diameter, and placed at high crustal levels, approximately 1-2 km beneath the sea floor.

10.5.3 Thermal Models

A model on the cooling of oceanic crust by conduction was developed by Sleep (1975, 1978). A different model was presented by Kusznir and Bott (1976). Both studies emphasize the very small spreading rates necessary for

maintaining steady state magma chambers. Sleep and Kuszniir & Bott calculated half-spreading rates of 0.9 cm/y (centimeters per year) and 0.45 cm/y respectively. The maximum width of a magma chamber according to Sleep's calculations is about 1 km for a half-spreading rate of 1 cm/y. The model of Kuszniir and Bott (*loc.cit.*) predicts a width of 6-8 km for a similar half-spreading rate. In a later communication, Kuszniir (1980) revised the minimum half-spreading rate to 0.65 cm/y. According to this later model, the width of a magma chamber could be not less than 3 km.

Lister (1983) modelled the cooling of the oceanic crust by sea water circulation. He concluded that the minimum half-spreading rate required for the existence of a magma chamber beneath the ridge axis is 5-6 cm/y.

10.5.4 Magma chamber models

Magma chamber models developed by Cann (1974) and Dewey and Kidd (1977). The "infinite onion" model of Cann envisages a high level magma chamber with inward dipping (towards the ridge axis) floor on which accumulative rocks form. The model successfully accomodates the seismic layering profile of oceanic crust. Dewey and Kidd (*loc.cit.*) suggested a wedge shaped magma chamber with flat floor. Cumulates segregate on the flat floor and massive gabbro plating occurs at the top. These models and earlier models based on ophiolite stratigraphy (Greenbaum, 1972; Vine and Moores, 1972) assumed large magma chambers, more than 20 km wide (Pallister and Hopson, 1981). Such magma chambers are not consistent however with geophysical constraints. Notwithstanding the geophysical evidence, several observations from ophiolite complexes are useful. The thickness of a magma chamber can be related to the thickness of the plutonic succession (cumulates) of ophiolites, which in the case of the Samail ophiolite ranges from 3 to 5 km. The shape of the chamber as

inferred from the Samail ophiolite must have been funnel-like according to Pallister and Hopson (1981).

A spreading ridge – magma chamber model has been proposed by Stakes et al. (1984). The various stages of magma chamber evolution according to this model are described here as they could apply to a Macquarie Island type magma chamber. In the initial stages of rifting, there is no magma reservoir beneath the rift valley. At the very early stages, the erupted melts are primitive because they have been derived directly from upper mantle peridotite assemblages, with minor only (if at all) crystal fractionation en route to the surface through the lithospheric fracture system. The most primitive (magnesian-rich) Macquarie Island basalts could be related to such early stages of rifting. A magma chamber begins to form and develop at some later stage. As the magma chamber augments in size, it achieves a steady state whereby input (continuous supply with primitive melts), output (lava extrusion) and crystallisation (segregation of plutonic rocks) are balanced. At steady state, the extruded melts are moderately fractionated. The formation of adcumulate rocks is believed to have taken place during this phase of magma chamber development. The Macquarie Island layered rocks must have been segregated in a magma chamber under such steady state conditions. The majority of the Macquarie Island basalts and dolerites (with mg* ratios of 62 ± 6) formed at this stage. When the replenishment rate decreases, the magma chamber starts solidifying progressively. In the advanced stages of magma chamber solidification, the extruded melts are evolved and resemble close-system differentiated liquids. Such silicic or very Fe-rich melts are not present in Macquarie Island and as a consequence it can be inferred that the exposed lithosphere on Macquarie Island is not representative of the later stages of magma chamber evolution; it rather represents the intermediate stages, when the magma chamber is well developed and the melts reaching the surface range from primitive to moderately differentiated.

10.5.5 Dynamics of magma chambers

Cumulate rocks from large continental layered intrusions have structures reminiscent of magmatic sedimentation. Their formation has been traditionally explained by crystal settling (Wager and Brown, 1967). The concept of crystal settling has been questioned and challenged much later. It has been shown that plagioclase accumulation through settling is unlikely to occur as that would involve plagioclase sinking in a less dense liquid, that magmas do not behave as simple Newtonian fluids, that crystals nucleate and grow against pre-existing crystals instead of nucleating within a liquid, and that the rate of crystal settling due to gravitational forces is much less than the velocities of the convection currents (Campbell, 1978; McBirney and Noyes, 1979; Chen and Turner, 1980; Sparks et al., 1984). Alternative processes have been proposed based on the dynamics of fluids. These processes are in-situ crystallisation and double-diffusive convection (McBirney and Noyes, 1979), and convective fractionation (Sparks et al., 1984).

Double-diffusive convection occurs in fluids when temperature and density change the buoyancy of these fluids. Because the magma density depends on temperature and composition at the same time, convection in magma chambers could be more complex than once thought. Turner and Gustafson (1978) suggested that double-diffusive convection could be important in magma chambers, and showed some effects in simple laboratory tank experiments. Such a process would result in stratified magma chambers, in both composition and temperature. Stratification because of double-diffusive convection could result from the upward flow of fluid (magma) which forms a boundary layer in contact to the nucleating and growing minerals, and the formation of a more differentiated (colder) fluid collecting at the roof of the magma chamber and overlying less differentiated (higher temperature) magma.

Sparks et al. (1984) introduced the concept of convective fractionation. Crystallisation at the walls and on the floor of the magma chamber would result in lighter magmas (more buoyant) which tend to rise and cause compositional convection. Compositional convection in magmas is important because it accounts for the separation of the liquid from the crystals and consequently drives crystal fractionation. Sparks and his colleagues argued that density changes during crystallisation have large compositional effects on the liquid. The formation of adcumulate rocks has been explained by such a process akin to compositional convection by Tait et al. (1984). The layered rocks of Macquarie Island are mostly adcumulates. They could have been formed by such a process, slightly off the ridge axis where there are non-turbulent conditions in the magma chamber. Immediately beneath the ridge axis, the environment is too turbulent to allow density and thermal processes to operate. Consequently, the adcumulate rocks must have formed slightly off this turbulent zone.

Huppert and Sparks (1980) presented a model for an oceanic ridge magma chamber and tried to explain why picritic magmas never (or very rarely) erupt. At the same time, Stolper and Walker (1980) suggested that MORBs erupt at their density minimum, through the "window of eruptibility". The model of Huppert and Sparks (1980) invokes picritic magmas entering the system and ponding at the floor of the chamber because they are denser than the overlying basaltic liquids. Heat is transferred from the lower picrite layer to the upper basaltic layer through a double-diffusive interface till the densities of the two layers become equal. When this happens, mixing occurs. In other words, the liquids become horizontally stratified and convective fractionation takes place till the "roll-over" of the chamber (Rice, 1981). When a less dense liquid enters the chamber system, immediate mixing occurs due to turbulent plume formation (Sparks and Huppert, 1984). In the case of denser liquid projecting upon entry into the chamber to higher levels due to its velocity momentum, it will always subside back to the bottom of the chamber (Turner and Gustafson, 1978). The dynamic

processes in MOR magma chambers predicted by such a model are compatible with petrologic models arguing for picritic parental magmas (Green et al., 1979). Following the discussion of chapter nine, it is very unlikely that picrites enter the magma chamber beneath the rift valley, and the "picrite paradox" is not a major problem in the basalt, in particular MORB, petrogenesis.

The presence of magmatic currents in the large basic continental layered complexes is well documented (Irvine, 1980). Although some structures of the Macquarie Island layered rocks resemble those structures, it is very unlikely that extensive magmatic current circulation and layer deposition took place immediately beneath the ridge axis. The occurrence of the uppermost laminated gabbros provides some evidence for the operation of such convection currents. The characteristics of these layers (isomodal with intrusive relations) indicate that crystallisation occurred in-situ and was frequently interrupted by new magma influxes. The small scale layering features can be explained by double-diffusive convection and bottom crystallisation (Irvine, 1980); here, it is assumed that individual layers or packets of layers belong to a single batch of magma input and crystallisation cycle. This involves the gravitational stratification of the liquid into horizontal layers and the development of convection cells in a layer-to-layer scale. Such a mechanism can account for the irregular distribution of olivine and plagioclase between adjacent layers.

10.6 Conclusions

The main conclusions of this section in conjunction with inferences from the previous chapters of this thesis have as follows:

1. The thickness of the Macquarie Island plutonic suite is about 2km. The exposed sequence of layered rocks is less thick (≤ 1.5 km) than that in other ophiolites. Pyroxenites, norites, podiform chromite deposits and late stage

felsic differentiates are very common in ophiolite complexes, but absent in Macquarie Island. In ophiolites, pyroxenes precede plagioclase crystallisation; in contrast, plagioclase always appears before clinopyroxene in Macquarie Island.

2. Thick sections of tectonised peridotites are exposed in many ophiolites. The harzburgite of Macquarie Island forms only a very narrow zone along the west coast. In both ophiolites and Macquarie Island, these peridotites are depleted and refractory in composition indicating a residual origin. The partial melting event which produced the Macquarie Island harzburgites was confined in the four phase volume Ol-En-Di-Sp, whereas the partial melting event(s) that produced the ophiolite peridotites advanced in the three phase volume Ol-En-Sp, eliminating so Di from the residue.

3. The Macquarie Island layered rocks are adcumulates. The compositions of their constituent cumulus minerals show limited variations. Compositionally, the cumulus minerals of the layered rocks and the phenocrysts of olivine/ spinel/ plagioclase/ clinopyroxene in the basalts-dolerites are identical. In addition, crystallisation modelling and least squares calculations also suggest that the major element compositions of basalts and dolerites are buffered by cumulus crystallisation in a crustal magma chamber.

4. The geochemical characteristics of the plutonic rocks (layered rocks and massive gabbros) are comparable to the high-Ti or MORB-type ophiolite plutonics. Such complexes originated in major oceanic basins, away from the influence of any subduction zones. The geochemical features are also supported by the crystallisation order Ol-→Plag-→Cpx which is similar to the low-pressure crystallisation order of MORBs.

5. The size of the magma chamber can be predicted by the thickness of the layered rocks. A total thickness of 1km to 1.5km is inferred from field relations. The lateral extent of such a magma chamber is difficult to evaluate due to the non-continuous lateral outcrop of the layered rocks. In any case, it cannot be of the order of 6km, as has been suggested by Kuszniir and Bott (1976). The more

likely magnitude is around 1km; the half-spreading rate for the existence of such a chamber width must be very small, possibly less than 1cm/year. Such a spreading rate however is too small for the existence and maintainance of a magma chamber according to Lister's (1983) calculations.

6. The magma chamber is an open plumbing system. Input of primitive basaltic melts, crystallisation, and extrusion of lavas are balanced in a steady state period. Primitive lavas mark the early stages of magma chamber formation and development. Crystallisation in the magma chamber occurs in-situ at the walls and on the floor. Accumulate rocks form through fractional crystallisation processes such as convective fractionation which are driven by convection.

7. The massive gabbros overlying the cumulates form a 500m to less than 1km thick horizon. They represent rocks crystallised at the roof of the magma chamber. Their position in the sequence and bulk rock chemistry indicate that they are liquids crystallising at the base of the dyke swarms (Sheeted Dykes), underplating so the upper crustal sequence and isolating the magma chamber beneath. Their stratigraphic position and thickness also suggests an inverted funnel-shaped magma chamber (see also Pallister and Hopson, 1981).

8. Pillow lavas and massive lava flows (mainly) make-up the volcanic section. Their mineralogy and geochemistry show a range from tholeiitic to alkalic compositions. Their geochemical characteristics as well as the composition of the spinel phenocrysts differ markedly to those of ophiolitic lavas, but are comparable to those of abyssal basalts.

9. The alkalic lavas sit on top of the tholeiitic lavas; they are also metamorphosed to lower grades than the tholeiitic ones. The alkalic basalts have incompatible element enrichments and incompatible element ratios similar to the "enriched" type MORBs. The obvious explanation would be their production by an "enriched" mantle. Very rarely, the alkalic basalts carry olivine and spinel "xenocrysts" which are more magnesian than those of the basal cumulate troctolites. Their spatial distribution and geochemical-mineralogic features

together with inferences from well constrained petrogenetic modelling on magma generation in the upper mantle by McKenzie and Bickle (1988) suggest that these alkalic basalts have been produced by small degrees of partial melting, possibly at more than 13kb pressure, of a homogeneous source. Their extrusion has taken place at the early rifting stages, when a magma chamber had not developed (or was in an immature stage) or/and at the closing stages of a volcanic cycle, when the magma chamber had solidified.

The tholeiitic basalts represent large degrees of partial melting, 20%-25%, at shallow depths, approximately <30km. Although some incompatible element concentrations of the tholeiitic and alkalic basalts can be explained by binary mixing of a "depleted" and an "enriched" component as shown in figure 9.14, it is more likely that the observed compositional range resulted from polybaric mixing of melts produced by different degrees of partial melting. This petrogenetic model provides an intergrated framework for basalt generation in a convecting upper mantle without resorting to mantle heterogeneity and ambiguous mantle metasomatism processes. However, isotopic data on Sr, Nd and Pb are required to corroborate this conclusion.

REFERENCES

- Abrajano, T.A., Pasteris, J.D. and Bacuta, G.C. (1989). Zambales ophiolite, Philippines, I. Geology and petrology of the critical zone of the Acoje massif. *Tectonophysics* 168, 65-100.
- Ahern, J.L. and Turcotte, D.A. (1979). Magma migration beneath an ocean ridge. *Earth Plan. Sci. Lett.* 45, 115-122.
- Anderson, D.L. (1983). Chemical composition of the mantle. *Proc. Lunar Sci. Conf. 4th. J. Geophys. Res.* 88 Suppl., B41-B52.
- Arculus, R.J. and Delano, J.W. (1981). Intrinsic oxygen fugacity measurements: Techniques and results for spinels from upper mantle peridotites and megacryst assemblages. *Geoch. Cosmoch. Acta* 45, 899-913.
- Atkins, F.B. (1969). Pyroxenes of the Bushveld intrusion. *J. Petrology* 10, 222-249.
- Aumento, F. (1968). The Mid-Atlantic Ridge near 45°N. II: Basalts from the Confederation Peak. *Can. J. Earth Sci.* 5, 1-21.
- Aumento, F. and Loubat, H. (1971). The Mid-Atlantic ridge near 45°16'N: serpentinised ultramafic intrusions. *Can. J. Earth Sci.* 8, 631-663.
- Banghar, A.R. and Sykes, L.R. (1969). Focal mechanisms of earthquakes in the Indian ocean and adjacent regions. *J. Geophys. Res.* 74, 632-649.
- Basaltic Volcanism Study Project (1981). Basaltic volcanism in the terrestrial planets. Pergamon Press.
- Beccaluva, L.D., Di Girolamo, P., Macchiotta, G. and Morra, V. (1983). Magma affinities and fractionation trends in ophiolites. *Ophioliti* 8, 307-324.
- Beccaluva, L., Ohnenstetter, D., Ohnenstetter, M. and Paupy, A. (1984). Two magmatic series with island arc affinities within the Yourinos ophiolite. *Contr. Mineral. Petrol.* 85, 253-271.
- Bence, A.E., Bayliss, D.M., Bender, J.F. and Grove, T.L. (1979). Controls on the major and minor element chemistry of mid-ocean ridge basalts and glasses. In: *Deep Drilling Results in the Atlantic Ocean: Ocean Crust*, M. Talwani, C.G. Harrison and D.E. Hayes (ed.), American Geophys. Union, 331-341.
- Bender, J.F., Hodges, F.N. and Bence, A.E. (1978). Petrogenesis of basalts from the project FAMOUS area: experimental study from 0 to 15 kbars. *Earth Plan. Sci. Lett.* 41, 277-302.
- Bender, J.F., Langmuir, C.H. and Hanson, G.N. (1984). Petrogenesis of basalt glasses from the Tamayo Region, East Pacific Rise. *J. Petrology* 25, 213-254.
- Beeson, M.H. and Jackson, E.D. (1969). Chemical composition of altered chromites from the Stillwater Complex, Montana. *Amer. Mineral.* 54, 1084-1100.

- Bickle, M.J., Ford, C.E. and Nisbet, E.G. (1977). The petrogenesis of peridotitic komatiites: evidence from high pressure melting experiments. *Earth Plan. Sci. Lett.* 37, 97-106.
- Biggar, G.M. (1983). Crystallization of plagioclase, augite and olivine in synthetic systems and in tholeiites. *Mineral. Mag.* 47, 161-176.
- Bonatti, E. and Honnorez, J. (1976). Sections of the Earth's crust in the Equatorial Atlantic. *J. Geophys. Res.* 81, 4104-4116.
- Bonatti, E., Ottonello, G., and Hamlyn, P.R. (1986). Peridotites from the island of Zabargad (St. John), Red Sea: petrology and geochemistry. *J. Geophys. Res.* 91, 599-631.
- Boudier, F. (1978). Structure and petrology of the Lanzo peridotite massif (Piedmont Alps). *Bull. Geol. Soc. Amer.* 89, 1574-1591.
- Boudier, F. and Coleman, R.G. (1981). Cross section through the peridotite in the Samail Ophiolite, Southeastern Oman Mountains. *J. Geophys. Res.* 86, 2573-2592.
- Bougault, H., Cambon, P., Corre, O., Joron, J-L. and Treuil, M. (1979a). Evidence for variability of magmatic processes and upper mantle heterogeneity in the axial region of the Mi-Atlantic Ridge near 22°N and 36°N. *Tectonophysics* 55, 11-34.
- Bougault, H., Joron, J-L. and Treuil, M. (1979b). Alteration, fractional crystallization, partial melting, mantle properties from trace elements in basalts recovered in the North Atlantic. In: *Deep Drilling Results in the Atlantic Ocean: Ocean Crust*, M. Talwani, C.G. Harrison and D.E. Hayes (ed.), American Geophys. Union, 352-368.
- Bowen, N.L. (1928). The evolution of the igneous rocks. Princeton University Press, 332p.
- Bratt, S.R. and Solomon, S.C. (1984). Compressional and shear wave structure of the East Pacific Rise at 11°20'N: constraints from three component ocean bottom seismometer data. *J. Geophys. Res.* 89, 6095-6110.
- Bryan, W.B. (1974). Fe-Mg Relationships in sector-zoned submarine basalt plagioclase. *Earth Plan. Sci. Lett.* 24, 157-164.
- Bryan, W.B. (1979). Regional variation and petrogenesis of basalt glasses from the FAMOUS area, Mid-Atlantic Ridge. *J. Petrology* 20, 293-325.
- Bryan, W.B. and Moore, J.G. (1977). Compositional variations of young basalts in the Mid-Atlantic Ridge rift valley near latitude 36°49'N. *Geol. Soc. Amer. Bull.* 88, 556-570.

- Bryan, W.B., Thompson, G., Frey, F.A. and Dickey, J.S. (1976). Inferred geologic settings and differentiation in basalts from the deep sea drilling project. *J. Geophys. Res.* 81, 4285-4304.
- Bryan, W.B., Thompson, G. and Frey, F.A. (1979a). Petrologic character of the Atlantic crust from DSDP and IPOD drill sites. In: *Deep Drilling Results in the Atlantic Ocean: Ocean Crust*, M. Talwani, C.G. Harrison and D.E. Hayes (ed.), American Geophys. Union, 273-284.
- Bryan, W.B., Thompson, G., and Michael, P.J. (1979b). Compositional variation in a steady state zoned magma chamber: mid-Atlantic ridge at 36°50'N. *Tectonophysics* 55, 63-85.
- Bryan, W.B., Thompson, G., and Ludden, J.N. (1981). Compositional variation in normal MORB from 22°-25°N: Mid-Atlantic Ridge and Kane Fracture zone. *J. Geophys. Res.* 86, 11815-11836.
- Buhl, P., Mutter, J.C., Vera, E.E., Barth, G.A., Detrick, R., Madsen, J., Orcutt, J.A. and Brocher, J. (1986). Along axis variability in the crustal magma chamber at the East Pacific Rise between 8°50'N and 13°30'N. *EOS (abstracts)*, 67, 1243.
- Burns, R.G. (1970). Site preferences of transition metal ions in silicate crystal structures. *Chem. Geology* 5, 275-283.
- Burns, R.G. (1973). The partitioning of trace transition elements in crystal structures: a provocative review with applications to mantle geochemistry. *Geoch. Cosmoch. Acta* 73, 2395-2403.
- Butler, R.F., Banerjee, S.K. and Stout, J.H. (1976). Magnetic properties of oceanic pillow basalts: evidence from Macquarie Island. *Geophys. J. Royal Astron. Soc.* 47, 179-196.
- Cameron, W.E. (1985). Petrology and origin of the primitive lavas from the Troodos ophiolite, Cyprus. *Contr. Mineral. Petrol.* 89, 239-255.
- Cameron, W.E., Nisbet, E.G. and Dietrich, V.J. (1980). Petrographic dissimilarities between ophiolitic and ocean-floor basalts. In: *Proceedings International Ophiolite Symposium, Cyprus 1979*, A. Panayiotou (ed.), Geological Survey Department of Cyprus, Nicosia, 182-192.
- Campbell, I.H. (1978). Some problems with the cumulus theory. *Lithos* 11, 311-323.
- Cann, J.R. (1974). A model for oceanic crustal structure developed. *Geophys. J. Royal Astron. Soc.* 39, 169-187.
- Carmichael, I.S.E., Turner, F.J. and Verhoogen, J. (1974). *Igneous Petrology*. McGraw-Hill Publ. Company.

- Cassard, D., Nicolas, A., Rabinovitch, M., Muette, J., Leblanc, M. and Prinzhofer, A. (1981). Structural classification of chromite pods in Southern New Caledonia. *Econ. Geol.* 76, 805-831.
- Ceuleneer, G. and Nicolas, A. (1985). Structures in podiform chromite from the Masqad district (Samail ophiolite, Oman). *Mineral. Deposita* 20, 177-185.
- Chen, C.F. and Turner, J.S. (1980). Crystallization in a double diffusive system. *J. Geophys. Res.* 85, 2573-2593.
- Christie, D.M. and Sinton, J.M. (1981). Evolution of abyssal lavas along propagating segments of the Galapagos spreading center. *Earth Plan. Sci. Lett.* 56, 321-335.
- Christie, D.M., Carmichael, I.S.E. and Langmuir, C.H. (1986). Oxidation states of mid-ocean ridge glasses. *Earth Plan. Sci. Lett.* 79, 397-411.
- Christodoulou, C. and Hirst, D.M. (1985). The chemistry of chromite from two mafic-ultramafic complexes in Northern Greece. *Chem. Geology* 49, 415-428.
- Coleman, R.G. (1977). *Ophiolites. Ancient Oceanic Lithosphere?* Springer-Verlag, 230p.
- Coleman, R.G. and Keith, T.E. (1971). A chemical study of serpentinization, Burro Mountain, California. *J. Petrology* 12, 311-328.
- Coleman, R.G. and Peterman, Z.E. (1975). Oceanic Plagiogranite. *J. Geophys. Res.* 80, 1099-1108.
- Davidson, P.M., Grover, J. and Lindsley, D.H. (1982). $(Ca,Mg)_2Si_2O_6$ Clinopyroxenes: A solution model based on nonconvergent site-disorder. *Contr. Mineral. Petrol.* 80, 88-102.
- Davis, B.T.C. and Boyd, F.R. (1966). The join $Mg_2Si_2O_6 - CaMgSi_2O_6$ at 30kbars pressure and its application to pyroxenes from kimberlites. *J. Geophys. Res.* 71, 3567-3576.
- Den Tex, E. (1969). Origin of ultramafic rocks, their tectonic setting and history: a contribution to the discussion of the paper "The origin of ultramafic and ultrabasic rocks" by P.J. Wyllie. *Tectonophysics* 7, 547-588.
- Dewey, J.F. and Kidd, W.S.F. (1977). Geometry of plate accretion. *Geol. Soc. Amer. Bull.* 88, 960-968.
- Dick, H.J.B. (1977). Partial melting in the Josephine peridotite I, the effect on mineral composition and its consequence for geobarometry and geothermometry. *Amer. J. Sci.* 277, 801-832.
- Dick, H.J.B. and Bryan, W.B. (1978). Variation of basalt phenocryst mineralogy and rock compositions in DSDP hole 396B. DSDP Leg 46, Initial Rep. DSDP Vol. 46, 215-225.

- Dick, H.J.B. and Bullen, T. (1984). Chromian spinel as a petrogenetic indicator in abyssal and alpine-type peridotites and spatially associated lavas. *Contr. Mineral. Petrol.* 86, 54-76.
- Dick, H.J.B. and Fisher, R.L. (1984). Mineralogic studies of the residues of mantle melting: Abyssal and alpine-type peridotites. In: J. Kornprobst (ed.), *Kimberlites II: The mantle and crust-mantle relationships*, 295-308. Elsevier Sci. Publ.
- Dick, H.J.B., Fisher, R.L. and Bryan, W.B. (1984). Mineralogic variability of the uppermost mantle along the mid-ocean ridges. *Earth Plan. Sci. Lett.* 69, 88-106.
- Dickey, J.S. Jr. (1975). An hypothesis of origin for podiform chromite deposits. *Geoch. Cosmoch. Acta* 39, 1061-1074.
- Dickey, J.S. Jr., Yoder, H.S. and Schairer, J.F. (1971). Chromium in silicate oxide systems. *Carnegie Instit. Washington Yearb.* 70, 118-122.
- Dmitriev, L.V., Sobolev, A.V., Uchanov, A.V., Malysheva, T.V. and Melson, W.G. (1984). Primary differences in oxygen fugacity and depth of melting in the mantle source regions for oceanic basalts. *Earth Plan. Sci. Lett.* 70, 303-310.
- Donaldson, C.H. and Brown, R.W. (1977). Refractory megacrysts and magnesium rich melt inclusions within spinel in oceanic tholeiites: indicators of magma mixing and parental magma composition. *Earth Plan. Sci. Lett.* 37, 81-89.
- Drake, M.J. and Holloway, J.R. (1981). Partitioning of Ni between olivine and silicate melt: the "Henry's law problem" re-examined. *Geoch. Cosmoch. Acta* 45, 431-437.
- Duncan, R.A. and Green, D.H. (1980). Role of multistage melting in the formation of oceanic crust. *Geology* 8, 22-26.
- Duncan, R.A. and Varne, R. (1988). The age and distribution of the igneous rocks of Macquarie Island. In: *Papers and Proceedings Royal Soc. Tasmania*, (ed.) M. R. Banks and S. J. Smith, Vol. 122 (Part I), 45-50.
- Dungan, M.A. and Rhodes, J.M. (1978). Residual glasses and melt inclusions in basalts from DSDP Legs 45 and 46: Evidence for magma mixing. *Contr. Mineral. Petrol.* 67, 417-431.
- Elthon, D. and Scarfe, C.M. (1984). High-pressure phase equilibria of a high-magnesia basalt and the genesis of primary oceanic basalts. *Amer. Mineral.* 69, 1-15.
- Engin, T. and Hirst, D.M. (1970). Serpentinization of harzburgites from the alpine peridotite belt of Southwest Turkey. *Chem. Geology* 6, 281-295.
- Engin, T. and Aucott, J.W. (1971). A microprobe study of chromites from the Andizlik-Zimparalik area, Southwest Turkey. *Mineral. Mag.* 38, 76-82.

- England, R.N. and Davies, H.L. (1973). Mineralogy of ultramafic cumulates and tectonites from Eastern Papua. *Earth Plan. Sci. Lett.* 17, 416-425.
- Erlank, A.J. and Kable, E.J.D. (1976). The significance of incompatible elements in Mid-Atlantic Ridge Basalts from 45°N with particular reference to Zr/Nb. *Contr. Miner. Petrol.* 54, 281-291.
- Evans, B.W. (1977). Metamorphism of alpine peridotite and serpentinite. *Ann. Reviews Earth Plan. Sci.* 5, 397-447.
- Evans, B.W. and Frost, B.R. (1975). Chrome-spinel in progressive metamorphism—a preliminary analysis. *Geoch. Cosmoch. Acta* 39, 959-972.
- Evans, B.W. and Wright, T.L. (1972). Composition of liquidus chromite from the 1959 (Kilauea Iki) and 1965 (Makaopuhi) eruptions of Kilauea volcano, Hawaii. *Amer. Mineral.* 57, 217-230.
- Evans, C. (1985). Magmatic "metasomatism" in peridotites from the Zambales Ophiolite. *Geology* 13, 166-169.
- Fabries, J. (1979). Spinel-olivine geothermometry in peridotites from ultramafic complexes. *Contr. Miner. Petrol.* 69, 329-336.
- Fisk, M.R. and Bence, A.E. (1980). Experimental crystallisation of chrome spinel in FAMOUS basalt 527-1-1. *Earth Plan. Sci. Lett.* 48, 111-123.
- Flower, M.F.J. (1980). Accumulation of calcic plagioclase in ocean ridge tholeiite: an indication of spreading rate? *Nature* 287, 530-532.
- Flower, M.F.J. and Robinson, P.T. (1979). Evolution of the FAMOUS ocean ridge segment: Evidence from submarine and deep sea drilling investigations. In: *Deep Drilling Results in the Atlantic Ocean: Ocean Crust*, M. Talwani, C.G. Harrison and D.E. Hayes (ed.), American Geophys. Union, 314-330.
- Frey, F.A. and Prinz, M. (1978). Ultramafic inclusions from San Carlos, Arizona: petrologic and geochemical data bearing on their petrogenesis. *Earth Plan. Sci. Lett.* 38, 129-176.
- Frey, F.A., Bryan, W.B. and Thompson, G. (1974). Atlantic ocean floor: geochemistry and petrology of basalts from Legs 2 and 3 of the Deep Sea Drilling Project. *J. Geophys. Res.* 79, 5507-5527.
- Fudali, R.F. (1965). Oxygen fugacities of basaltic and andesitic magmas. *Geoch. Cosmoch. Acta* 29, 10-63.
- Fujii, T. (1978). Fe-Mg partitioning between olivine and spinel. *Carnegie Instit. Washington Yearb.* 76, 563-569.
- Fujii, T. and Bougault, H. (1983). Melting of a magnesian abyssal tholeiite and the origin of MORBs. *Earth Plan. Sci. Lett.* 62, 283-295.
- Fujii, T. and Kushiro, I. (1977a). Melting relations and viscosity of an abyssal tholeiite. *Carnegie Instit. Washington Yearb.* 76, 461-465.

- Fujii, T. and Kushiro, I. (1977b). Density, viscosity and compressibility of basaltic liquid at high pressure. *Ann. Rep. Dir. Geophysical Lab. Carnegie Instit.* 76, 419-424.
- Fujii, T. and Scarfe, C.M. (1985). Composition of liquids coexisting with spinel lherzolite at 10 kbar and the genesis of MORBs. *Contr. Miner. Petrol.* 90, 18-28.
- Furuta, T. and Tokuyama, H. (1983). Chromian spinels in Costa Rica basalts, deep sea drilling project site 505. A preliminary interpretation of electron microprobe analyses. *DSDP Leg 69, Initial Rep. DSDP Vol. 69*, 805-810.
- Gass, I.G. (1958). Ultramafic pillow lavas from Cyprus. *Geol. Magazine* 95, 211-251.
- Gass, I.G. and Smewing, J.D. (1973). Intrusion, extrusion and metamorphism at constructive margins: evidence from the Troodos massif, Cyprus. *Nature* 242, 26-29.
- Gast, P.W. (1968). Trace element fractionation and the origin of tholeiitic and alkaline magma types. *Geoch. Cosmoch. Acta* 32, 1057-1068.
- Girardeau, J. and Nicolas, A. (1981). The structures of two ophiolite massifs, Bay of Islands, Newfoundland: a model for the oceanic crust and upper mantle. *Tectonophysics* 77, 1-34.
- Glazner, A.F. (1984). Activities of olivine and plagioclase components in silicate melts and their application to geothermometry. *Contr. Mineral. Petrol.* 88, 260-268.
- Green, D.H. and Ringwood, A.E. (1967). The genesis of basaltic magmas. *Contr. Mineral. Petrol.* 15, 103-190.
- Green, D.H., Ringwood, A.E., Ware, N.G. and Hibberson, W.D. (1972). Experimental petrology and petrogenesis of Apollo 14 basalts. *Proc. Lun. Sci. Conf. 3rd, Geoch. Cosmoch. Acta Suppl.* 3, 197-206.
- Green, D.H., Hibberson, W.D. and Jaques, A.L. (1979). Petrogenesis of mid-ocean ridge basalts. In: M.W. McElhinny (ed.), *The Earth, its origin, structure and evolution*. Academic Press, 165-299.
- Greenbaum, D. (1972). The geology and evolution of the Troodos plutonic complex and associated chromite deposits. Unpubl. Ph.D. thesis, University of Leeds, England.
- Greenbaum, D. (1977). The chromiferous rocks of the Troodos Ophiolite Complex, Cyprus. *Econ. Geology* 72, 1175-1194.
- Griffin, B.J. (1982). Igneous and Metamorphic petrology of lavas and dykes of the Macquarie Island ophiolite complex. Unpubl. Ph.D. thesis, University of Tasmania.

- Griffin, B.J. and Varne, R. (1980). The Macquarie Island ophiolite complex: mid-Tertiary oceanic lithosphere from a major ocean basin. *Chem. Geology* 30, 285-308.
- Grove, T.L. and Bryan, W.B. (1983). Fractionation of pyroxene-phyric MORBs at low pressure: An experimental study. *Contr. Mineral. Petrol.* 84, 293-309.
- Höckli, T.A. and Wright, T.L. (1967). The fractionation of nickel between olivine and augite as a geothermometer. *Geoch. Cosmoch. Acta* 31, 877-884.
- Hamlyn, P.R. and Bonatti, E. (1980). Petrology of mantle derived ultramafics from the Owen fracture zone, Northwest Indian ocean: Implications for the nature of the oceanic upper mantle. *Earth Plan. Sci. Lett.* 48, 65-79.
- Hanson, G.N. and Langmuir, C.H. (1978). Modelling of major elements in mantle-melt systems using trace element approaches. *Geoch. Cosmoch. Acta* 42, 725-741.
- Hart, S.R. and Davis, K.E. (1978). Nickel partitioning between olivine and silicate melt. *Earth Plan. Sci. Lett.* 40, 203-219.
- Hart, S.R., Erlank, A.J. and Kable, E.J.D. (1974). Sea floor basalt alteration: Some chemical and Sr isotopic effects. *Contr. Mineral. Petrol.* 44, 219-230.
- Hayes, D.E. and Talwani, M. (1972). Geophysical investigation of the Macquarie Ridge complex. In: D.E. Davies (ed.), *Antarctic Oceanology II, The Australian - New Zealand Sector*. Antarctic Res. Series 19, 211-234.
- Hebert, R., Bideau, D. and Hekinian, R. (1983). Ultramafic and mafic rocks from the Garret transform fault near 13°30'S on the East Pacific Rise: Igneous petrology. *Earth Plan. Sci. Lett.* 65, 107-125.
- Heirtzler, J.R., Dickson, G.O., Herron, E.M., Pitman, W.C. and LePichon, X. (1968). Marine magnetic anomalies, geomagnetic field reversals and motions of the ocean floor and continents. *J. Geophys. Res.* 73, 2119-2136.
- Hekinian, R. and Aumento, E. (1973). Rocks from the Gibbs Fracture zone and the Minia seamount near 53°N in the Atlantic ocean. *Mar. Geology* 14, 47-72.
- Herzberg, C.T. (1978). Pyroxene geothermometry and geobarometry: Experimental and thermodynamic evaluation of some subsolidus phase relations involving pyroxenes in the system CaO-MgO-Al₂O₃-SiO₂. *Geoch. Cosmoch. Acta* 42, 945-957.
- Hill, R.E. (1977). Three gabbros from DSDP Leg 37, site 334. Their petrography and pyroxene mineralogy. Initial Rep. DSDP Vol. 37, 763-768.
- Hill, R.E. and Roeder, P.L. (1974). The crystallisation of spinel from basaltic liquid as a function of oxygen fugacity. *J. Geology* 82, 709-72
- Hodges, F.N. and Papike, J.J. (1976). DSDP Site 334: Magmatic cumulates from oceanic layer 3. *J. Geophys. Res.* 81, 4135-4151.

- Hofmann, A.W. and Hart, S.R. (1978). An assessment of local and regional isotopic equilibrium in the mantle. *Earth Plan. Sci. Lett.* 38, 44-62.
- Holland, T.J.B., Navrotsky, A. and Newton, R.C. (1979). Thermodynamic parameters of $\text{CaMgSi}_2\text{O}_6$ - $\text{Mg}_2\text{Si}_2\text{O}_6$ pyroxenes based on regular solution and cooperative disordering models. *Contr. Mineral. Petrol.* 69, 323-344.
- Honnorez, J. and Bonatti, E. (1970). Nepheline gabbro from the Mid- Atlantic Ridge. *Nature* 228, 850-851.
- Honnorez, J. and Kiser, P. (1975). Petrology of rodingites from the equatorial mid-Atlantic fracture zone and their geotectonic significance. *Contr. Mineral. Petrol.* 49, 233-257.
- Hoover, J.D. and Presnall, D.C. (1982). Melting relations of simplified peridotite in the SiO_2 - CaO - Al_2O_3 - MgO - Na_2O system from 1 atm to 20 kb, II: Results and application to basalt generation. *Geol. Soc. Amer. Abstr. Program.* 14, 517.
- Hopson, C.A., Coleman, R.G., Gregory, R.T., Pollister, J.S., and Bailey, E.H. (1981). Geologic cross section through the Samail ophiolite and associated rocks along a Muscat-Ibra transect, Southeastern Oman Mountains. *J. Geophys. Res.* 86, 2527-2544.
- Houtz, R.E., Ewing, J. and Embley, R. (1972). Profiler data from the Macquarie ridge area. In: D.E. Davies (ed.), *Antarctic Oceanology II, The Australian - New Zealand Sector.* Antarctic Res. Series 15, 239-245.
- Humphris, S.E. and Thompson, G. (1983). Geochemistry of rare earth elements in basalts from the Walvis Ridge: implications for its origin and evolution. *Earth Plan. Sci. Lett.* 66, 223-242.
- Humphris, S.E., Thompson, G., Schilling, J-G. and Kingsley, R.H. (1985). Petrological and geochemical variations along the Mid-Atlantic Ridge between 46°S and 32°S : influence of the Tristan da Cunha mantle plume. *Geoch. Cosmoch. Acta* 49, 1445-1464.
- Huebner, J.S. (1980). Pyroxene phase equilibria at low pressure. *Reviews Mineral.* 7, 213-288.
- Huppert, H.E. and Sparks, R.S.J. (1980). Restrictions on the compositions of mid-ocean ridge basalts: a fluid dynamical investigation. *Nature* 286, 46-48.
- Huppert, H.E. and Turner, J.S. (1981). A laboratory model of a replenished magma chamber. *Earth Plan. Sci. Lett.* 54, 144-152.
- Irvine, T.N. (1965). Chromian spinel as a petrogenetic indicator. Part 1: Theory. *Can. J. Earth Sci.* 2, 648-672.
- Irvine, T.N. (1967). Chromian spinel as a petrogenetic indicator. Part 2: Petrologic applications. *Can. J. Earth Sci.* 4, 71-103.

- Irvine, T.N. (1970). Crystallization sequences in the Muskox intrusion and other layered intrusions. *Geol. Soc. South Africa Special Publ.* 1, 441-476.
- Irvine, T.N. (1977). Definition of primitive liquid compositions for basic magmas. *Carnegie Instit. Washington Yearb.* 76, 454-461.
- Irvine, T.N. (1980). Magmatic density currents and cumulus processes. *Amer. J. Sci.* 280-A, 1-58.
- Irvine, T.N. (1982). Terminology for layered intrusions. *J. Petrology* 23, 127-162.
- Irvine, T.N. and Findlay, T.C. (1972). Alpine type peridotites with particular reference to the Bay of Islands igneous complex. *Publ. Earth Physics Branch Dept. Energy & Mines Res. Canada* 42, 97-128.
- Irvine, T.N. and Kushiro, I. (1976). Partitioning of Ni and Mg between olivine and silicate liquids. *Carnegie Instit. Washington Yearb.* 75, 669-675.
- Ito, E. and Anderson, A.T. Jr. (1983). Submarine metamorphism of Gabbros from the Mid-Cayman Rise: Petrographic and mineralogic constraints on hydrothermal processes at slow spreading ridges. *Contr. Mineral. Petrol.* 82, 371-388.
- Jackson, E.D. (1969). Chemical variation in coexisting chromite and olivine in chromitite zone of the Stillwater Complex. In: *Magmatic Ore Deposits*, H.D.B. Wilson (ed.), *Econ. Geol. Mon.* 4, 41-71.
- Jackson, E.D., Green, H.W. and Moores, E.M. (1975). The Vourinos Ophiolite, Greece: Cyclic units of lineated cumulates overlying harzburgite tectonite. *Geol. Soc. Amer. Bull.* 86, 390-398.
- Jagoutz, E., Palme, H., Baddenhausen, H., Blum, K., Cendales, M., Dreibus, G., Spettel, B., Lorenz, V. and Wanke, H. (1979). The abundances of major, minor, and trace elements in the earth's mantle as derived from primitive ultramafic nodules. *Proc. Lunar Sci. Conf.* 10th, 2031-2050.
- Jaques, A.L. (1981). Petrology and petrogenesis of cumulate peridotites and gabbros from the Marum Ophiolite Complex, Northern Papua New Guinea. *J. Petrology* 22, 1-40.
- Jaques, A.L. and Green, D.H. (1980). Anhydrous melting of peridotite at 0-15 kbar pressure and the genesis of tholeiitic basalts. *Contr. Mineral. Petrol.* 73, 287-310.
- Johannes, W. (1968). Experimental investigation of the reaction $\text{fosterite} + \text{H}_2\text{O} \rightarrow \text{serpentine} + \text{brucite}$. *Contr. Mineral. Petrol.* 19, 75-98.
- Jenner, G.A. and Green, D.H. (1983). Equilibria in the Mg-rich part of the pyroxene quadrilateral. *Mineral. Mag.* 47, 153-160.
- Johnson, T. and Molnar, P. (1972). Focal mechanisms and plate tectonics of the southwest Pacific. *J. Geophys. Res.* 77, 5000-5050.

- Jones, J.H. (1984). Temperature- and pressure- independent correlation of olivine/liquid partition coefficients and their application to trace element partitioning. *Contr. Mineral. Petrol.* 88, 126-132.
- Jones, T.D. and McCue, K.F. (1988). The seismicity and tectonics of the Macquarie Ridge. In: *Papers and Proceedings Royal Soc. Tasmania*, (ed.) M. R. Banks and S. J. Smith, Vol. 122 (Part I), 51-57.
- Juteau, T. and Whitechurch, H. (1980). The magmatic cumulates of Antalya (Turkey): Evidence of multiple intrusions in a magma chamber. In: *Proceedings International Ophiolite Symposium, Cyprus, 1979*, A. Panayiotou (ed.), Geological Survey Department of Cyprus, Nicosia, 377-391.
- Kay, R., Hubbard, N.J. and Gast, P.W. (1970). Chemical characteristics and origin of ocean ridge volcanic rocks. *J. Geophys. Res.* 75, 1585-1613.
- Kilinc, A., Carmichael, I.S.E. and Sack, R.O. (1983). The ferric - ferrous ratio of natural silicate liquids equilibrated in air. *Contr. Mineral. Petrol.* 83, 136-140.
- Kretz, R. (1982). Transfer and exchange equilibria in a portion of the pyroxene quadrilateral as deduced from natural and experimental data. *Geoch. Cosmoch. Acta* 46, 411-421.
- Kuo, L.-C. and Kirkpatrick, R.J. (1982). Pre-eruption history of phyric basalts from DSDP Legs 45 and 46: Evidence from morphology and zoning patterns in plagioclase. *Contr. Mineral. Petrol.* 79, 13-27.
- Kushiro, I. (1960). Si-Al relation in clinopyroxenes from igneous rocks. *Amer. J. Sci.* 258, 548-554.
- Kushiro, I. and Thompson, R.N. (1972). Origin of some abyssal tholeiites from the mid-Atlantic ridge. *Carnegie Instit. Washington Yearb.* 71, 403-406.
- Kusznir, N.J. (1980). Thermal evolution of the oceanic crust: Its dependence on spreading rate and effect on crustal structure. *Geophys. J. Royal Astron. Soc.* 61, 167-181.
- Kusznir, N.J. and Bott, M.H.P. (1976). A thermal study of the formation of oceanic crust. *Geophys. J. Royal Astron. Soc.* 47, 83-95.
- Lago, B.J., Rabinowich, M. and Nicolas, A. (1982). Podiform chromite ore bodies: a genetic model. *J. Petrology* 23, 103-125.
- Langmuir, C.H. and Hanson, G.N. (1980). An evaluation of major element heterogeneity in the mantle sources of basalts. *Phil. Trans. Royal Soc. London A-* 297, 383-407.
- Langmuir, C.H. and Hanson, G.N. (1981). Calculating mineral-melt equilibria with stoichiometry, mass balance and single component distribution coefficients. S. K. Saxena (ed.), *Thermodynamics of minerals and melts*, 247-271, Springer-Verlag.

- Langmuir, C.H. and Bender, J.F. (1984). The geochemistry of oceanic basalts in the vicinity of transform faults: observation and implications. *Earth Plan. Sci. Lett.* 69, 107-127.
- Langmuir, C.H., Bender, J.F., Bence, A.E. and Hanson, G.N. (1977). Petrogenesis of basalts from the FAMOUS area: Mid-Atlantic Ridge. *Earth Plan. Sci. Lett.* 36, 133-156.
- Langmuir, C.H., Yocke, R.D., Hanson, G.N. and Hart, S.R. (1978). A general mixing equation with applications to Icelandic basalts. *Earth Plan. Sci. Lett.* 37, 380-392.
- Leake, B. (1978). Nomenclature of amphiboles. *Can. Mineral.* 16, 501-520.
- Leeman, W.P. (1978). Distribution of Mg^{2+} between olivine and silicate melt, and its implications regarding melt structure. *Geoch. Cosmoch. Acta* 42, 789-800.
- Leeman, W.P. and Lindstrom, D.J. (1978). Partitioning of Ni^{2+} between basaltic and synthetic melts and olivines. An experimental study. *Geoch. Cosmoch. Acta* 42, 801-816.
- Lehmann, J. (1983). Diffusion between olivine and spinel: application to geothermometry. *Earth Plan. Sci. Lett.* 64, 123-138.
- LeRoex, A.P. and Erlank, A.J. (1982). Quantitative evaluation of fractional crystallisation in Bouvet Island lavas. *J. Volcan. Geother. Res.* 13, 309-338.
- LeRoex, A.P., Erlank, A.J. and Needham, H.D. (1981). Geochemical and mineralogic evidence for the occurrence of at least three distinct magma types in the FAMOUS region. *Contr. Mineral. Petrol.* 77, 24-37.
- LeRoex, A.P., Dick, H.J.B., Erlank, A.J., Reid, A.M., Frey, F.A., and Hart, S.R. (1983). Geochemistry, mineralogy and petrogenesis of lavas erupted along the Southwest Indian Ridge between the Bouvet triple junction and 11 degrees east. *J. Petrology* 24, 267-318.
- LeRoex, A.P., Dick, H.J.B., Reid, A.M., Frey, F.A., Erlank, A.J., and Hart, S.R. (1985). Petrology and geochemistry of basalts from the American-Antarctic Ridge, Southern ocean: implications for the westward influence of the Bouvet mantle plume. *Contr. Mineral. Petrol.* 90, 367-380.
- Levi, S., Banerjee, S.K., Beske-Diehl, S. and Moskowitz, B. (1978). Limitations of ophiolite complexes as models for the magnetic layer of the oceanic lithosphere. *Geophys. Res. Letters* 5, 473-475.
- Lindsley, D.H. (1980). Phase equilibria of pyroxenes at pressures > 1 atm. *Reviews Mineral.* Vol. 7, 289-307.
- Lindsley, D.H. (1983). Pyroxene thermometry. *Amer. Mineral.* 68, 477-493.

- Lindsley, D.H. and Andersen, D.J. (1983). A two-pyroxene thermometer. *J. Geophys. Res.* 88, Supplement, A887-A906.
- Lindsley, D.H. and Dixon, S.A. (1976). Diopside - Enstatite equilibria at 850°C to 1400°C, 5 to 35 kbar. *Amer. J. Sci.* 276, 1285-1301.
- Lindsley, D.H., Grover, J.E. and Davidson, P.M. (1981). The thermodynamics of the $Mg_2Si_2O_6$ - $CaMgSi_2O_6$ join: A review and an improved model. In: *Thermodynamics of minerals and melts*, R. Newton, A. Navrotsky and B. J. Wood (eds.), 149-175, Springer-Verlag.
- Liou, J.G., Kuniyoshi, S. and Ito, K. (1974). Experimental studies on the phase relations between greenschist and amphibolite in a basaltic system, *Amer. J. Sci.* 274, 613-632.
- Lister, C. (1983). On the intermittency and crystallisation mechanisms of subseafloor magma chambers. *Geophys. J. Royal Astron. Soc.* 73, 351-356.
- Longhi, J., Walker, D. and Hays, J.F. (1975). Fe-Mg distribution between olivine and lunar basaltic liquids. *Amer. Geophys. Union Trans.* EOS 56, 471.
- Ludden, J.N. and Thompson, G. (1979). An evaluation of the behaviour of the rare earth elements during the weathering of the sea floor basalt. *Earth Plan. Sci. Lett.* 43, 85-92.
- Maeløe, S. (1979). Compositional range of primary tholeiitic magmas evaluated from major element trends. *Lithos* 12, 59-72.
- Maeløe, S. (1981). Magma accumulation in the ascending mantle. *J. Geol. Soc. London* 138, 223-236.
- Maeløe, S. and Aoki, K. (1977). The major element composition of the upper mantle estimated from the composition of lherzolites. *Contr. Mineral. Petrol.* 63, 161-173.
- Malpas, J. (1978). Magma generation in the upper mantle, field evidence from ophiolite suites and application to the generation of oceanic lithosphere. *Phil. Trans. Royal Soc. London A* 288, 527-545.
- Malpas, J. and Strong, D.F. (1975). A comparison of chrome spinels in ophiolites and mantle diapirs in Newfoundland. *Geoch. Cosmoch. Acta* 39, 1045-1060.
- Maurel, C. and Maurel, P. (1982a). Etude experimentale de la distribution de l'aluminium entre bain silicate basique et spinelle chromifere. Implications petrogenetiques: teneur en chrome spinelles. *Bull. Mineral.* 105, 197-202.
- Maurel, C. and Maurel, P. (1982b). Etude experimentale de la solubilité du chrome dans les bains silicates basiques et de sa distribution entre liquide et mineraux coexistants: conditions d'existence d spinelle chromifere. *Bull. Mineral.* 105, 640-647.

- Maurel, C. and Maurel, P. (1984a). Etude experimentale de la distribution de fer ferrique entre spinelle chromifere et silicate basique. Bull. Mineral. 107, 25-33.
- Maurel, C. and Maurel, P. (1984b). Etude experimentale de la distribution de fer ferreux et du magnesium entre spinelle chromifere et bain silicate basique. Bull. Mineral. 107, 767-776.
- Mawson, D. (1943). Macquarie Island, its geography and geology. Australasian Antarctic Expedition 1911-1914, Scientific Reports Series A5, 1-194p.
- McBirney, A.R. and Noyes, R.M. (1979). Crystallization and layering of the Skaergaard intrusion. J. Petrology 20, 487-554.
- McCulloch, M.T. and Cameron, W.E. (1983). Nd - Sr isotopic study of primitive lavas from the Troodos ophiolite, Cyprus: Evidence for a subduction related setting. Geology 11, 727-731.
- McKenzie, D. (1984). The generation and compaction of partially molten rock. J. Petrology 25, 713-765.
- McKenzie, D. (1985a). ^{230}Th - ^{238}U disequilibrium and the melting process beneath ridge axes. Earth Plan. Sci. Lett. 72, 149-157.
- McKenzie, D. (1985b). The extraction of magma from the crust and mantle. Earth Plan. Sci. Lett. 74, 81-91.
- McKenzie, D. and Bickle, M.J. (1988). The volume and composition of melt generated by extension of the lithosphere. J. Petrology 29, 625-679.
- Medaris, L.G. (1975). Coexisting spinel and silicates in alpine peridotites of the granulite facies. Geoch. Cosmoch. Acta 39, 947-958.
- Melson, W.G., Vallier, T.L., Wright, T.L., Buerly, G. and Nelen, J. (1976). Chemical diversity of abyssal volcanic glasses erupted along Pacific, Atlantic and Indian ocean-sea-floor spreading centres. Amer. Geophys. Union Monogr. 19, 351-368.
- Menzies, M. (1974). Petrogenesis of the Makirrakhi ultramafic complex. Unpubl. Ph.D. thesis, Cambridge University, England.
- Menzies, M. (1975). Spinel compositional variation in the crustal and mantle lithologies of the Othris Ophiolite. Contr. Miner. Petrol. 54, 303-309.
- Menzies, M. and Allen, C. (1974). Plagioclase lherzolite residual mantle relationships within two Eastern Mediterranean Ophiolites. Contr. Miner. Petrol. 45, 197-213.
- Michael, P.J. and Bonatti, E. (1985). Peridotite composition from the North Atlantic: Regional and tectonic variations and implications for partial melting. Earth Plan. Sci. Lett. 73, 91-104.
- Minster, J.B. and Jordan, T.H. (1978). Present day plate motions. J. Geophys. Res. 83, 5311-5354.

- Miyashiro, A. (1973). The Troodos ophiolite complex was probably formed in an island arc. *Earth Plan. Sci. Lett.* 19, 218-224.
- Miyashiro, A. and Shido, F. (1980). Differentiation of gabbros in the Mid-Atlantic Ridge near 24°N. *Geochemical Journal* 14, 145-154.
- Miyashiro, A., Shido, F. and Ewing, M. (1969a). Diversity and origin of abyssal tholeiite from the mid-Atlantic ridge near 24° and 30° north latitude. *Contr. Mineral. Petrol.* 23, 38-52.
- Miyashiro, A., Shido, F. and Ewing, M. (1969b). Composition and origin of serpentinites from the mid-Atlantic ridge near 24° and 30° north latitude. *Contr. Mineral. Petrol.* 23, 117-127.
- Miyashiro, A., Shido, F. and Ewing, M. (1970). Crystallization and differentiation in abyssal tholeiites and gabbros from mid-oceanic ridges. *Earth Plan. Sci. Lett.* 7, 361-365.
- Montigny, R., Bougault, H., Bottinga, Y., and Allegre, C.J. (1973). Trace element geochemistry and genesis of the Pindos ophiolite suite. *Geochim. Cosmoch. Acta* 37, 2135-47.
- Moody, J.B. (1976). Serpentinization: a review. *Lithos* 9, 125-138.
- Moody, J.B. (1979). Serpentinites, spilites and ophiolite metamorphism. *Can. Mineral.* 17, 871-887.
- Moody, J.B., Meyer, D. and Jenkins, J.E. (1983). Experimental characterization of the greenschist/amphibolite boundary in mafic systems. *Amer. J. Sci.* 283, 48-92.
- Moores, E.M. (1969). Petrology and structure of the Yourinos ophiolitic complex, Northern Greece. *Geol. Soc. Amer. Special Paper* 118, p.74p.
- Mori, T. and Green, D.H. (1975). Pyroxenes in the system $Mg_2Si_2O_6$ - $CaMgSi_2O_6$ at high pressure. *Earth Plan. Sci. Lett.* 26, 277-286.
- Morimoto, N., Fabries, J., Ferguson, A.K., Ginzburg, I.V., Ross, M., Seifert, F.A., Zussman, J., Aoki, K., Gottardi, G. (1988). Nomenclature of pyroxenes. *Amer. Mineral.* 73, 1123-1133.
- Morris, P.A. (1984). MAGFRAC: a basic program for least squares approximation of fractional crystallization. *Computers and Geoscience* 10, 437-444.
- Morse, S.A. (1980). *Basalts and Phase Diagrams*. Springer-Verlag.
- Mullen, E.D. (1983). MnO - TiO_2 - P_2O_5 : a minor element discriminant for basaltic rocks from oceanic environments and its implications for petrogenesis. *Earth Plan. Sci. Lett.* 62, 53-62.
- Mutter, J.C., Buhl, P., Vera, E.E., Barth, G.A., Orcutt, J.A. and Brocher, J. (1986). The shape and dimensions of axial magma chambers beneath the East Pacific Rise. *EOS (abstracts)*, 67, 1243.

- Mysen, B.O. (1975). Partitioning of iron and magnesium between crystals and partial melts in peridotite upper mantle. *Contr. Mineral. Petrol.* 52, 69-76.
- Mysen, B.O. (1979). Nickel partitioning between olivine and silicate melt: Henry's law revisited. *Amer. Mineral.* 64, 1107-1114.
- Mysen, B.O. and Kushiro, I. (1977). Compositional variation of coexisting phases with degree of melting of peridotite in the upper mantle. *Amer. Mineral.* 62, 843-856.
- Mysen, B.O. and Kushiro, I. (1979). Pressure dependence of nickel partitioning between olivine and aluminous silicate melt. *Earth Plan. Sci. Lett.* 42, 383-388.
- Nabelek, P.I. (1980). Nickel partitioning between olivine and liquid in natural basalts: Henry's law behaviour. *Earth Plan. Sci. Lett.* 48, 293-302.
- Nafziger, R.H. and Muan, A. (1967). Equilibrium phase compositions and thermodynamic properties of olivines and orthopyroxenes in the system MgO-FeO-SiO₂. *Amer. Mineral.* 52, 1364-1385.
- Natland, J.G. (1980). Effect of axial magma chamber beneath spreading centres on the composition of basaltic rocks. *Initial Rep. Deep Sea Drilling Project 54*, 833-850.
- Neary, C.R. and Brown, M.A. (1980). Chromites from the Al'ays Complex, Saudi Arabia, and th Samail Complex, Oman. In: Al-Shanti (ed.) *Evolution and mineralization of the Arabian Shield*, A.M.S., I.A.G. Bull. 2, 193-205.
- Nesbitt, R.W. and Sun, S.-S. (1980). Geochemical features of some Archaean and post Archaean high high magnesian - low alkali liquids. *Phil. Trans. Royal Soc. London A* 297, 365-381.
- Nicolas, A. and Jackson, E.D. (1972). Repartition et deux provinces des peridotites des chaines alpines longant la Mediterranee: implications geotectoniques. *Bull. Suis. Miner.* 52, 479-495.
- Nicolas, A. and LePichon, X. (1980). Thrusting of young lithosphere in subduction zones with special reference to structures in ophiolitic peridotites. *Earth Plan. Sci. Lett.* 46, 397-406.
- Nicolas, A. and Violette, J.F. (1982). Mantle flow at oceanic spreading centres: models derived from ophiolites. *Tectonophysics* 81, 319-339.
- Nicolas, A. and Prinzhofer, A. (1983). Cumulative or residual origin for the transition zone in ophiolites: Structural evidence. *J. Petrology* 24, 188-206.
- Nicolas, A., Boudier, F. and Bouchez, J.L. (1980). Interpretation of peridotite structures from ophiolitic and oceanic environments. *Amer. J. Sci.* 280-A, 192-210.

- Nisbet, E.G. and Fowler, C.M.R. (1978). The Mid-Atlantic Ridge at 37° and 45°N: some geophysical and petrological constraints. *Geophys. J. Royal Astron. Soc.* 54, 631-660.
- Noiret, G., Montigny, R. and Allegre, C.J. (1981). Is the Vourinos complex an island arc ophiolite? *Earth Plan. Sci. Lett.* 56, 375-386.
- Obata, M. (1980). The Ronda peridotite: garnet-, spinel- and plagioclase-herzolite facies and the P-T trajectories of a high temperature mantle intrusion. *J. Petrology* 21, 533-572.
- O'Donnell, T.H. and Presnall, D.C. (1980). Chemical variations of the glass and mineral phases in basalts dredged from 25°N-30°N along the Mid-Atlantic Ridge. *Amer. J. Sci.* 280-A, 845-868.
- O'Hara, M.J. (1968). The bearing of phase equilibria studies in synthetic and natural systems on the origin and evolution of basic and ultrabasic rocks. *Earth Sci. Reviews* 4, 69-133.
- O'Hara, M.J. (1977). Geochemical evolution during fractional crystallization of a periodically refilled magma chamber. *Nature* 266, 503-507.
- O'Hara, M.J. and Mathews, R.E. (1981). Geochemical evolution in an advancing, periodically replenished, periodically tapped, continuously fractionated magma chamber. *J. Geol. Soc. London* 138, 237-277.
- Osborne, M.D., Fleet, M.E. and Bancroft, G.M. (1981). Fe²⁺-Fe³⁺ ordering in chromite and Cr-bearing spinels. *Contr. Mineral. Petrol.* 77, 251-255.
- Ozawa, K. (1983). Evaluation of olivine-spinel geothermometry as an indicator of thermal history for peridotites. *Contr. Mineral. Petrol.* 82, 52-65.
- Ozawa, K. (1984). Olivine-spinel geospeedometry: Analysis of diffusion controlled Mg-Fe²⁺ exchange. *Geoch. Cosmoch. Acta* 48, 2597-2611.
- Onyeagocha, A.C. (1974). Alteration of chromite from the Twin Sisters Dunite, Washington. *Amer. Mineral.* 59, 608-612.
- Pallister, J.S. and Hopson, C.A. (1981). Samail Ophiolite plutonic suite: field relations, phase variation, cryptic variation and layering, and a model of a spreading ridge magma chamber. *J. Geophys. Res.* 86, 2593-2644.
- Panayiotou, A. (1978). The mineralogy and chemistry of the podiform chromite deposits in the serpentinites of the Limassol forest, Cyprus. *Mineral. Deposita* 13, 259-274.
- Pearce, J.A. and Cann, J.R. (1973). Tectonic setting of basic volcanic rocks determined using trace element analyses. *Earth Plan. Sci. Lett.* 19, 290-300.
- Pearce, J.A. and Norry, M.J. (1979). Petrogenetic implications of Ti, Zr, Y and Nb variations in volcanic rocks. *Contr. Mineral. Petrol.* 69, 33-47.

- Pearce, J.A., Gorman, B.E. and Brickett, T.C. (1975). The TiO_2 - K_2O - P_2O_5 diagram: a method of discriminating between oceanic and non-oceanic basalts. *Earth Plan. Sci. Lett.* 24, 419-426.
- Pearce, J.A., Gorman, B.E. and Brickett, T.C. (1977). The relationship between major element chemistry and tectonic environment of basic and intermediate volcanic rocks. *Earth Plan. Sci. Lett.* 36, 121-132.
- Pearce, J.A., Lippard, S.J. and Roberts, S. (1984). Characteristics and tectonic significance of supra-subduction zone ophiolites. In: *Ophiolites and Oceanic Crust*, I. G. Gass, S. J. Lippard and A. W. Shelton (ed.), 77-94.
- Perfit, M.R. and Fornari, D.J. (1983). Geochemical studies of abyssal lavas recovered by DSRV Alvin from Eastern Galapagos Rift, Inca Transform, and Ecuador Rift. 2. Phase chemistry and crystallisation history. *J. Geophys. Res.* 88, 10530-10550.
- Perfit, M.R., Fornari, D.J., Malahoff, A. and Embley, R.W. (1983). Geochemical studies of abyssal lavas recovered by DSRV Alvin from Eastern Galapagos Rift, Inca Transform, and Ecuador Rift. 3. Trace element abundances and petrogenesis. *J. Geophys. Res.* 88, 10551-10572.
- Pinsent, R.H. (1974). The emplacement and metamorphism of the Blue River ultramafic body, Cassiar district, British Columbia, Canada. Unpubl. Ph.D. thesis, University of Durham, England.
- Presnall, D.C. (1969). The geometrical analysis of partial fusion. *Amer. J. Sci.* 267, 1178-1194.
- Presnall, D.C. and Hoover, J.D. (1984). Composition and depth of origin of primary mid-ocean ridge basalts. *Contr. Mineral. Petrol.* 87, 170-178.
- Presnall, D.C., Dixon, S.E., Dixon, J.R., O'Donnell, T.H., Brenner, N.L., Schrock, R.L. and Dycus, D.W. (1978). Liquidus phase relations on the join diopside-fosterite-anorthite from 1atm to 20 kbar: Their bearing on the generation and crystallization of basaltic magma. *Contr. Mineral. Petrol.* 66, 203-220.
- Presnall, D.C., Dixon, J.R., O'Donnell, T.H. and Dixon, S.A. (1979). Generation of Mid-ocean Ridge Tholeiites. *J. Petrology* 20, 3-35.
- Prichard, H.M. and Cann, J.R. (1982). Petrology and mineralogy of dredged gabbro from Gettysburg bank, Eastern Atlantic. *Contr. Mineral. Petrol.* 79, 46-55.
- Prinz, M., Keil, K., Green, J.A., Reid, A.M., Bonatti, E. and Honnorez, J. (1976). Ultramafic and mafic dredge samples from the Equatorial Mid-Atlantic ridge and fracture zones. *J. Geophys. Res.* 81, 4087-4103.
- Prinzhofer, A., Nicolas, A., Cassard, D., Moutte, J., Leblanc, M., Paris, J.P. and Rabinowich, M. (1980). Structures in the New Caledonia peridotites-gabbros: implications for oceanic mantle and crust. *Tectonophysics* 69, 85-112.

- Prinzhofer, A. and Allegre, C.J. (1985). Residual peridotites and the mechanisms of partial melting. *Earth Plan. Sci. Lett.* 74, 251-265.
- Quick, J.E. (1981). Petrology and petrogenesis of the Trinity peridotite, an upper mantle diapir in the Eastern Klamath Mountains, Northern California. *J. Geophys. Res.* 86, 11837-11863.
- Quilty, P.G., Rubenach, M.J. and Wilcoxon, J.A. (1973). Miocene ooze from Macquarie Island. *Seacore* 4, 163-164.
- Rautenschlein, M., Jenner, G.A., Hertogen, J., Hofmann, A.W., Kerrich, R., Schmincke, H.-U. and White, W.M. (1985). Isotopic and trace element composition of volcanic glasses from the Akaki Canyon, Cyprus: implications for the origin of the Troodos ophiolite. *Earth Plan. Sci. Lett.* 75, 369-383.
- Rassios, A., Moores, E.M. and Green, H.W. (1983). Magmatic structure and stratigraphy of the Yourinos Ophiolite cumulate zone, Northern Greece. *Ophioliti* 8, 377-410.
- Rhodes, J.M. and Dungan, M.A. (1979). The evolution of ocean floor basaltic magmas. In: *Deep Drilling Results in the Atlantic Ocean: Ocean Crust, M.* Talwani, C.G. Harrison and D.E. Hayes (ed.), American Geophys. Union, 262-272.
- Rhodes, J.M., Dungan, M.A., Blanchard, D.P. and Long, P.E. (1979). Magma mixing at mid-ocean ridges: evidence from basalts drilled near 22°N on the mid-Atlantic Ridge. *Tectonophysics* 55, 35-61.
- Ribe, N.M. (1985). The generation and composition of partial melts in the earth's mantle. *Earth Plan. Sci. Lett.* 73, 361-376.
- Rice, A. (1981). Convective fractionation: A mechanism to provide cryptic zoning (macrosegregation), layering, crescumulates, banded tuffs and explosive volcanism in igneous processes. *J. Geophys. Res.* 86, 405-417.
- Ringwood, A.E. (1975). *Composition and petrology of the earth's mantle.* McGraw-Hill.
- Robinson, P.T., Melson, W.G., O'Hearn, T. and Schmincke, H-U. (1983). Volcanic glass compositions of the Troodos ophiolite, Cyprus. *Geology* 11, 400-404.
- Roden, M.F. and Murthy, V.R. (1985). Mantle metasomatism. *Ann. Rev. Earth Plan. Sci.* 13, p. 269-296.
- Roeder, P.L. (1975). Thermodynamics of element distribution in experimental mafic silicate-liquid systems. *Fortschr. Mineral.* 52, 61-73.
- Roeder, P.L. and Emslie, R.F. (1970). Olivine-liquid equilibrium. *Contr. Mineral. Petrol.* 29, 275-289.
- Roeder, P.L., Campbell, I.H. and Jamieson, H.E. (1979). A re-evaluation of the olivine spinel geothermometer. *Contr. Mineral. Petrol.* 68, 325-334.

- Roeder, P.L., Campbell, I.H. and Jamieson, H.E. (1980). Comment on discussion by Engi and Evans. *Contr. Mineral. Petrol.* 73, 205-206.
- Ross, M. and Huebner, J.S. (1975). A pyroxene geothermometer based on compositional temperature relationships of naturally occurring orthopyroxene, pigeonite, and augite. In: *International Conf. Geothermometry and Geobarometry*. Pennsylvania State University, P.A.
- Ross, J.V., Mercier, J.C., Ave Lallemand, H.G., Carter, N.L., Zimmerman, J. (1980). The Vourinos ophiolite complex, Greece: the tectonite suite. *Tectonophysics* 70, 63-82.
- Ruff, L. and Cozenave, A. (1985). SEASAT geoid anomalies and the Macquarie Ridge complex. *Physics Earth Plan. Interiors* 38, 59-69.
- Sack, R.D., Carmichael, I.S.E., Rivers, M. and Ghiorsio, M.S. (1980). Ferric - ferrous equilibria in natural silicate liquids at 1 bar. *Contr. Mineral. Petrol.* 75, 369-376.
- Sanford, R.E. (1981). Mineralogic and chemical effects of hydration reactions and applications to serpentinization. *Amer. Mineral.* 66, 290-297.
- Sato, H. (1977). Nickel content of basaltic magmas: Identification of primary magmas and a measure of the degree of olivine fractionation. *Lithos* 10, 113-120.
- Saunders, A.D., Tarney, J., Marsh, N.G. and Wood, D.A. (1980). Ophiolites as ocean crust or marginal basin crust: A geochemical approach. In: *Proceedings International Ophiolite Symposium, Cyprus, 1979*, A. Panayiotou (ed.), Geological Survey Department of Cyprus, Nicosia, 193-204.
- Schilling, J.-G. (1973). Iceland mantle plume: Geochemical study of Reykjanes Ridge. *Nature* 242, 565-572.
- Schilling, J.-G., Zajac, M., Evans, R., Johnston, T., White, W., Devine, J.D. and Kingsley, R. (1983). Petrologic and geochemical variations along the Mid-Atlantic Ridge from 29°N to 73°N. *Amer. J. Science* 283, 510-586.
- Sen, G. (1982). Composition of basaltic liquids generated from a partially depleted lherzolite at 9kbar pressure. *Nature* 299, 336-338.
- Sen, G. and Presnall, D.C. (1984). Liquidus phase relationships on the join anorthite-forsterite-quartz at 10kbar with applications to basalt petrogenesis. *Contr. Mineral. Petrol.* 85, 404-408.
- Serri, G. (1980). Chemistry and petrology of gabbroic complexes from the northern Apennine ophiolites. In: *Proceedings International Ophiolite Symposium, Cyprus, 1979*, A. Panayiotou (ed.), Geological Survey Department of Cyprus, Nicosia, 296-313.

- Serri, G. (1981). The petrochemistry of ophiolite gabbroic complexes: A key to classification of ophiolites into low-Ti and high-Ti types. *Earth Plan. Sci. Lett.* 52, 203-212.
- Seyfried, W.E.Jr. and Dibble, W.E.Jr. (1980). Seawater-peridotite interaction at 300°C and 500 bars: implications for the origin of oceanic serpentinites. *Geoch. Cosmoch. Acta* 44, 309-321.
- Seyler, M. and Mattson, P.H. (1989). Petrology and thermal evolution of the Tinaquillo peridotite (VENEZUELA). *J. Geophys. Res.* 94, 7629-7660.
- Shaw, D.M. (1970). trace element fractionation during anatexis. *Geoch. Cosmoch. Acta* 34, 237-243.
- Shervais, J. (1979). Thermal emplacement model for the alpine lherzolite massif at Balmuccia, Italy. *J. Petrology* 20, 795-820.
- Shervais, J. W. (1982). Ti-V plots and the petrogenesis of modern and ophiolitic lavas. *Earth Plan. Sci. Lett.* 59, 101-118.
- Shibata, T. and Thompson, G. (1986). Peridotites from the Mid-Atlantic Ridge at 43°N and their petrogenetic relation to abyssal tholeiites. *Contr. Mineral. Petrol.* 93, 144-159.
- Shibata, T., DeLong, S.E. and Walker, D. (1979a). Abyssal tholeiites from the Oceanographer Fracture zone. I. Petrology and Fractionation. *Contr. Mineral. Petrol.* 70, 89-102.
- Shibata, T., Thompson, G. and Frey, F.A. (1979b). Tholeiitic and alkali basalts from the Mid-Atlantic Ridge at 43°N. *Contr. Mineral. Petrol.* 70, 127-141.
- Shido, F., Miyashiro, A. and Ewing, M. (1971). Crystallisation of abyssal tholeiites. *Contr. Mineral. Petrol.* 31, 251-266.
- Sigurdsson, H. (1977). Spinels in Leg 37 basalts and peridotites: Phase chemistry and zoning. *DSDP Leg 37, Initial Rep. DSDP Vol.37*, 883-891.
- Sigurdsson, H. (1981). First order major element variation in basalt glasses from the Mid-Atlantic Ridge : 29°N to 73°N. *J. Geophys. Res.* 86, 9483-9502.
- Sigurdsson, H. and Schilling, J.G. (1976). Spinels in Mid-Atlantic Ridge basalts: Chemistry and occurrence. *Earth Plan. Sci. Lett.* 29, 7-20.
- Sinton, J.M. (1977). Equilibration history of the basal alpine-type peridotite, Red Mountain, New Zealand. *J. Petrology* 18, 216-246.
- Sinton, J.M. (1979). Petrology of alpine-type peridotites from site 395, DSDP Leg 45, *Initial Rep. DSDP Vol. 45*, 595-602.
- Sleep, N.H. (1975). Formation of oceanic crust: some thermal constraints. *J. Geophys. Res.* 80, 4037-4042.
- Sleep, N.H. (1978). Thermal structure and kinematics of mid-oceanic ridge axis: some implications to basaltic volcanism. *Geophys. Res. Lett.* , 426-428.

- Smewing, J.D. (1981). Mixing characteristics and compositional differences in mantle-derived melts beneath spreading axes: evidence from cyclically layered rocks in the ophiolite of North Oman. *J. Geophys. Res.* 86, 2645-2659.
- Smith, D. and Roden, M.F. (1981). Geothermometry and kinetics in a two spinel peridotite nodule, Colorado Plateau. *Amer. Mineral.* 66, 334-345.
- Sparks, R.S.J. and Huppert, H.E. (1984). Density changes during the fractional crystallization of basaltic magmas: fluid dynamic implications. *Contr. Mineral. Petrol.* 85, 300-309.
- Sparks, R.S.J., Meyer, P. and Sigurdsson, H. (1980). Density variation amongst mid-ocean ridge basalts: implications for magma mixing and the scarcity of primitive lavas. *Earth Plan. Sci. Lett.* 46, 419-430.
- Sparks, R.S.J., Huppert, H.E. and Turner, J.S. (1984). The fluid dynamics of evolving magma chambers. *Phil. Trans. Royal Soc. London A310*, 511-534.
- Spear, F.S. and Kimball, K.L. (1984). RECAMP: A fortran IV program for estimating Fe³⁺ contents in amphiboles. *Computers and Geoscience* 10, 317-325.
- Stakes, D.S., Shervais, J.W. and Hopson, C.A. (1984). The volcanic tectonic cycle of the FAMOUS and AMAR valleys, Mid-Atlantic Ridge (36°47'N): Evidence from basalt glass and phenocryst compositional variations for a steady state magma chamber beneath the valley midsections, AMAR 3. *J. Geophys. Res.* 89, 6995-7028.
- Stern, C.R. (1979). Open and closed system igneous fractionation within two Chilean ophiolites and the tectonic implication. *Contr. Mineral. Petrol.* 68, 243-258.
- Stern, C.R. and Elthon, D. (1979). Vertical variations in the effects of hydrothermal metamorphism in Chilean ophiolites: their implications for ocean floor metamorphism. *Tectonophysics* 55, 179-213.
- Stolper, E. (1980). A phase diagram for mid-ocean ridge basalts: preliminary results and implications for petrogenesis. *Contr. Mineral. Petrol.* 74, 13-27.
- Stolper, E. and Walker, D. (1980). Melt density and the average composition of basalt. *Contr. Mineral. Petrol.* 74, 7-12.
- Summerhayes, C.P. (1967). Note on Macquarie ridge and the Tonga -Kermadec complex. Are they parts of the mid-ocean ridge system? *New Zealand J. Sci.* 10, 808-812.
- Summerhayes, C.P. (1969). Marine geology of the New Zealand subantarctic sea-floor. *New Zealand Dept. Sci. Ind. Res. Bull.* , 190.
- Sun, S.S., Nesbitt, R.W. and Sharaskin, A. Ya. (1979). Geochemical characteristics of mid-ocean ridge basalts. *Earth Plan. Sci. Lett.* 44, 119-138.

- Sykes, L.R. (1967). Mechanism of earthquakes and nature of faulting on the mid-oceanic ridges. *J. Geophys. Res.* 72, 2131-2121.
- Sykes, L.R. (1970). Seismicity of the Indian ocean and a possible nascent island between Ceylon and Australia. *J. Geophys. Res.* 75, 5041-5055.
- Tait, S.R., Huppert, H.E. and Sparks, R.S.J. (1984). The role of compositional convection in the formation of adcumulate rocks. *Lithos* 17, 139-146.
- Takahashi, E. (1978). Partitioning of Ni^{2+} , Co^{2+} , Fe^{2+} , Mn^{2+} and Mg^{2+} between olivine and silicate melts: Compositional dependence of partition coefficients. *Geoch. Cosmoch. Acta* 42, 1829-1844.
- Takahashi, E. (1980). Thermal history of lherzolite xenoliths I. Petrology of lherzolite xenoliths from the Ichinomegata crater, Oga peninsula, Northeast Japan. *Geoch. Cosmoch. Acta* 44, 1643-1653.
- Takahashi, E. and Kushiro, I. (1983). Melting of a dry peridotite at high pressures and basalt magma genesis. *Amer. Mineral.* 68, 859-879.
- Tarney, J., Wood, D.A., Yaret, J., Saunders, A.D. and Cann, J.R. (1979). Nature of mantle heterogeneity in the North Atlantic: Evidence from Leg 49 basalts. In: *Deep Drilling Results in the Atlantic Ocean: Ocean Crust*, M. Talwani, C.G. Harrison and D.E. Hayes (ed.), American Geophys. Union, 285-301.
- Tiezzi, L.J. and Scott, R.B. (1980). Crystal fractionation in a cumulate gabbro, Mid-Atlantic Ridge, 26°N. *J. Geophys. Res.* 85, 5438-5454.
- Thayer, T.P. (1966). Serpentinization considered as a constant volume metasomatic process. *Amer. Mineral.* 51, 685-709.
- Thompson, G. and Humphris, S.E. (1984). Petrology and geochemistry of rocks from the Walvis Ridge: Deep Sea Drilling Project Leg 74, sites 525, 527 and 528. *Init. Rep. DSDP Vol. 74*, 755-764.
- Thompson, R.N. (1972). Melting behaviour of two Snake River lavas at pressures up to 35 kb. *Carnegie Instit. Washington Yearb.* 71, 406-410.
- Thompson, R.N. (1984). Dispatches from the basalt front, I: Experiments. *Proc. Geol. Assoc.* 95, 249-262.
- Thompson, R.N. (1987). Phase equilibria constraints on the genesis and magmatic evolution of oceanic basalts. *Earth Science Reviews* 24, 161-210.
- Thompson, R.N., Morrison, M.A., Hendry, G.L. and Parry, S.J. (1984). An assessment of the relative roles of crust and mantle in magma genesis: an elemental approach. *Phil. Trans. Royal Soc. London A.310*, 549-590.
- Thy, P., Brooks, C.K. and Walsh, J.N. (1985). Tectonic and petrogenetic implications of major and trace element chemistry of Troodos glasses, Cyprus. *Lithos* 18, 165-178.

- Turner, J.S. and Gustafson, L.B. (1978). The flow of hot saline solutions from vents in the sea floor. Some implications for exhalative massive sulphide and other ore deposits. *Econ. Geology* 73, 1082-1100.
- Upadhyay, H.D. and Neale, E.R.W. (1979). On the tectonic regimes of ophiolite genesis. *Earth Plan. Sci. Lett.* 43, 93-102.
- Yanko, D.A. and Batiza, R. (1982). Gabbroic rocks from the Mathematician Ridge failed rift. *Nature* 300, 742-744.
- Vannier, M. (1977). Modélisation de la solution spinelle naturelle. *Bull. Soc. Fr. Minéral. Cristallogr.* 100, 239-245.
- Varne, R. and Rubenach, M.J. (1972). Geology of Macquarie Island and its relationship to oceanic crust. In: D.E. Davies (ed.), *Antarctic Oceanology II, The Australian - New Zealand Sector*. Antarctic Res. Series 19, 251-261.
- Vine, F.J. and Moores, E.M. (1972). A model for the gross structure, petrology and magnetic properties of oceanic crust. *Geol. Soc. Amer. Mem.* 132, 195-205.
- Wager, L.R., Brown, G.M. and Wadsworth, W.J. (1960). Types of igneous cumulates. *J. Petrology* 1, 73-85.
- Wager, L.R. and Brown, G.M. (1967). *Layered igneous rocks*. Oliver and Boyd Publ. Co.
- Walker, D., Shibata, T. and DeLong, S.E. (1979). Abyssal tholeiites from the Oceanographer fracture zone. II. Phase equilibria and mixing. *Contr. Mineral. Petrol.* 70, 111-125.
- Watkins, N.D. and Gunn, B.M. (1970). Petrology, geochemistry and magnetic properties of some rocks dredged from the Macquarie Ridge. *New Zealand J. Geol. Geophys.* 14, 153-163.
- Weissel, J.K. and Hayes, D.E. (1971). Asymmetric spreading south of Australia. *Nature* 23, 517-521.
- Weissel, J.K., Hayes, D.E. and Herron, E.M. (1977). Plate tectonic synthesis: The displacement between Australia, New Zealand and Antarctica since the late Cretaceous. *Marine Geology* 25, 231-277.
- Wells, P.R.A. (1977). Pyroxene thermometry in simple and complex systems. *Contr. Mineral. Petrol.* 62, 129-139.
- Wicks, F.J. and Whittaker, E.J.W. (1977). Serpentine textures and serpentinization. *Can. Mineral.* 15, 459-488.
- Wilkinson, J.F.G. (1982). The genesis of Mid-Ocean Ridge Basalt. *Earth Sci. Reviews* 18, 1-57.
- Williamson, P. (1974). Recent studies on Macquarie Island and the Macquarie Ridge Complex. *Bull. of the Australian Soc. of Exploration Geophysicists* 5, 19-22.

- Williamson, P. (1978). The paleomagnetism of outcropping oceanic crust on Macquarie Island. *J. Geol. Soc. Australia* 25, 387-394.
- Williamson, P. (1988). Origin, structural and tectonic history of the Macquarie Island Region. In: *Papers and Proceedings Royal Soc. Tasmania*, (ed.) M. R. Banks and S. J. Smith, Vol. 122 (Part I), 27-43.
- Williamson, P. and Johnson, B.D. (1974). Crustal structure of the central region of the Macquarie Ridge Complex from gravity studies. *Marine Geophys. Res.* 11, 127-132.
- Williamson, P. and Rubenach, M.J. (1972). Preliminary report on geophysical studies of Macquarie Island. In: D.E. Davies (ed.), *Antarctic Oceanology II, The Australian - New Zealand Sector*. Antarctic Res. Series 19, 165-196.
- Williamson, P., Hawkins, L.V. and Long, B. (1981). An examination of the possible occurrence of sea-floor spreading magnetic anomalies on Macquarie Island. *Marine Geophys. Res.* 5, 139-155.
- Wilson, A.H. (1982). The geology of the Great "Dyke", Zimbabwe: The ultramafic rocks. *J. Petrology* 23, 240-292.
- Wood, B.J. and Banno, S. (1973). Garnet-orthopyroxene and orthopyroxene - clinopyroxene relationships in simple and complex systems. *Contr. Mineral. Petrol.* 42, 109-124.
- Wood, D.A. (1979). A variably veined sub-oceanic upper mantle - genetic significance for mid-ocean ridge basalts from geochemical evidence. *Geology* 7, 499-503.
- Wood, D.A., Tarney, J., Yaret, J., Saunders, A.D., Bougault, H., Joron, J.-L., Treuil, and Cann, J.R. (1979). Geochemistry of basalts drilled in the North Atlantic by IPOD Leg 49: Implications for mantle heterogeneity. *Earth Plan. Sci. Lett.* 42, 77-97.
- Wright, T.L. (1973). Magma mixing as illustrated by the 1959 eruption Kilauea volcano, Hawaii. *Geol. Soc. Amer. Bull.* 84, 84-858.
- Yoder, H.S.Jr. and Tilley, C.E. (1962). Origin of basalt magmas: an experimental study of natural and synthetic rock systems. *J. Petrology* 3, 342-532.

FIGURES

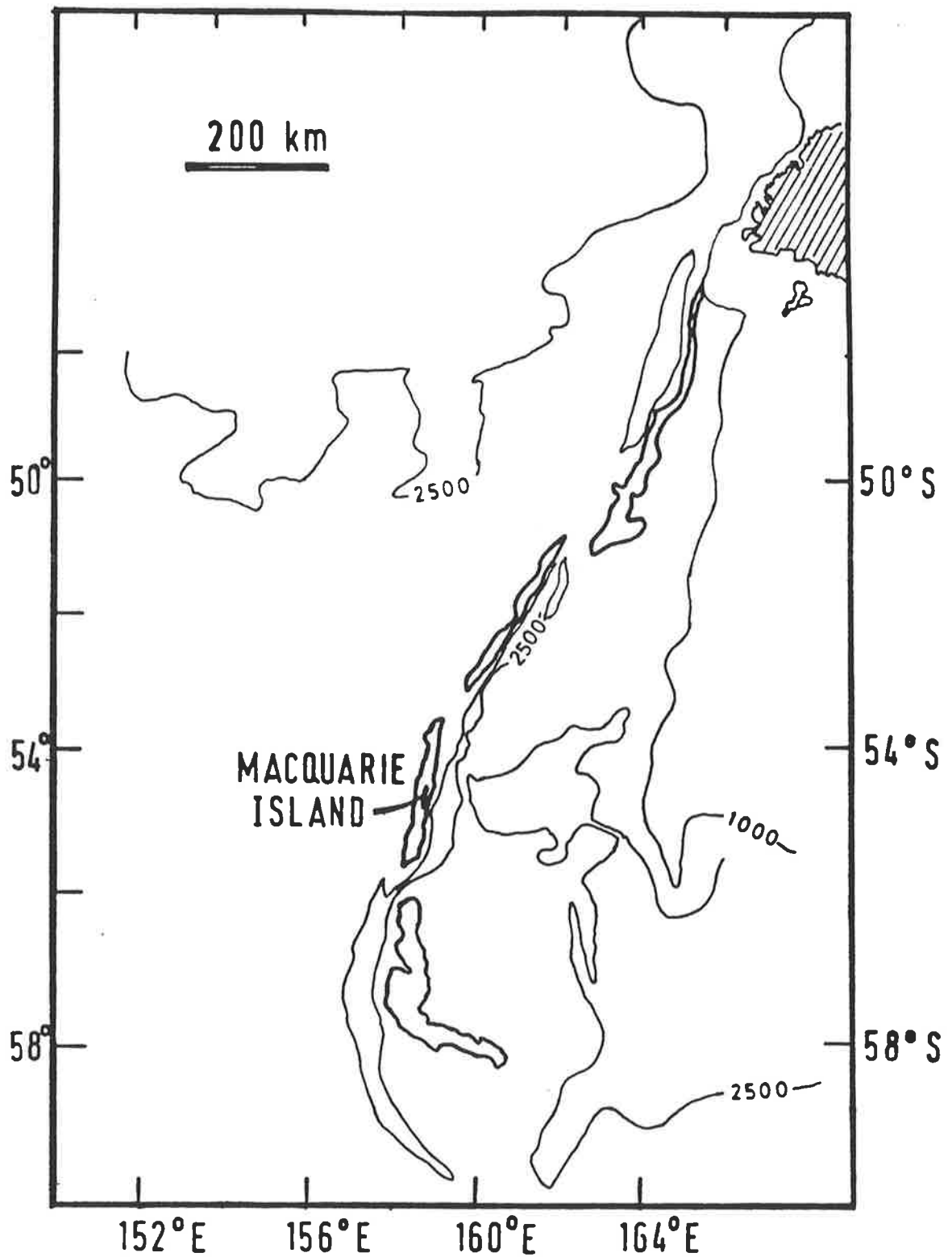


Figure 2.1. Regional setting of Macquarie Island. The Macquarie Ridge is shown by thick pencil. Isobath contours (1000 and 2500) in fathoms. Hatched area (top right) is the southern island of New Zealand.

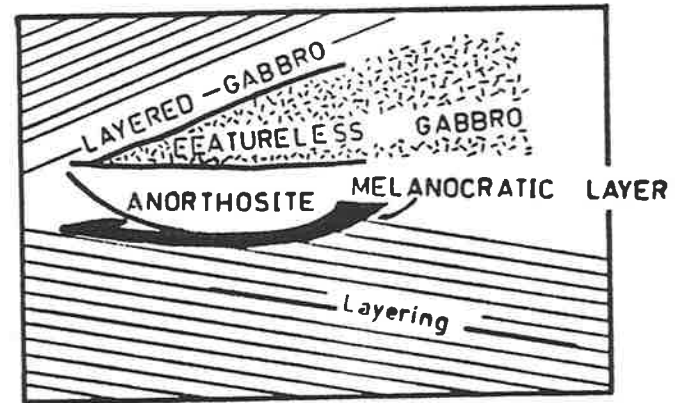
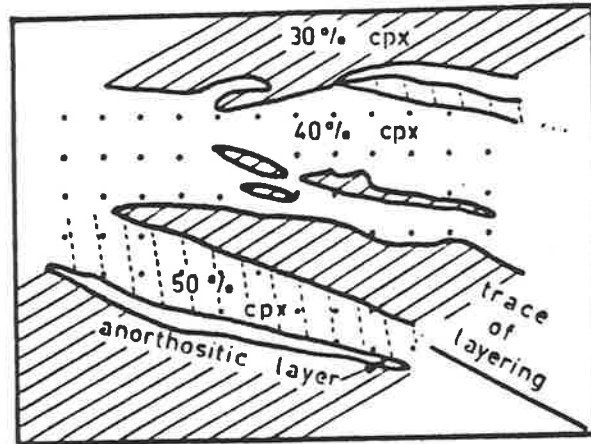
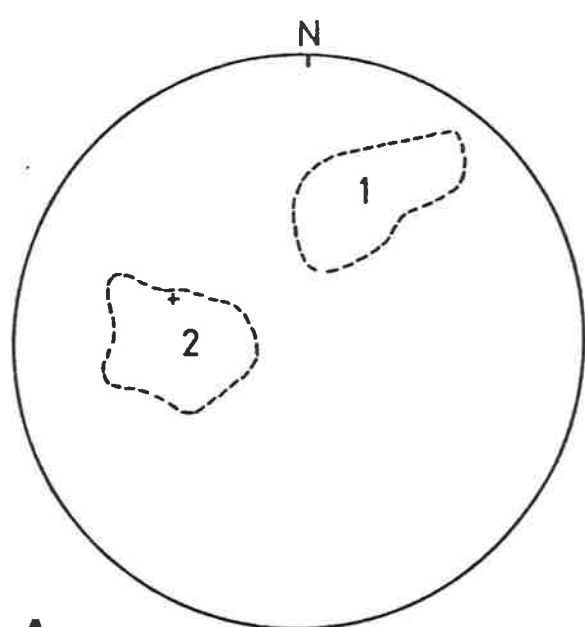


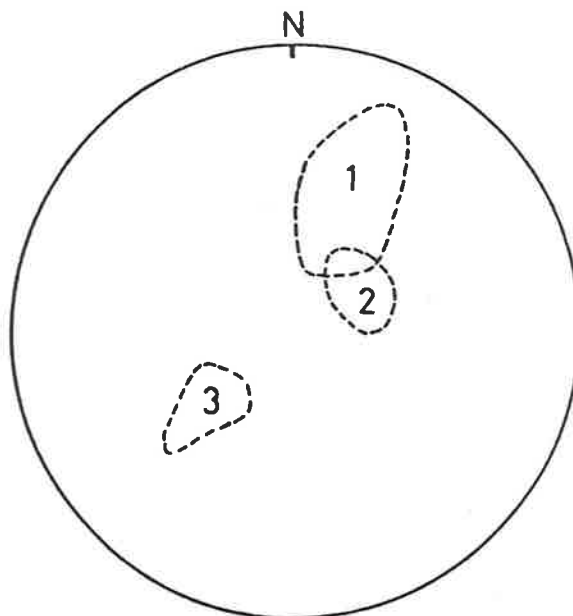
Figure 2.2. Alternations of discontinuous, truncated, intrusive and texturally and mineralogically distinct layers. Sketches redrawn after outcrop photographs. Northern side of Handspike Point.



A.

LAYERED TROCTOLITES & GABBROS.

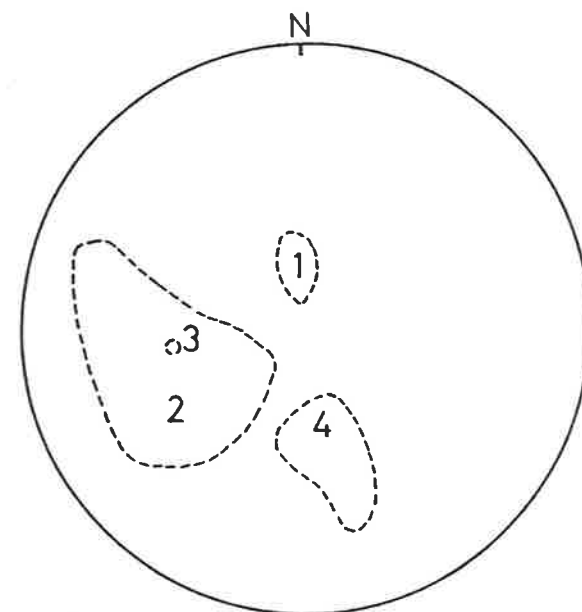
- 1. HANDSPIKE PT. 110/60 SW
- 2. EAGLE & HALF-MOON BAYS. 006/38 ESE
- + . COMPOSITIONAL LAYERING IN HARZBURGITE, EAGLE PT.



B.

DOLERITE DYKE SWARMS.

- 1. HASSELBOROUGH BAY & GADGETS GULLY 115/40 SW
- 2. LUSITANIA BAY. 150/32 SW
- 3. NT. MARTIN 136/42 NE



C.

PILLOW LAVAS

- 1. MAWSON PT. 78 / 22 SE
- 2. SOUTH ISLAND LAVAS 170 / 42 ENE
- 3. LANGDON PT. 168 / 50 NE
- 4. GREEN GORGE 78 / 50 SW

Figure 2.3. Equal area projections of structural measurements according to locality. A: Layering in troctolites and olivine-gabbros. B: Attitude of dolerite dykes from the dyke swarms. C: Bedding measurements in pillow basalts.

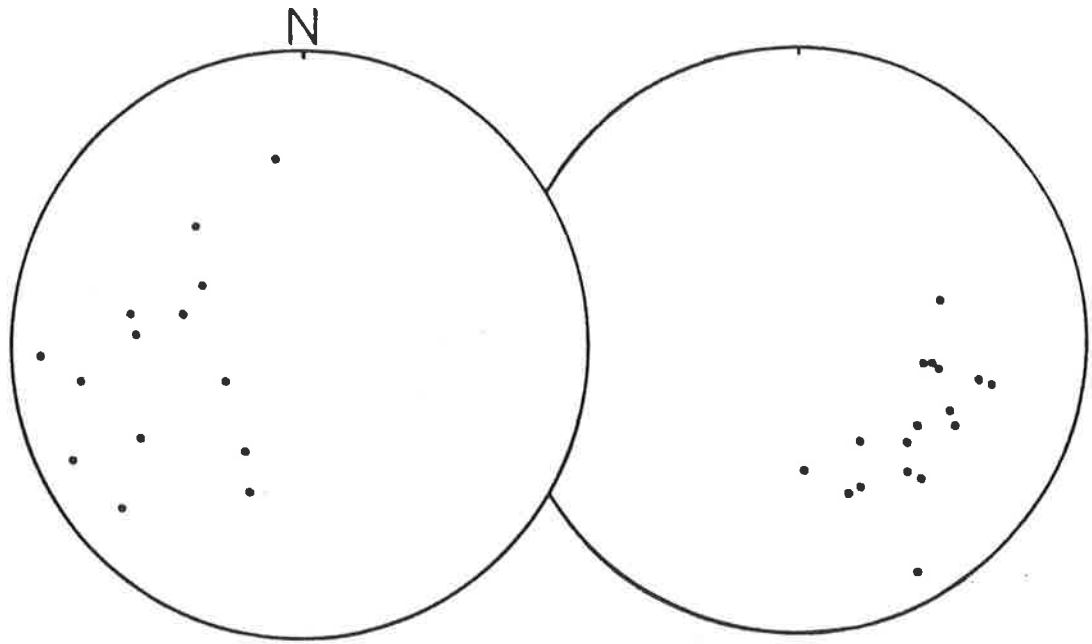
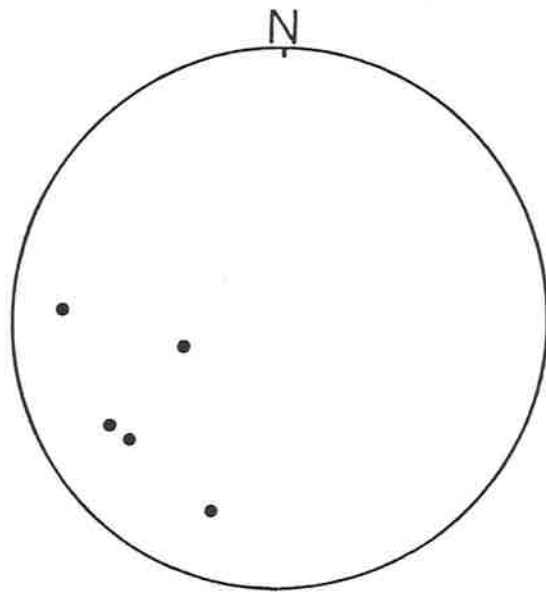
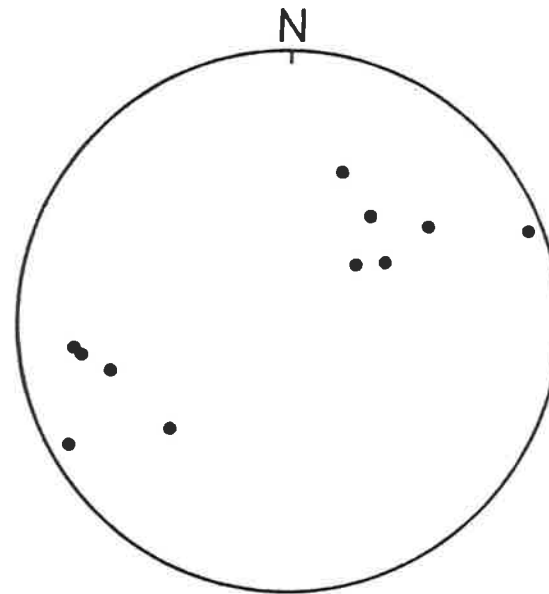


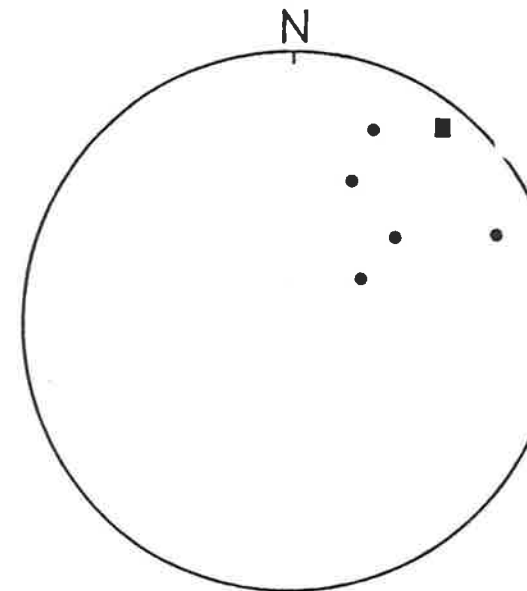
Figure 2.4. Measurements of harzburgite faulting, east of Langdon Point.



A.
DOLERITE DYKES IN HARZBURGITE



B.
GABBROIC DYKES IN HARZBURGITE.

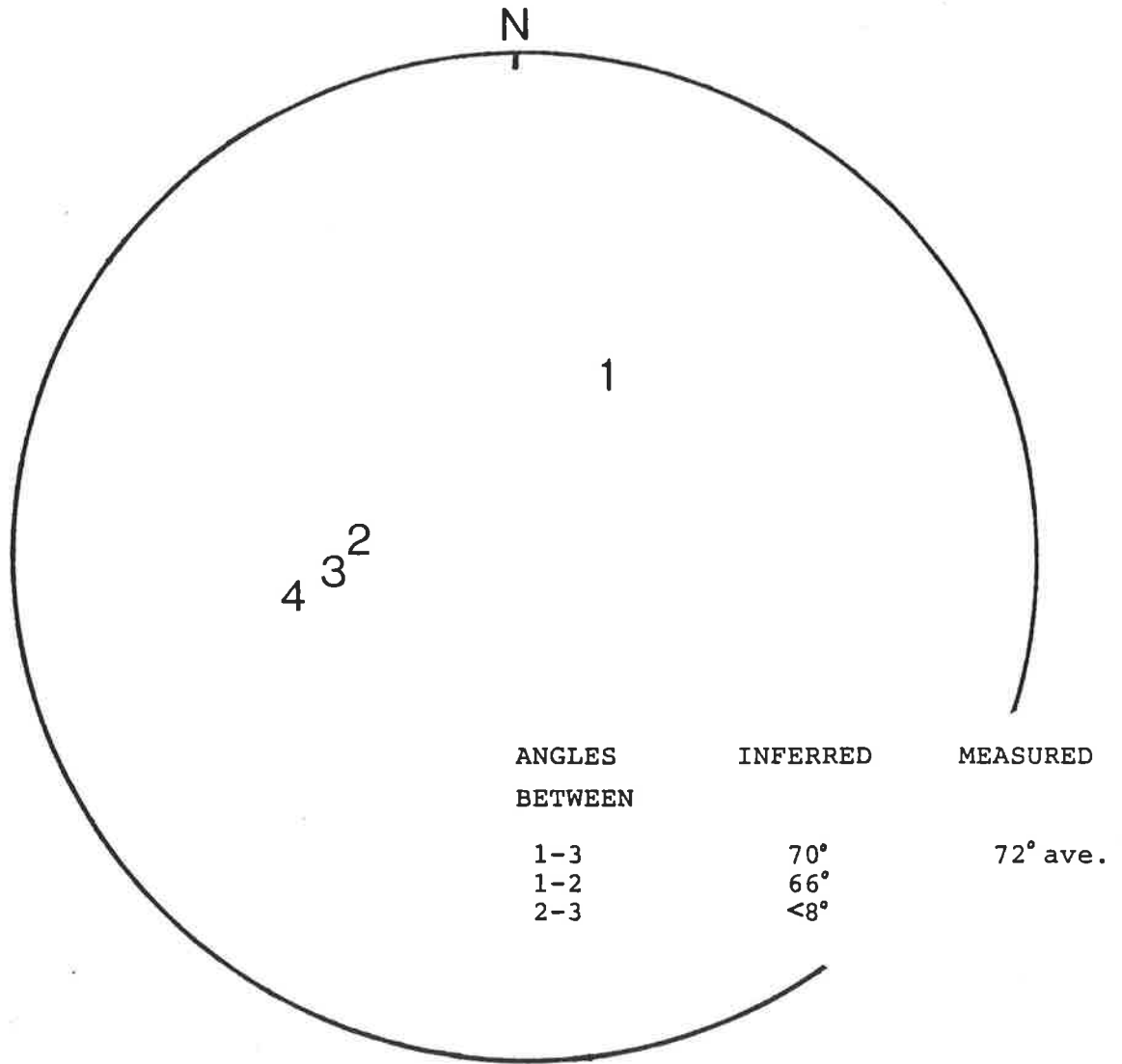


C.
FOLIATION IN GABBRO
CATACLASITE ZONE(■) AVER.

Figure 2.5A. Lower hemisphere equal area projection of the orientation of dolerite dykes crosscutting the harzburgite outcrop at Langdon Bay.

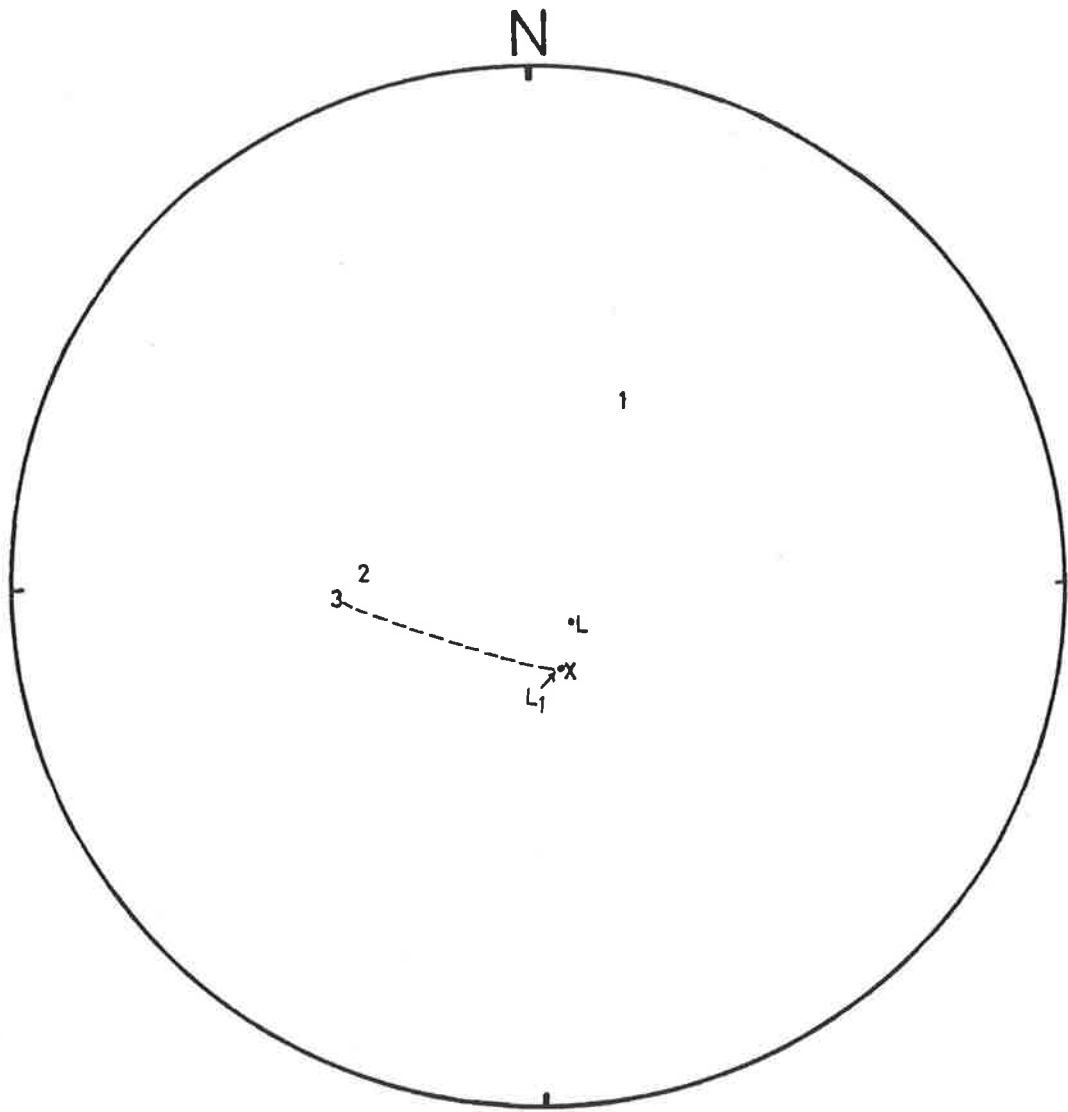
2.5B. Orientation of gabbroic dykes crosscutting harzburgite at Langdon Bay and Eagle Point.

2.5C. Orientation of the gabbro foliation (from gabbroic mylonites) south-west of Eagle Bay. The square is the average orientation of the cataclasite zone exposed to the west of Langdon Point.



1. DYKE SWARM COMPLEX, NORTHERN ISLAND.
2. TROCTOLITE LAYERING, EAGLE BAY.
3. LAVA BEDDING, SOUTHERN ISLAND.
4. LAVA BEDDING, LANGDON PT.

Figure 2.6. Orientation maxima of the various rock units according to locality.



1. DOLERITE DYKES
 2. TROCTOLITES-LAYERING
 3. LAVAS
 X. AXIS 70° S, 160° E
 L. LAYERING $N55E, 10^{\circ}$ NW
 L_1 . POSITION OF L AFTER ROTATION AROUND
 AXIS X BY 10° .

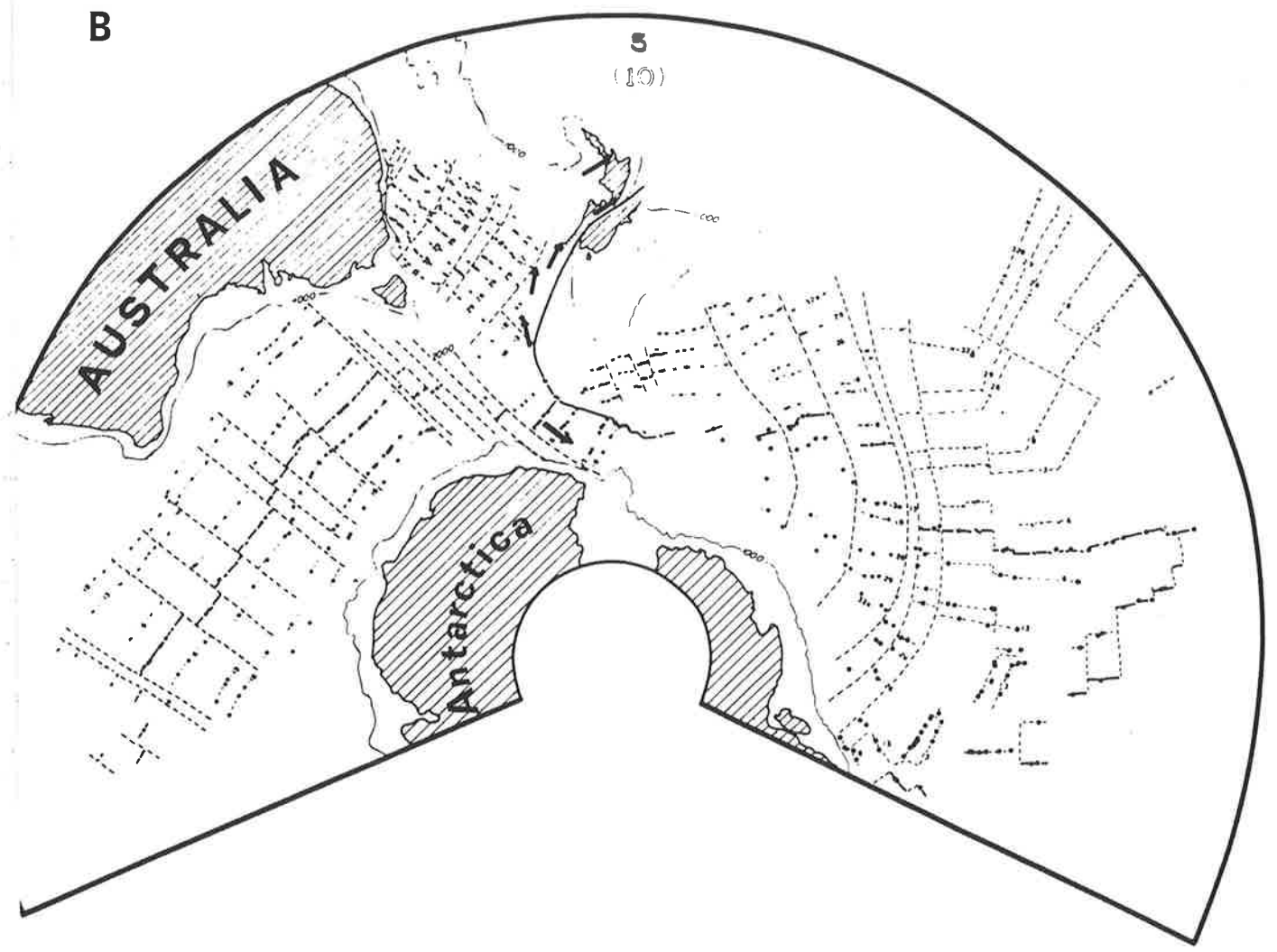
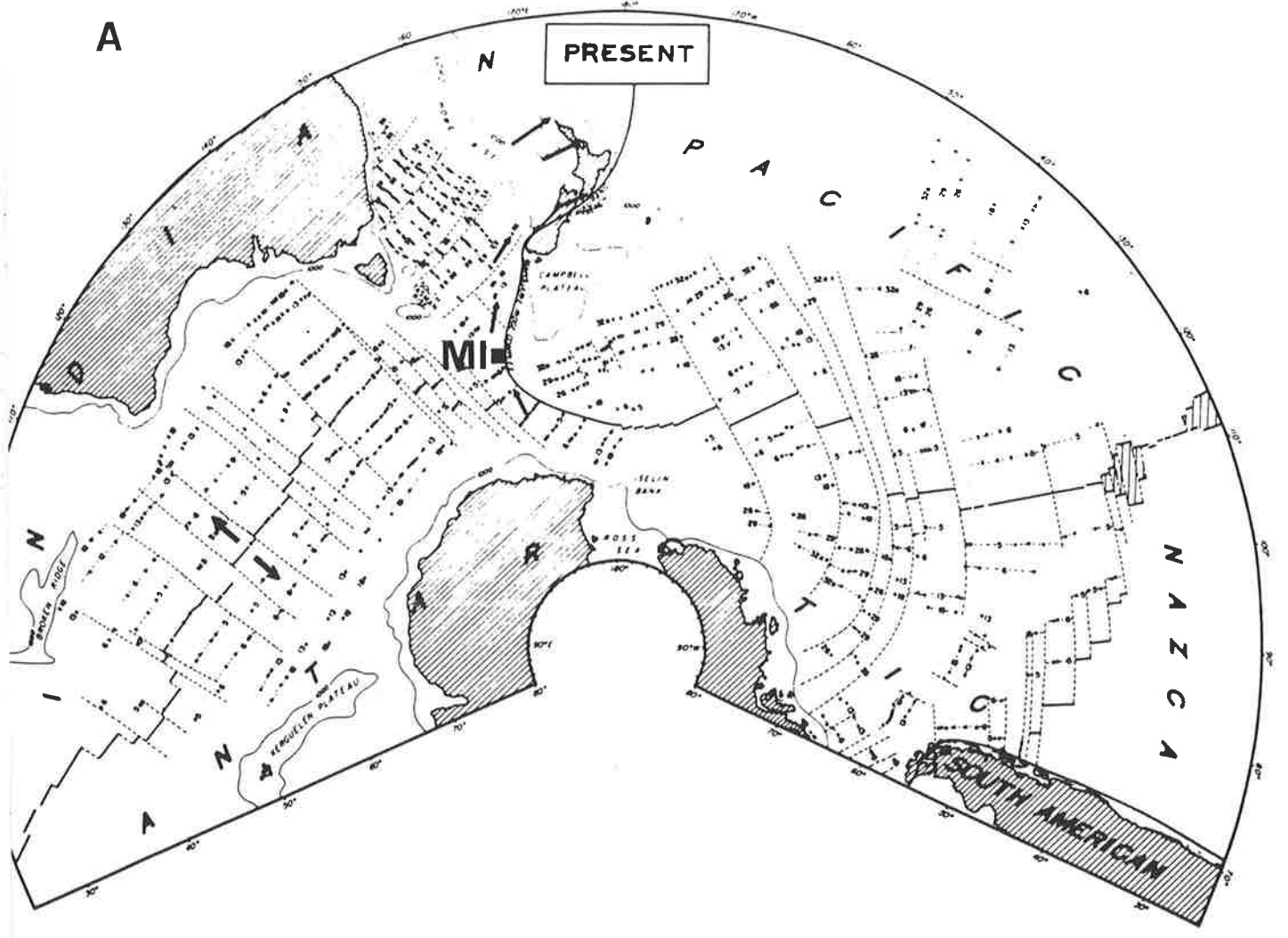
Figure 2.7. Synthesis of structural data.

Figure 2.0. Geotectonic features in the Southern Pacific. Australia, Antarctica, New Zealand and a portion of South America are shown by the shaded areas (from Hayes and Talwani, 1972).

A. Present day plate configuration.

The Macquarie Ridge Complex is shown by the solid curve. The relative motions of Indian, Antarctic and Pacific plates are indicated by arrows. The extension-accretion boundary between Indian-Australian and Antarctic plates is also marked. The magnetic lineations are marked on each side of a spreading ridge. MI indicates the location of Macquarie Island. Dashed lines indicate transcurrent faults.

B. Positioning of plates at Anomaly time 5. The Macquarie Ridge Complex is also shown by the solid curve. The motion of the Indian-Australian plate relative to the Pacific plate is indicated by the arrows. The Indian-Australian - Pacific spreading ridge is now shown by Anomaly 5.



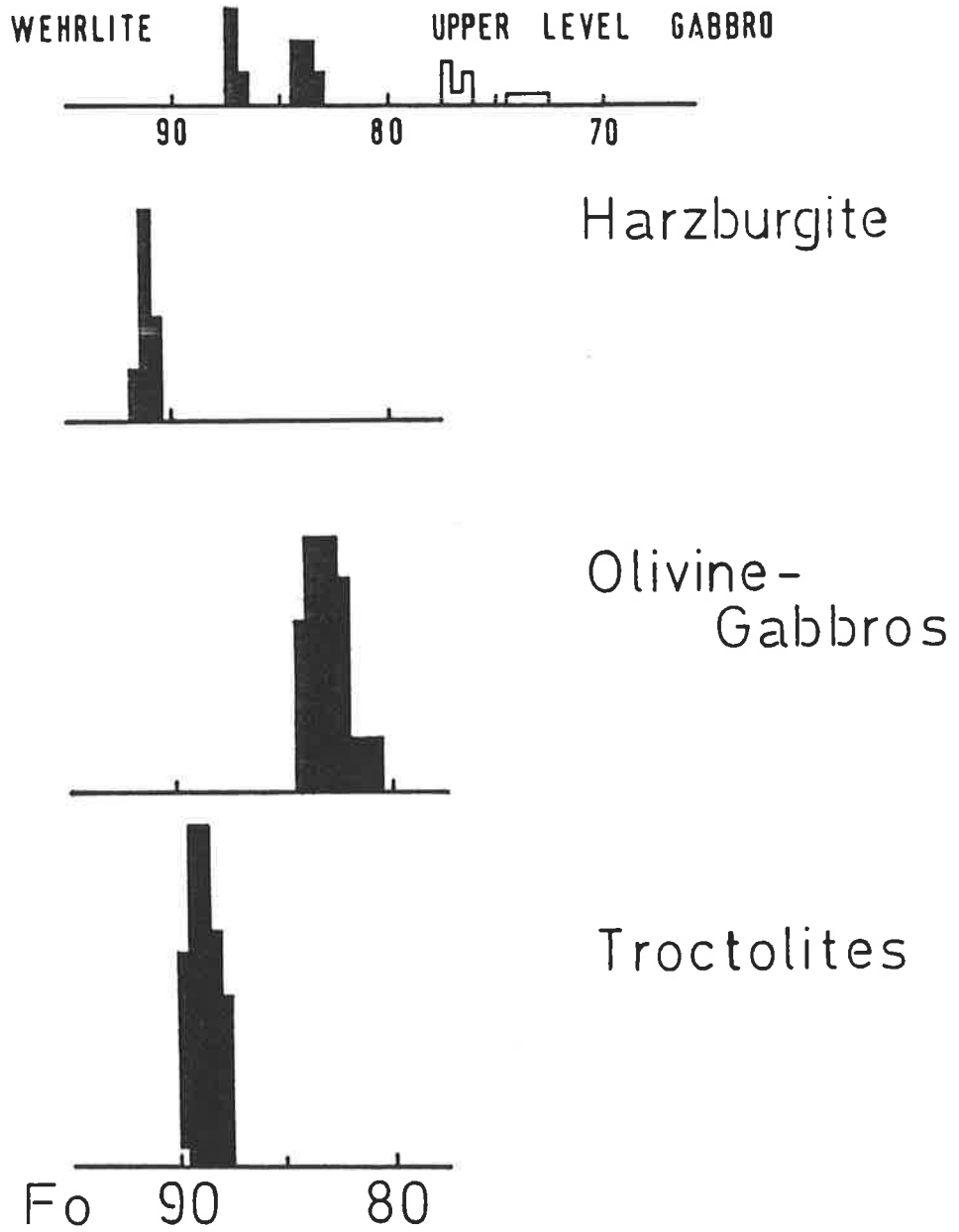
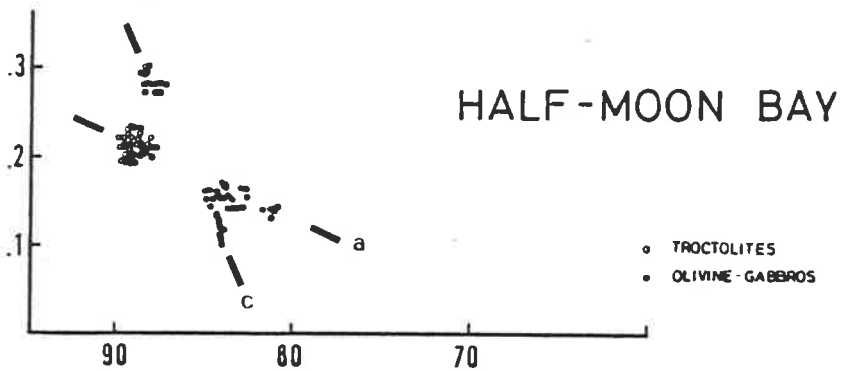
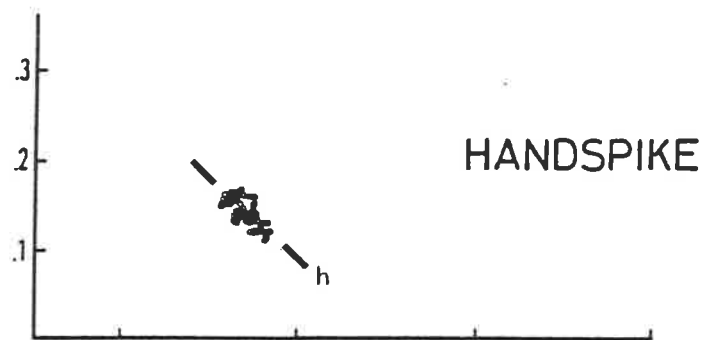


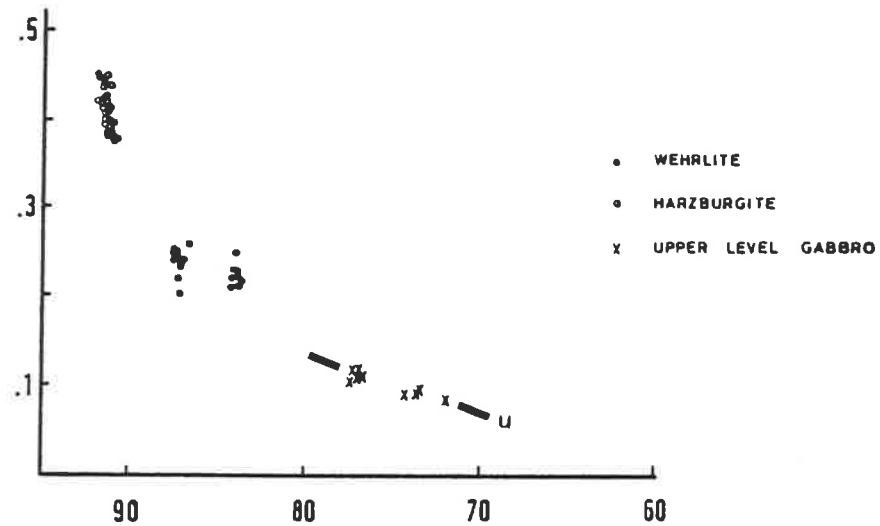
Figure 4.1. Olivine composition histograms for the plutonic rocks. Fo=forsterite content.

Figure 4.2. A NiO versus Fo-content plot of Macquarie Island olivines from the plutonic rocks. NiO in weight percent. Representative analyses are plotted only. Data from the olivine-gabbros from Handspike area are shown in the "HANDSPIKE" plot. They define trend h. Data from the troctolites and olivine-gabbros at Langdon Bay and Half-Moon Bay are shown in the "HALF-MOON BAY" plot. Two trends with different slopes, a and c, are defined in this plot. Data from the harzburgites, the North Mountain wehrlite and the Upper Level Gabbro are shown in the right-hand side plot. Olivines in the Upper Level Gabbro define trend u. This trend has similar slope to trend a.

NiO



NiO



Fo - content

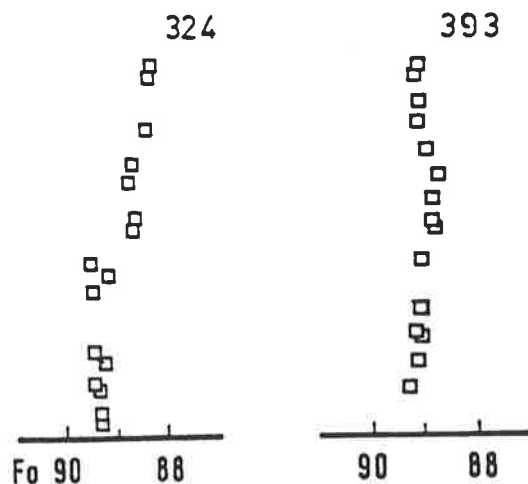


Figure 4.3A. Compositional variation in olivine, in terms of its forsterite content (Fo), in two layered troctolites from the Eagle Bay outcrop. Samples 324 and 393. Each specimen was cut normal to layering first. Then, two polished-thin sections were made from each slab. One polished-thin section from the upper part and a second from the lower part of each slab. The vertical distance from the base of the lower part thin section to the top of the upper part thin section is 8-9cm. Each square is the average of two or more microprobe analyses. The stratigraphic variation in the olivine Fo-content is limited to less than 1mol% in both samples. Fo-content decreases slightly with stratigraphic height in sample 324, whereas it initially decreases but then increases in sample 393. It is emphasized here that the analytical precision is $\pm 1\%$ for major elements; replicate analyses are also accurate within $\pm 1\%$.

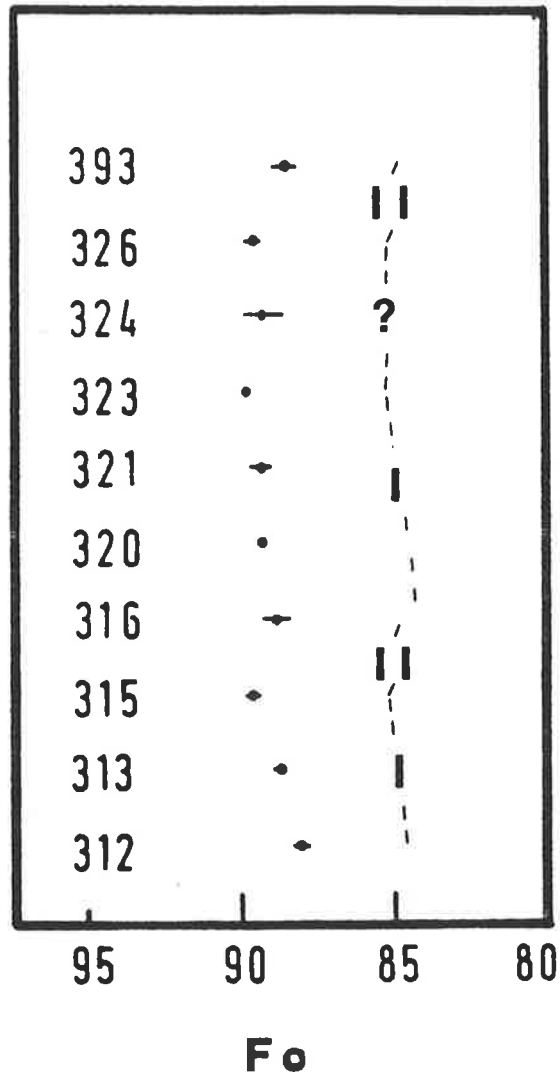
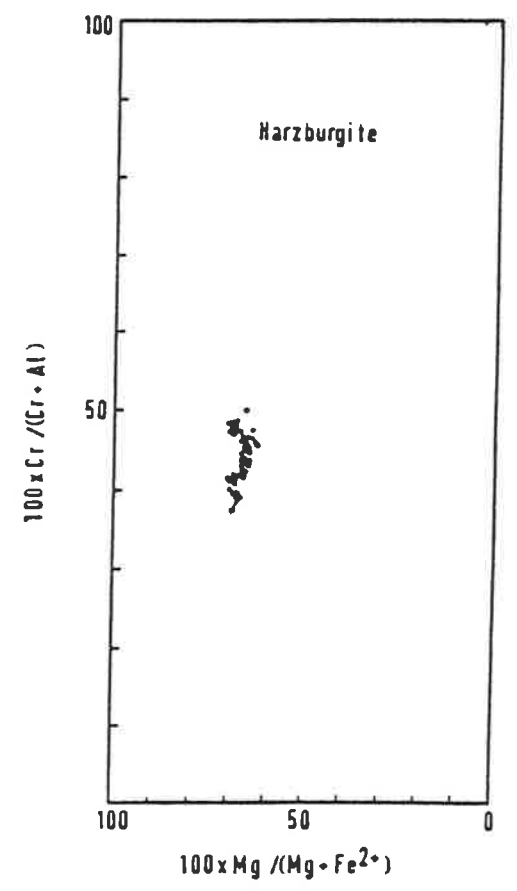
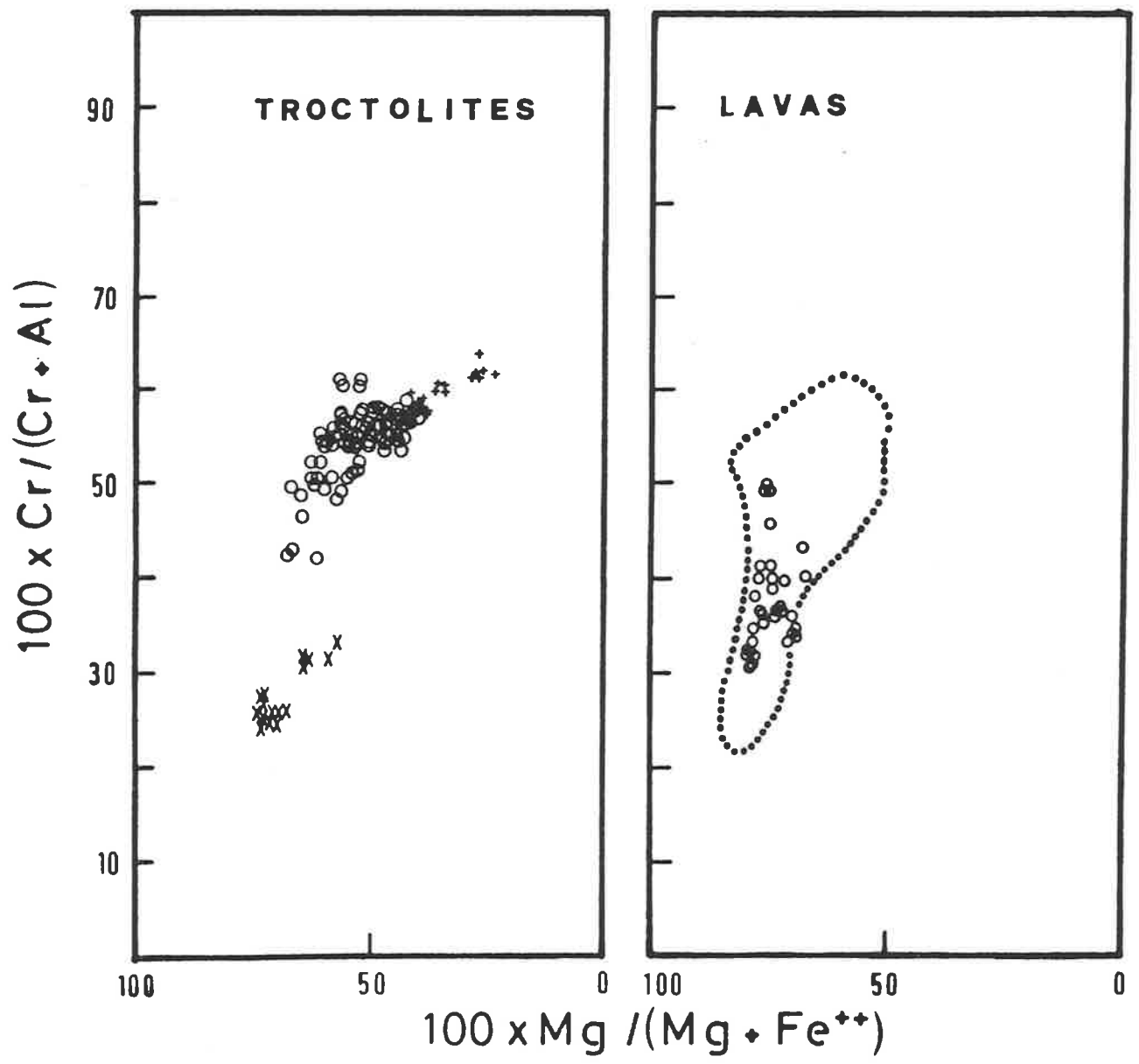


Figure 4.3B. Stratigraphic composition variation in olivine from troctolites (Eagle Bay exposure). Fo is the forsterite content of olivine. Numbers on the left hand side are the studied troctolite specimens. The true distance from sample 312 to sample 393 is approximately 100 meters. The overall variation in the composition of olivine from the base of the section (sample 312) to the top (sample 393) is limited to 2.5mol%. Horizontal bars indicate the observed range within sample; it is always less than 1mol%. Two patterns are developed. Pattern I defines a trend of decreasing Fo-content, whereas pattern II indicates increasing Fo-content with stratigraphic height. No pattern is clearly defined between sample 323 and 326, marked as ?.

Figure 4.4.A. Macquarie Island spinel compositions plotted in the $100\text{Mg}/(\text{Mg}+\text{Fe}^{2+}) - 100\text{Cr}/(\text{Cr}+\text{Al})$ projection of the spinel compositional prism. In the "TROCTOLITES" plot, Cr-spinels from troctolites are shown by open circles. The North Mountain wehrlite spinels are shown by X, and spinels from the mafic intrusive layers at Handspike Point by crosses (mainly sample 358). In the "LAVAS" plot, core spinel compositions (phenocrysts or xenocrysts) from the lavas are only included (open circles). The area defined by the dotted curve indicates the field of spinel phenocrysts from abyssal basalts (after Dick and Bullen, 1984). The "Harzburgite" plot presents selected data of Cr-spinels from the Macquarie island harzburgites.

A.



B.

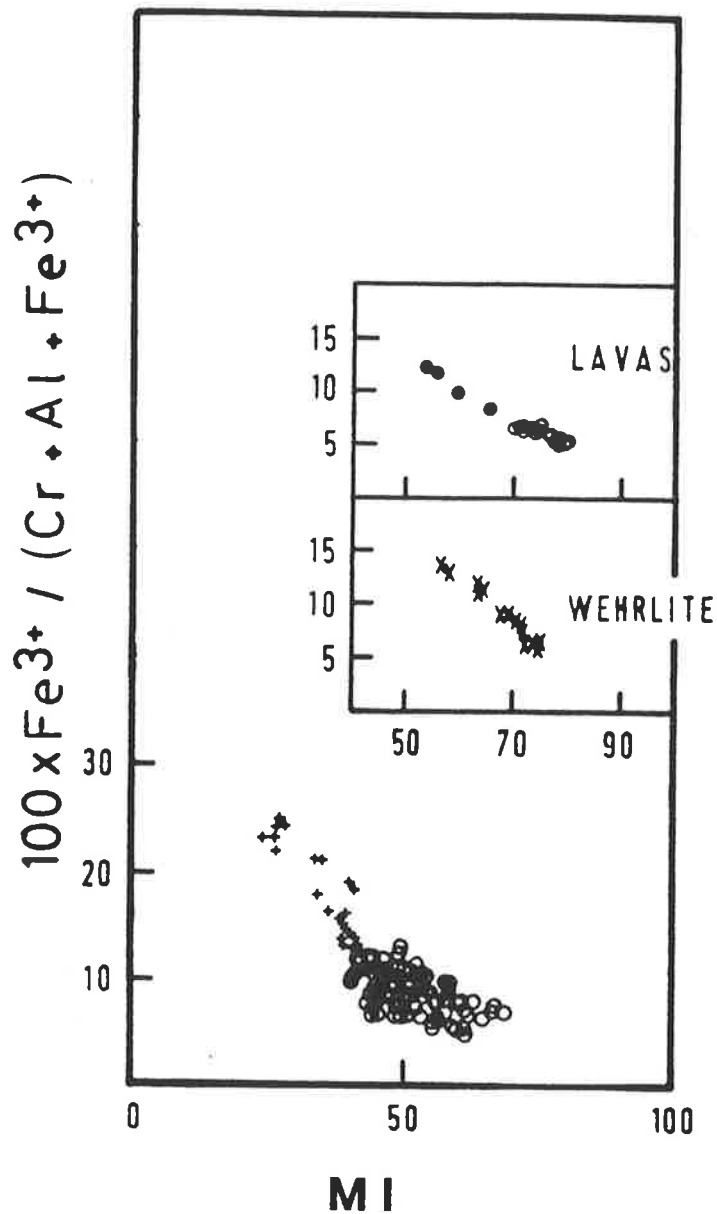
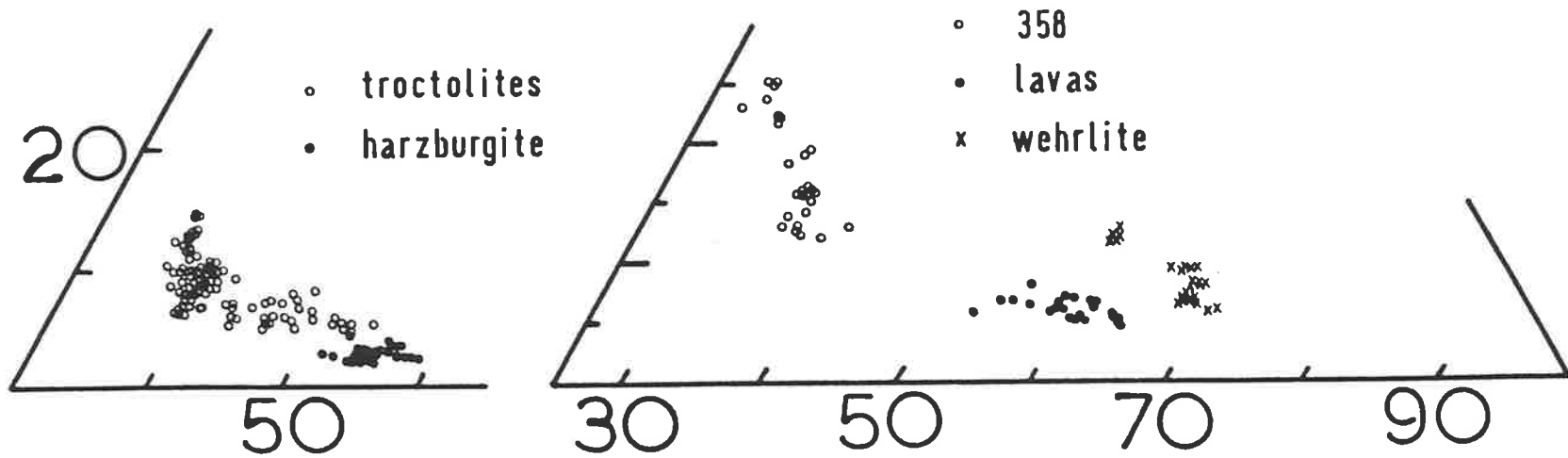
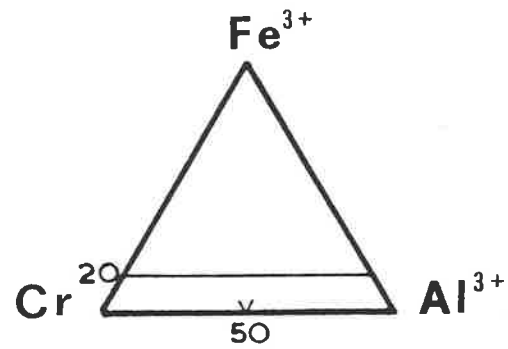


Figure 4.4.B. A $100\text{Mg}/(\text{Mg} + \text{Fe}^{2+})$ (MI) versus $100\text{Fe}^{3+}/(\text{Cr} + \text{Al} + \text{Fe}^{3+})$ plot of Macquarie Island Cr-spinels. Cr-spinels in troctolites are shown by open circles; crosses are spinels from sample 358. In the "LAVAS" inset, the core compositions of spinel xenocrysts are shown by open circles, and the rim compositions by filled circles. The "WEHRLITE" inset shows the spinel trend from the North Mountain wehrlite unit.

Figure 4.4.C. Projection of the trivalent cations Cr^{3+} - Al^{3+} - Fe^{3+} of Macquarie Island spinels. Spinel in harzburgite has the lowest ferric iron content and plots in the chromian spinel field (not shown). Spinel in lavas and the North Mountain wehrlite plot in the same field, and have higher Fe^{3+} content. Spinel in troctolites and sample 358 (an intrusive layer in the Handspike Point olivine-gabbros) show an initial enrichment in Cr, followed by Cr and Fe^{3+} increases; the ferric iron increase is better pronounced by spinels from sample 358. These spinels plot in the aluminian chromite field.

4.4.C.



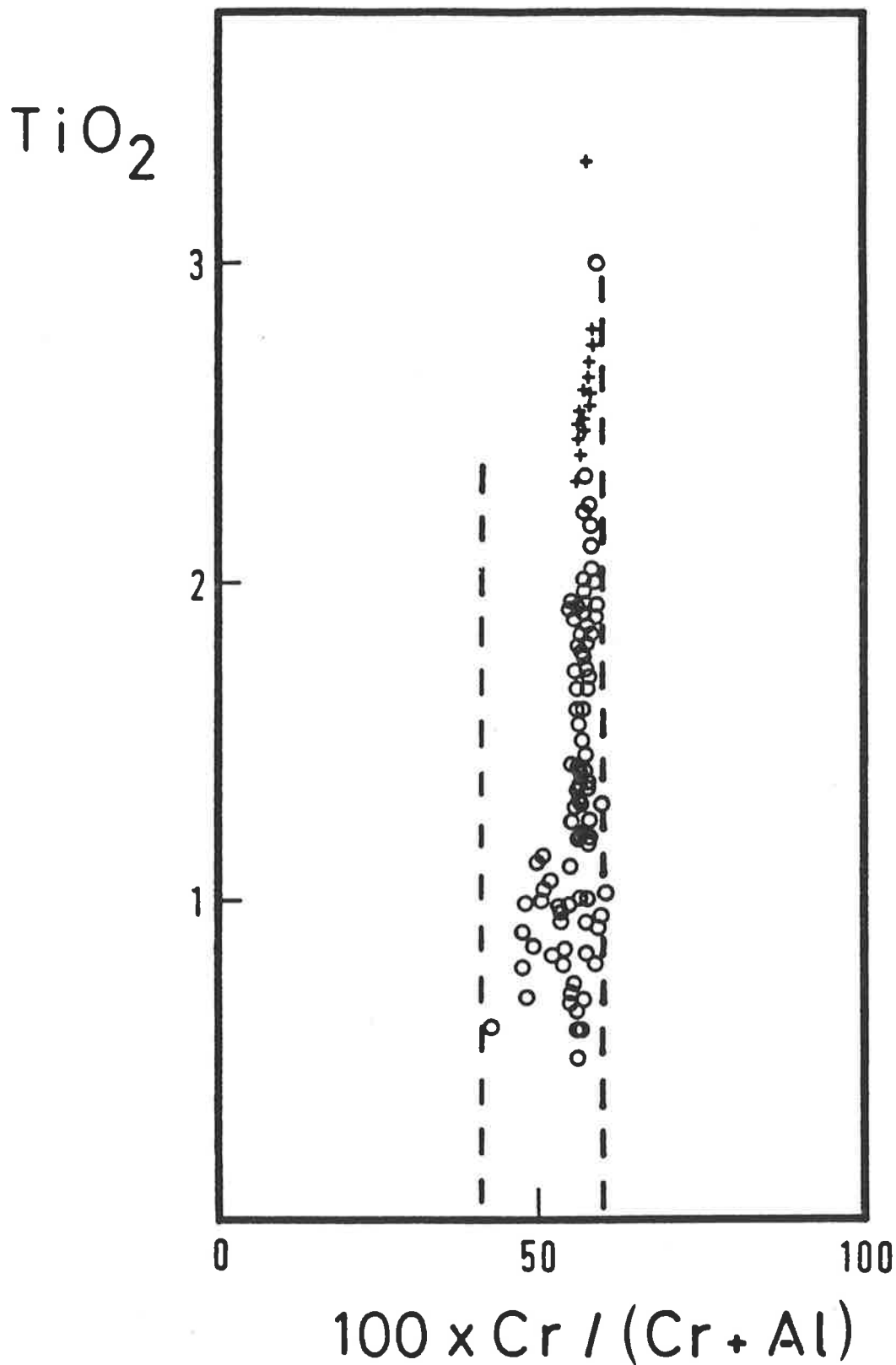
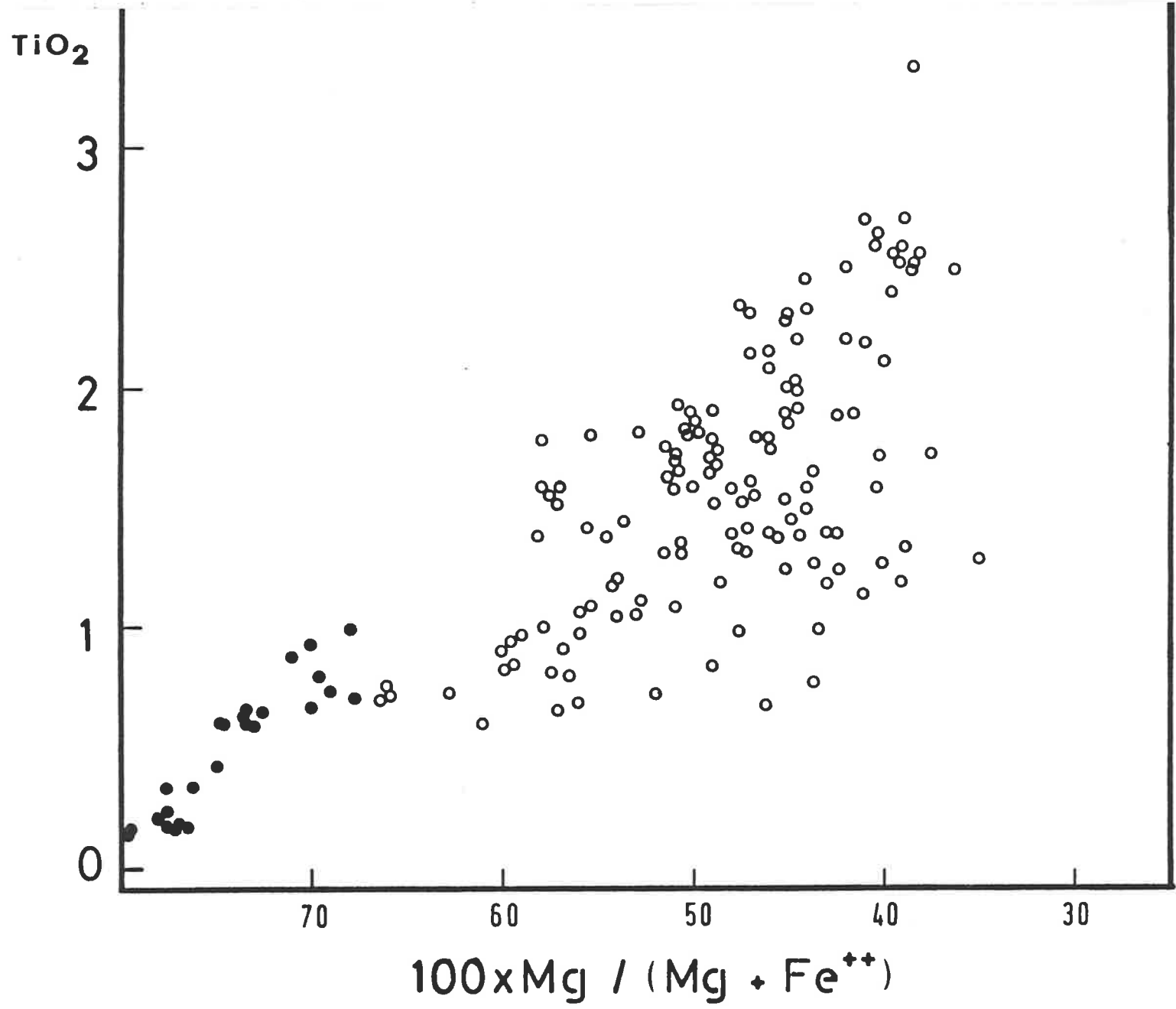


Figure 4.5. TiO_2 content (wt%) versus Cr-ratios of the cumulus spinels. Open circles are Cr-spinels from troctolites and crosses from the mafic intrusive layers. The two vertical lines outline the field of plagioclase herzolite spinels (from Dick and Bullen, 1984).

Figure 4.6. A TiO_2 versus $100 \cdot \text{Mg}/(\text{Mg} + \text{Fe}^{2+})$ plot of Macquarie Island Cr-spinels. TiO_2 is in weight percent. Open circles represent Cr-spinels from the cumulate troctolites and the intrusive melanocratic layers from Handspike Pt. Cr-spinels in these intrusive layers have the highest TiO_2 contents and the lowest $100 \cdot \text{Mg}/(\text{Mg} + \text{Fe}^{2+})$ ratios. Filled circles are Cr-spinel xenocrysts from lava M14; data on spinel phenocryst compositions from Cameron et al. (1980) are also included.



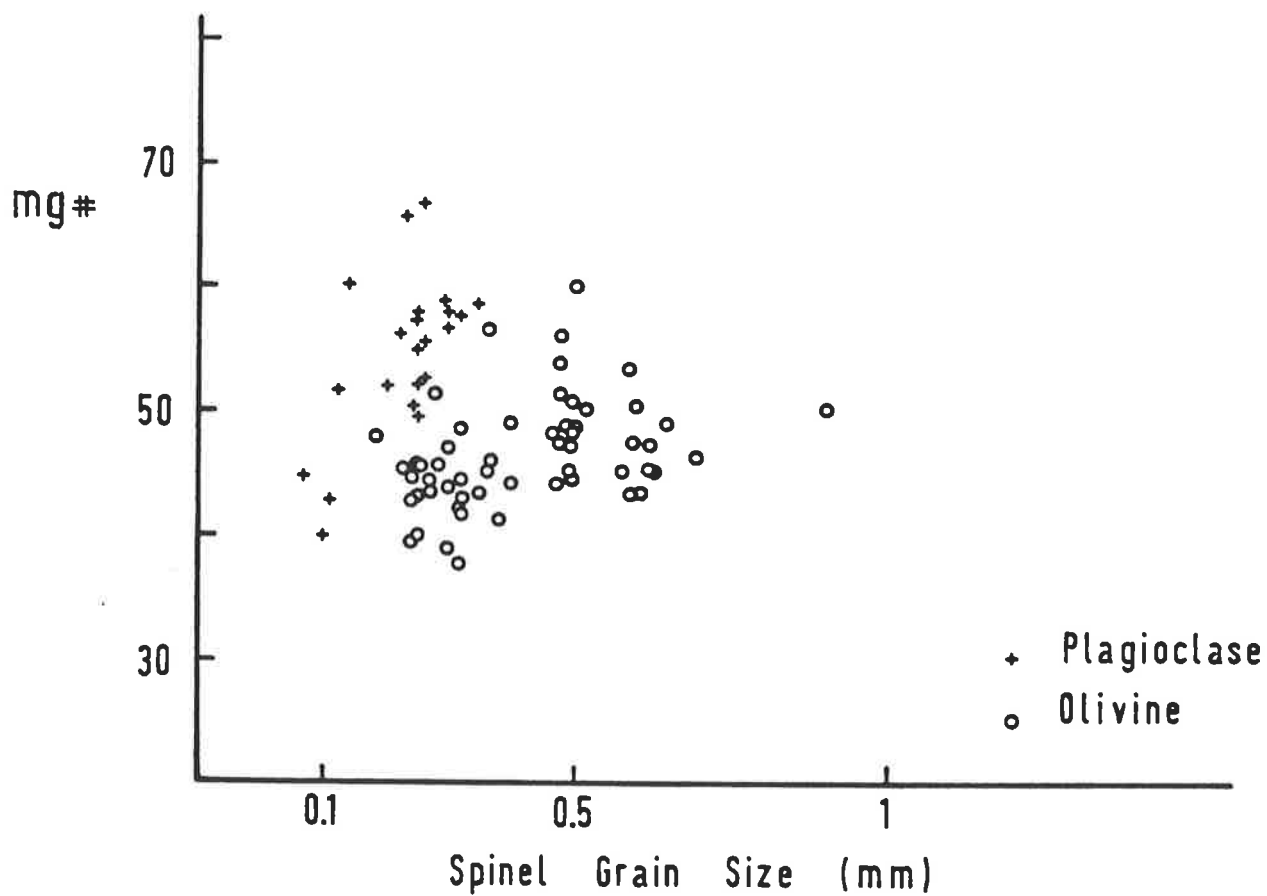


Figure 4.7. Variation of the spinel $mg\#$ in terms of its grain size and host phase. Spinel included in plagioclase are shown by crosses.
 $mg\# : 100 \cdot Mg / (Mg + Fe^{2+})$.

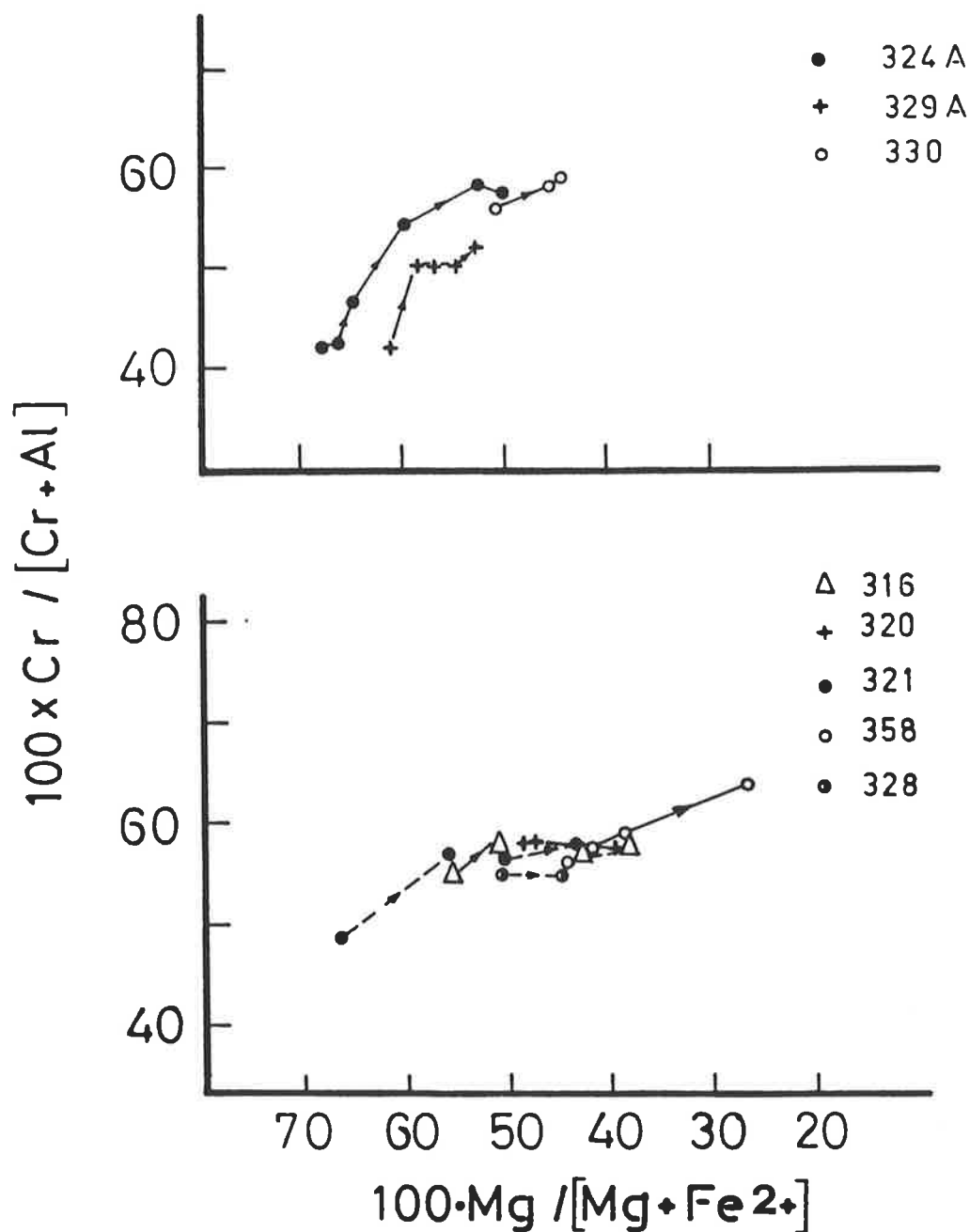


Figure 4.8A. The top diagram illustrates the changing spinel composition as the crystal size decreases (direction of the arrows). The lower plot represents the changes in spinel Mg# and Cr# from core to rim (broken lines with arrows pointing towards the rim). Solid lines show again compositional variation with decreasing grain size.

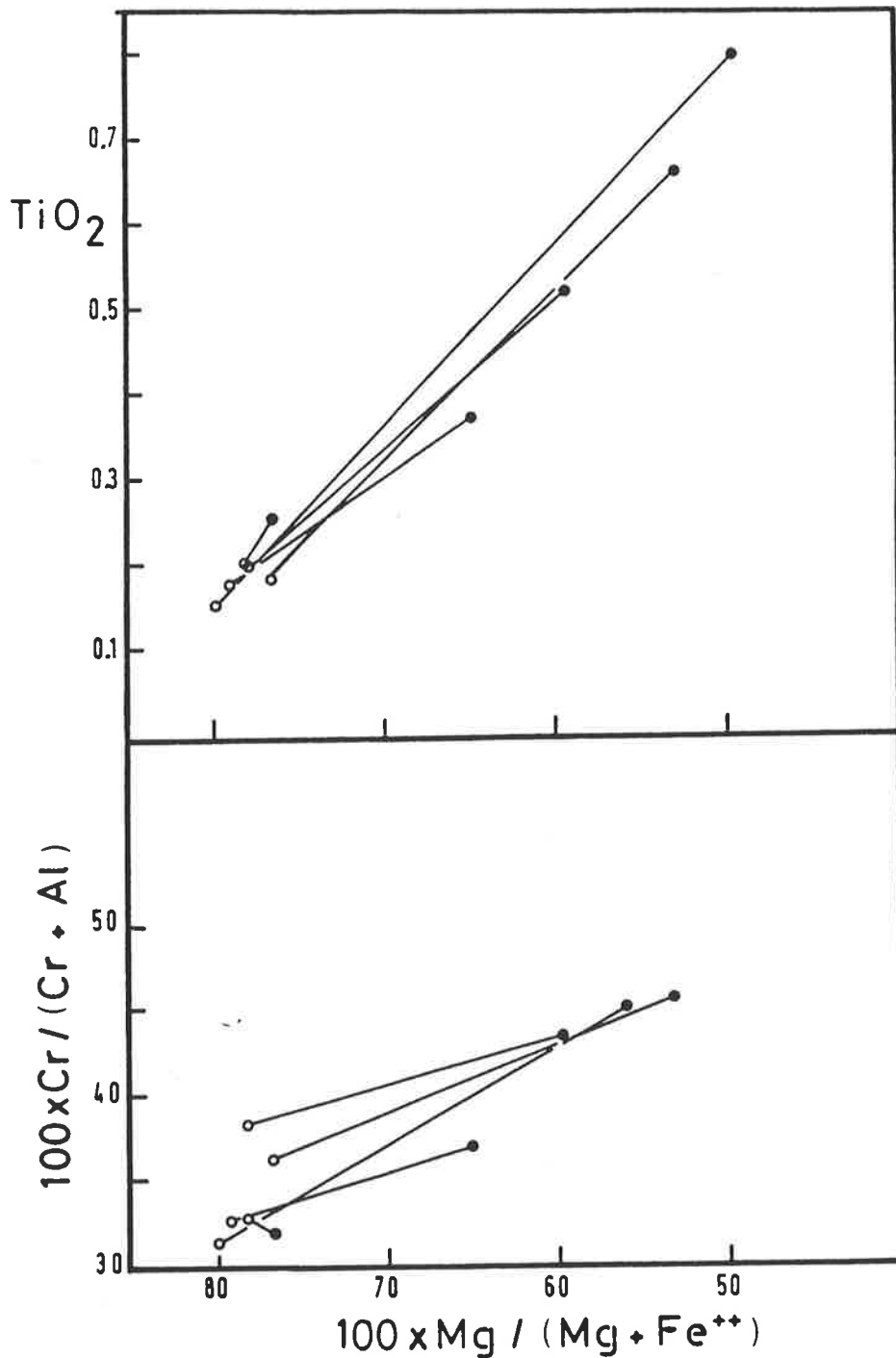
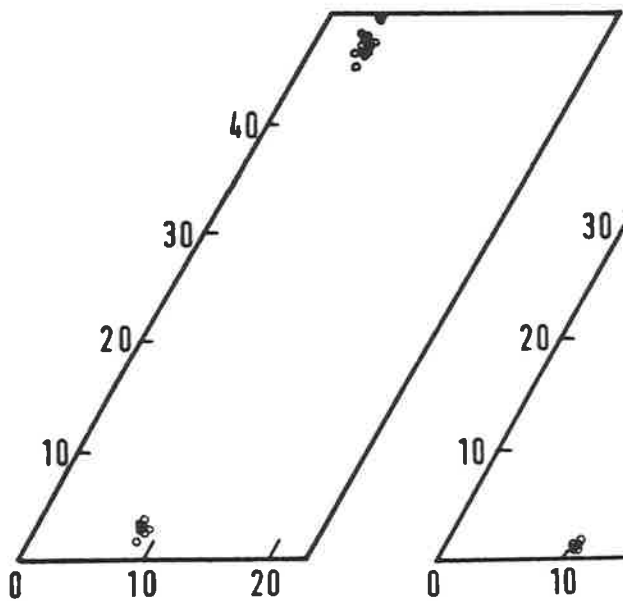


Figure 4.8B. Core - rim composition variations in spinel xenocrysts from the lavas. All analysed rims are black, contrasting the typically reddish-brown cores. Open circles represent core compositions and filled circles the rim compositions. Significant increases in TiO_2 (Wt%) and decreases in the $100\text{Mg}/(\text{Mg}+\text{Fe}^{++})$ ratio from core to rim, suggest that these spinels are not in equilibrium with the host basalt.

Figure 4.9A. Macquarie Island pyroxene compositions plotted in the enstatite-ferrosilite-wollastonite (Mg-Fe-Ca) ternary. Orthopyroxene compositions represent exsolution lamellae, more than $5\mu\text{m}$ in width, from clinopyroxene in the layered rocks. Clinopyroxenes in harzburgite and the layered rocks are diopsides. The orthopyroxenes in harzburgite and the exsolved orthorhombic Ca-poor phase (from clinopyroxenes) in the rocks of the layered sequence are enstatites, following the classification of Morimoto et al. (1988).

A.

HARZBURGITE

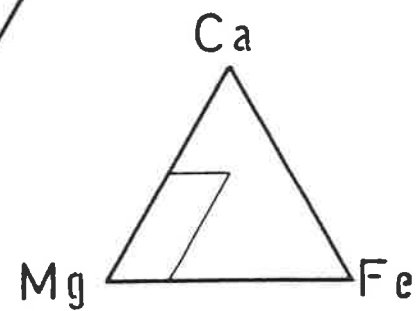
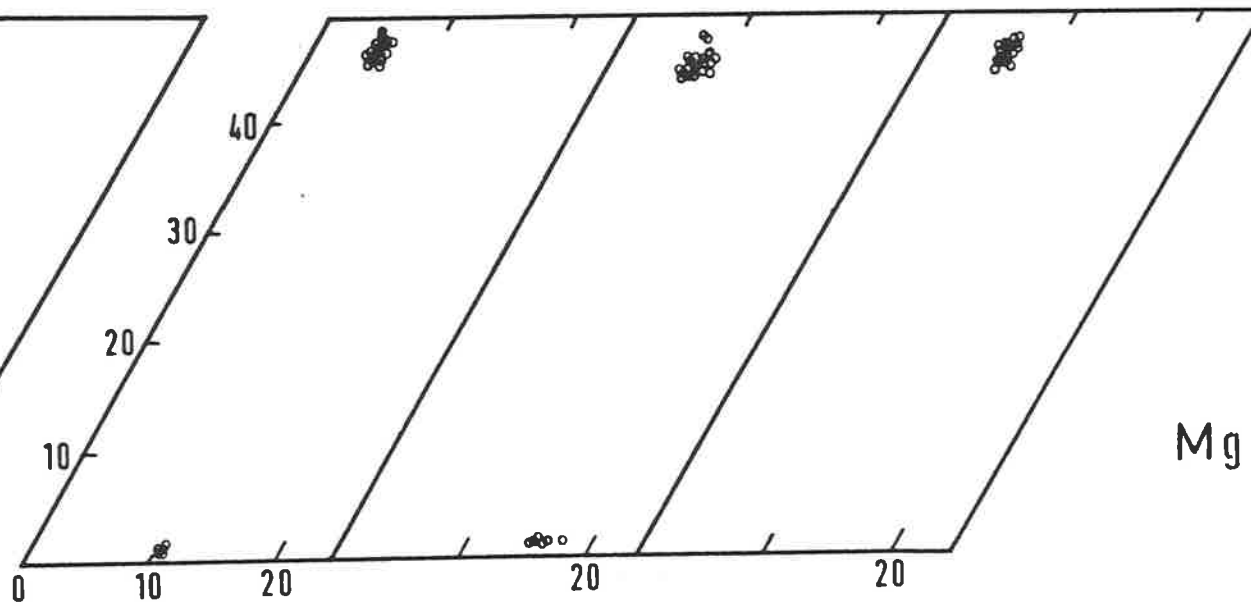


LAYERED SEQUENCE

TROCTOLITES

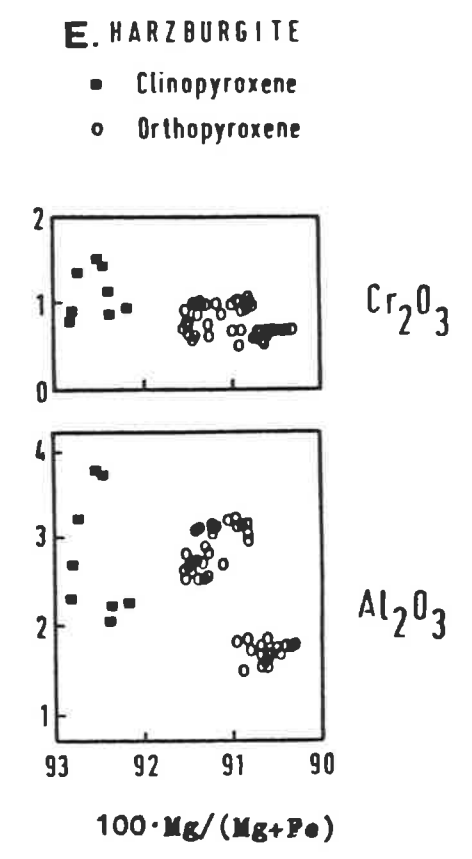
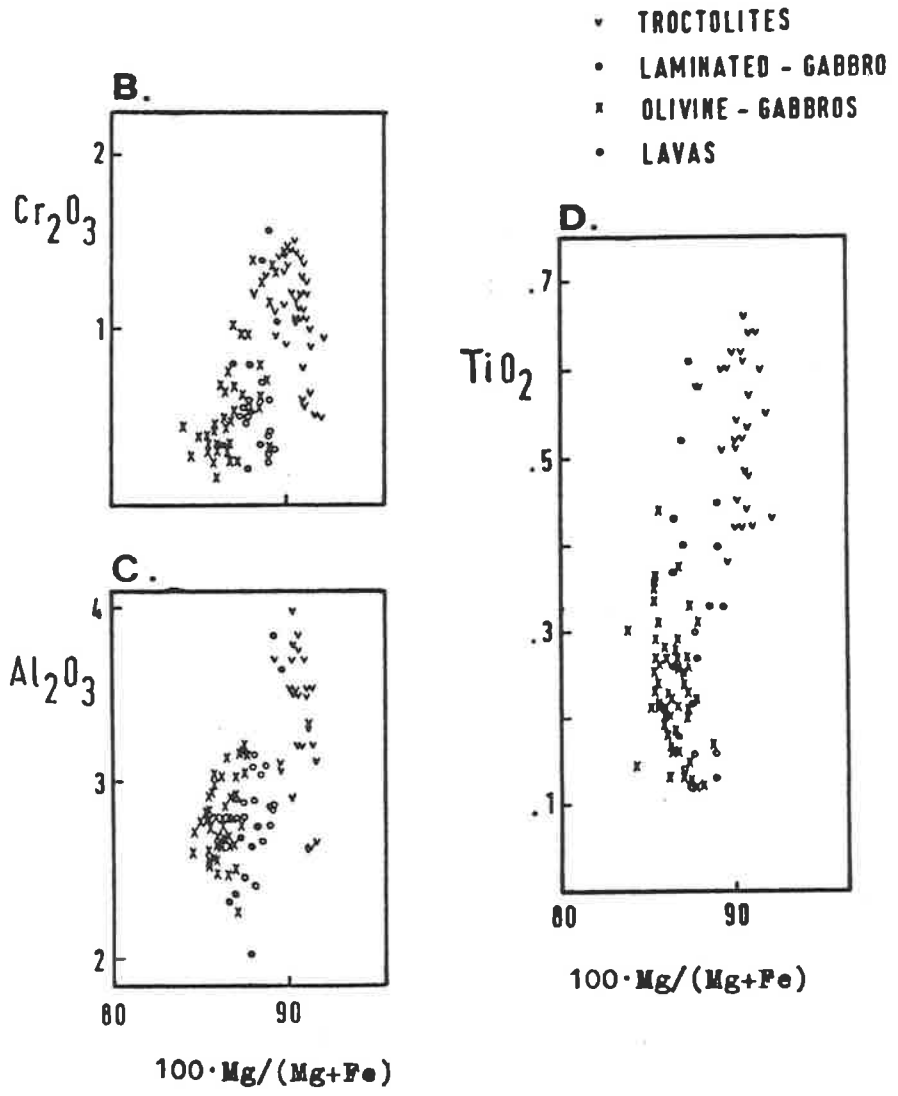
OL - GABBROS

GABBROS



Figures 4.9B to E. Compositional characteristics of plutonic clinopyroxenes, harzburgite pyroxenes and clinopyroxene phenocrysts (lavas only) from Macquarie Island.

- 4.9B. A plot of Cr_2O_3 (wt%) against atomic $100 \cdot \text{Mg}/(\text{Mg}+\text{Fe})$ for plutonic clinopyroxenes, and clinopyroxene phenocrysts in the lavas. Plutonic clinopyroxenes are from the layered troctolites, olivine-gabbros and laminated gabbros; the laminated (also lineated) gabbros are the uppermost rock type from the layered sequence. The data for clinopyroxene phenocrysts are taken from Griffin (1982).
- 4.9C. Correlation of Al_2O_3 contents (wt%) with $100 \cdot \text{Mg}/(\text{Mg}+\text{Fe})$. Symbols as in 4.9B.
- 4.9D. TiO_2 versus $100 \cdot \text{Mg}/(\text{Mg}+\text{Fe})$ plot. Symbols as in 4.9B.
- 4.9E. Correlation of Cr_2O_3 and Al_2O_3 contents (wt%) of harzburgite pyroxenes with their $100 \cdot \text{Mg}/(\text{Mg}+\text{Fe})$ ratios. Clinopyroxenes (squares) are distinctly more magnesian than the coexisting orthopyroxenes. Clinopyroxenes represent interstitial material and exsolved phases.



F.

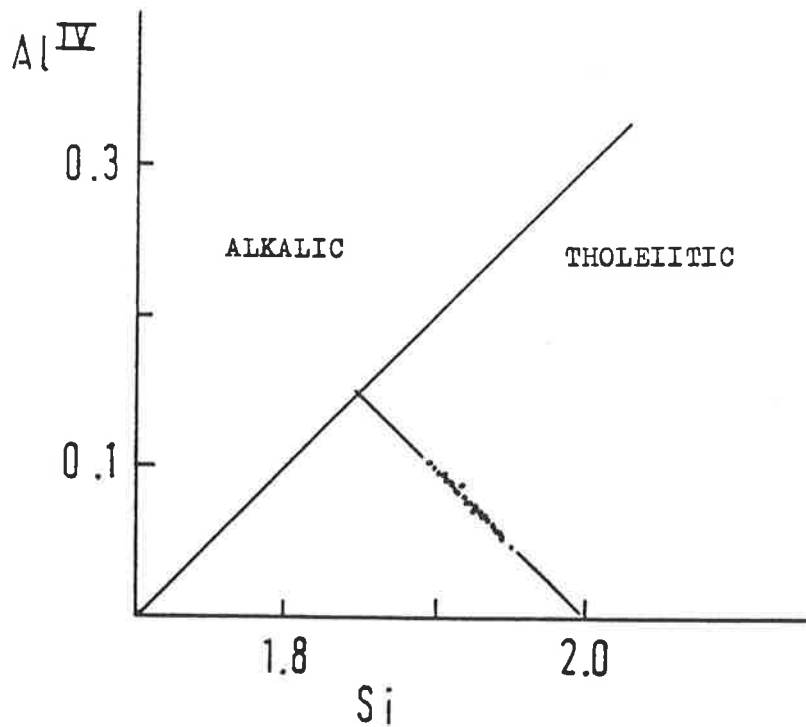


Figure 4.9F. Cation plot of Si versus tetrahedral Al (Al^{IV}) for clinopyroxenes in the layered troctolites and olivine-gabbros. Clinopyroxenes derived from tholeiitic melts are chemically different from those derived from alkalic melts. The division between tholeiitic and alkalic clinopyroxenes is based on Kushiro (1960). The Macquarie Island clinopyroxenes (small filled circles) plot in the tholeiitic field.

G.

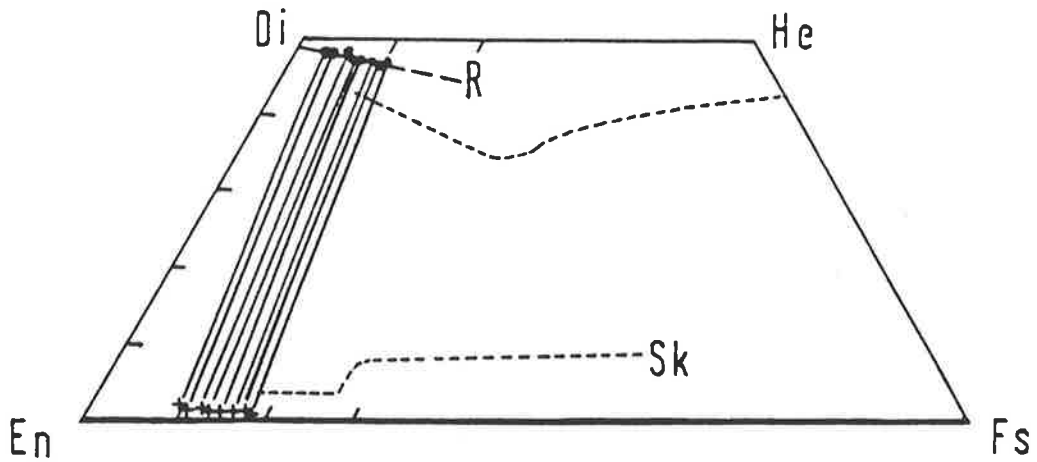


Figure 4.9G. Coexisting clinopyroxene (filled circles) and exsolved low-Ca pyroxene (crosses) compositions from the layered rocks. Tie lines connect clinopyroxene and the exsolved low-Ca phase. Sk is the Skaergaard pyroxene trend. R is the 800°C solvus of Ross and Huebner (1975).

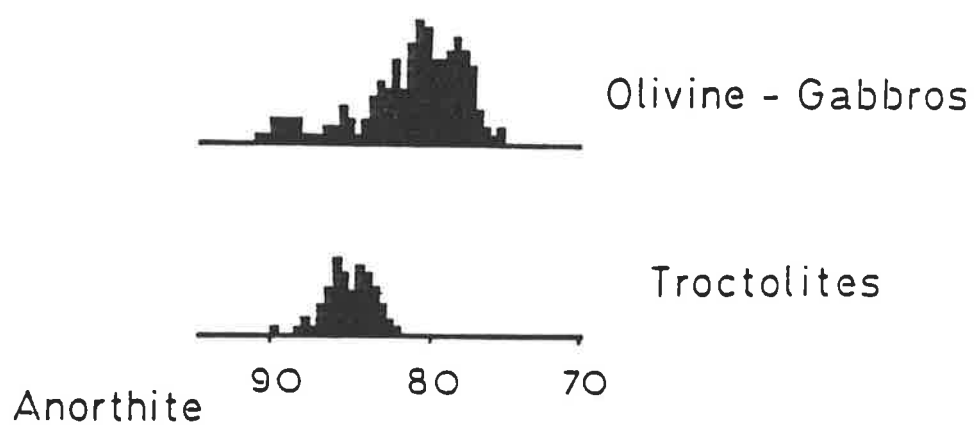
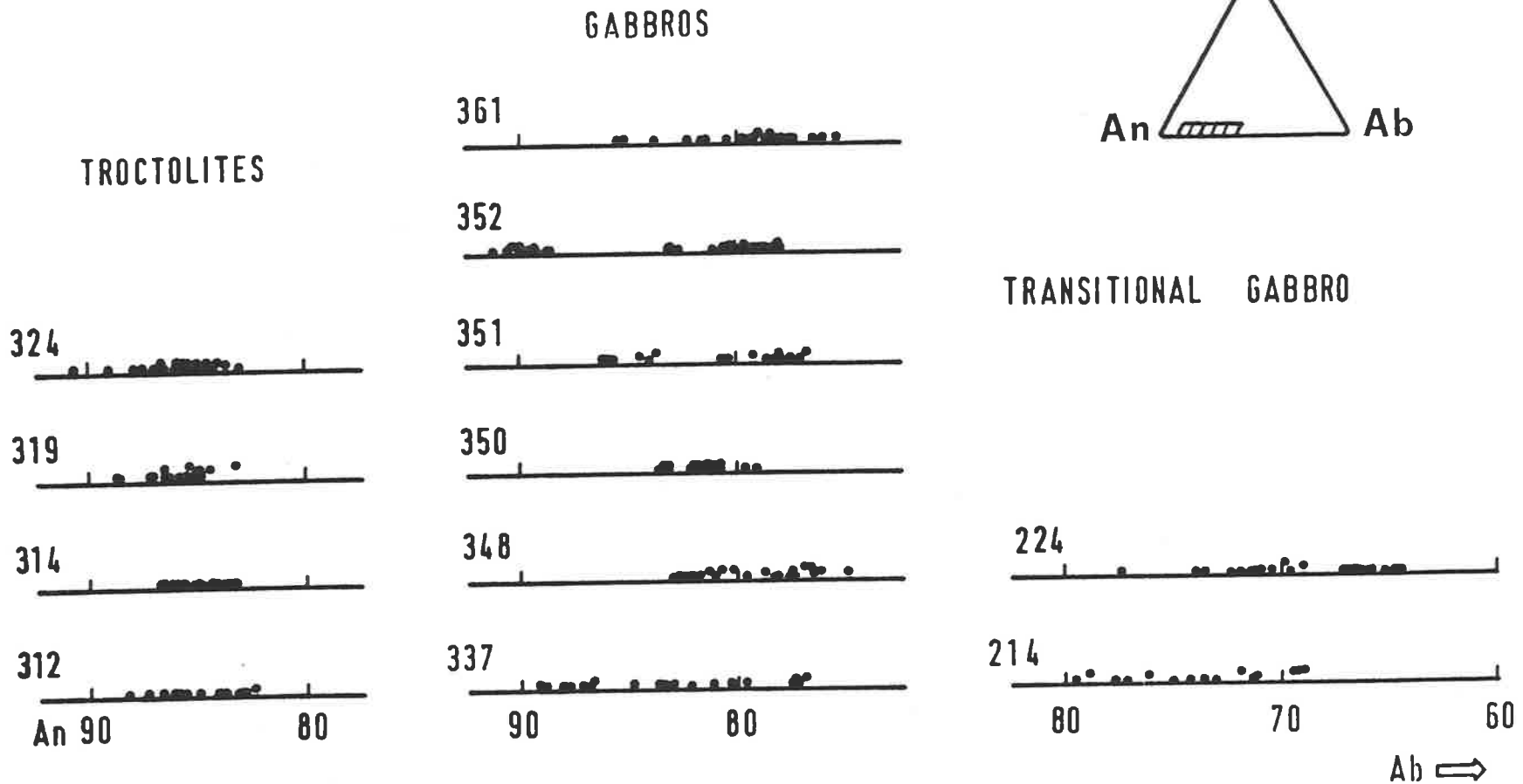


Figure 4.10. Histogram of plagioclase compositions from the olivine gabbros and troctolites. Total number of plotted analyses for olivine gabbros 200, for troctolites 100.

Figure 4.11A. Plutonic plagioclase analyses plotted in the An-Ab-Or ternary. The compositional variation observed in four troctolites, and six olivine-gabbros and olivine-free gabbros (GABBROS) is shown. Both, core and rim compositions are plotted. The transitional gabbro (samples 214 and 224) is the uppermost layered rock type; it shows well developed igneous lamination.

Layered sequence



Upper level gabbro

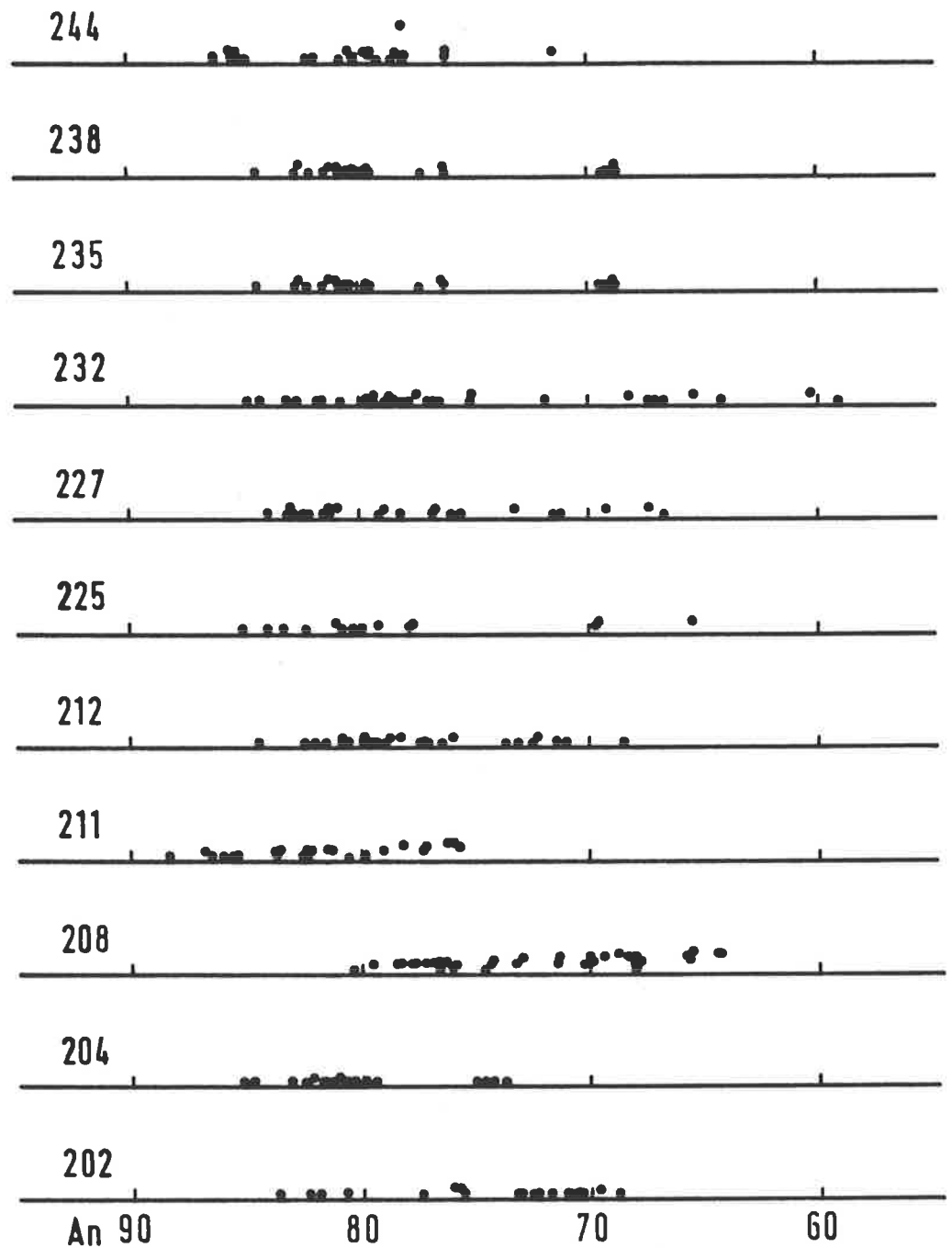


Figure 4.11B. Range in plagioclase composition within individual samples from the Upper Level Gabbro.

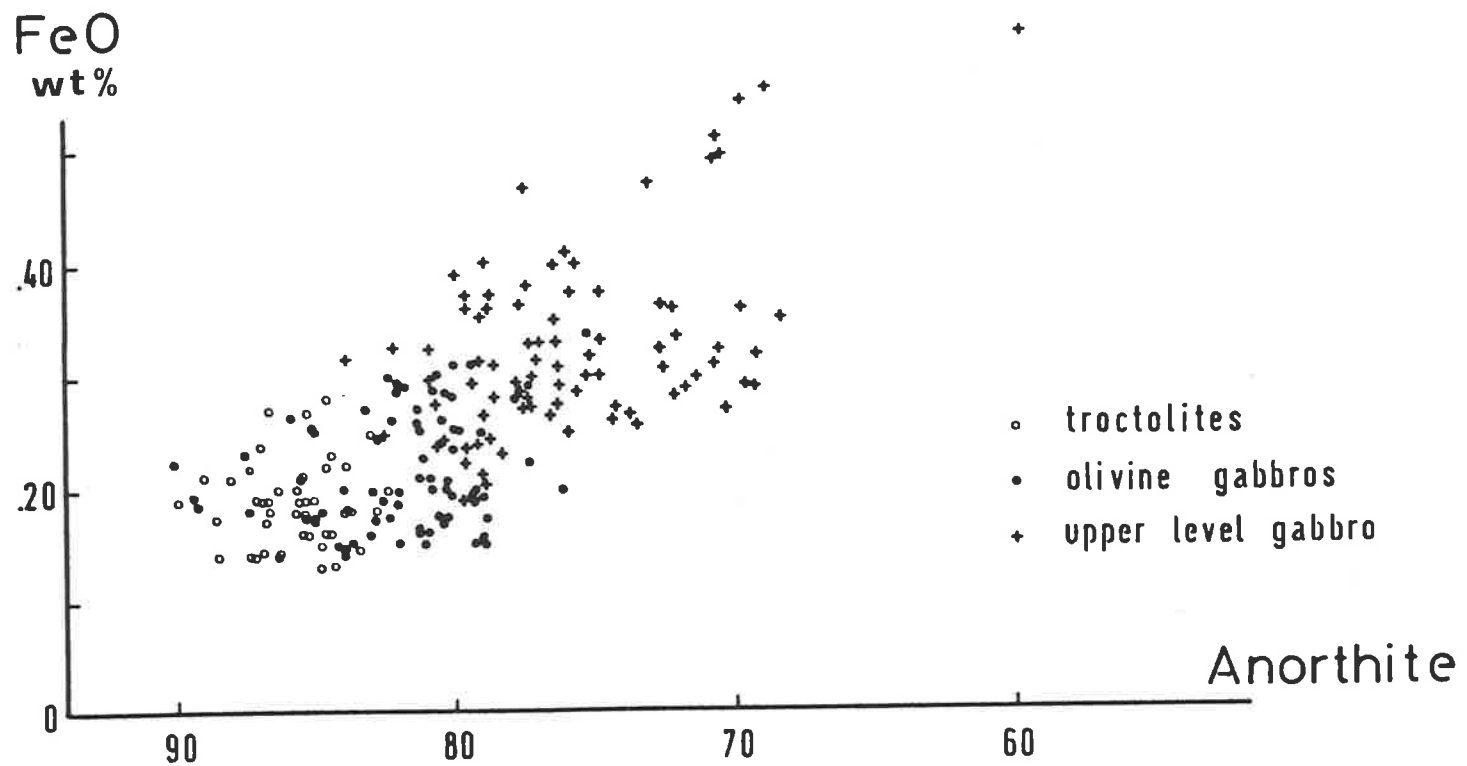


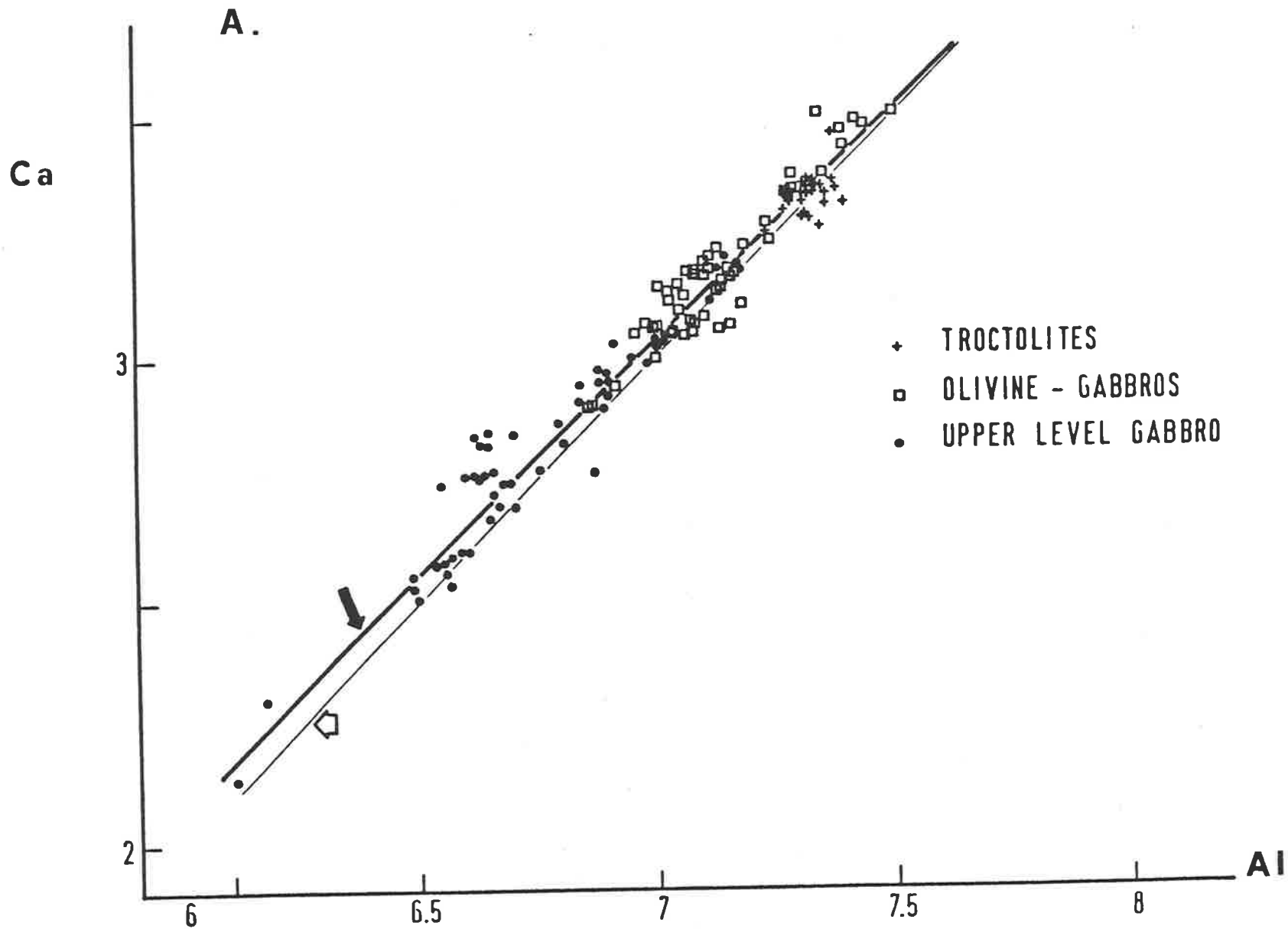
Figure 4.12. The iron content of the plutonic plagioclases as a function of the anorthite content. An overall positive variation is demonstrated by the data.

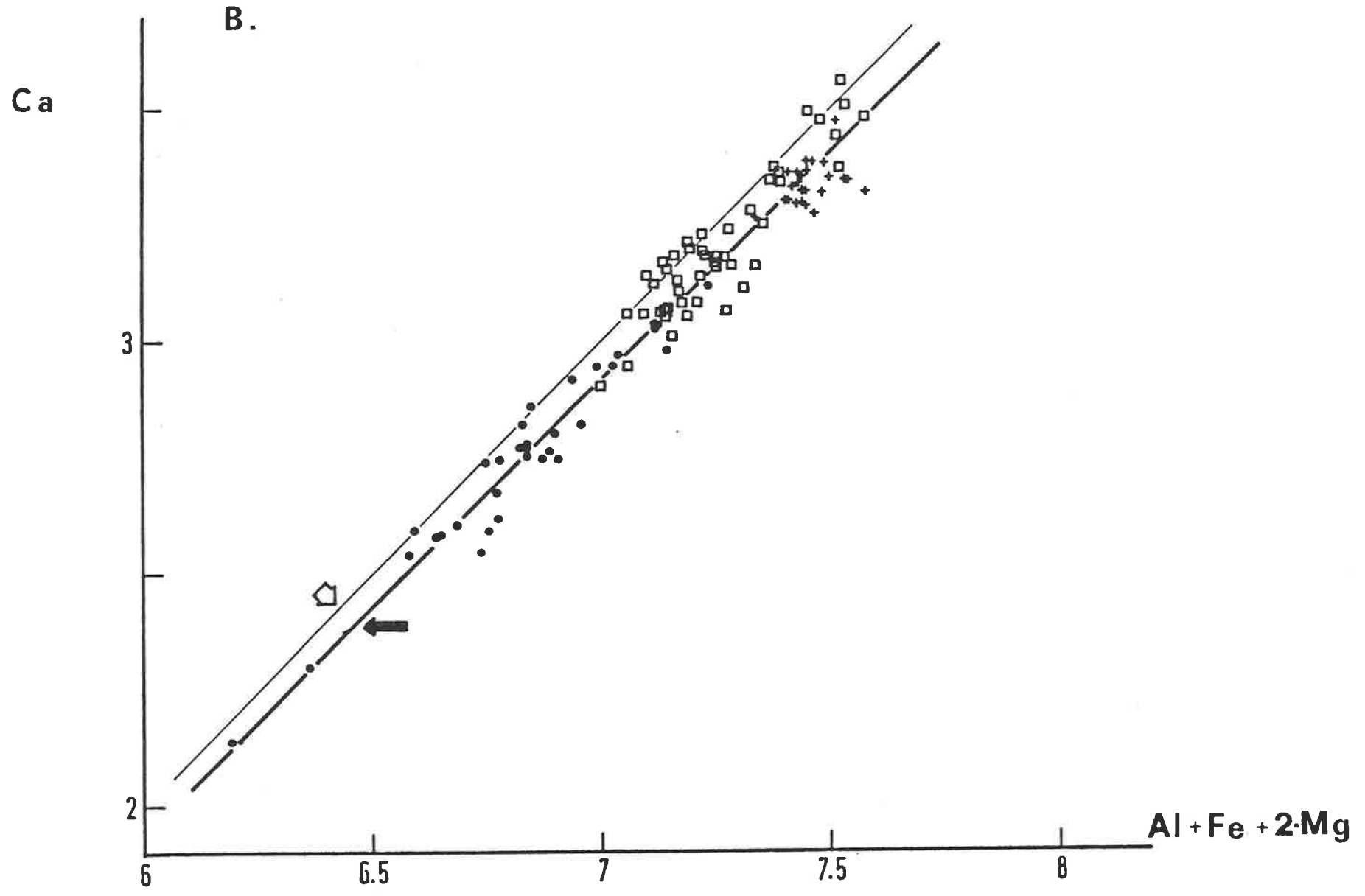
Figure 4.13A. Cation correlation in plutonic plagioclases. A Ca versus Al plot of plagioclase from troctolites (crosses), layered olivine-gabbros (open squares) and Upper Level gabbro (filled circles). Thick line (pointed by the solid arrow) is the best fit line to Macquarie Island data. Thin line (indicated by the short open arrow) is the predicted line from feldspar stoichiometry.

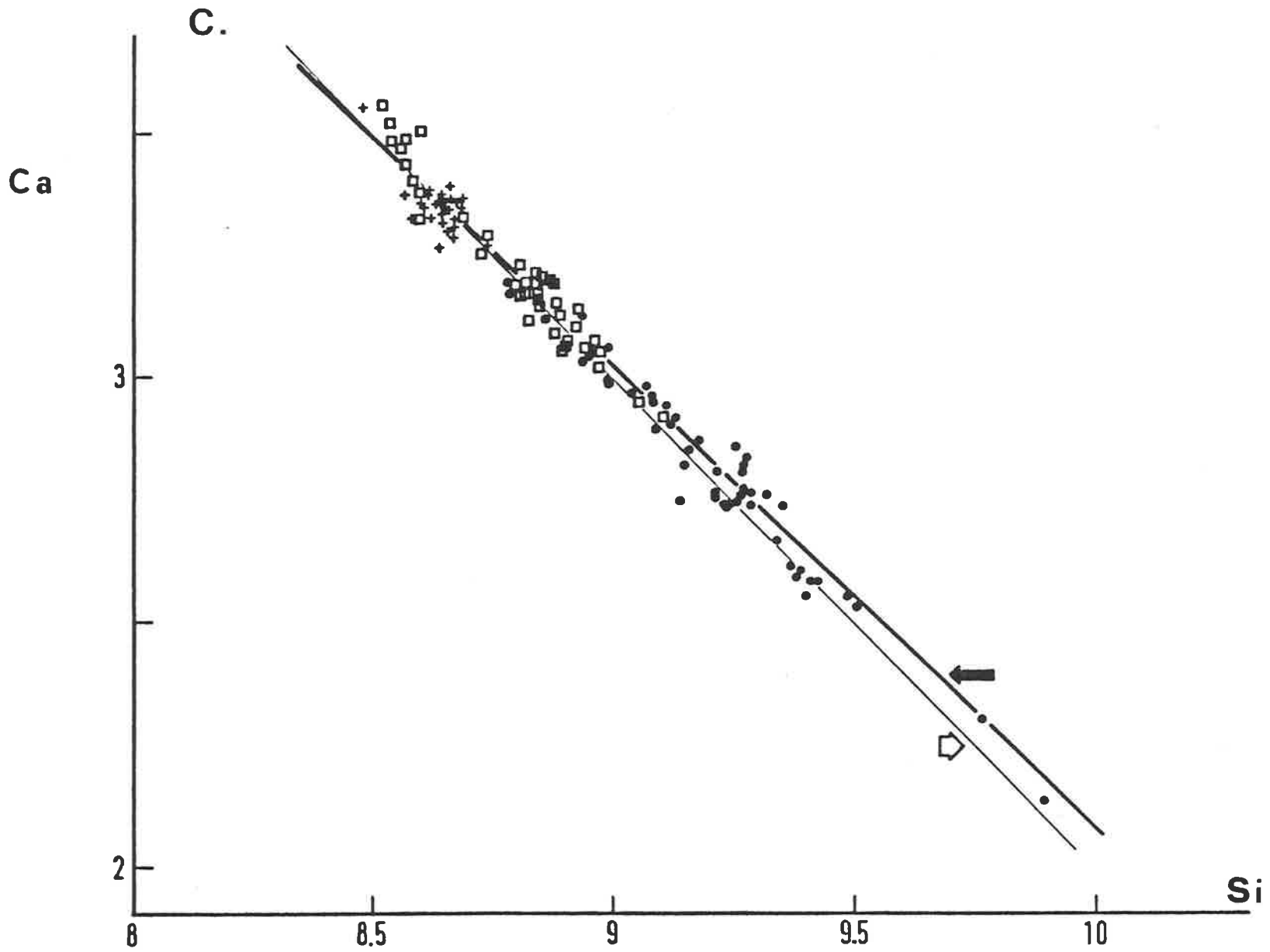
4.13B. A Ca versus $Al+Fe+2Mg$ plot.

4.13C. A Ca versus Si plot.

4.13D. A Ca versus Si-Mg-Fe plot.







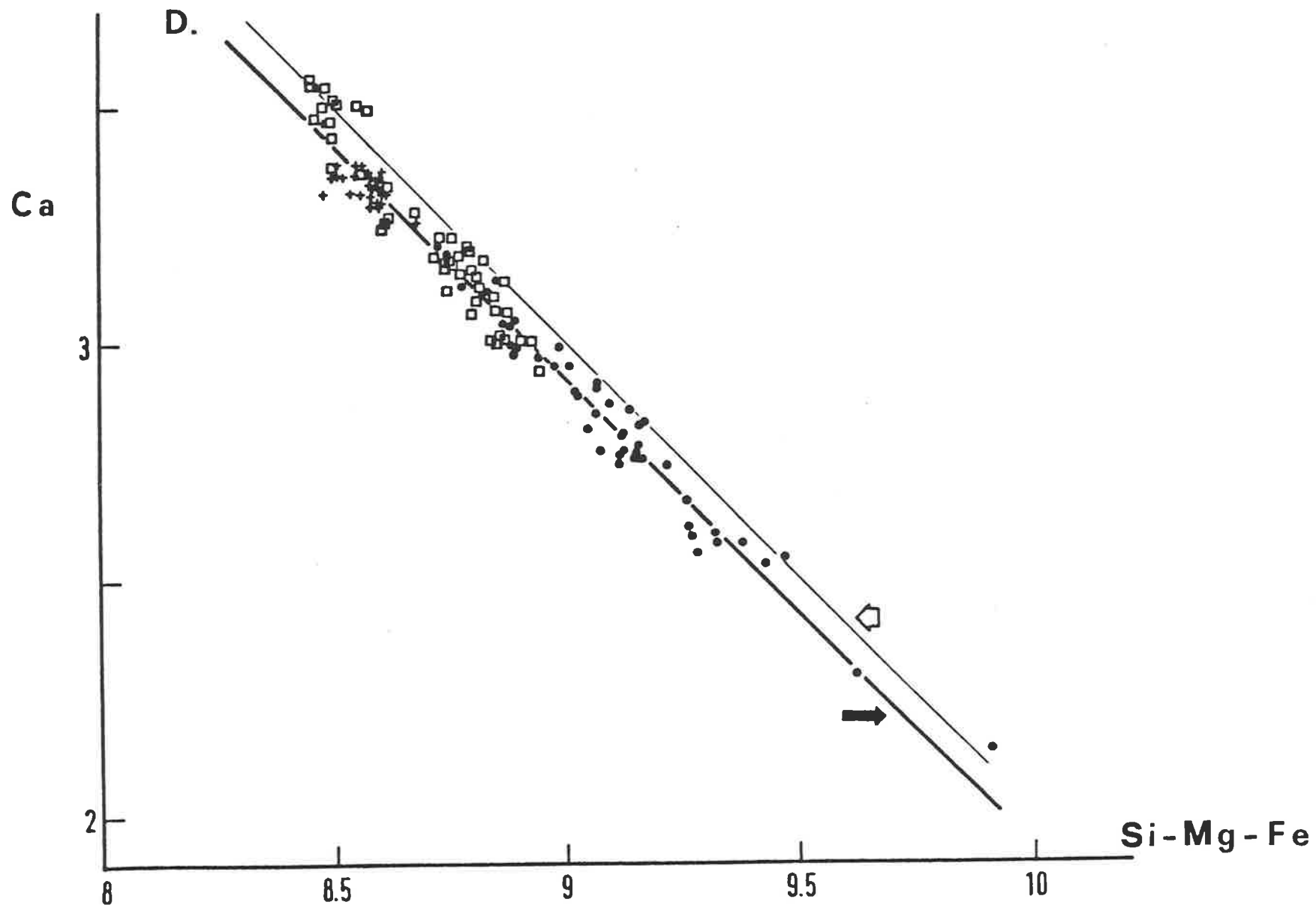


Figure 4.14.

Olivine, plagioclase and clinopyroxene cryptic variation in a section through the Macquarie Island plutonic suite. Sample 358 is an intrusive mafic layer in the olivine-gabbros at Handspike Point. Sample 202 is a gabbroic screen from the dyke swarm at Gadgets Gully. Horizontal bars indicate the compositional range observed in each sample. The range in plagioclase compositions is greater in the Upper Level gabbro than in troctolites and olivine-gabbros; core and rim compositions are plotted.

R-H: residual harzburgite, ot: olivine-rich troctolite segregations (MgO more than 30%wt).

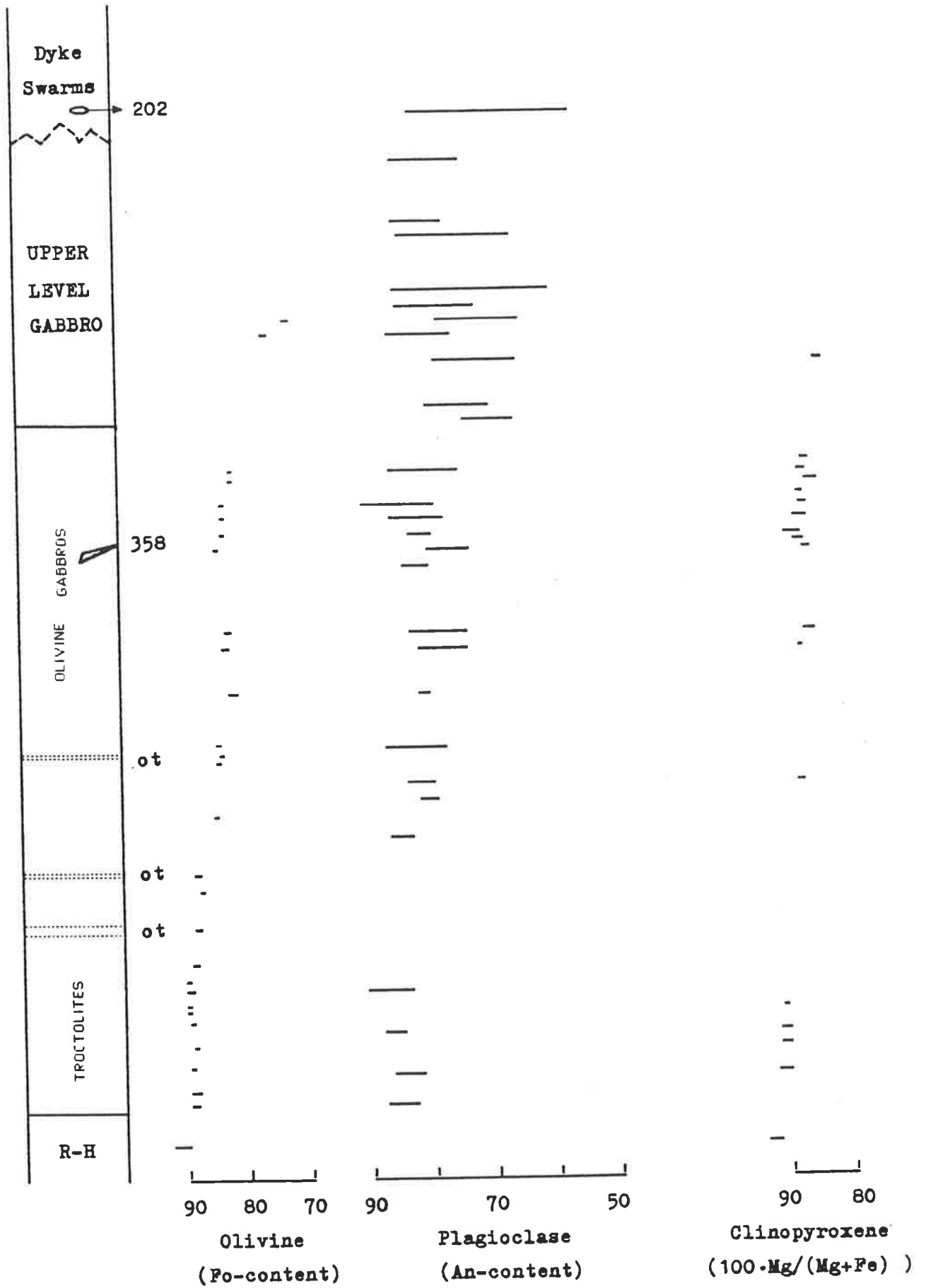


Figure 5.1. Representative analyses of amphiboles from the plutonic rocks, are plotted in a Si versus $Mg/(Mg+Fe^{2+})$ diagram. The upper plot is for amphiboles with a cation sum of Na and K in A sites of less than 0.5. The lower plot is for amphiboles with total Na+K cations in A sites of less or equal to 0.5. The classification is based on Leake (1978).

Upper plot: Filled circles are pale green to colourless amphiboles in the Upper Level gabbro. They form euhedral fringes around clinopyroxene, possibly as a replacement phase. Stars are well developed green hornblendes in sample 726. Semi-filled circles are strongly pleochroic green amphiboles from a secondary monomineralic vein in Upper Level Gabbro. Open circles are colourless amphiboles from the layered troctolites; they plot in the tremolite field. The fields from the left hand side to the right hand side, for $Mg/(Mg+Fe^{2+})$ ratios of more than 0.5, are actinolite, actinolitic hornblende (A.HB.), magnesio-hornblende (MG-HB), tschermakitic hornblende and tschermakite.

Lower plot: A Si versus $Mg/(Mg+Fe^{2+})$ plot for colourless to pale green amphiboles from layered troctolites. The sum of Na and K in A sites is greater than 0.5, and Fe^{3+} is greater than Al^{vi} in all amphiboles. E.HB.: edenitic hornblende, P.HB.: pargasitic hornblende, PARG: pargasitic hornblende. Cation recalculation on the basis of 23 oxygens.

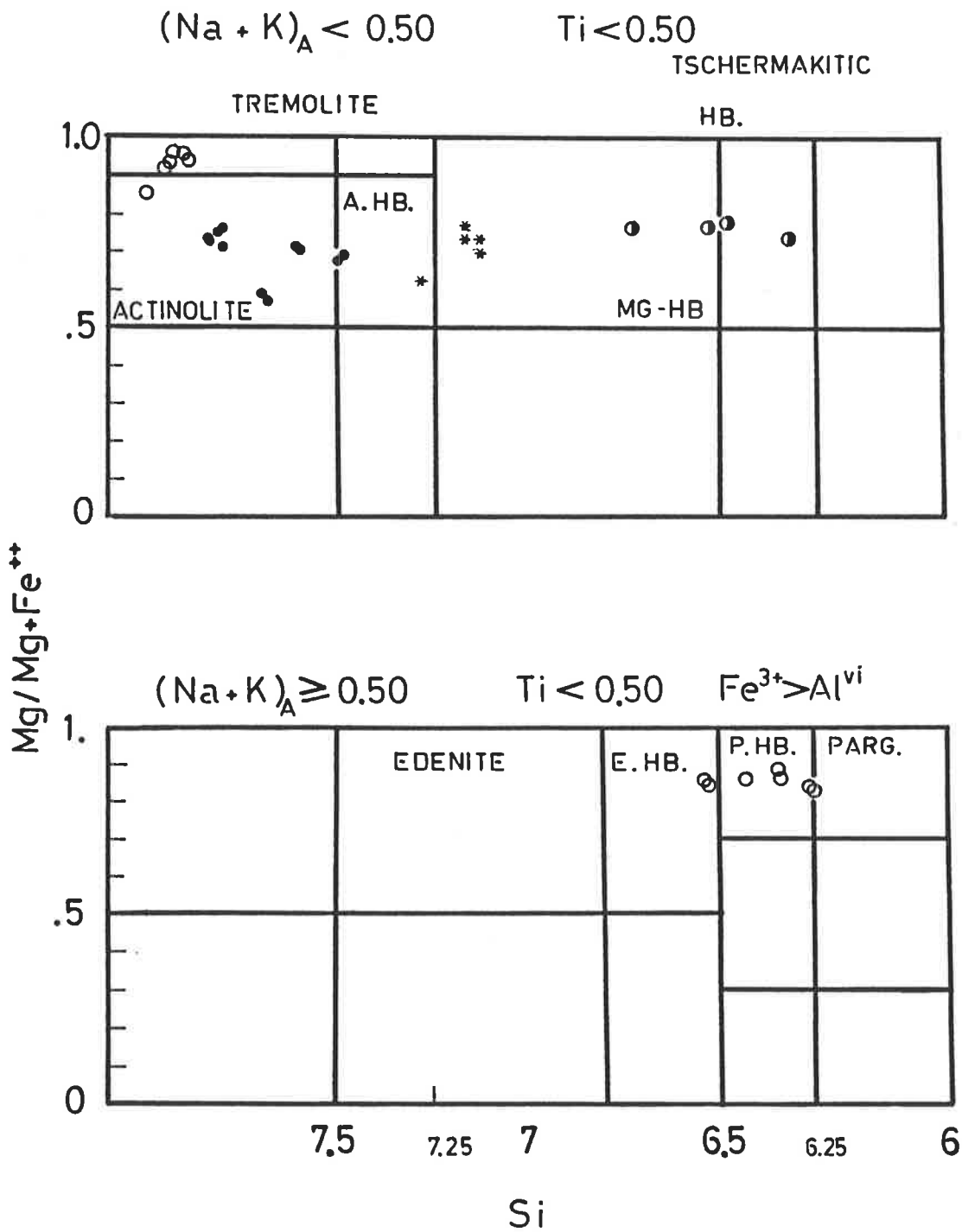
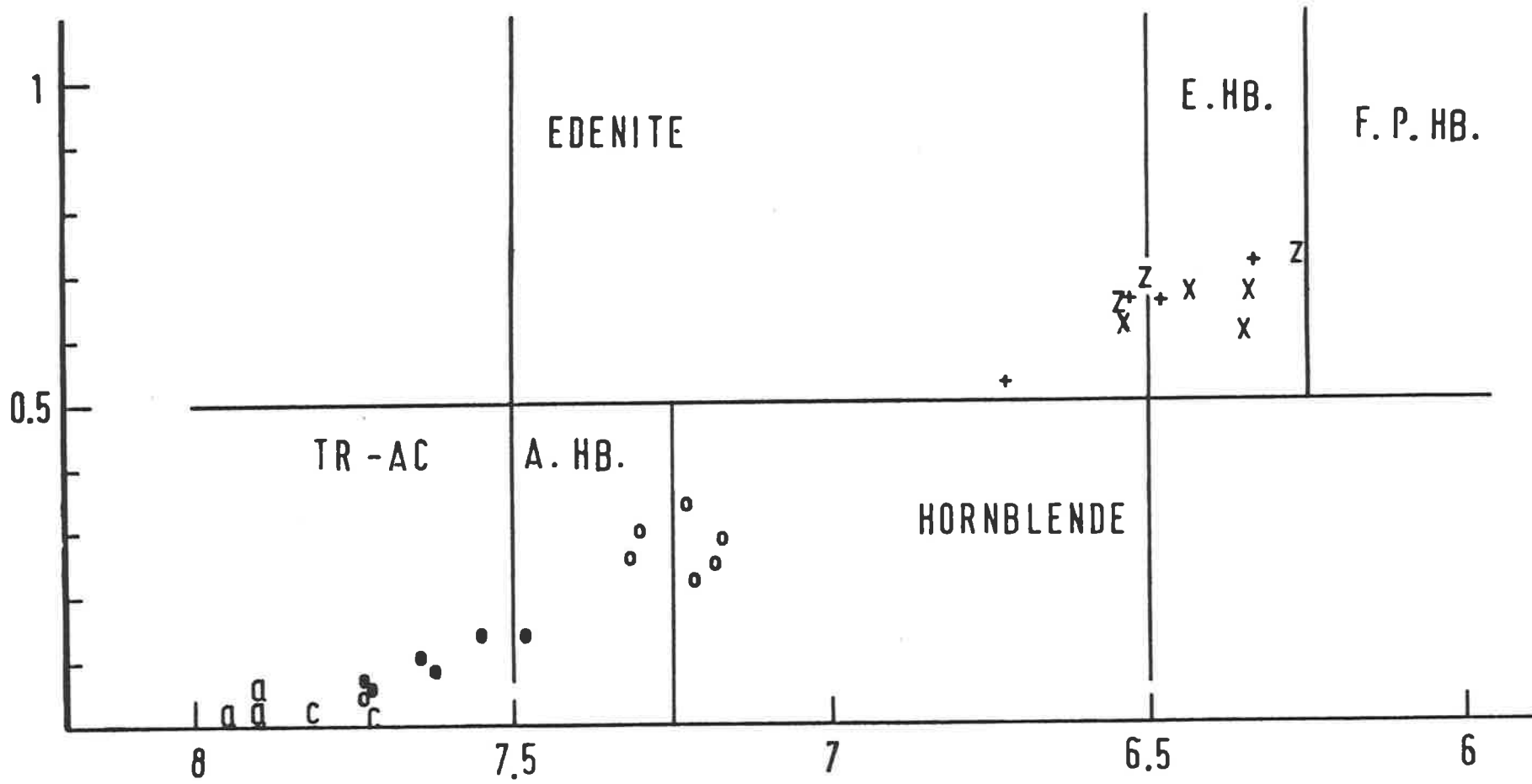


Figure 5.2. A plot of Si cations versus the Na+K cations in A sites for plutonic amphiboles. Symbols are as follows, a: colourless amphibole in layered troctolites, c: colourless amphibole in Upper Level Gabbro, filled circles: colourless to pale green amphibole replacing primary clinopyroxene in Upper Level Gabbro, open circles: bright green hornblende in doleritic gabbro (sample 726), X: pleochroic amphibole in troctolites, Z: colourless amphibole in troctolites, +: strongly pleochroic amphibole from a secondary vein in Upper Level Gabbro.

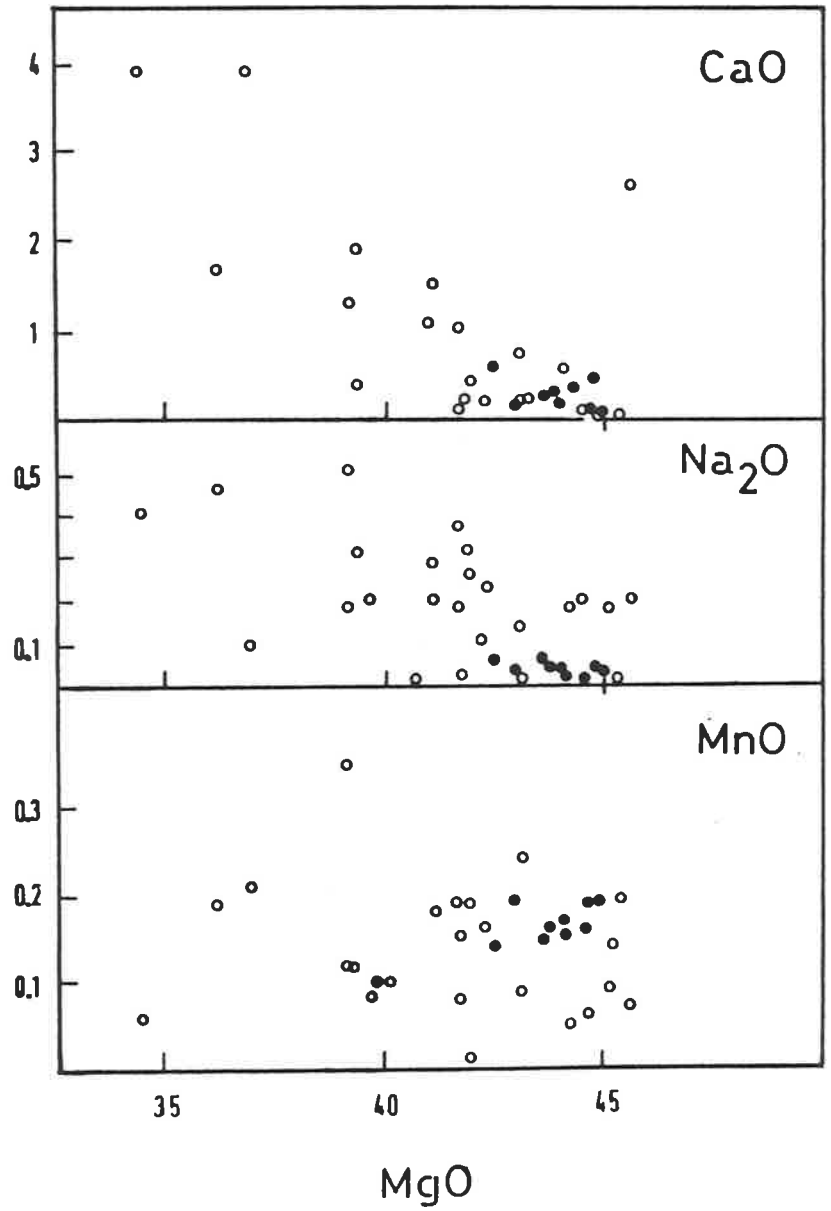
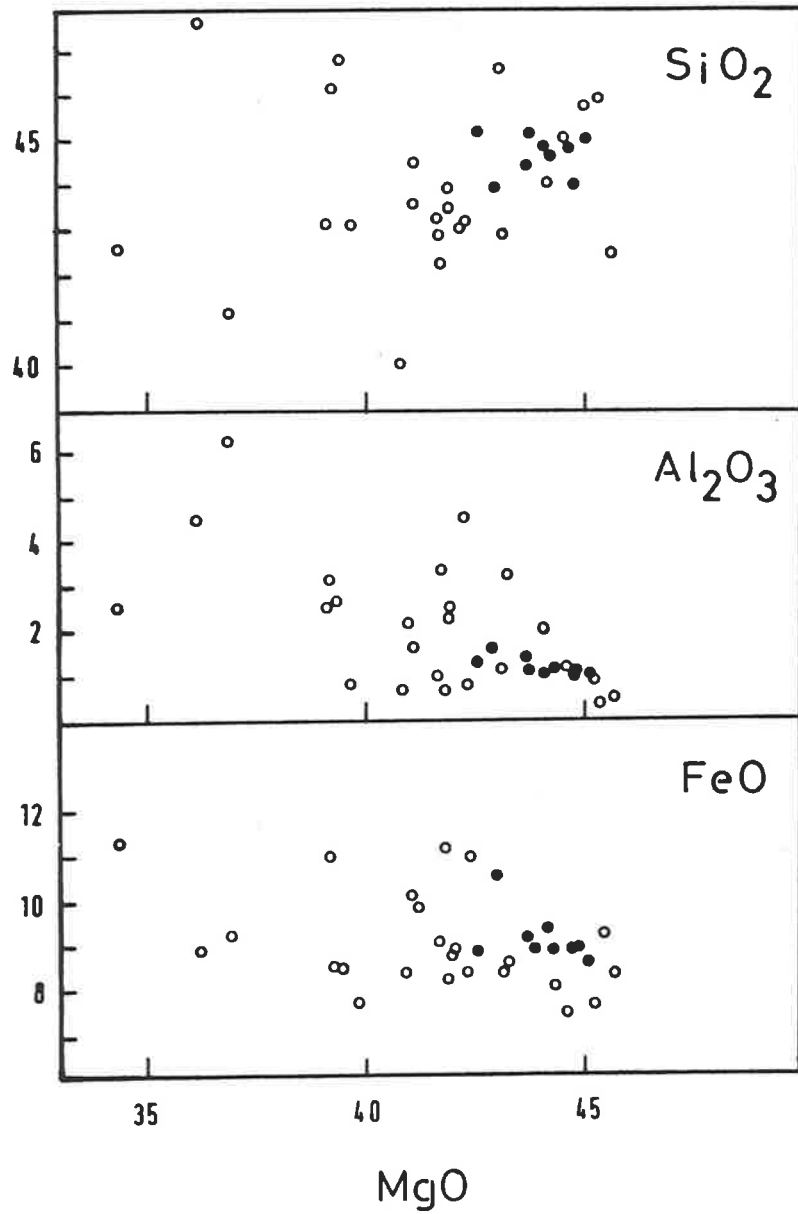
Classification according to Leake (1978). The pleochroic amphiboles plot in the edenitic hornblende (E.HB.) field, the colourless in the tremolite-actinolite (TR-AC) field, and the bright green hornblende ifrom sample 726 in the hornblende and actinolitic hornblende (A.HB) fields. F.P.HB. is ferroan pargasitic hornblende. (Analyses recalculated on 23 oxygens).

$(Na+K)_A$



Si

Figure 6.1. Variation of the major oxide content (wt%) with the MgO content (wt%) in Macquarie Island harzburgites (shown by filled circles). The compositional variation in abyssal peridotites (open circles) is significantly greater. The Macquarie Island rocks plot towards the high-MgO end of the abyssal peridotite field, and lower Na₂O and CaO contents. Data sources for abyssal peridotites: Aumento and Loubat (1971), Hekinian and Aumento (1973), Prinz et al. (1976), Shibata and Thompson (1986).



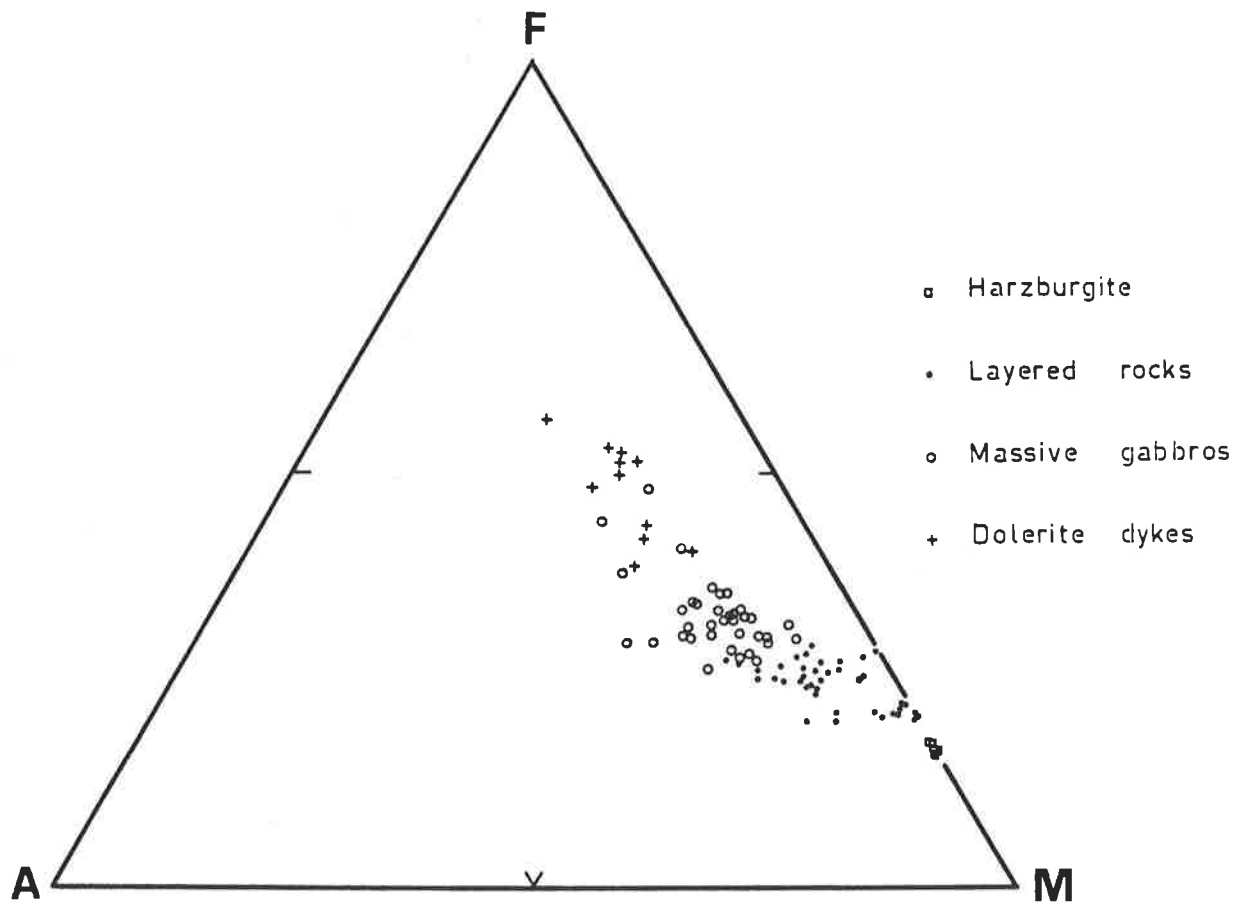


Figure 6.2. AFM plot for plutonic rocks and dolerite dykes in the layered sequence and massive gabbros.

A = Na₂O+K₂O, F = total Fe and M = MgO.

All oxides in weight percent.

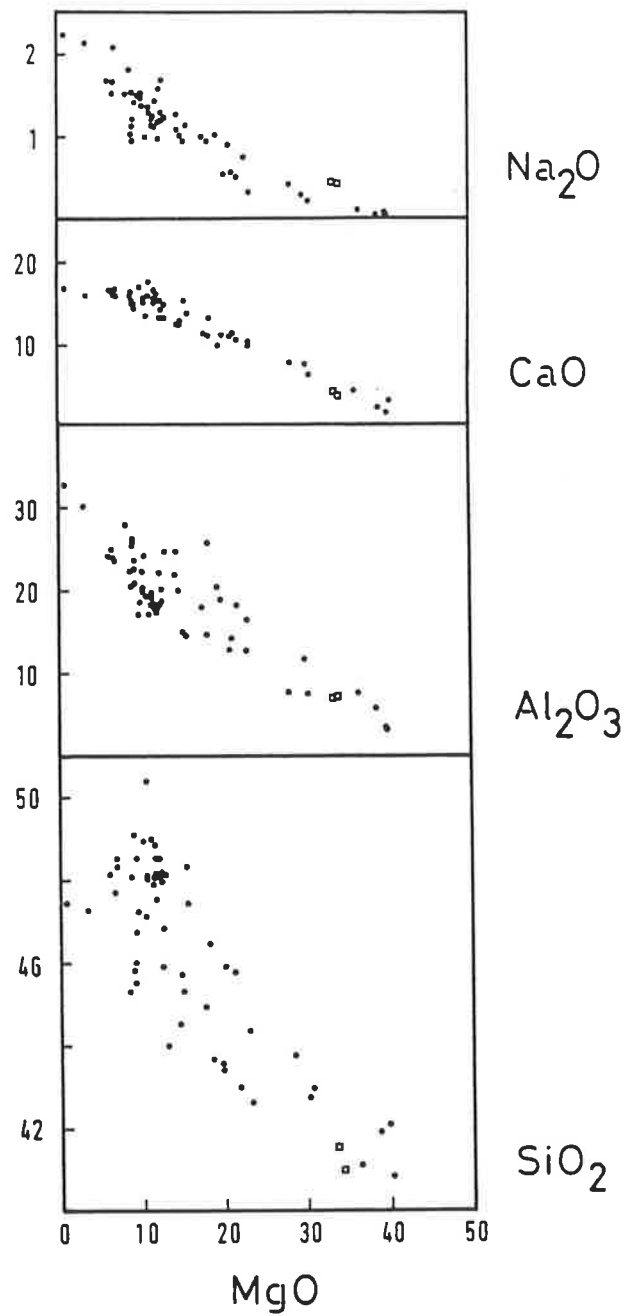


Figure 6.3. MgO variation diagrams for the layered rocks (dots). Two samples from the North Mt. wehrlite are shown by squares. The oxides in weight percentages.

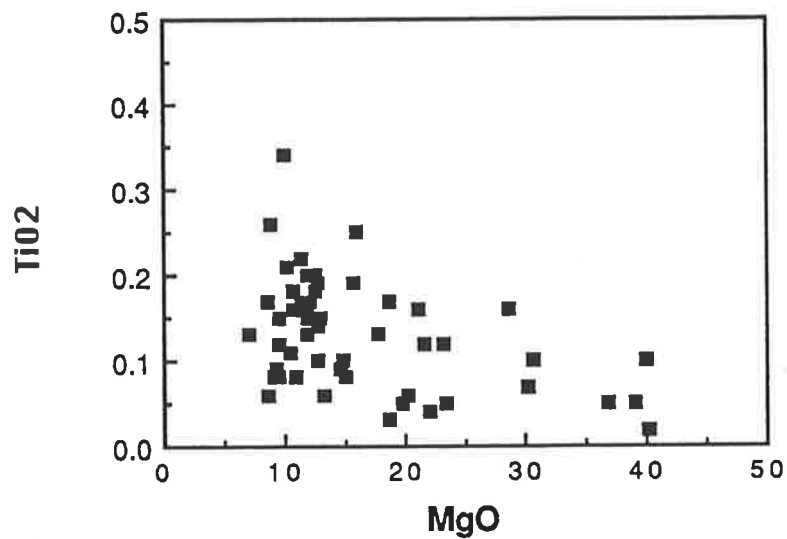


Figure 6.4. A TiO₂ versus MgO plot of Macquarie Island layered rocks. Both oxides in weight percentages. Anorthosites from the layered sequence are not plotted.

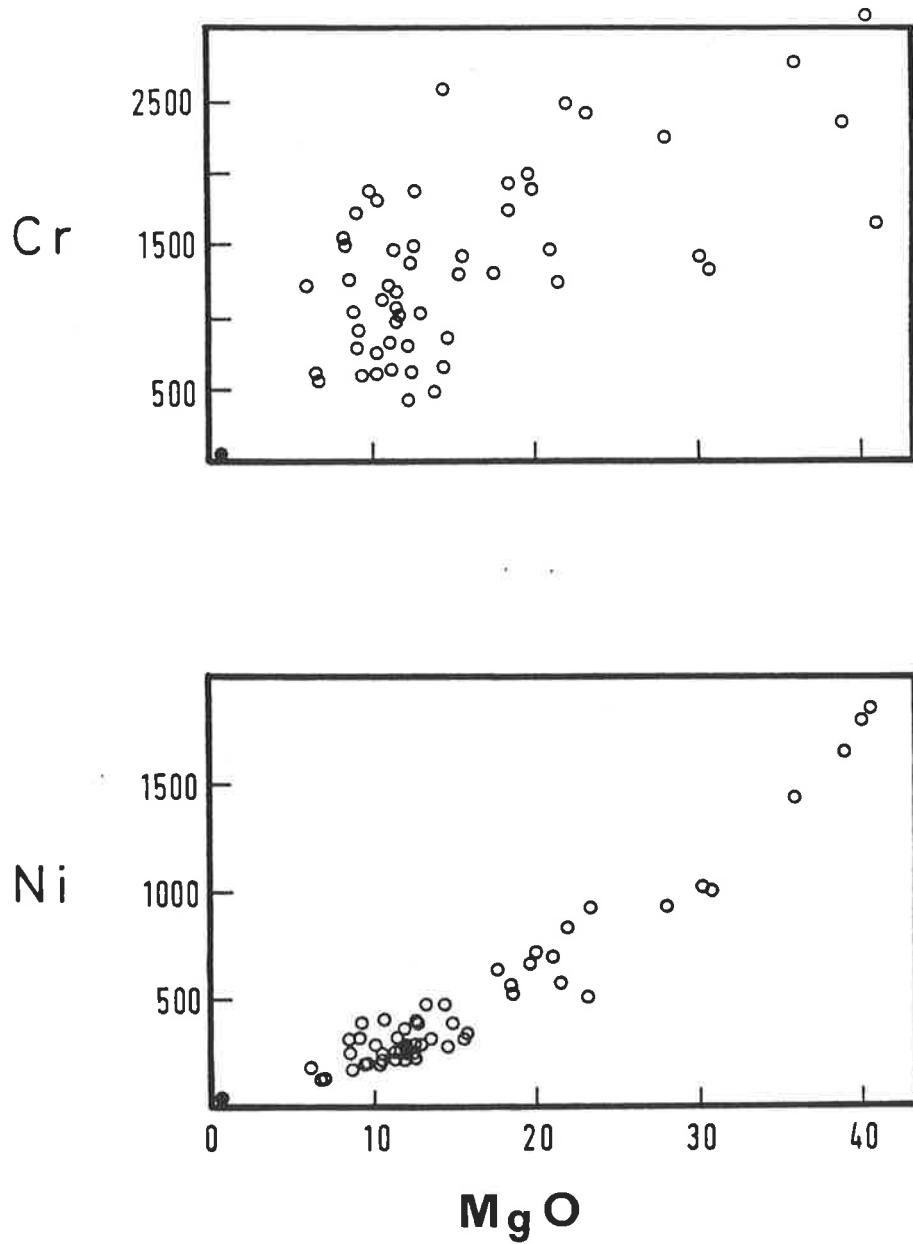


Figure 6.5. Concentrations of Ni and Cr (in ppm) relative to MgO (in wt%) in the layered rocks. The filled circle represents an anorthositic layer.

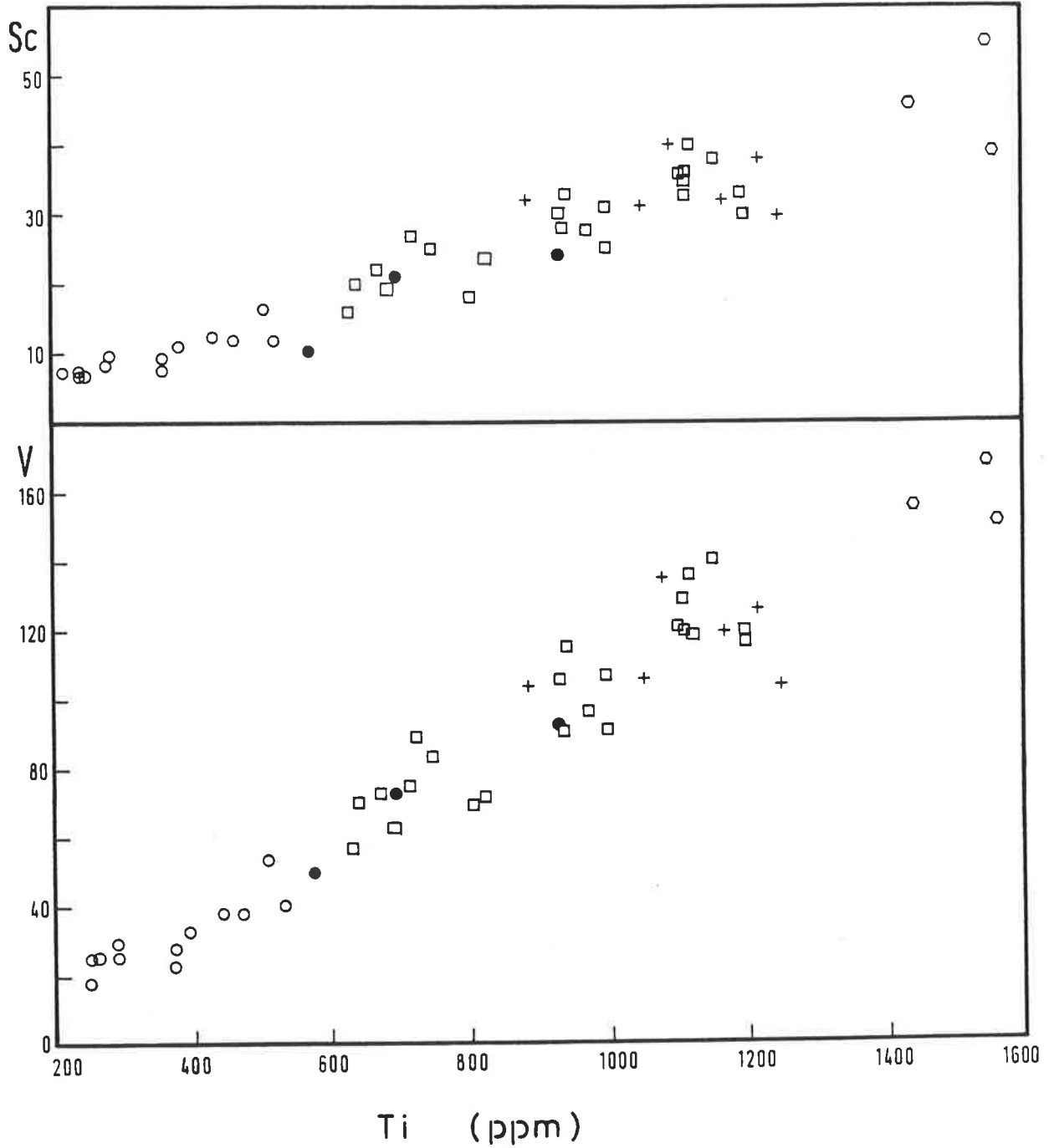


Figure 6. 6. Correlation of the Sc and V abundances (ppm) with those of Ti in the layered series. Open circles: troctolites, filled circles: mafic intrusive layers in olivine- gabbros, squares: olivine- gabbros, hexagons: laminated gabbros, crosses: structureless gabbros.

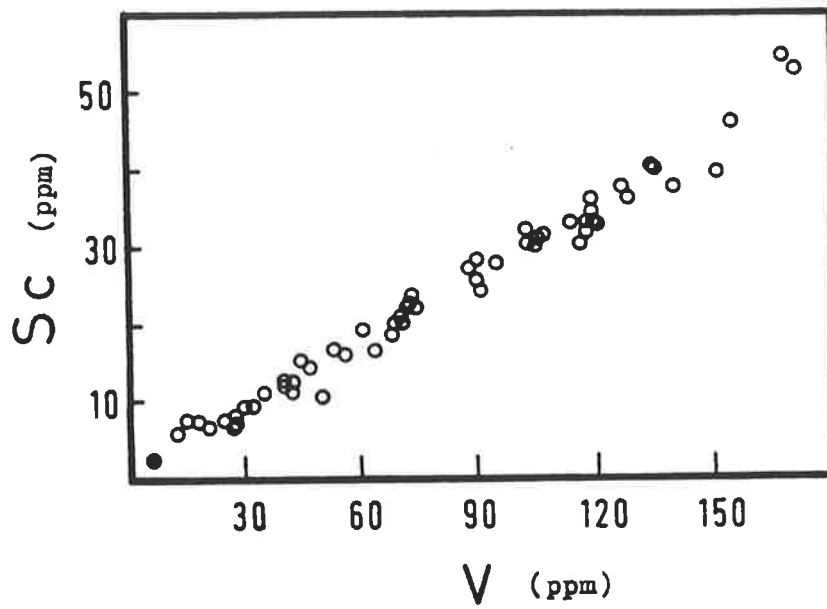


Figure 6.7. Sc-V covariance in layered rocks. The sample with the lowest concentrations (filled circle) is an anorthosite.

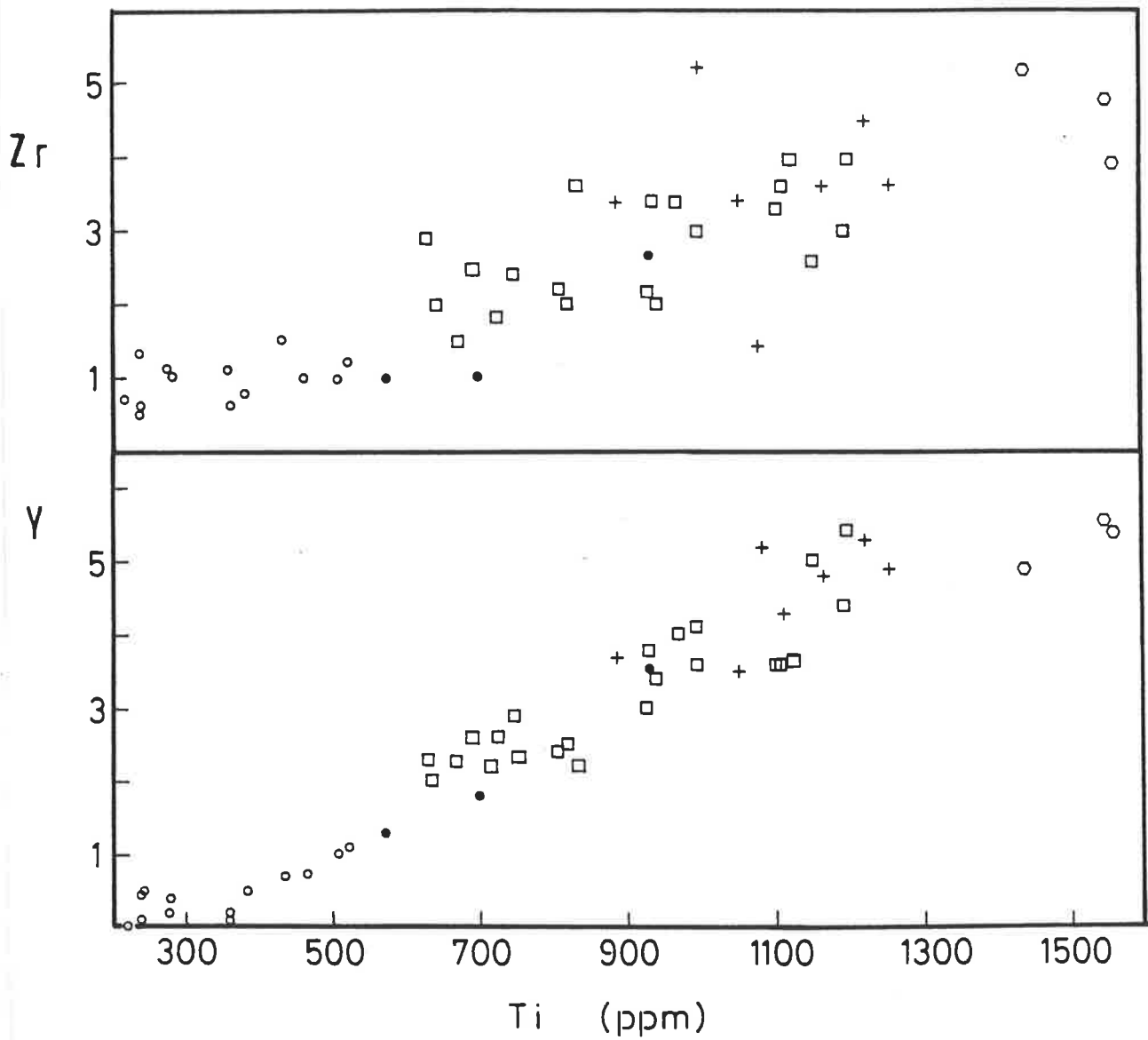


Figure 6.8. Correlation of the incompatible Zr and Y (ppm) to the Ti concentrations, layered sequence. Symbols as in 6.6.

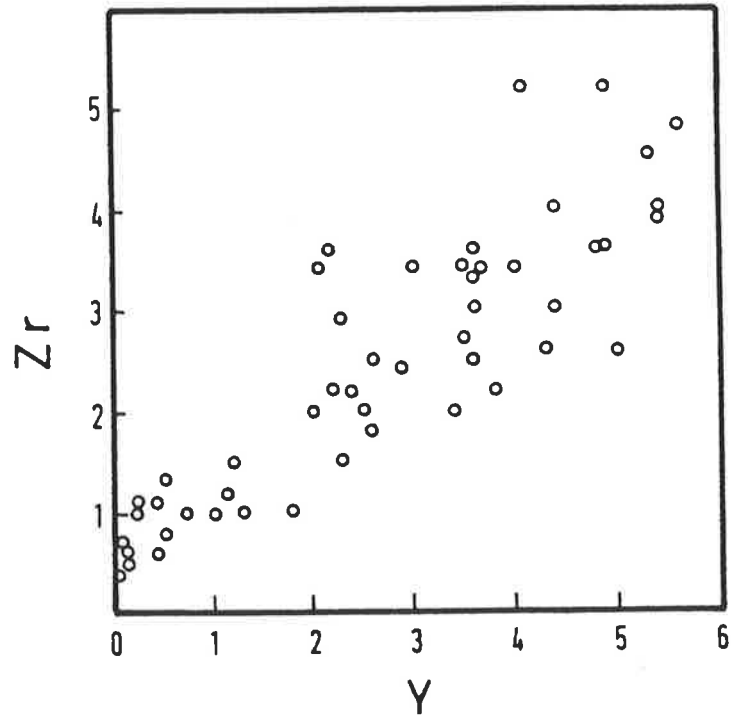


Figure 6.9. Covariance of Zr (ppm) and Y (ppm) in the rocks of the layered sequence.

Anorthosites are not included.

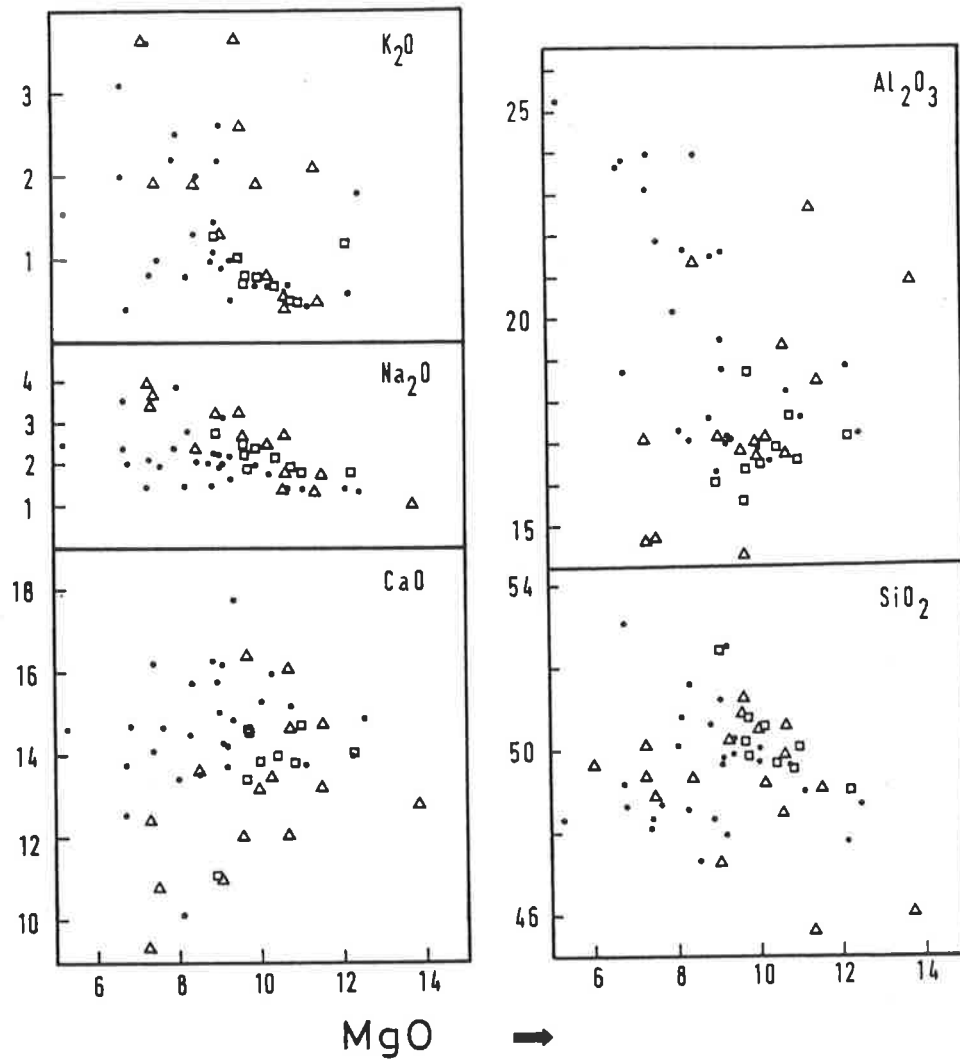


Figure 6.10. MgO variation diagrams for the massive gabbros. Squares: Island Lake Gabbro, filled circles: Upper Level Gabbro, open triangles: other massive gabbroic units.

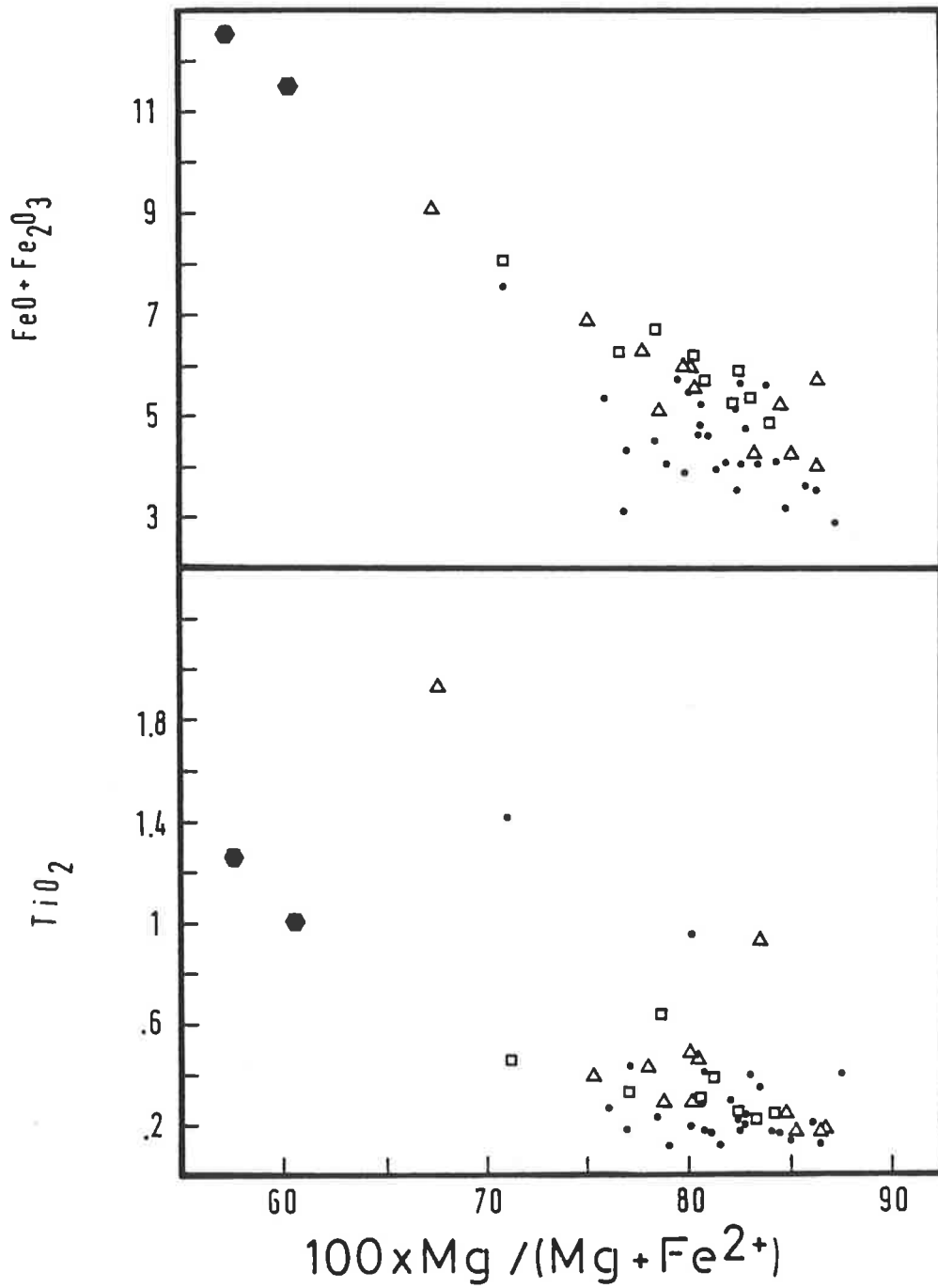


Figure 6.11. Total Fe ($\text{FeO} + \text{Fe}_2\text{O}_3$) and TiO_2 contents of the massive gabbros in terms of Mg-values. Solid hexagons represent the two North Mt. gabbro samples. Other symbols as in figure 6.10.

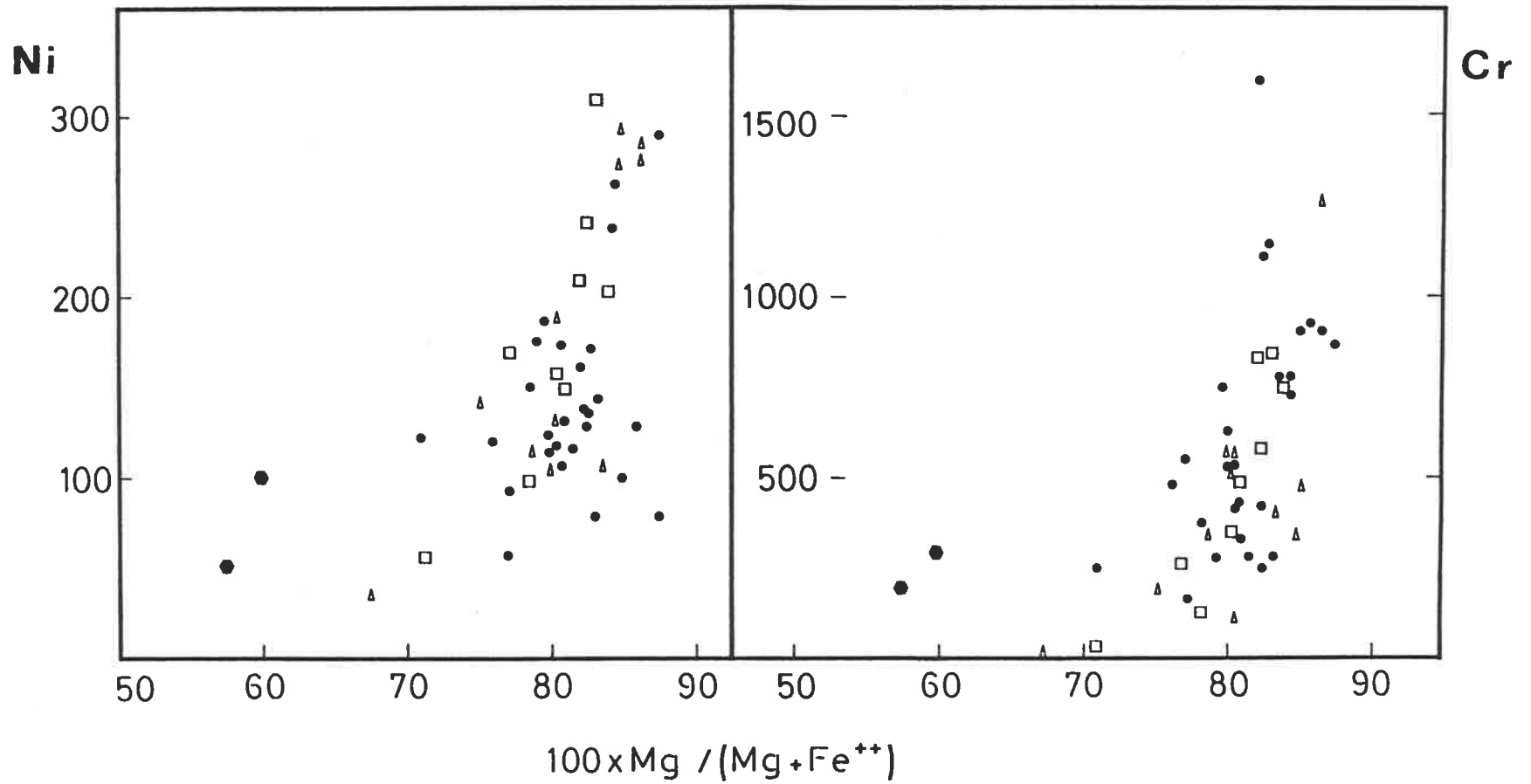


Figure 6.12. Cr and Ni concentrations (ppm) versus $100\text{Mg}/(\text{Mg}+\text{Fe}^{2+})$ in the massive gabbros. Symbols as in figure 6.11.

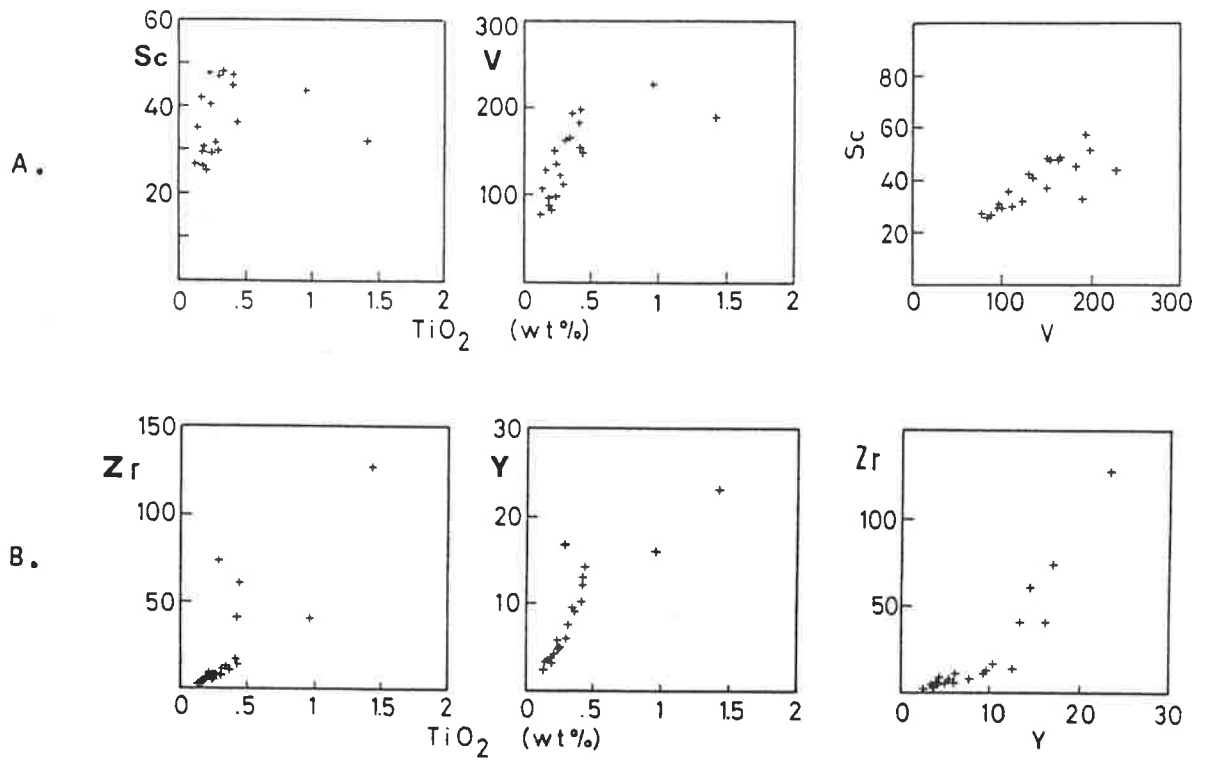


Figure 6.13A. Dependence of Sc and V (ppm) on the TiO₂ content (wt%) of the Upper Level Gabbro. The Sc-V covariance is also shown.

Figure 6.13B. Variation of Zr and Y (ppm) with TiO₂ in Upper Level Gabbro. The Zr-Y correlation is also shown.

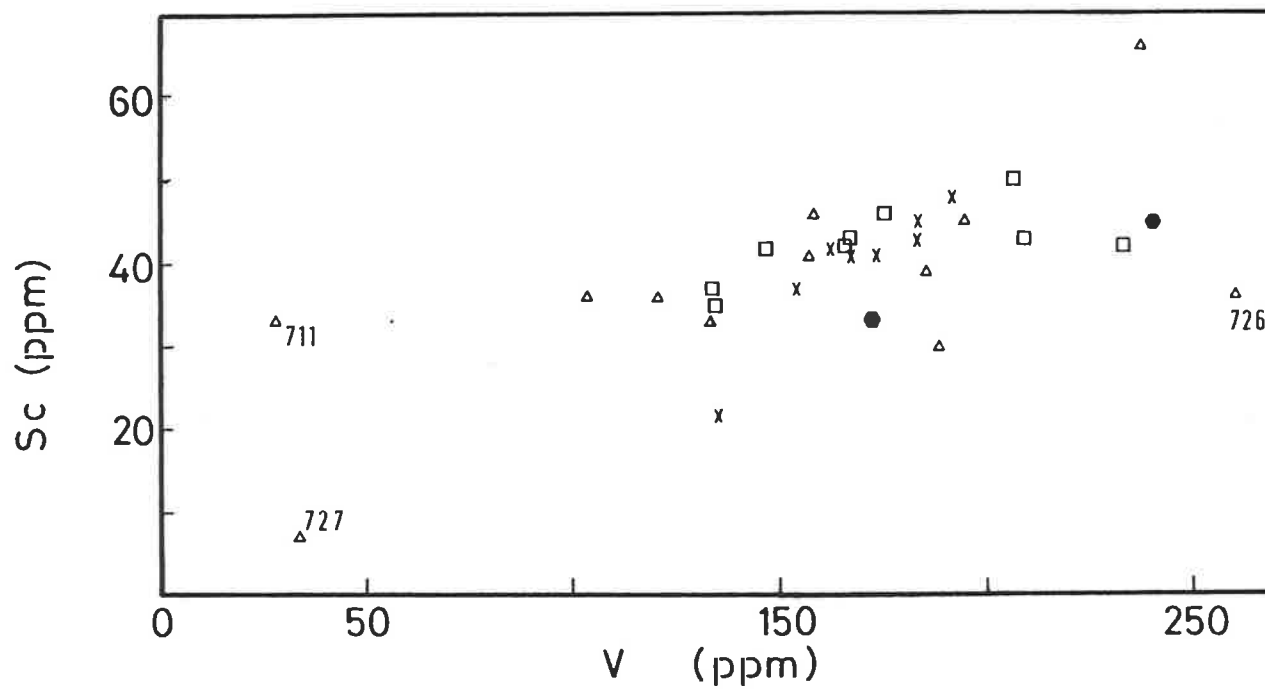


Figure 6.14. Sc and V abundances (ppm) in the massive gabbros. Squares: Island Lake Gabbro, filled hexagons: North Mt. Gabbro, triangles: massive gabbros on the east coast, X: Sandy Bay Gabbro.

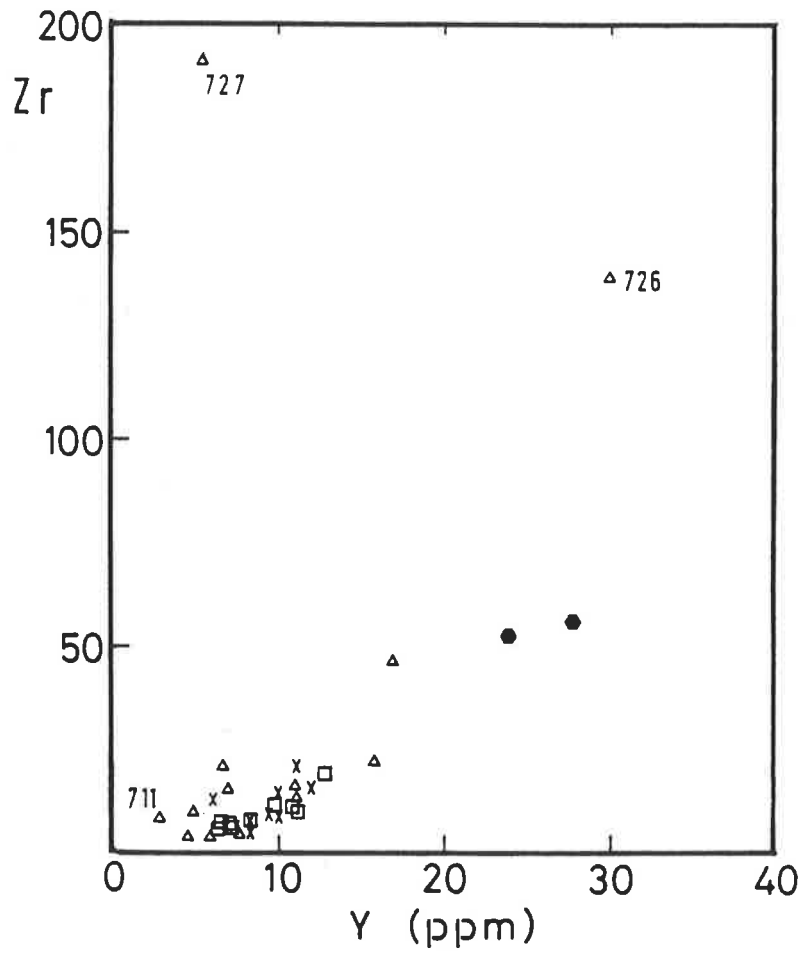


Figure 6.15. Concentrations of Zr and Y (ppm) in the massive gabbros. Symbols in figure 6.14.

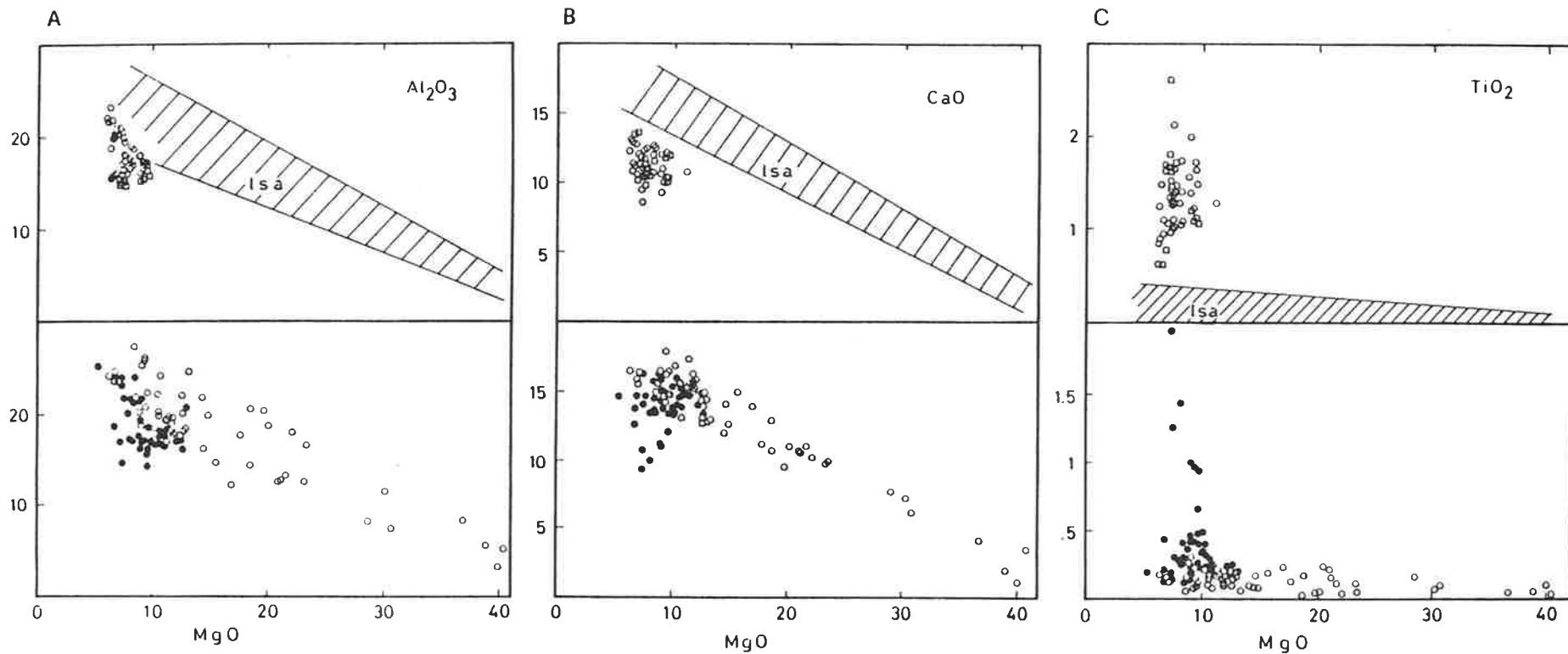


Figure 6.16. Oxide weight percents plotted against MgO weight percent.

A: Al_2O_3 - MgO plots. In the bottom diagram, layered rocks (open circles) and massive gabbros (filled circles) are plotted. In the top diagram, dolerite dykes from the dyke swarms (open squares), tholeiitic lavas (open hexagons) and alkalic lavas (open circles) are plotted; the shaded area "lsa" is the layered sequence array, as defined in the bottom plot.

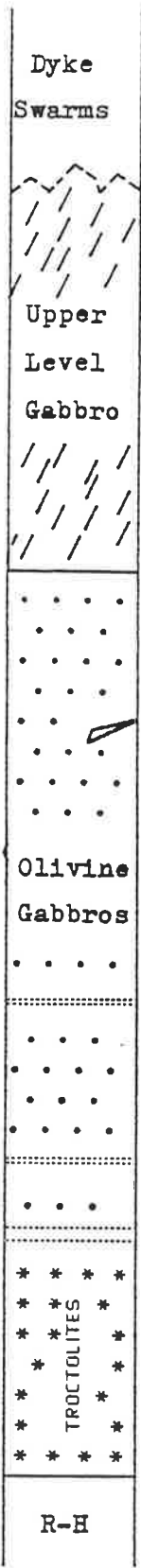
B: CaO -MgO plot. Symbols as in 6.16A.

C: TiO_2 - MgO plot. Symbols as in the previous diagrams.

Figure 6.17.

Stratigraphic variation of nickel, titanium and zirconium in the Macquarie Island plutonic rock types. The harzburgites (R-H) have the highest Ni-content and negligible Ti and Zr contents. In the rocks of the layered sequence, Ni is highest in the troctolites; Ni content reduces gradually up-section and approaches the lowest concentrations in the uppermost olivine-gabbros and laminated olivine-free gabbros. In the olivine-rich segregations (ot), Ni shows considerable increases. The concentrations of Ti and Zr in the layered rocks are constantly very low; Ti shows minor increases in the uppermost layered olivine-gabbros and laminated gabbros. Sample 358 is an intrusive mafic layer in the olivine-gabbros at Handspike Point. In the Upper Level Gabbros, the concentration of Ni is maintained uniformly low; Ti and Zr contents increase progressively up-section, and reach the highest concentrations in the upper parts of the unit and on nearing the Dyke Swarm - U.L.Gb. contact.

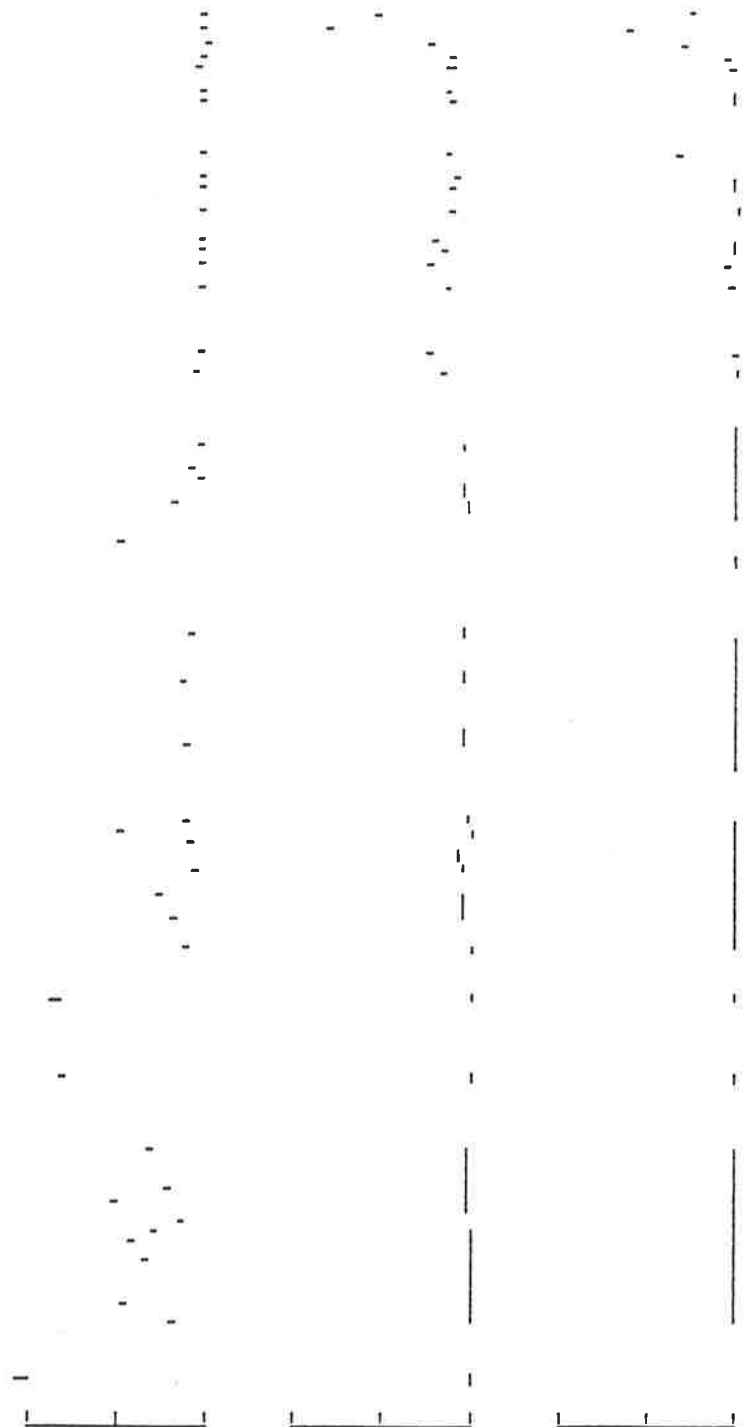
LAYERED SEQUENCE



20 10 0
Ni x100
(ppm)

10 5 0
Ti x1000
(ppm)

200 0
Zr
(ppm)



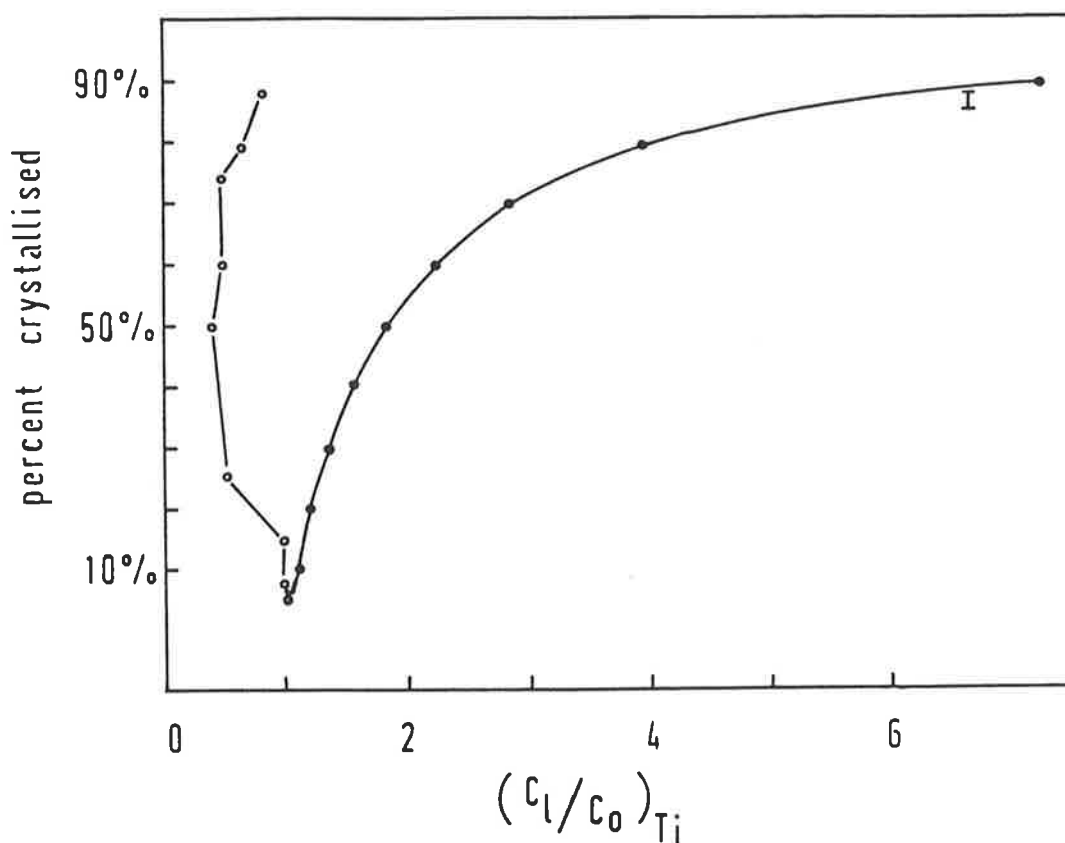


Figure 6.18. The normalised Ti concentration in liquids coexisting with the layered rocks $(C_l/C_o)_{Ti}$ is plotted against the percentage of crystallisation. The Ti content of the liquids (open circles) coexisting with the layered rocks has been calculated from the Ti-content of the clinopyroxene assuming a $K_D^{Ti}(\text{cpx-liq}) = 0.3$ (Pearce and Norry, 1979); then the Ti values were normalised to the Ti-content of the liquid coexisting with the lowermost troctolites. Curve I represents the variation in the liquid Ti-content during fractional crystallisation in a closed system; the curve has been calculated from the equation of fractional crystallisation assuming a fractionating assemblage of $ol_{20}plag_{45}cpx_{35}$, which is the observed average assemblage of the cumulates.

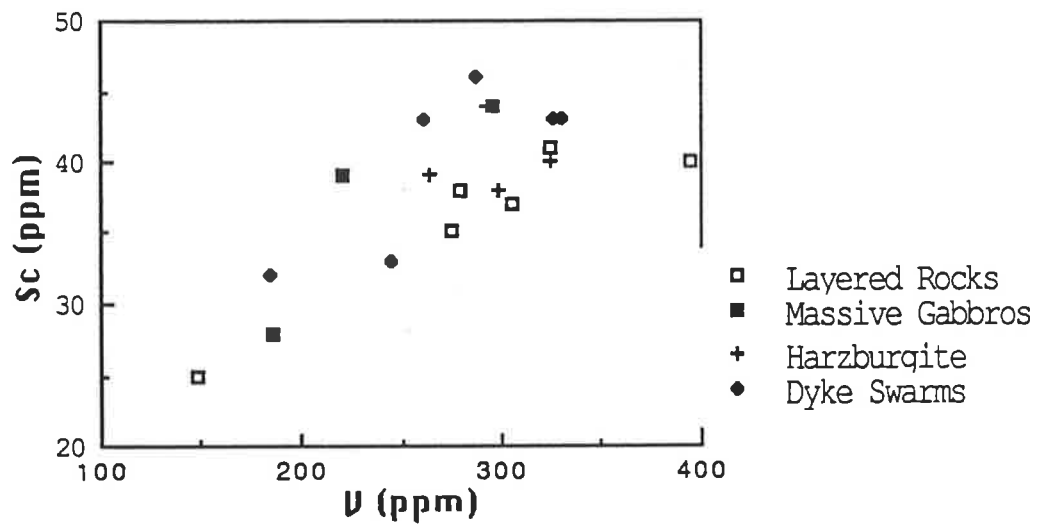


Figure 7.1. A plot of the Sc against V concentrations (in ppm) of Macquarie Island dolerite dykes. Dolerite dykes from different stratigraphic horizons are plotted. Symbols according to the legend. Dolerites from different levels of the crustal section have comparable Sc and V contents.

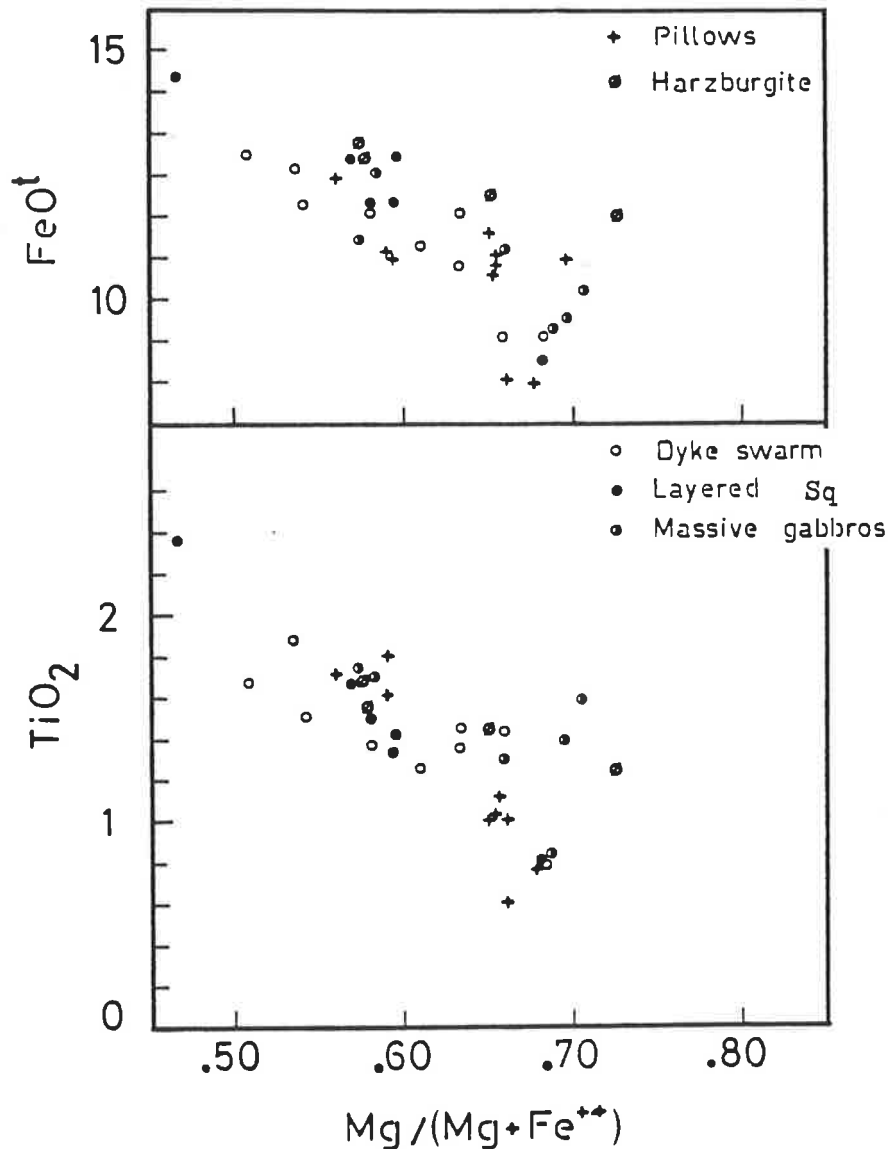


Figure 7.2. Plots of $Mg/(Mg+Fe^{++})$ ratios versus TiO_2 content and total iron content for Macquarie Island dolerite dykes. The dolerites are plotted according to their host lithology. Dolerite dykes crosscutting layered rocks are shown by filled circles (Layered Sq). Dolerites cutting pillow lavas and lava flows are shown by crosses (+ Pillows).

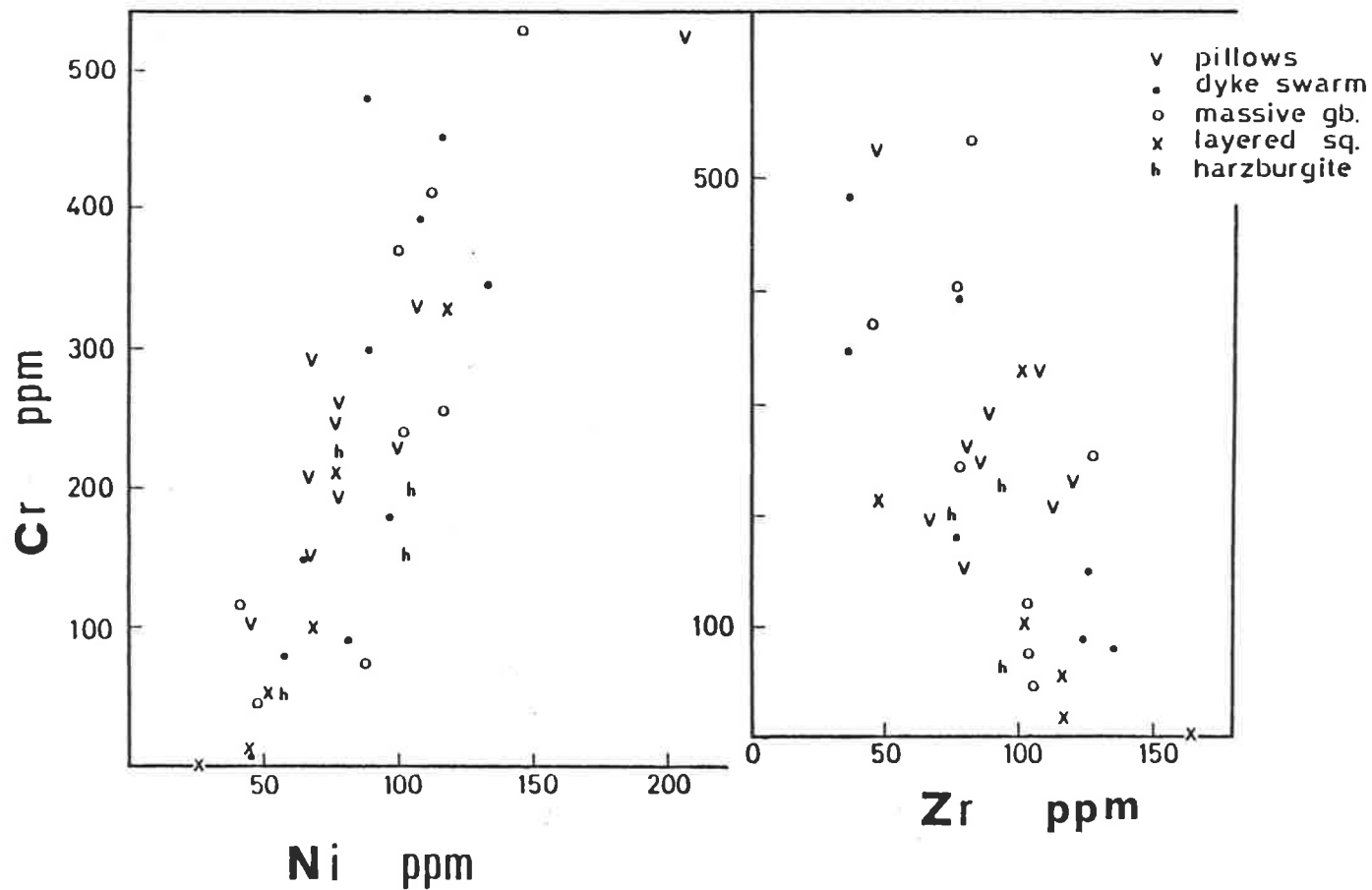


Figure 7.3. A plot of the abundances of the ferromagnesian trace elements Cr and Ni of Macquarie Island dolerite dykes. All dolerites are plotted according to their stratigraphic position. A positive correlation is shown. A plot of Cr versus Zr of the dolerites shows a broad negative correlation.

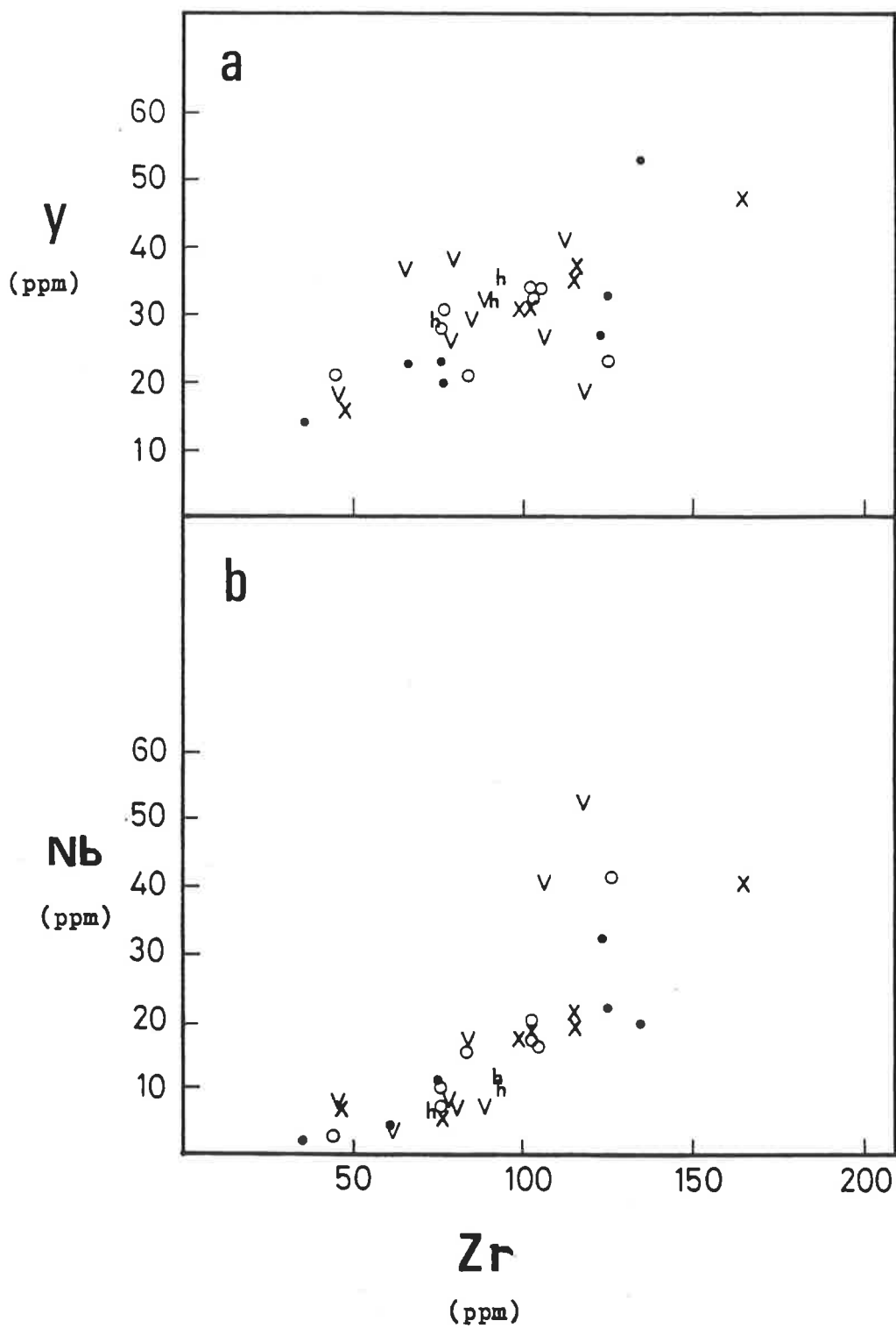


Figure 7.4. (a): Y and Zr exhibit positive correlation for dykes encountered in different rock lithologies. (b): the Zr-Nb correlation is good only for samples with less than 30ppm Nb. Symbols as in figure 7.3.

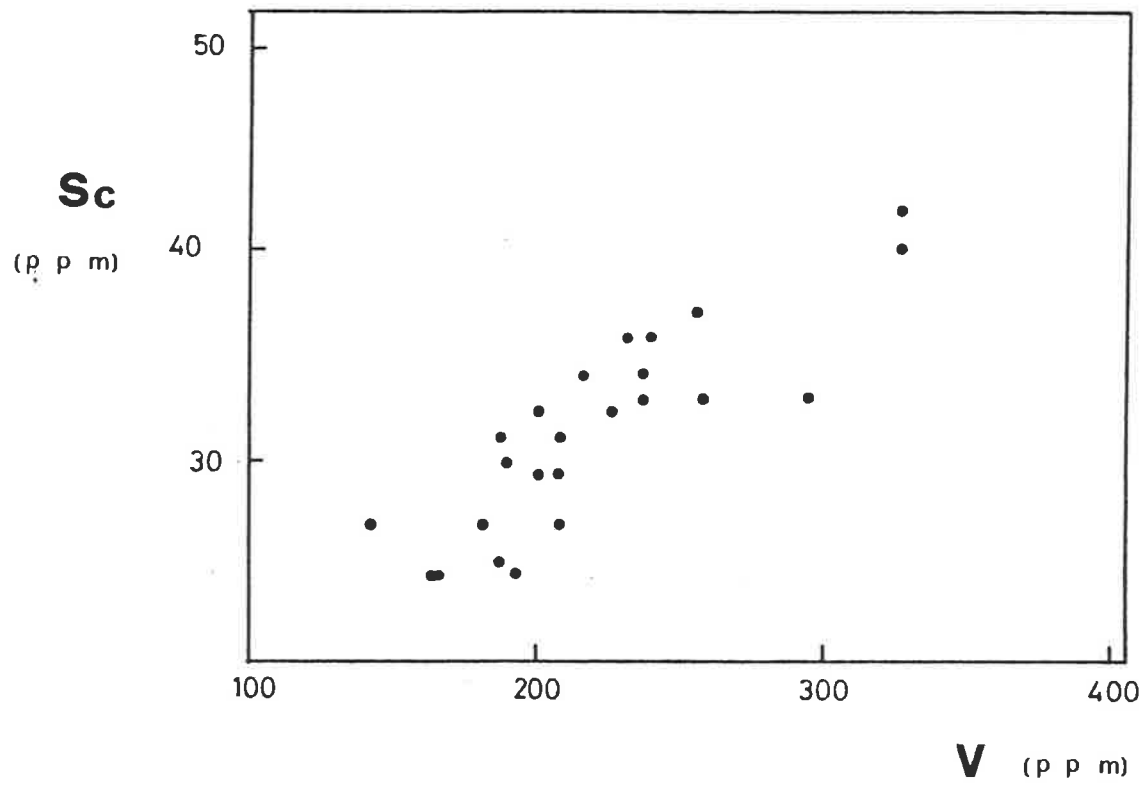


Figure 7.5. Covariance of Sc and V abundances in basalts.

Figure 7.6A. Variation of MnO and TiO₂ (both oxides in weight percent) with the Mg# ratio of basalts and dolerite dykes from Macquarie Island. Both oxides show a typical negative correlation with the Mg# ratio. Open circles: dolerite dykes, filled rhombs: alkalic basalts, open squares with dot in the centre: tholeiitic basalts.

The variation of the transition elements with the Mg# ratio is shown for all analysed samples. Ni and Cr decrease with differentiation, while V increases. Sc shows a broadly defined decrease with decreasing Mg#. The dolerite dykes have characteristically higher Sc contents than the basalts. Also, the dykes have as a group consistently higher V content than the basalts. Concentrations of Ni, Cr, Sc, V in ppm.
 $Mg\# = 100 \cdot Mg / (Mg + Fe)$.

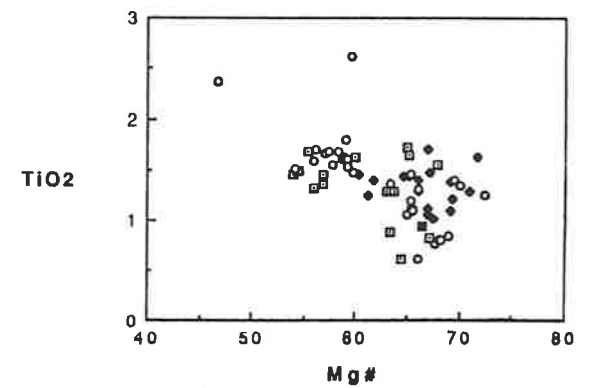
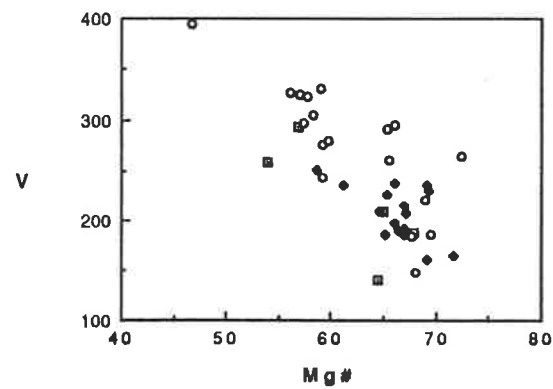
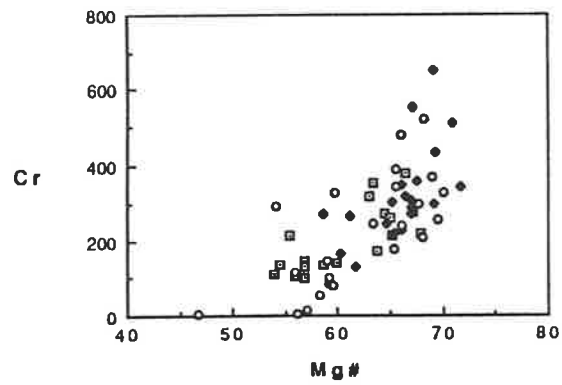
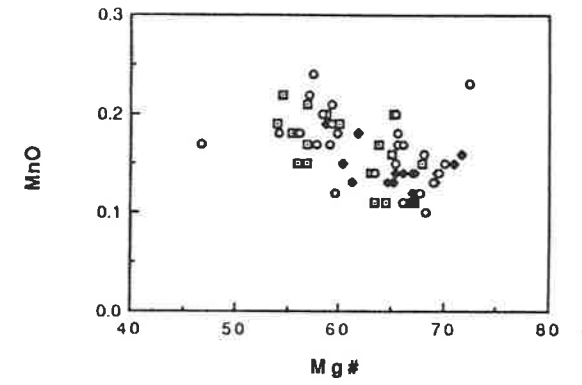
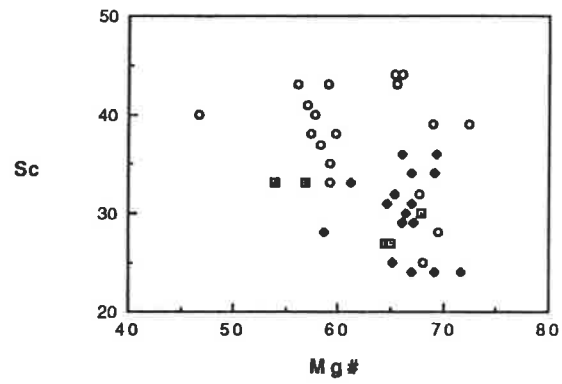
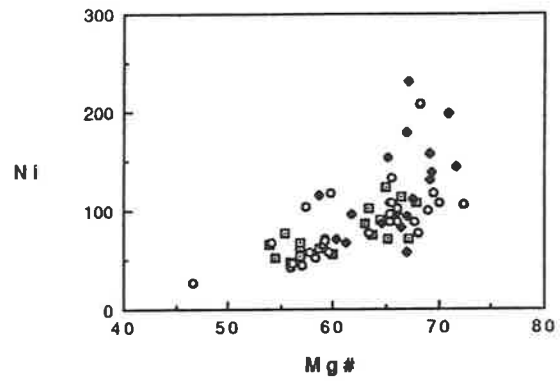
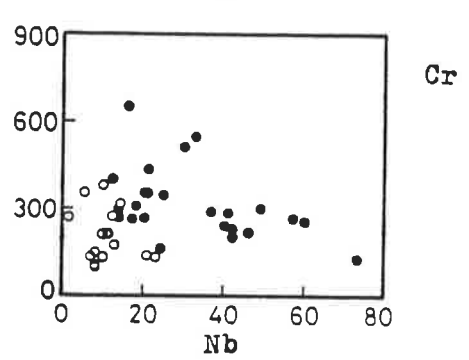
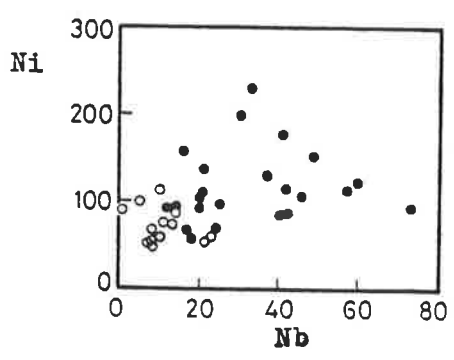
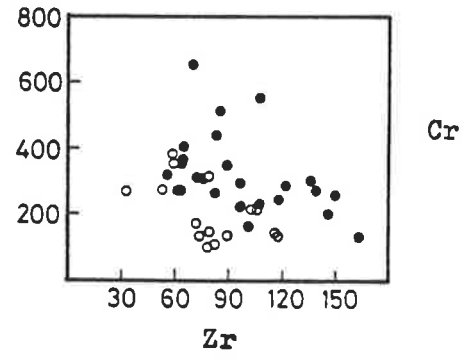
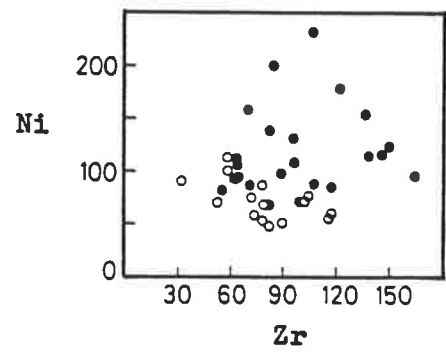
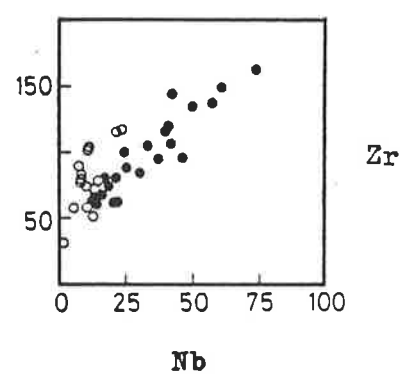
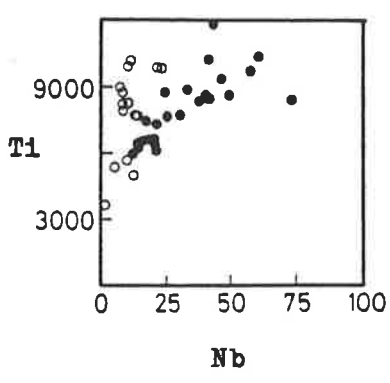
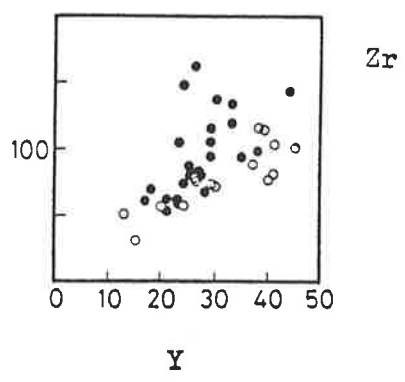
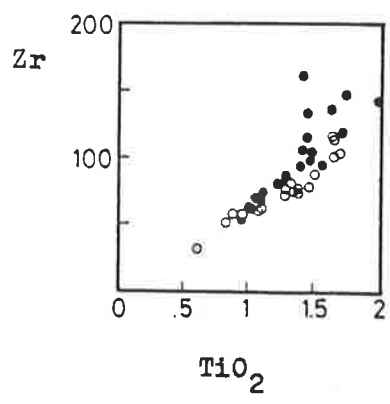
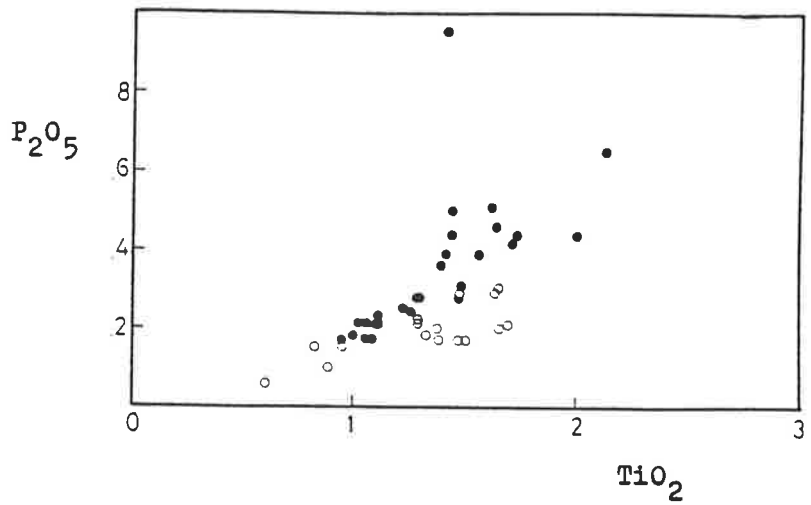


Figure 7.6B. Summary of minor oxide contents and trace elements abundances of the Macquarie Island basalts. P_2O_5 and TiO_2 are expressed in weight percentages. Trace elements Zr, Y, Nb, Cr, Ni, Ti are all expressed in ppm. The alkalic basalts (Ne-normative) are shown by filled circles and the tholeiitic -type (Hy-normative) by open circles. Good positive correlations are shown by the alkalic lavas in the incompatible- incompatible element ($P_2O_5-TiO_2$, $Zr-TiO_2$, $Ti-Nb$ and $Zr-Nb$) plots. In the compatible- incompatible element plots ($Ni-Zr$, $Ni-Nb$, $Cr-Zr$, $Cr-Nb$), the dispersion of the data points is not consistent with possible crystallisation or melting trends. The tholeiitic basalts show good positive correlations in the $Zr-TiO_2$ and $P_2O_5-TiO_2$ plots, and poorly defined negative correlations in the $Ni-Zr$ and $Zr-Cr$ plots.



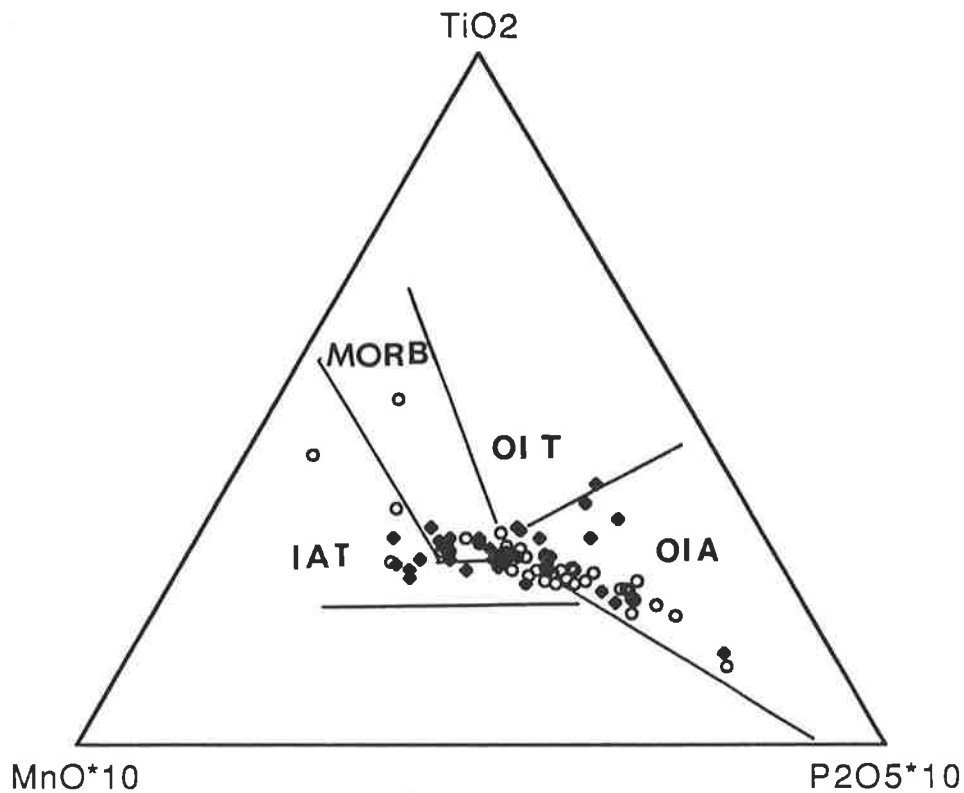


Figure 7.7.

A TiO_2 - $\text{MnO} \cdot 10$ - $\text{P}_2\text{O}_5 \cdot 10$ ternary diagram for the Macquarie Island basalts and dolerites. Open circles=basalts, filled rhombs=dolerites. The fields of basalts and basaltic andesites are from Mullen (1983); MORB= mid-ocean ridge basalts, IAT= island arc tholeiites, OIT= ocean island tholeiites, OIA= ocean island alkalic basalts. The Macquarie Island rocks extend from the MORB field to the ocean island rock field; the high P_2O_5 content of the alkalic basalts indicates small percentages of partial melting, a characteristic feature of ocean island tholeiitic and alkalic basalts.

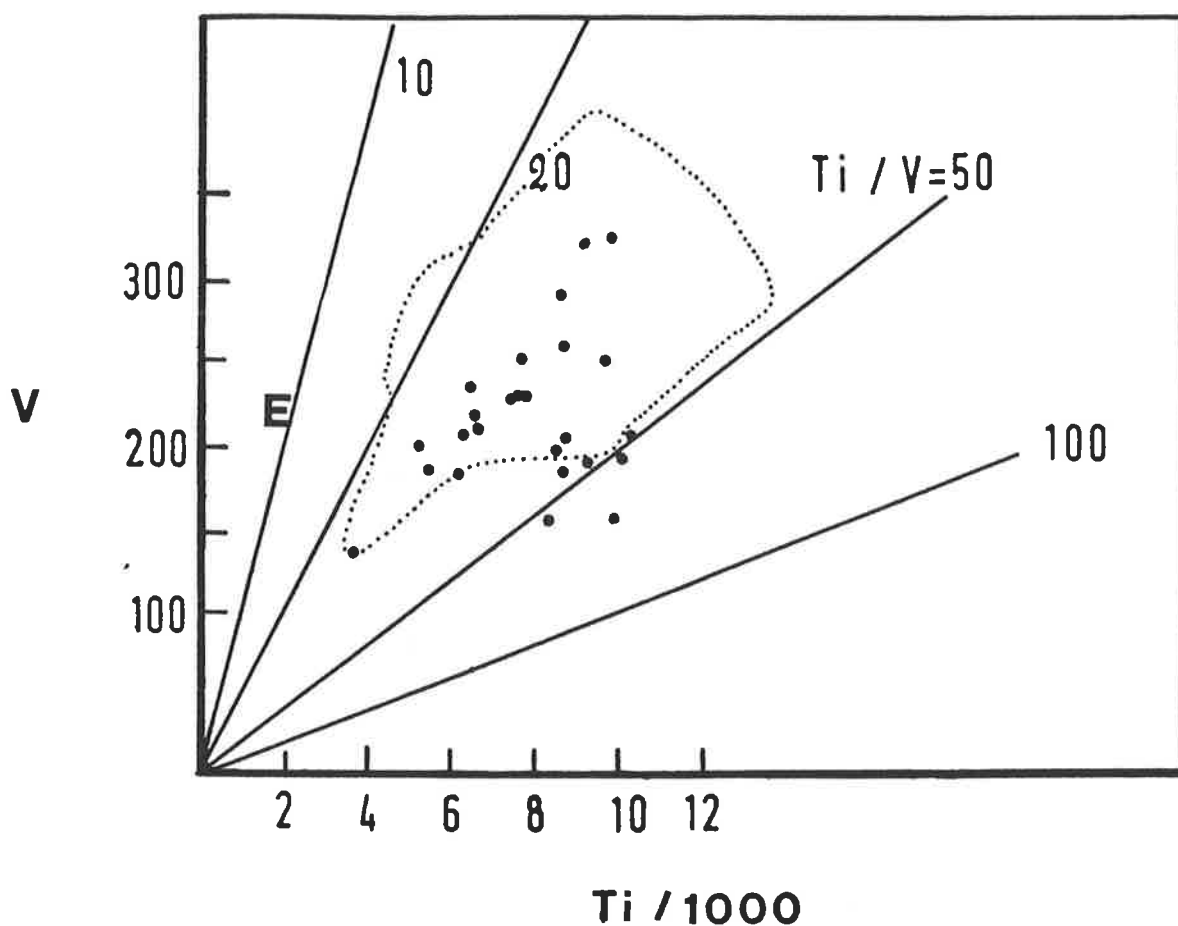


Figure 7.8. A V (ppm) versus Ti (ppm)/1000 plot for the Macquarie Island lavas (filled circles). The trend lines for constant Ti/V ratios of 10, 20, 50, 100 are also shown. The majority of the lavas have Ti/V ratios between 25 and 50. The field of mid-Atlantic ridge basalts is shown for comparison; MORB from the Atlantic ocean have Ti/V ratios between 20 and 50. E is the mean value for Ti and V abundances from the Upper pillow lavas of the Troodos Ophiolite complex.

FIGURE 7.9.

- A. A Ti versus V plot for the Macquarie Island intrusive and extrusive rocks. Filled squares: cumulates, crosses: massive gabbros (Upper Level Gabbro samples), open squares: dolerite dykes, filled circles: tholeiitic basalts, rhombs: alkalic basalts. Line c is the constant Ti/V ratio of 29. Trend line a is the olivine+plagioclase fractionation trend from 0% to 40% fractionation; initial Ti and V contents are 4000 ppm and 140 ppm respectively. The proportions of olivine and plagioclase adopted in the calculations were 25% and 75% respectively, very similar to the average mode of troctolites. Trend b is the olivine+plagioclase+clinopyroxene fractionation trend; the percentages of these minerals employed in the calculations were 15%, 70% and 25%. Such a mode is similar to the average olivine-gabbro of the layered sequence. The Ti and V contents in the initial melt were chosen to be 6000 and 200 ppm. Fractionation trend b is shown from 0% to 40% ol+plag+cpx fractionation. Trend d is the trend defined by the Macquarie Island alkalic basalts.
- B. A logTi versus logV plot of Macquarie Island intrusive and extrusive rocks. Symbols as in legend.

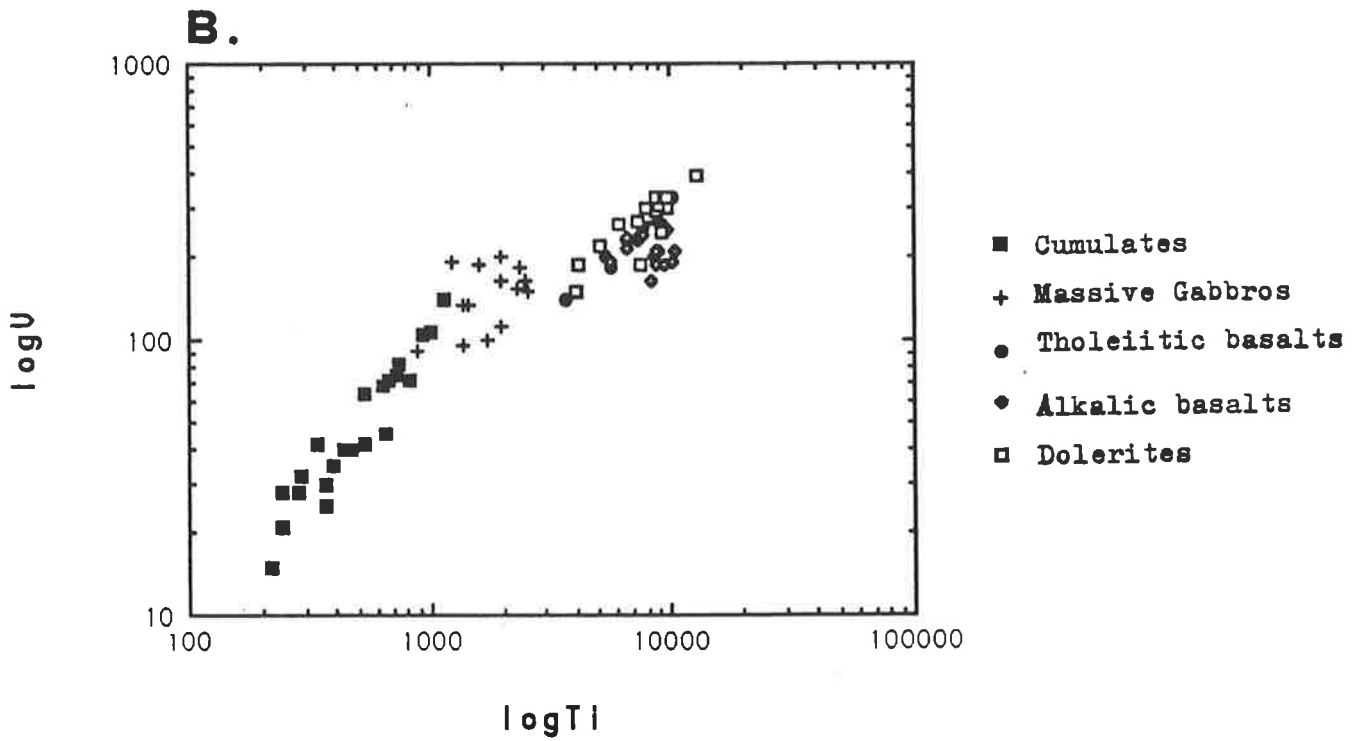
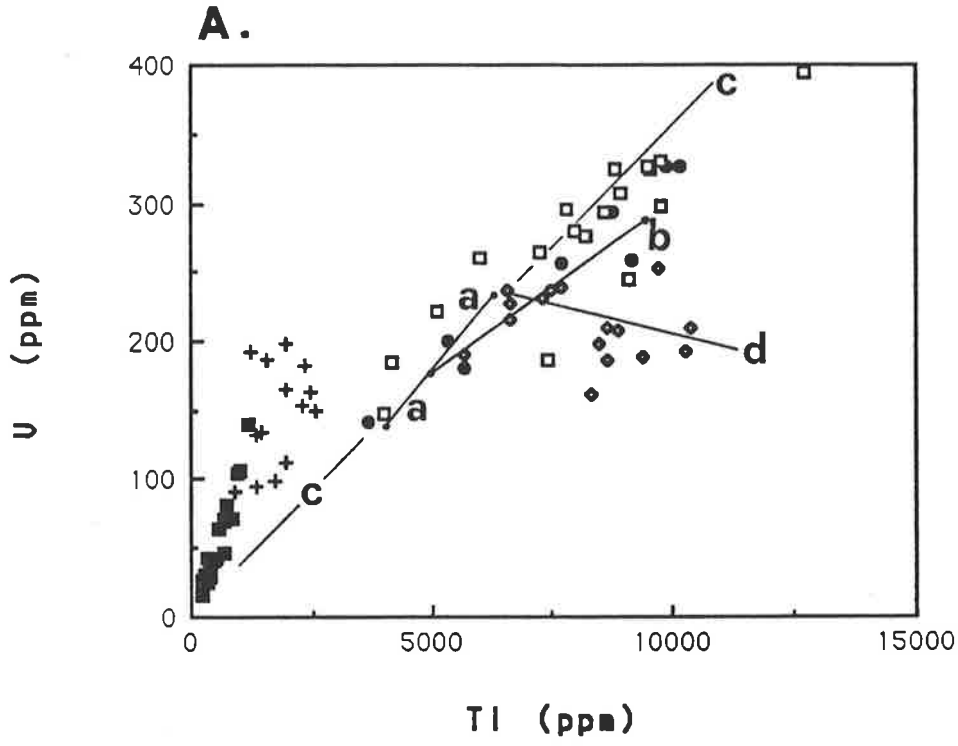
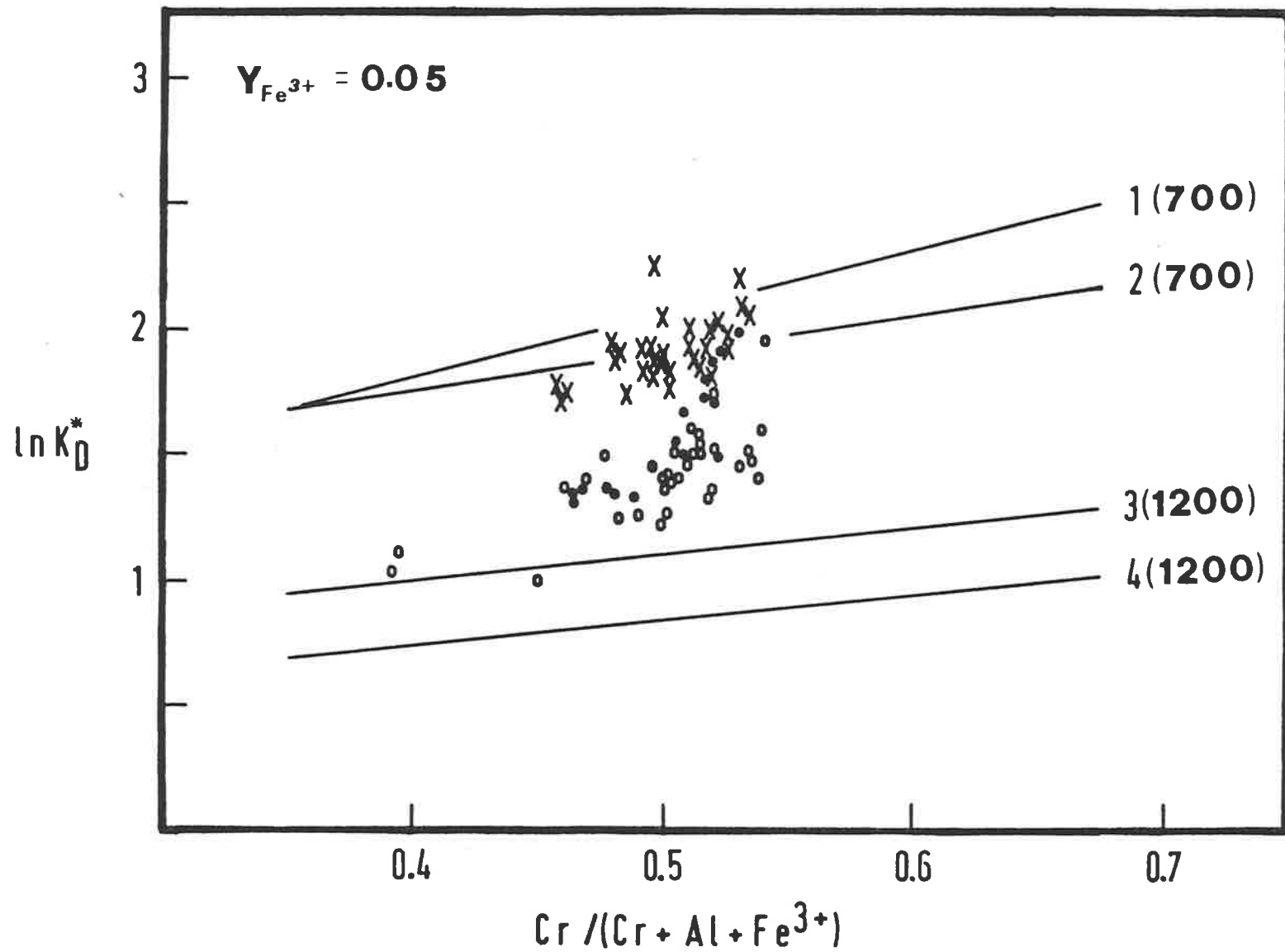
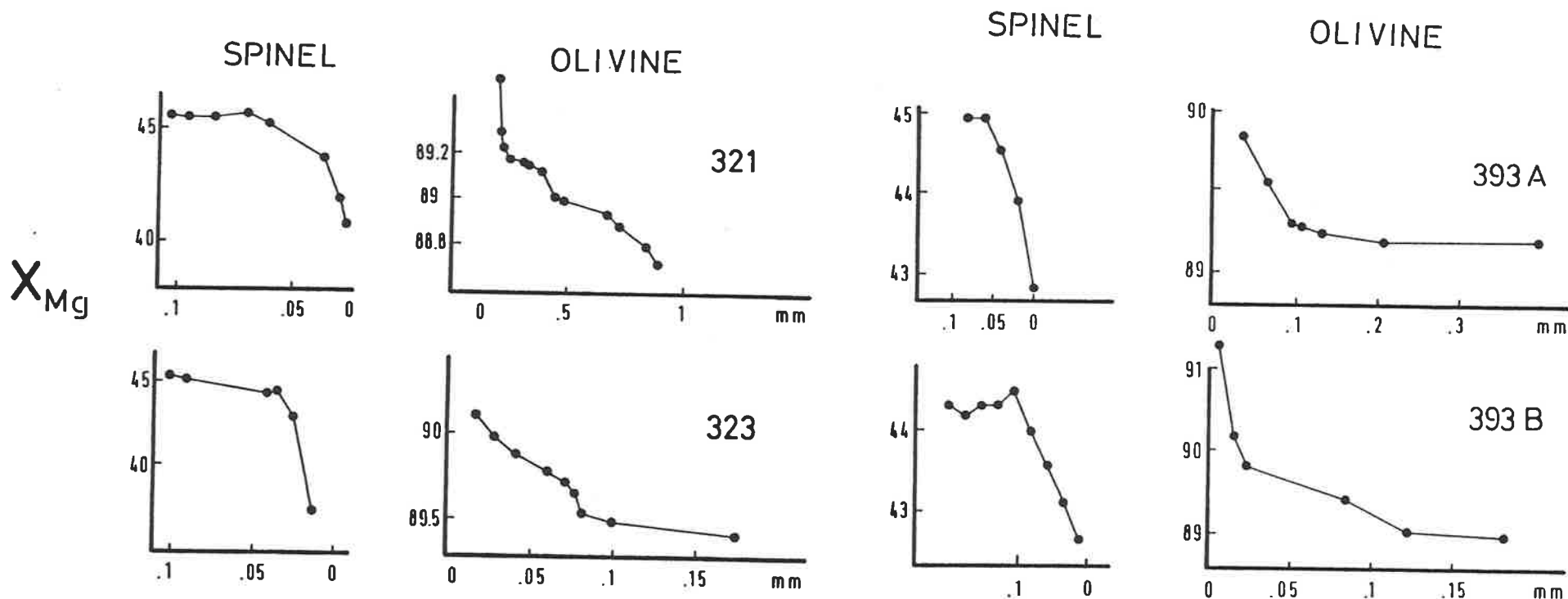


Figure 8.1.

Plot of the normalised Fe^{2+} -Mg olivine-spinel distribution coefficient $\ln K_D^*$ versus the $\text{Cr}/(\text{Cr}+\text{Al}+\text{Fe}^{3+})$ ratios of the Macquarie Island Cr-spinels. The $Y_{\text{Fe}^{3+}}$ of Cr-spinels was taken as 0.05. The plotted data are from olivine-spinel pairs in troctolites. Open circles are pairs of Cr-spinels included in plagioclases and olivines in contact with these plagioclases. **X** represents pairs of large olivines and Cr-spinels included in these olivines. Filled circles are pairs of Cr-spinels lying at the boundaries of plagioclase - olivine crystals and adjacent olivines. Lines **1** and **2** are the 700°C isotherms of Evans and Frost (1975) and Roeder et al. (1979) respectively. Lines **3** and **4** are the 1200°C isotherms of Roeder et al. (1979) and Evans and Frost (1975) respectively.





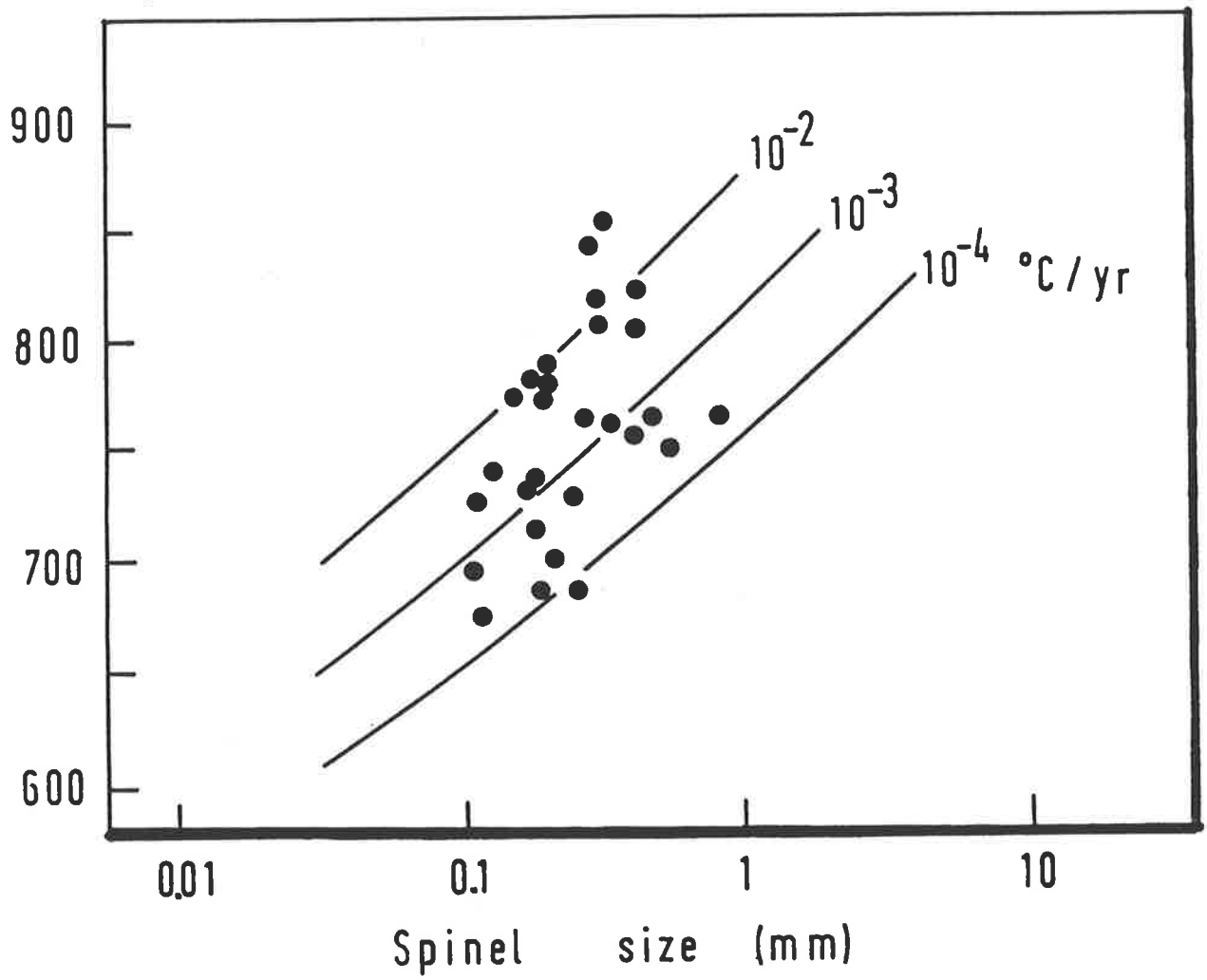
Distance from the olivine-spinel boundary.

Figure 8.2. Measured X_{Mg} ($100 \cdot Mg / (Mg + Fe^{2+})$) values of adjacent spinels and olivines from troctolites. The samples presented are 321, 323, 393A and 393B. Along the axis-x, the distance of either olivine or spinel from their mutual contact is given in mm.

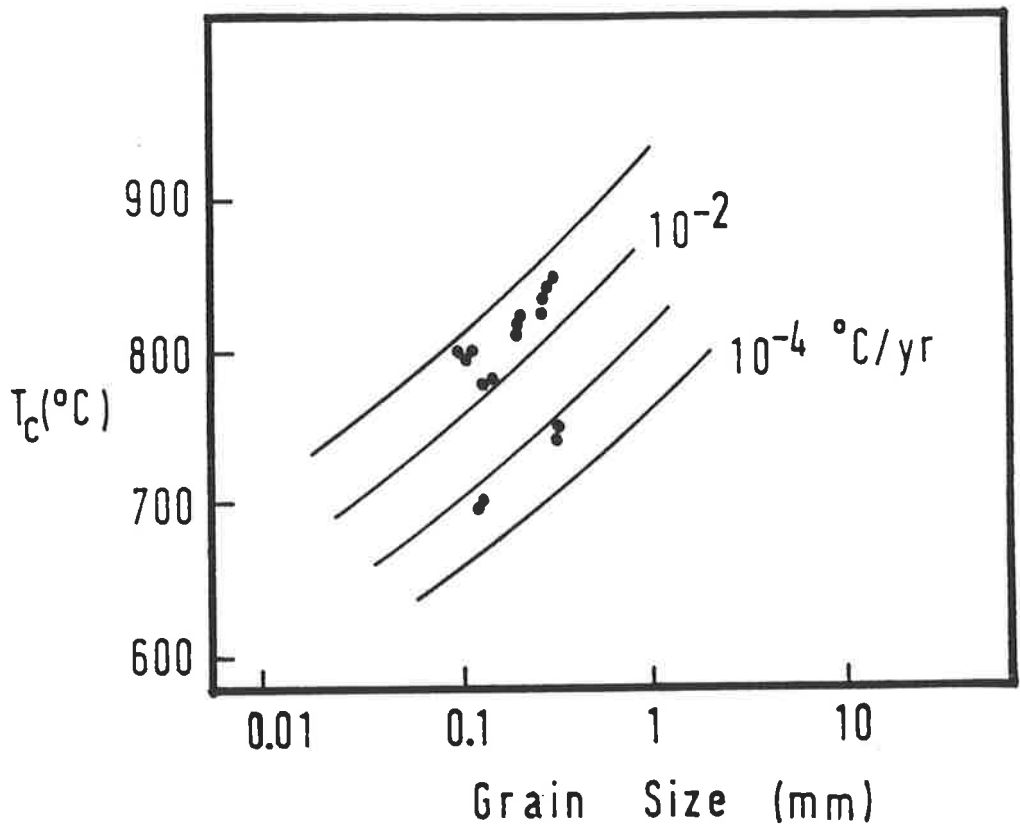
Figure 8.3. Plots of spinel grain size (diameter in mm) against the calculated equilibration temperature T_c (in degrees Celcius) from the olivine-spinel thermometric expression of Roeder et al. (1979). Selected data from the different rock types.

- (A). Relationship of spinel grain size and T_c in troctolites. The spinel crystals chosen for projection in this diagram have Y_{Cr} ratios as close as possible to 0.5 and $Y_{Fe^{3+}}$ ratios of 0.05. The core spinel chemical composition and the olivine X_{Mg} ratio away from the spinel-olivine interface are used. The preferred spinel crystals have diameters between 0.1mm and 1mm (as shown in the diagram), because for smaller spinel size than 0.01mm and larger than 1mm, the olivine X_{Mg} is independent of the cooling rate (Ozawa 1984). The curves represent computed cooling rates assuming that the Y_{Cr} of spinel equals 0.5 and its $Y_{Fe^{3+}} = 0.0$; the olivine X_{Mg} (initial ratio) is taken as 0.9. These values correspond or are in good agreement with the spinel and olivine compositions from troctolites. The cooling rates are indicated in degrees Celcius per year ($^{\circ}C/yr$). Most of the data plot between the 10^{-2} and 10^{-4} $^{\circ}C/yr$ curves. For such small cooling rates, the spinel X_{Mg} is more sensitive than that of olivine. The data from troctolites therefore demonstrate that these rocks cooled very slowly to their present state.
- (B). A T_c - spinel grain size plot for mineral pairs from the Macquarie Island harzburgites. Most of the spinels are included in enstatites and plot between the 10^{-2} and 10^{-1} $^{\circ}C/yr$ cooling curves. Smaller spinels enclosed in olivines have lower X_{Mg} and hence the temperatures T_c are lower; the cooling rate indicated by these spinels is significantly lower.
- (C). A T_c -spinel grain size plot for the North Mt. wehrlite and the lava M14. Mineral data from the wehrlite suggest cooling rates of about 10^3 $^{\circ}C/yr$, and from the lava more than 10^4 $^{\circ}C/yr$. The olivine and spinel compositions from the lava represent well developed phenocrysts (xenocrysts) only.

A.



B.



C.

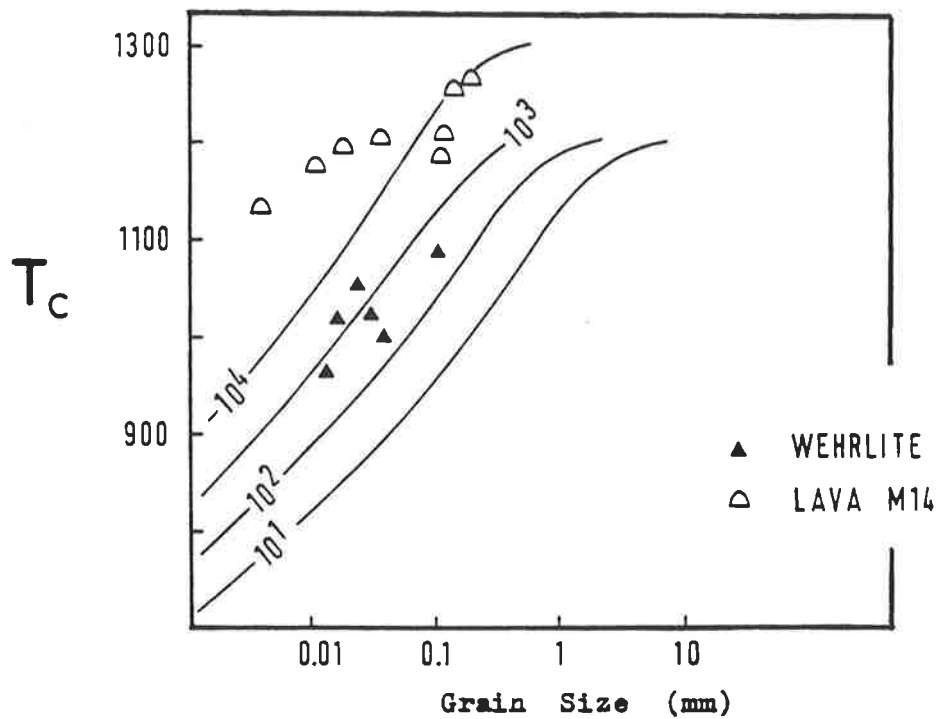
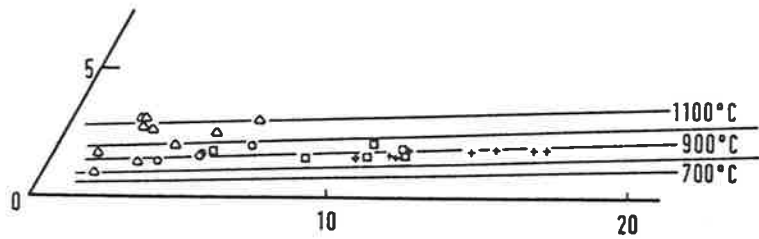
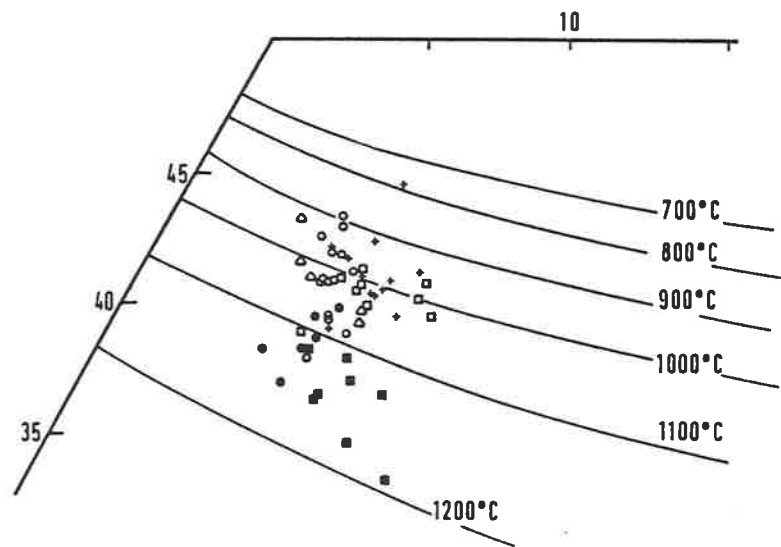


Figure 8.4.

Clinopyroxene and orthopyroxene compositions from the Macquarie Island plutonic rocks are plotted in the Mg-rich portion of the pyroxene quadrilateral. The compositions of pyroxenes were first recalculated by the method of Lindsley and Anderson (1983), and then projected in the quadrilateral. The isotherms are taken from Lindsley and Anderson (1983) as well. Filled symbols represent "bulk" pyroxene compositions obtained with defocused electron beam. Orthopyroxenes in troctolites, olivine-gabbros and massive gabbros represent exsolved phases only.

The large enstatites from harzburgites indicate temperatures of 900°C to 1100°C, and the interstitial clinopyroxene temperatures between 900°C and 1060°C.

The clinopyroxenes from the layered troctolites and olivine-gabbros point to temperatures of 900°C to about 1100°C. "Bulk" clinopyroxene compositions indicate temperatures of 1100°C-1200°C.



- TROCTOLITES
- OLIVINE - GABBROS
- ✦ MASSIVE GABBROS
- △ HARZBURGITE

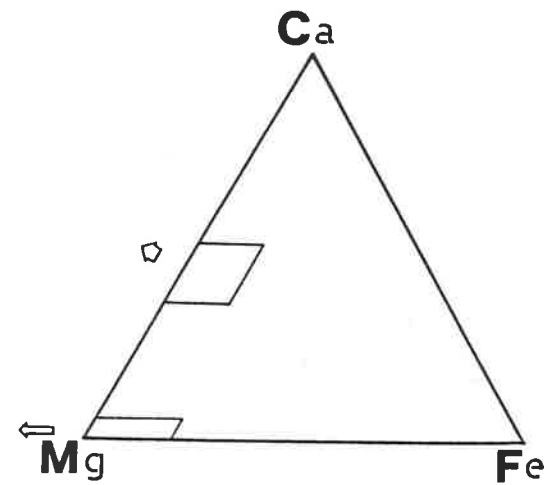


Figure 8.5.

A plot of the $\text{Cr}/(\text{Cr}+\text{Al}+\text{Fe}^{3+})$ versus $\text{Mg}/(\text{Mg}+\text{Fe}^{2+})$ ratios of selected spinels from troctolites and lavas. The spinels from troctolites are large crystals, unzoned, euhedral to subhedral and are not included in olivines. The spinels from the lavas are euhedral phenocrysts. The fields of temperature and oxygen fugacity ($f\text{O}_2$) of Fisk and Bence (1980) are also shown. The logarithmic value of $f\text{O}_2$ is given.

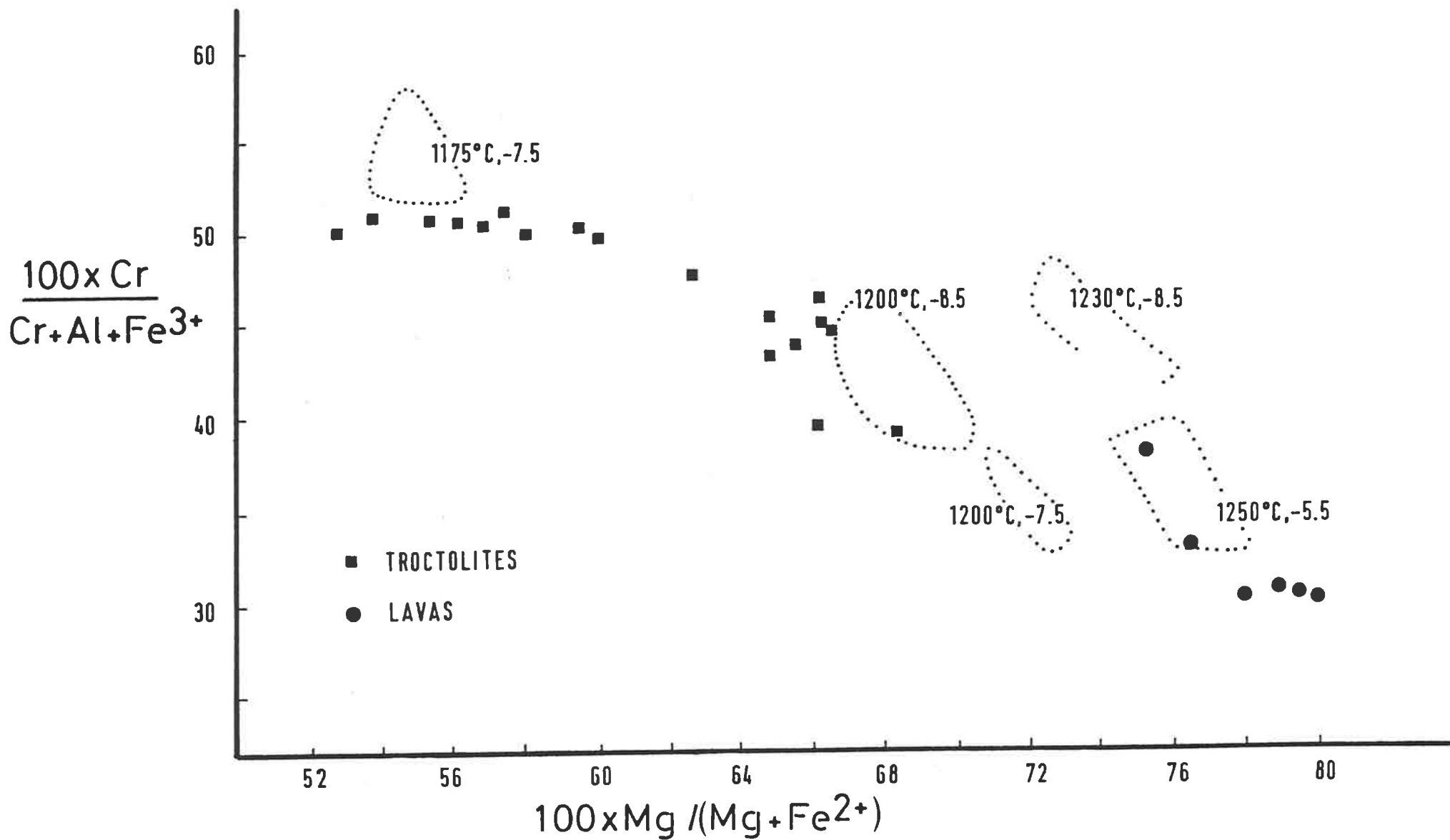


Figure 8.6 Calculated liquid trends after olivine equilibrium crystallisation from initial liquids 1 and 2, and $Mg/(Mg+Fe^{2+})$ ratios and Ni-contents of Macquarie Island basalts. The $Mg/(Mg+Fe^{2+})$ ratios and Ni-contents of initial liquids 1 and 2 (marked as \emptyset) have been calculated as those in-equilibrium with olivine $Fo_{89.7}$ (0.22%wt NiO). The $Mg/(Mg+Fe^{2+})$ ratio and Ni-content of liquid 1 has been calculated at a temperature of 1280°C and of liquid 2 at 1220°C. The changing liquid composition during olivine equilibrium crystallisation from these two liquids is shown by the curves, which are marked for an increment of 1% olivine crystallisation. Macquarie Island basalts are plotted as open circles (tholeiitic-type basalts) and filled squares (alkalic-type basalts). The best fit curve S-S to the basalt data points has the following format,
 $y=9.2578-0.308x+2.7 \cdot 10^{-3}x^2$.

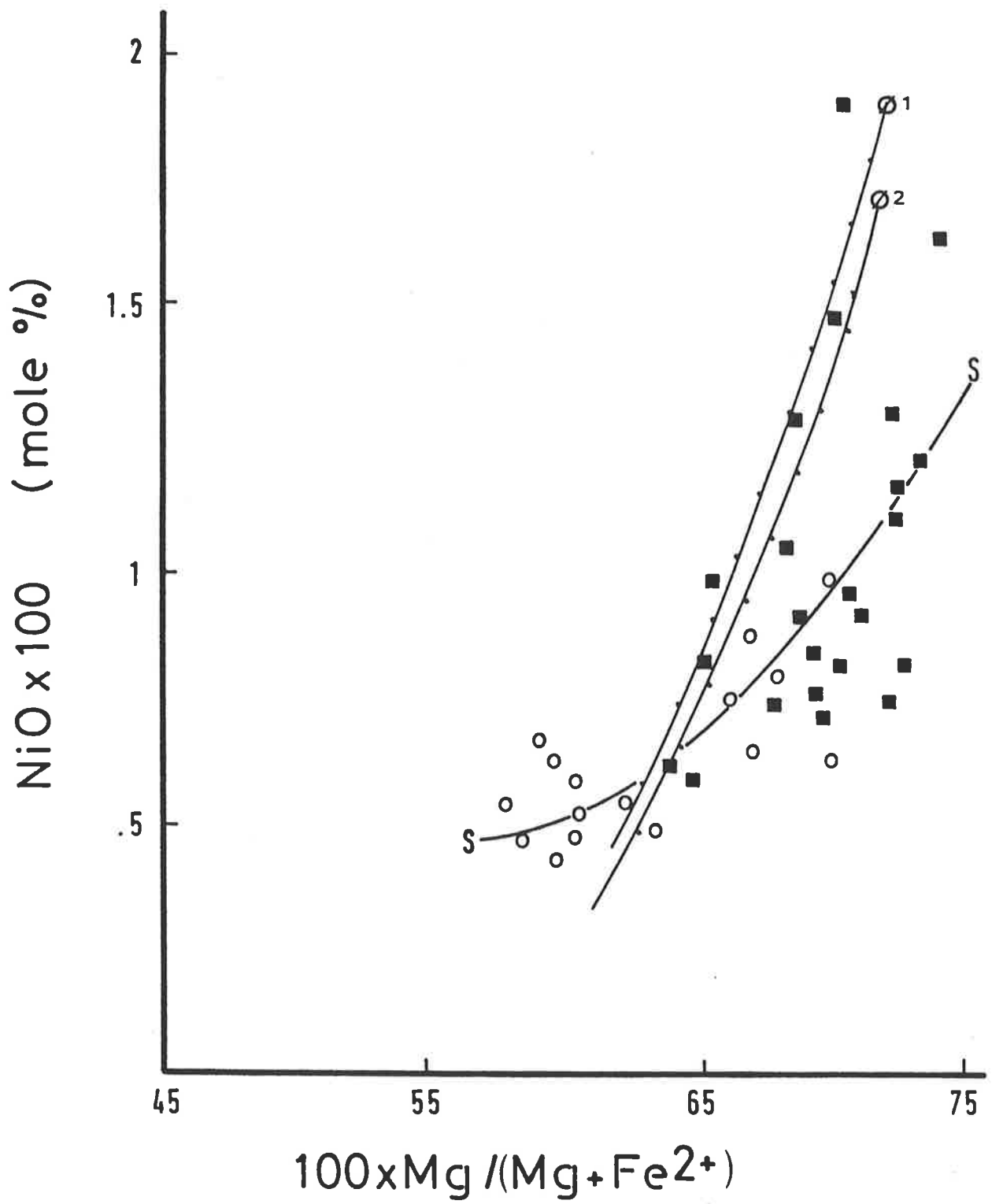


Figure 8.7a. A Mg# versus Ni-content plot of Macquarie Island basalts (crosses) and a superimposed calculated liquid line of descent during fractional crystallisation of olivine from a possible parental liquid, basalt 236. The increment of olivine fractionation is 2%, and is marked by small solid circles on the calculated liquid path. Maximum olivine fractionation marked on the liquid curve is 10%. Almost all basalts are produced by 1% to 10% fractionation from basalt 236. $Mg\# = Mg / (Mg + Fe^{2+})$.

Figure 8.7b. A Mg# versus Ni-content plot of Macquarie Island dolerites (open circles) and the calculated liquid line of descent of figure 8.7a, from basalt 236. The increment of olivine fractionation is again 2%, and is marked by small solid circles on the calculated liquid curve. The most evolved dolerite is sample 391 with 0.467 $Mg\# = Mg / (Mg + Fe^{2+})$.

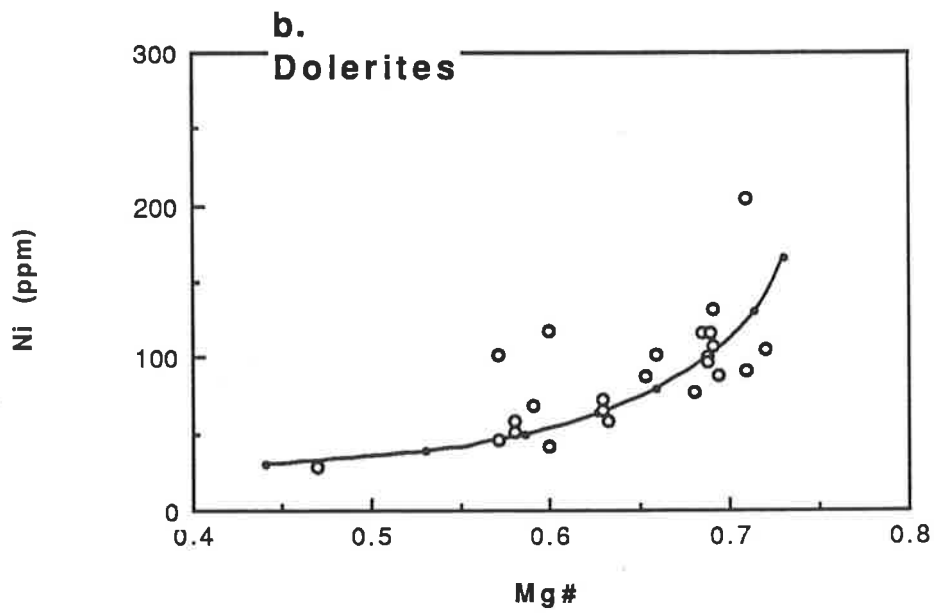
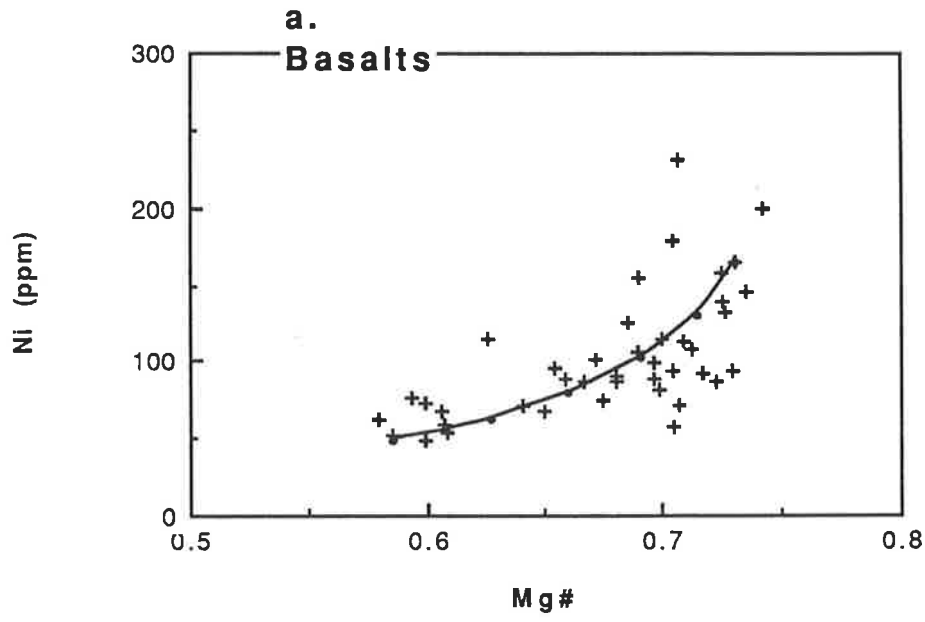
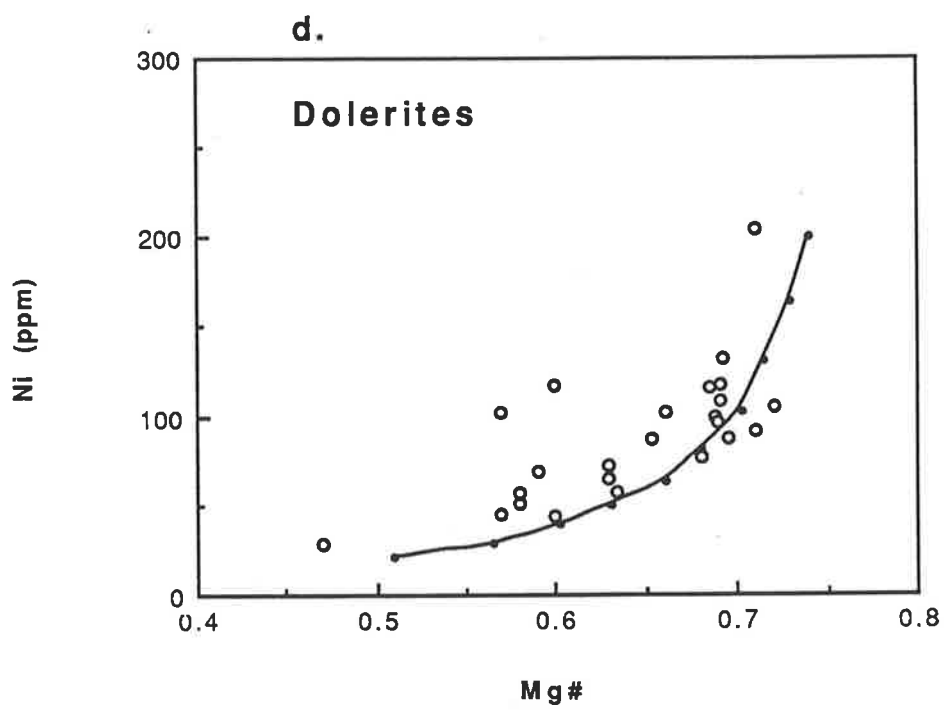
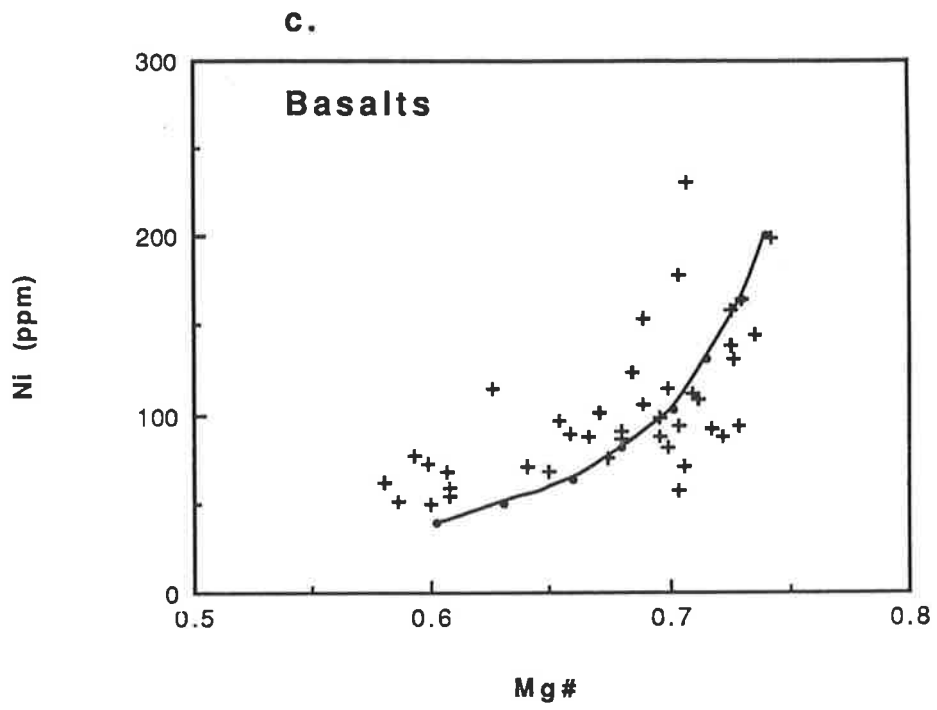


Figure 8.7c. A Mg# versus Ni-content plot of Macquarie Island basalts (crosses) and a superimposed calculated liquid line of descent during fractional crystallisation of olivine from a possible parental liquid, basalt 38188. The increment of olivine fractionation is 2%, and is marked by small solid circles on the calculated liquid path. Maximum olivine fractionation marked on the liquid curve is 14%. The liquid path approximates the basalt trend. Most of the basalts can be derived by 2% to 14% fractionation from basalt 38188.
 $Mg\# = Mg / (Mg + Fe^{2+})$.

Figure 8.7d. A Mg# versus Ni-content plot of Macquarie Island dolerites (open circles) and the calculated liquid line of descent of figure 8.7c, from basalt 38188. The increment of olivine fractionation is again 2%, and is marked by small solid circles on the calculated liquid curve. All dolerites can be related to such a parental liquid by 4-12% fractionation, and the most evolved dolerite by more than 16%.
 $Mg\# = Mg / (Mg + Fe^{2+})$.



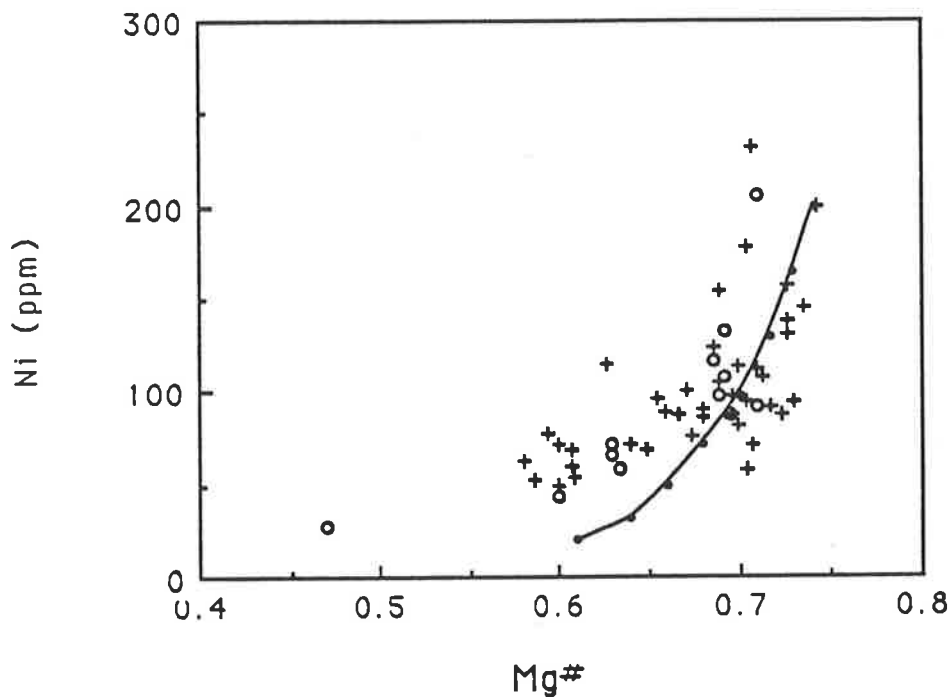
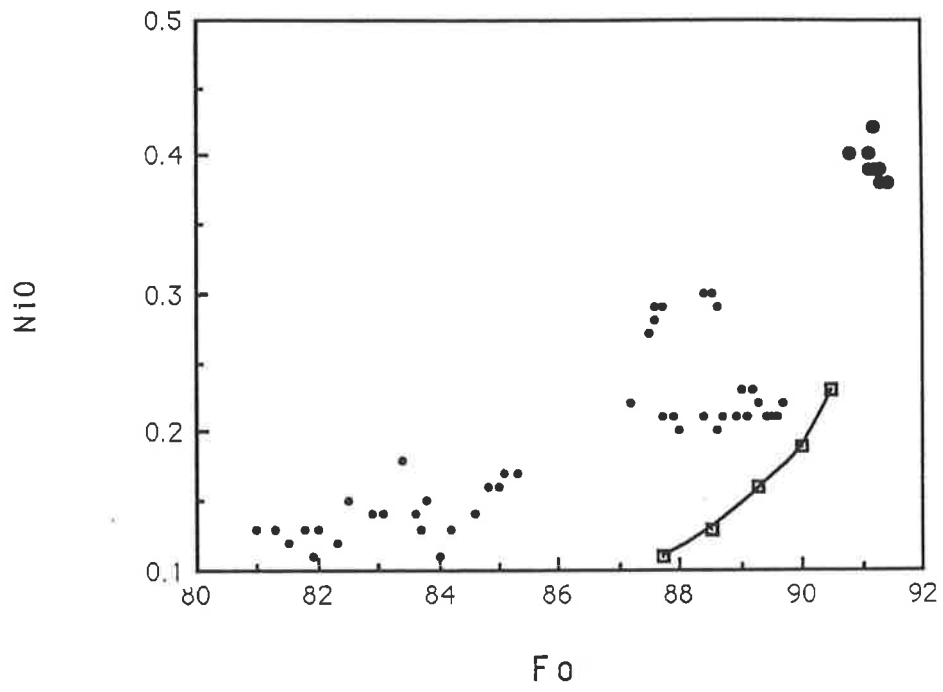


Figure 8.8. A Mg#ratio versus Ni-content plot of Macquarie Island basalts (crosses) and dolerites (open circles). Superimposed is the calculated liquid line of descent of basalt 38188 during olivine fractional crystallisation. D^{Ni} calculated from expression 8.15b for temperatures ranging from 1265°C to 1200°C. K^{Fe-Mg} is 0.3. $Mg\# = Mg/(Mg+Fe^{2+})$. The increment of olivine fractionation is 2%, and is marked on the calculated liquid curve by small solid circles. The liquid path crosses the basalt - dolerite cluster at $Mg\# \approx 0.70 \pm 0.3$. The more differentiated basalts and dolerites ($Mg\# \approx 0.60 \pm 0.02$) have higher Ni-contents than those predicted by this fractionation model.

Figure 8.9. Fo versus NiO (wt%) plots of representative Macquarie Island olivines from the layered rocks (small filled circles) and harzburgites (large filled circles). Calculated olivine composition paths during fractionation of basalt 38188 are superimposed (shown by solid curves). Each square represents the calculated olivine composition after an interval of 2% fractionation. The first olivine to crystallise is the in-equilibrium olivine with this basalt. $K^{\text{Fe-Mg}}$ is taken constant at 0.3. The olivine path shown in figure 8.9a, was calculated using a D^{Ni} of 9; in figure 8.9b, the D^{Ni} equals 12. After 8% fractionation (the maximum plotted value), the calculated olivine NiO content reduces to 0.11%. Calculated trends are not in agreement with the observed trends of olivines from the layered rocks.

a.



b.

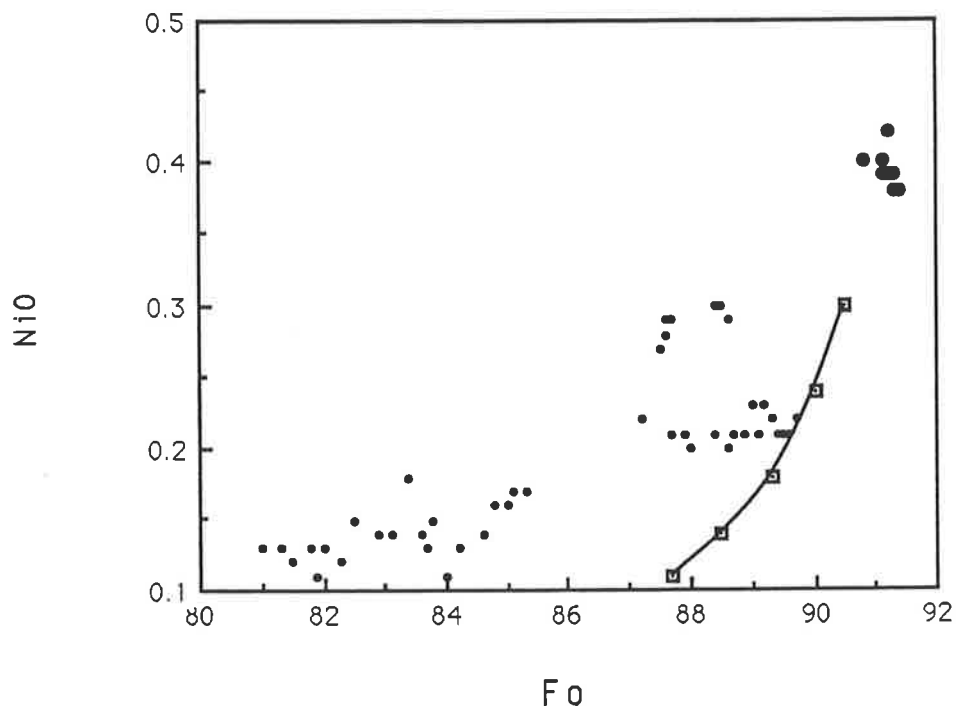


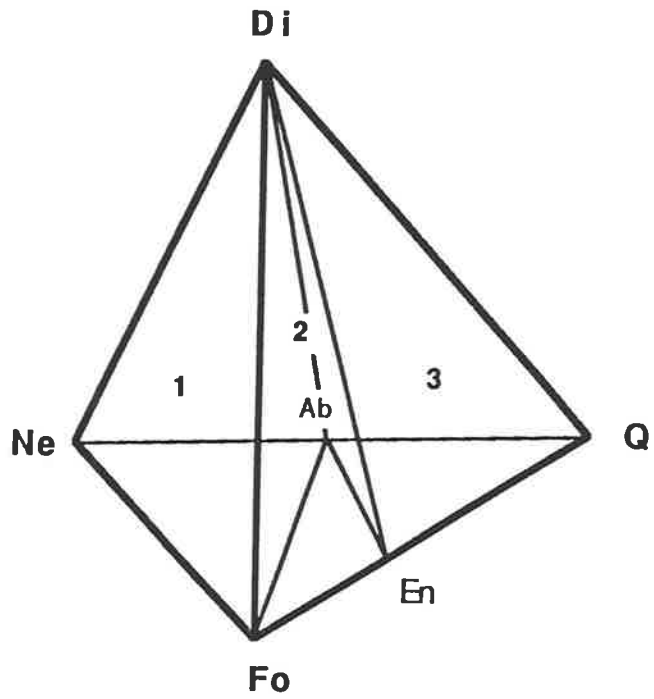
Figure 9.1.

(a). The normative basalt tetrahedron nepheline-forsterite-diopside-quartz of Yoder and Tilley (1962). Symbols as follows, Di=diopside, Ne=nepheline, Q=quartz, Fo=forsterite, En=enstatite, Ab=albite. The volumes (1), (2) and (3) within the tetrahedron define the fields occupied by alkali basalts, olivine-basalts and tholeiites. The plane Di-Fo-Ab is the plane of silica undersaturation and separates alkali basalts from olivine-tholeiites. The plane Di-Ab-En is the silica saturation surface and separates olivine-tholeiites from quartz-tholeiites.

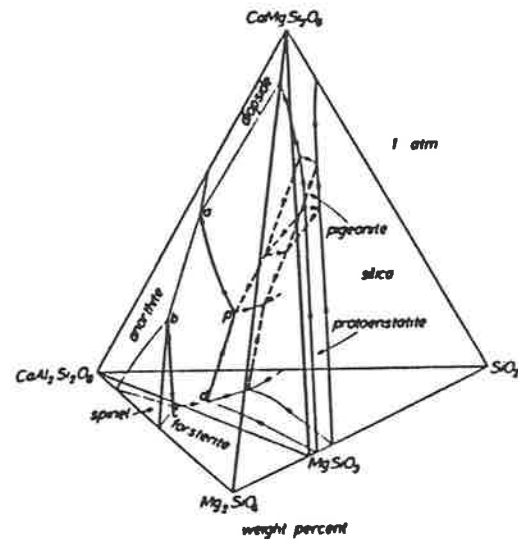
(b). Phase relations in the system Fo-Di-An-SiO₂, part of the larger CaO-MgO-Al₂O₃-SiO₂ quaternary system, at 1 atm (from Presnall et al., 1978). The Mg₂SiO₄-CaAl₂Si₂O₈-CaMgSi₂O₆ (Fo-An-Di) plane is equivalent to the Di-Ab-Fo plane of the normative basalt tetrahedron and the CaMgSi₂O₆ - CaAl₂Si₂O₈-MgSiO₃ (Di-An-En) plane is equivalent to the Di-Ab-En.

(c). Liquidus phase relations in the An-Di-Fo and An-Fo-SiO₂ joins of the Fo-Di-An-SiO₂ system at 1 atm pressure. Dashed phase boundaries after Osborne and Tait (1952) (from Morse, 1980).

a



b



c

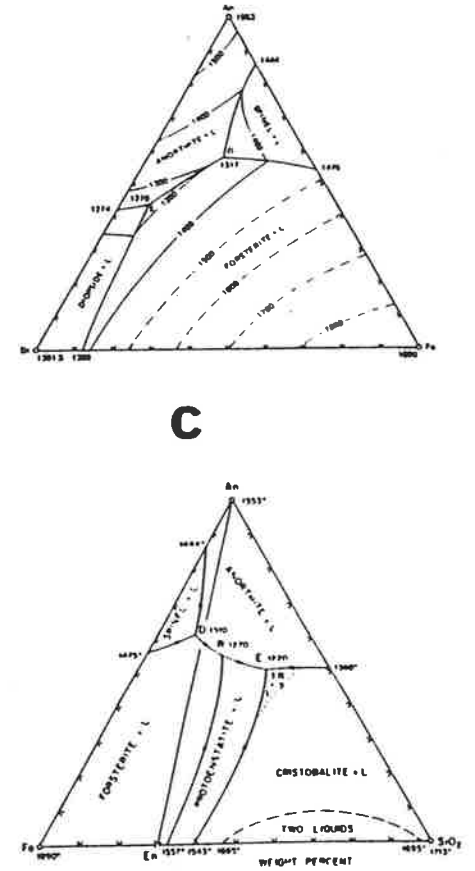
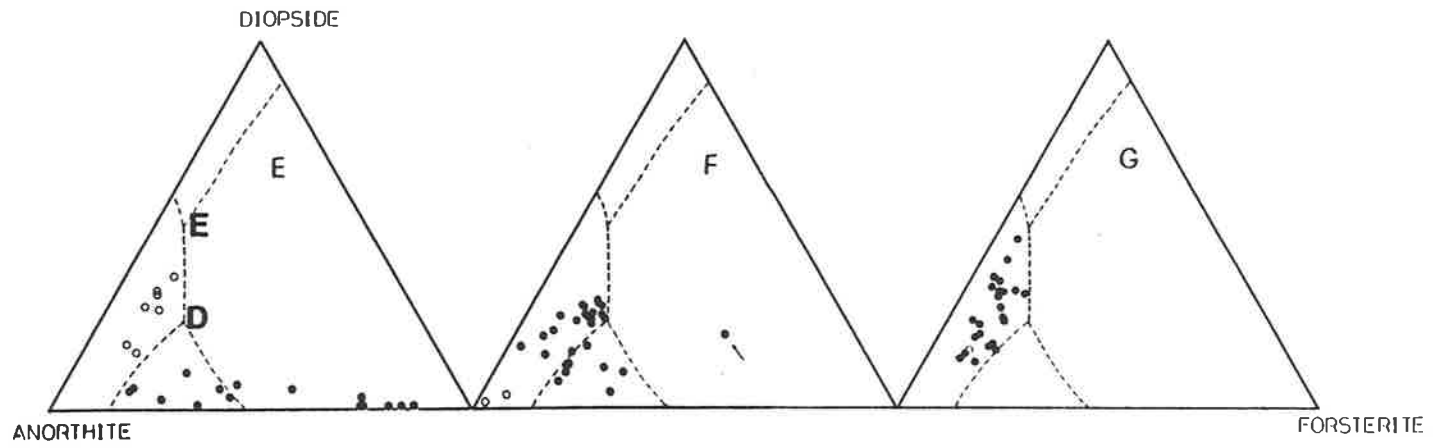
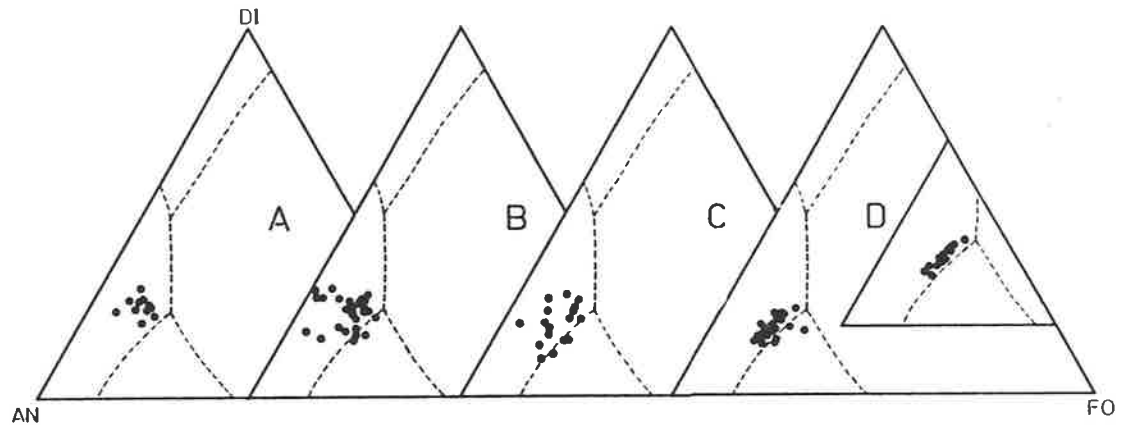


Figure 9.2. Macquarie Island rock data projected on the An-Di-Fo join of the An-Di-Fo-SiO₂ synthetic system. The four primary fields at 1atm pressure are from figure 9.1c.

- (A). Volcanic glass compositions plot in the anorthite+liquid field (An+L).
- (B). Dolerite dykes from the dyke swarms, layered rocks and massive gabbros. Three dykes plot in the forsterite+liquid field (Fo+L).
- (C). Projection of lavas with tholeiitic chemistry. They plot mostly in the An+L field.
- (D). Projection of alkalic lavas (nepheline normative). The inset diagram is a plot of aphyric lavas or close to aphyric lavas containing less than 10% phenocrysts. They plot in the An+L field but very near the univariant curve representing equilibrium of coexisting Fo+An+L.
- (E). Projection of the layered rocks. Solid circles are troctolites; open circles are the uppermost strongly laminated gabbros, olivine-free types, of the layered sequence.
- (F). Projection of olivine-gabbros (solid circles). Two anorthosites are also plotted (open circles). The rock pointed by the arrow in the Fo+L field is a mafic intrusive layer in the olivine-gabbros at Handspike Point (sample 380).
- (G). Massive gabbros. Mainly Upper Level gabbros and selected samples from other massive gabbro occurrences. The open circle is a doleritic gabbro from a minor outcrop on the east coast (sample 726). All rocks plot in the An+L field.



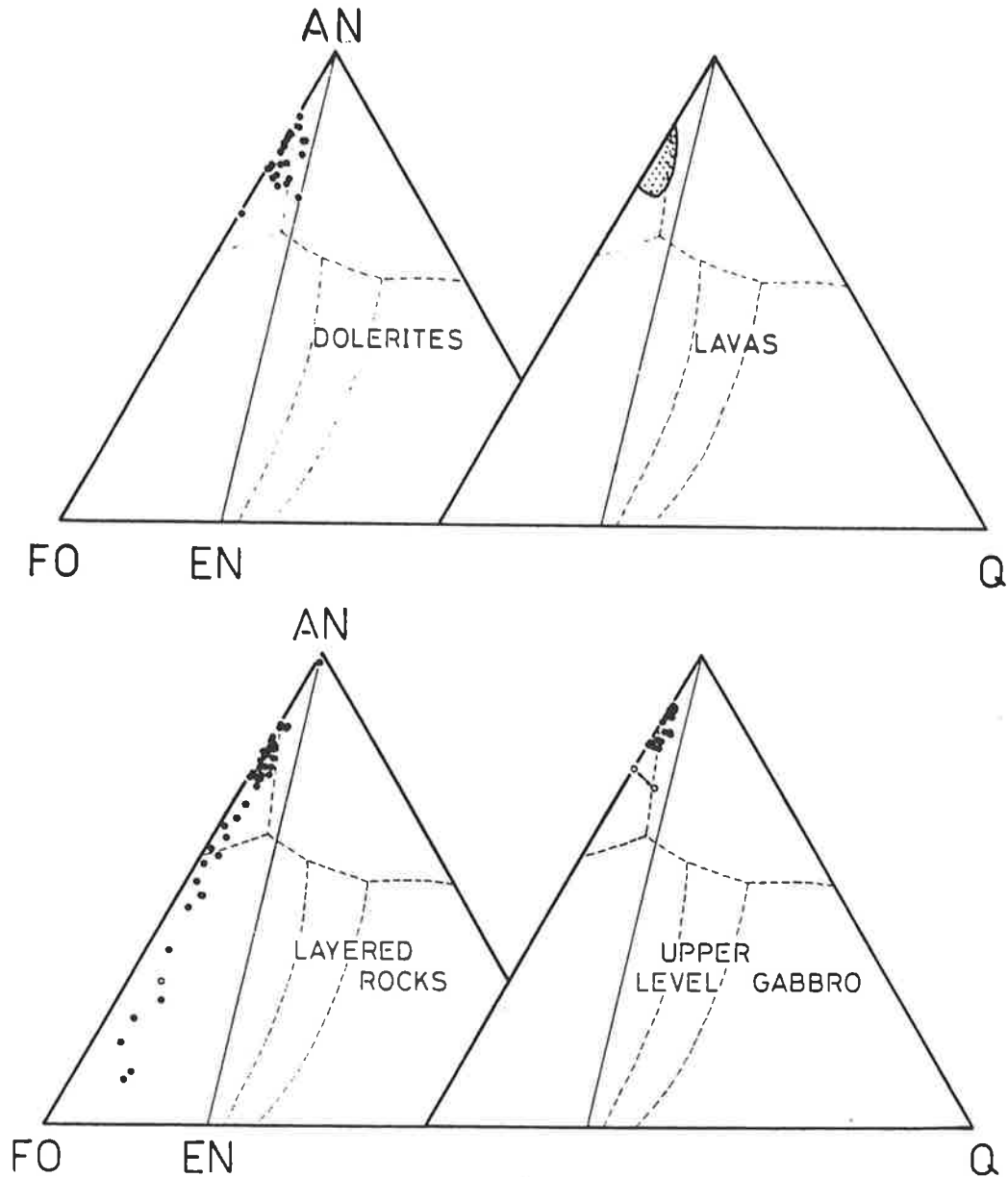


Figure 9.3. Projection of Macquarie Island rock data in the Fo-An-SiO₂ join of the Fo-Di-An-SiO₂ tetrahedron. Q=SiO₂. In the "LAVAS" diagram, the dotted field includes both tholeiitic and alkalic lavas. In the "LAYERED ROCKS" diagram, the open circle is sample 380. In the "UPPER LEVEL GABBRO" diagram, the two open circles joined together by double arrow represent a dolerite dyke and a massive gabbro showing mutually intrusive relations. The dolerite dyke lies on the spinel-anorthite cotectic.

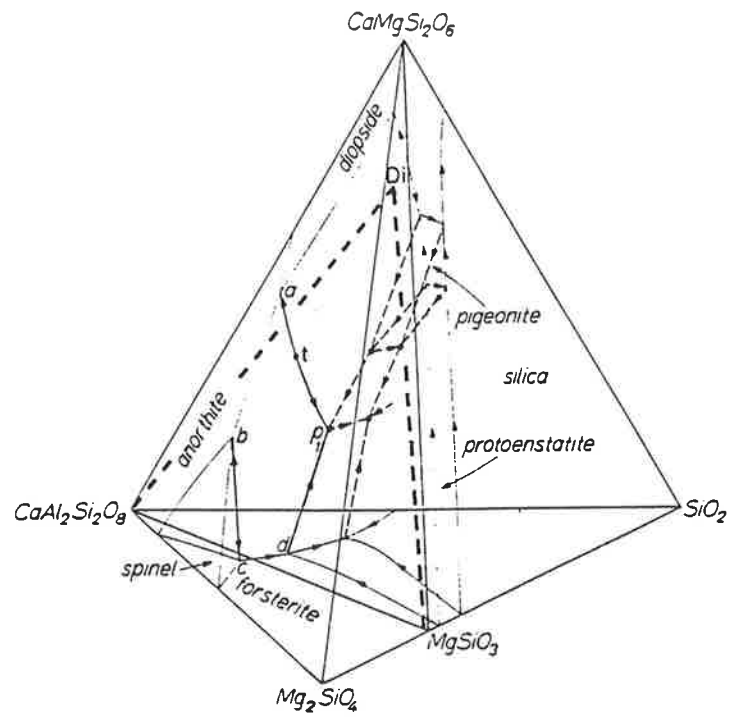


Figure 9.4. Phase relations in the Mg_2SiO_4 - $\text{CaAl}_2\text{Si}_2\text{O}_6$ - $\text{CaMg}_2\text{SiO}_6$ - SiO_2 quaternary. Phase boundaries after Presnall et al. (1978). Arrows on cotectics indicate direction of dropping temperature. Points **a** and **b** are the two piercing points on the Mg_2SiO_4 - $\text{CaAl}_2\text{Si}_2\text{O}_6$ - $\text{CaMg}_2\text{SiO}_6$ ternary. Point **p** is the invariant point of the system. The temperature maximum on the cotectic **a-p** is marked by **t**. **Di** is the diopside solid solution (it is referred in the text as Di_{ss}). The plane Mg_2SiO_4 - $\text{CaAl}_2\text{Si}_2\text{O}_6$ -**Di** lies to the silica- rich side of the Mg_2SiO_4 - $\text{CaAl}_2\text{Si}_2\text{O}_6$ - $\text{CaMg}_2\text{SiO}_6$ plane.

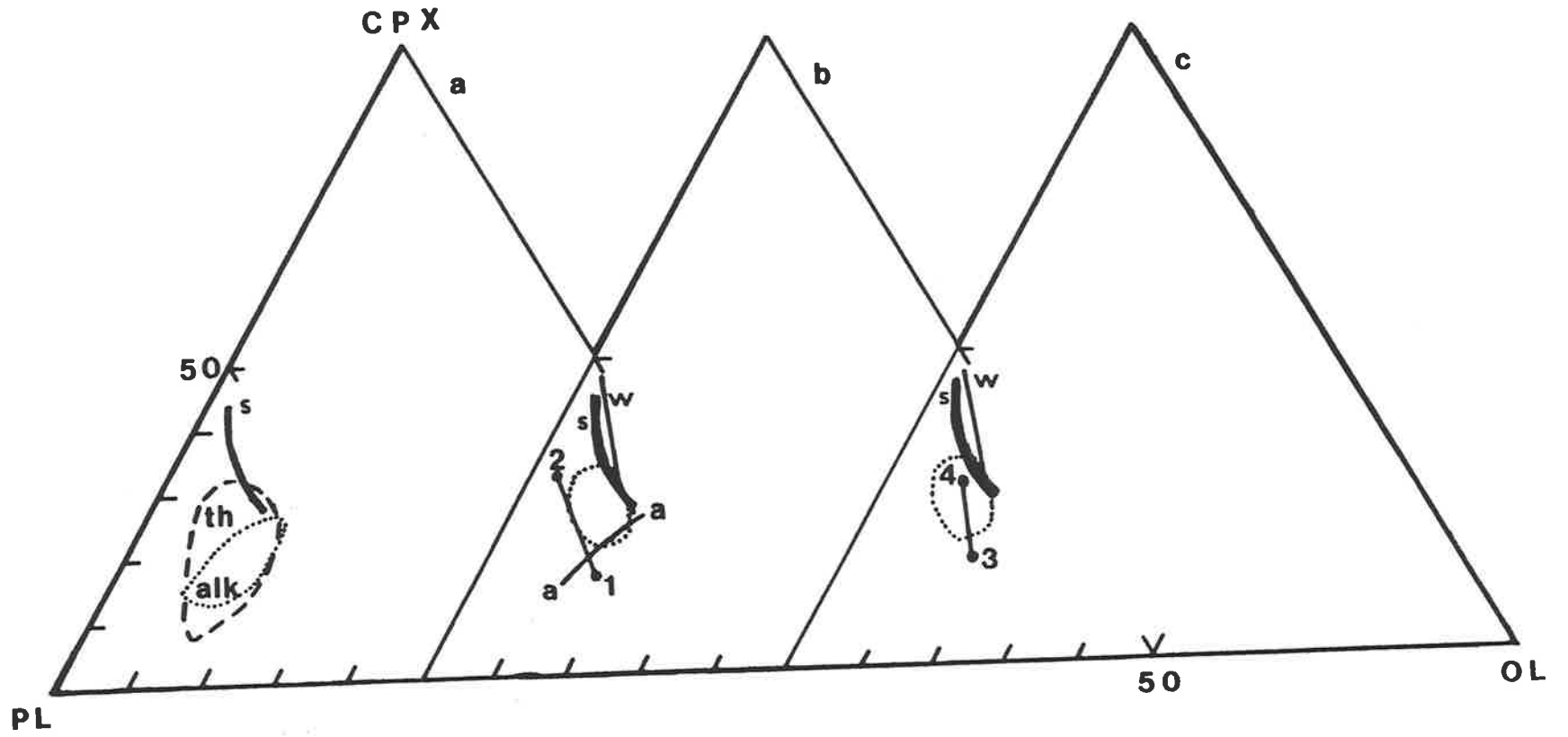
Figure 9.5

Projection of selected Macquarie Island data in the normative clinopyroxene- plagioclase- olivine (CPX-PL-OL) ternary.

(a). The fields of Macquarie Island basalts are shown by the dashed and dotted curves; **th** is the field of the tholeiitic and **alk** is the field of the alkalic basalts. **s** is the olivine-plagioclase cotectic of Shido et al. (1971).

(b). The field of Macquarie Island glasses is shown by the dotted curve. The trend or cotectic-like boundary defined by the aphyric alkalic basalts is shown by the **a-a** curve. Solid circles **1** and **2** represent the magnesian and evolved dolerites 220 and 153 respectively. **w** is the inferred plagioclase-olivine cotectic of Bryan (1983) from FAMOUS glasses, and **s** the cotectic of Shido et al. (loc.cit.).

(c). The field of Macquarie Island glasses and the cotectics **s** and **w** as in (b). Point **3** is the magnesian basalt 38284 and point **4** is the differentiated basalt 108C.



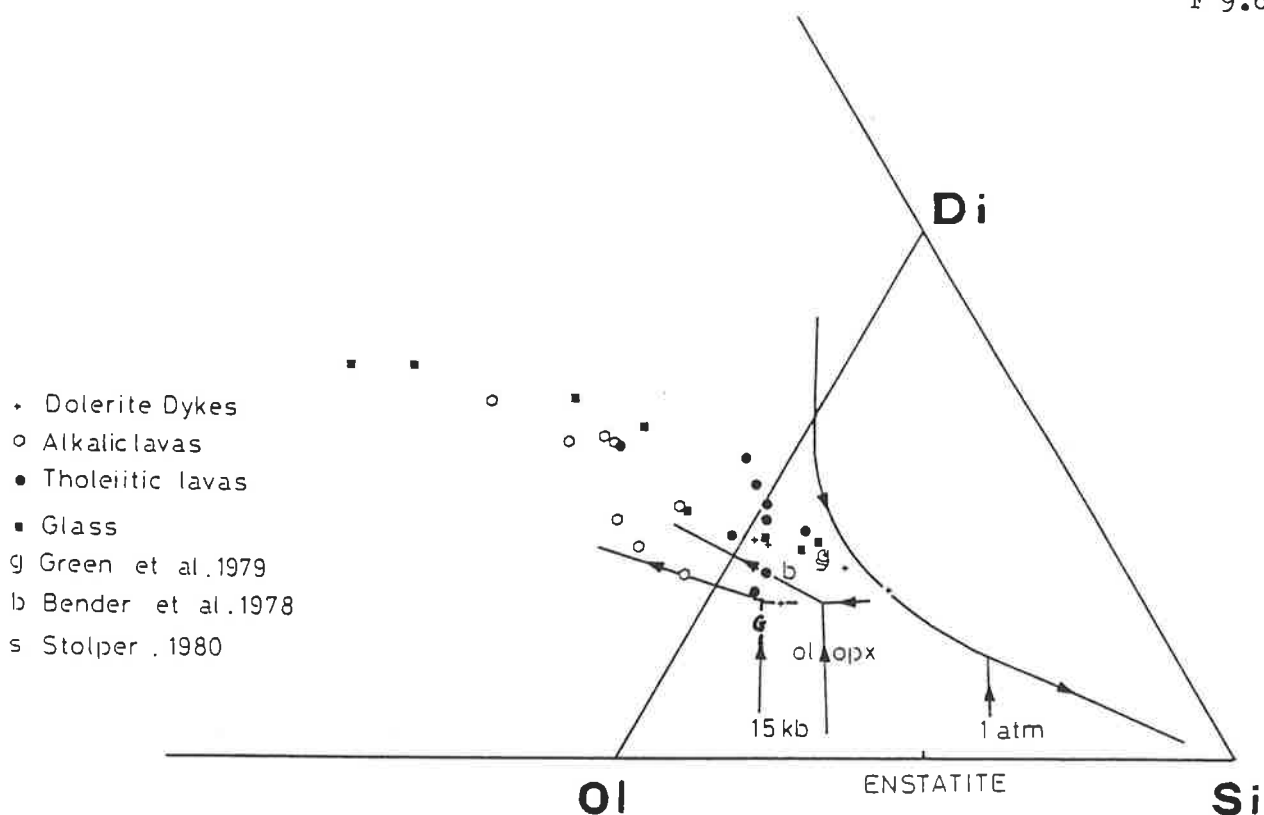


Figure 9.6. Projection from the plagioclase into the diopside-olivine-silica plane of the olivine-plagioclase-diopside-silica (Ol-Pl-Di-Si) tetrahedron of Walker et al. (1979). The phase boundaries and the positioning of the cotectics at different pressures are those of Walker et al. Arrows indicate the direction of falling temperature. The 10kbar cotectic is shown in this diagram between the 1atm and 15kbar cotectics.

Selected Macquarie Island data are plotted. These include dolerite dykes from the dyke swarms, tholeiitic and alkalic lavas, and glasses.

Compositions g, b and s are the primitive basaltic glasses whose phase relations were studied experimentally by Green et al. (1979), Bender et al. (1978) and Stolper (1980) respectively. Composition (G) is a mixture of the basaltic glass 3-18-7-1 plus 17% olivine utilized by Green et al. (1979).

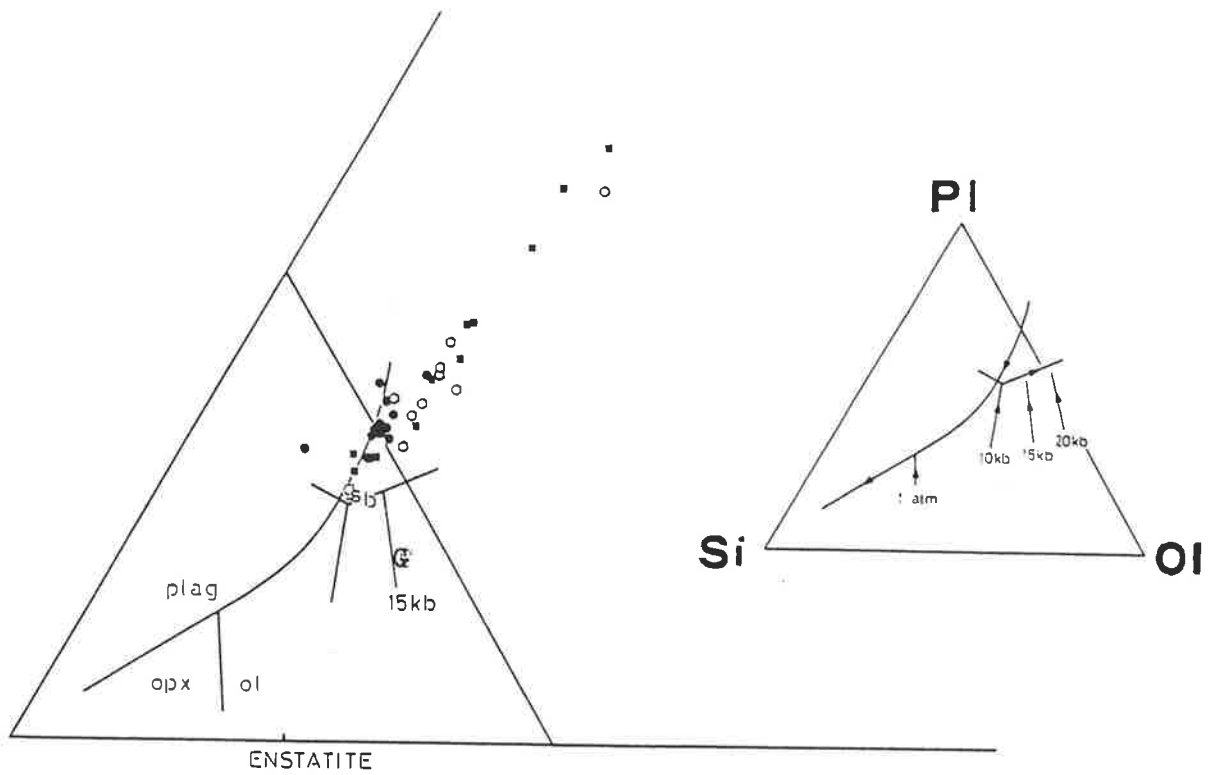
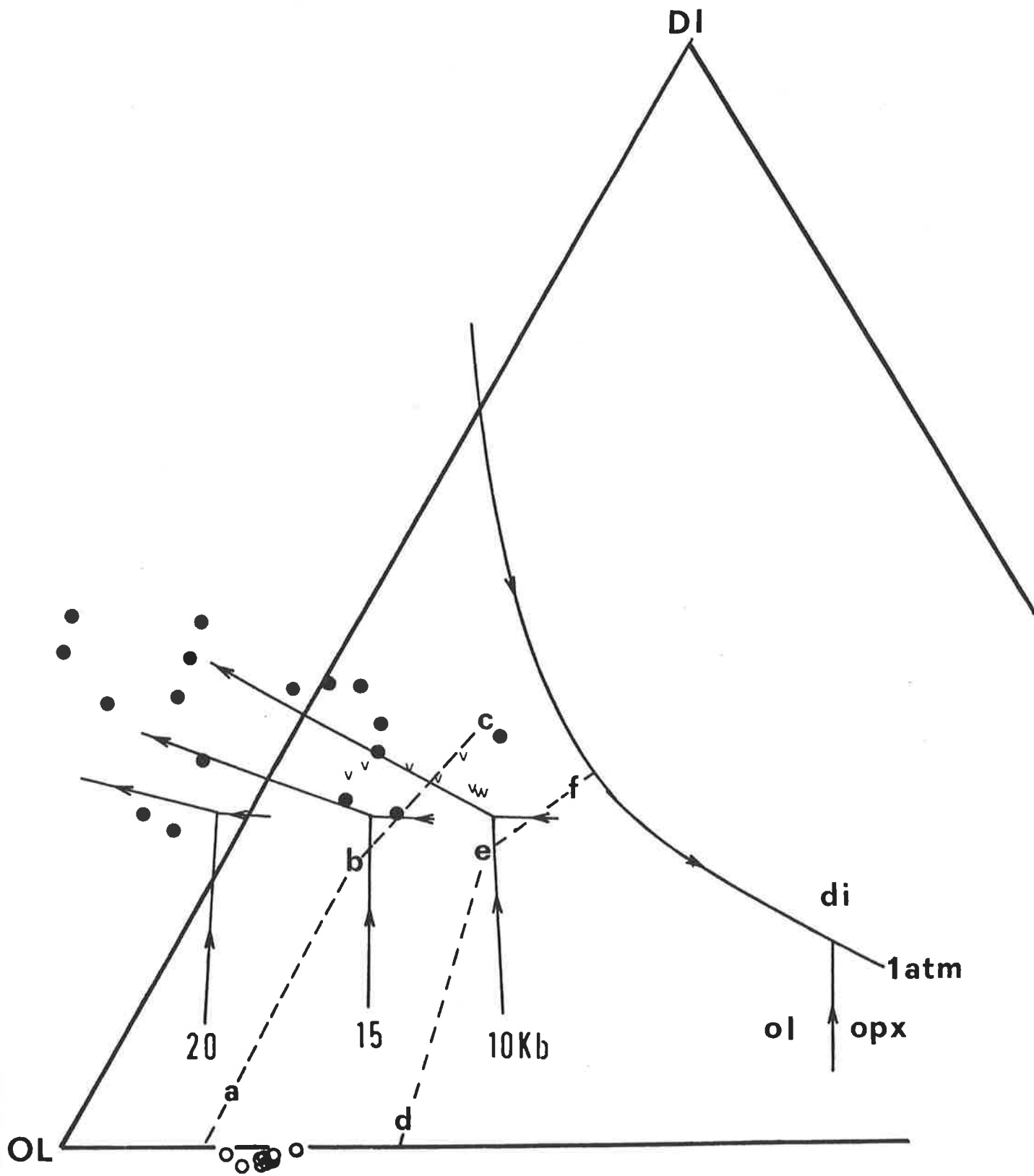


Figure 9.7. Projection from the diopside into the Ol-Pl-Si plane of the Ol-Pl-Di-Si tetrahedron. Phase boundaries from Walker et al. (1979). Arrows again indicate falling temperature. Symbols as in figure 9.6.



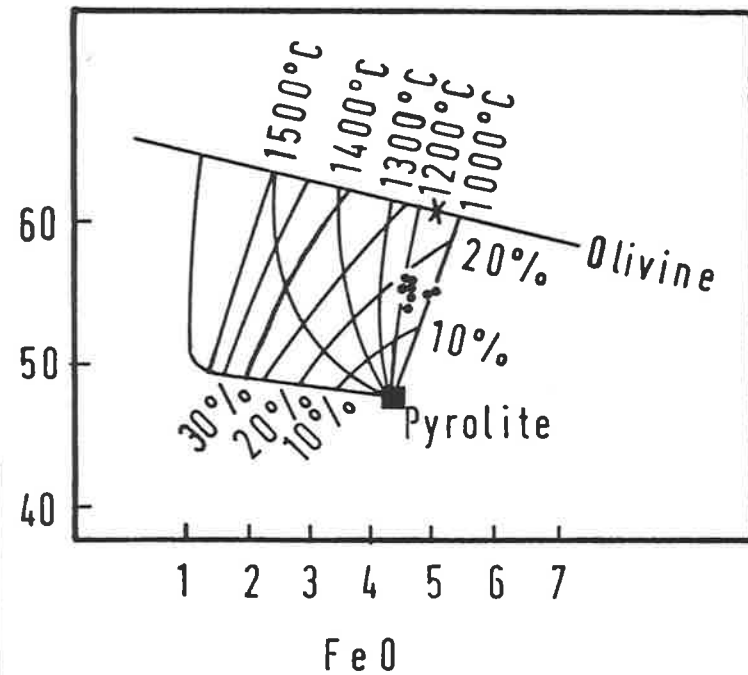
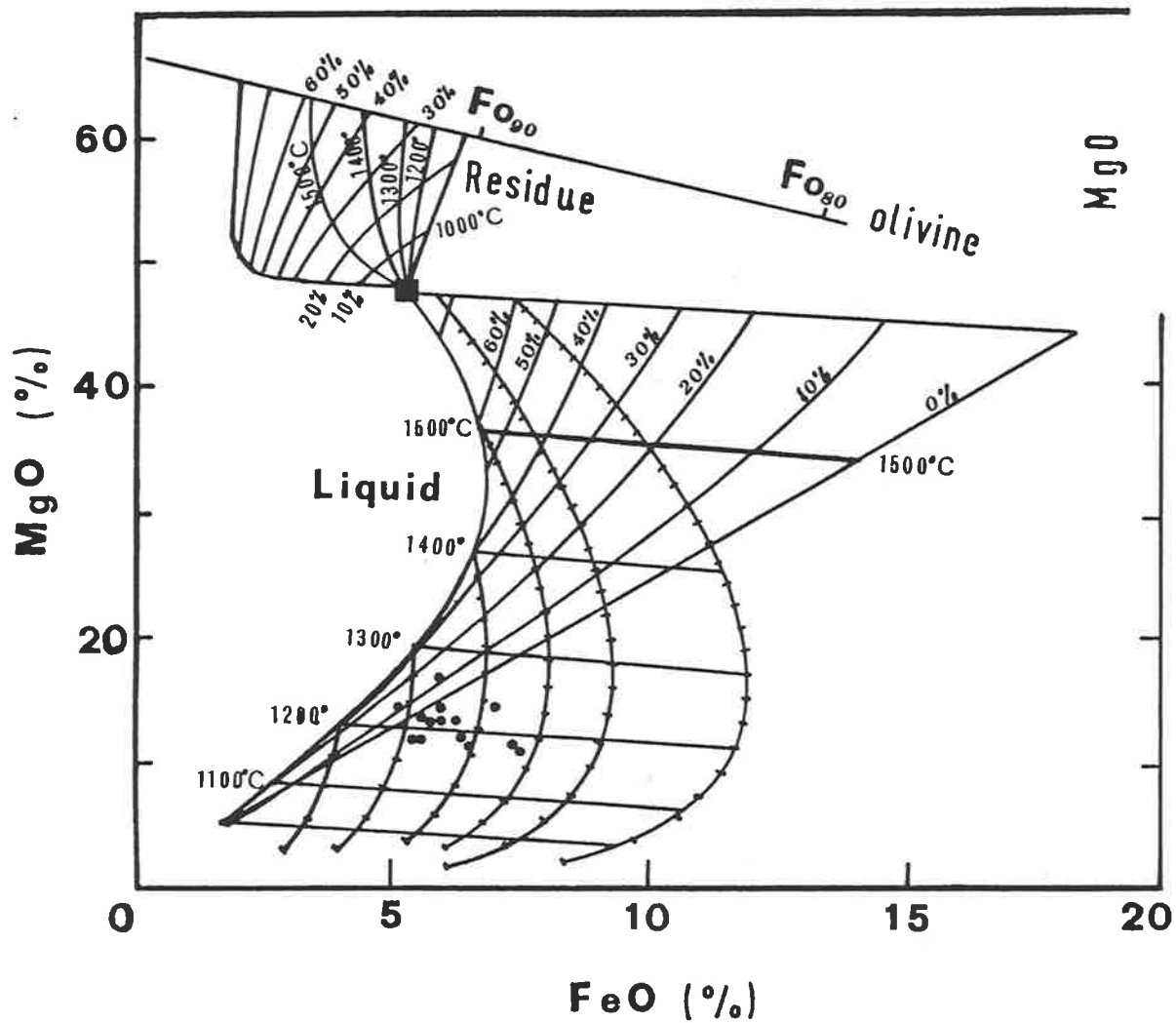


Figure 9.10.

(A). Normalised patterns (to CI chondrites) of transition element abundances from the Macquarie Island harzburgites and basalts. The majority of analysed basalts define field **B**; **H** is the field of all analysed harzburgites apart from sample 163. The pattern of sample 163 is shown by heavy line and is marked as **HT**.

(B). The calculated TM abundances in melts and residues during batch melting of a source lherzolite consisting of 70% olivine, 12% opx, 16% cpx and 2% spinel are normalised to chondrites and plotted. Patterns 1-1 and 2-2 show the calculated liquid and residue patterns respectively for 20% partial melting. Pattern 3-3 is displayed by the source lherzolite. The very good agreement between the observed and calculated patterns in basalts and harzburgites suggests that the observed TM abundances in the Macquarie Island volcanics and residual peridotites could have been produced by moderate (15%-20%) degrees of melting of a lherzolite source.

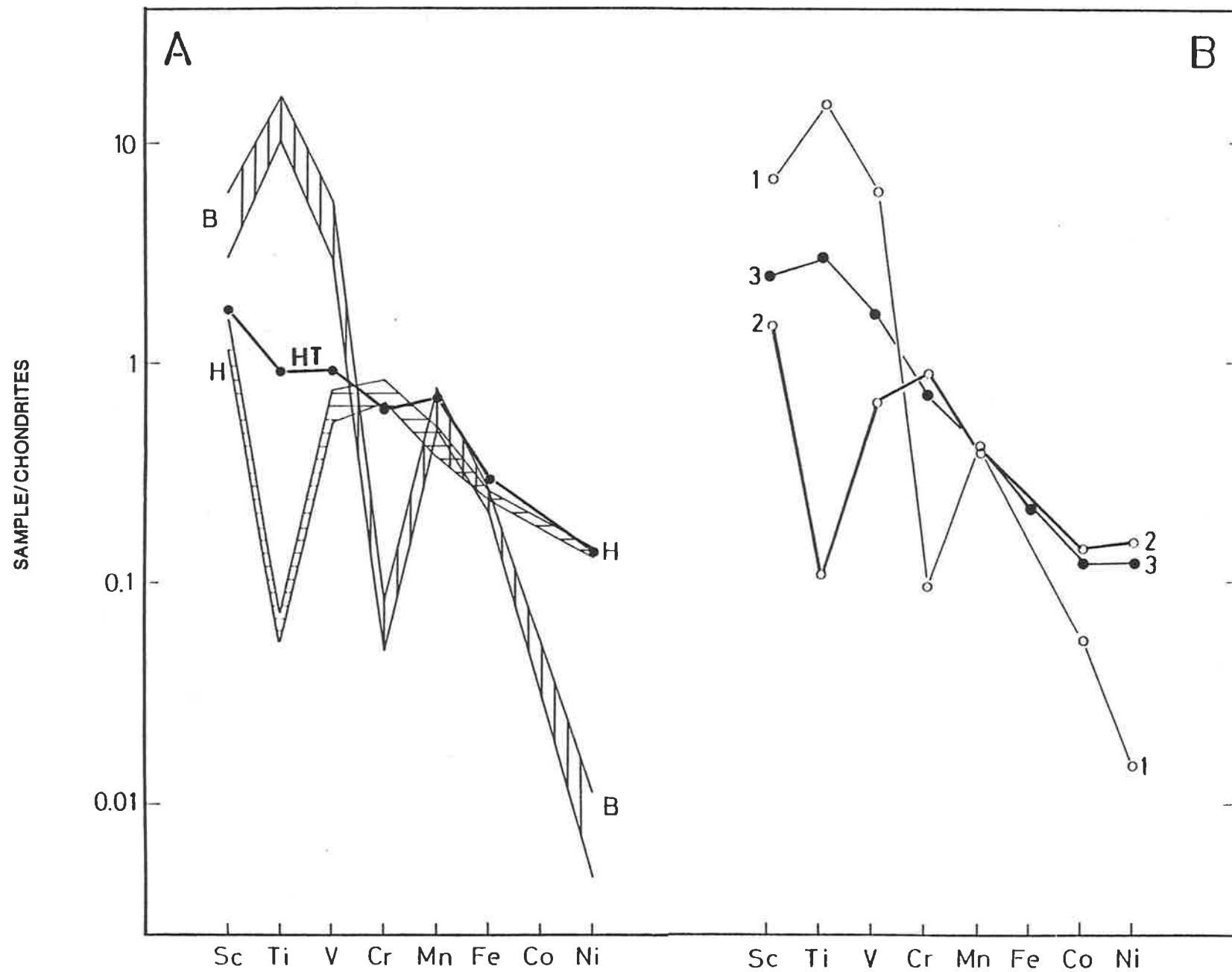


Figure 9.11.**A.**

Calculated liquid Zr content (in ppm) as a function of the percentage of partial melting (% melt). The trends have been calculated for increments of 2% to 30% of batch melting for two different source mineralogies and two different mantle source Zr concentrations; a primordial mantle source with an initial Zr concentration of 11 ppm (Tarney et al., 1980) and an upper mantle source having a Zr content of 27 ppm (Anderson, 1983).

Mineral composition of source mineralogies:

mineralogy 1: 70%olivine+25%orthopyroxene+4%clinopyroxene+1%spinel,

mineralogy 2: 70%olivine+12%orthopyroxene+16%clinopyroxene+2%spinel.

Curves 1, 2, 3 and 4 have been calculated as follows:

- 1: mineralogy 1 and 27 ppm Zr in the mantle source,
- 2: mineralogy 2 and 27 ppm Zr in the mantle source,
- 3: mineralogy 1 and 11 ppm Zr in the mantle source and
- 4: mineralogy 2 and 11 ppm Zr in the mantle source.

B.

Calculated liquid Nb content (in ppm) as a function of the percentage of partial melting (% melt). The trends have been calculated for increments of 2% to 30% of batch melting from the two source mineralogies as before (figure 9.11A). Primordial mantle Nb content is 0.62 (Tarney et al., loc. cit.) and upper mantle Nb content is 6.03 ppm (Anderson, loc. cit.).

Curves 1, 2, 3 and 4 have been calculated as follows,

- 1: mineralogy 1 and 6.03 ppm Nb in the mantle source,
- 2: mineralogy 2 and 6.03 ppm Nb in the mantle source,
- 3: mineralogy 1 and 0.62 ppm Nb in the mantle source and
- 4: mineralogy 2 and 0.62 ppm Nb in the mantle source.

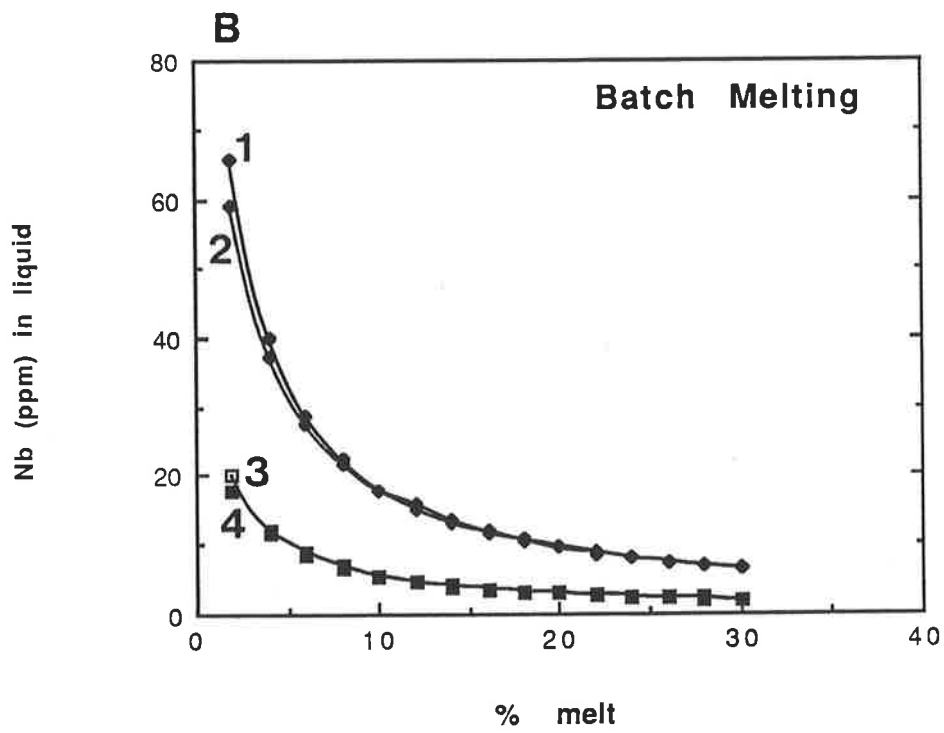
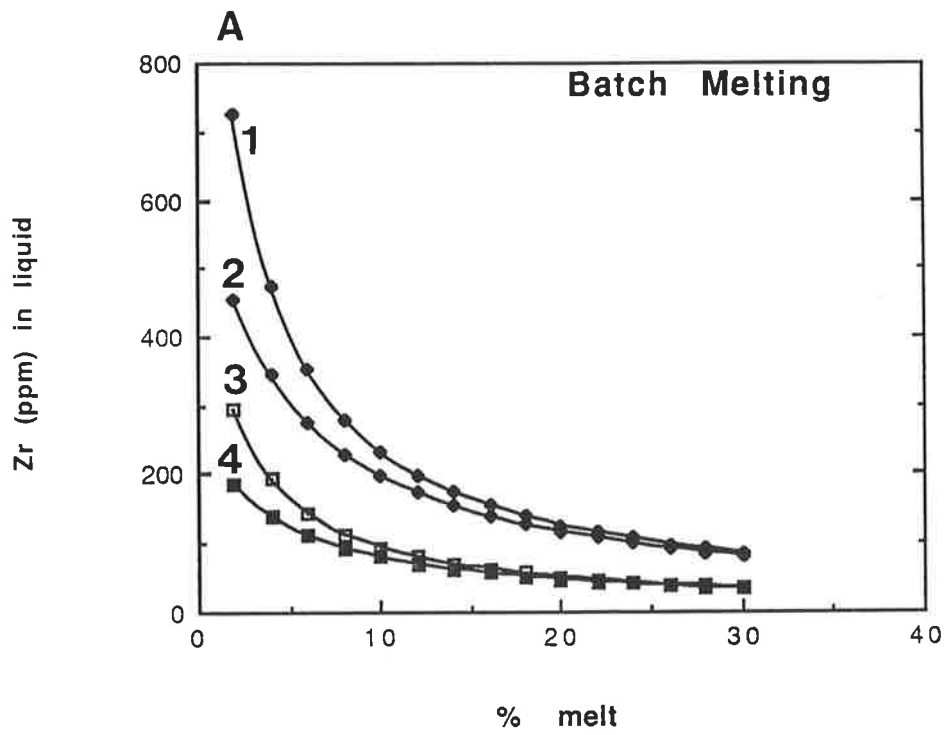


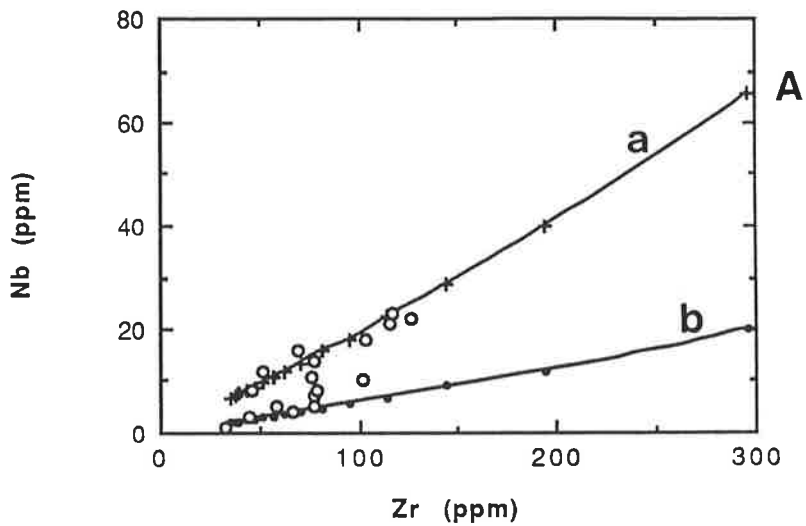
Figure 9.12.

A. A Zr versus Nb plot of Macquarie Island tholeiitic basalts shown by open circles. Batch partial melting curves **a** and **b** have been estimated from the source mantle mineralogy 1 and for 2.03 and 0.62ppm Nb in the source respectively. The source Zr content was 11ppm. The minimum and maximum percent of melting is 2% and 30% respectively; the marks on both curves (**a** and **b**) indicate an interval of 2% melting.

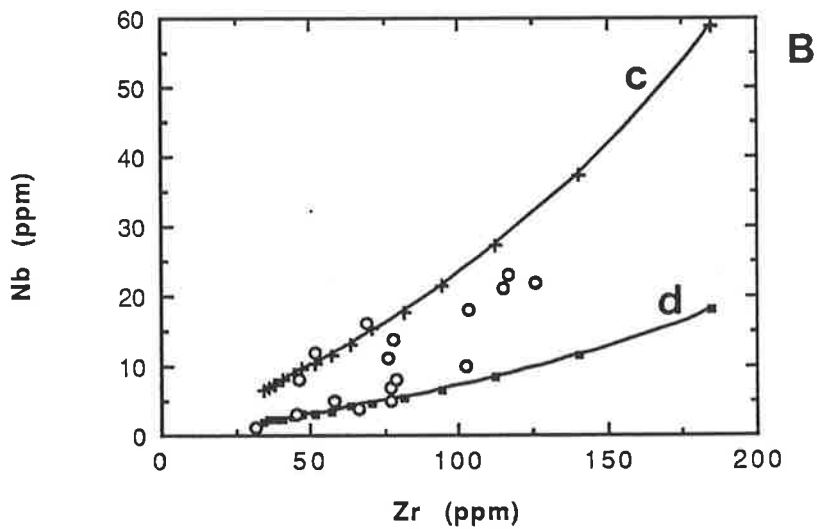
B. A plot similar to **A**, but for the source mineralogy 2. Batch partial melting curves **c** and **d** represent 2.03 and 0.62ppm Nb in the source respectively.

C. A plot similar to **A**, but for a high Zr source (27ppm) and for the source mineralogy 2. Batch partial melting curves **e** and **f** represent 2.03 and 0.62ppm Nb in the source respectively.

Source Mineralogy 1



Source Mineralogy 2



Source Mineralogy 1

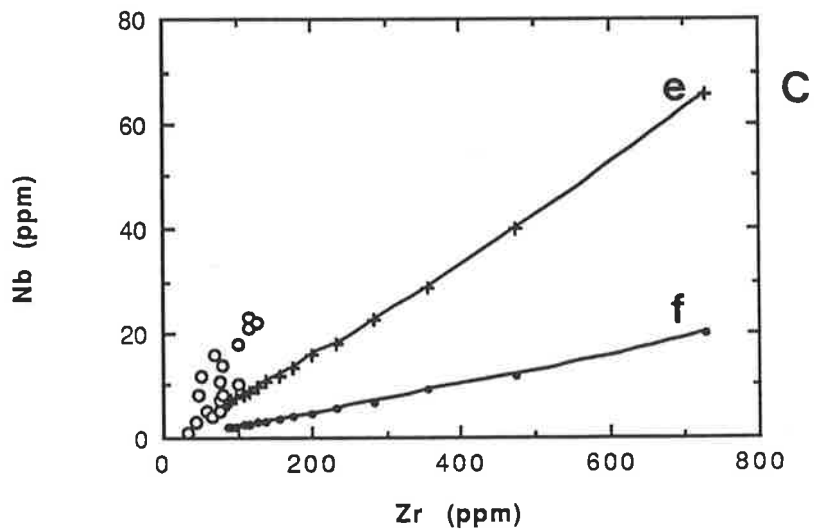


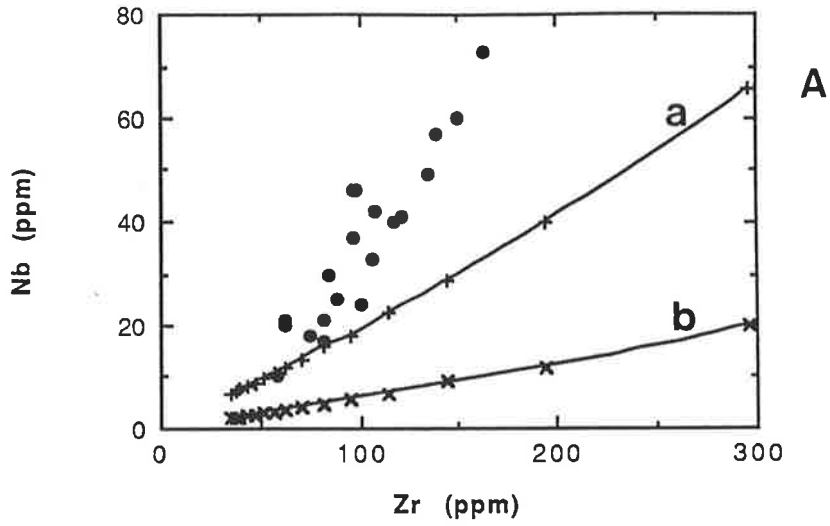
Figure 9.13.

A. A Zr versus Nb plot for the Macquarie Island alkalic basalts (filled circles). Batch melting curves **a** and **b** were calculated assuming a source mineralogy 1, low Zr content in the source (11 ppm), and source Nb contents of 2.03 and 0.62 ppm respectively. The melting curves are drawn for a minimum percent of melting of 2% and a maximum percent of 30%. The increment of melting is marked on each curve for an interval of 2% melting.

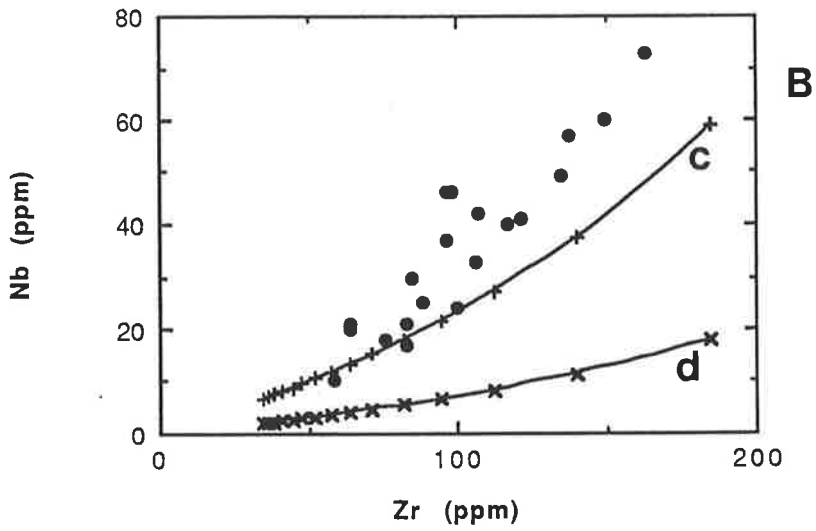
B. A plot similar to **A**, but for different source mineralogy (2). Batch melting curves **b** and **d** were calculated assuming low Zr content in the source (11 ppm), and source Nb contents of 2.03 and 0.62 ppm respectively.

C. A plot similar to **A**, but for different source mineralogy (2). Batch melting curves **e** and **f** were calculated assuming a high Zr content in the source (27 ppm). The source Nb contents for the melting curves **e** and **f** was 2.03 and 0.62 ppm respectively.

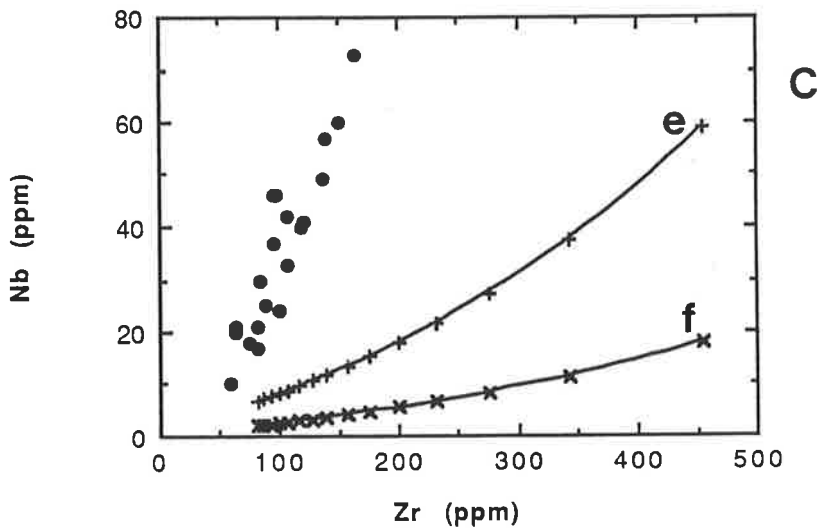
Source Mineralogy 1



Source Mineralogy 2



Source Mineralogy 2



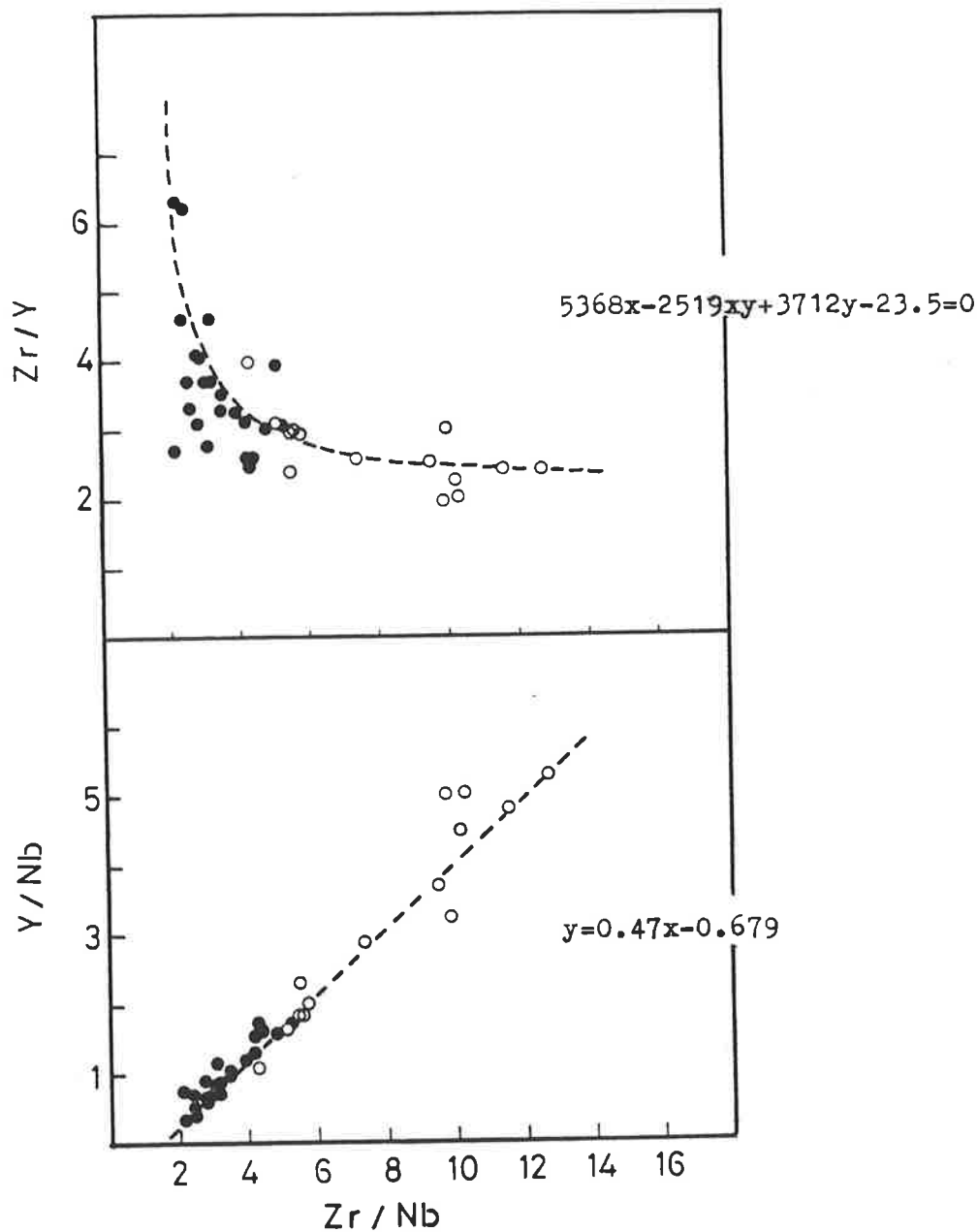


Figure 9.14. Zr/Y versus Zr/Nb and Y/Nb versus Zr/Nb plots of lavas. Open circles are lavas with tholeiitic affinities and filled circles represent the alkalic type lavas. The mixing lines were calculated from samples 38280 and 210 using the equation of Langmuir et al. (1978). The Zr/Nb of lava 38280 is 2.2, while that of lava 210 is 12.7. The derived mixing equations are also shown on each diagram. The best fit line to the data in the Y/Nb vs Zr/Nb diagram is $y=0.48x-0.637$, very similar to the calculated mixing line.

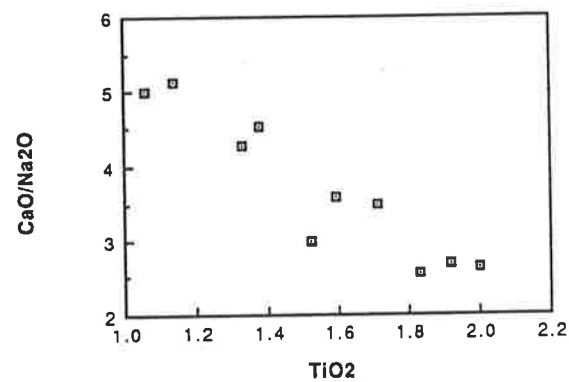
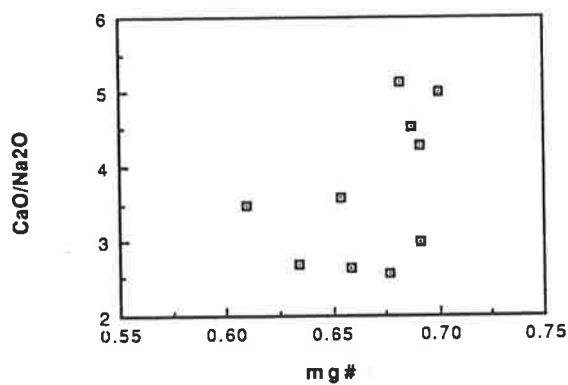
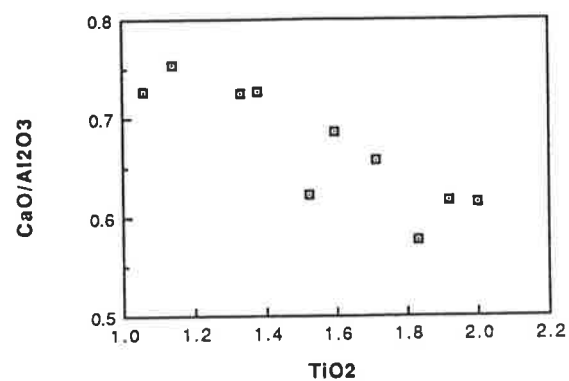
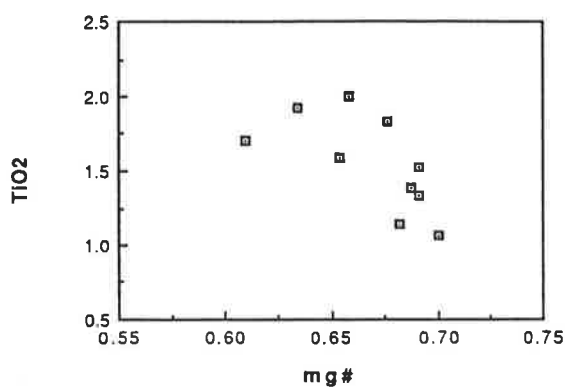
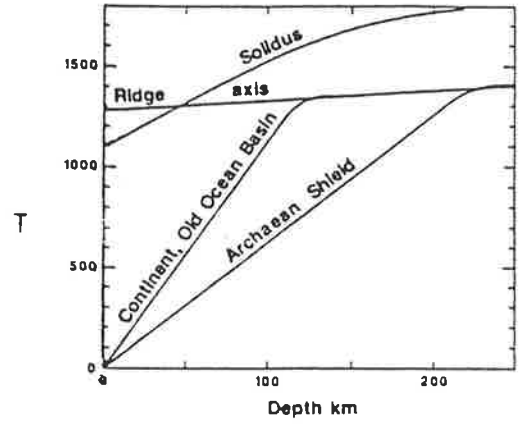


Figure 9.15. CaO/Al₂O₃ and CaO/Na₂O variation in respect to TiO₂ and $mg\# = Mg/(Mg+Fe)$ for Macquarie Island glasses.

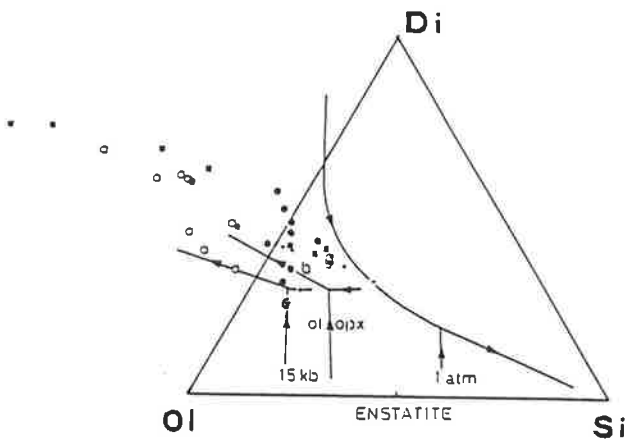
Figure 9.16.

- A. The convective geotherms of McKenzie and Bickle (1988). Depth in km, temperature T in $^{\circ}\text{C}$.
- B. The diopside-olivine-quartz projection of Walker et al. (1979) for Macquarie Island basalts, dolerites and glasses.
- C. A Di-Ol-Q projection (similar to B) for the calculated melt compositions of McKenzie and Bickle (1988).
- D. The lithosphere structure model beneath a spreading ridge of Ahern and Turcotte (1979). Solid curve is the solidus; thin lines with marked percentages indicate the degrees of partial melting as a function of depth.
- E. Temperature distribution beneath a ridge axis according to McKenzie and Bickle (1988), calculated for a potential mantle temperature of 1280°C .

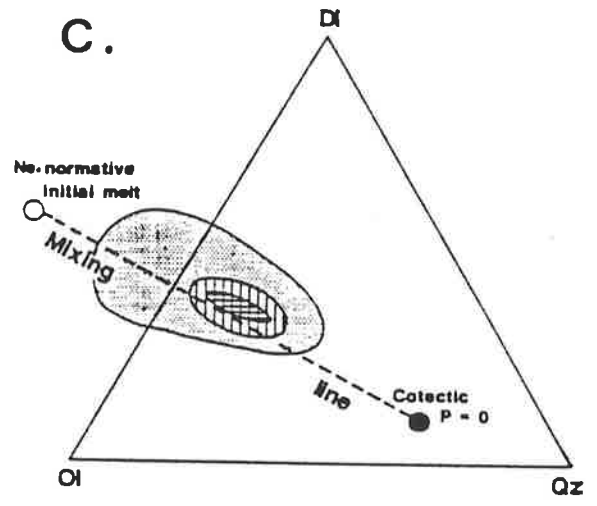
A.



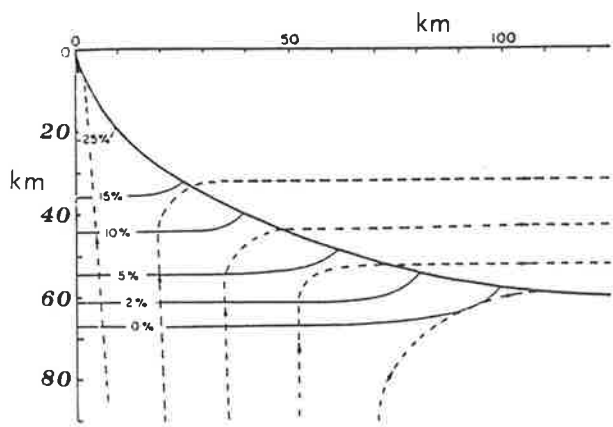
B.



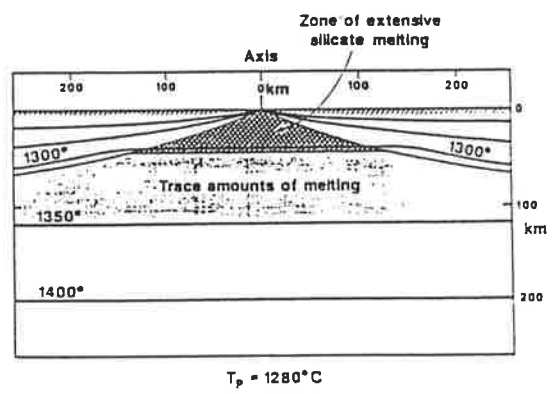
C.



D.



E.



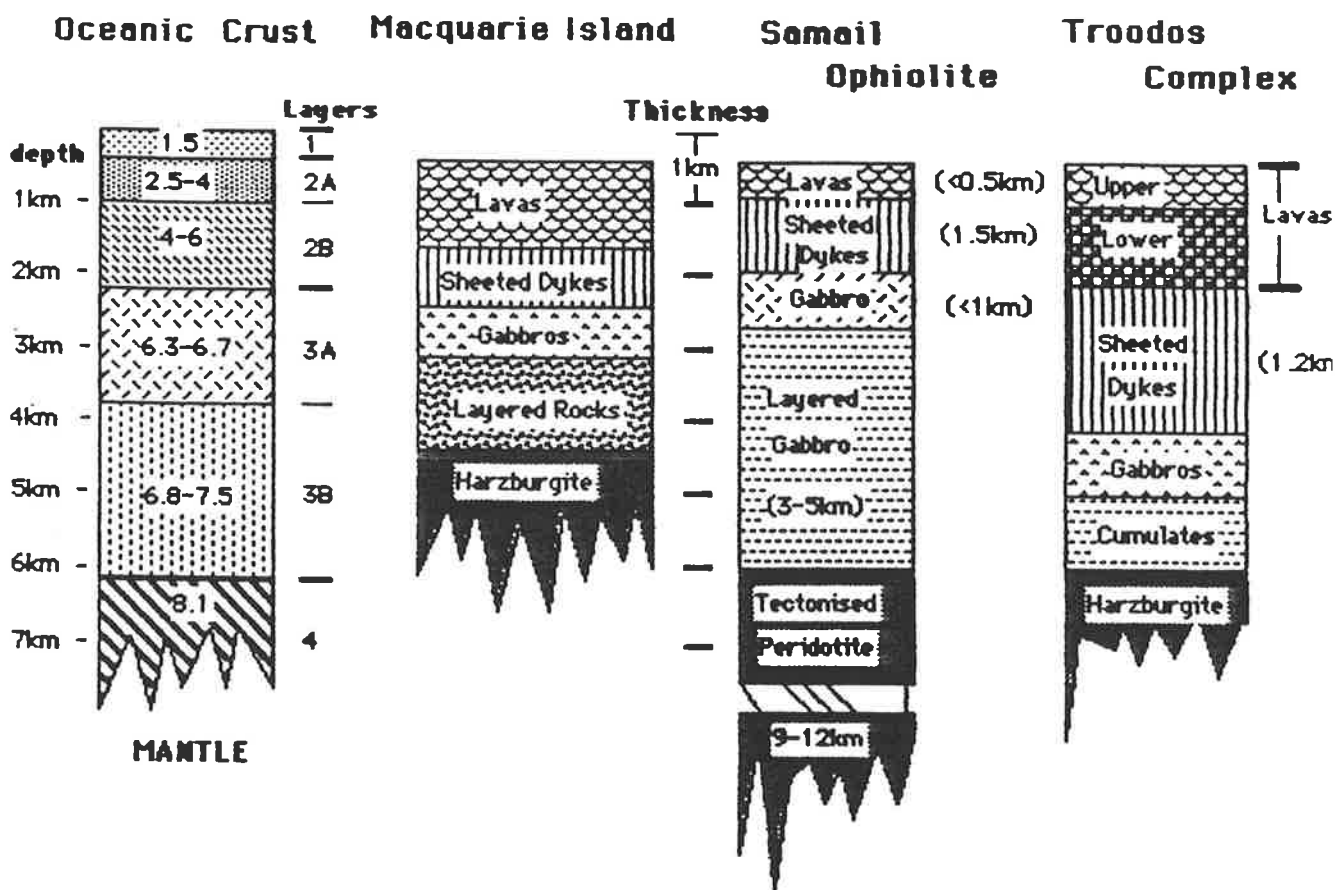


Figure 10.1. Lithostratigraphy of oceanic crust, Macquarie Island and the two better exposed ophiolite complexes, Samail ophiolite and Troodos complex. The stratigraphy of oceanic crust is based on seismic refraction data. The layers of oceanic crust are defined by their different seismic velocities (V_p) - km/sec - shown within each layer. The seismic velocities and the magnetization of the layers as well as sampling by dredge hauls suggest that layer 1 is made of sediments, layer 2 consists of pillow lavas, and layer 3 is chiefly gabbroic rocks. The Mohorovicic discontinuity marks the boundary between layer 3 and layer 4. Layer 4 is believed to consist of residual mantle peridotite. The cross section of Samail ophiolite is from Hopson et al. (1981); that of Troodos complex is from Gass and Smewing (1973). The stratigraphy of Macquarie Island is based on several traverses in the northern part of the island. By comparison, the Macquarie Island plutonic section is thinner than that in Samail ophiolite.

Figure 10.2. Compositional variation of spinel from ophiolitic peridotites and Macquarie Island harzburgites in terms of its $\text{Cr}/(\text{Cr}+\text{Al})$ and $\text{Mg}/(\text{Mg}+\text{Fe}^{2+})$ ratios.

(a). Shaded area defines the spinel field from the Macquarie Island harzburgites. Solid circles represent individual spinel compositions from the Samail ophiolite, tectonite peridotite unit (Pallister and Hopson, 1981). The alpine-type field is indicated by a (Irvine and Findlay, 1972). p and j indicate the spinel fields from the Blue River ultramafics (Pinsent, 1974) and the Josephine peridotite (Dick, 1977). The small field inside field p, is the spinel field from the Othris peridotites (Menzies, 1974). Field c is defined by the spinels in the Chalkidiki ophiolite (Christodoulou and Hirst, 1985). The field of spinels from the Troodos ophiolite complex is marked by t; data from Greenbaum (1977) and Panayiotou (1978).

(b). Compositional variation of spinel in abyssal basalts (solid line) and abyssal peridotites from the world's ridge system. Data source, Dick and Bullen (1984). Selected microprobe analyses of spinels from the Macquarie Island harzburgites are also plotted for comparison.

(c). Spinel composition in the lherzolite massifs from Southern Europe. Individual spinel analyses are plotted. Data from Boudier (1978), Shervais (1979) and Dick and Bullen (1984).

- r - Ronda
- x - Ligurian
- o - Lanzo
- . - Balmuccia
- + - Baldisarro

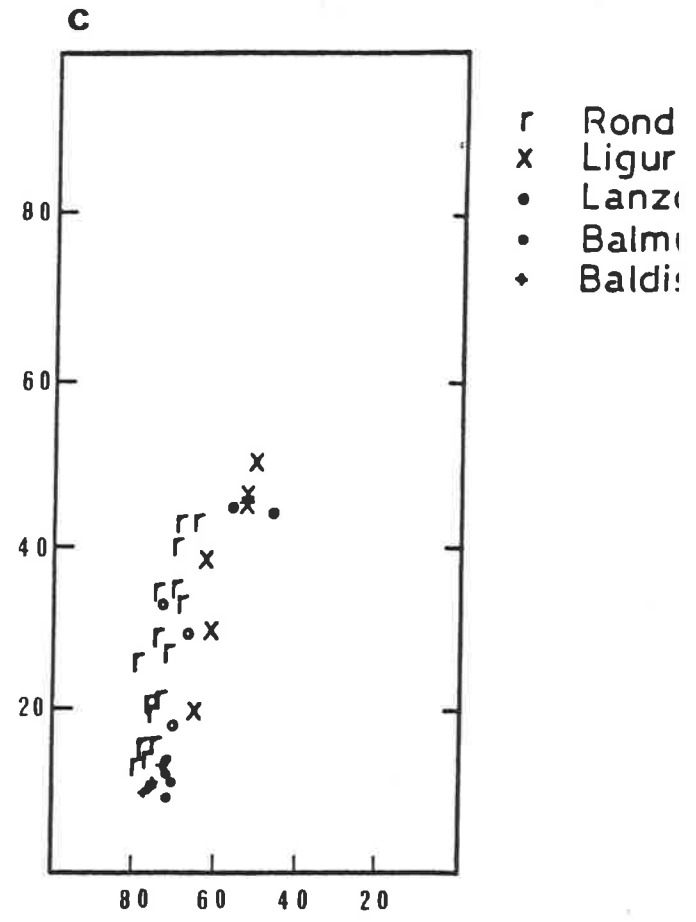
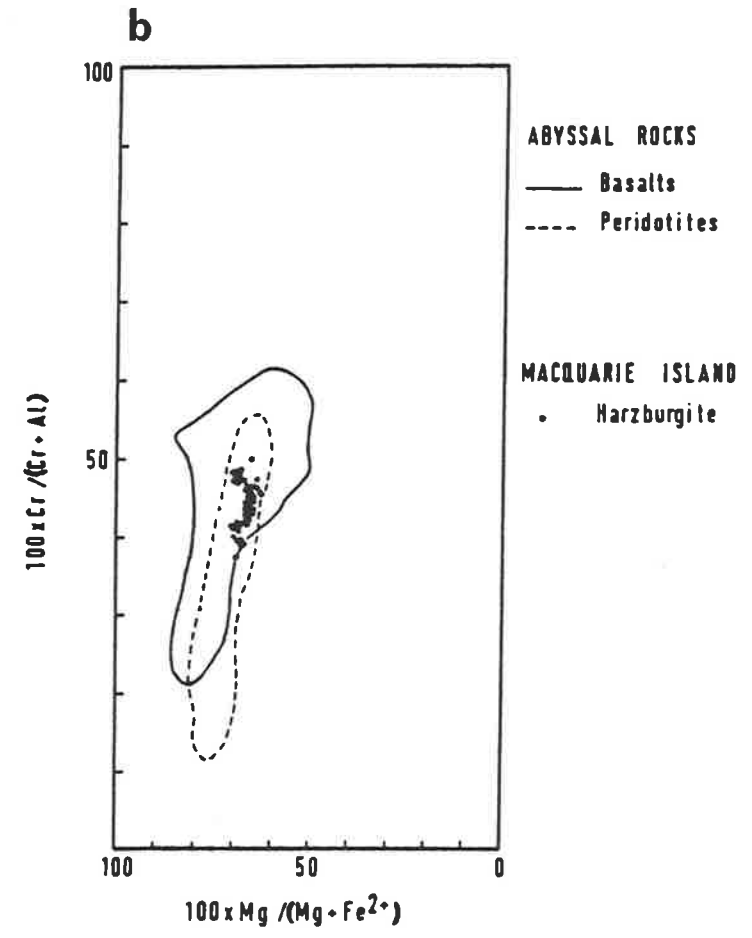
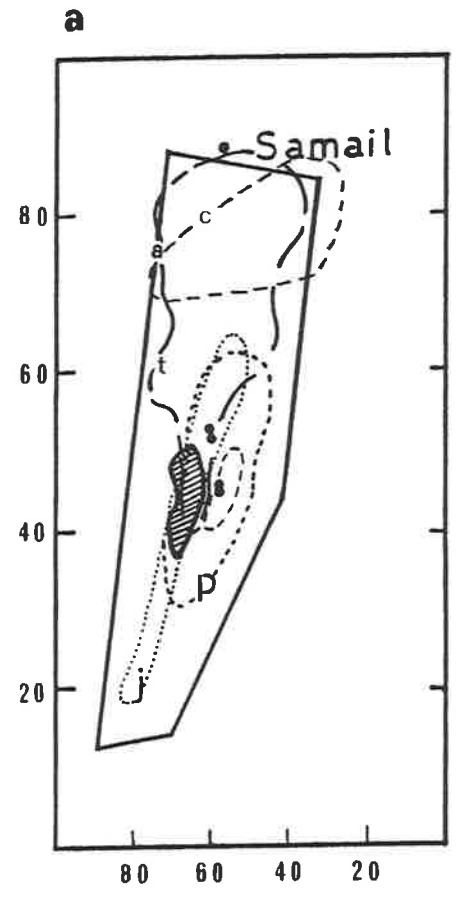
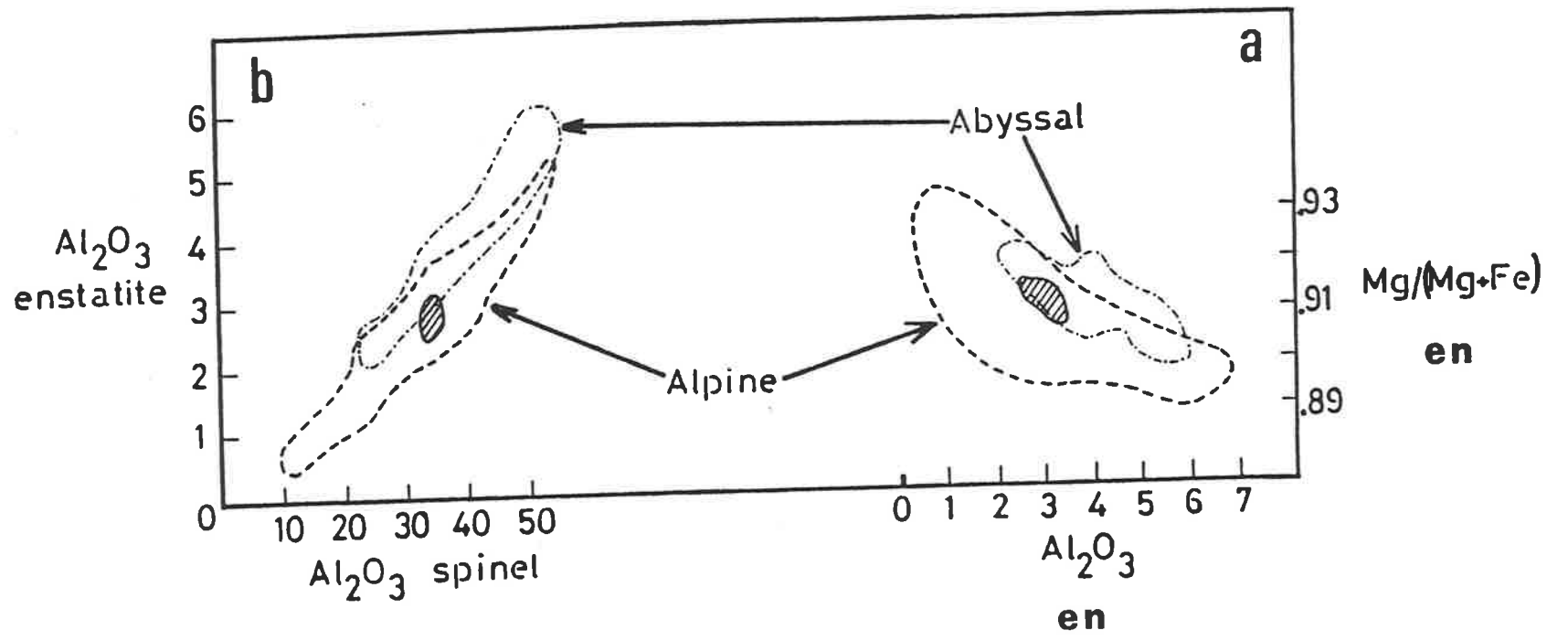


Figure 10.3a.

A plot of Al_2O_3 (in wt%) against the $\text{Mg}/(\text{Mg}+\text{Fe})$ ratio of enstatites from the Macquarie Island harzburgites, the alpine-type and abyssal type peridotites. The Macquarie Island field is shown by the shaded area. The alpine and abyssal fields are from Dick and Fisher (1984).

Figure 10.3b.

A plot of the Al_2O_3 contents (wt%) of coexisting enstatite and spinel from Macquarie Island harzburgites and abyssal and alpine-type peridotites. The shaded area is the Macquarie Island field. A good positive correlation is demonstrated by the data. The alpine-type enstatite and spinel extend to more refractory compositions than their abyssal counterparts. The Macquarie Island field overlaps both, abyssal and alpine-type, fields. Data for the abyssal and alpine fields are taken from Dick and Fisher (1984).



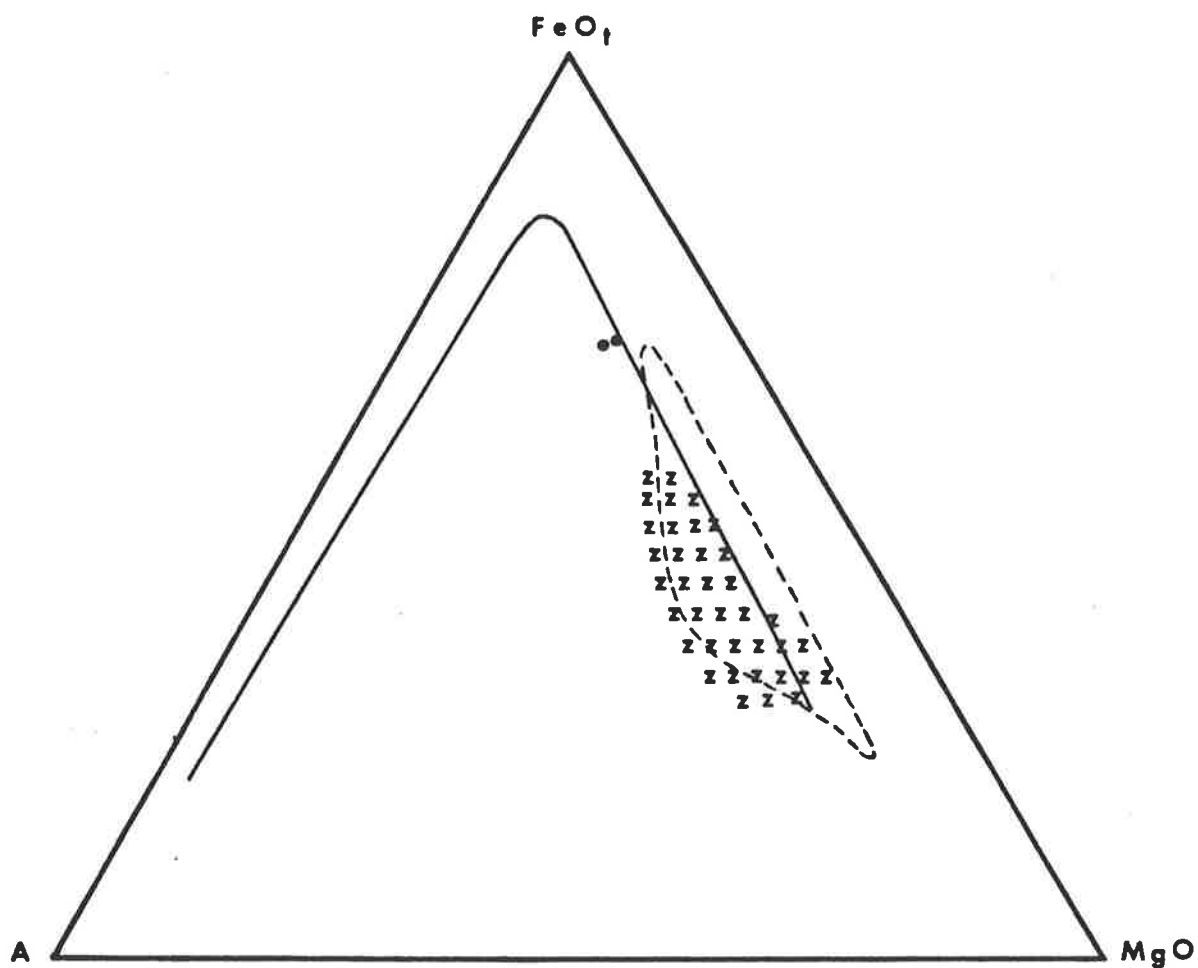


Figure 10.4. $\text{A}=\text{Na}_2\text{O}+\text{K}_2\text{O}$. Solid line is the Skaergaard rock trend and dashed line is the field of gabbros from Mid-Atlantic. The two solid circles are two ilmenite-gabbros from the Equatorial Mid-Atlantic. Data sources: Prinz et al. (1976), Serri (1980). The field of massive gabbros from Macquarie Island is indicated by z.

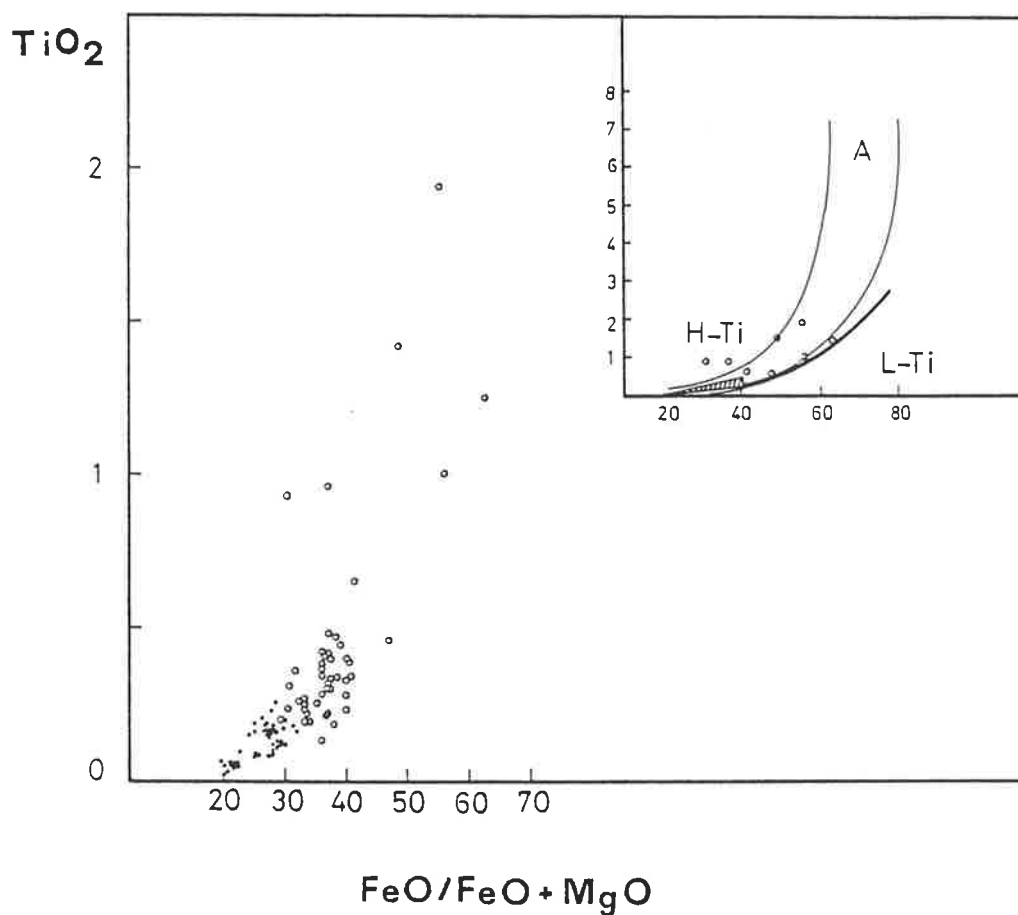


Figure 10.5. A $\text{FeO}/(\text{FeO}+\text{MgO})$ versus TiO_2 discriminating plot for gabbroic rocks from ophiolite complexes (according to Serri, 1981) and Macquarie Island. All oxides in wt%. FeO is the total iron content. Macquarie Island layered rocks and massive gabbros are shown by small filled circles and open circles respectively.

Upper right inset: the fields of high titanium (H-Ti) and low titanium (L-Ti) ophiolites are separated by the thick curve. Field A, defined by the two finer curves, represents the compositional span of gabbroic rocks from the Atlantic and Indian oceans. Open circles are the most evolved Macquarie Island massive gabbros. The hatched area is the field of the layered gabbros and troctolites from Macquarie Island.

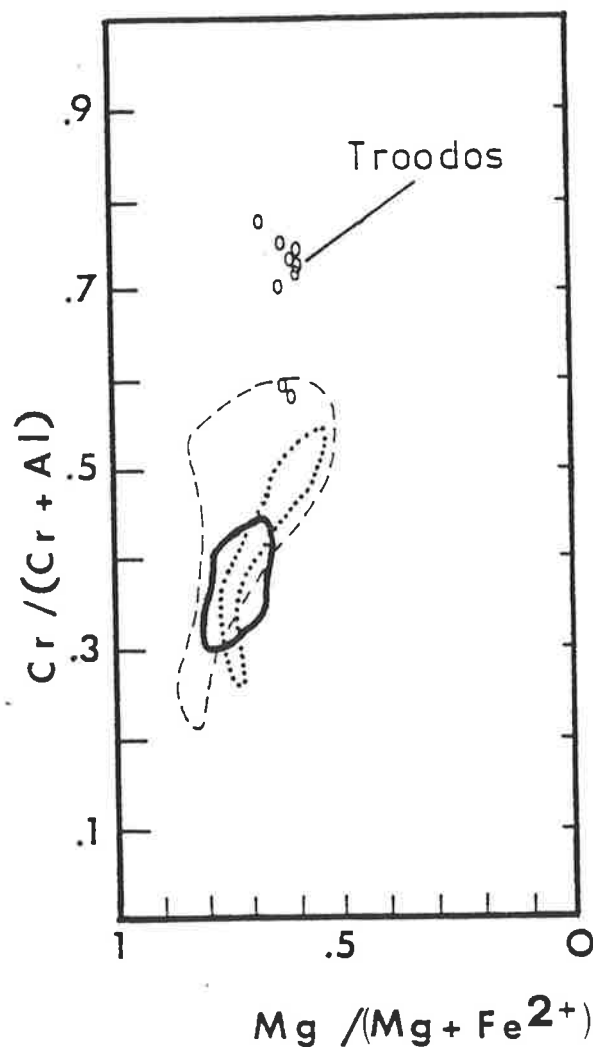


Figure 10.6. Spinel compositions from ophiolitic volcanic rocks are plotted in a $Cr/(Cr+Al) - Mg/(Mg+Fe^{2+})$ diagram. The Macquarie Island field is shown by the thick curve. The compositional fields of spinels from the Mid-Atlantic Ridge and East Pacific Rise are shown by the dashed and dotted curves respectively. Data from Sigurdsson and Schilling (1976), and Dick and Bullen (1984). The compositions of spinel phenocrysts from the Troodos lavas are also plotted in this diagram; sources, Greenbaum (1972) and Cameron (1985).

TABLES

	Olivine	Serpentine	Iddingsite		Talc	
SiO ₂	39.63	40.49	40.81	40.98	62.71	62.54
Al ₂ O ₃	-	-	-	0.13	1.18	1.13
FeO	12.27	2.64	18.45	21.18	2.98	2.62
MnO	0.16	-	0.20	0.19	-	-
MgO	47.25	40.42	22.54	20.35	30.11	30.60
NiO	0.30	0.25	-	0.32	-	-
CaO	-	0.07	0.46	0.65	-	-
Na ₂ O	-	0.35	0.25	0.24	-	0.27
SUM	99.62	84.21	82.83	84.04	96.79	97.14

Table 5.2

Zeolite veins in sample 319

	4,v/1	4,v/2	4,v/3	4,v/4	2,v/1	2,v/2
SiO ₂	37.37	37.69	38.73	39.36	40.17	37.83
Al ₂ O ₃	28.44	28.88	28.18	28.58	29.27	29.52
MgO	0.11	0.15	0.00	0.28	0.26	0.25
CaO	11.39	12.00	11.09	10.72	10.93	11.66
Na ₂ O	4.81	4.44	4.88	3.45	3.03	2.82
SUM	82.12	83.26	82.89	82.38	83.65	82.09

Table 5.3

	Epidote	Clinozoisite	Clinozoisite	
Sample:	726	726	205	205
SiO ₂	37.81	38.28	37.09	37.24
TiO ₂	-	-	-	-
Al ₂ O ₃	24.02	27.79	27.10	26.49
Cr ₂ O ₃	0.15	-	-	0.12
FeO	11.03	7.03	6.76	7.51
MnO	-	-	0.15	-
MgO	0.13	0.25	0.10	0.24
CaO	23.95	24.09	23.06	22.95
SUM	97.09	97.43	94.28	94.54

Lizardite after Olivine

SiO ₂	41.61	41.75	41.66	42.02	41.51
Al ₂ O ₃	0.27	0.38	0.32	0.16	0.17
FeO	2.25	1.93	1.81	1.60	1.48
MgO	40.52	41.16	41.13	41.26	41.59
NiO	-	0.26	0.20	0.16	0.25
Na ₂ O	0.52	1.00	0.57	0.46	0.71
K ₂ O	-	0.06	-	0.07	0.18
TOTAL	85.17	86.54	85.69	85.72	85.90

Number of ions recalculated on 9 oxygens

Si	2.5566	2.2559	2.5432	2.5592	2.5320
Al	0.0196	0.0273	0.0228	0.0113	0.0121
Fe	0.1154	0.0977	0.0922	0.0815	0.0757
Mg	3.7110	3.7112	3.7431	3.7454	3.7810
Ni	-	0.0128	0.0100	0.0077	0.0124
Na	0.0616	0.1176	0.0680	0.0541	0.0834
K	-	0.0045	-	0.0057	0.0141

Table 5.5

Bastites after Orthopyroxene

SiO ₂	36.85	36.23	38.26	36.76	36.29
Al ₂ O ₃	2.39	2.40	2.60	2.63	2.63
Cr ₂ O ₃	0.96	0.96	1.00	1.03	1.06
FeO	3.68	3.82	3.67	3.74	3.92
MgO	37.08	37.43	36.92	37.29	37.58
MnO	0.11	-	0.13	0.15	0.16
Na ₂ O	0.57	0.47	0.19	0.17	0.29
Cl	0.51	0.62	-	0.54	0.60
TOTAL	82.14	81.92	82.76	82.39	82.54

Cations on 9 oxygens

Si	2.4024	2.3753	2.4476	2.3890	2.3606
Al	0.1835	0.1851	0.1957	0.2018	0.2020
Cr	0.0495	0.0498	0.0504	0.0529	0.0545
Fe	0.2005	0.2094	0.1961	0.2035	0.2131
Mg	3.6034	3.6578	3.5205	3.6126	3.6440
Mn	0.0060	-	0.0070	0.0081	0.0089
Na	0.0718	0.0593	0.0242	0.0216	0.0367
Cl	0.0568	0.0693	-	0.0599	0.0656

LAVAS

	<u>Mg/(Mg+Fe²⁺)</u>	<u>Zr/Nb</u>	<u>Zr/Y</u>	<u>Y/Nb</u>	<u>Ti/Zr</u>	<u>Ti/Nb * 10²</u>	<u>Ti/Y</u>
108C	0.608	9.8	1.95	5.0			
108E	0.60	10.3	2.0	5.1			
119	0.674	5.5	2.4	2.3	112	6.2	269
139	0.70	5.8	2.9	2.0	100.6	5.8	292
147	0.599	10.2	2.3	4.5	99.6	10.2	226
151	0.706	4.3	4.0	1.08			
199	0.593	9.5	2.5	3.73	94.5	8.9	240
202	0.671	11.6	2.4	4.8	104.3	12.1	252
206	0.666	5.6	3.0	1.86			
210	0.586	12.7	2.4	5.28			
212	0.681	3.2	2.1	15.0	118.7	37.9	253
214	0.608	7.4	2.55	2.9			
38335	0.607	9.9	3.0	3.25	110.8	10.9	336
56I	0.717	4.4	2.65	1.64	96.8	4.2	256
38265	0.685	2.5	6.2	0.4	69.6	1.7	432
38314	0.712	2.1	2.7	0.76	97.4	2.03	267
38315	0.699	-	2.6	-	103.5	-	271
38310	0.696	2.5	3.7	0.69	79.0	2.0	291
38188	0.742	2.8	3.1	0.9	92.1	2.57	286
38291	0.735	-	-	-	-	-	427
38292	0.704	4.2	3.13	1.33	88.7	3.7	277
38297	0.723	3.9	3.28	1.19	89.2	3.5	292
38288	0.723	2.6	3.3	0.78	86.8	2.25	287
38280	0.654	2.2	6.3	0.35	51.8	1.16	325
38331	0.689	2.8	4.1	0.67	63.9	1.76	261
38325	0.64	4.2	2.6	1.58	88.1	3.6	232
38284	0.704	2.95	3.66	0.8	84.7	2.5	310
38301	0.696	3.5	3.5	1.0	87.2	3.06	306
38303	0.649	4.8	3.04	1.59	91.4	4.4	277
38306	0.707	3.2	4.6	0.7	83.7	2.7	386
38307	0.626	2.4	4.6	0.53	70.4	1.7	323
38297	0.727	3.9	3.3	1.2	89.2	3.5	292
60	0.729	5.3	3.05	1.75	95.4	5.1	290
233	0.68	2.9	4.0	0.72	73.8	2.2	297
234	0.725	4.3	2.4	1.75	95.5	4.1	235
G-7	0.689	2.1	2.74	0.76	69.3	1.4	190
157	0.709	3.0	3.7	0.81	97.1	2.9	358

Table 7.1 (cont.)

DOLERITE DYKES

	<u>Zr/Nb</u>	<u>Zr/Y</u>	<u>Y/Nb</u>	<u>Ti/Zr</u>	<u>Ti/Nb*10²</u>	<u>Ti/Y</u>
303 (*)	6.9	2.9	2.35	85.1	5.9	250
325	5.9	3.2	1.8	80.0	4.7	258
372D	6.1	3.1	1.9	81.5	5.0	257
379C	5.7	3.3	1.7	79.6	4.55	264
213D	10.0	2.5	4.4	101.5	11.2	252
221D	3.1	5.5	0.56	58.3	1.8	322
111A (@)	11.8	2.4	4.8	102.0	12.1	250
115D	9.4	2.7	3.5	93.5	8.8	251
127	8.45	2.9	2.9	92.6	7.8	269
233 (D)	2.7	4.0	0.67	75.2	2.0	298
124	12.7	2.8	4.6			
139	11.4	2.2	5.3			
38133	5.4	3.1	1.7	85.5	4.6	267
38137	6.4	2.6	2.44	91.1	5.8	240
38223	2.3	6.6	0.35	70.9	1.6	469
38273	3.9	4.6	0.84	73.5	2.8	337
38320	16.5	2.9	5.75	91.1	15.0	261
38425	5.7	3.8	1.5	77.3	4.4	295
38449	6.5	3.3	2.1	87.3	6.0	288
38334	15.4	3.85	4.0			

(*) : Dolerite dykes in the layered rocks and massive gabbros

(@) : Dolerite dykes in harzburgite

(D) : Dolerites from the dyke swarms

	<u>Ti/Zr</u>	<u>Zr/Nb</u>	<u>Zr/Y</u>	<u>Y/Nb</u>	<u>Reference</u>
Typical MORBs		37	3.8	9.7	Erlank & Kable (1976)
N-type MORBs	110	18-55	2.5		Sun et al (1979)
MAR 45°N		6.4			Erlank & Kable (1976)
MAR 46°S-32°S					
Depleted		32	2.7	11.5	Humphris et al (1985)
Enriched		15	3.1	5.1	#
AAR (54°S-59°S)					
N-type (average)		27	3.4	9.1	leRoex et al (1985)
(range)		17-78	2.2-4.2	4.6-23	#
T-type		9-15	3-5	2-4	#
P-type		6.3	7.1	0.9	#
FAMOUS area					
olivine-basalts	106	8.4	2.6	3.3	leRoex et al (1981)
plag-pyx basalts	106	6	2.6	2.3	#
picritic basalts	113	10.5	1.8	5.67	#
SWIR (53°S-55°S)					
N-type		17-64	2-3.6	>8	leRoex et al (1983)
T-type		8-12	3.6-6.2	1.3-3	#
P-type		6-7	6-8	0.9-1.2	#
Oceanic islands		6.6			Erlank & Kable (1976)
Tristan da Cunha		0.29	7.2	0.4	Humphris & Thompson (1983)
Bouvet Island		6.4	6.8	0.9	leRoex & Erlank (1982)
Chondrites	110	16			Sun et al (1979)
Macquarie Island (means from table 7.1)					
Basalts	89.5	5	3.2	2.25	
Dolerites	84	7.8	3.4	2.66	

MAR : Mid-Atlantic Ridge

AAR : American Antarctic Ridge 54°S

SWIR : Southwest Indian Ridge

TABLE 7.3Least Squares Calculations

<u>Parent</u>	<u>Daughter</u>	<u>% Liquid</u>	<u>Cumulate %</u>			<u>Squared Residuals</u>
			<u>Olivine</u>	<u>Plag.</u>	<u>Cpx</u>	
38188	38434	72.5	26.3	48.7	25	0.119
38188	38303	79.3	54.8	17	28.2	0.69
38188	38307	65.5	33.3	48.4	18.3	0.356
38288	38307	65.5	21.5	65.4	13.1	0.13
38284	38434	81	15.8	61.6	22.6	0.10
47979	38390	68.6	18.1	52.2	29.6	0.18
47979	38389	94	21.6	30.8	47.6	0.58
213D	153D	97.3	100			0.23
213D	379D	81.3	19.6	45	35.4	0.166
213D	391D	62	12.7	46	41.3	0.64
38288	199	67.1	26.3	68.8	4.9	0.753
38288	43B	68.6	26.7	67.9	5.4	0.13
38188	199	68.8	39.8	51.5	8.7	0.71
38188	214	70.1	41.1	58.1	0.8	0.267
38288	147	58.5	19.6	68.4	12	0.286
47979	38325	76.8	20.3	55.3	24.4	0.986
38188	38325	77.9	47.6	50.3	2.1	0.045

Least squares mixing calculations for Macquarie Island basalts and dolerites (D). The mineral compositions used in the calculations are actual compositions from the cumulate troctolites - olivine-gabbros. Calculations carried out using the computer program of Morris (1984).

Table s.1a

 Estimated temperatures in degrees Centigrade for troctolites

Sample	Jackson	Fujii	Fabries	Roeder	Mg# sp	Mg# olivine
313	1421	1006	930	966	58.3	89.4
313	1368	937	898	915	57.4	89.4
313	1198	818	838	818	51.5	89.2
315	977	615	721	645	43.4	89.2
315	970	610	717	640	43.4	89.4
315	949	594	707	626	43.4	89.7
321	1073	759	805	763	45.7	88.6
321	1015	711	777	722	44.5	89.1
324A	1549	1179	997	1125	68.3	89.6
324A	1428	1041	939	1027	66.3	#
324A	1448	1033	938	1010	64.8	#
324A	1407	989	922	954	59.7	#
324A	1338	933	896	911	58.1	#
324A	1234	844	853	830	52.8	#
324A	950	636	732	666	44.4	#

Table s.1b

 Estimated temperatures (degrees C) for harzburgites

Sample	Jackson	Fujii	Fabries	Roeder	Mg# Spinel
179	1300	852	849	889	68.5
179	1290	830	840	866	67.3
179	1278	823	836	855	66.3
179	1250	815	832	835	64.9
179	1052	678	754	735	59.0
179	1030	660	743	720	58.4
179	956	602	707	669	55.0
110	1354	904	878	913	67.0
128	1255	801	824	838	65.8
182	1348	893	870	925	70.2

Mg#: atomic $100 \cdot \text{Mg} / (\text{Mg} + \text{Fe}^{2+})$

$$T(^{\circ}\text{K}) = \frac{5580(Y_{\text{Cr}})^{\text{sp}} + 1018(Y_{\text{Al}})^{\text{sp}} - 1720(Y_{\text{Fe}^{3+}})^{\text{sp}} + 2400}{0.90(Y_{\text{Cr}})^{\text{sp}} + 2.56(Y_{\text{Al}})^{\text{sp}} - 3.08(Y_{\text{Fe}^{3+}})^{\text{sp}} - 1.47 + 1.987 \ln K_{\text{D}}} \quad (8.3)$$

$$T(^{\circ}\text{K}) = \frac{775 + 2010(Y_{\text{Cr}})^{\text{sp}}}{\ln K_{\text{D}}^* - 4(Y_{\text{Fe}^{3+}})^{\text{sp}} - 0.006 - 0.003(Y_{\text{Cr}})^{\text{sp}}} \quad (8.5)$$

$$T(^{\circ}\text{K}) = \frac{4250(Y_{\text{Cr}})^{\text{sp}} + 1343}{\ln K_{\text{D}}^* + 1.825(Y_{\text{Cr}})^{\text{sp}} + 0.571} \quad (8.6)$$

$$T(^{\circ}\text{K}) = \frac{3840(Y_{\text{Cr}})^{\text{sp}} + 1018(Y_{\text{Al}})^{\text{sp}} - 1720(Y_{\text{Fe}^{3+}})^{\text{sp}} + 2400}{2.33(Y_{\text{Cr}})^{\text{sp}} + 2.56(Y_{\text{Al}})^{\text{sp}} - 3.08(Y_{\text{Fe}^{3+}})^{\text{sp}} - 1.47 + 1.987 \ln K_{\text{D}}^*} \quad (8.7)$$

$$T(^{\circ}\text{K}) = \{3621 + \{(1 - [\text{Fe}]_{\text{ol}})^2 - (1 - [\text{Mg}]_{\text{ol}})^2\} \cdot (457 + 1.83p) + (\Delta G_1[\text{Fe}^{3+}]_{\text{sp}} - \Delta G_2[\text{Al}]_{\text{sp}}) \cdot \{([\text{Mg}]_{\text{sp}} + [\text{Fe}^{2+}]_{\text{sp}})/R\} + 1636\{([\text{Fe}^{2+}]_{\text{sp}})^2 - ([\text{Mg}]_{\text{sp}})^2\}\} \cdot \left(0.685 + \ln \frac{[\text{Mg}]_{\text{ol}}/[\text{Fe}]_{\text{ol}}}{[\text{Mg}]_{\text{sp}}/[\text{Fe}^{2+}]_{\text{sp}}}\right) - 1 \quad (8.8)$$

$$T(^{\circ}\text{K}) = \{2585.5 + \{(1 - [\text{Fe}]_{\text{ol}})^2 - (1 - [\text{Mg}]_{\text{ol}})^2\} \cdot (457 + 1.83p) + (\Delta G_2[\text{Cr}]_{\text{sp}} - \Delta G_3[\text{Fe}^{3+}]_{\text{sp}}) \cdot \{([\text{Mg}]_{\text{sp}} + [\text{Fe}^{2+}]_{\text{sp}})/R\} + 1636\{([\text{Fe}^{2+}]_{\text{sp}})^2 - ([\text{Mg}]_{\text{sp}})^2\}\} \cdot \left(0.745 + \ln \frac{[\text{Mg}]_{\text{ol}}/[\text{Fe}]_{\text{ol}}}{[\text{Mg}]_{\text{sp}}/[\text{Fe}^{2+}]_{\text{sp}}}\right) - 1 \quad (8.9)$$

Sample
no./

	Mg/(Mg+ΣFe)	Mg/(Mg+Fe ²⁺)	Ni (ppm)	Cr (ppm)
<u>LAVAS</u>				
38188@	0.71	0.742	199	514
38291@	0.70	0.735	145	343
236*	0.70	0.732	164	663
234*	0.69	0.725	158	652
56A*	0.69	0.722	87	311
38306@	0.67	0.706	231	552
38284@	0.67	0.704	178	189
 <u>DYKES</u>				
233*	0.695	0.729	107	330
220*	0.68	0.716	207	523
38237@	0.68	0.711	89	299
38320@	0.65	0.692	133	346
38334@	0.65	0.691	108	392
 <u>BASALTIC GLASS</u>				
47979*	0.667	0.70		
155*	0.655	0.688		

@: sample numbers from the Macquarie Island rock collection of the
Geology Department, University of Tasmania

*: Griffin's (1982) field sample numbers

TABLE 9.1

Compositions of Macquarie Island harzburgites and basalts used in the following calculations

Harzburgites			Basalts				
Sample:	107	163	38188	38284	47979	234	OL(Added olivine)
SiO ₂	44.81	43.79	48.42	48.95	49.24	50.23	39.65
Al ₂ O ₃	1.00	1.57	16.40	17.07	17.20	17.32	-
FeO*	8.87	10.57	8.29	8.41	8.24	7.65	9.92
MnO	0.11	0.19	0.15	0.14	-	0.13	0.15
MgO	44.77	43.01	11.17	9.39	9.27	9.45	49.53
CaO	0.13	0.13	10.71	10.28	12.50	10.46	NiO 0.30
Na ₂ O	0.02	0.04	2.89	2.73	2.50	2.79	
TiO ₂	0.00	0.00	1.29	1.71	1.06	1.10	
Ni	2087	2061	199	178	-	158	
Ti	32	619	7733	10250	-	6594	
Normative minerals:			Ne:				
			0.4%	Ol:			
				15%	10%	12%	
				Hy:			
				4.5%	7%	8.5%	

Ni and Ti contents in ppm.
FeO* : total iron.

TABLE 9.1 (cont.)

Recalculated basalt compositions after olivine OL addition

Sample:	38188	38284	38284	47979	47979	234	234
Percent added							
olivine OL:	2%	2%	5%	2%	5%	2%	5%
SiO ₂	48.55	49.39	49.11	49.05	48.79	50.44	50.13
Al ₂ O ₃	16.18	16.95	16.46	16.86	16.38	17.12	16.63
FeO*	8.37	8.55	8.58	8.27	8.32	7.76	7.82
MnO	0.15	0.14	0.14	-	-	0.13	0.13
MgO	12.00	10.30	11.44	10.06	11.91	10.32	11.45
CaO	10.56	10.20	9.91	12.25	11.91	10.34	10.04
Na ₂ O	2.85	2.71	2.63	2.45	2.38	2.76	2.68
TiO ₂	1.27	1.70	1.65	1.04	1.01	1.09	1.06
Ni	246	225	296	-	-	205	276

(Ni in ppm)

TABLE 9.1 (cont.)

Calculated source compositions from Macquarie Island basalts and harzburgites

Basalt:	38188	38188	38188	38188	38284	38284	38284	38284	47979	47979	47979	47979	234	234
Harzburgite:	163	163	107	107	163	163	107	107	163	163	107	107	107	163
Percent OL added:	0%	2%	0%	2%	2%	5%	2%	5%	2%	5%	2%	5%	5%	5%
Mixing proportions:	85% harzburgite + 15% basalt													
SiO ₂	44.53	44.50	45.40	45.37	44.63	44.59	45.50	45.45	44.60	44.54	45.45	45.40	45.61	44.74
Al ₂ O ₃	3.81	3.76	3.32	3.28	3.87	3.80	3.39	3.32	3.86	3.79	3.38	3.30	3.34	3.83
FeO*	10.23	10.24	8.79	8.80	10.27	10.27	8.82	8.83	10.22	10.23	8.78	8.79	8.71	10.16
MnO	0.18	0.18	0.11	0.11	0.18	0.18	0.11	0.11	0.16	0.16	0.09	0.09	0.11	0.18
MgO	38.24	38.35	39.74	39.85	38.09	38.26	39.60	39.77	38.07	38.23	39.56	39.73	39.77	38.27
CaO	1.73	1.69	1.72	1.69	1.64	1.60	1.64	1.60	1.95	1.90	1.95	1.90	1.61	1.62
Na ₂ O	0.47	0.46	0.45	0.44	0.44	0.43	0.42	0.41	0.40	0.39	0.38	0.37	0.42	0.43
TiO ₂	0.23	0.23	0.19	0.19	0.34	0.34	0.26	0.26	0.23	0.23	0.16	0.16	0.16	0.23
NiO	0.22	0.23	0.23	0.23	0.23	0.23	0.23	0.23	0.22	0.22	0.23	0.23	0.23	0.23

TABLE 9.2

Peridotite compositions

	(1)	(2)	(3)	(4)	(5)	(6)	(7)	(8)	(9)	(10)
SiO ₂	45.20	48.02	43.46	44.15	47.90	47.50	45.10	44.60	43.70	44.95
Al ₂ O ₃	3.54	4.88	3.66	1.96	5.91	5.35	9.93	6.59	2.75	3.22
FeO*	8.52	9.90	7.60	8.28	8.83	7.52	7.25	8.05	10.19	7.67
MnO	0.14	0.14	0.12	0.12	0.13	0.18	0.15	0.16	0.14	0.14
MgO	37.50	32.35	42.42	42.25	28.80	32.80	27.88	33.28	37.22	40.03
CaO	3.08	2.97	2.00	2.08	5.14	4.97	7.28	5.46	3.26	2.99
Na ₂ O	0.57	0.66	0.02	0.18	0.96	0.30	0.63	0.53	0.33	0.18
TiO ₂	0.71	0.22	0.07	0.07	1.18	0.13	0.24	0.21	0.25	0.08
NiO	0.20		0.27		0.13	0.43	0.30	0.28	-	0.26

(FeO* = total iron)

(1): Pyrolite, Ringwood (1975)

(2): Spinel-lherzolite HK66, Takahashi & Kushiro (1983)

(3): Spinel-lherzolite 77PAII-1, Sen (1982)

(4): Average spinel-lherzolite of Maaloe & Aoki (1977)

(5): Pyrolite minus 40%olivine, Jaques & Green (1980)

(6): Tinaquillo lherzolite minus 40%olivine, Jaques & Green (1980)

(7) & (8): Peridotite-basalt mixtures SM2 and SM4 of Fujii & Scarfe (1985)

(9): Garnet-lherzolite PHN 1611, Mysen & Kushiro (1977)

(10): Tinaquillo lherzolite, Jaques & Green (1980)

Table 9.3

Selected compositions of experimentally produced basaltic melts
equilibrated with peridotites at around 10 kbar pressure

Sample number:	S210	S275	SM2/1	SM2/3	SM4/6	TK31
SiO ₂	50.61	51.65	48.80	48.90	48.90	51.74
Al ₂ O ₃	17.73	15.06	17.50	16.40	17.40	15.23
FeO*	7.14	7.50	7.77	6.79	7.25	9.41
MnO	-	-	0.26	0.16	0.23	0.19
MgO	8.52	12.03	9.82	12.00	10.30	9.81
CaO	13.26	13.29	10.80	12.40	11.20	10.38
Na ₂ O	0.48	0.44	3.11	1.93	2.82	2.34
K ₂ O	0.10	0.05	0.16	0.08	0.16	0.08
TiO ₂	0.36	0.34	0.88	0.56	0.86	1.07
Cr ₂ O ₃	-	-	-	-	-	0.08
Mg/(Mg+ΣFe)	0.68	0.74	0.69	0.76	0.72	0.65

FeO* : total iron content

S210	1210 °C, 9 kbar (Sen, 1982)
S275	1275 °C, 9 kbar (Sen, 1982)
SM2/1	1250 °C, 10 kbar (Fujii and Scarfe, 1985)
SM2/3	1290 °C, 10 kbar (Fujii and Scarfe, 1985)
	SM2: mixture of 15% basalt and 85% peridotite PPM-1
SM4/6	1250 °C, 10 kbar (Fujii and Scarfe, 1985)
	SM4: mixture of 15% basalt and 85% peridotite PPM-2
TK31	1250 °C, 8 kbar (Takahashi and Kushiro, 1983)
	Sandwich of basalt L45 and peridotite HK66

	PPM-1	PPM-2
<i>SiO₂</i>	44.20	43.70
<i>TiO₂</i>	0.13	0.09
<i>Al₂O₃</i>	8.94	5.01
<i>FeO*</i>	7.11	8.05
<i>MnO</i>	0.14	0.15
<i>MgO</i>	30.90	37.30
<i>CaO</i>	6.41	4.27
<i>Na₂O</i>	0.37	0.25
<i>NiO</i>	0.26	0.33
<i>Cr₂O₃</i>	1.36	0.75

Table 9.4a

Averaged mineral analyses from Macquarie Island harzburgites

	Olivine	Orthopyroxene	Clinopyroxene	Spinel
SiO ₂	40.20	55.31	54.00	-
Al ₂ O ₃	-	2.50	2.25	31.56
FeO*	8.80	5.64	2.33	15.90
MnO	0.11	0.13	0.10	0.20
MgO	50.25	33.80	17.00	15.00
CaO	-	0.85	23.45	-
TiO ₂	-	-	0.03	0.03
NiO	0.40	0.11	-	0.14
Cr ₂ O ₃	-	0.50	0.90	36.30

Calculated harzburgite composition from the mineral compositions according to the listed mode and average whole rock composition from 9 harzburgite samples

	"Estimated" Harzburgite	Average Harzburgite	Modal mineral percentages
SiO ₂	44.36	44.62	
Al ₂ O ₃	0.92	1.14	
FeO*	7.80	9.09	
MnO	0.12	0.13	
MgO	44.63	44.04	OL: 70%
CaO	1.02	0.27	OPX: 26%
Ti (ppm)	<10	116	CPX: 3.4%
Ni (ppm)	2430	2107	SPIN: 0.6%
Cr (ppm)	2590	2548	

FeO*: Total iron as FeO

Table 9.4b

Calculated source composition from the calculated harzburgite composition (table 9.4a) and basalts 38188, 38284 and 234 (table 9.1). The percentage of added olivine (OL, table 9.1) to each basalt is shown in parentheses. The source composition was estimated for 85 parts harzburgite and 15 parts basalt.

Basalt :	38188 (+2% OL)	38284 (+5% OL)	234 (+5% OL)
SiO ₂	42.24	42.26	42.27
TiO ₂ (**)	0.24	0.30	0.20
Al ₂ O ₃	3.60	3.64	3.68
FeO*	7.43	7.43	7.43
MnO	0.11	0.11	0.11
MgO	42.50	42.52	42.53
CaO	2.74	2.63	2.66
Na ₂ O	0.48	0.44	0.45
NiO	0.29	0.29	0.29
Cr ₂ O ₃	0.37	0.37	0.38

FeO* : total iron

(**) The Ti value used in the is the average harzburgite content of 116ppm from table 9.4a

Table 9.5

Crystal fractionation modelling for Zr and Nb (Rayleigh fractionation)

Initial composition is the most primitive Macquarie Island basalts

Calculated values of Zr and Nb in residual liquid
f= fraction of initial liquid remaining

Initial composition:	Estimated Zr content in ppm				Estimated Nb content in ppm				Crystal Extract
	f=0.6	f=0.7	f=0.8	f=0.9	f=0.6	f=0.7	f=0.8	f=0.9	
38288 Zr=96 ppm Nb=37 ppm	157	135	119	106	61	53	46	41	Gabbro 64%plag+22%ol+14%cpx
38284 Zr=121 ppm Nb=41 ppm		169	149	141	58	51	45	42	Gabbro 62%plag+15%ol+22%cpx
234 Zr=69 ppm Nb=16ppm	112	97	85	76	26	23	20	18	Gabbro 62%plag+15%ol+22%cpx
38188 Zr=84 ppm Nb=30 ppm	136	118	104	93	82	43	37	33	Gabbro 62%plag+15%ol+22%cpx

Table 9.6

Geochemical characteristics of primitive Macquarie Island basalts and dolerites

Sample No.:	234	38314	38265	38288	38306	38334*	38188	38297	220*
Zr (ppm)	69	96	149	96	106	77	84	82	46
Nb (ppm)	16	46	60	37	33	5	30	21	8
Ni (ppm)	158	108	124	131	231	108	199	138	207
Mg/(Mg+ Σ Fe)	0.69	0.68	0.65	0.69	0.67	0.655	0.71	0.69	0.716
Zr/Nb	4.3	2.1	2.5	2.6	3.2	15.4	2.8	3.9	5.8
<i>Normative Hy</i>	8.5	1.5	-	-	-	11	-	-	0.4
<i>Normative Ne</i>	-	-	0.9	0.3	1.5	-	0.42	5.4	-

*: Dolerite

Table 9.7

Comparative major element concentrations of the primitive Macquarie Island basalts and the 10 kbar melts of Fujii and Scarfe (1985)

Sample:	MI 234	F&S 1	MI 38334	F&S 6	MI 38288	MI 38291
SiO ₂	50.23	48.80	49.86	48.90	48.86	49.26
Al ₂ O ₃	17.32	17.50	16.42	17.40	18.25	17.25
FeO*	7.65	7.77	8.99	7.25	7.20	7.14
MnO	0.13	0.26	0.17	0.23	0.13	0.16
MgO	9.45	9.82	9.52	10.30	9.00	9.38
CaO	10.46	10.80	10.32	11.20	11.05	10.08
Na ₂ O	2.79	3.11	2.21	2.82	2.79	2.30
TiO ₂	1.10	0.88	1.12	0.86	1.39	1.64

MI: Macquarie Island

F&S: Fujii and Scarfe (1985)

Samples 1 and 6 are compositions 1 and 6 respectively from table 6 of Fujii and Scarfe (1985)

Table 9.8

Comparative major element composition of natural peridotites and calculated Macquarie Island source peridotite

	1	2	3	4	5
SiO ₂	44.64	44.40	43.79	44.65	44.5-45.6
Al ₂ O ₃	2.26	2.38	2.60	3.85	3.3-3.8
FeO*	8.27	8.31	7.98	8.63	8.7-10.3
MgO	42.36	42.06	41.25	38.00	38.1-39.9
CaO	1.85	1.34	2.41	3.18	1.6-2.0
Na ₂ O	0.05	0.27	0.17	0.34	0.37-0.47
TiO ₂	0.03	0.13	0.08	0.15	0.16-0.23
Cr ₂ O ₃	0.49	0.44	0.43	-	0.37
NiO	-	0.31	0.26	-	0.23

1: Less refractory abyssal peridotite, Michael and Bonatti (1985)

2: Average oceanic spinel-lherzolite, Maaloe and Aoki (1977)

3: Mean composition of Tinaquillo lherzolite, Seyler and Mattson (1989)

4: Mean composition of Zabargad spinel-lherzolite, Bonatti et al. (1986)

5: Range of estimated source peridotite composition from the combined Macquarie Island basalt-harzburgite mixes

Table 9.9a

DATA: 38284=38434+Ol+Plag+Cpx

	OBSERVED	ESTIMATED	RESIDUALS
	38284		
SiO2	48.95	48.90	0.0503
TiO2	1.71	1.62	0.0929
Al2O3	17.07	17.10	-0.0326
FeO	8.40	8.60	-0.2078
MnO	0.14	0.17	-0.0273
MgO	9.39	9.36	0.0223
CaO	10.28	10.37	-0.0917
Na2O	2.73	2.54	0.1877
K2O	-	-	-

	Component	Proportion	Squared Residuals
Liquid	38434	80.94%	
Olivine	Fo85	3.04%	0.1003
Plagioclase	An85	11.68%	
Clinopyroxene	mg# 86	4.34%	

DATA: 38284=147+Ol+Plag+Cpx

	OBSERVED	ESTIMATED	RESIDUALS
	38284		
SiO2	48.95	49.04	-0.0862
TiO2	1.71	1.05	0.6611
Al2O3	17.07	17.02	0.0438
FeO	7.03	6.95	0.0838
MnO	0.14	0.14	-0.0034
MgO	9.39	9.34	0.0473
CaO	10.28	10.14	0.1443
Na2O	2.73	2.67	0.0623
K2O	0.88	0.68	0.1987

	Component	Proportion	Squared Residuals
Liquid	147	64.83%	
Olivine	Fo85	8.60%	0.5199
Plagioclase	An85	22.13%	
Clinopyroxene	mg#86	4.44%	

Table 9.9b

DATA: 38188=38303+Ol+Plag+Cpx

	OBSERVED	ESTIMATED	RESIDUALS
	38188		
SiO ₂	48.42	48.59	-0.1722
TiO ₂	1.29	0.99	0.2955
Al ₂ O ₃	16.40	16.30	0.0975
FeO	8.92	7.67	0.6193
MnO	0.15	0.13	0.0239
MgO	11.17	11.21	-0.0476
CaO	10.71	10.40	0.3072
Na ₂ O	2.89	3.18	-0.2936
K ₂ O	-	-	-

	Component	Proportion	Squared Residuals
Liquid	38303	79.32%	
Olivine	Fo85	11.29%	0.69
Plagioclase	An85	3.55%	
Clinopyroxene	mg# 86	5.84%	

DATA: 38188=38307+Ol+Plag+Cpx

	OBSERVED	ESTIMATED	RESIDUALS
	38188		
SiO ₂	48.42	48.58	-0.1658
TiO ₂	1.29	1.07	0.2233
Al ₂ O ₃	16.40	16.33	0.0666
FeO	8.92	8.01	0.2828
MnO	0.15	0.15	0.0212
MgO	11.17	11.12	0.0528
CaO	10.71	10.42	0.2923
Na ₂ O	2.89	2.56	0.3265
K ₂ O	-	-	-

	Component	Proportion	Squared Residuals
Liquid	38307	65.53%	
Olivine	Fo85	11.46%	0.3566
Plagioclase	An85	16.75%	
Clinopyroxene	mg# 86	6.26%	

Table 9.9c

DATA: 38288=38307+Ol+Plag+Cpx

	OBSERVED	ESTIMATED	RESIDUALS
	38288		
SiO ₂	48.86	48.86	-0.0045
TiO ₂	1.39	1.06	0.3232
Al ₂ O ₃	18.25	18.25	-0.0008
FeO	7.24	7.35	-0.1106
MnO	0.13	0.14	-0.0096
MgO	8.99	8.95	0.0387
CaO	11.05	11.05	0.0026
Na ₂ O	2.79	2.66	0.125
K ₂ O	-	-	-

	Component	Proportion	Squared Residuals
Liquid	38307	65.59%	
Olivine	Fo85	7.37%	0.134
Plagioclase	An85	22.49%	
Clinopyroxene	mg#86	4.55%	

DATA: 38288=38307+Ol+Plag+Cpx

	OBSERVED	ESTIMATED	RESIDUALS
	38288		
SiO ₂	48.86	48.77	0.091
TiO ₂	1.39	1.17	0.2206
Al ₂ O ₃	18.25	18.27	-0.0243
FeO	7.24	7.55	-0.3117
MnO	0.13	0.14	-0.0171
MgO	8.99	8.99	0.0014
CaO	11.05	11.20	-0.1571
Na ₂ O	2.79	2.84	-0.0524
K ₂ O	-	-	-

	Component	Proportion	Squared Residuals
Liquid	38307	69.54%	
Olivine	Fo88	6.34%	0.1825
Plagioclase	An85	19.62%	
Clinopyroxene	mg# 88	4.50%	

Table 9.9d

DATA: 47979=38390+Ol+Plag+Cpx

	OBSERVED	ESTIMATED	RESIDUALS
	47979		
SiO2	49.24	49.31	-0.0736
TiO2	1.06	1.21	-0.1577
Al2O3	17.20	17.18	0.0181
FeO	7.00	6.71	0.2896
MnO	-	-	-
MgO	9.27	9.28	-0.0103
CaO	12.50	12.37	0.1268
Na2O	2.50	2.42	-0.0757
K2O	0.20	0.40	-0.2114

	Component	Proportion	Squared Residuals
Liquid	38390	68.57%	
Olivine	Fo88	5.72%	0.1812
Plagioclase	An85	16.36%	
Clinopyroxene	mg#88	9.35%	

DATA: 47979=38389+Ol+Plag+Cpx

	OBSERVED	ESTIMATED	RESIDUALS
	47979		
SiO2	49.24	49.03	0.2047
TiO2	1.06	1.39	-0.3355
Al2O3	17.20	17.24	-0.0365
FeO*	8.24	8.46	-0.2165
MnO	-	-	-
MgO	9.27	9.39	-0.1162
CaO	12.50	12.85	-0.3559
Na2O	2.50	2.98	-0.4851
K2O	-	-	-

	Component	Proportion	Squared Residuals
Liquid	38389	94.00%	
Olivine	Fo88	1.30%	0.578
Plagioclase	An85	1.85%	
Clinopyroxene	mg# 86	2.85%	

FeO*: Total iron

PLATES

Plate 2.1A. Alternations of olivine-rich (top) and plagioclase-rich (bottom) layers. There is a sharp contact surface between the two layers.

A thin olivine-rich segregation occurs in the middle of the felsic layer.

Plate 2.1B. Displacement of layers along a fault plane, left of the picture.

Plate 2.1C. Small scale drag faulting of isomodal layers. Eagle Bay outcrop.

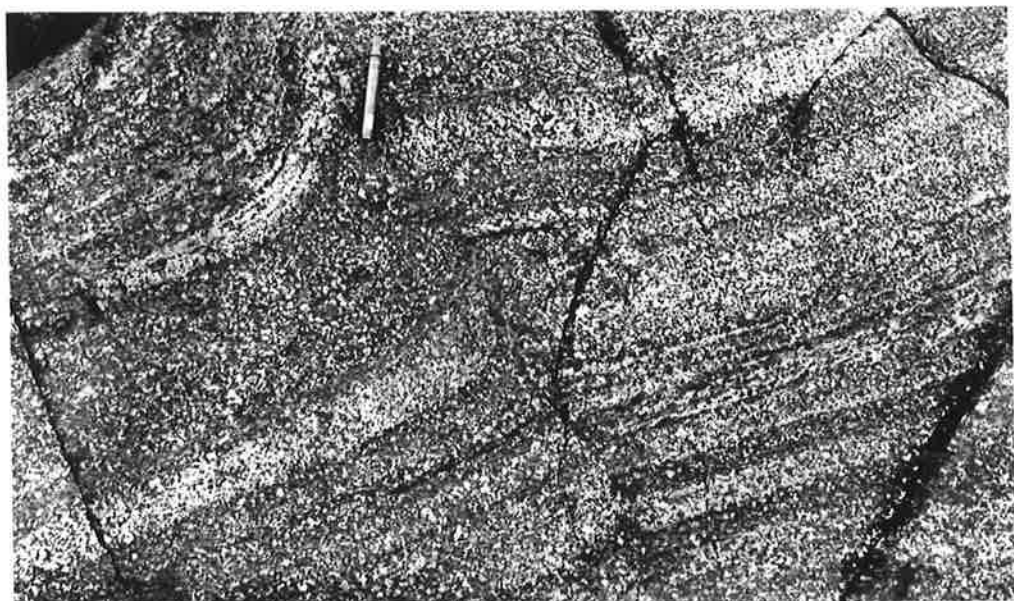
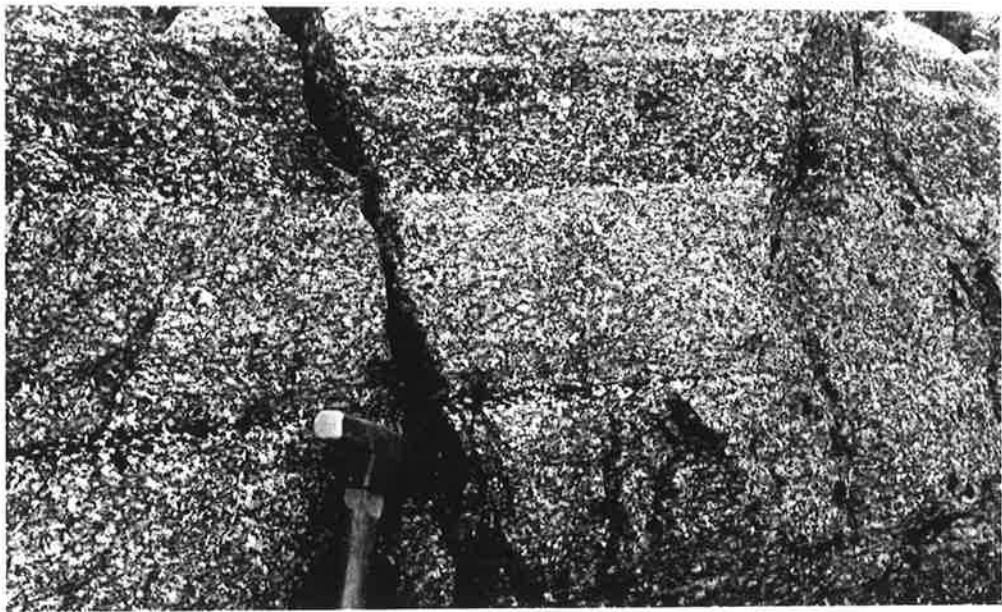
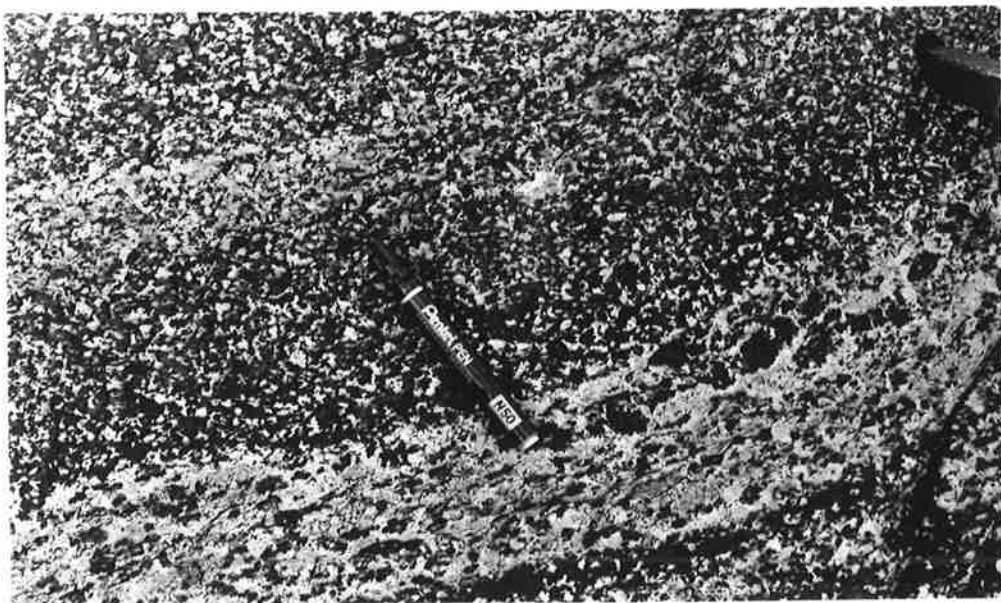
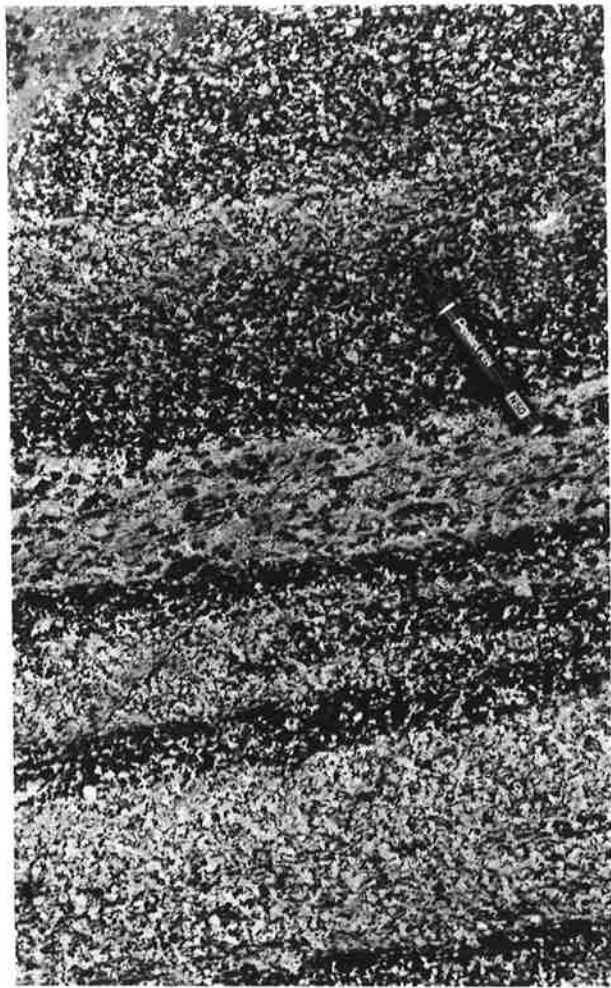


Plate 2.2A. Changes in the proportions of olivine and plagioclase across successive layers. Note the larger size of olivines from the olivine-rich layers.

Plate 2.2B. Alternations of mafic and felsic layers with modal contacts. In the plagioclase-rich layer (centre of the picture), the olivines show elongation and alignment on the plane of layering.

Plate 2.2C. Close-up of the previous photograph. Planar lamination is well defined by the larger olivine crystals. Troctolites from the Eagle Bay outcrop.



Plates 2.3A and B. Upper left and right. Troctolite sample 324. Plate A shows a section cut perpendicular to the layering, and plate B parallel to the layering orientation. In the first section, the olivine crystals show alignment on the plane of layering, whereas in the second section the crystals are tabular. The layers are not clearly defined at the lower part of the first section. Scale bar is 2cm long.

Plate 2.3C. Bottom left. Small scale layering. Three successive layers are marked. Olivines from the plagioclase-rich layer have distinctly smaller size than those from the olivine-rich layers.

Plate 2.3D. Bottom right. Unmodal layers. The section to the left is cut normal and the other parallel to the layering. There are two thin plagioclase-rich layers marked. Also, the upper and the lower olivine-rich layers are more mafic in character than the central layer.

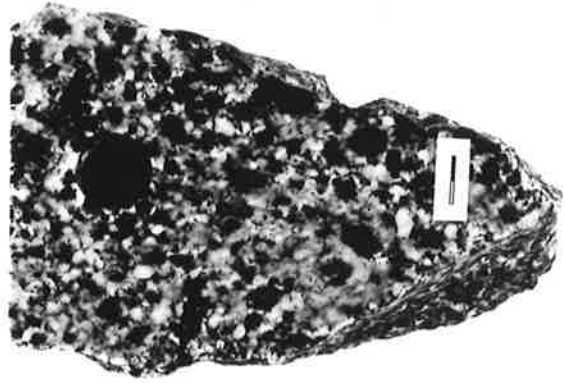
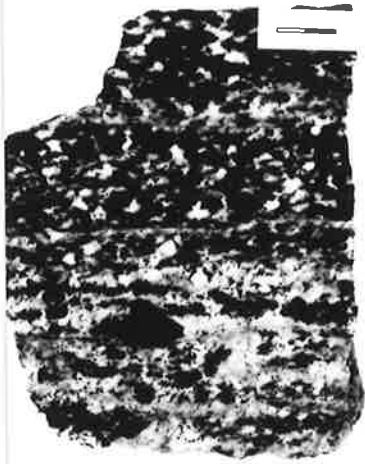


Plate 2.4A. Troctolite layering at the Eagle Bay outcrop. The layers are continuous over the outcrop, but there is no rhythmic repetition. A set of plagioclase-rich layers (in the upper centre of the photograph) shows a basin-like structure.

Plate 2.4B. A general view of the layering at Eagle Bay. The continuity of the individual layers is well illustrated. Although some layers are traced for several meters, others "phase out" in less than two meters. No grain size gradation is observed within a layer or across sets of layers.

Plate 2.4C. Anorthositic layers in melatroctolite. They show irregular thickness and limited lateral extent, while maintaining sharp contacts with the melatroctolite.



Plate 2.5A. Intrusion of a mafic layer into modally layered olivine-gabbro. The layer is injected at an angle to the layering plane and has not been spread or mixed with the overlying olivine-gabbro. The shape of the layer as well as its intrusive style are reminiscent of the layer patterns produced by "surge type" density currents (Irvine, 1980). Boulder at Half Moon Bay.

Plate 2.5B. Detail of the lower contact face of the mafic layer. A plagioclase-rich segregation was formed together with detached wedges from the mafic layer. The contact between olivine-gabbro and mafic layer is sharp. So is the contact between the plagioclase-rich segregation and the olivine-gabbro. The irregular shape of this intrusion and lower interface, as well as its sharply defined contact to the overlying layered rocks and the lack of chilled margins suggest a plastic environment at hypersolidus conditions.

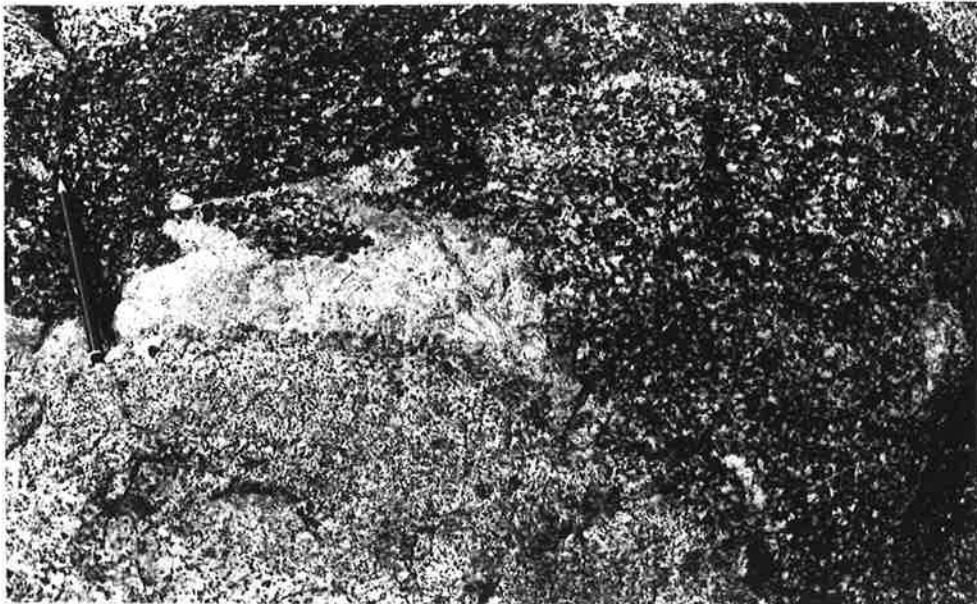
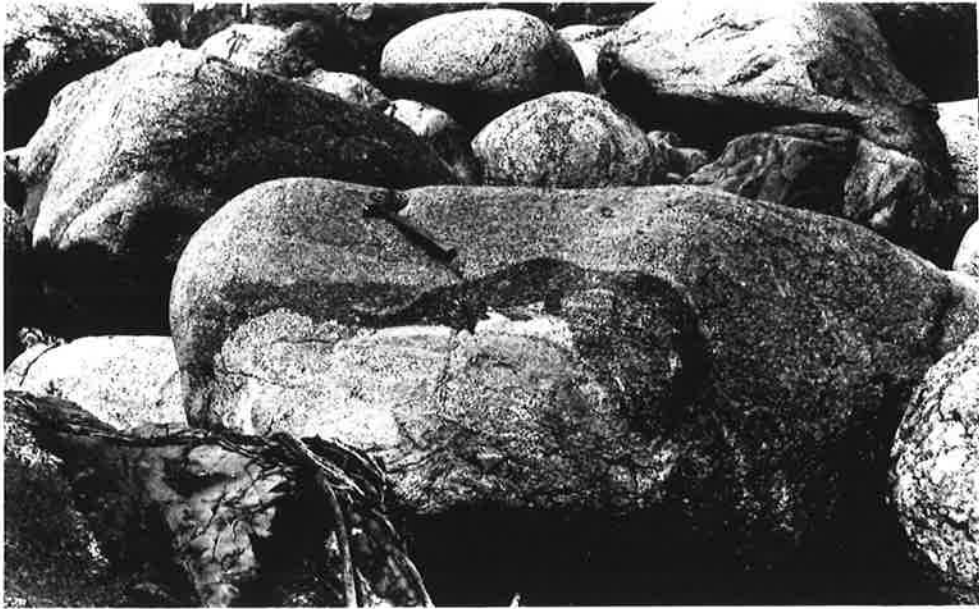


Plate 2.6A. An olivine-rich intrusion into layered olivine gabbros. The intrusive layer is 1m thick and massive. The contact between the two lithologies is strikingly sharp. No thermal effects have been observed. Outcrop from the Handspike Pt. layered rock series.

Plate 2.6B. A wedge-like more melanocratic layer to the left, penetrates the more felsic olivine-gabbro to the right of the photograph. Handspike Pt.

Plate 2.6C. Laminated olivine-gabbro outcrop from Handspike Pt. The trace of the plane of layering is marked by the red line. The top of this section is pointed by the pencil. An olivine-rich layer crosscuts the layering at an angle. It is more coarse-grained than the olivine-gabbro. It also shows a sharp contact with the olivine-gabbro to the right.



Plate 2.7A. A coarse-grained olivine-gabbro layer (centre) is sandwiched between a medium-grained olivine-gabbro. The layer is thin and of limited lateral extent. The medium-grained olivine-gabbro layer is overlain by a layer richer in olivine, and underlain by another modally uniform olivine-gabbro layer. Handspike Pt.

Plate 2.7B. Laminated olivine-gabbro. Red lines delineate layer boundaries. The felsic layer in the centre shows variable thickness. Small blocks of this layer are cut off and incorporated into the overlying layer. These features could be indicative of the existence of magmatic currents, which detach and transport highly solidified material. Handspike Pt.

Plate 2.7C. Detail of the contact between two intrusive layers. Wedge shaped apophyses of the layer in the centre penetrate the layer to the left. The plagioclase segregation (centre) is worth noting. This monomineralic plagioclase segregation displays sharp interfaces to the surrounding olivine-gabbro, and an intrusive contact relationship to the right-hand side. To the left, it thins and tapers out to a modally different olivine-gabbro. These features suggest flow in the system and not gravitational sorting at a convection-free melt body. Convection currents could be responsible for the accumulation of these layers.



Plate 2.8A. Small scale boudin-like faulting in harzburgite from the Eagle Bay exposure. Foliated metagabbroic material interleaves with harzburgite preferentially along displacement surfaces.

Plate 2.8B. Successions of olivine-rich (black) and enstatite-rich (light grey) layers define banding. Harzburgite outcrop at Eagle Pt.



Plate 2.9A. Contact relationship between an aphyric dolerite dyke and a massive medium-grained gabbro. Outcrop to the south of Nuggets Pt. from the transitional zone between dyke swarm complex and Upper Level gabbro.

Plate 2.9B. Injection of gabbroic material into a set of parallel dolerite dykes. The gabbroic intrusion crosscuts the dolerite dykes and is penecontemporaneously displaced. Note the very sharply defined contacts between gabbro and dolerite.

Plate 2.9C. Plagioclase segregation in the Upper level gabbro. Outcrop on the coast line and to the south of Nuggets Pt.



Plate 2.10A. Pillow lava outcrop at North Head. Note the variable size of the individual pillows.

Plate 2.10B. Dolerite dykes from the dyke swarm complex. Note the interchange between the aphyric and plagioclase-phyric types. Hasselborough Bay outcrop.

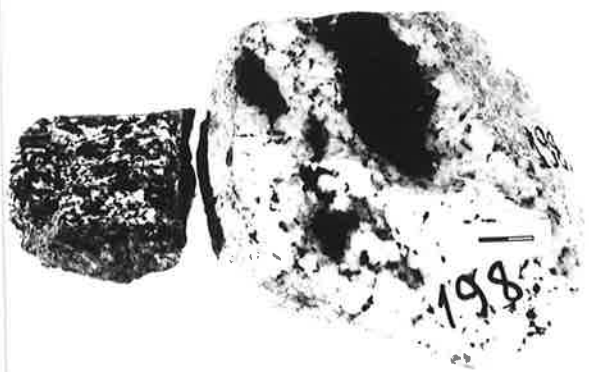
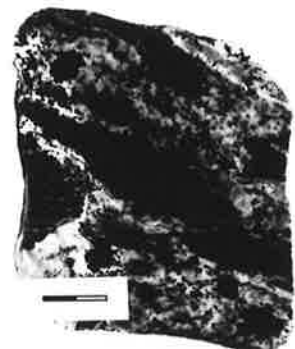


Plate 2.11A. Upper left. Cataclasite from the exposure to the east of Langdon Bay. This is a fine-grained and totally recrystallised rock. Striations are clearly defined.

Plate 2.11B. Upper right. Mylonites from Eagle Bay. Foliation is defined by the recrystallised pyroxene augens.

Plate 2.11C. Bottom left. Two mylonite specimens from Eagle Pt. A well banded mylonite (left-hand side) and a leucocratic- metagabbroic mylonite with incorporated harzburgite blocks (right-hand side) are shown.

Plate 2.11D. Bottom right. Black outcrop of harzburgite (with grey-green enstatites); harzburgite is cut by a vein of recrystallised gabbroic material now containing biotite.



APPENDICES

APPENDIX 1 : SAMPLE DESCRIPTIONS

Descriptions of all studied samples are primarily based on petrography. Grouping of samples to different categories focused on field relations only.

The freshness of the specimens is divided to four categories according to the extent of alteration products:

fresh : secondary products usually less than 10%,

r-fresh : alteration by-products limited to less than 25%,

m-altered : replacement of primary minerals ranges from 25 to

55%, altered : extensive alteration, more than 55%. Primary minerals are completely replaced or pseudomorphed.

Mineral grain sizes range from more than 5mm in the coarse - grained rocks to 1mm - 5mm in the medium - grained ones.

Abbreviations of minerals are as follows: act= actinolite, epid=epidote, hornb= hornblende, zois= zoisite, chlor= chlorite, biot= biotite and sulph= sulphides.

The abbreviations adopted for rock textures are:

hypid=hypidiomorphic granular, adcum= adcumulate texture, lamin= planar lamination of igneous minerals and incip. rercy.=

recrystallization along crystal boundaries with the development of somehow granoblastic polygonal texture. When the degree of preferred orientation is strong the term good lamination is used. Otherwise, the lamin. abbreviation refers to poorly developed planar orientation of the crystals.

(A) LAYERED SEQUENCE

<u>Sample No.</u>	<u>Rock Type</u>	<u>Primary Minerals</u>	<u>Texture</u>
186	Sheared troctolite	Basal thrust zone of the	
311	Sheared troctolite	layered sequence	
301	Gabbro	plag, cpx	coarse, massive
303	Dolerite dyke	plag phen	
304	Gabbro	plag, cpx	coarse, massive
305	Gabbro	plag, cpx	good lamination
306	Gabbro	plag, cpx	medium, massive
307	Gabbro	plag, cpx	good lamination
308	Gabbro	plag, cpx	good lamination
309	Ol-gabbro	plag, cpx, ol	medium, adcum
310	Gabbro	plag, cpx	coarse, adcum
312	Troctolite	plag, ol, sp, cpx	adcum
313	Troctolite	plag, ol, sp	adcum
314	Troctolite	plag, ol	adcum
315	Troctolite	plag, ol, cpx, sp	adcum
316	Troctolite	plag, ol, cpx, sp	adcum
317	Ol-gabbro	plag, cpx, ol	good lamination
318	Sp-gabbro	plag, cpx, sp	altered
319	Sp-gabbro	plag, cpx, sp	altered
320	Troctolite	plag, ol, cpx, sp	adcum, lamin
321	Troctolite	plag, ol, sp	adcum, lamin
322	Troctolite	plag, ol, sp	adcum
323	Troctolite	plag, ol, sp	adcum, lamin
324	Troctolite	plag, ol, sp, cpx	adcum
325	Dolerite dyke	plag phen	
326	Gabbro	plag, cpx, sp	sheared, m-altered

(A) continued

327	Dolerite dyke	aphyric	altered
328	Melatroctolite	ol, plag, sp	adcum
329A	Melatroctolite	ol, plag, sp	adcum
329B	Dolerite dyke	plag, hornb	fine, holocrystalline
330	Melatroctolite	ol, plag, cpx, sp	adcum
331	Melatroctolite	ol, plag, cpx, sp	adcum
331A	Melatroctolite	ol, plag, cpx, sp	adcum
332	Troctolite	plag, ol, cpx	adcum
333A	Ol-gabbro	plag, ol, cpx	adcum
333B	Ol-gabbro	plag, cpx, ol	altered
334	Ol-gabbro	plag, cpx, ol, sp	coarse, adcum
335	Gabbro	plag, cpx	good lamination
336	Gabbro	plag, cpx	coarse, massive
337	Ol-gabbro	plag, cpx, ol, sp	coarse, adcum
338	Troctolite	ol, plag, cpx, sp	coarse
339	Troctolite	plag, ol, cpx, sp	adcum
340	Gabbro	plag, cpx	coarse, sheared
341	Gabbro	plag, cpx	sheared
342	Ol-gabbro	plag, cpx, ol	adcum
343	Gabbro	plag, cpx	m-altered, massive
344	Gabbro	plag, cpx	good lamination
345	Ol-gabbro	plag, cpx, ol	medium, adcum
346	Ol-gabbro	plag, cpx, ol	adcum
347	Gabbro	plag, cpx	strongly sheared
348A	Ol-gabbro	plag, cpx, ol	adcum
348B	Ol-gabbro	plag, cpx, ol	coarse, adcum
349	Gabbro	plag, cpx	coarse to very coarse
350	Ol-gabbro	plag, cpx, ol	adcum

(A) continued

351	Ol-gabbro	plag, cpx, ol	adcum, lamin
352	Ol-gabbro	plag, cpx, ol	good lamination
353	Ol-gabbro	plag, cpx, ol	good lamination
355	Ol-gabbro	plag, cpx, ol	adcum, lamin
356	Ol-gabbro	plag, cpx, ol	adcum
357	Ol-gabbro	plag, cpx, ol	mesocumulate
358	Troctolite	plag, ol, cpx, sp	intrusive layer
359	Gabbro	plag, cpx	good lamination
360	Ol-gabbro	plag, cpx, ol	adcum, good lamination
361A	Gabbro	plag, cpx	good lamination
361BA	Ol-gabbro	plag, cpx, ol	adcum, good lamination
361BB	Ol-gabbro	plag, cpx, ol	good lamination
370	Ol-gabbro	plag, cpx, ol	adcum
371	Ol-gabbro	plag, cpx, ol	adcum
372	Dolerite dyke	aphyric	
373	Ol-gabbro	plag, cpx, ol	coarse, adcum
374	Ol-gabbro	plag, cpx, ol	adcum
375	Ol-gabbro	plag, cpx, ol	coarse, lamin
376	Gabbro	plag, cpx	good lamination
377	Dolerite dyke	aphyric	
378	Anorthosite	plag	cumulate, m-altered
379C, R	Dolerite dyke	aphyric	centre (C), rim (R)
380	Ol-gabbro	plag, cpx, ol	intrusive layer
381	Ol-gabbro	plag, cpx, ol	good, lamination
383	Anorthosite	plag	cumulate, good lamin
384	Ol-gabbro	plag, cpx, ol	adcum, good lamin
390	Anorthosite	plag	thin layer, altered
391	Dolerite dyke	aphyric	

(A) continued

392	Troctolite	plag, ol, sp	adcum
393	Troctolite	plag, ol, sp	adcum
394	Microgabbro	cpx, plag	recrystallized, mortar texture, //fault plane
601	Ol-gabbro	plag, cpx, ol	adcum
661	Troctolite	ol, plag, cpx, sp	intrusive layer
663	Troctolite	plag, ol, cpx, sp	adcum
664	Troctolite	plag, ol, sp	adcum
665	Troctolite	ol, plag, cpx, sp	intrusive layer
666	Anorthosite	plag	altered, thin layer
530	Ol-gabbro	plag, cpx, ol	adcum
531	Ol-gabbro	plag, cpx, ol	adcum
532	Ol-gabbro	plag, cpx, ol	adcum
534	Gabbro	plag, cpx	good lamination
535	Gabbro	plag, cpx	good lamination
536	Gabbro	plag, cpx	good lamination
537	Ol-gabbro	plag, cpx, ol	adcum
538	Gabbro	plag, cpx	massive
539	Gabbro	plag, cpx	good lamination
540	Gabbro	plag, cpx	coarse, massive

(B) UPPER LEVEL GABBRO

<u>Sample No.</u>	<u>Rock Type</u>	<u>Primary Minerals</u>	<u>Remarks</u>
2	Gabbro	plag, cpx	coarse, r-fresh
200	Gabbro	plag, cpx	screen in dol. dyke swarm, r-fresh, epid. zois. veins
201	Gabbro	plag, cpx	screen in dyke swarm
202	Gabbro	plag, cpx	altered, brown-green hornb. zois. veins, plag-phen dyke
203	Gabbro	plag, cpx	incip. recry., hornb.
204	Gabbro	plag, cpx	altered, hornb., sulph. prehnite veins, coarse
205	Gabbro	plag, cpx	r-fresh, zois. veins
206	Gabbro	plag, cpx	r-fresh, hornb, act.
207	Gabbro	plag, cpx	r-fresh, hornb, zois. epid. veins
208	Gabbro	plag, cpx	altered, hornb, medium cpx lamination
209A	Gabbro	plag, cpx	r-fresh, incip. recry.
209B	Gabbro	plag, cpx	r-fresh, medium
210	Gabbro	plag, cpx	r-fresh, hornb
211	Ol-gabbro	plag, cpx, ol	r-fresh, hypid.
212	Gabbro	plag, cpx, ol	r-fresh, relict ol.
213D1	Felsic dyke	plag	altered
213D2	Dolerite dyke	plag phen	ophitic
213D3	Dolerite dyke		aphyric
214	Gabbro	plag, cpx	r-fresh, cpx lamination
215	Gabbro	plag, cpx	coarse, r-fresh
216	Gabbro	plag, cpx	m-altered
218	Gabbro	plag, cpx	altered, recrystallized porphyroblastic texture

(B) continued

219	Gabbro	plag, cpx	incip. recr., zois, green hornb.
220	Gabbro	plag, cpx	fresh, coarse, brown hornb.
221A	Gabbro	medium, hornb, plag, Fe-Ti oxides	subophitic texture
221B	Dolerite dyke	micro-	holocrystalline, r-fresh
222A	Gabbro	plag, cpx	coarse, m-altered
223B	Gabbro	plag, cpx	r-fresh, coarse, chlor.
224	Gabbro	plag, cpx	r-fresh, cpx lamination
225	Ol-gabbro	plag, cpx, ol	r-fresh, hornb, talc?
227	Gabbro	plag, cpx	m-altered, hornb, chlor.
228	Gabbro	plag, cpx	m-altered, incip. recr. prehnite veins, hornb, Fe-Ti oxides
229	Gabbro	plag, cpx	r-fresh,
230	Gabbro	plag, cpx	m-altered, hornb, epid.
233	Ol-gabbro	plag, cpx, ol	m-altered, cumulate
234	Gabbro	plag, cpx	altered
235	Ol-gabbro	plag, cpx, ol	r-fresh, cumulate
236	Gabbro	plag, cpx	m-altered, coarse
238	Ol-gabbro	plag, cpx, ol	coarse, cumulate
239	Gabbro	plag, cpx	fresh, medium
240	Gabbro	plag, cpx	r-fresh, hornb, epid.
241	Gabbro	plag, cpx	m-altered, hornb.
243	Gabbro	plag, cpx	r-fresh, coarse, hornb, chlor.
244	Gabbro	plag, cpx	coarse, m-altered, sulph.
604	Gabbro	plag, cpx	r-fresh, hornb, chlor.
605	Ol-gabbro	plag, cpx, ol	r-fresh, cumulate
606	Gabbro	plag, cpx	coasre, altered
607	Gabbro	plag, cpx	coarse, m-altered

(C) PERIDOTITES AND GABBROIC MYLONITE

<u>Sample No.</u>	<u>Rock Type</u>	<u>Primary Minerals</u>	<u>Remarks</u>
Langdon Bay - Eagle Point			
102	Cataclasite	plag, act, hornb	fine matrix
103	Harzburgite	ol, en	serpentinized
105	Gabbroic mylonite	plag, cpx	massive
106	Harzburgite	ol, en, sp	serpentinized
107	Harzburgite	ol, en, sp	serpentinized
109	Harzburgite	ol, en	serpentinized
110	Harzburgite	ol, en, sp	serpentinized
111A	Dolerite dyke	aphyric	< 5cm wide
112	Harzburgite	ol, en, sp, cpx	serpentinized
113	Gabbroic dyke	altered	1 cm wide
115	Dolerite dyke	aphyric	plus a felsic dyke
116	Dolerite dyke	plag phen.	holocrystalline
117	Harzburgite	ol, en, sp	serpentinized
118	Harzburgite	ol, en, sp	serpentinized
119	Harzburgite	ol, en, sp	serpentinized
119A	Gabbroic dyke	altered	< 2 cm wide
121	Harzburgite	ol, en	serpentinized
122	Harzburgite	ol, en	serpentinized
123	Harzburgite	ol, en, sp	serpentinized
125	Harzburgite	ol, en, sp	serpentinized
126	Gabbroic mylonite	plag, cpx	coarse, massive
127	Dolerite dyke	aphyric	< 10 cm wide
128	Harzburgite	ol, en, sp	sheared serpentinite

(C) continued

131	Harzburgite	ol, en	serpentinized
132	Gabbroic mylonite	plag, cpx	coarse, massive
134	Harzburgite	ol, en	serpentinized
135	Harzburgite	ol, en	serpentinized
136	Harzburgite	ol, en	serpentinized
137	Gabbroic mylonite	plag, cpx	coarse, massive
140	Harzburgite	ol, en	serpentinized
142	Gabbroic mylonite	plag, cpx	coarse, massive
143	Harzburgite	ol, en	serpentinized
145	Gabbro	plag, cpx	recrystallized
146	Harzburgite	ol, en, sp	serpentinized
150	Gabbroic mylonite	plag, cpx, ol	coarse
151	Harzburgite	ol, en, sp	serpentinized
152	Harzburgite	ol, en, sp	serpentinized
153P	Harzburgite	ol, en	serpentinized
153M	Gabbroic mylonite	plag, cpx, biot	mortar texture
155	Gabbroic mylonite	plag, cpx	good foliation
157	Harzburgite	ol, en	serpentinized
158	Gabbroic mylonite	plag, cpx	coarse, massive
160	Dolerite dyke	aphyric	
161	Harzburgite	ol, en, sp	partly serpentinised
163	Harzburgite	ol, en	serpentinized
164	Harzburgite	ol, en, sp	serpentinized
165	Harzburgite	ol, en, sp	serpentinized
167	Serpentinite		serpentine
168	Sheared Serpentinite		

(C) continued

169	Harzburgite	ol, en, sp	serpentinite
170	Gabbroic dyke	altered	
171	Gabbroic mylonite	plag, cpx	coarse to very coarse
172	Harzb.+ Gb. dyke	altered	
173	Gabbroic dyke	altered	
174	Harzb.+ Gb. dyke	altered	
175A	Gabbroic mylonite	plag, cpx	good foliation
176	Harzburgite	ol, en, sp	serpentinized
177	Harzb.+ Gb. dyke	altered	
178	Harzburgite	ol, en	serpentinized
179	Harzburgite	ol, en, sp	serpentinized
180	Gabbroic mylonite	plag, cpx	foliated
181	Harzburgite	ol, en, sp	serpentinized
182	Harzburgite	ol, en, sp, cpx	partly serpentinised
183	Harzburgite	ol, en	serpentinized
184	Gabbroic mylonite	plag, cpx, hornb	mortar texture
185	Harzburgite	ol, en, sp	serpentinized
187	Harzburgite	ol, en	serpentinized
191	Gabbroic mylonite	plag, cpx	medium, cpx-foliation
193	Dolerite dyke	aphyric	
401	Gabbroic dyke		altered
402	Gabbroic dyke		altered
403	Gabbroic dyke		altered
404	Gabbroic dyke		altered
405	Gabbroic mylonite	plag, cpx, ol	mylonite, brown hornb.

(C) continued

<u>Sample No.</u>	<u>Rock Type</u>	<u>Primary Minerals</u>	<u>Remarks</u>
Boot Hill Peridotite			
506	Harzburgite	ol, en	serpentinite
509	Harzburgite	ol, en	serpentinite
511	Harzburgite	ol, en, sp	serpentinite
678	Harzburgite	ol, en	partly serpentinised
Central Plateau Peridotite			
27	Harzburgite	ol, en	serpentinite
30	Harzburgite	ol, en	serpentinite
31	Harzburgite	ol, en	serpentinite
50	Harzburgite	ol, en	serpentinite
541	Harzburgite	ol, en	serpentinite
Mount Blair Peridotite			
40	Harzburgite	ol, en	serpentinite
54	Harzburgite	ol, en	serpentinite
55	Harzburgite	ol, en	serpentinite
58	Harzburgite	ol, en, sp	serpentinite
60	Harzburgite	ol, en	serpentinite
62	Harzburgite	ol, en	serpentinite
63	Harzburgite	ol, en, sp	felsic 5mm vein

(D) ISLAND LAKE GABBRO

<u>Sample No.</u>	<u>Rock Type</u>	<u>Primary Minerals</u>	<u>Remarks</u>
21	Gabbro	plag, cpx	coarse, r-fresh, horn, actinolite
22	Gabbro	plag, cpx	medium, r-fresh
23	Ol-gabbro	plag, cpx, ol	medium, fresh, hypid.
24	Gabbro	plag, cpx	medium, altered, zois, hornb, chlor.
25	Gabbro	plag, cpx	coarse, r-fresh
26	Gabbro	plag, cpx	coarse, r-fresh, hornb.
32	Gabbro	plag, cpx	medium, r-fresh, hornb.
33	Gabbro	plag, cpx	coarse, m-altered, act.
34	Gabbro	plag, cpx	medium, subophitic
35	Gabbro	plag, cpx	coarse, r-fresh, hypid.
36	Gabbro	plag, cpx	medium, fresh, hypid.
37	Gabbro	plag, cpx	medium, r-fresh, hornb.
39	Ol-gabbro	plag, cpx, ol	coarse, r-fresh, hypid.
43	Gabbro	plag, cpx	medium, r-fresh
46	Gabbro	plag, cpx	coarse, altered
47	Gabbro	plag, cpx	medium, altered
673	Gabbro	plag, cpx	medium, fresh
675	Ol-gabbro	plag, cpx, ol	coarse, fresh
651	Gabbro	plag, cpx	recrystallized, hornb, mortar texture

continued

652	Gabbro	plag, cpx
653A	Gabbro	plag, cpx recrystallized, mortar texture, hornb, sulph.
653B	Dol. dyke	plag, hornb, Fe-Ti oxides, holocrystalline recryst. subophitic

(E) SANDY BAY GABBROIC UNIT

<u>Sample No.</u>	<u>Rock Type</u>	<u>Primary Minerals</u>	<u>Remarks</u>
65	Gabbro	plag, cpx	fresh, coarse
66	Gabbro	plag, cpx	medium, fresh, hypid.
67	Gabbro	plag, cpx	medium, r-fresh, hornb
68	Ol-gabbro	plag, cpx, ol	medium, fresh
69	Ol-gabbro	plag, cpx, ol	coarse, m-altered, brown hornb, chlor.
70	Gabbro	plag, cpx	medium, r-fresh
71	Gabbro	plag, cpx	medium, r-fresh, hypid., hornb
72	Gabbro	plag, cpx	medium, r-fresh
73	Gabbro	plag, cpx	coarse, altered
74	Gabbro	plag, cpx	coarse, m-altered
75	Gabbro	plag, cpx	fresh, hypid.
76	Gabbro	plag, cpx	coarse, altered
78	Ol-gabbro	plag, cpx, ol	medium, r-fresh, green hornb.
79	Ol-gabbro	plag, cpx, ol	medium to coarse, r-fresh, idding.
80	Gabbro	plag, cpx	medium, r-fresh
81	Ol-gabbro	plag, cpx, ol	coarse, m-altered, hornb, act, talc

(F) NORTH MT. - MT. BLAIR: GABBROS AND WERHLITE

<u>Sample No.</u>	<u>Rock Type</u>	<u>Primary Minerals</u>	<u>Remarks</u>
North Mountain Gabbro			
501	Gabbro	plag, cpx	m-altered, medium
502	Gabbro	plag, cpx	altered, subophitic
503	Gabbro	plag, cpx	altered, subophitic
504	Gabbro	plag, cpx	completely altered
505	Gabbro	plag, cpx	altered, zeolites
Boot Hill Gabbro			
508	Gabbro	plag, cpx	altered, medium to coarse, hypid.
510	Gabbro	plag, cpx	altered
512	Gabbro	plag, cpx	microgabbro, zeolite and epidote veins
514	Gabbro	plag, cpx	m-altered, medium
542	Gabbro	plag, cpx	altered
Rookery Creek			
524	Ol-gabbro	plag, cpx, ol	r-fresh, medium, cumulate
525	Gabbro	plag, cpx	m-altered, medium

(F) continued

Mount Blair Gabbro

51	Gabbro	plag, cpx	m-altered, medium
52	Gabbro	plag, cpx	m-altered, medium sulphides
53	Gabbro	plag, cpx	r-fresh, coarse
57	Gabbro	plag, cpx	r-fresh, medium
59	Gabbro	plag, cpx	m-altered, medium, hornb.
61	Gabbro	plag, cpx	altered, medium
515	Gabbro	plag, cpx	altered, coarse, hornb.
520	Gabbro	plag, cpx	altered, medium, epidote veins
521	Ol-gabbro	plag, cpx, ol	fresh, medium, cumulate
522	Gabbro	plag, cpx	entirely replaced, hornb, albite?

North Mountain Wehrlite

671	Plag-wehrlite	ol, plag, cpx, sp	cumulus ol and sp, postcumulus plag and cpx
672	Plag-wehrlite	ol, plag, cpx, sp	

(G) EAST COAST: NUGGETS PT. - SANDY BAY

<u>Sample No.</u>	<u>Rock Type</u>	<u>Primary Minerals</u>	<u>Remarks</u>
701	Gabbro	plag, cpx	m-altered, medium, subophitic
702	Ol-gabbro	plag, cpx, ol	fresh, medium
703	Gabbro	plag, cpx	r-fresh, medium, brown hornb.
704	Gabbro	plag, cpx	altered, zois. vein
705	Gabbro	plag, cpx	m-altered, coarse, hypid, hornb.
706	Gabbro	plag, cpx	m-altered, medium
707	Gabbro	plag, cpx	r-fresh, igneous lamination
708	Gabbro	plag, cpx	altered
709	Gabbro	plag, cpx	m-altered, sulph, hornb, chlor.
710	Gypsum		vein in dykes
711	Felsic layer	plag, act	altered
713	Dolerite dyke		aphyric
715	Ol-gabbro	plag, cpx, ol	r-fresh, medium green hornb, idding
716	Gabbro	plag, cpx	altered, coarse
720	Gabbro	plag, cpx	altered, coarse
721	Gabbro	plag, cpx	altered
722	Gabbro	plag, cpx	r-fresh, medium
723	Microgabbro	plag, cpx	r-fresh, hornb, Fe-Ti oxides, subophitic
724	Gabbro	plag, cpx	altered
725	Dolerite dyke	cpx, plag	ophitic
726	Alkali gabbro	plag, cpx, horn, kaersutite	subophitic, sulph, prehnite, epid.
727	Felsic layer	plag	altered

Table (H): Lavas and Dykes

<u>Sample No.</u>	<u>Remarks</u>
M14	Pillow lava. North of Mt. Gwynn. Sample number in Griffin's field collection 235.
234	Basalt. North of Aurora Pt.
236	Basalt. North of Mt. Gwynn.
38188	Pillow lava. Green Gorge.
38291	Basalt. North of Green Gorge.
38284	Basalt. ESE of Davis Pt.
38306	Basalt. South of Green Gorge.
38280	Basalt. South of Cape Toucher.
210	Pillow lava. North of Cape Star.
38237	Dolerite dyke from dyke swarms. Gadgets Gully.
38320	Dolerite dyke from dyke swarms. Double Pt.
38334	Dolerite dyke from dyke swarms. South of Lucitania bay.
233	Dyke in pillows. North of Aurora Pt.
220	Dyke in pillows. SW of Mt. Hamilton.
NH2	Basaltic glass. North Head.

APPENDIX 2: X-Ray Fluorescence Analysis and Atomic Absorption Analysis, Techniques and Results.

(A). Preparation of samples.

Carefully selected troctolites, olivine-gabbros, massive gabbros, harzburgites, dolerite dykes and small gabbroic veins in harzburgite were prepared for whole rock analysis. The specimens were sizable because of their coarse character and the presence of layering. Two to five kilograms from each sample were used. Firstly, the samples were cleaned off from the weathering cover by sawing the outer crust, and then they were split to smaller fragments using a hydraulic splitter. The rock fragments were then passed through a jaw crusher, so that their size would be reduced to less than 10 mm. The crushed sample was then cleaned by hand of any weathered pieces. Special precaution was taken for the small dykes in harzburgite; all pieces showing weathering effects were removed using a hand lense. The clean separate of each sample was then ground in a tungsten carbide mill in batches of 100 gr at a time. The average weight of each sample was approximately 200gr. For the very coarse rocks, up to four runs were carried to ensure homogeneity of the samples. The resulted powders were used for major and trace element analysis. W and Co were not analysed.

(B). Analytical techniques for major element analysis.

Sample powders were put in an oven for two hours at 98°C. A sample of three to five grams of the dried powder was weighed in pure silica crucibles (alumina crucibles were also used) and then placed in a furnace at 960°C for for twelve hours. The ignited sample was then weighed as soon as was recovered from the furnace and weighed. The weight difference between pre-ignition and after-ignition values was employed to estimate the loss on ignition values (L.O.I.).

Na and K determinations were carried out by atomic absorption

spectrophotometry techniques. 30 mg of sample was weighed in teflon beakers using a Mettler analytical balance. The sample was then dissolved in 2 ml of H_2SO_4 (50% v/v) and 10 ml of HF (50% w/w); it was then placed on a hot plate at 120°C for twelve hours. When digestion was completed, the digested sample was diluted to a solution up to 100 ml by volume. In a group of 25 samples, two internal standard samples (BHN II) and three blanks were prepared. Details on the technique can be found in Turnbull and McDuie (1979). The solution were run in the Varian Techtron AA6D spectrophotometer of the Geology Department, University of Adelaide.

The other major elements, Si, Ti, Al, Fe, Mg, Mn, Ca, and P were analysed in glass disks using a Siemens SRS-1 spectrometer. The glass disks were prepared using the method of Norrish and Hutton (1969). 0.28 gr of ignited sample, 0.02 gr of NaNO_3 and 1.5 gr of lithium borate flux (Norrish formula) were weighed and mixed thoroughly. The mixture was then fused in Pt-Au crucibles (at 1070°C); the molten mix was poured in a graphite disk and pressed.

(C). Analytical techniques for trace elements.

Pressed powder pellets were prepared for trace element analysis and then run in the Siemens spectrometer for Ni, Cr, Sr, Rb, Ba, Y, Zr, Nb, Ti, Sc, V, Zn and Cu. Unignited sample powder was pressed in a hydraulic presser at 5 t/sq.in.

(D). FeO determination.

Unignited sample powder was weighed in Pt crucibles and then dissolved in 10 ml of H_2SO_4 (50% v/v) and 5ml of HF (50% A.R.). The mixture was placed on a hot plate (asbestos plate) at 320°C for 20-25 minutes. When the mixture simmered, the crucible was carefully immersed in a beaker containing a solution of 10 ml H_2SO_4 (50% v/v) and 30 ml H_3BO_3 previously prepared. The sample was then titrated against standard ceric sulphate solution (0.025 N) using ten drops of N-phenyl anthranilic

acid as indicator. Ferrous iron was then determined on the basis of 1 ml
1N Ce-solution is equivalent to 71.85 mg of FeO.

(E). Results and CIPW norms.

A group of 165 rock samples from the layered rocks, the harzburgites, the various massive gabbros, the North Mt. wehrlite and dolerite dykes were selected for major and trace element analysis. The samples of the layered rocks were prepared in duplicates in order to assess analytical inconsistencies; some samples were prepared in triplicates as well. Minor deviation was detected for the concentration of Cr and Ni in the troctolites, $\pm 3\%$, due the high Cr and Ni contents in these rocks. The results are the average values of the duplicates. Major element data on basalts and dolerites from the dyke swarms are from Griffin (1982).

ANALYTICAL RESULTS IN MICROFICHE (BACK POCKET)

Abbreviations in the following tables,

na: not analysed

nd: not determined

FeO - : ferric iron not determined

LAYERED SEQUENCE

Sample No:	319	320	322	323	326	328	331	332	333A	333B
SiO2	45.30	42.76	43.96	43.65	46.00	41.89	42.14	45.85	54.84	48.05
Al2O3	27.28	11.50	24.60	20.64	25.74	5.74	3.36	25.27	24.20	19.60
Fe2O3	0.62	4.72	1.91	2.54	0.32	7.47	11.48	0.56	0.96	1.34
FeO	1.73	2.70	1.79	2.37	2.82	3.57	-	2.58	3.19	2.88
MnO	0.05	0.12	0.06	0.07	0.06	0.18	0.17	0.06	0.08	0.09
MgO	8.59	30.24	13.27	18.63	9.36	38.98	40.04	9.17	10.83	11.49
CaO	14.95	7.24	12.88	10.67	14.57	1.90	1.49	14.59	13.09	15.24
Na2O	1.51	0.28	1.20	0.93	0.93	0.02	0.08	1.03	0.97	1.13
K2O	0.13	0.02	0.49	0.08	0.40	0.005	0.01	0.38	0.74	0.06
TiO2	0.06	0.07	0.06	0.03	0.08	0.05	0.10	0.08	0.08	0.17
P2O5	0.01	0.02	0.01	0.01	0.01	0.01	0.01	0.03	0.01	0.01
L.O.I.	3.86	10.04	5.90	6.03	5.03	11.25	11.26	2.88	3.70	4.15
TOTAL	100.23	99.67	100.23	99.62	100.29	99.82	98.88	99.60	99.99	100.06

Trace Elements in ppm

Sr	210	20	148	134	97	3.6	1.2	116	96	127
Rb	1.7	0.7	7.3	7.1	1.5	0.6	0.5	7.2	7.5	12.8
Y	0.1	1.2	2.1	0.2	0	0.4	2.2	0.7	2.5	1
Zr	0.6	1.5	3.4	1.1	0.7	0.6	1	1	2	2
Nb	0.2	0.4	0.4	0.3	0	0	0.1	0.5	0.7	0.4
Ba	27	7	44	92	15	2	3	78	142	169
Sc	9.3	12.6	11	7.7	7.6	7.2	17	12	20	15
V	30	40	42	25	15	28	64	40	71	46
Ti	363	437	849	360	217	240	534	467	823	652
Cr	1531	1413	1010	1730	777	2343	3152	1022	1121	632
Ni	310	1020	477	530	621	1643	1783	320	410	318
Cu	37	61	57	52	55	45	na	64	90	92
Zn	13	34	19	21	22	47	na	15	28	23

CIPW Norm

C	-	-	-	-	-	2.27	0.53	-	-	-
OR	0.77	0.12	2.90	0.47	2.36	0.03	0.06	2.25	4.37	0.35
AB	7.85	2.37	4.99	7.87	7.87	0.17	0.68	8.72	8.21	9.56
AN	67.28	30.06	60.29	51.91	64.88	9.36	7.33	63.21	59.50	48.23
NE	2.67	-	2.80	-	-	-	-	-	-	-
DI	Wo	2.85	2.39	1.48	0.40	3.06	-	-	3.75	2.25
	En	2.25	2.04	1.23	0.33	2.28	-	-	2.84	1.70
	Fs	0.28	0.03	0.06	0.02	0.48	-	-	0.53	0.32
HY	En	-	11.28	-	2.53	1.63	28.33	26.87	1.14	2.03
	Fs	-	0.17	-	0.13	0.34	0.19	0.56	0.21	0.38
OL	Fo	13.41	43.44	22.30	30.51	13.59	48.17	51.05	13.22	16.29
	Fa	1.84	0.74	1.28	1.69	3.14	0.35	1.16	2.71	3.38
MT		0.90	6.84	2.77	3.86	0.46	10.83	10.44	0.81	1.39
IL		0.11	0.13	0.11	0.06	0.15	0.09	0.19	0.15	0.15
AP		0.02	0.05	0.02	0.02	0.02	0.02	0.02	0.07	0.02
TOTAL		100.23	99.67	100.23	99.62	100.29	99.82	98.88	99.60	99.99
Mg#		89.85	95.23	92.96	93.34	85.54	95.11	94.34	86.37	85.82

LAYERED SEQUENCE

Sample No:	351	352	353	356	357	358	359	360	371	374
SiO2	44.35	47.14	48.51	48.32	48.07	44.49	47.24	48.52	45.73	48.57
Al2O3	12.59	22.13	20.76	14.80	20.20	21.83	22.40	23.55	19.74	17.35
Fe2O3	3.66	1.46	1.56	1.09	1.09	1.02	1.26	0.78	5.54	4.85
FeO	5.33	2.78	2.00	4.10	3.00	4.58	2.92	2.16	-	-
MnO	0.19	0.09	0.09	0.11	0.09	0.10	0.08	0.07	0.09	0.11
MgO	23.27	10.54	9.44	15.65	10.59	14.46	9.64	7.05	14.85	12.40
CaO	9.64	14.57	16.16	14.99	15.55	11.93	14.72	16.34	12.22	15.51
Na2O	0.72	1.44	1.44	0.92	1.34	1.23	1.40	1.63	1.06	1.16
K2O	0.04	0.03	0.03	0.04	0.03	0.03	0.03	0.03	0.12	0.06
TiO2	0.12	0.11	0.15	0.19	0.16	0.09	0.12	0.13	0.10	0.18
P2O5	0.01	0.01	0.01	0.01	0.01	0.02	0.01	0.01	0.0	0.0
L.O.I.	3.98	1.70	1.05	2.85	1.45	3.43	1.55	0.80	3.26	1.74
TOTAL	99.90	100.30	100.15	100.22	100.13	99.78	99.82	100.26	99.74	100.18

Trace Elements in ppm

Sr	89	158	167	83	122	100	136	153	96	117
Rb	0.7	1.2	0.8	1	0.8	0	0.5	0.3	2	0.8
Y	2	2.3	3.8	5	3.6	1.3	2.2	2.9	2.6	4.4
Zr	2	1.5	2.2	2.6	3	1	2.2	2.4	2.5	4
Nb	0.5	1	0.8	0	0.6	0.4	0.3	0.6	1	0.4
Ba	4	5	6	14	15	10	12	12	18	18
Sc	20	22	30	38	31	10	22	25	20	35
V	69	72	105	140	106	50	74	82	62	119
Ti	643	673	932	1151	996	573	717	745	693	1114
Cr	457	611	900	1287	738	2587	593	555	311	676
Ni	408	196	190	319	207	479	198	122	487	213
Cu	90	53	96	143	95	149	98	70	na	na
Zn	47	21	16	30	22	27	21	14	na	na

CIPW Norm

OR	0.24	0.18	0.18	0.24	0.18	0.18	0.18	0.18	0.71	0.35
AB	6.09	12.19	12.19	7.78	11.34	9.87	11.85	13.79	8.97	9.82
AN	31.00	53.83	50.10	36.14	49.02	53.96	54.75	56.86	48.75	41.96
NE	-	-	-	-	-	0.29	-	-	-	-
DI	Wd	7.00	7.68	12.53	15.94	11.72	2.13	7.60	10.08	4.96
	En	5.54	5.96	10.08	12.22	8.96	1.58	5.79	7.64	3.70
	Fs	0.66	0.88	0.99	2.04	1.53	0.33	1.03	1.41	0.77
HY	En	6.96	2.10	3.41	5.02	2.89	-	3.75	1.62	3.95
	Fs	0.83	0.31	0.33	0.84	0.49	-	0.67	0.30	0.83
OL	Fo	31.85	12.74	7.02	15.23	10.18	24.12	10.14	5.82	20.56
	Fa	4.19	2.08	0.76	2.81	1.92	5.61	1.99	1.18	4.74
MT		5.31	2.12	2.26	1.58	1.58	1.48	1.83	1.13	1.62
IL		0.23	0.21	0.28	0.36	0.30	0.17	0.23	0.25	0.19
AP		0.02	0.02	0.02	0.02	0.02	0.05	0.02	0.02	-
TOTAL		99.92	100.30	100.15	100.22	100.13	99.78	99.82	100.27	99.75

Mg#	88.61	87.11	89.38	87.18	86.29	84.91	85.47	85.33	84.86	84.98
-----	-------	-------	-------	-------	-------	-------	-------	-------	-------	-------

LAYERED SEQUENCE

Sample No:	378B	380	381	383	394A	601	662	665
SiO2	47.25	43.71	46.76	47.40	49.46	47.67	40.87	41.12
Al2O3	29.96	7.72	23.40	32.56	17.10	24.64	5.69	7.68
Fe2O3	1.68	11.49	4.08	0.69	6.04	0.38	10.11	9.55
FeO	-	-	-	-	-	2.44	-	-
MnO	0.02	0.18	0.06	0.0	0.09	0.05	0.13	0.14
MgO	3.43	28.65	9.62	0.95	10.02	6.86	40.23	36.82
CaO	15.49	7.70	14.35	16.32	14.66	15.87	3.04	4.01
Na2O	2.11	0.41	1.48	2.20	2.11	1.47	0.02	0.08
K2O	0.04	0.02	0.09	0.12	0.09	0.17	0.02	0.03
TiO2	0.06	0.16	0.12	0.04	0.34	0.13	0.02	0.05
P2O5	0.0	0.0	0.01	0.0	0.01	0.01	0.0	0.0
L.O.I.	1.37	6.17	1.55	0.88	1.59	1.45	12.04	10.34
TOTAL	100.03	100.03	99.97	100.28	99.92	99.69	100.14	99.48

Trace Elements in ppm

Sr	185	45	138	199	142	178	1.3	3.2
Rb	0.6	0.2	0.8	1.4	0.8	2.6	0.2	0.5
Y	0	3.5	2.3	0	9.7	2.2	0	0.5
Zr	1.2	2.7	7.2	1.3	7.1	3.6	0.4	1.4
Nb	0.1	0.3	1.2	0.1	0.4	1.2	0	0
Ba	7	4	9	5	16	26	1	1
Sc	8	24	15	3.8	38	24	6	7
V	19	92	52	6	163	72	14	28
Ti	417	930	757	306	1870	837	107	243
Cr	99	2251	519	8	424	431	1634	2846
Ni	85	916	254	28	146	170	1792	1452
Cu	na	na	na	na	na	79	na	na
Zn	na	na	na	na	na	75	na	na

CIPW Norm

C	-	-	-	-	-	-	0.11	0.23
OR	0.24	0.12	0.53	0.71	0.53	1.00	0.12	0.18
AB	16.23	3.47	12.52	15.35	17.85	12.44	0.17	0.68
AN	72.16	19.17	56.94	78.62	36.92	60.14	15.08	19.89
NE	0.88	-	-	1.77	-	-	-	-
DI Wb	1.96	7.95	5.92	0.98	14.92	7.74	-	-
En	1.50	6.60	4.47	0.65	10.39	5.67	-	-
Fs	0.25	0.36	0.85	0.26	3.30	1.34	-	-
HY En	-	14.66	1.21	-	0.11	1.29	13.87	12.53
Fs	-	0.80	0.23	-	0.04	0.31	0.02	0.40
OL Fo	4.93	35.11	12.80	1.20	10.13	7.10	60.49	55.48
Fa	0.91	2.11	2.67	0.52	3.55	1.85	0.09	1.96
MT	0.87	9.41	1.57	0.14	1.51	0.55	10.15	8.05
IL	0.11	0.30	0.23	0.08	0.65	0.25	0.04	0.09
AP	-	-	0.02	-	0.02	0.02	-	-
TOTAL	100.04	100.04	99.97	100.28	99.92	99.69	100.13	99.48

Mg#	84.99	91.11	85.11	74.15	78.12	83.36	95.84	94.25
-----	-------	-------	-------	-------	-------	-------	-------	-------

LAYERED SEQUENCE

Sample No:	530	531	532	533	534	535	537	538	539	540
SiO ₂	45.89	44.90	48.56	48.03	49.08	48.32	45.95	48.13	48.88	47.39
Al ₂ O ₃	22.04	17.78	17.86	21.87	20.21	23.57	12.69	24.08	18.10	14.36
Fe ₂ O ₃	1.85	3.32	1.42	1.45	1.11	0.75	2.78	0.42	1.17	1.71
FeO	3.05	4.07	3.78	2.26	2.40	2.55	5.46	2.48	2.76	5.10
MnO	0.07	0.13	0.10	0.05	0.07	0.06	0.14	0.06	0.10	0.18
MgO	12.63	17.71	11.85	8.71	8.90	6.91	21.13	6.32	11.75	15.87
CaO	13.08	11.17	15.24	15.57	16.42	15.49	10.52	16.42	16.25	13.62
Na ₂ O	0.96	0.97	1.23	1.53	1.79	2.04	0.89	1.67	1.10	1.12
K ₂ O	0.19	0.07	0.06	0.04	0.03	0.04	0.06	0.03	0.03	0.08
TiO ₂	0.10	0.13	0.20	0.17	0.26	0.16	0.16	0.18	0.16	0.25
P ₂ O ₅	0.01	0.02	0.02	0.02	0.02	0.01	0.02	0.02	0.01	0.02
L.O.I.	3.51	4.69	1.89	2.01	1.71	1.77	4.15	1.32	1.66	3.51
TOTAL	99.87	100.26	100.32	99.70	100.29	99.90	99.80	99.81	100.31	99.70

Trace Elements in ppm

Sr	95	118	101	146	120	185	73	148	98	88
Rb	3.5	1.2	0.7	0.4	0.6	0.6	0.8	0.4	0.3	1.5
Y	2.3	2.4	5.4	4.1	5.4	3.5	4	4.9	5.2	7.6
Zr	2.9	2.2	4	5.2	3.9	3.4	3.4	3.6	1.4	3.4
Nb	0.7	0.7	0.7	1.7	0.4	1	0.5	0.7	0.1	0.8
Ba	34	29	31	55	26	36	28	47	17	31
Sc	16	18	30	25	39	31	28	30	40	53
V	56	68	116	90	151	105	95	103	134	171
Ti	633	807	1197	995	1559	1048	969	1248	1078	1572
Cr	1373	1285	1048	1503	1249	604	1460	1207	1470	1414
Ni	398	633	247	255	179	117	693	172	257	339
Cu	79	69	125	69	222	4	104	104	114	30
Zn	26	38	26	21	20	16	45	15	21	59

CIPW Norm

OR	1.12	0.41	0.35	0.24	0.18	0.24	0.35	0.18	0.18	0.47
AB	8.12	8.21	10.41	12.95	14.64	16.04	7.53	14.13	9.31	9.48
AN	55.27	43.96	43.04	52.69	47.02	55.04	30.46	58.12	44.36	33.92
NE	-	-	-	-	0.28	0.66	-	-	-	-
DI Wo	3.99	4.73	13.55	10.20	14.32	9.08	9.02	9.69	15.11	14.00
En	3.14	3.78	10.22	8.03	11.16	6.69	7.01	7.01	11.82	10.50
Fs	0.40	0.41	1.95	1.02	1.61	1.52	1.03	1.79	1.63	2.09
HY En	6.39	6.34	5.37	3.61	-	-	8.67	0.14	5.47	4.17
Fs	0.89	0.68	1.09	0.46	-	-	1.27	0.04	0.75	0.83
OL Fo	14.98	23.82	9.50	7.04	7.71	7.37	25.89	6.02	8.39	17.41
Fa	2.12	2.83	1.99	0.99	1.22	1.85	4.19	1.69	1.27	3.82
MT	2.68	4.81	2.06	2.10	1.61	1.09	4.03	0.61	1.70	2.48
IL	0.19	0.25	0.38	0.32	0.49	0.30	0.30	0.34	0.34	0.47
AP	0.02	0.05	0.05	0.05	0.05	0.02	0.05	0.05	0.02	0.05
TOTAL	99.87	100.27	100.32	99.70	100.29	99.90	99.80	99.81	100.31	99.70
Mg#	88.07	88.58	84.82	87.29	86.86	82.85	87.34	81.96	88.36	84.72

HARZBURGITE

Sample No:	107	112	134	146	161	163	169	182	185
SiO ₂	44.81	45.25	44.85	44.34	45.08	43.79	44.96	43.84	44.65
Al ₂ O ₃	1.00	1.20	0.99	1.29	1.07	1.57	1.01	1.05	1.09
Fe ₂ O ₃	8.87	8.83	9.38	9.11	8.98	10.57	8.57	8.71	8.83
FeO	-	-	-	-	-	-	-	-	-
MnO	0.11	0.14	0.10	0.10	0.11	0.19	0.14	0.14	0.12
MgO	44.77	42.63	44.12	43.74	43.88	43.01	45.13	44.85	44.25
CaO	0.13	0.61	0.15	0.25	0.28	0.13	0.06	0.45	0.37
Na ₂ O	0.02	0.06	0.04	0.06	0.04	0.04	0.04	0.04	0.01
K ₂ O	0.0	0.01	0.01	0.01	0.02	0.01	0.02	0.0	0.01
TiO ₂	0.0	0.0	0.0	0.0	0.0	0.11	0.0	0.0	0.0
P ₂ O ₅	0.0	0.01	0.01	0.01	0.0	0.0	0.0	0.0	0.0
L.O.I.	12.32	11.78	12.10	11.95	11.81	11.91	12.27	11.76	12.49
TOTAL	99.71	98.74	99.65	98.93	99.47	99.44	99.94	99.08	99.33

Trace Elements in ppm

Sr	1.2	4	1.9	2.5	3.4	0.9	2.2	2.6	1.5
Rb	0	0.4	0.2	0	0.6	0	0.6	0	0
Y	0.7	0.2	0	1.7	0.2	2.7	0.3	0	0
Zr	0.3	1.6	0	5	3	3.9	0	0.1	0
Nb	0	0	0	0.6	0	0.2	0.2	0	0
Ba	3	2	3	7	3	3	4	3	5
Sc	11	13	11	9	11	14	9.6	9	12
V	40	47	41	34	40	58	33	36	45
Ti	32	47	41	149	46	619	46	36	34
Cr	2492	2758	2830	2316	2278	2191	2950	2378	2742
Ni	2087	2000	2179	2206	2119	2061	2056	2169	2092
Cu	na	na	na	na	na	na	na	na	na
Zn	na	na	na	na	na	na	na	na	na

CIPW Norm

C	0.73	0.01	0.66	0.75	0.47	1.26	0.81	0.17	0.39
OR	-	0.06	0.06	0.06	0.12	0.06	0.12	-	0.06
AB	0.17	0.51	0.34	0.51	0.34	0.34	0.34	0.34	0.08
AN	0.64	2.96	0.68	1.17	1.39	0.64	0.30	2.23	1.84
HY En	24.68	26.92	25.11	23.72	25.79	22.95	24.53	19.22	23.89
Fs	2.92	3.34	3.18	2.95	3.15	3.35	2.79	2.24	2.85
OL Fo	60.84	55.53	59.40	59.71	58.50	58.98	61.57	64.80	60.49
Fa	7.93	7.59	8.29	8.18	7.87	9.49	7.73	8.32	7.95
MT	1.80	1.80	1.90	1.84	1.83	2.15	1.74	1.77	1.80
IL	-	-	-	-	-	0.21	-	-	-
AP	-	0.02	0.02	0.02	-	-	-	-	-
TOTAL	99.71	98.74	99.65	98.91	99.46	99.42	99.93	99.08	99.33
Mg#	91.27	90.92	90.69	90.86	91.01	89.40	91.60	91.43	91.22

Sample No:	2	205	209A	209B	210	211	212	214	215	220
SiO ₂	48.11	51.62	52.49	50.61	48.27	48.58	48.71	49.66	51.27	49.71
Al ₂ O ₃	23.12	17.09	16.97	17.63	25.26	21.67	21.82	18.71	16.23	16.88
Fe ₂ O ₃	0.80	1.73	0.59	0.94	0.42	1.02	1.32	0.48	1.38	1.11
FeO	2.33	3.02	2.34	3.11	2.81	3.05	3.31	3.56	3.82	4.57
MnO	0.05	0.07	0.07	0.10	0.06	0.07	0.10	0.09	0.12	0.12
MgO	7.38	8.36	9.21	8.87	5.31	8.27	7.64	9.14	9.03	10.02
CaO	16.22	14.48	14.21	16.27	14.66	15.74	14.64	16.21	15.01	15.30
Na ₂ O	1.50	2.88	3.21	2.08	2.52	1.55	2.03	1.98	2.35	2.03
K ₂ O	0.08	0.20	0.26	0.10	0.13	0.08	0.10	0.09	0.12	0.07
TiO ₂	0.14	0.41	0.42	0.36	0.19	0.25	0.30	0.31	0.42	0.34
P ₂ O ₅	0.01	0.03	0.01	0.02	0.01	0.02	0.03	0.02	0.03	0.02
L.O.I.	1.39	1.46	1.78	1.04	2.28	0.86	1.55	1.72	0.84	1.63
TOTAL	99.74	99.87	99.79	100.09	99.64	100.30	100.00	100.25	99.78	100.17
Trace Elements in ppm										
Sr	124	176	206	127	185	149	135	139	154	112
Rb	1	2.3	2	1.4	1.7	1.3	0.7	1	1	1
Y	3.7	10.3	13	9.3	3.8	5.3	6	7.7	12.4	9.6
Zr	3.4	17.6	41	11.6	5.3	8.6	11.5	8.9	15	13.6
Nb	0.7	2	3	1	0.7	1.5	1.6	1.3	1.9	1.8
Ba	15	39	61	20	27	22	18	17	37	22
Sc	30	45	47	57	30	29	30	47	51	48
V	91	182	153	193	95	99	112	163	198	165
Ti	897	2361	2297	1236	1361	1719	1969	2481	1973	1973
Cr	912	294	875	782	555	430	422	1600	441	751
Ni	100	79	80	144	94	136	118	161	107	187
Cu	84	6	3	115	35	82	98	80	7	132
Zn	16	11	13	19	19	22	24	21	16	37
CIPW Norm										
OR	0.47	1.18	1.54	0.59	0.77	0.47	0.59	0.53	0.71	0.41
AB	12.69	24.37	25.07	17.60	17.80	13.12	17.18	14.86	19.89	17.18
AN	56.12	33.12	31.13	38.48	57.23	51.94	50.13	41.90	33.38	36.74
NE	-	-	1.13	-	1.91	-	-	1.03	-	-
DI Wo	10.14	16.09	16.41	17.58	6.44	10.86	9.31	16.03	17.07	16.30
En	7.66	12.30	12.80	13.15	4.40	8.06	6.78	11.61	12.47	11.57
Fs	1.45	2.11	1.81	2.69	1.53	1.75	1.67	2.96	3.00	3.31
HY En	1.98	0.81	-	0.65	-	3.47	2.48	-	4.28	0.07
Fs	0.37	0.14	-	0.13	-	0.75	0.61	-	1.03	0.02
OL Fo	6.12	5.40	7.10	5.81	6.18	6.35	6.85	7.82	4.02	9.33
Fa	1.28	1.02	1.11	1.31	2.38	1.52	1.86	2.19	1.06	2.94
MT	1.16	2.51	0.86	1.36	0.61	1.48	1.91	0.70	2.00	1.61
IL	0.27	0.78	0.80	0.68	0.36	0.47	0.57	0.59	0.80	0.65
AP	0.02	0.07	0.02	0.05	0.02	0.05	0.07	0.05	0.07	0.05
TOTAL	99.74	99.89	99.78	100.09	99.64	100.30	100.00	100.25	99.78	100.17
g#	84.95	83.15	87.52	83.56	77.11	82.86	80.45	82.07	80.82	79.62
SiO ₂ /MgO	0.42	0.57	0.32	0.46	0.61	0.49	0.61	0.44	0.57	0.57

UPPER LEVEL GABBRO

Sample No:	221A	223B	224	225	227	228	229	230	232	233
SiO ₂	50.83	48.61	50.04	49.00	47.94	53.05	49.17	50.10	50.28	47.82
Al ₂ O ₃	17.26	23.83	16.55	17.61	21.66	18.71	23.69	20.16	17.05	18.82
Fe ₂ O ₃	1.72	1.15	1.18	1.51	0.89	0.77	3.86	0.83	0.89	1.55
FeO	5.84	2.74	3.93	4.14	3.88	3.56	-	4.50	2.72	4.05
MnO	0.16	0.06	0.13	0.12	0.12	0.09	0.09	0.10	0.10	0.10
MgO	8.09	6.85	10.34	11.18	9.18	6.77	6.73	8.01	9.39	12.19
CaO	10.04	14.68	15.93	14.77	13.77	12.57	13.77	13.41	17.80	14.02
Na ₂ O	3.93	2.09	1.83	1.45	2.08	3.60	2.44	2.41	1.69	1.45
K ₂ O	0.25	0.04	0.07	0.04	0.14	0.31	0.20	0.22	0.05	0.07
TiO ₂	1.42	0.13	0.23	0.22	0.19	0.44	0.21	0.28	0.23	0.19
P ₂ O ₅	0.39	0.01	0.01	0.01	0.02	0.05	0.02	0.04	0.01	0.01
L.O.I.	1.86	1.93	1.59	1.55	2.58	1.61	1.76	1.50	1.36	1.35
TOTAL	99.93	100.19	100.24	100.04	99.87	99.92	100.16	100.04	100.21	100.27

Trace Elements in ppm

Sr	299	140	125	117	171	197	160	152	150	129
Rb	1.5	0.4	0.9	0.7	1.8	3.7	1.5	3.2	0.9	0.6
Y	23	2.5	6.8	4.9	4	14	4.3	17	5.9	4.6
Zr	127	2.6	2.4	4.5	7.3	61	9.4	74	5.8	4.3
Nb	42	0.4	1.3	0	1	4	1.8	4	0.3	1
Ba	73	20	21	12	62	52	27	52	26	14
Sc	32	27	61	40	26	36	25	32	48	34
V	189	77	187	133	88	149	84	123	150	109
Ni	8119	881	1588	1356	1069	2546	1256	1688	1360	1168
Cr	257	291	1111	1151	538	169	628	487	1726	781
Mn	122	116	137	171	173	58	114	119	128	239
Cu	7	38	21	96	18	42	40	17	43	79
Zn	46	27	23	29	59	21	30	22	22	29

IPW Norm

R	1.48	0.24	0.41	0.24	0.83	1.83	1.18	1.30	0.30	0.41
B	33.26	17.69	15.49	12.27	16.75	30.46	20.65	20.39	13.34	12.27
N	28.72	55.53	36.74	41.43	49.35	33.98	53.10	43.54	38.79	44.64
E	-	-	-	-	0.46	-	-	-	0.52	-
I Wo	7.74	7.20	17.63	13.27	7.86	11.71	6.30	9.49	20.65	10.38
En	5.25	5.28	12.91	9.81	5.62	8.16	4.50	6.41	15.76	7.79
Fs	1.89	1.23	3.06	2.19	1.55	2.58	1.24	2.35	2.74	1.55
Y En	2.41	2.04	1.37	7.07	-	2.41	0.89	3.76	-	3.86
Fs	0.87	0.48	0.32	1.58	-	0.76	0.24	1.37	-	0.77
L Fo	8.75	6.82	8.04	7.69	12.08	4.41	7.97	6.85	5.34	13.11
Fa	3.47	1.75	2.10	1.89	3.67	1.54	2.42	2.76	1.02	2.87
T	2.49	1.67	1.71	2.19	1.29	1.12	1.25	1.20	1.29	2.25
L	2.70	0.25	0.44	0.42	0.36	0.84	0.40	0.53	0.44	0.36
P	0.91	0.02	0.02	0.02	0.05	0.12	0.05	0.09	0.02	0.02
TOTAL	99.93	100.19	100.24	100.05	99.87	99.92	100.18	100.06	100.21	100.27
#	71.17	81.67	82.42	82.79	80.83	77.22	79.99	76.03	86.02	84.28
Ca*/MgO	0.93	0.57	0.49	0.50	0.52	0.64	0.57	0.66	0.38	0.46

UPPER LEVEL GABBRO

Sample No:	234	235	236	238	242	243	244	604	606	607
SiO2	49.80	45.92	49.92	48.13	48.33	48.09	48.37	48.74	47.35	49.65
Al2O3	19.45	12.61	17.14	12.29	21.52	16.25	23.96	17.20	23.97	18.20
Fe2O3	0.09	2.92	1.34	2.28	3.49	1.77	0.72	0.61	4.03	0.12
FeO	4.45	5.60	4.12	4.99	-	3.83	2.77	4.04	-	4.51
MnO	0.10	0.15	0.09	0.15	0.08	0.12	0.07	0.10	0.07	0.10
MgO	9.10	21.00	9.34	16.95	8.97	14.62	7.41	12.52	8.57	10.77
CaO	14.25	10.64	14.81	13.89	15.76	14.07	14.11	14.90	13.51	15.22
Na2O	2.30	0.88	2.25	0.91	1.57	1.21	2.20	1.42	2.15	1.49
K2O	0.22	0.06	0.10	0.03	0.11	0.13	0.36	0.18	0.13	0.07
TiO2	0.24	0.22	0.96	0.24	0.14	0.17	0.19	0.18	0.12	0.18
P2O5	0.02	0.02	0.07	0.01	0.01	0.01	0.02	0.01	0.01	0.02
L.O.I.	2.19	3.42	1.28	2.36	1.86	3.08	2.76	2.45	3.39	1.49
TOTAL	100.07	100.02	100.18	99.87	99.98	100.27	100.18	99.88	99.92	100.08

Trace Elements in ppm

Sr	150	75	129	72	138	94	205	117	197	92
Rb	1.9	1.9	1	0.9	1.7	1.6	5	3.1	2.3	1
Y	5	4.8	16	6.3	3.4	3.9	3.3	3.3	2	6
Zr	6.5	7.9	41	6	2.5	4.5	5.9	3.2	2.4	4.5
Nb	1	1.3	6.4	0.8	0.7	0	0.8	1.2	0	0.2
Ba	21	11	19	11	20	14	65	22	29	10
Sc	40	27	43	43	35	42	30	45	21	40
V	134	89	227	149	107	129	96	134	67	131
Ti	1443	1242	5541	1354	1006	1150	1229	1222	714	1148
Cr	384	1368	544	929	912	740	261	730	287	336
Ni	149	573	124	293	289	307	128	262	155	130
Cu	100	122	8	113	195	45	58	49	24	107
Zn	23	47	17	37	16	30	19	24	30	19

CIPW Norm

OR	1.30	0.35	0.59	0.18	0.65	0.77	2.13	1.06	0.77	0.41
AB	18.58	7.45	19.04	7.70	13.29	10.24	16.82	12.02	15.15	12.61
AN	42.10	30.28	36.38	29.36	51.35	38.53	54.44	40.03	55.37	42.77
NE	0.48	-	-	-	-	-	0.97	-	1.63	-
DI Wo	11.89	9.34	15.30	16.49	11.18	13.03	6.44	14.12	4.84	13.62
En	8.12	7.25	11.36	12.62	8.59	10.10	4.73	10.47	3.31	9.58
Fs	2.83	1.08	2.45	2.14	1.41	1.53	1.10	2.28	1.14	2.88
HY En	-	8.47	2.20	8.84	1.20	4.95	-	1.90	-	4.93
Fs	-	1.26	0.47	1.50	0.20	0.75	-	0.41	-	1.48
OL Fo	10.19	25.63	6.80	14.54	8.79	14.97	9.62	13.18	12.63	8.63
Fa	3.91	4.21	1.61	2.72	1.59	2.50	2.47	3.17	4.78	2.86
MT	0.13	4.23	2.00	3.31	1.45	2.57	1.04	0.88	-	0.17
IL	0.46	0.42	1.82	0.46	0.27	0.32	0.36	0.34	0.23	0.34
AP	-	0.05	0.16	0.02	0.02	0.02	0.05	0.02	0.02	0.05
TOTAL	100.02	100.02	100.18	99.87	99.98	100.27	100.18	99.90	99.91	100.33

Mg#	78.47	86.98	80.16	85.82	86.52	87.18	82.66	84.67	79.12	80.97
FeO*/MgO	0.49	0.41	0.58	0.43	0.39	0.38	0.47	0.37	0.47	0.43

& GABBROIC MYLONITE (150, 158, 171)

Sample No:	673	675	150	158	171
SiO ₂	49.08	49.78	50.47	51.60	45.93
Al ₂ O ₃	16.26	18.71	17.78	16.79	14.84
Fe ₂ O ₃	1.57	1.23	6.57	6.43	7.20
FeO	4.70	4.51	-	-	-
MnO	0.12	0.11	0.14	0.13	0.17
MgO	12.70	9.74	8.95	8.47	9.78
CaO	13.33	13.21	12.71	12.56	19.51
Na ₂ O	1.72	2.70	2.80	2.96	0.86
K ₂ O	0.04	0.07	0.11	0.20	0.14
TiO ₂	0.25	0.23	0.38	0.38	1.26
P ₂ O ₅	0.02	0.02	0.02	0.03	0.25
L.O.I.	1.32	0.66	0.67	0.71	2.87
TOTAL	99.79	100.31	99.93	99.57	99.93

Trace Elements in ppm

Sr	147	184	210	180	81
Rb	0.7	0.5	1.6	2.2	1.2
Y	7.2	4.6	9	12	79
Zr	5.2	3.9	9.6		95
Nb	0.2	0.7	0.3	na	27
Ba	20	25	38	54	64
Sc	38	31	32	41	62
V	137	113	149	177	349
Ti	1520	1320	2218	2422	9591
Cr	534	294	178	104	246
Ni	246	183	139	80	212
Cu	91	84	na	na	na
Zn	31	29	na	na	na

CIPW Norm

OR	0.24	0.41	0.65	1.18	0.66
AB	14.55	21.89	23.69	25.05	-
AN	36.53	38.73	35.62	31.94	36.22
NE	-	0.52	-	-	3.94
DI Wo	12.31	11.14	11.40	12.60	24.61
En	9.08	7.88	7.70	8.45	17.18
Fs	2.05	2.30	2.83	3.21	5.38
HY En	7.14	-	2.58	4.94	-
Fs	1.61	-	0.95	1.88	-
OL Fo	10.80	11.48	8.42	5.40	5.03
Fa	2.69	3.70	3.42	2.26	1.74
MT	2.28	1.78	1.90	1.86	2.09
IL	0.47	0.44	0.72	0.72	2.39
AP	0.05	0.05	0.05	0.07	0.58
TOTAL	99.79	100.31	99.93	99.55	99.94
Mg#	82.81	79.38	75.20	74.56	75.16

Sample No:	68	69	70	75	76	78	79	80	81
SiO ₂	48.92	50.62	49.77	52.23	51.20	49.21	50.07	49.38	50.15
Al ₂ O ₃	19.45	18.24	17.43	16.26	17.67	15.94	15.89	16.08	16.71
Fe ₂ O ₃	0.87	0.59	1.23	0.33	1.06	1.13	0.49	1.63	0.68
FeO	5.76	5.12	4.70	6.36	4.84	5.25	5.62	5.02	4.85
MnO	0.12	0.12	0.13	0.15	0.13	0.11	0.11	0.13	0.11
MgO	9.93	8.32	9.82	10.01	8.67	11.45	10.73	11.78	9.78
CaO	12.06	13.87	14.66	11.76	12.80	13.92	14.51	13.59	14.90
Na ₂ O	2.25	2.68	2.14	2.45	3.12	1.81	1.94	2.07	2.07
K ₂ O	0.14	0.09	0.07	0.05	0.09	0.07	0.07	0.11	0.07
TiO ₂	0.23	0.39	0.33	0.33	0.34	0.36	0.41	0.29	0.38
P ₂ O ₅	0.03	0.01	0.11	0.01	0.01	0.04	0.04	0.01	0.01
L.O.I.	1.45	1.81	1.82	0.38	2.47	0.79	0.63	2.39	1.33
TOTAL	99.76	99.96	100.29	99.94	99.93	99.29	99.88	100.09	99.71

Trace Elements in ppm

Sr	197	186	166	163	212	140	145	153	174
Rb	2.5	0.8	0.7	0.7	0.9	0.9	1.6	1.4	1.2
Y	6	10	10	7.7	8.3	11	12	8.2	9.5
Zr	13	9.2	15		5.5	22	16	7.9	10
Nb	2.2	1.7	1.7		0.8	2.8	1.6	1.2	1
Ba	44	33	43	22	34	35	34	42	27
Sc	22	44	41	37	48	37	41	42	45
V	85	183	167	160	192	154	173	162	183
Ti	1330	2398	1932	1783	2096	2166	2433	1799	2302
Cr	359	756	384	76	100	777	391	576	787
Ni	195	151	153	81	83	221	165	217	171
Cu	51	36	74	na	15	69	79	97	67
Zn	38	31	31	na	33	38	32	40	28

CIPW Norm

OR	0.83	0.53	0.41	0.30	0.53	0.41	0.41	0.65	0.41
AB	19.04	22.68	18.11	20.73	26.40	15.32	16.42	17.52	17.52
AN	42.56	37.48	37.75	33.22	33.95	35.16	34.44	34.26	36.10
DI Wo	7.13	13.06	14.58	10.46	12.31	14.04	15.57	13.82	15.77
En	4.75	8.60	10.27	6.75	8.37	9.93	10.60	9.97	10.92
Fs	1.86	3.53	3.07	3.02	2.98	2.90	3.75	2.59	3.55
HY En	4.56	0.60	1.24	13.28	0.73	5.20	3.73	2.45	2.48
Fs	1.79	0.24	0.37	5.93	0.26	1.52	1.32	0.64	0.81
OL Fo	10.81	8.07	9.08	3.44	8.75	9.38	8.68	11.85	7.68
Fa	4.67	3.65	2.99	1.69	3.44	3.01	3.38	3.40	2.75
MT	1.26	0.86	1.78	0.48	1.54	1.64	0.71	2.36	0.99
IL	0.44	0.74	0.63	0.63	0.65	0.68	0.78	0.55	0.72
AP	0.07	0.02	0.02	0.02	0.02	0.09	0.09	0.02	0.02
TOTAL	99.76	100.05	100.29	99.94	99.93	99.29	99.88	100.09	99.71

Mg#	75.45	74.33	78.83	73.72	76.15	79.54	77.29	80.70	78.23
-----	-------	-------	-------	-------	-------	-------	-------	-------	-------

MASSIVE GABBROS (501 - 521) & WERHLITE (671,2)

Sample No:	501	502	508	524	52	53	521	671	672
SiO ₂	48.88	47.23	49.26	46.19	49.28	49.95	46.02	41.52	40.91
Al ₂ O ₃	14.64	17.05	18.41	7.99	17.12	16.73	20.78	6.81	7.05
Fe ₂ O ₃	2.72	1.00	0.71	4.92	0.89	5.56	1.92	4.65	4.96
FeO	9.84	10.50	3.54	4.27	5.98	-	3.86	8.35	7.50
MnO	0.25	0.18	0.09	0.16	0.15	0.13	0.11	0.22	0.19
MgO	7.50	9.05	11.47	23.63	10.25	10.71	13.81	33.87	34.69
CaO	10.79	10.98	14.75	12.18	13.46	14.60	12.81	4.06	3.62
Na ₂ O	3.64	3.21	1.81	0.39	2.49	1.88	1.14	0.43	0.41
K ₂ O	0.19	0.13	0.05	0.04	0.08	0.06	0.19	0.05	0.03
TiO ₂	1.25	0.99	0.19	0.24	0.40	0.29	0.20	0.29	0.21
P ₂ O ₅	0.10	0.08	0.01	0.01	0.02	0.01	0.02	0.03	0.02
L.O.I.	2.74	3.01	1.98	5.44	2.10	1.54	2.97	5.08	6.99
TOTAL	99.81	100.22	100.29	100.02	100.12	99.92	100.14	100.27	99.59
Trace Elements in ppm									
Sr	171	182	151	37	166	153	110	45	58
Rb	1.9	0.9	1.2	0.2	0.2	0.9	2.3	2.7	2.2
Y	28	24	4.5	6	11	7.4	5	5.6	3.5
Zr	56	53	3.5	4.2	12	5.4	9.4	13	9
Nb	3.9	3.6	0.4	0.6	0.5	0	0.6	1.9	1.3
Ba	51	41	18	19	32	24	34	8	6
Sc	45	33	36	46	45	41	18	15	12
V	240	172	121	158	194	157	73	70	53
Ti	6029	4696	1154	1560	2527	1796	1238	1326	894
Cr	216	300	489	1801	201	515	1271	2463	2309
Ni	52	101	291	716	140	188	275	1274	1376
Cu	79	110	72	81	73	81	74	38	29
Zn	76	74	20	44	35	28	32	63	58
CIPW Norm									
OR	1.12	0.77	0.30	0.24	0.47	0.35	1.12	0.30	0.18
AB	27.60	19.54	15.32	3.30	19.33	15.91	9.65	3.64	3.47
AN	23.05	31.73	41.96	19.93	35.30	37.04	51.02	16.50	17.31
NE	1.74	4.13	-	-	0.94	-	-	-	-
DI	12.45	9.28	13.01	16.88	13.09	14.75	5.18	1.44	0.22
Wo	6.82	5.08	9.74	13.93	8.74	10.52	4.00	1.13	0.17
En	5.19	3.86	1.97	0.87	3.38	2.93	0.63	0.15	0.02
Fs	-	-	1.34	11.53	-	4.61	3.25	8.31	8.35
HY	-	-	0.27	0.72	-	1.28	0.51	1.13	0.94
En	8.31	12.24	12.25	23.40	11.76	8.09	19.02	52.50	54.57
Fo	6.98	10.26	2.73	1.61	5.01	2.48	3.28	7.83	6.74
Fa	3.94	1.45	1.03	7.13	1.29	1.39	2.78	6.74	7.19
MT	2.37	1.88	0.36	0.46	0.76	0.55	0.38	0.55	0.40
IL	0.23	0.19	0.02	0.02	0.05	0.02	0.05	0.07	0.05
AP	0.23	0.19	0.02	0.02	0.05	0.02	0.05	0.07	0.05
TOTAL	99.80	100.40	100.29	100.02	100.12	99.92	100.86	100.28	99.59
Mg#	57.59	60.57	85.24	90.79	75.34	80.58	86.44	87.85	89.18

Sample No:	702	703	706	707	708	709	711	7130*	7136
SiO2	45.57	50.86	51.35	48.48	50.50	49.29	47.03	50.19	50.57
Al2O3	22.60	14.25	16.78	19.32	16.91	21.27	29.56	15.59	16.65
Fe2O3	1.64	0.87	1.83	1.09	1.56	1.09	0.55	8.19	6.31
FeO	3.62	3.38	4.13	2.95	4.44	4.05	-	-	-
MnO	0.06	0.09	0.11	0.08	0.14	0.10	0.04	0.09	0.10
MgO	11.41	9.68	9.61	10.68	10.01	8.47	2.97	9.34	10.71
CaO	13.24	16.39	11.99	16.03	13.28	13.59	14.02	12.08	12.07
Na2O	1.35	2.65	3.25	1.42	2.47	2.40	2.60	2.29	2.75
K2O	0.21	0.26	0.37	0.04	0.19	0.19	1.09	0.43	0.49
TiO2	0.25	0.93	0.47	0.18	0.48	0.30	0.15	1.60	0.43
P2O5	0.02	0.17	0.03	0.01	0.02	0.02	0.0	0.20	0.01
L.O.I.	2.51	1.05	2.40	2.25	2.09	2.72	2.50	1.76	2.85
TOTAL	99.97	99.51	99.91	100.28	99.99	99.99	100.26	100.01	100.08

Trace Elements in ppm

Sr	136	282	159	120	149	155	365	170	188
Rb	2.8	3.7	4.6	0.6	1.2	2.6	14	6	5
Y	6.7	17	11	4.9	16	6.9	2.7	34	13
Zr	21	47	16	2.4	22	15	8	103	17
Nb	3.4	9	2	0.7	2.8	1.5	0.9	17	2.6
Ba	38	83	45	18	34	31	170	40	57
Sc	15	66	39	43	30	9.6	33	47	48
V	58	237	185	133	188	112	28	307	184
Ti	1423	5946	2560	1222	2691	1512	888	9211	2429
Cr	354	414	122	1367	572	358	8	76	492
Ni	271	106	130	283	104	113	48	88	117
Cu	4	5	6	142	19	123	3	na	na
Zn	18	10	19	29	49	40	10	na	na

CIPW Norm

OR	1.24	1.54	2.19	0.24	1.12	1.12	6.44	2.54	2.90
AB	11.42	16.93	27.50	12.02	20.90	18.69	12.94	19.38	23.22
AN	54.99	26.22	30.11	46.23	34.49	46.71	65.77	30.99	31.64
NE	-	2.97	-	-	-	0.88	4.91	-	0.03
DI Wo	4.41	22.54	12.18	13.88	13.05	8.60	1.58	11.54	11.76
En	3.36	17.24	8.96	10.66	9.45	6.07	1.34	7.65	8.18
Fs	0.59	2.95	2.06	1.75	2.40	1.79	0.03	3.05	2.62
HY En	0.29	-	0.45	1.12	4.14	-	-	9.76	-
Fs	0.05	-	0.10	0.18	1.05	-	-	3.90	-
OL Fo	17.35	4.81	10.18	10.38	7.95	10.53	4.24	4.10	12.96
Fa	3.36	0.91	2.58	1.88	2.22	3.43	0.11	1.80	4.57
MT	2.38	1.26	2.65	1.58	2.26	1.58	0.36	1.78	1.38
IL	0.47	1.77	0.89	0.34	0.91	0.57	0.28	3.04	0.82
AP	0.05	0.40	0.07	0.02	0.05	0.05	-	0.46	0.02
TOTAL	99.97	99.53	99.92	100.28	100.00	100.00	100.26	100.00	100.09
Mg#	84.88	83.62	80.57	86.58	80.00	78.85	94.63	70.51	78.07

* : Dolerite dyke

EAST COAST

.16-

Sample No:	715	723A	726	727
SiO ₂	47.03	49.32	50.16	56.21
Al ₂ O ₃	14.99	14.60	17.00	22.12
Fe ₂ O ₃	1.75	11.01	2.83	0.44
FeO	4.78	-	6.23	1.10
MnO	0.10	0.20	0.14	0.04
MgO	15.68	7.33	7.33	2.66
CaO	13.72	12.46	9.33	9.01
Na ₂ O	0.95	3.41	3.92	6.21
K ₂ O	0.05	0.03	0.36	0.37
TiO ₂	0.16	1.71	1.94	0.97
P ₂ O ₅	0.01	0.20	0.40	0.24
L.O.I.	1.94	2.76	2.06	1.06
TOTAL	99.22	100.27	99.64	99.37

Trace Elements in ppm

Sr	91	145	316	394
Rb	1.4	0.5	5.2	3.7
Y	3.2	34	30	5.6
Zr	2.9	105	139	191
Nb	0.9	16	45	67
Ba	12	44	121	99
Sc	36	30	36	5.9
V	104	301	260	34
Ti	928	8830	8674	4855
Cr	1346	na	<5	25
Ni	359	48	37	38
Cu	114	na	3	10
Zn	32		26	6

CIPW Norm

OR	0.30	0.18	2.13	2.19
AB	8.04	25.86	33.17	51.01
AN	36.49	24.44	27.73	31.39
NE	-	-	-	0.83
DI Wo	13.16	15.06	6.66	4.90
En	9.96	8.36	4.58	4.17
Fs	1.85	6.11	1.55	0.08
HY En	5.87	-	5.24	-
Fs	1.09	-	1.77	-
OL Fo	16.27	6.93	5.91	1.72
Fa	3.33	5.59	2.20	0.04
MT	2.54	2.41	4.10	0.64
IL	0.30	3.25	3.68	1.84
AP	0.02	0.46	0.93	0.56
TOTAL	99.22	100.27	99.64	99.37

Mg#	85.39	58.28	67.70	81.15
-----	-------	-------	-------	-------

Sample No:	38236	38237	38242	38449	38451	153	38334	38273	38320	38425
SiO ₂	51.53	49.41	48.97	51.11	48.96	50.57	49.86	50.17	50.51	51.38
Al ₂ O ₃	14.76	21.01	15.91	15.38	21.80	14.98	16.42	16.17	15.57	15.42
Fe ₂ O ₃	1.79	0.97	1.56	1.42	0.98	1.46	1.49	1.49	1.44	1.48
FeO	9.11	4.95	7.93	7.24	5.02	7.44	7.58	7.60	7.36	7.52
MnO	0.18	0.12	0.16	0.15	0.11	0.12	0.17	0.19	0.18	0.17
MgO	7.68	6.83	9.69	8.98	6.43	7.21	9.52	7.24	9.26	7.15
CaO	9.73	13.62	11.97	12.07	13.52	11.79	10.32	11.19	11.86	11.31
Na ₂ O	7.10	2.09	2.51	2.13	2.41	3.19	2.21	3.37	2.44	3.14
K ₂ O	0.11	0.11	0.12	0.15	0.08	0.31	1.16	0.68	0.18	0.37
TiO ₂	1.72	0.77	1.05	1.20	0.61	2.61	1.12	1.62	1.09	1.81
P ₂ O ₅	0.29	0.11	0.13	0.16	0.07	0.32	0.14	0.29	0.12	0.26
L.O.I.	3.26	1.82	2.28	0.94	2.42	5.03	3.39	2.38	2.50	1.34

Trace Elements in ppm

Sr	157	135		144	148	199	163	280	160	191
Rb	0.6	0.6		2	2	0	29	12	2	6
Y	37	17		23	14	53	20	27	23	33
Zr	na	na		76	36	135	77	124	66	126
Nb				11	2	19	5	32	4	22
Ba	59	15	na		na	na	na	187	41	69
Sc	43	32			na	na	na	33	43	43
V	326	185			na	na	na	245	261	330
Ti	9488	4179						9110	6015	9738
Cr	7	299		180	480	80	392	89	346	150
Ni	46	89		97	88	58	108	72	133	65
Cu	na	na		na	na	na	na	na	na	na
Zn	na	na		na	na	na	na	na	na	na

CIPW Norm

QR	-	-	-	0.41	-	-	-	-	-	-
OR	0.65	0.65	0.71	0.89	0.47	1.83	6.86	4.02	1.06	2.19
AB	27.97	17.69	21.24	18.02	20.39	26.99	18.70	28.33	20.65	26.57
AN	8.08	47.62	31.79	31.96	48.43	25.64	31.46	26.99	31.00	26.89
NE	17.39	-	-	-	-	-	-	0.10	-	-
DI Wo	15.99	8.03	11.17	11.22	7.59	12.84	7.86	11.12	11.30	11.49
En	9.17	5.24	7.03	7.16	4.82	8.19	5.00	6.68	7.19	6.98
Fs	6.11	2.23	3.45	3.34	2.29	3.82	2.35	3.85	3.39	3.88
HY En	-	8.31	3.89	15.20	3.19	6.19	7.98	-	10.08	8.41
Fs	-	3.54	1.91	7.08	1.52	2.88	3.75	-	4.75	4.68
OL Fo	6.98	2.42	9.26	-	5.61	2.51	7.52	7.96	4.06	1.70
Fa	5.12	1.14	5.01	-	2.94	1.29	3.90	5.06	2.11	1.04
MT	2.60	1.41	2.26	2.06	1.42	2.12	2.16	2.16	2.09	2.15
IL	3.27	1.46	1.99	2.28	1.16	4.96	2.13	3.08	2.07	3.44
AP	0.67	0.26	0.30	0.37	0.16	0.74	0.33	0.67	0.28	0.60
TOTAL		99.99	100.00	99.99	99.99	100.00	99.99	100.01	100.01	100.01
Mg#	56.10	67.70	64.90	65.30	66.00	59.50	65.50	59.10	65.60	59.00
FeO*/MgO	1.42	0.87	0.98	0.96	0.93	1.23	0.95	1.25	0.95	1.26

I) DOLERITE DYKES IN LAYERED SEQUENCE (303 - 3910)

& UPPER LEVEL GABBRO (21301 - 221B)

Sample No:	303	325	37200	379C	379R	3910	21301*	21302	21303	221B
SiO2	48.30	49.18	49.98	49.69	51.01	50.71	58.26	50.26	50.55	49.75
Al2O3	21.09	16.01	15.05	15.72	15.01	14.31	22.68	18.32	15.30	17.42
Fe2O3	1.14	11.44	11.41	10.47	10.32	13.33	0.71	7.26	9.16	7.48
FeO	5.35	-	-	-	-	-	-	-	-	-
MnO	0.16	0.18	0.22	0.21	0.20	0.17	0.03	0.13	0.17	0.14
MgO	6.37	7.87	7.21	7.25	6.86	5.58	2.02	7.65	8.48	8.11
CaO	13.61	10.73	11.13	11.39	10.23	7.88	8.03	12.40	11.31	10.35
Na2O	2.79	3.00	3.20	3.44	4.23	4.84	6.73	3.05	3.34	3.80
K2O	0.10	0.13	0.09	0.08	0.06	0.15	0.39	0.24	0.15	0.23
TiO2	0.81	1.48	1.67	1.54	1.70	2.36	0.10	0.85	1.31	1.40
P2O5	0.10	0.21	0.24	0.24	0.26	0.39	0.0	0.07	0.12	0.39
L.O.I.	2.07	1.43	0.64	1.80	1.68	1.46	0.99	1.30	0.97	1.52
TOTAL	99.82	100.23	100.19	100.03	99.88	99.72	99.41	100.23	99.89	99.07

Trace Elements in ppm

Sr	228	263	189	240	248	168	430	171	139	318
Rb	1.4	0.7	0.6	0.9	0.3	0.1	3.6	3.4	2.8	1.3
Y	16	31	37	31	35	47	4.7	21	31	23
Zr	47	100	117	103	116	165	9.5	45	77	127
Nb	6.8	17	19	18	21	40	0.3	2.5	7	41
Ba	45	62	73	84	74	51	98	54	42	80
Sc	25	38	41	35	37	40	13	39	44	28
V	148	280	325	276	306	395	21	221	296	186
Ti	4000	8001	9532	8201	8905	12741	577	5123	7812	7407
Cr	212	329	14	100	54	<5	211	369	243	257
Ni	77	118	45	69	52	27	19	100	102	117
Cu	18	na	na	na	na	na	na	na	na	na
Zn	55	na	na	na	na	na	na	na	na	na

CIPW Norm

OR	0.59	0.77	0.53	0.47	0.35	0.89	2.30	1.42	0.89	1.36
AB	20.69	25.39	27.08	29.11	35.79	40.96	56.69	25.81	28.26	31.53
AN	44.73	29.84	26.44	27.22	21.79	16.88	30.53	35.59	26.31	29.80
NE	1.58	-	-	-	-	-	0.14	-	-	0.34
DI Wo	9.24	9.20	11.36	11.57	11.38	8.21	3.89	10.63	12.11	7.93
En	5.81	5.11	6.15	6.48	6.34	3.83	3.30	6.71	7.44	5.16
Fs	2.87	3.73	4.82	4.63	4.60	4.29	0.08	3.26	3.99	2.23
HY En	-	4.47	4.62	0.64	-	1.11	-	0.41	2.10	-
Fs	-	3.27	3.62	0.46	-	1.24	-	0.20	1.12	-
OL Fo	7.05	7.02	5.03	7.66	7.53	6.28	1.22	8.36	8.12	10.53
Fa	3.84	5.65	4.35	6.03	6.02	7.75	0.03	4.47	4.80	5.00
MT	1.65	2.49	2.46	2.28	2.25	2.90	0.58	1.59	1.99	1.62
IL	1.54	2.81	3.17	2.92	3.23	4.48	0.19	1.61	2.49	2.66
AP	0.23	0.49	0.56	0.56	0.60	0.91	-	0.16	0.28	0.91
TOTAL	99.82	100.23	100.20	100.03	99.88	99.72	98.95	100.23	99.89	99.07
Mg#	67.97	59.66	56.95	59.21	58.23	46.74	92.07	68.87	65.98	69.44

* : Gabbroic dyke

IN HARZBURGITE

Sample No:	111A	113	11500	1158	116	119A	127	401	403
SiO ₂	43.37	42.85	49.68	58.61	49.06	44.70	42.10	52.62	41.78
Al ₂ O ₃	14.00	21.50	15.07	24.15	15.30	23.00	16.13	14.48	16.45
Fe ₂ O ₃	10.07	2.85	11.40	0.94	11.74	0.43	10.39	0.61	4.40
FeO	-	-	-	-	-	0.11	-	-	-
MnO	0.23	0.20	0.22	0.01	0.20	0.09	0.20	0.03	0.19
MgO	12.62	13.92	7.38	0.62	7.52	8.46	8.85	1.81	10.73
CaO	18.32	18.57	10.83	7.41	9.95	23.10	20.60	27.58	26.20
Na ₂ O	0.14	0.12	3.17	7.32	3.72	0.08	0.21	2.79	0.13
K ₂ O	0.01	0.03	0.25	0.08	0.32	0.01	0.01	0.02	0.01
TiO ₂	1.25	0.16	1.56	0.16	1.69	0.15	1.46	0.24	0.19
P ₂ O ₅	0.13	0.05	0.17	0.02	0.24	0.02	0.15	0.06	0.0
L.O.I.	4.41	6.93	1.02	1.01	1.44	6.28	4.43	3.02	3.39
TOTAL	100.14	100.25	99.73	99.32	99.74	100.15	100.10	100.24	100.08

Trace Elements in ppm

Sr	9.7	15	210	610	238	22	13	58	83
Rb	0.8	0.8	3.7	1.1	6.2	0.2	0.2	0.3	0
Y	29	4.6	35	44	36	29	32	21	3.8
Zr	71	116	94	178	na	116	93	116	3.7
Nb	6	16	10	88		35	11	83	0.3
Ba	1	8	93	52	111	2	6	94	7
Sc	39	2.5	40	4.7	38	2.6	44	0	37
V	265	9	324	27	298	4	293	11	155
Ti	7242	1177	8785	864	9756	857	8611	1669	1640
Cr	na	na	na	na	na	na	na	na	na
Ni	105	237	58	8	103	30	88	75	340
Cu	-	-	-	na	-	-	-	-	-
Zn	-	-	-	na	-	-	-	-	-

CIPW Norm

OR	-	-	1.48	0.47	1.89	-	-	0.12	-
AB	-	-	26.82	61.47	29.82	-	-	19.97	-
AN	37.54	58.04	26.15	32.80	24.11	62.37	43.04	26.93	44.27
LC	0.05	0.14	-	-	-	0.05	0.05	-	0.05
NE	0.64	0.55	-	0.26	0.90	0.37	0.96	1.97	0.60
DI	Wo	17.13	5.49	11.05	1.60	9.89	10.92	14.56	5.22
	En	11.29	4.48	6.05	1.20	5.40	9.44	8.96	4.51
	Fs	4.61	0.35	4.60	0.24	4.14	-	4.76	1.01
HY	En	-	-	3.66	-	-	-	-	-
	Fs	-	-	2.79	-	-	-	-	-
WO	-	-	-	-	-	-	-	40.51	-
OL	Fo	14.11	21.15	6.07	0.24	9.34	8.15	9.17	14.43
	Fa	6.35	1.80	5.09	0.05	7.89	-	5.37	2.61
CS	-	3.55	6.38	-	-	-	8.03	7.22	20.62
MT	-	2.19	1.45	2.61	0.64	2.61	0.21	2.90	0.40
IL	-	2.37	0.30	2.96	0.30	3.21	0.28	2.77	0.46
HM	-	-	-	-	-	-	0.28	-	0.02
AP	-	0.30	0.12	0.40	0.05	0.56	0.05	0.35	0.14
TOTAL		100.14	100.25	99.73	99.32	99.74	100.15	100.10	100.24

Mg#	72.43	93.06	57.80	68.85	57.41	99.27	65.27	91.22	86.44
FeO*/MgO	0.80	0.20	1.54	1.51	1.56	0.06	1.17	0.34	0.41

APPENDIX 3: Electron Microprobe Analysis and Results

Instrumentation and precision levels of wavelength (WDS) and energy (EDS) dispersive systems

The mineral compositions were determined using a JEOL 733 automated microanalyser at the Electron Optical Centre of the University of Adelaide. The instrument was equipped with three spectrometers for WDS analysis and a Kevex Si(Li) crystal detector for EDS analysis. The operating conditions for EDS were 15 KV accelerating voltage and 5 nA beam current; for WDS, 15 KV and 3 nA respectively. The beam diameter was maintained at 10 μm , except when analysing for exsolution lamellae in pyroxenes; in the latter case, the beam was reduced to a minimum of 2-3 μm .

The KEVEX EDS system was calibrated on oxide and mineral standards and checked on pure copper standards. The counting time was 60 seconds. In WDS analysis, the peak counting time was 100 seconds and background position counting time 60 seconds. Oxides and pure metal standards as well as a set of mineral standards were used for calibration. On line data correction was carried out using the JEOL supplied software package "jastran".

Polished thin sections were prepared for 85 selected samples from harzburgites, troctolites, olivine-gabbros, massive gabbros from the major exposures, wehrlite, and a few basalts and dolerites.

A spinel composition determined by WDS and EDS methods is given in table 1. There is good agreement between the two methods with the only discrepancy being the vanadium content. No vanadium has been detected by the WDS method. Ni has not been detected by the EDS method. Spinel composition in troctolites determined by EDS. Additionally, spinels analysed by WDS in 10 samples. The composition of spinel phenocrysts/

megacrysts in the lavas obtained by WDS. The detection limits of the WDS method for all analysed elements, are lower than those of the EDS method. This is particularly important for minor elements. Detection limits for both methods are given in table 2. The major elements of olivine (Si, Mg, Fe) were determined by EDS and the minor elements (Ni, Mn, Al, Cr, Ti) by WDS. Olivine compositions used for olivine composition profiles in the geothermometry-geospeedometry section were analysed by WDS. Pyroxenes from the troctolites and gabbros analysed by EDS, and enstatites and clinopyroxenes from harzburgites by WDS. Plagioclase compositions obtained by EDS.

Tables of microprobe analyses from representative phases in Microfiche.

FIG. 12A

MACQUARIE ISLAND.

54° 30'

35'

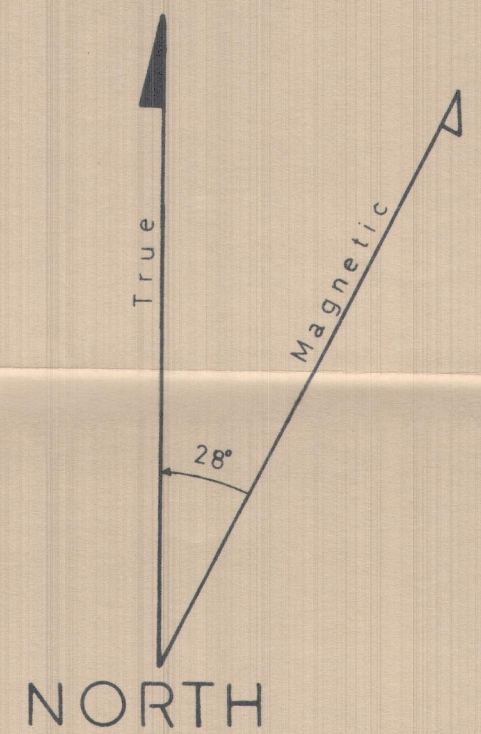
40'

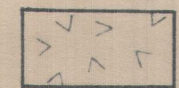

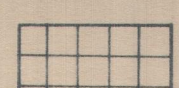



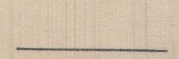

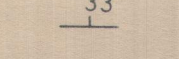
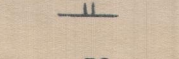

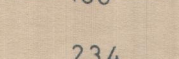


45'

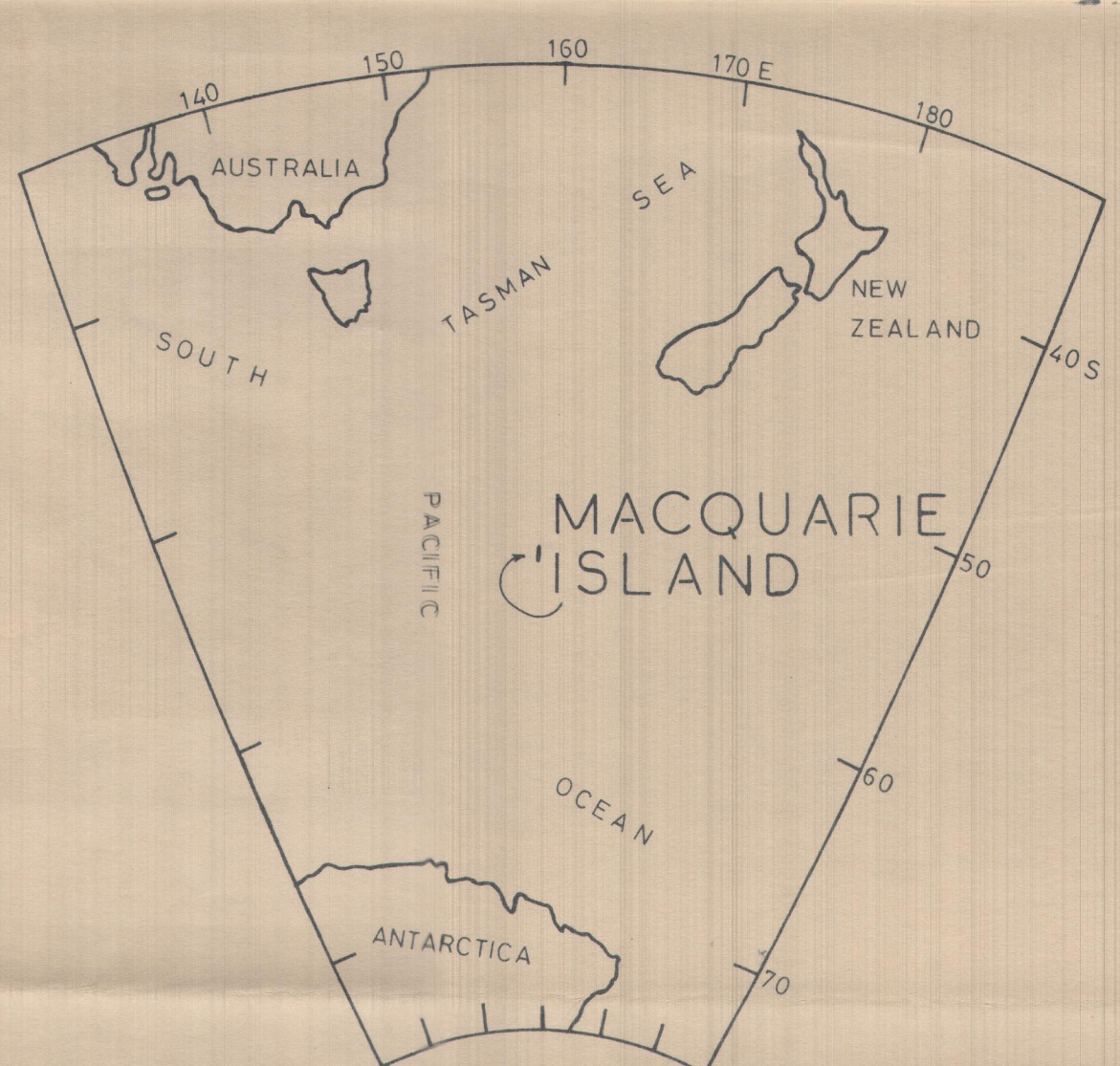
50'

55'

159°00'

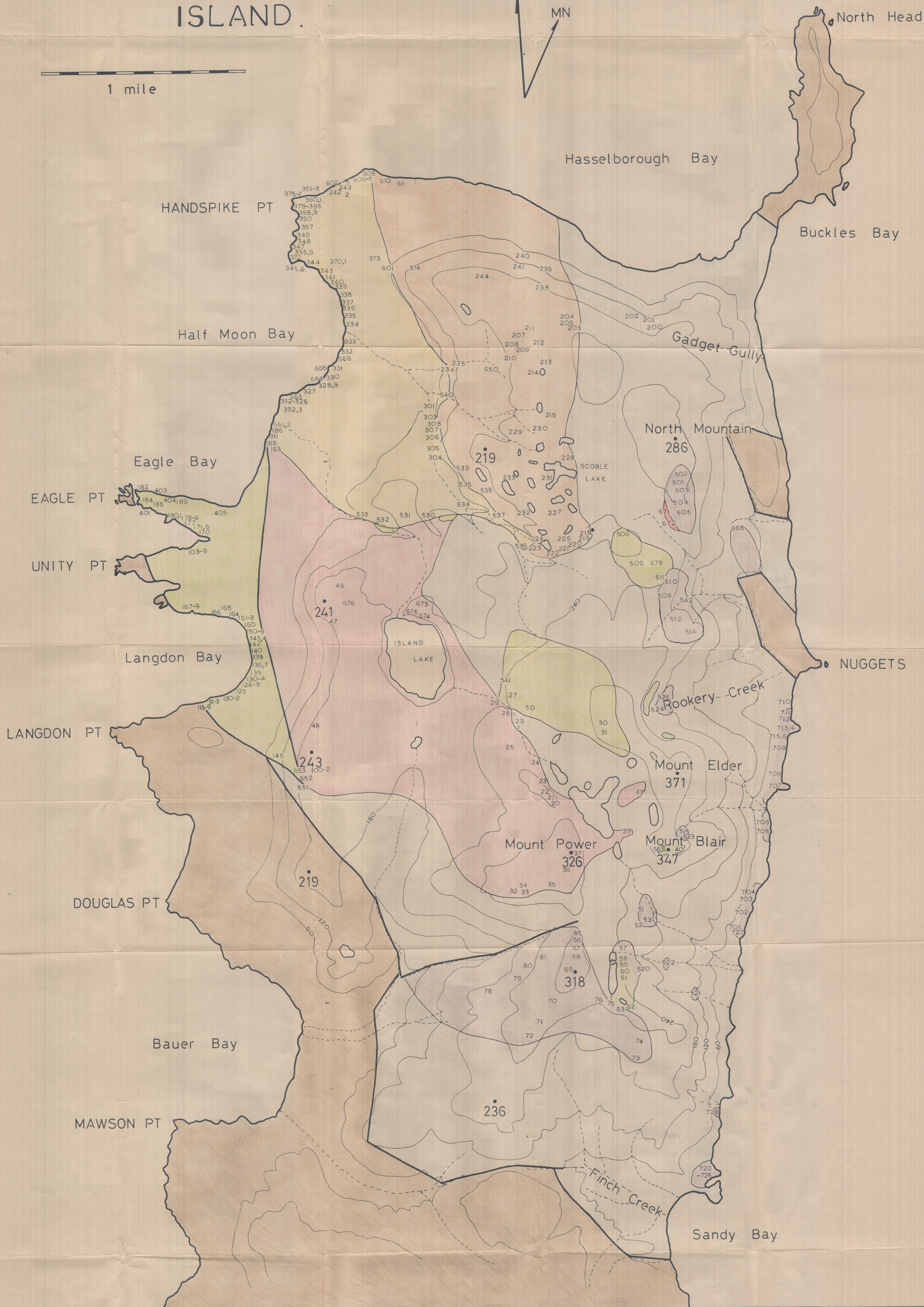


-  PILLOW BASALTS
-  DOLERITE DYKES
-  UPPER LEVEL GABBRO
-  SEQUENCE OF LAYERED GABBROS
-  ULTRAMAFIC ROCKS
-  MASSIVE GABBROIC ROCKS
-  GEOLOGICAL BOUNDARIES
-  FAULTS
-  BEDDING OF LAVAS
-  ATTITUDE OF DYKE SWARMS
-  LAYERING OF GABBROS-TROCTOLITES
-  CONTOURS (METRES)
-  SPOT HEIGHT (METRES)
-  LAKES



MACQUARIE ISLAND.

1 mile



	Geological Boundaries		Lavas
	Faults		Dolerite dike swarms
	Sample Sites		Upper level gabbro
	Contours (meters)		Layered sequence
	Creeks		Peridotites
	Spot Heights (meters)		Island lake gabbro
	Lakes		Massive gabbros
			Wehrlite

LOCALITY

5 KM